Exploring the Genetics of Primary Open-angle Glaucoma with Next Generation Sequencing

By

Dr Tiger Zhou, BPhysio (Hons), BMBS

Thesis
Submitted to Flinders University
for the degree of Doctor of Philosophy

College of Medicine and Public Health

Awarded 7th May 2021

Table of Contents

Declaration and acknowledgments

I certify that this thesis:

1. does not incorporate without acknowledgment any material previously submitted for a degree or diploma in any university; and

2. to the best of my knowledge and belief, does not contain any material previously published or written by another person except where due reference is made in the text.

First and foremost, I would like to acknowledge and thank my principle supervisor Prof Jamie Craig for his guidance, mentorship and tutelage. He has been the most instrumental person in my professional life, without whom I would not have achieved the accomplishments in my career to

date. I would also like to extend my most heartfelt gratitude to my supervisors Dr Shiwani Sharma and Associate Prof Kathryn Burdon for teaching me the skills and knowledge required on the journey that was the PhD candidature. Their instruction and feedback helped me forward whenever I encountered roadblocks. Acknowledgement and many thanks also goes to Prof David Lynn who taught and helped me with RNA sequencing and pathway analysis; Dr Andrew Dubowsky for teaching me skills in mutation analysis; Dr Mark Van der Hoek for technical support with RNA sequencing; And last but not least, Ms Deb Sullivan for helping me deal with the many administrative challenges of the process. Finally, the emotional support from my family and fiancé Belinda has kept me happy and sane throughout these demanding times.

I would like to dedicate this work to my patients and participants for they made this research possible. It is my greatest hope that this research can benefit them and humanity in return.

Signed Dr Tiger Zhou

25/09/2020

Summary of thesis

Primary open-angle glaucoma (POAG) is a common complex eye condition that leads to blindness if left untreated. Important risk factors for developing POAG are positive family history and high intraocular pressure (IOP). Patients with high IOP are said to have high tension glaucoma, while those with normal IOP have normal tension glaucoma. The precise pathophysiology of POAG remains elusive despite advances in understanding of its genetic risk factors. Around five percent of POAG cases have been linked to known monogenic Mendelian inherited genes found predominantly by familial linkage studies. Common risks alleles for POAG have been identified via genome wide association studies. These single nucleotide polymorphisms individually increase the risk of developing POAG by around 50 percent each at best. The unidentified genetic causes of POAG likely include rare disease-causing variants that are not detected by genome wide association studies or familial linkage studies.

The advent of next generation high-throughput massively parallel sequencing, such as whole exome and RNA sequencing, has made comprehensive investigation of rare disease-causing variants possible. Using whole exome sequencing, this thesis found the genetic contributions of all known monogenic glaucoma disease-causing genes in a cohort with extreme phenotypic POAG of severe disease and younger onset to be 22.9 percent. This thesis also identified one gene associated with genome wide association loci (*CARD10*) that demonstrated enrichment of rare disease-causing variants. However, the presence of rare disease-causing variants in genes with genome wide association was not the norm, as no enrichment of rare-disease causing variants was found in the remaining one hundred genes examined.

Using rare variant SKAT analysis on the whole exome data, we identified neuroglobin as a POAG candidate gene. Neuroglobin is a highly conserved protein with neuroprotective properties shown to

act in cerebral and retinal ischaemia. Three predicted pathogenic variants were identified in the exome sequenced advanced glaucoma cohort of 187 participants with none in our control cohort of 1096 participants. However, further functional experimentation of the three variants is required to confirm pathogenicity.

Using network and pathway analysis of the exome data from the high tension and normal tension POAG participants, this thesis identified potentially differing biological mechanisms involved in each disease subtype. Participants with high tension glaucoma showed significant enrichment of rare predicted pathogenic variants in genes associated with unfolded protein response, the biological pathway responsible for removal of misfolded insoluble gene products, while participants with normal tension glaucoma had enrichment of variants in genes associated with transmembrane transport homeostasis, a deficiency of which leads to susceptibility to apoptosis.

The ocular gene expression data acquired in this thesis through RNA sequencing was found to have a greater dynamic range and sensitivity than previously published microarray ocular expression data. Archetypical high tension glaucoma genes were found to be selectively expressed within the trabecular meshwork, peripheral iris and ciliary body, which are tissues associated with IOP regulation. Network and pathway analysis of gene expression of IOP related tissues identified focal adhesion and extracellular matrix interactions to be the pathways selectively enriched in these tissues.

Chapter 1: Introduction

1.1 Glaucoma

Glaucoma is the leading cause of irreversible blindness worldwide and accounted for 6.6-8% of all blindness in 2010 (Pascolini and Mariotti, 2012, Bourne et al., 2013). An estimated 79 million people in the world will be affected by glaucoma in 2020 (Quigley and Broman, 2006) rising to 111.8 million by 2040 (Tham et al., 2014). Glaucoma is an optic neuropathy caused by loss of retinal ganglion cells leading to well-defined optic nerve damage, characteristic optic disc cupping, visual field deficits and ultimately blindness if untreated (Foster et al., 2002). There are many subtypes of glaucoma, which fall under the umbrellas of open-angle, angle closure or congenital glaucoma (Quigley, 2011). Open-angle glaucoma is the most common subtype (Bengtsson, 1981, Weinreb et al., 2014), which can be secondary to pigment dispersion or pseudoexfoliation syndromes, or primary where no contributing aetiology can be found (Kwon et al., 2009, Musch et al., 2012). Regardless, the common trait of all open-angle glaucoma is the presence of a macroscopically unobstructed iridocorneal angle (Figure 1). The iridocorneal angle is formed by the root of the iris and the peripheral cornea as it transitions to the sclera at the limbus. The most predominant glaucoma subtype in all ethnicities is primary open-angle glaucoma (POAG) accounting for 69.3% of all glaucoma burden worldwide (Tham et al., 2014). The proportion of glaucoma due to POAG varies by geography with the rates lowest in Asians (61.2%) and highest in North America (89.3%) (Tham et al., 2014). Primary open-angle glaucoma (POAG) can be further subdivided into high tension glaucoma (HTG) in those patients with high intraocular pressure (IOP) and normal tension glaucoma (NTG) in those with normal IOP. However the two subtypes of POAG are not mutually exclusive and the cut-off IOP is set arbitrarily at 21mmHg with the HTG designation assigned to glaucoma patients with IOP that is greater than the cut-off at two standard deviations higher than the population mean. NTG is much more common in Asian populations comprising 52% to 92% of all POAG cases, and less common in Caucasian populations accounting for 30% to 38.9% (Cho and Kee, 2014).

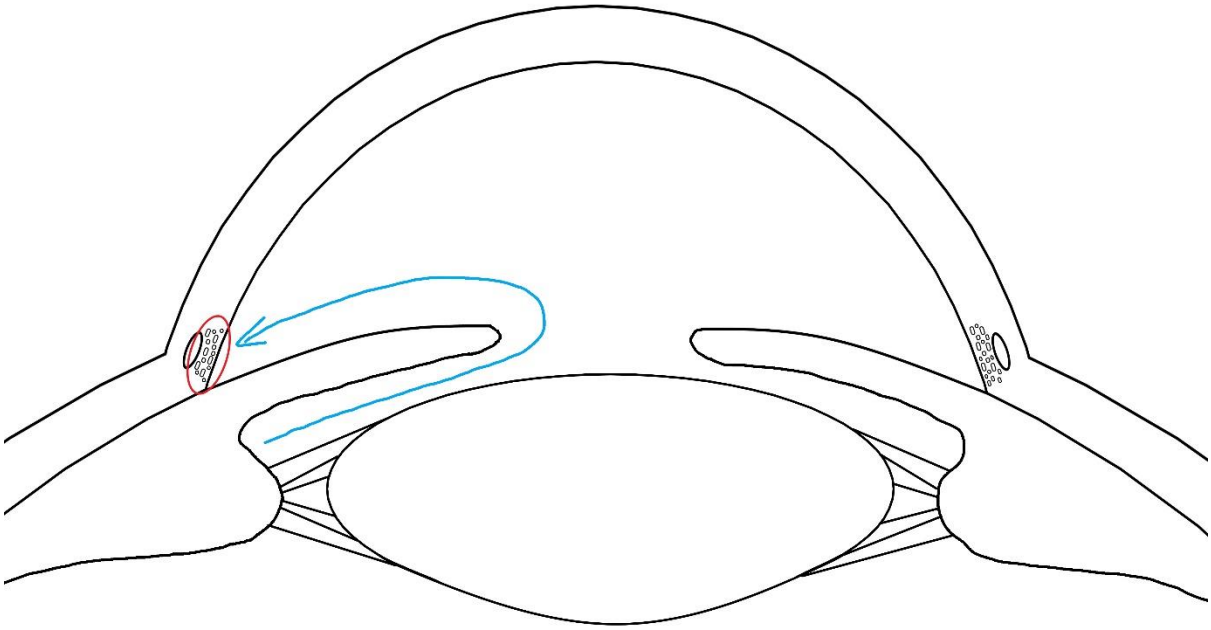

Figure 1: Diagram showing the course of aqueous humour produced by the non-pigmented epithelial cells of the ciliary body and drained by the trabecular meshwork with the blue arrows depicting the direction of flow. The red circle highlights the trabecular meshwork situated at the iridocorneal angle which is open in this diagram and in patients with open-angle glaucoma.

1.1.1 Epidemiology and disease burden

Population studies around the world have indicated the worldwide prevalence of primary open-angle glaucoma between the ages of 40 to 80 years to be 3.05% ranging from 2.31% in Asia to 4.2% in Africa (Tham et al., 2014). The estimated disease prevalence for ages between 40 and 80 years in Oceania is 2.63% (1.16%-4.83%), and detailed glaucoma population screening in Australia revealed an overall prevalence of 3.0% (Mitchell et al., 1996). Average prevalence of glaucoma within European descendants is 2.37% (Tham et al., 2014). Yearly incidence of glaucoma has been reported at 0.49-1% in the African population (Leske et al., 2007b, Nemesure et al., 2007), and 0.34% per

annum in Australian Caucasians (Burdon et al., 2015). These figures are conservative representations of actual global disease burden as population based epidemiological studies have shown a ten percent diagnosis rate worldwide (Quigley, 2011). Even developed nations have an estimated 50% or lower diagnosis rate (Mitchell et al., 1996, Wensor et al., 1998, Weih et al., 2001, Heijl et al., 2013).

Prevalence of glaucoma is dependent on several cofactors. Age plays an important role in the prevalence of glaucoma. Accounting for all other factors, the prevalence of glaucoma increases with age at 1.73 times per decade (Tham et al., 2014). The rate of age-related increase in glaucoma was the highest for people of European ancestry at 2.05 times per decade (Rudnicka et al., 2006) and the Oceania region at 2.81 times per decade (Tham et al., 2014). Age also increases the risk of glaucoma progression among glaucoma patients at 7% per year (Spry et al., 2005).

The effect of sex on POAG prevalence is ambiguous with no difference and biases in both directions being reported in different population studies (Vajaranant et al., 2010). Although the Blue Mountain Eye Study (BMES) in Australia (Mitchell et al., 1996) reported a 50% higher prevalence of glaucoma in females in a predominantly Caucasian population over the age of 49, Bayesian meta-analysis found that males have a 37% higher prevalence when adjusted for age and other co-factors (Rudnicka et al., 2006). Experimental studies seems to infer a protective effect of oestrogen, which is lost in post-menopausal women (Vajaranant et al., 2010). By examining HTG and NTG separately, ANZRAG data showed that females were significantly more prevalent in the advanced NTG cohort, while males were overpresented in the HTG cohort (Ng et al., 2014).

1.1.2 Pathophysiology

The exact pathogenesis of all glaucoma still evades elucidation but there has been progress in the understanding of disease physiology. The end result of glaucoma is well established and that is the apoptosis of retinal ganglion cells leading to the characteristic cupped appearance of the optic disc and vision loss (Weinreb et al., 2014). Visual loss occurs secondary to loss of retinal ganglion cells, corresponding to the location of cell death. Progression from normal vision to complete blindness in glaucoma takes on average 25 years without treatment (Heijl et al., 2009). Even with treatment, 50-68% of glaucoma patients will experience worsening of visual field loss, albeit at slower rates and with 9-19% reaching legal blindness (Kwon et al., 2001, Eid et al., 2003). Intraocular pressure (IOP) elevation remains the only known modifiable risk factor in glaucoma (Sommer, 1996, Bahrami, 2006) although other sources of retinal ganglion cell damage have been proposed.

Aqueous humour homeostasis regulates and maintains the IOP (Figure 1). This clear serous fluid also provides nourishment to the transparent avascular cornea and crystalline lens. Non-pigmented epithelial cells located at the ciliary processes of the pars plicata produce the aqueous humour via active secretion of serum products (Goel et al., 2010). Drainage of the aqueous occurs via the trabecular meshwork (TM) and uveoscleral outflow pathways with the TM contributing 75% of the total resistance in humans (Goel et al., 2010). Intraocular pressure regulation occurs by altering outflow and is increased due to higher trabecular meshwork resistance particularly in glaucoma (Weinreb et al., 2014).

Lamina cribrosa is the sieve-like structure at the optic nerve head through which axons of all retinal ganglion cells exit the globe and is thought to be the site of initial damage in glaucoma (Figure 2) (Kwon et al., 2009). Elevation or fluctuations in IOP can instigate axonal damage at the lamina cribrosa through mechanical stress, alterations in perfusion and astrocyte activation (Bahrami,

2006). Mechanical stress causes damage by inhibiting retrograde axonal transport of vital survival molecules such as brain-derived neurotrophic factor (BDNF) to the retinal ganglion cells (Quigley et al., 2000, Almasieh et al., 2012). Pressure-related reduction in optic nerve head perfusion promote the generation of reactive oxygen species (ROS) (Kwon et al., 2009). Activated astrocytes at the lamina cribrosa trigger remodelling of extracellular matrix, which alters the biomechanics at the optic disc, further exacerbating mechanical stress on the ganglion cell axons. Additionally, astrocytes experience impaired debris clearance capacity and secrete neurotoxic molecules in response to raised IOP (Almasieh et al., 2012). All pressure related damage to the ganglion cell axons has the potential to lead to apoptosis of the retinal ganglion cell, activation of complement cascade, scarring and eventually cupping of optic disc (Kwon et al., 2009).

Figure 2: Microscopy sections of optic nerve head located at the posterior pole of the eye where the optic nerve exits the globe (Quigley 2011, Glaucoma. Lancet, 377, 1367-77). The area between the red curved lines denotes the lamina cribrosa. A = Normal optic nerve head, B = Glaucomatous optic nerve head.

Although raised IOP is the cause of glaucoma in some patients, patients with NTG have IOPs within the normal range. Traditionally, disease progression is measured by the rate of change in the mean threshold of minimal detectable light stimulus in affected eyes. Progression of disease in NTG

appears to occur at a slower rate than high-tension glaucoma (HTG), at -0.36 dB/year versus -1.31 dB/year respectively according to the Early Manifest Glaucoma Trial (Heijl et al., 2009). The Collaborative Normal-Tension Glaucoma Study Group calculated a similar progression rate for NTG at -0.41 dB/year, with half of the patients progressing by 5-7 years (Anderson et al., 2001). Understanding of the aetiology of NTG is not as comprehensive and more speculative, nonetheless much research has been dedicated to ascertain the mechanisms involved in non-pressure dependent ganglion cell damage.

Low systemic blood pressure is correlated with NTG via vascular dysregulation causing reduced ocular blood flow, tissue ischaemia and increased oxidative stress (Osborne, 2008, Mi et al., 2014). Proximal to the lamina cribrosa, RGCs are neurons with unmyelinated axons. Consequently they have the highest oxygen demand in the body due to their reliance on aerobic respiration to generate the considerable energy required for maintaining transmembrane gradients that allow action potential propagation (Lee et al., 2011, Lascaratos et al., 2012). Unsurprisingly, there are abundant mitochondria in the RGC. Mitochondria are major cellular sites of ROS generation, which is further elevated in dysfunction, especially of Complex I and III (Lee et al., 2011). Energy depletion and ROS-induced oxidative stress from ischaemia or mitochondrial dysfunction are involved in RGC damage and glaucoma incidence, which shares a common pathway to IOP-related damage (Tezel, 2006). A study of mitochondrial sequencing in 27 POAG patients identified 22 predicted pathogenic mutations in 14 patients with none found in 159 controls (Abu-Amero et al., 2006) suggesting a possible role for mitochondrial dysfunction in POAG pathogenesis.

Neurotrophins are a group of molecules that regulate the growth and survival of mature neurons including those in the retina. Brain derived neurotrophic factor (BDNF) is the best studied of these molecules associated with the retina. Its expression is elevated shortly after increased intraocular

pressure or optic nerve axotomy in animal models of glaucoma (Almasieh et al., 2012). Retrograde transportation via RGC axons deliver this critical growth factor to the retina, with the remaining retinal supply produced locally (Wilson and Di Polo, 2012). Hence there may be some ability of the retina to compensate for the initial deprivation of neurotrophic factors from early glaucomatous processes, which could explain the gradual nature of the deterioration in the natural disease course. Animal experiments have also shown a delayed RGC apoptosis with adeno-associated viral (AAV) BDNF gene therapy (Wilson and Di Polo, 2012). However, BDNF was unable to prevent eventual RGC death or promote axonal regrowth. It is likely that the internalization and downregulation of the downstream TrkB surface receptor diminishes the long-term effects of BDNF (Almasieh et al., 2012). Functions of the other neurotrophic factors may not be as straightforward as BDNF.

Nerve growth factor (NGF) is another neurotrophin in the same family as BDNF. Its complex effect on RGC survival has shed light on the downstream signalling of the neurotrophins through selective activation of its two surface receptors TrkA and p75 (Almasieh et al., 2012). TrkA activation promotes RGC survival while p75 activation stimulates apoptosis. The reverse outcomes were ascertained when the two receptors were inhibited. All neurotrophins bind one of the Trk receptors (TrkA, TrkB or TrkC) as well as p75, but their precursor forms are highly selective for p75 (Almasieh et al., 2012). Following optic nerve transection, the ratio of pro-neurotrophin to neurotrophin is drastically increased triggering apoptosis. Other notable neurotrophic and growth factors have been identified, with differing actions. Ciliary neurotrophic factor (CNTF) is a neurotrophin that not only confers neuroprotection but also supports axonal regeneration in mature neurons (Wilson and Di Polo, 2012). Fibroblast growth factor-2 (FGF-2) upregulation led to a 10-fold increase in axonal regeneration (Wilson and Di Polo, 2012). Glial cell line-derived neurotrophic factor (GDNF) had a lesser neuroprotective effect than BDNF, but was additive when combined.

1.1.3 Current therapies

Currently, the only effective treatment target relies on the principle of IOP lowering even in NTG patients (Leske et al., 1999). Most contemporary regimens for glaucoma management start with medical IOP lowering drops including prostaglandin analogue and β-adrenergic antagonists (National Health and Medical Research Council (NHMRC) level 1 evidence (van der Valk et al., 2005, Vass et al., 2007)). The effectiveness of pressure lowering drops have been well studied and approximately halves the risk of developing glaucoma and glaucoma progression. The Ocular Hypertension Treatment Study (Kass et al., 2002) showed pressure lowering drops reduced the incidence of developing glaucoma by 53% (from 9.5% to 4.4%) after 5 years of treatment. The Latanoprost for open-angle glaucoma trial (UKGTS) found that prostaglandin analogue latanoprost reduced glaucomatous visual field progression by 40.6% (from 25.6% to 15.2%) after 2 years of treatment (Garway-Heath et al., 2015). Adjuvant laser trabeculoplasty can be added for additional pressure lowering by increasing the trabecular meshwork outflow in patients with high IOP (Weinreb et al., 2014). In recent years, laser trabeculoplasty has been shown to be a cost effective, non-inferior equivalent 1st line therapy for the management of early glaucoma (Gazzard et al., 2019). Failing those options, trabeculectomy is the current gold standard for IOP control with 2.2 mmHg lower IOP than medicated drops sustained over 9 years (Zaidi, 1980, Shigeeda et al., 2002, Musch et al., 2008). Early detection in POAG is vital and has vast benefits. With appropriate treatment, disease progression risk can be halved in POAG (Leske et al., 2007a). Recently, there has also been heightened interest in neuroprotective primary therapies in glaucoma prevention. Preventative strategies are based on altering disease pathology through lowering IOP or molecular pathways via drugs or gene therapy (Osborne, 2008, Almasieh et al., 2012, Wilson and Di Polo, 2012). A Cochrane review failed to identify any effective neuroprotective agents in glaucoma prevention from the only RCT conducted which compared the supposed neuroprotective agent brimonidine to the timolol

control (Sena and Lindsley, 2013). Oral memantine has since been trialed as a neuroprotective agent in glaucoma, however it was not shown to be more effective than placebo in reducing glaucoma progression over 4 years of therapy (Weinreb et al., 2018). All other work on neuroprotection in glaucoma has come from experiments in animal models involving promoting neurotropic factors and inhibiting apoptotic signals on a protein or genetic level (Wilson and Di Polo, 2012).

1.2 Endophenotypes and risk factors for primary open-angle glaucoma

1.2.1 Intraocular pressure

There is indisputable evidence that IOP is the most important risk factor in glaucoma (Kass et al., 2002, Le et al., 2003, Garway-Heath et al., 2015). Coincidentally, the Ocular Hypertension Treatment Study and Early Manifest Glaucoma Trial report an identical 11% increase in glaucoma risk for one mmHg increase of IOP (Gordon et al., 2002, Bengtsson et al., 2007). The Barbados Eye Study found a similar 12% increase in risk per mmHg (Nemesure et al., 2007) while the Los Angeles Latino Eye Study recorded a higher 18% elevation per mmHg (Jiang et al., 2012). Among glaucoma patients in a retrospective study of case notes, 1 mmHg increase in IOP may raise the risk of disease progression by 7%, although the result was not statistically significant (Spry et al., 2005). Conversely, lowering IOP by 1 mmHg reduces the risk of disease progression by 10% in the EMGT (Leske et al., 2003). Overall, 37% of the attributable risk of glaucoma was from IOP (for patients with an IOP greater than 21 mmHg), with a relative risk of 7.9 (3.8-16.2), making it the greatest modifiable risk factor (Nemesure et al., 2007). Genetic correlation between IOP and glaucoma is the highest for any endophenotype at 0.801 (Charlesworth et al., 2010). High IOP not only increases the risk of developing glaucoma, it is also strongly associated with more severe and rapid disease progression (Kwon et al., 2001, Medeiros et al., 2009, Jiang et al., 2012). Furthermore, IOP susceptibility was also evident in the subset of patients with blinding NTG (Oliver et al., 2002). Every one mmHg increase in IOP in HTG patients corresponded on average to a 0.07 point decrease in visual field score (Kwon et

al., 2001) or 0.05µm thinning of retinal nerve fibre layer (RNFL) thickness formed by retinal ganglion cell axons (Medeiros et al., 2009).

1.2.2 Optic disc parameters

Optic disc morphology is used in the diagnosis of glaucoma and also predicts future disease progression. Optic disc haemorrhage or Drance haemorrhage is the best disc parameter for predicting presence and progression of glaucoma (Drance et al., 2001, Leske et al., 2003, Uhler and Piltz-Seymour, 2008, De Moraes et al., 2013, Hollands et al., 2013). The presence of this subtle sign (Uhler and Piltz-Seymour, 2008) suggests inadequate management of IOP and heralds worsening of glaucoma (Drance et al., 2001, De Moraes et al., 2013). Data from the population-based Baltimore Eye Study was the first to show a weak but non-significant link between optic disc area and glaucoma (Quigley et al., 1999). The neuroretinal rim represents the sum of the RGC axons traversing the lamina cribrosa to exit the eye. Neuroretinal rim thinning translates to increased cup-to-disc ratio (CDR) and indicates worsening glaucoma. Glaucoma patients who underwent disease progression had 19.2% (p=0.001) thinner neuroretinal rims than those who did not progress (Jonas et al., 2005). Similarly, higher CDR and cup asymmetry were found to be risk factors for glaucoma incidence (Le et al., 2003, Miglior et al., 2007, Hollands et al., 2013). Participants with a CDR of greater than 0.7 had a 7.9 times relative risk of developing glaucoma (Le et al., 2003). Every increment in horizontal and vertical CDR of 0.1 infers 25% and 32-34% increased risk of developing glaucoma respectively (Gordon et al., 2002, Miglior et al., 2007). Total optic disc area also seemed to be associated with glaucoma risk. Patients with POAG on average have a larger optic disc as discovered in two studies in Caucasian populations (Healey and Mitchell, 1999, Wang et al., 2003), with POAG discs being 0.05 mm and 0.33 mm larger respectively. While statistically significant, this difference in optic disc area may be confounded by the reliance of glaucoma diagnosis upon CDR. Cup-to-disc ratio is positively correlated with optic disc area as RGCs exiting the lamina cribrosa will

leave a larger central cup if the circumference of the aperture is enlarged due to geometry. This correlation may lead to a higher rate of diagnosis for glaucoma in people with larger optic disc area.

1.2.3 Central corneal thickness

Inverse correlation between central corneal thickness (CCT) and glaucoma risk was first reported by the Ocular Hypertension Treatment Study and has been reproduced since (Gordon et al., 2002, Herndon et al., 2004, Sullivan-Mee et al., 2006, Dueker et al., 2007, Miglior et al., 2007, Francis et al., 2008, Fernandez-Bahamonde et al., 2011, Jiang et al., 2012, Wang et al., 2014). Even within the same patient, the eye with the thinner CCT was associated with the worse pattern standard deviation on visual field testing (Rogers et al., 2007). However, the association was not found in several Asian populations including Chinese, Indian and Japanese participants (Xu et al., 2008, Lin et al., 2009, Day et al., 2011, Wang et al., 2011, Natarajan et al., 2013). While thinner CCT increases risk of developing glaucoma by 30-71% for every 40µm reduction (Gordon et al., 2002, Miglior et al., 2007, Jiang et al., 2012), its contribution to glaucoma progression is minor at best (Kim and Chen, 2004, Chauhan et al., 2005, Jonas et al., 2005, Cao et al., 2012, Viswanathan et al., 2013). Despite a strong genetic heritability estimate of 0.72, bivariate analysis of quantitative traits from 1181 Caucasians failed to reveal any significant genetic correlation of POAG with CCT (Charlesworth et al., 2010). This result was corroborated by a SNP-based genetic association study of 1759 Australian Caucasian participants (Dimasi et al., 2012).

Processes by which thin cornea induce glaucoma are not well understood. Selection bias may contribute partly to the interplay between CCT and glaucoma. As the measurement of IOP by the gold standard Goldmann applanation tonometry assumes a CCT of 500µm, thinner CCT leads to underestimation of actual IOP thereby over-calling the effect of CCT on glaucoma rates (Manni et al., 2008). True biological influences of CCT have been suggested. The relationship between CCT and

optic disc area in glaucoma patients is a central hypothesis linking CCT to glaucoma (Pakravan et al., 2007, Gunvant et al., 2008, Insull et al., 2010). Patients with thinner CCTs have larger optic discs which experience greater displacement of the lamina cribrosa with IOP changes. Retinal ganglion cell axons encounter greater stress at the lamina cribrosa under such conditions leading to heightened susceptibility for glaucoma. However the influence of CCT on the optic disc may be limited to glaucoma patients as there was no correlation between CCT and optic disc parameters in unaffected individuals (Carbonaro et al., 2014). Recent evidence indicates that biomechanical properties of the cornea such as hysteresis may play a bigger role in glaucoma pathogenesis than thickness alone (Deol et al., 2015). Hysteresis describes the viscoelastic property of the cornea where there is a loss of mechanical energy that is absorbed by the tissue during its compression and distention. Given the significant correlation between CCT and corneal hysteresis (Mangouritsas et al., 2009, Carbonaro et al., 2014), there may well be a biomechanical role for CCT in glaucoma that has yet to be elucidated.

1.2.4 Myopia

Short-sightedness or myopia is a condition of refractive error where the focal point of the ocular optical system falls in front of the sensory retina thereby causing blurring of the image seen. The degree of refractive error can be measured in spherical equivalent units of dioptres (D), which is the inverse of the distance from the lens to the point of focus (focal distance). Myopia has been shown to be a significant risk factor for glaucoma in epidemiological studies across the world. However, changes in disc appearance associated with myopia often complicate the diagnosis of glaucoma. Furthermore, damage to RGC seen in glaucoma also occurs in myopia alone and may cause over-diagnosis of glaucoma (Hsu et al., 2015). The earliest population-based epidemiology studies to identify the link between myopia and POAG were published in 1999 (Mitchell et al., 1999, Wu et al., 1999). The highest reported odds ratio (OR) of glaucoma came from the Blue Mountain Eye Study of Australian Caucasians, at 2.3 (1.3-4.1) and 3.3 (1.7-6.4) for myopia with spherical equivalent of -3.0

to -1.0D and ≤ -3.0D respectively (Mitchell et al., 1999). The Barbados Eye Study (Wu et al., 1999) and Beaver Dam Eye Study (Wong et al., 2003) discovered similar glaucoma ORs of 1.48 (1.12-1.95) and 1.6 (1.1-2.3) for myopia with spherical equivalent units of ≤ -0.5D and ≤ -1.0D respectively. Amongst Asian people with myopia, the Singapore Malay Eye Study (Perera et al., 2010) and the Beijing Eye Study (Xu et al., 2007) noted glaucoma ORs of 2.87 (1.09-7.53) and 2.28 (0.99-5.25) for spherical equivalent of ≤ -4.0D and ≤ -6.0D respectively. Long axial length, a related measure of myopia, was found to increase risk of glaucoma by 48% for every millimetre of increment (Jiang et al., 2012). In meta-analyses, the OR for glaucoma from myopia was found to be 1.88 (1.6-2.2) (Marcus et al., 2011), while severe myopia of spherical equivalent ≤ -6.0D increased the OR to 5.7 (3.1-11) (Hollands et al., 2013). One population survey in the United States detected significant difference in the degree of visual field defects between non-myopic participants and participants with myopia but no difference in the incidence of glaucoma, hinting at possible underreporting of glaucoma (Qiu et al., 2013).

Normal tension glaucoma was more significantly associated with myopia in studies which measured IOP. The Early Manifest Glaucoma Trial found that the prevalence of glaucoma in people with myopia (spherical equivalent of ≤ -1.0D) was highest for IOP ≤ 20mmHg and diminished to background levels by IOP of 30mmHg (Grodum et al., 2001). In a Japanese cohort of predominantly NTG patients (92%), the Tajimi Study identified glaucoma ORs of 1.85 (1.03-3.31) and 2.6 (1.56-4.35) using the same myopia cut-offs as the BMES, spherical equivalent of -3.0 to -1.0D and ≤ -3.0D respectively (Suzuki et al., 2006). Another Asian study of NTG patients found high myopia of ≤ -6.0D to be significantly associated with glaucoma at an OR of 3.54 in Koreans aged between 19 to 39 (Kim et al., 2014). These findings particularly in Asians, may explain the coincidence of prevalent NTG and myopia in this ethnicity (Doss et al., 2014).

1.2.5 Systemic factors

Numerous non-ocular risk factors such as diabetes mellitus and hypertension have been examined in relation to POAG but conflicting evidence exists for their correlation (Quigley et al., 1994, Boland and Quigley, 2007, Kwon et al., 2009). Proliferative diabetic retinopathy causes secondary neovascular glaucoma, but diabetes itself was anecdotally thought to increase the risk of developing POAG (Sommer, 1996, Boland and Quigley, 2007). In the Korea National Health and Nutrition Examination Survey, a fasting capillary glucose of ≥ 200mg/dL was associated with increased risk of NTG (OR = 12.65, 2.63–60.94]) (Kim et al., 2014). Diabetes risk in POAG was also nominally higher in the Baltimore Eye Survey but was due to strong selection bias (Sommer, 1996). Patients with diabetes were having more regular eye examinations with their ophthalmologist, which led to a higher diagnosis rate of POAG. However other studies such as The Rotterdam Study failed to find any statistical evidence linking diabetes to POAG incidence (de Voogd et al., 2006). A 2014 systematic review found that overall, diabetes increased the rate of POAG by 34% (Zhou et al., 2014). The authors did notice significant heterogeneity within the case-control studies and consequently excluded them from the analysis, although the OR for the case-control studies also favoured a positive association between diabetes and POAG.

Cardiovascular risk factors also contribute to glaucoma risk. Presence of cardiac disease increases the risk of POAG incidence by 54-71% (Gordon et al., 2002, Miglior et al., 2007). Likewise, the risk of glaucoma progression is amplified 2.44 fold with cardiac disease history in patients with HTG (IOP ≥ 21 mmHg) (Leske et al., 2007a). Low levels of high-density lipoprotein cholesterol also slightly elevated POAG risk (Kim et al., 2014). The effect of blood pressure on POAG pathogenesis is complex. Intraocular pressure was positively associated with body mass index (BMI) and hypertension (Wang et al., 2011). Hypertension was found to be significantly associated with POAG itself in Chinese cohorts (Fan et al., 2004, Sun et al., 2012). Conversely, systolic blood pressures

lower than 125 mmHg increased glaucoma progression risk in NTG patients (Leske et al., 2007a). Other studies have found that initially hypertension may be protective for POAG by increasing optic nerve head perfusion, but prolonged hypertension and therefore atherosclerosis increases risk of glaucoma by reducing ocular perfusion (Sommer, 1996, Boland and Quigley, 2007).

1.2.6 Family history

Family history is a major risk factor for glaucoma that is well-recognized within numerous ethnicities (Wolfs et al., 1998, Nemesure et al., 2001, Weih et al., 2001, Le et al., 2003, Sung et al., 2006, Green et al., 2007, Sun et al., 2012, Kong et al., 2013). However the exact mode of inheritance for POAG rarely conforms to a pure Mendelian pattern (Charliat et al., 1994, Nemesure et al., 2001, Gong et al., 2007, Wang et al., 2010c). Genetic load of common POAG risk alleles is positively correlated with the number of affected relatives in a pedigree (Mabuchi et al., 2015). Having a positive family history of glaucoma confers a 9.2 times risk of developing glaucoma (Wolfs et al., 1998). The presence of a first-degree relative with glaucoma increases the risk of incident glaucoma 7.67-8.3 fold (Charliat et al., 1994, Kong et al., 2013). The risk was highest for siblings at 67.4% and lesser for offspring at 13.2% (Nguyen et al., 2000). The number of siblings with POAG significantly increases the odds of having glaucoma. Having more than 2 siblings with POAG increases the odds 5.64 times while having only one sibling heightens it by 3.08 fold (Doshi et al., 2008).

Although mathematical modelling estimates that around 72% of all people with glaucoma have a positive family history (Gong et al., 2007), actual familial studies report lower rates. Around 16.1% of 1st degree relatives (Tielsch et al., 1994), 24.5% including 2nd degree relatives (Budde and Jonas, 1999), 21.5% including up to 4th degree relatives (Kong et al., 2011) and 30.2-59.6% of unspecified blood relatives (Nguyen et al., 2000, Green et al., 2007, Gramer et al., 2014) also have POAG. The difference between theoretical and recorded rates can easily be explained by the well documented

underreporting of family history in glaucoma (McNaught et al., 2000, Mitchell et al., 2002). The heritability and influence of family history is the highest for juvenile-onset POAG and weaken with age for adult onset disease (Budde and Jonas, 1999). While 35.8% of patients under 50 years old have a positive family history, the rate falls to 11.7% in patients over 70 years old (Budde and Jonas, 1999).

There is conflicting evidence regarding the relationship between a positive family history and the severity of glaucoma. Two studies have found having a family history of glaucoma led to more severe disease at diagnosis (Deva et al., 2008, Wu et al., 2006) while others reported no association (Quigley et al., 1994, Landers et al., 2003). However when Landers and colleagues (Landers et al., 2003) only examined the cohort under 50 years of age, visual field loss was lesser in the patients with a positive family history by two thirds (OR = 0.3). This phenomenon is likely due to better recognition and earlier diagnosis of glaucoma in people with a family history (Gramer et al., 2014). Similarly, having a positive POAG family history was associated with a significant 71% reduction in the odds of late presentation to an ophthalmologist with advanced visual field loss in the UK (Fraser et al., 1999). It should be noted that this beneficial effect of family history in the UK is likely a result of free vision screening for first-degree relatives of people with glaucoma which allowed for earlier disease detection than other study cohorts. This finding further underscores the importance and advantages of a comprehensive screening program.

1.3 Genetic sequencing

1.3.1 Human genome and disease

The task of unravelling the genetic sequence of our own species became the Holy Grail in molecular genetics following the initial successes in the sequencing of genomes of simpler species. It was a massive undertaking considering that the human genome comprises approximately 3 billion base

pairs. The Human Genome Project distributed the sequencing load between many global participating nations in a collective human effort by fragmenting the genome into segments. This was achieve by cutting the genome using different restriction enzymes and thereby generating unique fingerprint contigs, which was later used to map the completed sequences (Lander et al., 2001). Using a shotgun sequencing approach based on improved versions of Sanger sequencing, both a public multinational and a privately funded effort achieved this monumental task in 11 years at a cost of around 3 billion dollars (Lander et al., 2001, Venter et al., 2001). The project revealed that only 1.1% of the human genome encodes for any protein (i.e. exons) while 24% is non-coding (i.e. introns in genes) and 75% is intergenic (Venter et al., 2001). It also showed that random single nucleotide polymorphisms (SNPs) are common within the human genome, occurring at an average rate of 1 per 1250 base pairs, but less than 1% of these SNPs would ever result in a change in the encoded amino acid residue. The human genome project provided valuable insight into the architecture of the genetic makeup of our species and formed a template upon which future human genome sequences could be aligned.

With the human genome mapped, the next challenge became identifying the frequency of the random SNPs that pepper the genome in the world's populations with a view to better understand phenotypic variance in health and disease. The 1000 genomes project was one of the first databases to record the frequencies of SNPs within the genome of 1092 participants from 14 different ethnicities using whole genome and whole exome sequencing methods (Abecasis et al., 2012). This resource was able to capture 98% of common human SNPs which occur in the population at a 1% frequency or higher. While these common variants likely accounted for a large proportion of the phenotypic variation between ethnicities, they alone are unlikely to be the sole cause of most human genetic disorders, which occur at much rarer frequencies. Hence the next step in the search for the genetic aetiology of human disease lay in sequencing of larger cohorts. Due to the expenses

of whole genome sequencing, it was felt that the most cost-effective strategy was to target genetic sequencing toward exons, the 1.1% of the genome which encoded for proteins.

The National Heart, Lung, and Blood Institute (NHLBI) funded Exome Sequencing Project (ESP) sequenced the exons of 1351 European and 1088 African participants (Tennessen et al., 2012). The results demonstrated that while 86% of single nucleotide variants (SNV) in any given human genome were rare (< 0.5%), only 2.3% of these variants were predicted to alter protein function. However, the majority (95.7%) of potentially damaging variants were indeed rare. The large burden of rare SNVs in any given individual represented a high degree of background signal noise, which combined with the rarity of potentially disease causing variants, make discovery of rare disease causing variants challenging. This was evident in the failure of whole exome sequencing studies to identify rare SNV causes in common complex diseases such are autism spectrum disorder (Liu et al., 2013a) and schizophrenia (Purcell et al., 2014), involving 1036 and 2536 participants respectively.

Established in 2014, the largest public domain database of human exomes is available from the Exome Aggregation Consortium (ExAC) (Lek et al., 2016). This collection houses the exomes of 60706 unrelated participants with no severe paediatric disease and may be used as a useful population control cohort for severe disease phenotypes. The participants from the 1000 genome project and ESP were all incorporated into the ExAC and joint-called. Participants from a number of ethnicities were involved in this database including 5203 African Americans, 5789 Latinos, 4327 East Asians, 3307 Finnish, 33370 non-Finnish Europeans, 8256 South Asians and 454 unspecified. This resource provided the most useful tool available at the time of this thesis to filter of potentially disease causing variants. At the time of writing, the ExAC database has been integrated into and succeed by the Genome Aggregation Database (gnomAD) consortium which includes a total of 125748 exomes (Koch, 2020).

1.3.2 First generation DNA sequencing

Following the discovery of the 3-dimensional structure of DNA by Watson and Crick in 1953, the next great hurdle in human understanding of molecular genetics lay in unravelling the sequence of the 4 basic codes of life in organisms. The first successful attempts in revealing the sequence of nucleic acids were achieved using the single-stranded RNA of viral bacteriophages with the first complete gene ever sequenced coming from bacteriophage MS2 (Min Jou et al., 1972). It wasn't until 1975 that the first ever DNA genome was sequenced from the bacteriophage PhiX174 using the 'plus and minus' system (Sanger and Coulson, 1975). The derivatives of this method using chain terminating modified di-deoxynucleotidetriphosphates (ddNTP) was the ground breaking discovery that is in widespread use still today and has been named 'Sanger sequencing' (Sanger et al., 1977). Sanger sequencing uses the fact that ddNTPs lacking a 3-hydroxl group are unable to form phosphodiester bonds with other nucleotides and therefore cause termination of DNA chain elongation. By labelling the ddNTPs, the exact positions of each base may be determined using gel and more recently capillary electrophoresis (Sanger et al., 1977).

1.3.3 Next generation sequencing

First generation Sanger sequencing involved ascertainment of the nucleotide sequence in a linear fashion. While its high accuracy ensures it is still the gold standard in DNA resequencing, direct Sanger sequencing is too slow and costly to be employed for genome-wide analysis on a commercial scale (Johar et al., 2015). The essence of next-generation sequencing (NGS) is to sequence segments of the genome in parallel thereby reducing time and cost (Mardis, 2008). Entire genomes are divided into 50-350bp fragments depending on the sequencing platform and attached to a library of adapters before undergoing priming and modified polymerase chain reactions (PCR) (Ratan et al., 2013, van Dijk et al., 2014). Although many platforms for NGS exist, all rely on the massively parallel sequencing principle where any given base pair in a target region is sequenced multiple times

denoted by the metric read depth. The proportion of the target regions adequately sampled by sequencing is termed the coverage. Due to the different sequencing chemistries, coverage is platform-specific and at least 1.4% of total SNVs may be missed due to coverage issues (Ratan et al., 2013). Furthermore, experimental error may occur within the same platform due to mis-priming events (McCall et al., 2014). By comparing NGS with Sanger sequencing, McCall and colleagues identified false-positive variant calls frequently occur within 10 bases from either end of any read, at base substitutions and short insertions, within non-full length amplicon reads, and sequences sharing homology with panel primers (McCall et al., 2014).

Due to the varying capture and priming errors described previously, quality control and calibration is critical during raw data generation in minimizing false-positives. The raw reads (in FASTQ format) generated by sequencing are aligned to one another using overlapping sequences and mapped to a reference genome to produce BAM files. FASTQ files stores the raw sequence of nucleotides along with their quality obtained by sequencing. BAM files are binary files that contain the sequence alignment data. Due to the large number of reads produced per sequencing run, alignment and mapping is only made possible by the use of automated algorithms (Fonseca et al., 2012). Many mapping programs or mappers exist, but all function using the same basic principles. Mappers locate the true position of the experimental sequences on the reference genome to allow further sequence analysis. This is achieved while allowing flexibility to account for single nucleotide polymorphisms (SNP) and multi-nucleotide insertion and deletions (indels). Hence sequence mapping depends on constraint parameters of the mapper.

After the generation of raw data, bioinformatics analysis is essential to all next generation sequencing pipelines due to the complexity of the enormous quantities of experimental output. Discrepancies between the sequence data and the reference genome are identified by variant calling

software to generate variant call files (VCF). These variants are annotated for final analysis and reporting. In order to detect allelic heterozygosity and to reduce error rates, next generation sequencing requires multiple copies of the same fragment to be captured to be confident of the findings at probabilities usually greater than 99.9%.

1.3.4 Whole exome capture

The earliest paper to describe the complete human exome was published in 2008 based on the genome of biologist John Craig Venter (Levy et al., 2007, Ng et al., 2008). However, the genome was sequenced by the relatively slow and costly Sanger method. This work did reveal some interesting facts about the human exome and foreshadowed the dawn of 'next generation sequencing'. The first protocol describing selective massively parallel sequencing of the human coding exome came in 2007 (Hodges et al., 2007). Combining traditional microarray technology as a capture platform to massively parallel next generation sequencing, the human exome was covered at 1.19 times by 1.99 million reads (Hodges et al., 2007). Of the 5604 nonsynonymous variants in the first published human exome, rare variants were the most likely to harbour damaging protein coding changes as determined by the 'Sorting Intolerant From Tolerant' (SIFT) algorithm (Ng et al., 2008). Potentially damaging insertions and deletions (indels) are most commonly a single nucleotide long. Non-frameshift and therefore likely non-damaging indels are preserved 54% of the time compared to only 6% of frameshift indels exhibiting selection pressure against the theoretically more damaging frameshifts (Ng et al., 2008).

Currently, most successful discoveries using whole exome sequencing (WES) have been made with family linkage studies. Due to the low frequency of the alleles of interest, the large sample sizes required to detect statistical significance on a variant-by-variant basis in case-control studies have been prohibited by cost. Two whole exome sequencing studies achieved genome-wide significance

at the time of this thesis. One was the 2015 study published in Science linking TBK1 to amyotrophic lateral sclerosis (ALS) (Cirulli et al., 2015). A total of 2874 patients with ALS and 6405 controls were sequenced with whole exome capture. The qualifying variants for analysis were filtered for rarity (minor allele frequency less than 0.05%) and predicted pathogenicity based on PolyPhen HumVar and protein truncating changes. The other was published in Nature Genetics in 2016 (Huang et al., 2016) linking FGD6 to polypoidal choroidal vasculopathy in ethnically Chinese populations. 194 cases with polypoidal choroidal vasculopathy, 155 cases with choroidal neovascularization and 1602 unaffected controls were sequenced with whole exome capture. All exonic variants were included for analysis regardless of predicted pathogenicity or rarity in a manner similar to GWAS SNP array studies.

1.3.5 RNA sequencing

Progress in next-generation massively parallel sequencing have enabled the use of case-control study design for the discovery of rare disease-causing genes in common diseases (Bamshad et al., 2011, Chiang et al., 2012, Cirulli et al., 2015). In many cases, the hypothesis-free discovery studies will highlight a shortlist of potential candidates and requires supporting functional evidence to pinpoint the causative gene. Tissue-based gene expression profiling is often the first-line in biological analysis of any candidate gene. Traditionally, profiling techniques included expressed sequenced tags (EST) (Boguski et al., 1993) and serial analysis of gene expression (SAGE) (Yamamoto et al., 2001). These are now less commonly used than newer, wholistic and/or cheaper technologies including cDNA microarray hybridization approach (Duggan et al., 1999) and most recently next-generation RNA sequencing (RNAseq) (Ozsolak and Milos, 2011).

For most applications, RNAseq offers superior performance to gene expression microarray technology as it lacks the experimental issues of cross-hybridisation, non-specific hybridisation and

variable probe performance (Zhao et al., 2014). The output of RNAseq is completely digital, in the form of counts, whereas microarray is based on hybridization fluorescence intensity and is dependent upon tag performance and imaging capabilities (Hitzemann et al., 2013). This difference in data acquisition modality offers many advantages to RNAseq. Firstly, detection of transcripts in RNAseq is not limited to the probes set by the microarray and therefore allows for the capture of novel transcripts (Hitzemann et al., 2013, Zhao et al., 2014). Similarly, the effect of transcript polymorphism is reduced and can be further circumvented by bioinformatic mapping algorithms following data acquisition. Secondly, sensitivity to detect differential expression is greater with RNAseq (Marioni et al., 2008, Sirbu et al., 2012, Mantione et al., 2014). Microarray technology is capable of reliably detecting as small as 2 fold changes in magnitude. By contrast RNAseq is able to distinguish as little as a 1.25 fold change in expression (Mantione et al., 2014). Thirdly, the signal dynamic range of RNAseq is greater than microarray due to the lack of a ceiling effect from probe saturation and floor effect from non-specific hybridisation (Sirbu et al., 2012, Zhao et al., 2014). Furthermore, RNAseq has improved discriminating power at lower expression values without the limitation of signal-to-noise ratio of fluorescence-based technology (Marioni et al., 2008, Sirbu et al., 2012, Zhao et al., 2014). Finally and perhaps most importantly, RNAseq was shown to provide more accurate absolute transcript level quantification than microarray technology when both methodologies were tested using proteomics (Fu et al., 2009) or qPCR (Marioni et al., 2008) as a third independent measure.

1.4 Gene discovery techniques in glaucoma

1.4.1 Linkage studies

Almost all disease causing genes in glaucoma to date have been identified through the use of parametric linkage analysis studies. In brief, by examining the co-segregation of genetic loci with disease in large families, linkage study design enables the mapping of disease locus to a specific

chromosome location (Dawn Teare and Barrett, 2005, van Koolwijk et al., 2013). The benefit of the linkage study design is that no prior knowledge of gene function is required. Hence it is superior to candidate gene studies for gene discovery and is non-hypothesis driven. However, parametric linkage analysis does require assumptions of the disease model. The best model for gene discovery using linkage design would entail Mendelian inheritance of disease with monogenic, high penetrance, rare and pathogenic mutations.

Rationale for linkage analysis relies upon the knowledge that co-segregation is a measure of genetic distance in organisms that undergo meiotic reproduction (van Koolwijk et al., 2013). Proximity between two loci reduces the chance of recombination during meiosis and therefore increases the chance of co-segregation. This idea not only applies to two physical genetic loci, but can be extrapolated in the same way to incorporate a disease phenotype and genetic loci. Magnitude or significance or genetic linkage is measured with the logarithm of odds (LOD) score. Traditionally, statistically significant linkage is obtained at a LOD score of 3 or 1000:1 ratio of probability favouring linkage. However, this is only equivalent to a genome-wide significance of 0.09 (Dawn Teare and Barrett, 2005). A LOD score of 3.3 is required to achieve a genome-wide significance of 0.05.

Linkage studies have achieved mixed success in identifying highly penetrant Mendelian genes in primary open-angle glaucoma. A total of 16 glaucoma loci have been flagged to date with linkage designs. Only seven of these loci in POAG and two in primary congenital glaucoma (PCG) have been pinpointed to the gene level with the majority remaining unsolved. The challenge in discovering new genes in the unsolved loci and future loci using linkage analysis will no doubt be hindered by its rigid assumptions. Due to the relative late onset of glaucoma, many patients may be deceased at the time of sample collection. This prohibits genotyping of large number of affected family members critical for successful linkage analysis. Additionally, some mutation carriers within affected families may be

too young to exhibit signs of glaucoma and therefore be falsely designated as unaffected. This will introduce false negative errors in the linkage analysis, thereby underestimating the LOD score and reducing sensitivity to detect causative genes.

It is becoming ever more apparent that even disease causing mutations in the archetypal Mendelian glaucoma genes exhibit incomplete penetrance (Allingham et al., 1998, Craig et al., 2001, Williams et al., 2015). Furthermore, results from recent genome-wide associate studies (GWAS) provide evidence supporting the complex non-Mendelian genetic nature of glaucoma. As many central tenets of traditional parametric linkage-based studies do not apply to a significant proportion of glaucoma disease burden, its role in gene discovery although important will be limited to a selected minority of cases. The total POAG disease burden accounted for by the known and validated monogenic Mendelian disease genes is around 5% in the world (Fingert, 2011).

1.4.2 Genome-wide association studies

Genome wide association studies (GWAS) have been a major breakthrough in the investigation of genetic aetiology of glaucoma (Thorleifsson et al., 2010, Burdon et al., 2011, Janssen et al., 2013). It was apparent that the use of linkage analysis in POAG was never going to account for the majority of genetic burden in the disease. The challenge lay in both the rarity of large families with segregating glaucoma and the scarcity of pathogenic mutations in the identified genes in the POAG cohort in general. This realization shifted some emphasis onto the common disease common variant (CDCV) hypothesis. The rationale for this hypothesis is based on the “Out of Africa” theory of human evolution (Gong et al., 2004). Common diseases such as POAG are present worldwide, albeit at different frequencies. Any common variant associated with disease in multiple ethnicities must have been in linkage disequilibrium with the disease causing variant before the modern human exited Africa some 120,000 years ago (Stringer, 2003). However any common variants associated with

disease in independent ethnicities will allow the mapping of causative loci to nearby genes due to the short period of recombination events (Gong et al., 2004). The CDCV hypothesis forms the basis for GWAS and conversely the success of GWAS strengthens the hypothesis (Ramdas et al., 2011a).

Since the advent of GWAS, numerous common susceptibility loci have been identified in many common complex diseases including in POAG (Hemminki et al., 2008, Burdon, 2012, Mackey and Hewitt, 2014). The success of the GWAS in gene discovery can be attributed to its many advantages over the linkage study design (Hirschhorn and Daly, 2005). No assumptions are made about the model of inheritance in the GWAS making it truly non-hypothesis driven. Heritability and penetrance of diseasing causing alleles in common complex disease is seldom complete; linkage studies rely heavily on high penetrance whereas GWAS is able to identify genes with much lower penetrance. GWAS are able to map association loci to a much smaller region than linkage studies relying upon the principles of linkage disequilibrium. Furthermore, GWAS are able to detect alleles with small effect sizes and large population frequency with sufficiently powered study samples that no other study design can achieve giving them high external validity. Finally, there is no dependence on large families with segregating disease rather having study samples with high inter-relatedness and population stratification will introduce false positives.

At the most fundamental level, all GWAS are case-control designs that compare the frequency of particular alleles at sites of common polymorphisms between disease cohort and population controls. They commonly involve substantial cohorts numbering in the thousands to overcome the relatively small effect size of each locus and the stringent level of multiple testing correction required for the large number of SNPs genotyped in these studies. Even though the human genome contains around 3 billion bases, around 1 million “tag” SNP markers are sufficient to cover its entirety when distributed along the genome. This is due to the phenomenon of linkage

disequilibrium (LD) where SNP with a LD block are associated more frequently than random recombination dictates. Correspondingly linkage disequilibrium is often an indicator of genetic proximity. Only a few tagging SNPs need to be genotyped for an entire LD block, which are 200 kb long on average (Wang et al., 2005). Linkage disequilibrium is pertinent among common SNPs and occurs within much of the human genome (Hirschhorn and Daly, 2005, Wang et al., 2005). By combining SNP genotype data and linkage disequilibrium information, un-genotyped allele frequencies can be imputed. The standard threshold of significance for GWAS is set at 5×10^{-8} to account for around 10^6 SNPs genotyped on a standard microarray chip (Burdon, 2012, Mackey and Hewitt, 2014). Furthermore, the standard scientific practice recommends replication of any gene found to be significantly associated with disease in a separate cohort. Owing to the design of the GWAS, genotyped alleles are rarely within protein coding regions.

Though highly successful, there are gaps in the knowledge provided by GWAS. Firstly, a large proportion of SNPs are non-exonic and therefore of unknown function (Hemminki et al., 2008, Manolio et al., 2009). The genotyped SNPs are not putatively disease causing, but rather in linkage disequilibrium with nearby functional alleles that are pathogenic, although exactly which nearby allele is pathogenic is not obvious. Secondly, the magnitude of odds ratios for these disease association polymorphisms are less than two for the strongest candidate genes with a significant proportion of normal controls harbouring aforementioned polymorphisms (Mackey and Hewitt, 2014). Within replication cohorts, the relative risk further decreases due to the “winner’s curse” statistical phenomenon. Finally, while disease association SNPs in GWAS often account for > 10% of disease causality, they do not yet explain the majority of familial disease (Hemminki et al., 2008).

1.5 Monogenic causes of glaucoma

1.5.1 Glaucoma locus GLC1A – Myocilin

1.5.1.1 Discovery

Myocilin was the first gene to be linked to autosomal dominant primary open-angle glaucoma. It was initially mapped to GLC1A locus at 1q21-q31 (LOD score 6.5) in a large American pedigree of 37 members with 22 glaucoma patients (Sheffield et al., 1993). This family had a consistent phenotype of high intraocular pressure and young age-of-onset, prior to 30-years of age. Linkage to this locus was replicated in other American (Richards et al., 1994, Wiggs et al., 1994), French (Meyer et al., 1994), Danish (Graff et al., 1995) and British families (Stoilova et al., 1997). Analysis of haplotype markers from multiple large families with juvenile-onset glaucoma narrowed the shared locus to a region encompassing only 3 genes - Trabecular Meshwork-induced Glucocorticoid Response Protein (*TIGR*) also known as Myocilin (*MYOC*), Apoptosis (*APO-1*) Antigen Ligand 1 (*APT1LG1*) and Tax-Transcriptionally Activated Glycoprotein 1 (*TXGP1*) (Stone et al., 1997). Genotype screening in more glaucoma patients combined with functional evidence highlighted *MYOC* as the causative gene at glaucoma locus GLC1A.

1.5.1.2 Mutation prevalence

After identifying three *MYOC* mutations (G357V, Q368X and Y430H) in 227 familial glaucoma cases, 103 unselected glaucoma cases, 380 general population participants and 91 normal controls, Stone and colleagues (1997) observed a *MYOC* mutation prevalence of 4.4%, 2.9%, 0.3% and 0% respectively. In accordance with the initial discovery of myocilin, its prevalence is the highest among cases of juvenile onset glaucoma. For predominantly Caucasian cohorts with the age of diagnosis under 35 and 40 years, the prevalence rate of myocilin glaucoma is 36% and 17% respectively (Shimizu et al., 2000, Souzeau et al., 2013). The most common mutation within *MYOC* is the Q368X variant with a frequency ranging from 1.6-4.27% (Fingert et al., 1999, Mataftsi et al., 2001, Ennis et

al., 2010). However this mutation is absent in glaucoma in the African population (Sale et al., 2002, Melki et al., 2003). In the largest cohort of advanced glaucoma cases (1108 Australian Caucasians), the frequency of Q368X and all *MYOC* mutations were 2.64% and 4.25% respectively (Souzeau et al., 2013). The preponderance of *MYOC* mutations in glaucoma, especially of the Q368X mutation begs the question regarding the presence of Founder effects. The common Q368X mutation found in 15 Australian families was indeed linked to a common European ancestor in the 1800s (Baird et al., 2003). Further analysis revealed that the same haplotype was found in a large French Canadian family implying a potential Founder effect in both populations (Baird et al., 2005). Similar founder effects have been demonstrated with the less common T377M *MYOC* mutation worldwide (Hewitt et al., 2007) and six different mutations in French-Canadian cases (Faucher et al., 2002).

1.5.1.3 Mutation penetrance

The penetrance of *MYOC* disease causing variants vary for each mutation and rises with increasing age in-keeping with a progressive degenerative optic neuropathy (Shimizu et al., 2000, Gong et al., 2004). In general, *MYOC* disease causing variants have high penetrance. However, no disease causing variant is fully penetrant at age 30, with the T377M variant having the highest rate at 88% in Australian Caucasians (Mackey et al., 2003). By contrast, a Greek study showed complete penetrance of T377M variant by age 80, but much lower penetrance at 30-years (Wirtz et al., 2010). Other variants with reported penetrance include G367R (Iliev et al., 2008), Q368X (Angius et al., 2000, Craig et al., 2001, Hewitt et al., 2008), D380H (Wirtz et al., 2007), K423E (Morissette et al., 1998), C433R (de Vasconcellos et al., 2003, Povoa et al., 2006), W453del (Williams et al., 2015) and N480K (Brezin et al., 1998) (Figure 3). Of note, the most common variant Q368X is also one of the least penetrant, and potentially displays the mildest phenotype of all myocilin glaucoma (Graul et al., 2002, Hogewind et al., 2010).

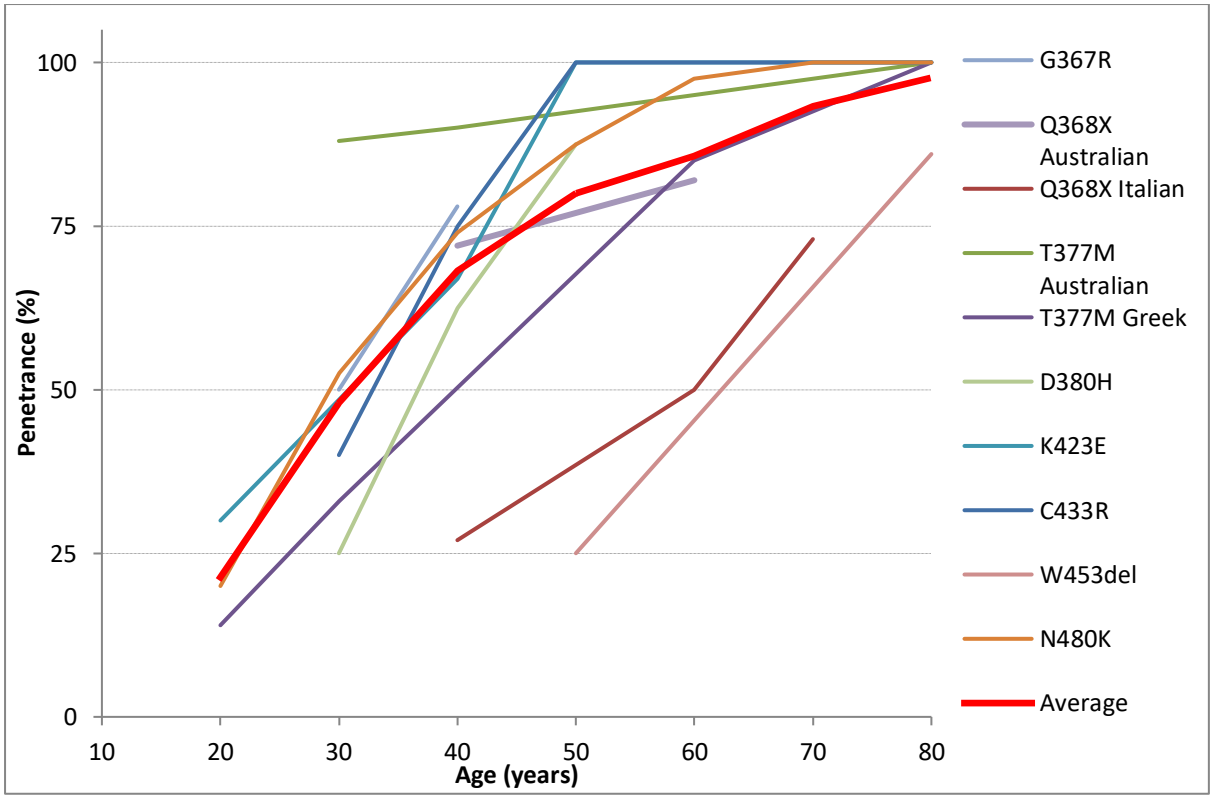

Figure 3: Progressive penetrance rate (%) of MYOC mutations by participant age generated from previously published data detailed in the paragraph above. Different Q368X and T377M variant penetrance was reported by separate studies in different populations. The Red dashed line indicates the average penetrance by age.

1.5.1.4 Structure and location

The *MYOC* gene encodes the 504-amino acid polypeptide myocilin and has 3 exons. The protein contains a leucine zipper-like motif towards the N-terminal and an olfactomedin-like domain towards the C-terminal. By far the majority of all disease-causing mutations in the *MYOC* gene are located within the evolutionary conserved olfactomedin-like domain in exon 3 (Adam et al., 1997, Rozsa et al., 1998, Fingert et al., 2002). Ubiquitously expressed throughout the human body, myocilin is also highly expressed in numerous eye tissues (Abu-Amero et al., 2012, Fingert et al., 2002). Its expression within the eye is the highest in the trabecular meshwork (Resch and Fautsch, 2009). The highest intracellular location of the protein was in the perinuclear region corresponding

to the area abundant in mitochondria (Wentz-Hunter et al., 2002). Within trabecular meshwork cells, myocilin is also localized to the golgi apparatus and endoplasmic reticulum, where it is actively secreted from the cell via exosomes by exocytosis (Hardy et al., 2005, Joe and Tomarev, 2010).

1.5.1.5 Function of wildtype myocilin protein

Despite many years of research, the physiologic function of myocilin and its role in glaucoma is still not entirely clear (Gobeil et al., 2004, Resch and Fautsch, 2009, Menaa et al., 2011). True to the name of trabecular meshwork inducible glucocorticoid response (TIGR) gene, myocilin protein expression increased significantly over baseline levels after prolonged exposure to the steroid dexamethasone in human cultured trabecular meshwork cells (Nguyen et al., 1998). Post steroid induction and *MYOC* overexpression, trabecular meshwork cells were significantly more susceptible to apoptosis while losing actin stress fibres, cellular adhesion and spreading (Wentz-Hunter et al., 2004). Loss of actin stress fibres is activated by Wnt signalling pathway as evident in the ability of Wnt inhibitors to preserve actin fibres (Shen et al., 2012). By sustaining cadaveric human anterior segments in organ culture solution, administering recombinant *MYOC* increased the IOP up to threefold more than control (Fautsch et al., 2000). Conflictingly, the degree of steroid-induced IOP elevation does not correlate to the level of *MYOC* expression stimulation in cultured human TM cells, therefore suggesting that upregulation of myocilin may not account for the elevation of IOP in glaucoma (Sohn et al., 2010). Recently, gene expression profiling of myocilin-expressing HEK293 cells revealed a role in cell survival and death. Myocilin-expressing cells showed higher cell proliferation and lower cell apoptosis via ERK signalling pathway (Joe et al., 2014).

1.5.1.6 Myocilin mutants

Disease causing variants within *MYOC* may act via a dominant negative or neomorphic gain-of-function effect as reduced expression of the wildtype *MYOC* does not confer disease (Kim et al.,

2001, Menaa et al., 2011). There is much experimental evidence examining the effect of *MYOC* expression on POAG pathogenesis. Deletion of one copy of the *MYOC* gene secondary to complex deletion of chromosome 1 (1q23-1q25) failed to cause the IOP elevation and optic nerve damage characteristic of myocilin glaucoma in a patient with developmental delay (Wiggs and Vollrath, 2001). Complete loss of *MYOC* expression in myocilin knockout mice does not show any glaucoma phenotype either (Kim et al., 2001). In humans, the severe truncating mutation *MYOC* R46X removed more than 90% of the protein effectively causing a loss of expression of the affected allele. This variant was found in 3% of the control population and was not associated with glaucoma in an affected Chinese family in its heterozygous or homozygous form (Lam et al., 2000). Participants with homozygous K423E mutation of *MYOC* did not develop glaucoma whereas those from the same family with heterozygous mutations did, further confirming that its pathogenesis is not via genetic haploinsufficiency (Morissette et al., 1998). Similarly, a woman with homozygous *MYOC* Q368X mutation did not exhibit glaucoma at age of 49 despite her heterozygous mother having glaucoma (Hewitt et al., 2006a). Taken together, these experiments illustrate that the most likely genetic mechanism of myocilin related pathogenesis in glaucoma is via a dominant negative or neomorphic effect.

While the function of wildtype myocilin is debated, *MYOC* mutant-triggered biological cascade leading to glaucoma is well studied. Mutation-derived structural change alters the physical properties of myocilin protein causing misfolding, intracellular aggregation, cellular stress and damage (Liu and Vollrath, 2004, Resch and Fautsch, 2009). Myocilin is detected in the aqueous humour in cataract and glaucoma patients (Russell et al., 2001). Within the aqueous, myocilin is secreted as an oligomer or bound to other proteins as its discovered size of 250kDa was much larger than its actual size of 56kDa. Successful secretion of myocilin relies on the biochemical properties of its oligomers, namely solubility. In Triton X-100 detergent, wildtype myocilin is completely soluble

while mutant variants are substantially insoluble (Zhou and Vollrath, 1999). The severity of different myocilin mutations have been compared by cloning recombinant mutants into Rosetta-Gami 2(DE3)pLysS cells (Burns et al., 2011). Myocilin variants associated with early-onset glaucoma, K423E, Y437H and I477N, exhibited the greatest misfolding and thermal instability while forming insoluble aggregates. In contrast, wildtype myocilin and non-pathogenic variants had the highest thermal stability and solubility. These results indicate that the pathogenicity of myocilin mutations is dependent on the solubility of the mutant protein. Furthermore, myocilin mutants undergo hetero-oligomerization with wildtype myocilin forming insoluble Russell bodies and providing an explanation for a dominant negative mechanism (Joe et al., 2003, Gobeil et al., 2004, Yam et al., 2007a).

A direct consequence of the formation of insoluble mutant myocilin aggregates is a sequestration and accumulation of these oligomers within intracellular compartments. *In vitro* studies identified the greatest accumulation of the Russell body aggregates in the endoplasmic reticulum, congruent with the active secretion of myocilin from the cell (Joe et al., 2003, Liu and Vollrath, 2004, Yam et al., 2007a). Mutant myocilin bound the wildtype protein in most cases and significantly reduced the secretion of all myocilin from the affected cells (Joe et al., 2003, Liu and Vollrath, 2004). Russell body formation within the endoplasmic reticulum produces reactive oxygen species, reduces cell proliferation and instigates apoptosis via activation of caspases and expression of CHOP/GADD153 (Joe et al., 2003, Yam et al., 2007a, Joe and Tomarev, 2010). Trabecular meshwork cell death from myocilin aggregate accumulation may reduce aqueous outflow and increase IOP as determined with human T377M mutation carriers even before the onset of glaucoma (Wilkinson et al., 2003). The mutation carriers with reduced outflow facility developed glaucoma more rapidly than the carriers that had normal aqueous regulation. Transgenic mouse models have been developed for the human *MYOC* Y437H mutation with mouse and human recombinant *MYOC* (Senatorov et al., 2006, Zhou et

al., 2008). In both cases, the cascade of intracellular accumulation, reduced secretion, increased IOP and glaucomatous RGC damage were observed.

1.5.1.7 Potential therapies for myocilin glaucoma

The pathogenicity of myocilin mutations could be reversed experimentally by increasing the solubility of mutant proteins. By lowering culture temperature to 30°C to increase thermal stability and therefore solubility, *MYOC* P370L-transfected human TM cells accumulated less misfolded aggregates, secreted more myocilin and survived longer (Liu and Vollrath, 2004). Another way to improve protein solubility was found by treating *MYOC* mutant-transfected human TM cells with molecular chaperone osmolyte trimethylamine N-oxide (TMAO) (Jia et al., 2009) or phenylbutyrate (PBA) (Yam et al., 2007b, Zode et al., 2011, Zode et al., 2012). This method was more effective than low-temperature culture for myocilin mutants with more severe misfolding. Chaperone therapy is able to correct protein misfolding, thereby facilitating the secretion of Russell bodies from the endoplasmic reticulum. *In vitro* treatment of *MYOC* mutant transfected TM cell culture with TMAO or PBA was able to rescue the cells from apoptosis (Jia et al., 2009, Yam et al., 2007b). *In vivo* treatment of *MYOC* mutant transgenic mice with PBA both topically and systemically showed similar anti-apoptotic effects (Zode et al., 2011, Zode et al., 2012).

1.5.2 Glaucoma locus GLC1C – IL20RB

The glaucoma locus GLC1C was originally mapped to 3q21-q24 between markers D3S3637 and D3S1744 via linkage in a family with twelve affected members from the US with adult onset POAG with predominantly high IOP (Wirtz et al., 1997). It was not until 2014 that the causative variant for the original linkage signal was identified in *IL20RB* (Interleukin 20 Receptor Subunit Beta) p.Thr104Met via Sanger sequencing (Keller et al., 2014). Keller and colleagues established that IL20RB was expressed in a primary culture of human trabecular meshwork cells from cadaveric

donors. Normal human dermal fibroblasts demonstrated increased phosphorylation of downstream target (STAT3) of *IL20RB* protein upon exposure for 24 hours to cytokines IL-19, IL-20, and IL-24 (Keller et al., 2014). In dermal fibroblasts of participants with *IL20RB* p.Thr104Met mutation, phosphorylation of STAT3 was reduced upon exposure to the cytokine cocktail. The functional evidence suggests that IL20RB may play a role in IOP regulation via signalling matrix metalloproteinase activity which was reduced by the p.Thr104Met variant in the discovery pedigree (Keller et al., 2014). However, *IL20RB* disease causing variants are exceedingly rare with none identified in the 230 random POAG cases screened (Keller et al., 2014).

1.5.3 Glaucoma locus GLC1E – Optineurin

1.5.3.1 Discovery

Optineurin (*OPTN*) was the second gene to be identified in POAG that is inherited in a classical Mendelian pattern albeit that the phenotype associated with *OPTN* is distinct from *MYOC* and is typically characterized by normal or near-normal IOP. The genetic locus was narrowed down to 10p14-15 via linkage (LOD score 10) in a large British family with 19 affected patients from a 51-member pedigree (Sarfarazi et al., 1998). The critical region was 5cM in size and encompassed five genes. Optineurin was the optimal candidate based on its position and expression within the retina (Rezaie et al., 2002). At the time, *OPTN* was also known as FIP-2 and NRP. By screening a total of 54 families with predominantly NTG cases, the authors reported a remarkable 16.7% carrier rate of disease-causing *OPTN* mutations within this highly selected cohort. Three causative and one risk associated mutations were reported at discovery with the most prevalent being the causative E50K (13.5%) and disease-associated M98K (13.6%) variants. Later replication studies have found a much lower prevalence.

1.5.3.2 Mutation prevalence

Out of all *OPTN* variants, the E50K variant is the most consistently replicated variant in other cohorts with POAG (Alward et al., 2003, Ayala-Lugo et al., 2007). *OPTN* E50K mutant has the greatest pathogenicity risk in NTG. However its occurrence is exceedingly rare with reported frequencies of 0% in Brazilian and Australian POAG cohorts (Baird et al., 2004, Caixeta-Umbelino et al., 2009), 0.1% in a Caucasian all POAG cohort (Iowa) with enrichment to 3.5% in NTG with positive family history (Alward et al., 2003). In NTG cohorts, the prevalence is around 1.5% in a predominantly Caucasian cohort (Hauser et al., 2006b) and 3% in an ethnically mixed cohort (Ayala-Lugo et al., 2007). The most frequent polymorphism in *OPTN,* the M98K variant, is often found at similar rates in case and control cohorts across different ethnicities (Alward et al., 2003, Baird et al., 2004, Ayala-Lugo et al., 2007) and therefore may not be pathogenic. Similarly, the R545Q variant was not significantly enriched in replication cohorts (Alward et al., 2003, Ayala-Lugo et al., 2007).

1.5.3.3 Structure and location

The *OPTN* gene encodes for a 577 amino-acid polypeptide and consists of a total of 16 exons with the first codon located within exon 4 (Chalasani et al., 2009). Although 4 different transcripts of *OPTN* have been identified, all known transcripts have the same open reading frame and encode for the same polypeptide (Ying and Yue, 2012). *OPTN* contains several functional domains including 1 bZIP motif, 2 leucine zippers, 3-4 coiled-coil domains and a C-terminal zinc finger domain (Chalasani et al., 2009, Kachaner et al., 2012). It shares strong homology with NF-κB modulator NEMO with 53% similarity with the main difference being the insertion of a 166-residue sequence which includes a leucine zipper repeat (Kachaner et al., 2012). Notable variant E50K is located within the bZIP motif; M98K is located within the first coiled-coil domain; R545Q situated within the C-terminal zinc finger (Chalasani et al., 2009). Within the eye, optineurin is predominantly expressed in the ganglion cells of the mouse retina (De Marco et al., 2006, Kroeber et al., 2006). Within cells, it is localized to the

cytoplasm (Park et al., 2007, Gao et al., 2014) and especially associated with the golgi apparatus (De Marco et al., 2006, Chi et al., 2010).

1.5.3.4 Function of wildtype optineurin protein

Normal optineurin is known to be involved in protein transportation intracellularly by linking myosin IV to golgi apparatus via Rab8 and transferrin receptor (Sahlender et al., 2005, Park et al., 2006, Ying et al., 2010); it is crucial in exocytosis. Golgi fragmentation occurs when functioning *OPTN* is knocked down experimentally followed by cell death (Sippl et al., 2014, Turturro et al., 2014). Additionally, wildtype *OPTN* may counter apoptosis by buffering against TNF-α mediated NF-κB activation due to its similar homology to the NF-κB upstream modulator NEMO (Zhu et al., 2007, Kachaner et al., 2012). Upregulation of *OPTN* increases the mRNA expression of *MYOC* but did not affect the levels of two other glaucoma genes (*CYP1B1* and *WDR36*) in transfected human trabecular meshwork, rat PC12 and mice retinal photoreceptor (RGC5) cells (Park et al., 2007). The increase in *MYOC* mRNA levels resulted from improved mRNA stability and half-life and not from upregulation of *MYOC* transcription. Functional work on *MYOC* emphasized the pathogenicity of instability in myocilin protein. It stands to reason that *OPTN* overexpression should increase cell viability. Indeed this has been validated experimentally where upregulation of *OPTN* protected against hydrogen peroxide damage (De Marco et al., 2006). Under apoptotic conditions, optineurin is upregulated two-fold and transported from the golgi apparatus to the nucleus via Rab8 GTPase activity. Correspondingly, siRNA knockdown of *OPTN* in rat PC12 and RGC5 cells inhibited cell growth and amplified apoptosis via downregulation of numerous neurotrophic factors including BDNF and neurotrophin-3 (NTF3) (Li et al., 2011, Sippl et al., 2011). Optineurin is also known to interact with TANK (TRAF-associated NF-κB activator) binding kinase 1, huntingtin, transferrin receptor, transcription factor IIIA, metabotropic glutamate receptors 1 and 5 amongst others to regulate autophagy and apoptosis (Chi et al., 2010, Ying and Yue, 2012, Kachaner et al., 2012).

1.5.3.5 Optineurin mutants

The most studied mutation in *OPTN* is the highly pathogenic E50K variant. The hypothesized genetic mechanism for this mutation is a dominant negative model (Rezaie et al., 2002). Toxicity of *OPTN* mutations may arise from increased reactive oxygen species (ROS) production, disruption to cellular processes, autophagy and amyloidogenesis. Variant E50K is located within the bZIP domain which regulates DNA transcription, binding and protein polymerisation (Chalasani et al., 2009). When the *OPTN* E50K mutation was introduced into RGC5, it triggers production of ROS and induces apoptotic cell death (Chalasani et al., 2007). When the same mutation was induced in other cell lines including human HeLa (cervix), monkey Cos-1 (kidney) and human IMR32 (neuroblastoma) lines, no survival difference was noted, indicating a selective pro-apoptotic effect of the mutation in the RGC5 cells. Optineurin E50K mutation completely disrupts the interaction with Rab8 GTPase which controls its translocation to the nucleus under metabolic stress (Chi et al., 2010). In effect, this leads to inability to respond to stress and impaired intracellular trafficking of vital molecules such as transferrin receptor leading to loss of RGC and glaucoma (Nagabhushana et al., 2010, Park et al., 2010).

Autophagy is a potential cause of apoptosis involved in *OPTN* pathogenicity (Shen et al., 2011, Sirohi et al., 2013, Wong and Holzbaur, 2014). The microtubule-associated protein 1 light chain 3 (LC3) interaction region (LIR) of optineurin recruits LC3, inducing autophagosome formation (Wong and Holzbaur, 2014). The Optineurin mutants E50K and M98K have both been implicated in enhancing autophagy related apoptosis in the RGC5 cell line (Shen et al., 2011, Sirohi et al., 2013). Recent revelations revealed that the supposed rat RGC5 cell line, which much of *in vitro OPTN* studies utilized, is in fact mouse in origin (Van Bergen et al., 2009). Upon further characterization, RGC5 cells were determined to be the photoreceptor cell line 661W (Wood et al., 2010, Krishnamoorthy et al., 2013). Despite the problem of RGC5 misidentification, retinal ganglion cells of E50K transgenic mice demonstrated *in vivo* evidence of autophagy stimulation via upregulation of autophagy marker LC3

(Shen et al., 2011). Intravitreal delivery of adeno-associated type 2 viral (AAV2) vectors carrying wildtype and E50K mutant *OPTN* in the rat model confirmed induced autophagic processes leading to loss of RGC and retinal thinning previously documented in RGC5 cells (Ying et al., 2015). The loss of RGC was greater in the E50K mutant when compared to the wildtype *OPTN*, 11.7% ± 1.9 and 6.2% ± 0.4, respectively. Rapamycin was able to supress *OPTN* E50K overexpression and counter the induced apoptosis (Shen et al., 2011, Ying et al., 2015).

Another possibly related biochemical action of the *OPTN* E50K mutation is amyloidogenesis secondary to abnormal protein oligomerization. While wildtype optineurin forms non-covalently bonded oligomers that dissociate with a reducing agent, the E50K mutation generates resilient covalent-bonded trimers via ROS production (Gao et al., 2014). These covalent trimers cause accumulation of abnormal protein in a similar manner to the misfolded *MYOC* protein and have been detected in the retinas of *OPTN* E50K transgenic mice (Minegishi et al., 2013). Therefore aggregation of amyloid may lead to optic nerve damage in people with *OPTN* E50K mutations.

1.5.4 Glaucoma locus GLC1F – *ASB10*

1.5.4.1 Discovery

Ankyrin repeat and SOCS box containing 10 (*ASB10*) gene was first described as a potential glaucoma linked locus in 1999 (Wirtz et al., 1999). Using genome-wide microsatellite screening in a Caucasian family of 25 with 10 members affected with HTG, the glaucoma locus GLC1F was identified as the region on chromosome 7q35-36 bound by markers D7S2442 and D7S483. Screening of the GLC1F locus in a Japanese NTG cohort showed significant association of the D7S1277i locus (Murakami et al., 2010). Pinpointing the gene responsible for the linkage signal proved difficult as no rare nonsynonymous variants were found in 42 genes at the locus (Pasutto et al., 2012). The only rare variant which segregated in the original discovery family members and was absent in controls was

the novel synonymous variant c.765C>T p.255T>T. Despite being non-protein changing, the synonymous variant was experimentally shown to cause alternate splicing and premature termination of the *ASB10* protein. Hence by the process of elimination, *ASB10* was attributed as the causative gene. Immunofluorescence work in human trabecular meshwork cells has implicated *ASB10* in ubiquitin-mediated autophagy-lysosomal degradation pathways (Keller et al., 2013).

1.5.4.2 Mutation prevalence

Three case-control studies have examined the association between ASB10 and POAG. The prevalence of ASB10 potentially deleterious nonsynonymous variants was significantly higher in POAG cases ($p = 0.008$) at 6% (70 out of 1172) and 2.8% (13 out of 461) in controls within a study of 195 US and 977 German Caucasian cases (Pasutto et al., 2012). Opposing evidence for the role of ASB10 was published in a candidate study of US Caucasian POAG patients where the rate of rare nonsynonymous ASB10 variants (13 out of 158, 7.0%) in cases was not significantly higher than that in controls (3 out of 82, 3.7%) (Fingert et al., 2012). A more recent Pakistani study of 238 cases found a significant association of ASB10 rare nonsynonymous variants in POAG with 9.7% (23 out of 238) prevalence in cases compared to 1.3% (2 out of 151) in controls (Micheal et al., 2015). The overall global prevalence of ASB10 from these 3 studies is 7.2% (106 out of 1468), which is significantly higher than the pooled control prevalence of 2.6% (18 out of 694, $p = 0.000006$).

1.5.5 Glaucoma locus GLC1G – *WDR36*

1.5.5.1 Discovery

The GLC1G locus was mapped to the 5q22.1 region in two large POAG families in the US (Monemi et al., 2005). After direct sequencing of a total of seven candidate genes within the 35Mb linkage region in the discovery cohort, the only gene with rare potentially pathogenic mutations was *WDR36* (WD Repeat Domain 36). The proposed variant in question, D658G, was found in seven affected

family members but none of the 9 unaffected members or 238 normal controls. Further screening of *WDR36* in 129 unrelated probands yielded 3 other novel variants (N355S, A449T, R529Q) (Monemi et al., 2005). Replication studies examining the prevalence of *WDR36* in POAG have varied outcomes in different ethnicities.

1.5.5.2 Replications

One of the first replication studies came from another US cohort of 126 affected probands and 108 controls (Hauser et al., 2006a). Although the investigators identified 17 nonsynonymous variants in *WDR36*, no variant demonstrated segregation in affected pedigrees or statistically significant difference to controls including the most prevalent and significant D658G variant from the discovery study. In the Australian population, a case-control study of 249 POAG participants and 217 age-matched controls found no significant enrichment of D658G in POAG (Hewitt et al., 2006b). Another US replication study containing an Iowa cohort of 409 POAG patients and 421 controls (Fingert et al., 2007) found no significant difference between the cases and controls in the frequency of any *WDR36* variant including the D658G variant. Therefore all replication studies from US and Australian Caucasian cohorts with similar ethnicities to the discovery study did not support the notion that *WDR36* is a POAG disease-causing gene.

Within the HTG phenotype, there is more supportive evidence for *WDR36* in pathogenesis, albeit only in the form of SNP association studies. Within a Japanese cohort of 136 HTG and 103 NTG patients, the rate of mutations were significantly higher in the HTG group than controls for p.I264V and c.1965-30A>G variants, but not higher in the NTG cases (Miyazawa et al., 2007). In a German study, there was significant enrichment of *WDR36* putative disease-causing variants with 80% of the variants present in HTG patients, which accounted for 80% of the cohort (Pasutto et al., 2008). Similarly in a Chinese case-control study, *WDR36* rare disease-causing variants were significantly

associated with HTG but not NTG or JOAG (Fan et al., 2009). Employing a common variant analysis, an Indian study genotyped ten common SNPs in *WDR36* and found the exon 5-linked rs10038177 to be associated with HTG, but no SNPs were associated with POAG or NTG (Mookherjee et al., 2011). A linkage study in the Mongolian population mapped the 5q22.1 region to IOP (Lee et al., 2010). From the available evidence, *WDR36* may be a rare cause of HTG and high IOP and therefore studies with POAG consisting of a larger proportion of NTG may be diluting any small enrichment.

1.5.6 Glaucoma locus GLC1O – *NTF4*

Neurotrophin 4 (*NTF4*) is the only glaucoma gene listed in the OMIM database not to be discovered via linkage study. Instead *NTF4* was an excellent candidate gene for glaucoma pathogenesis and was found to be significantly associated with POAG in a case-control association study with two replication cohorts (Pasutto et al., 2009). The discovery cohort contained 399 European Caucasians where 2.26% carried a heterozygous nonsynonymous variant in *NTF4*. Total mutation carrier frequency was 1.7% after combining all three cohorts. Various other authors have attempted to replicate these results with mixed success. Case-control studies of European Caucasians (Liu et al., 2010) and Indians (Rao et al., 2010) found no significant difference in the rate of *NTF4* mutation carriers between POAG patients and controls. It was noted that the control cohort used in the European study (Liu et al., 2010) were significantly younger than the original discovery cohort and may include future glaucoma patients. Meanwhile, two separate studies in Chinese populations have identified very low rates of nonsynonymous mutations in *NTF4* from 0.3-0.6% in POAG cases and none in controls suggesting that it may be a rare cause of POAG in Chinese people (Chen et al., 2012, Vithana et al., 2010).

1.5.7 Glaucoma locus GLC1P – *TBK1*

1.5.7.1 Discovery

TBK1 is unique amongst all Mendelian causes of POAG. It is the only POAG locus known to date that causes disease through copy number variation. GLC1P was mapped to 12q14 from linkage study of a pedigree of African American ancestry with 10 affected members out of 12 examined participants (Fingert et al., 2011). All affected members from the pedigree had NTG. The linked locus was 9.47Mb long and was bound by rs12227270 centromerically and rs7488555 telomerically. Copy number assays indicated the presence of a large duplicated region spanning 4 genes (*TBK1*, *XPOT*, *RASSF3* and *GNS*) (Fingert et al., 2011). *TBK1* was selected as the causative candidate as it was the only gene that instigated an expression level change in its duplicated form. Further screening of NTG cases in the Iowa discovery cohort revealed another segregating duplication within *TBK1*, which generates a prevalence rate of 1.3% in the NTG cohort (Fingert et al., 2011).

1.5.7.2 Mutation prevalence

TBK1 has been replicated in several other cohorts around the world although only as a rare cause of NTG. The reported rate from the discovery study was 1.3% of NTG in the US (Fingert et al., 2011). The largest number of *TBK1* carriers was found in the Australian and New Zealand Registry of Advanced Glaucoma (ANZRAG) cohort with a total of 4 probands and rate of 1.2% amongst NTG patients (Awadalla et al., 2015). The ANZRAG cohort study also reported the only case of *TBK1* triplication in the literature to date. Three other studies have found TBK1 duplications to date with 0.4% in a Japanese NTG cohort (Kawase et al., 2012), 1% in a Caucasian NTG cohort from New York (Ritch et al., 2014) and 1.4% in the Indian NTG cohort (Kaurani et al., 2016). No cases of *TBK1* duplication have been reported yet in HTG or normal controls. The overall rate of *TBK1* duplication from all studies worldwide is 0.8% (10 out of 1222 NTG cases).

1.5.8 Glaucoma locus GLC3A – *CYP1B1*

1.5.8.1 Discovery

The GLC3A locus was initially mapped using family-based linkage studies on large primary congenital glaucoma (PCG) pedigrees. Subsequently, phenotypic heterogeneity of the locus has been demonstrated via its association with POAG of juvenile or adult-onset as well as digenic interaction with other POAG genes namely *MYOC*. Using a discovery cohort of 17 Turkish families with 40 affected individuals, the GLC3A locus was localized to 2p21 (Sarfarazi et al., 1995). They also revealed genetic heterogeneity in PCG by finding that 6 out of the 17 families did not link to locus GLC3A. The remaining 11 families showed perfect linkage to three closely linked markers D2S177, D2S1346 and D2S1348. A later study of 25 Saudi Arabian families found the strongest linkage signal to the marker D2S177 (Bejjani et al., 1998). With the larger cohort, Bejjani and colleagues narrowed the linked region to between D2S2186 and D2S1356. Meanwhile, using the data from Saudi Arabia (Bejjani et al., 1998) a US group was able to further narrow the disease locus to between D2S2186 and D2S1346 (Stoilov et al., 1997). A total of three potential candidate genes were located within the region of interest - *hSOS1*, *PRKR* and *CYP1B1* (Stoilov et al., 1997). Direct sequencing of cDNA from skin fibroblasts of affected individuals ruled out coding mutations in *hSOS1*, *PRKR* and discovered a 13bp homozygous deletion in exon 3 of *CYP1B1* (Cytochrome P450, Family 1, Subfamily B, Polypeptide 1) (Stoilov et al., 1997). This deletion caused a frameshift and truncation due to the insertion of a premature stop codon which corresponds to functional knockout. Twenty-four out of 25 Saudi Arabian families carried homozygous or compound heterozygous missense mutations in *CYP1B1* with complete cosegregation (Bejjani et al., 1998).

1.5.8.2 Mutation prevalence

CYP1B1 mutations are the predominant genetic cause of PCG, but prevalence varies greatly between ethnicities. In populations with higher rates of consanguinity, *CYP1B1* accounts for the majority of

PCG, such as 100% in Slovak Gypsies (Plasilova et al., 1999), 96% in Saudi Arabia (Bejjani et al., 2000) and 70% in Iran (Chitsazian et al., 2007). The global mutational prevalence of *CYP1B1* in PCG is lower at around 20% in countries such as Pakistan (17%) (Bashir et al., 2014), China (17.2%) (Chen et al., 2014a), Germany (18%) (Weisschuh et al., 2009), Japan (20%) (Mashima et al., 2001), Australia (21.6%) (Dimasi et al., 2007), Korea (25.9%) (Kim et al., 2011) and India (46%) (Tanwar et al., 2009).

The rates of *CYP1B1* mutations in POAG are significantly lower than in PCG. The first study to report the mutation load of *CYP1B1* in POAG was in a French population. A total of 4.6% of unrelated French POAG patients carried mutations in *CYP1B1* compared to 2.2% of controls (Melki et al., 2004). These *CYP1B1* carrying patients were characterized by having a younger age of diagnosis (13-52 years). In-keeping with the PCG rates, the rate of *CYP1B1* mutations in Saudi Arabian POAG patients was the highest at 85.7% (Abu-Amero et al., 2013). Globally, the prevalence of *CYP1B1* mutations in POAG fluctuates while remaining lower than that in PCG for any given ethnicity, ranging from 4.5%, 10.76% to 18.6% in Indian studies (Acharya et al., 2006, Chakrabarti et al., 2007, Kumar et al., 2007), 4.62% in a Taiwanese study (Su et al., 2012), 6.1% in a New Zealand POAG cohort (Patel et al., 2012), 6.8% in Australia JOAG cohort (Souzeau et al., 2015), 10.9% in a Spanish POAG cohort (Lopez-Martinez et al., 2007), and 11.1% in an Iranian cohort (Suri et al., 2008). Through measuring ethoxyresorufin O-deethylation activity, a measure of CYP1B1 catalytic activity, and *CYP1B1* stability, *CYP1B1* mutants present in the Spanish cohort were shown to be hypomorphic with a 40-80% reduction in catalytic activity (Lopez-Garrido et al., 2010). Heterozygous mutations in *CYP1B1* may be sufficient to be a risk factor for POAG (Pasutto et al., 2010). In the Australian ANZRAG cohort of severe POAG patients, *CYP1B1* mutations were associated with a younger age of onset (mean = 23.1 vs 31.5, $p = 0.008$) and more severe disease as measured by mean deviation on visual field testing (-24.5 vs -15.6, $p = 0.02$) (Souzeau et al., 2015). These data support the notion that primary congenital glaucoma is a more severe manifestation on the same disease spectrum as POAG.

1.5.9 Glaucoma locus GLC3D – LTBP2

1.5.9.1 Discovery

The cause of autosomal recessive primary congenital glaucoma in 2 consanguineous Pakistani families was mapped to the region between 14q24.2 and 14q24.3 and coined the GLC3D locus (Firasat et al., 2008b). The linkage region is 4.2 Mb long and encompasses 97 genes. In the follow up study, *LTBP2* (Latent transforming growth factor beta binding protein 2) was selected as the most probable candidate following a review of all 97 potential genes based on its expression in the anterior segment (Ali et al., 2009). In a total of 4 consanguineous Pakistani families, premature termination codon causing null mutations in *LTBP2* were found to co-segregate and elicited as the cause of PCG in these families (Ali et al., 2009). The culpability of *LTBP2* was further supported by the finding of homozygous premature termination codons in 2 other consanguineous Iranian families with PCG (Narooie-Nejad et al., 2009).

1.5.9.2 Mutation prevalence

Screening of unrelated Gypsy individuals with PCG uncovered one of the null mutations (p.Arg299X) from a consanguineous Pakistani family in 8 out of 15 cases (Ali et al., 2009) suggesting a founder effect within this population. The authors predict that the Arg299X mutation accounts for 40% of all PCG in this Gypsy population and ranks as the second commonest cause of PCG after *CYP1B1*. In a screening study of PCG in Roma/Gypsy population, the rate of *LTBP2* p.Arg299X truncating mutations was 33.8% (Azmanov et al., 2011). Similar to *CYP1B1*, potential disease-causing *LTBP2* variants have been also implicated in POAG, albeit at a lower prevalence. In a study of 42 Iranian individuals with POAG, the carrier rate of novel *LTBP2* coding variants was 11.9% (5 out of 42) (Jelodari-Mamaghani et al., 2013). However, a WES study failed to detect any *LTBP2* variants in 340 Chinese POAG, JOAG and PCG patients (Huang et al., 2014).

1.6 Rationale and hypotheses for research

Linkage analysis studies have identified the most prevalent high penetrance Mendelian disease alleles. However, the percentage of glaucoma cases attributed to highly penetrant genes is around 3.6% (Huang et al., 2014) to 5% (Fingert, 2011, Gemenetzi et al., 2012) with the majority of glaucoma disease load unaccounted for. The quest to explain the remaining missing heritability has continued during the era of genome-wide association studies (GWAS) using DNA microarray technology. Assuming a common disease, common variant model, this approach has been successful with several disease associated genes discovered (Burdon et al., 2011, Gharahkhani et al., 2014). However, the greatest risk effect of any disease associated single nucleotide polymorphism (SNP) is substantially less than 2 fold in magnitude (Burdon et al., 2011, Mackey and Hewitt, 2014). Many people without POAG also carry disease-associated alleles while never developing the condition, indicating that these SNPs are associated risk factors for POAG, but are not sufficient to cause disease. This makes gaining a functional understanding of each locus and developing gene-targeted therapeutic approaches difficult (Bodmer and Bonilla, 2008).

Rare disease-causing variants should in theory account for a proportion of the missing heritability (Cirulli and Goldstein, 2010). The advent of next generation sequencing has introduced a useful tool in tackling the conundrum of the common disease rare variant hypothesis in glaucoma. Next-generation sequencing offers new ways to identify rare disease-associated variants with fewer restrictions than traditional linkage studies, which generally require large pedigrees. The optimal conditions of high penetrance and large affected families may not be present for the majority of these rare variants to be detected on traditional family linkage studies. Indeed, even in the presence of families with numerous affected members, the success of linkage analysis is not guaranteed. The inadequacies of the linkage study design are evident in the abundance of inconclusive glaucoma loci and non-replicated disease genes within the published medical literature (GLC1B, GLC1D, GLC1H,

GLC1I, GLC1J, GLC1K, GLC1M, GLC1N) (Stoilova et al., 1996, Trifan et al., 1998, Wiggs et al., 2004, Allingham et al., 2005, Pang et al., 2006, Wang et al., 2006, Suriyapperuma et al., 2007).

Rare variants are likely to have larger effect sizes than common variants (Bansal et al., 2010) and thus are more likely to lead to disease. In terms of clinical application, rare variants may have much greater positive predictive values than associated SNPs from GWAS. Enrichment of rare deleterious mutations have been demonstrated in other complex neurological conditions including the common disease schizophrenia (Purcell et al., 2014) and the rare amyotrophic lateral sclerosis (Cirulli et al., 2015). These elusive mutations are often missed by GWAS design owing to their rarity as DNA microarrays used in GWAS target reasonably common single nucleotide changes with population minor allele frequencies of greater than one per cent (Siu et al., 2011). Furthermore, common and rare variants exhibit low levels of linkage disequilibrium rendering imputation of rare variants from GWAS microarray uninformative. Currently next-generation sequencing techniques are able to accurately capture the whole exome encompassing the significant proportion of rare variants (Pengelly et al., 2015).

For the first time, the cost of sequencing all the protein changing mutations within the human genome for a large number of cases is no longer prohibitive. This allowed for the catalogue of rare human mutations as seen in the completed and publically available 1000 Genomes project (Abecasis et al., 2012) and NHLBI GO Exome Sequencing Project (ESP) (Tennessen et al., 2012). Therefore by extension, NGS technology also facilitates association studies of rare genetic variants in disease phenotypes in the same way as DNA microarray chips allowed for GWAS of common SNPs. The drawback to rare variant analysis is the need for large sample sizes potentially in the magnitude of thousands to achieve statistical significance at a genome-wide level for the discovery of a single causative gene (Gorlov et al., 2008). Using even the economical next-generation sequencing

technique of whole exome sequencing (WES), the current costs and bioinformatics challenges of this venture are far from trivial.

1.6.1 Aims

The primary aim of this thesis was to identify novel genetic causes of POAG using a rare variant approach by whole exome sequencing in a Caucasian cohort of participants with advanced disease. Secondly, we aim to explore the genetic contributions of rare pathogenic variants in known disease-causing genes in primary open-angle glaucoma. This thesis also aims to use next generation RNA sequencing (RNAseq) to examine genes and pathways with enrichment in tissues implicated in glaucoma pathogenesis. Finally, the RNAseq derived ocular tissue expression dataset will serve as a foundation for future research in tissue expression in ocular disease.

Chapter 2: Whole exome sequencing case-control study for rare potentially disease-causing monogenic variants in primary open-angle glaucoma

2.1 Ethics

This study adhered to the principles listed by the revised Declaration of Helsinki and the Australian National Health and Medical Research Council (NHMRC) statement of ethical conduct in research involving humans. Ethical approval was obtained from the Southern Adelaide Clinical Human Research Ethics Committee, SA Health, South Australia. Written informed consent was obtained from all participants following explanation for the use and storage of DNA for the purpose of research. All peripheral blood samples were collected for genomic DNA extraction as a part of the ANZRAG as previously described (Souzeau et al., 2012).

2.2 Participant recruitment

The individuals comprising the study cohort were Caucasian participants from the Australian and New Zealand Registry of Advanced Glaucoma (ANZRAG) database, which were recruited in a prospective consecutive manner and previously analysed for common disease-associated variants in genome-wide association studies (GWAS) (Burdon et al., 2011, Gharahkhani et al., 2014, Springelkamp et al., 2015, Hysi et al., 2014). Full recruitment details for the ANZRAG were previously published (Souzeau et al., 2012) and are reiterated herein. The majority of participants for this study were recruited by practitioner referral with the remaining participants self-referring from word of mouth. Catchment areas include all of Australia, New Zealand and internationally located relatives of the probands. Contact was made with the potential participants and consent obtained. Empty blood tubes were posted to each participant with provisions made for return postage after a blood sample was collected by a local phlebotomist. Each participant's clinical details were obtained from their

treating ophthalmologist. Written and signed consent was obtained from all participants and stored within the ANZRAG database.

2.3 Selection of participants for whole exome sequencing

Inclusion criteria for the present studies selected for participants with primary open-angle glaucoma with exclusion of participants having concurrent diagnoses of any other subtype of glaucoma such as anterior segment dysgenesis, pseudoexfoliation and pigment dispersion syndromes. Furthermore only participants with 'advanced' glaucoma were included. Advanced glaucoma was defined as having glaucomatous visual field loss of two or more of the four central squares having a pattern standard deviation (PSD) <0.5% on a Humphrey 24-2 field or a mean deviation of ≤22 dB. They must also have evidence of glaucomatous optic nerve cupping on fundoscopy in order to be included. For participants without formal visual field testing, their best-corrected visual acuity had to be worse than 20/200 owing to glaucomatous damage. The less affected eye was also required to have glaucomatous optic neuropathy as measured by a reliable Humphrey 24-2 field, with corresponding neuroretinal rim thinning. Using available clinical information, efforts were made for the study in this thesis to ensure a comparable split of participants with high and normal IOP for genotyping with whole exome sequencing. High-tension glaucoma (HTG) was defined as having a maximum recorded IOP of greater than 21 mmHg and normal tension glaucoma (NTG) encompassed the remaining participants with maximum recorded IOP of 21 mmHg or less. All participants were also screened for mutations in the myocilin gene. 29 Individuals with disease-causing *MYOC* variants detected by sanger sequencing were not analyzed by whole exome sequencing as the genetic cause of their glaucoma was known (Souzeau et al., 2013) (Appendix Table 1), but were included for analysis to enable relative proportions of POAG cases potentially explained by each individual gene to be assessed. 187 cases with advanced glaucoma were analysed, 84 of which were male (45%) and 103 of which were female (55%). 103 local non-glaucomatous participants served as both technical and

phenotypic controls. The local control cohort was clinically examined to ensure absence of any glaucoma related phenotype and included 51 keratoconus patients, 32 congenital cataract patients and 20 normal controls without ocular disease.

2.4 Whole exome sequencing

DNA was extracted from peripheral blood samples using the QIAamp® DNA blood kit (Qiagen, Hilden, Germany) following the manufacturer's protocol. Sequencing was outsourced to Macrogen Next Generation Sequencing Services. Samples were prepared with SureSelect Human All Exon V4 enrichment kit (Agilent, Santa Clara, USA) as per manufacturer's protocol for whole exome capture and enrichment. Enriched DNA was sequenced on a HiSeq2000 (Illumina, San Diego, USA) with 100bp paired end reads. Firstly, the sequencing platform generated raw sequencing images, which the instrument control software used to locate clusters, and outputs the cluster intensity, X and Y positions, and an estimate of the noise for each cluster. The output from image analysis provided the input for the next step of base calling. Base calling used cluster intensities and noise estimates to output the sequence of bases read from each cluster, a confidence level for each base, and whether the read passes filtering. This was performed by internal platform control software Real Time Analysis (RTA) v1.12.4 (Illumina, San Diego, California, USA) and generated BCL files. The BCL files were converted into FASTQ files using Consensus Assessment of Sequence and Variation (CASAVA) v1.8.2 to generate raw sequencing data. Multiplexed samples were demultiplexed during this step.

Local controls served as both technical and phenotypic controls. Furthermore, raw sequencing data were used to generate BAM files and joint-called with 993 previously sequenced Australian Osteoporosis Genetics Consortium (AOGC) exomes that were captured with the Nimblegen Human Exome Capture V2 (Roche) and sequenced on the HiSeq2000 (Illumina) at the University of Queensland Centre for Clinical Genomics, Brisbane, Australia in collaboration with Prof Matthew A.

Brown (Estrada et al., 2012). All AOGC participants (n = 993) were females with either high or low bone mass and were otherwise self-identified as healthy. FASTQ files were aligned to human genome build hg19 with novoalign (version 3.02.08). Duplicate reads were marked with Picard MarkDuplicates (version 1.124). Local indel realignment and base quality recalibration were performed with GATK (McKenna et al., 2010) (version 3.2-2). Variant calling of single nucleotide variants and small indels was performed with the UnifiedGenotyper module in GATK and variant quality scores were recalibrated according to the GATK "Best Practices Guidelines" (DePristo et al., 2011, Van der Auwera et al., 2013). Top candidates identified on whole exome sequencing were validated with sanger sequencing.

2.5 Post sequencing bioinformatics analysis

2.5.1 Variant annotation

Variant annotation was performed with ANNOVAR (Wang et al., 2010b) software using refGene, variant function prediction software including SIFT (Sorting Intolerant From Tolerant) (Kumar et al., 2009) and PolyPhen2 (Polymorphism Phenotyping v2) HVAR (Adzhubei et al., 2010), as well as publically available population frequency databases including NHLBI GO Exome Sequencing Project (ESP) (http://evs.gs.washington.edu/EVS/), 1000 Genomes Project (http://www.1000genomes.org/), and Exome Aggregation Consortium (ExAC) databases (exac.broadinstitute.org/). Only the non-Finnish Caucasian population frequencies from the public domain genetic frequency databases were used to closely approximate the genetic background of our study cohort. Annotation enables understanding of the significance and identity of the variants found by exome sequencing as well as further variant filtering for analysis.

The following codes were used to generate filtered variant count summary data using variant call files (VCF) in UNIX operating system or its emulation. The codes were designed to minimize the

computer processor time and memory required for completion while sacrificing parsimony in certain steps. Prior to the annotation process, indexing software Tabix (Li, 2011) and VCF processing software VCFtools (Danecek et al., 2011) were installed. PLINK toolset (Purcell et al., 2007) was also installed for creating variant count summaries.

Firstly, single nucleotide variant and indel calls were merged to allow simultaneous processing. The "$" sign at the start of a new line denotes the beginning of the code in UNIX and was not included in the actual input into UNIX.

```
$ vcf-concat SNV.vcf.gz INDEL.vcf.gz > Jointcall.SNVindel.vcf
```

A VCF header file was constructed from the top 67 lines of the VCF file that included information on the samples, sequencing and filtering processes. This header was later reattached to the filtered variants to reconstruct a valid VCF file.

```
$ head -n 67 Jointcall.SNVindel.vcf > Jointcall.SNVindel.header.vcf
```

Only variants that passed the filter for sequencing quality control was included in the analysis. The output from filtering lacked a VCF header, hence the header generated in the previous step needed to be concatenated in ordered to generate a complete VCF file.

```
$ awk -F'\t' '$7 == "PASS"' OFS='\t' Jointcall.SNVindel.vcf | cat Jointcall.SNVindel.header.vcf - >
Jointcall.SNVindel.PASS.vcf
```

The first 8 columns of the VCF file contains all the variant information required for annotation and only accounts for a small fraction of the entire VCF file as the majority of the data stored within pertains to the genotype of each sample sequenced. Therefore a VCF without genotype was generated for faster annotation.

```
$ cut -f-8 Jointcall.SNVindel.PASS.vcf > Jointcall.SNVindel.PASS.no.geno.vcf
```

ANNOVAR converts VCF files into tab-delimited text, but only the first 5 columns of the text file was required for annotation. Annotation was performed using the first 5 columns of the ANNOVAR .txt file.

```
$ perl convert2annovar.pl -format vcf4old Jointcall.SNVindel.PASS.no.geno.vcf >
Jointcall.SNVindel.PASS.no.geno.txt
$ cut -f-5 Jointcall.SNVindel.PASS.no.geno.txt > Jointcall.SNVindel.PASS.no.anno.txt
$ perl table_annovar.pl Jointcall.SNVindel.PASS.no.anno.txt humandb/ -buildver hg19 -out
Jointcall.SNVindel.PASS -remove -protocol
refGene,ljb26_sift,ljb26_pp2hvar,ljb26_gerp++,ljb26_phylop100way_vertebrate,esp6500siv2_ea,10
00g2014oct_eur,exac03,clinvar_20150330 -operation g,f,f,f,f,f,f,f,f -nastring .
```

The header from full VCF file was removed to allow joining with annotation.

```
$ tail -n +68 Jointcall.SNVindel.PASS.vcf > Jointcall.SNVindel.PASS.noheader.txt$ sed 1d
Jointcall.SNVindel.PASS.hg19_multianno.txt | paste - Jointcall.SNVindel.PASS.noheader.txt >
Jointcall.SNVindel.PASS.anno.noheader.txt
```

A header was then made for the annotated .vcf file.

```
$ paste <(head -n 1  Jointcall.SNVindel.PASS.hg19_multianno.txt) <(tail -n 1
Jointcall.SNVindel.header.vcf) > Jointcall.SNVindel.PASS.anno.header.txt
```

2.5.2 Variant filtering

With all variants in the VCF annotated, filtering can be applied to selectively analyse only functionally significant variants. Firstly, only exonic and splicing variants were selected for analysis.

```
$ grep -v ^# Jointcall.SNVindel.PASS.anno.noheader.txt | grep -v intronic | grep -v UTR3 | grep -v UTR5 | grep -v intergenic | grep -v upstream | grep -v downstream | grep -v ncRNA_ | grep -v nonframeshift | grep -v UNKNOWN >> Jointcall.SNVindel_exonic.txt
```

A minor allele frequency filter was then applied. In the example codes below, a public domain cut-off MAF of less than or equal to 0.1% was used.

```
$ awk -F'\t' '(($17 <= 0.001 && $18 <= 0.001 && $24 <= 0.001) || ($17 >= 0.999 && $18 >= 0.999 && $24 >= 0.999) || ($17 == "." && $18 >= 0.999 && $24 >= 0.999) || ($17 >= 0.999 && $18 == "." && $24 >= 0.999) || ($17 == "." && $18 == "." && $24 >= 0.999))' OFS='\t' Jointcall.SNVindel_exonic.txt > Jointcall.SNVindel_maf0.001.txt
```

Functional filtering was applied by selecting for predicted deleterious variants using filters of SIFT <=0.05 or PolyPhen2 >=0.909.

```
$ awk -F'\t' '(($9 ~ /^nonsyn/ && $11 <= 0.05 && $11 != ".") || ($9 ~ /^nonsyn/ && $13 >= 0.909) || ($9 ~ /^nonsyn/ && $11 == "." && $13 == ".") || $9 ~ /^stop/ || $6 ~ /splicing/ || $9 ~ /^frameshift/)' OFS='\t' Jointcall.SNVindel_maf0.001.txt > Jointcall.SNVindel_maf0.001_filter0.05.txt
```

Alternatively, canonical loss of function variants could be selected by filter for only frameshift, stop gain and splicing variants.

```
$ awk -F'\t' '($9 ~ /^stopgain/ || $6 ~ /splicing/ || $9 ~ /^frameshift/)' OFS='\t' Jointcall.SNVindel_maf0.001_filter0.05.txt > Jointcall.SNVindel_maf0.001_LoF.txt
```

When the VCF files for SNV and indels were concatenated, any variants with single base frameshift that also have multiple nucleotide frameshift will have duplicated entries. Due to the order of concatenation, the SNV variant always comes before the multiple nucleotide indel, therefore the

following command will always retain the SNV indel variant rather than the multi-nucleotide variant. This is logically the better option as SNV indels occur much more frequently than multiple nucleotide indels (Levy et al., 2007) and both single nucleotide frameshift and multiple base frameshifts cause disruption of amino acid residues distal to the mutation.

```
$ cut -f28,29 Jointcall.SNVindel.noXY_maf0.001_LoF.txt | paste -
Jointcall.SNVindel.noXY_maf0.001_LoF.txt | awk '!x[$1,$2]++' - | cut -f3- - >
Jointcall.SNVindel.noXY_maf0.001_LoF_nodup.txt
```

A file with ANNOVAR annotation and vcf coordinates was made by cutting the annotated file without duplicates and sorting by VCF coordinate.

```
$ paste <(awk -F'\t' '{print substr($28,4)}' OFS='\t' Jointcall.SNVindel.noXY_maf0.001_LoF_nodup.txt)
<(cut -f-34 Jointcall.SNVindel.noXY_maf0.01_LoF_nodup.txt) | sort -t$'\t' -k 1,1n -k 30,30n - | cut -f2-
- > LoF_maf0.001_nodup_anno.txt
```

A filtered VCF file was made by removing the annotation and adding back the VCF header.

```
$ cut -f28- LoF_maf0.001_nodup_anno.txt | cat Jointcall.SNVindel.header.vcf - >
Jointcall.SNVindel_maf0.001_LoF_nodup.vcf
```

Reads from chromosomes X and Y were removed due to the large discrepancy in the sex of the ANZRAG and AOGC cohorts, whereby the AOGC control cohort consisted entirely of female participants.

```
$ awk -F'\t' '($1 != "chrX" && $1 != "chrY")' OFS='\t' Jointcall.SNVindel_maf0.001_LoF_nodup.vcf >
Jointcall.SNVindel_maf0.001_LoF_nodup.noXY.vcf
```

2.5.3 Counting minor alleles

PLINK was used to count minor allele frequencies. It requires two input files (.fam and .ped) which can be generated from the VCF file using VCFtools. Note, filenames in PLINK cannot have the period sign amongst other prohibited symbol. The .ped file contains the following information in 6 columns:

1. Family ID
2. Sample ID
3. Father ID
4. Mother ID
5. Sex (1=male, 2=female)
6. Phenotype (1=unaffected, 2=affected)

This information was manually entered into the corresponding columns and saved as a tab-delimited .txt file. When Microsoft Excel creates tab-delimited .txt files, it generates \newline character as the end of each row which causes malalignment of the output file and was removed using sed command in UNIX.

```
$ sed 's/\n//g' input.txt > Joint_FAM_file.txt
```

VCFtools was used to generate .ped and .fam files.

```
$ vcftools --vcf Jointcall_SNVindel_maf001_LoF_nodup_noXY.vcf --plink --out
Jointcall_SNVindel_maf001_LoF_nodup_noXY
$ cut -f7- Jointcall_SNVindel_maf001_LoF_nodup_noXY.ped | paste Joint_FAM_file.txt - >
Jointcall_SNVindel_maf001_LoF_nodup_noXY_correct.ped
```

The filename of Jointcall_SNVindel_maf001_LoF_nodup_noXY_correct.ped was changed to Jointcall_SNVindel_maf001_LoF_nodup_noXY.ped to match the .fam file.

PLINK software was used to calculate the minor allele count per variant and genomic inflation factor (λ) to examine for the presence of population stratification.

```
$ plink --bfile filedirectory\Jointcall_SNVindel_maf001_LoF_nodup_noXY --assoc --counts --adjust --out filedirectory\Jointcall_SNVindel_maf001_LoF_nodup_noXY_counts
```

The number of samples with missing capture per variant was calculated to determine the adequacy and quality of exome capture for any given variant.

```
$ plink --bfile filedirectory\Jointcall_SNVindel_maf001_LoF_nodup_noXY --test-missing --out filedirectory\Jointcall_SNVindel_maf001_LoF_nodup_noXY_missing
```

The number of carriers of SNV per variant was also calculated using an autosomal dominant model in PLINK.

```
$ plink --bfile filedirectory\Jointcall_SNVindel_maf001_LoF_nodup_noXY --model --adjust --model-dom --out filedirectory\Jointcall_SNVindel_maf001_LoF_nodup_noXY_case
$ grep -e DOM -e TEST filedirectory\Jointcall_SNVindel_maf001_LoF_nodup_noXY_case.model | sed 's/[ ][ ]*/\t/g' - | sed 's|/|\t|g' - | cut -f2- - > filedirectory\Jointcall_SNVindel_maf001_LoF_nodup_noXY_model.txt
```

All outputs from PLINK were passed through the following UNIX command for conversion to tab-delimited .txt files.

```
$ sed 's/[ ][ ]*/\t/g' [Plink output] | cut -f2- - > Output.txt
```

Allele counts per subgroup (HTG, NTG, local controls and AOGC controls) could be calculated by the addition of a cluster file. A cluster file contains the first 2 columns (family ID and individual ID) of the

Joint_FAM_file.txt as well as a third column containing the subgroup ID (1=HTG, 2=NTG, 3=local controls, 4=AOGC controls).

```
$ plink --bfile filedirectory\Jointcall_SNVindel_maf001_LoF_nodup_noXY --freq --nonfounders --within filedirectory\cluster.txt --out filedirectory\Jointcall_SNVaindel_maf001_LoF_nodup_noXY_clusteredcounts
$ sed 's/[ ][ ]*/\t/g' Jointcall_SNVindel_maf001_LoF_nodup_noXY_counts.txt | cut -f2- - > Jointcall_SNVindel_maf001_LoF_nodup_noXY_clusteredcounts.txt; cut -f2,3,7,8 Jointcall_SNVindel_maf001_LoF_nodup_noXY_clusteredcounts.txt | head -n 1 - | awk -F'\t' '{print $1,$2,$3,$4,$1,$2,$3,$4,$1,$2,$3,$4,$1,$2,$3,$4}' OFS='\t' - > All_counts_LoF.txt; paste <(cut -f2,3,7,8 Jointcall_SNVindel_maf001_LoF_nodup_noXY_clusteredcounts.txt | awk -F'\t' '$2 == "HTG"' OFS='\t' -) <(cut -f2,3,7,8 Jointcall_SNVindel_maf001_LoF_nodup_noXY_clusteredcounts.txt | awk -F'\t' '$2 == "NTG"' OFS='\t' -) <(cut -f2,3,7,8 Jointcall_SNVindel_maf001_LoF_nodup_noXY_clusteredcounts.txt | awk -F'\t' '$2 == "CTRL"' OFS='\t' -) <(cut -f2,3,7,8 Jointcall_SNVindel_maf001_LoF_nodup_noXY_clusteredcounts.txt | awk -F'\t' '$2 == "AOGC"' OFS='\t' -) >> All_counts_LoF.txt
```

The final summary file was generated by pasting the columns of the annotation file with the counts per variant files. The variant burden per gene was calculated using pivot tables in Microsoft Excel. In order to compare the gene mutation burden of our cases with the largest available public domain database (ExAC V3, accessed 20/07/2015), the raw data file “ExAC.r0.3.sites.vep.vcf.gz” was downloaded from the ExAC website (exac.broadinstitute.org). The VCF file was modified using UNIX commands to allow manipulation to extract the necessary information, namely the variant information and frequency data from the European American and Non-Finnish European cohorts.

```
$ awk -F'\t' '$34 == "PASS"' input.txt > output.txt
$ sed -e 's/;/\t/g' ExAC.r0.3.sites.vep.vcf > ExAC.r0.3_tab.vcf
```

```
$ awk '{print $1, $2, $3, $4, $5, $6, $7, $8, $16, $26, $11, $23, $15}' OFS='\t' ExAC.r0.3_tab.vcf >
ExAC.r0.3_NFE_all.vcf
```

The variants were annotated using the same pipeline in ANNOVAR as the study cohort after the VCF file was manipulated into the appropriate format.

```
$ perl convert2annovar.pl -format vcf4old -includeinfo ExAC.r0.3_NFE_all.vcf >
ExAC.r0.3_NFE_all_ANNOVAR.txt
$ cut -f-5 ExAC.r0.3_NFE_all_ANNOVAR.txt > ExAC.r0.3_NFE_all_noanno.txt
```

A column ID header file “Col_ID.txt” was constructed with the following headers “#CHROM, POS ID, REF, ALT, QUAL, FILTER, INFO, AC_Adj, AN_Adj, AC_Hom, AC_NFE, AN_NFE” and concatenated with the ANNOVAR pre-annotation text file. #CHROM = chromosome number, POS ID = variant starting base location, REF = reference allele, ALT = alternate allele, QUAL = call quality, AC_adj = adjusted allele count, AN_adj = adjusted allele captured, AC_Hom = homozygous alternate allele count, AC_NFE = allele count in Non-Finnish Europeans, AN_NFE = allele captured in Non-Finnish Europeans.

```
$ cut -f6- ExAC.r0.3_NFE_all_ANNOVAR.txt | cat Col_ID.txt - > ExAC.r0.3_NFE_all_counts.txt
$ paste <(tail -n +2 ExAC.r0.3_NFE_all_counts.txt | cut -f-8 -) <(tail -n +2
ExAC.r0.3_NFE_all_counts.txt | awk -F'\t' '{print substr($9,8), substr($10,8), substr($11,8),
substr($12,8), substr($13,8)}' OFS='\t' -) > ExAC.r0.3_NFE_all_counts_clean_noheader.txt; paste
<(cut -f-8 ExAC.r0.3_NFE_all_counts_clean_noheader.txt) <(cut -f9
ExAC.r0.3_NFE_all_counts_clean_noheader.txt | awk -F, '{for(i=1;i<=NF;i++) x+=$i; print x; x=0}' -)
<(cut -f10 ExAC.r0.3_NFE_all_counts_clean_noheader.txt) <(cut -f11
ExAC.r0.3_NFE_all_counts_clean_noheader.txt | awk -F, '{for(i=1;i<=NF;i++) x+=$i; print x; x=0}' -)
<(cut -f12 ExAC.r0.3_NFE_all_counts_clean_noheader.txt | awk -F, '{for(i=1;i<=NF;i++) x+=$i; print x;
```

```
x=0}' -) <(cut -f13 ExAC.r0.3_NFE_all_counts_clean_noheader.txt) | cat Col_ID.txt >
ExAC.r0.3_NFE_all_counts_summed.txt
$ perl table_annovar.pl ExAC.r0.3_NFE_all_noanno.txt humandb/ -buildver hg19 -out
ExAC.r0.3_NFE_all -otherinfo -remove -protocol
refGene,ljb26_sift,ljb26_pp2hvar,ljb26_gerp++,ljb26_phylop100way_vertebrate,esp6500siv2_ea,10
00g2014oct_eur,exac03,clinvar_20150330 -operation g,f,f,f,f,f,f,f,f -nastring .
```

Following annotation, the allele count information from the relevant ExAC controls was added to called variants.

```
$ cut -f-27 ExAC.r0.3_NFE_all.hg19_multianno.txt | paste - ExAC.r0.3_NFE_all_counts_summed.txt >
ExAC.r0.3_NFE_all.txt
```

Only exonic or splicing variants were included using the same filter in UNIX as the study cohort.

```
$ grep -v ^# ExAC.r0.3_NFE_all.txt | grep -v intronic | grep -v UTR3 | grep -v UTR5 | grep -v
intergenic | grep -v upstream | grep -v downstream | grep -v ncRNA_ | grep -v nonframeshift | grep
-v UNKNOWN >> ExAC.r0.3_NFE_all_exonic.txt
```

The same cut-off for minor allele frequency and predicted pathogenicity filters (SIFT <=0.05 orPolyPhen2 >=0.909) was applied.

```
$ awk -F'\t' '(($17 <= 0.001 && $18 <= 0.001 && $24 <= 0.001) || ($17 >= 0.999 && $18 >= 0.999 &&
$24 >= 0.999) || ($17 == "." && $18 >= 0.999 && $24 >= 0.999) || ($17 >= 0.999 && $18 == "." &&
$24 >= 0.999) || ($17 == "." && $18 == "." && $24 >= 0.999))' OFS='\t' ExAC.r0.3_NFE_all_exonic.txt
> ExAC.r0.3_NFE_all_maf0.001.txt
$ awk -F'\t' '(($9 ~ /^nonsyn/ && $11 <= 0.05 && $11 != ".") || ($9 ~ /^nonsyn/ && $13 >= 0.909) ||
($9 ~ /^nonsyn/ && $11 == "." && $13 == ".") || $9 ~ /^stop/ || $6 ~ /splicing/ || $9 ~
```

```
/^frameshift/)' OFS='\t' ExAC.r0.3_NFE_all_maf0.001.txt >
ExAC.r0.3_NFE_all_maf0.001_filter0.05.txt
```

As per the study cohort, the alternative canonical loss of function variants only (frameshifts, stop gains and splicing variants) filter was also applied.

```
$ awk -F'\t' '($9 ~ /^stopgain/ || $6 ~ /splicing/ || $9 ~ /^frameshift/)' OFS='\t'
ExAC.r0.3_NFE_all_maf0.001_filter0.05.txt > ExAC.r0.3_NFE_all_maf0.001_LoF.txt
```

A header file was constructed by joining the top row of annotated position file with the previously generated “Col_ID.txt”. The header was added to each output file by concatenation.

```
$ head -n 1 ExAC.r0.3_NFE_all.hg19_multianno.txt | cut -f-28 - | paste - Col_ID.txt >
ExAC.r0.3_NFE_all_header.txt
$ cat ExAC.r0.3_NFE_all_header.txt input.txt > output.txt
```

With all variants from the ExAC database filtered and annotated with the same criteria and categories as the experimental data, the gene mutation burden in ExAC could be calculated using a pivot table equivalent command in UNIX. Firstly the filtered annotated file was manipulated into the appropriate format and a pivot table header file (Pivot_header.txt) was made with the following headings: Gene.name, chr, AC_adj, AN_adj, HOM, AC_NFE, AN_NFE.

```
$ cut -f7 ExAC.r0.3_NFE_all_maf0.001_LoF.txt | sed 's/,/\t/g;s/(/\t/g;s/;/\t/g' - | cut -f1 - | paste -
ExAC.r0.3_NFE_all_maf0.001_LoF.txt > LoF_pivot_input.txt
$ awk 'BEGIN {FS=OFS="\t"} NR>1 {AC[$1]+=$37} {AN[$1]+=$38} {HOM[$1]+=$39} {NFEC[$1]+=$40}
{NFEN[$1]+=$41} {count[$1]+=1} {chr[$1]=$2} END {for (i in AC) {print
i,chr[i],AC[i],AN[i]/count[i],HOM[i],NFEC[i],NFEN[i]/count[i]}}' LoF_pivot_input.txt | sort - | cat
Pivot_header.txt - > LoF_pivot_output.txt
```

2.5.4 SKAT analysis

Sequence or SNP kernel association testing (SKAT) analysis performs association testing with weighted linear kernel function by measuring the genetic similarity among samples and controls (Wu et al., 2011). Traditional gene burden tests collapse all variants within a gene to produce one test statistic per gene. However, this makes the assumption that all variants within a gene are either protective or deleterious without the possibility of a combination thereof. SKAT does not collapse variants in a gene and therefore can detect both deleterious and protective variants improving its sensitivity. Overall, SKAT is reported to have higher power than gene collapsing burden testing while controlling for type I error (Tachmazidou et al., 2012).

SKAT requires four input files (.bed, .fam, .bim, .setID). The .bed, .fam, .bim files are binary coded files that could be generated in PLINK while simultaneously applying threshold for Hardy-Weinberg Equilibrium (HWE) and max internal minor allele frequency (MAF).

```
$ plink --max-maf 0.01 --hwe 0.05 --file filedirectory\Jointcall.SNVindel_maf0.001_LoF_nodup.noXY --make-bed --tab --out filedirectory\Jointcall.SNVindel_maf0.001_LoF_nodup.noXY
$ plink --keep filedirectory\Jointcall.SNVindel_maf0.001_LoF_nodup.noXY.list  --bfile filedirectory\Jointcall.SNVindel_maf0.001_LoF_nodup.noXY --make-bed --tab --out filedirectory\Jointcall.SNVindel_maf0.001_LoF_nodup.noXY
```

The .bim file was used to generate a variant coordinates file.

```
$ awk -F'\t' '{print "chr"$1,$4,$2}' OFS='\t' Jointcall.SNVindel_maf0.001_LoF_nodup.noXY.bim > Bim_LoF_coord.txt
```

Corresponding variants from the VCF annotation file matching the variants in the .bim file was selected for annotation at a later stage:

```
$ awk -F'\t' 'FILENAME=="Bim_LoF_coord.txt"{A[$1$2]=$1$2}
FILENAME=="LoF_nodup_anno.txt"{if(A[$28$29]){print}}' OFS='\t' Bim_LoF_coord.txt
LoF_maf0.001_nodup_anno.txt > Bim_LoF_hwe_intmaf01_anno.txt
```

Unlike the three binary files, the .setID file had to be manually created. The two columns of the .setID file was manually constructed using the following code which carried out the following functions. The gene column from the .bim file matched annotation file was selected as the SNP_set. The gene column was split based on ",", ";" and "(" delimiters. The gene column was cleaned up by only printing the gene name and removing the header. SNP_ID column from .bim coordinate file was appended to complete the .setID file for SKAT analysis.

```
$ cut -f7 Bim_LoF_hwe_intmaf01_anno.txt | sed 's/"//g;s/,/\t/g;s/(/\t/g;s/;/\t/g' - | cut -f1 - | paste -
Bim_LoF_coord.txt | cut -f1,4 - > Jointcall_SNVindel_noXY_maf001_LoF_hwe_intmaf01.setID
```

Using the four input files (.bed, .bim, .fam, .setID), SKAT generates two intermediate files that are used for final analysis (.ssd and .info). SKAT also applies Bonferroni multiple testing correction to the output p values.

```
library(SKAT)
Generate_SSD_SetID("Jointcall.AG.CTRL.AOGC_filter0.05_maf0.01.bed",
"Jointcall.AG.CTRL.AOGC_filter0.05_maf0.01.bim",
"Jointcall.AG.CTRL.AOGC_filter0.05_maf0.01.fam",
"Jointcall.AG.CTRL.AOGC_filter0.05_maf0.01.setID",
"Jointcall.AG.CTRL.AOGC_filter0.05_maf0.01.ssd",
"Jointcall.AG.CTRL.AOGC_filter0.05_maf0.01.info")
FAM<-Read_Plink_FAM("Jointcall.AG.CTRL.AOGC_filter0.05_maf0.01.fam", Is.binary=TRUE)
y<-FAM$Phenotype
```

```
SSD.INFO<-Open_SSD("Jointcall.AG.CTRL.AOGC_filter0.05_maf0.01.ssd",
"Jointcall.AG.CTRL.AOGC_filter0.05_maf0.01.info")
obj<-SKAT_Null_Model_MomentAdjust(y ~ 1, is_kurtosis_adj=TRUE)
out.SKATO.bin<-SKATBinary.SSD.All(SSD.INFO, obj, method="SKATO")
output.SKATO.bin.df = out.SKATO.bin$results
write.table(output.SKATO.bin.df, file="Output_SKATO_bin.txt", col.names=TRUE, row.names=FALSE)
Get_EffectiveNumberTest(out.SKATO.bin$results$MAP, alpha=0.05)
```

Within SKAT, there is the option to generate a QQ plot of the p values for all genes tested. This gives a graphical representation of genomic inflation factor λ.

```
QQPlot_Adj(out.SKATO.bin$results$P.value, out.SKATO.bin$results$MAP)
```

2.6 Results

The sequencing strategy utilized for ANZRAG cases (n = 187) and local controls (n = 103) in the current study yielded good read quality, coverage and depth. Mean percentage of mappable reads was high at 99.4% with an average total on-target reads per sample of 4.12×10^9 and an average depth of 73 reads per target base. Average coverage at greater than 10× depth was 97.9% of all targeted exonic regions. The average total number of coding SNPs and indels per participant was 19,605 and 465, respectively. This was similar to published exome data from 1000 Genome Project (Abecasis et al., 2012). AOGC controls (n = 993) had an average depth of 24 reads per target base and 10× coverage of 75.1%. After filtering for rare predicted pathogenic variants only, there was an average of 159 qualifying variants per participant.

QQ plot of all variants surviving the filter for predicted deleterious function and rare population minor allele frequency (MAF <0.1%) demonstrated that there was no population stratification of our dataset, which is concordant with the calculated genomic inflation of λ = 1.00 (Figure 4).

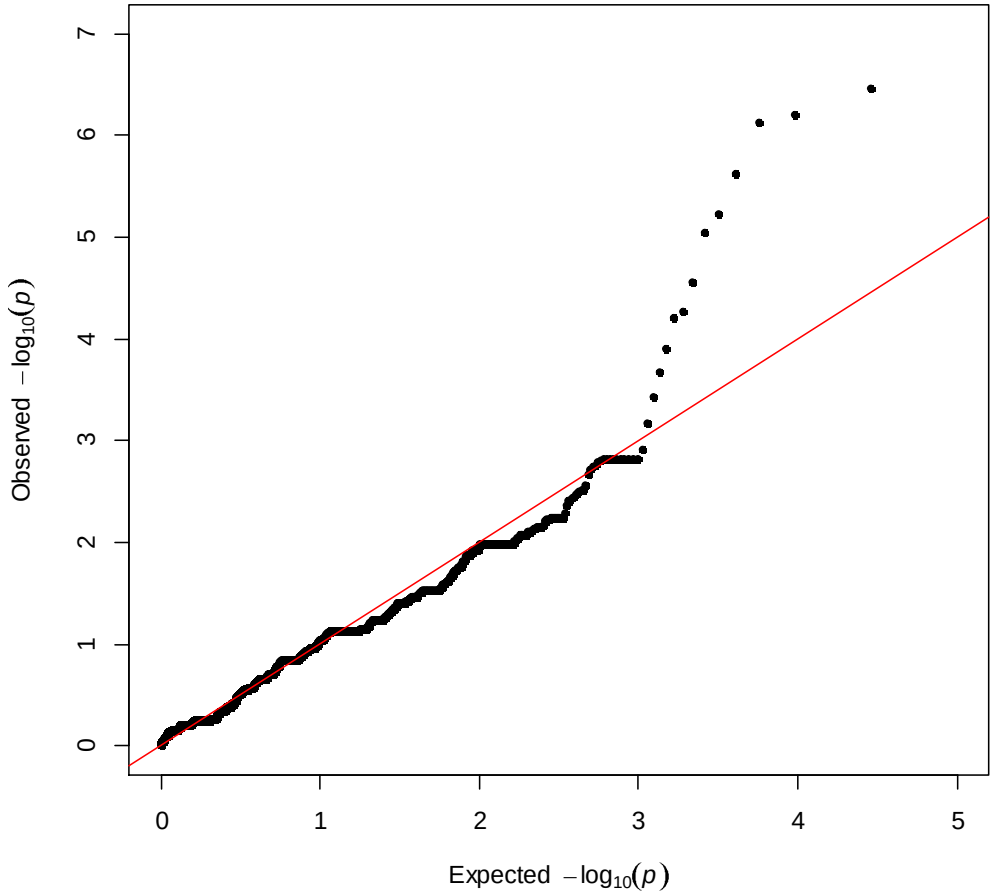

Figure 4: QQ plot of genes with variants that passed the filter of predicted pathogenic by SIFT or PolyPhen2 and having population minor allele frequency of less than 0.1% from whole exome sequencing.

The calculated multi-testing significance cut-off for whole exome analysis by SKAT was $p < 8.98 \times 10^{-6}$. The p-value of the top five candidates exceeded the statistical threshold (Table 1). However the control cohort harboured the same predicted pathogenic variants in all five candidates as the POAG cases. A true rare pathogenic variant is unlikely to be found in any of the 1096 joint-called controls. Furthermore, within a cohort of 187 POAG cases, it was unlikely that a single rare variant gene signal

would account for more than 10 participants or more than 5 per cent of the total cohort. Examination of the most promising signal within the top 10, *MTCH2*, by sanger sequencing via capillary electrophoresis (performed by IMVS Sequencing Facility, Flinders Medical Centre, South Australia) showed that the signal detected by WES was a technical sequencing artefact. Nine genes contained the most promising signals whereby three rare predicted pathogenic variants (1.6% frequency) were identified in the POAG cases and none were identified in the controls. The top candidate of the nine was neuroglobin (*NGB*), which has previously been identified as potential glaucoma candidate gene from rodent studies (Lechauve et al., 2013, Lechauve et al., 2014). All three *NGB* variants identified on WES were validated using sanger sequencing. Two of the three variants were predicted pathogenic variants in exon 2 (NM_021257, c. T163C, p.C55R and NM_021257, c.C173G, p.S58W) while the final variant involved the loss of the splice acceptor site for exon 3 (NM_021257, c.202-1G>C) resulting in the omission of the entire third exon from the final gene product. These three variants were extremely rare in public domain population database ExAC with allele frequencies of 8.49×10^{-5}, 4.78×10^{-5} and 6.4×10^{-6} for the C55R, S58W and exon 3 splice acceptor variants respectively.

Table 1: Top 30 hits from the SKAT analysis of whole exome sequencing using a predicted deleterious model with population minor allele frequency cut-off of 0.1%.

HGNC Gene name	Allele count in cases	Allele count in controls	P value
CDC27	10	3	3.49E-07
MUC16	110	385	6.32E-07
PABPC1	20	11	7.45E-07
OR4A16	24	22	2.40E-06
WDR89	11	7	5.84E-06
CTBP2	23	62	9.07E-06
MTCH2	6	1	2.81E-05
PRSS48	7	3	5.44E-05
HLA-DRB1	21	47	6.21E-05
TMEM82	11	10	0.000125058
APBB1	5	3	0.000213165
KIAA1468	10	13	0.000365625
ZNF717	18	34	0.000682476
FAM151A	5	5	0.001221755
NKTR	5	8	0.001507031
DDRGK1	3	0	0.001526977
GPBAR1	3	0	0.001526977
KCNH1	3	0	0.001526977
NGB	3	0	0.001526977
RFX6	3	0	0.001526977
SMIM3	3	0	0.001526977
TAS2R10	3	0	0.001526977
TMC4	3	0	0.001526977
ZBED2	3	0	0.001526977
OR2J2	4	1	0.001567584
DSCAML1	7	8	0.001616472
GXYLT1	18	27	0.001756603
TTC28	9	43	0.00179942
KIAA1614	5	3	0.001934783
ZDBF2	6	6	0.002169421

Neuroglobin (*NGB*) is a 151 amino acid globin protein that was discovered 20 years ago (Burmester et al., 2000). It is well conserved across species and archaic in evolutionary origin (Droge et al., 2012). Its expression is limited to some endocrine tissues and neural tissue in the brain and the eye (Brittain, 2012). The highest expression is in the retina and is approximately 100 times that of its expression in brain tissue (Schmidt et al., 2003).

Although its mechanism of action is debated, there is good *in vitro* (Sun et al., 2001, Schmidt-Kastner et al., 2006, Fordel et al., 2007) and *in vivo* (Li et al., 2006, Schmidt-Kastner et al., 2006, Greenberg et al., 2008, Li et al., 2010, Raida et al., 2013) evidence that upregulation of wildtype neuroglobin confers neuroprotection through increasing resistance to ischaemic injury. The response of *NGB* to hypoxia is dependent on cell type and degree of oxygen deprivation with the greatest upregulation achieved under the highest degree of hypoxia. In a 0% oxygen environment, primary cortical neuron cultures from Charles River CD1 mouse embryos after 16 hours of exposure showed maximum upregulation of approximately 250% in NGB expression (Sun et al., 2001). In 0.3% oxygen environment, *NGB* upregulation after 24 hours was around 210% and 150% in cultured mouse hippocampal neuronal cells (HN33) and rat adrenal pheochromacytoma cells (PC12) with neural characteristics, respectively (Schmidt-Kastner et al., 2006). The human neuroblastoma cell line SH-SY5Y is relatively resistant to hypoxia with 98% of cells remaining viable and minimal *NGB* expression change after 36 hours of anoxia (Fordel et al., 2007). However, after culture under combined oxygen and glucose deprivation for 32 hours, only 46% of cells remained viable with around 400% upregulation of NGB (Fordel et al., 2007).

In vivo, upregulation of wildtype neuroglobin secondary to injury has been shown in rat cortical neurons (Schmidt-Kastner et al., 2006, Li et al., 2006). Cerebral hypoxia has been induced experimentally by bilateral occlusion of common carotid arteries for 12.5 minutes or by keeping the

animals in hypoxic chambers. Occlusion induced transient ischaemia failed to produce any noticeable wildtype *NGB* overexpression in the non-transgenic rat model (Schmidt-Kastner et al., 2006). Sustained exposure to hypoxia at 10% oxygen concentration induced a 250% increase in NGB mRNA expression in the rat cortex after 3 days (Li et al., 2006). Whereas intermittent hypoxia alternating between 10% and room oxygen every 90 seconds managed to trigger a maximal upregulation of NGB of just 175% after 1 day, followed by no significant elevation of NGB from days 3 to 14 (Li et al., 2006). These findings may suggest that 12.5 minutes of neuronal ischaemia or intermittent hypoxia at 10% oxygen content may be insufficient to induce a maximal NGB injury response.

Experimental evidence in animal models implicates *NGB* in glaucoma pathogenesis. Within the retina, neuroglobin is localized abundantly to mitochondria-rich cells including the ganglion cell layer (Bentmann et al., 2005, Lechauve et al., 2012), which is the main tissue contributing disease phenotype in glaucoma. Studies in rodent models of glaucoma have demonstrated that overexpression of *NGB* prevents ganglion cell death induced by high intraocular pressure (Wei et al., 2011, Chan et al., 2012). Adeno-associated viral gene therapy with *NGB* protected ganglion cell loss in the harlequin rat model characterized by mitochondrial respiratory chain defect (Lechauve et al., 2014) and in DBA/2J mice that spontaneously develop glaucoma (Cwerman-Thibault et al., 2017). Conversely NGB knockdown caused retinal ganglion cell loss as occurs in glaucoma in otherwise normal rats (Lechauve et al., 2012).

2.6.1 Functional analysis of the top candidate - Neuroglobin

Given the statistical signal from exome sequencing and compelling results from previous functional studies of *NGB*, a functional study of the three *NGB* variants identified in our glaucoma cohort was performed with the aim of assessing their effect on human neuronal cell viability. The hypothesis

was that the three *NGB* variants (C55R, S58W and exon 3 splice site) produced polypeptides with reduced function compared to that of the wildtype *NGB*, thereby reducing cellular tolerance to oxidative stress. By inference, the increased susceptibility of retinal ganglion cells in the participants carrying these variants may have led to the pathogenesis of primary open-angle glaucoma.

2.6.2 Generation of wildtype and mutant constructs

2.6.3 Reverse transcription

Total RNA from cadaveric human retina was available in our laboratory for use in this study. The retina was obtained from deceased donor through the Eye Bank of South Australia following ethical approval by the SAC HREC, SA, Australia. From total RNA, genomic DNA was removed by treatment with recombinant RNase-free DNase (Invitrogen, California, USA). 6.8µg of human retinal RNA in 17µL was mixed with 1µL of rDNase I (Invitrogen, California, USA) and 2µL of 10X DNase I buffer and then incubated at 37°C for 30 minutes for degradation of gDNA and then the enzyme was inactivated with 2µL of DNase Inactivation Reagent (Invitrogen, California, USA) by incubating at room temperature for 2 minutes with regular mixing. After that the mixture was centrifuged at 10000g for 1.5 minutes and supernatant collected in a fresh tube. The concentration of RNA was measured with Nanodrop 2000 (Thermo Fisher, Massachusetts, USA).

For reverse transcription reaction, 1µg of DNase-free RNA was mixed with 1 µL of random hexamer primer (50µM) (Invitrogen, California, USA) and 1µL of dNTP (10mM) (Invitrogen, California, USA). The reaction volume was made up to 13µL with RNase free Milli-Q water. A second identical reaction was set up to be used as a reverse transcriptase negative control (RT-). The reagents were mixed by pipetting and the reaction mix incubated at 65°C for 5 minutes for denaturation of RNA. Immediately after that, the reaction mixtures were chilled on ice for 1 minute and then spun down by a brief centrifugation. While the RNA mixtures were incubating, two reverse transcription reaction mixtures

were prepared. Both mixtures contain 4µL of 5X 1st strand buffer (Invitrogen, California, USA), 1µL of 0.1M DTT (Invitrogen, California, USA) and 1µL of RNase inhibitor (Invitrogen, California, USA). 1µL of Superscript III reverse transcriptase (200U/µL) (Invitrogen, California, USA) was added to the reverse transcription reaction mixture while 1µL of water was added to the control reagent mixture to make 7µL of reaction mixtures. The reaction mixtures were added to each chilled RNA mixture to make two 20µL reactions and incubated at room temperature for 5 minutes. Both tubes were incubated at 50°C for 1 hour for cDNA synthesis before being inactivated at 70°C for 15 minutes. The resulting cDNA and RT- control were used for polymerase chain reaction (PCR).

2.6.4 Polymerase chain reaction for amplification of full length *NGB*

NGB specific primers were designed using Primer3 webtool (http://bioinfo.ut.ee/primer3-0.4.0/) for amplifying the *NGB* (NM_021257.3) cDNA; the primers flanked the coding region of the gene and introduced restriction enzyme sites (Table 2). DNA restriction enzymes which digest the vector plasmid (pcDNA 3.1 myc-His(-) A vector (Invitrogen, California, USA)) in the multiple cloning site at two sites but did not digest the *NGB* construct were selected using NEB cutter webtool (http://nc2.neb.com/NEBcutter2). The two restriction enzymes that best fulfilled the requirements were EcoRI-HF and BamHI-HF (NEB, Massachusetts, USA). The optimized reaction contained 10.9µL of MilliQ water, 2µL of 10X PCR buffer, 4µL of Q solution (QIAgen, Hilden, Germany), 0.5µL of dNTP (4mM) (Invitrogen, California, USA), 1µL each of forward and reverse primer (10µM), 0.5 µL of cDNA and 0.1µL Hot Star Taq DNA polymerase (5U/µL) (QIAgen, Hilden, Germany). PCR conditions were as follows: denaturation at 95°C for 15 minutes; 40 cycles of denaturation at 95°C for 30 seconds, annealing at 62°C for 30 seconds and extension at 72°C for 30 seconds with final extension phase at 72°C for 5 minutes. PCR products were analysed by gel electrophoresis on 1.0% agarose gel with ethidium bromide at 130V and 400mA for 30 minutes and showed a single band at approximately 450bp confirming the specificity of the PCR. 5µL of PCR product was cleaned by incubating with

0.5µL 20U/µL Exonuclease I (NEB, Massachusetts, USA) and 2µL of 1U/µL shrimp alkaline phosphatase (Invitrogen, California, USA) at 37°C for 60 minutes followed by inactivation at 80°C for 20 minutes. The exonuclease degrades the remaining primers, while the shrimp alkaline phosphatase dephosphorylated remaining dNTPs in the reaction mix to prevent ligation and thus remove sources of interference for sanger sequencing. Sanger sequencing by capillary electrophoresis with NGB_clone_F primer (by IMVS Sequencing Facility, Flinders Medical Centre, South Australia) was performed for validating specificity of the amplified cDNA. The PCR was repeated 5 times and the products cleaned with Wizard® PCR clean-up system (Promega, Wisconsin, USA) to generate sufficient cDNA for further experimentation.

Table 2: Primers used to amplify *NGB* from human retinal cDNA. Red highlighted sequence denotes the restriction site for EcoRI-HF. Blue highlighted sequence denotes the restriction site for BamHI-HF.

Primer	Sequence	Expected product size (bp)
NGB_clone_F	5'ATCGACTCAAGAATTCgacagcatggagcgcccggagcccga3'	453
NGB_clone_R	5'TACCGAGCTCGGATCCctcgccatcccagcctcgactcatg3'	

2.6.5 Site directed mutagenesis

Site directed mutagenesis was performed using custom designed primers to induce the mutations detected in cases by whole exome sequencing of the advanced glaucoma cohort (C55R, S58W and exon 3 deletion) in the amplified wildtype cDNA (Table 3). To generate each NGB mutant cDNA, two rounds of PCR were carried out. In the first round, cDNA was amplified in two overlapping fragments on either side of the mutation of interest as shown in Figure 5. The second round of PCR was

performed to produce full length cDNA product containing the desired mutation from the two fragments from the first round.

Table 3: Primers used for site directed mutagenesis. Red and underlined bases indicate the site of introduced mutation.

NGB site directed mutagenesis primers			
Primer	**Sequence**	**GC content**	**Melting temp**
	C55R		
NGB.C55R_F	5'ctccagcccagaggaccgtctctcct3'	65%	70°C
NGB.C55R_R	5'actcaggcgaggagagacggtcctct3'	62%	69°C
	S58W		
NGB.S58W_F	5'agaggactgtctctcctggcctgagt3'	58%	68°C
NGB.S58W_R	5'tccaggaactcaggccaggagagaca3'	58%	68°C
	Exon 3 splice acceptor		
NGB.ex3.del_F	5'accacatcaggaagacagtgggtgagtct3'	52%	68°C
NGB.ex3.del_R	5'agactcacccactgttcttcctgatgtggt3'	52%	68°C

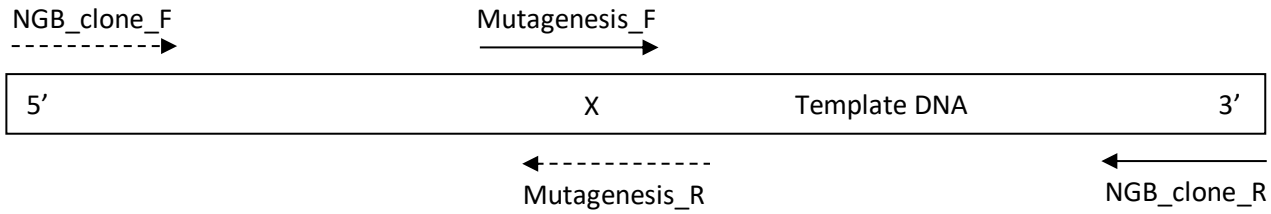

Figure 5: Schematic diagram showing the first stage polymerase chain reactions for site directed mutagenesis. X denotes the targeted base for mutagenesis. There were two PCRs in the first stage producing two fragments of the final construct; one on each side of the mutation of interest

represented by reactions between primers NGB_clone_F & Mutagenesis_R (dotted lines) and Mutagenesis_F & NGB_clone_R (solid lines).

For first round PCR, 6 reactions were optimized to produce the two overlapping fragments for each of the three mutant cDNA (Table 4). For this, each PCR reaction contained 13.4µL of Milli-Q water, 2µL of 10X PCR buffer, 0.5µL of 4mM dNTP mix, 1µL each of forward and reverse primers (10µM) (Table 3), 0.1µL of Hot Star Taq DNA polymerase and 50ng of template cDNA. The PCR conditions were as described above and the annealing temperature for each PCR was 62°C with amplification for 30 cycles. All PCR products from the 1st round PCRs were cleaned with Wizard® PCR clean-up system as per manufacturer's protocol and concentrations of cleaned products quantified with Nanodrop 2000.

Table 4: Primer combinations used for first round PCR for site directed mutagenesis. Product sizes and annealing temperature for each combination are indicated.

Primer pairs:	Product size (bp)	Optimal annealing temp.
NGB_clone_F & NGB.C55R_R	187	62°C
NGB.C55R_F & NGB_clone_R	307	62°C
NGB_clone_F & NGB.S58W_R	194	62°C
NGB.S58W_F & NGB_clone_R	298	62°C
NGB_clone_F & NGB.ex3.del_R	222	62°C
NGB.ex3.del_F & NGB_clone_R	146	62°C

The second round PCR amplified the full length cDNA using the two overlapping fragments carrying the same mutation from the first round PCRs as templates by using the outer primers NGB_clone_F and NGB_clone_R. Each reaction contained 9.4µL of Milli-Q water, 4µL of Q solution, 2µL of 10X PCR

buffer, 0.5µL of 4mM dNTP, 1µL each of NGB_clone_F and NGB_clone_R primers (10µM), 0.1µL Hot Star Taq DNA polymerase and 1µL each of the overlapping products from the first round of PCR. A concentration of 5ng/µL of template DNA was used for overlapping fragments carrying the C55R and S58W mutation, and 25ng/µL for those carrying exon 3 deletion. All 2nd round PCRs were performed at an annealing temperature of 62°C for 25 cycles. The final products were analysed by gel electrophoresis using 1% agarose gel and found to be of the predicted sizes.

2.6.6 Recombinant DNA cloning

Each NGB mutant cDNA and the wildtype NGB cDNA were independently cloned into the pcDNA 3.1myc-His(-) A vector (Invitrogen, California, USA) at EcoRI and BamHI restriction sites. For this, the vector and each cDNA (mutant and wildtype) were digested with EcoRI-HF and BamHI-HF (NEB, Massachusetts, USA) restriction enzymes. The digestion reactions of the inserts (cDNA) contained approximately 500ng of insert DNA, 2µL of 10X Cutsmart buffer (NEB, Massachusetts, USA), 1µL of 20000U/mL each of EcoRI-HF and BamHI-HF (NEB, Massachusetts, USA) and Milli-Q water in a final volume of 20µL. The digestion reactions of the vector were similarly set-up using approximately 2µg of pcDNA 3.1myc-His(-) A vector. All digestion reactions were incubated at 37°C for 1 hour. The digested vector DNA was treated with shrimp alkaline phosphatase (SAP) for dephosphorylation of the digested ends to prevent re-ligation. All digested insert and vector products were size separated on a 0.8% preparatory agarose gel using 1kb marker ladder (NEB, Massachusetts, USA); electrophoresis was performed at 80V for 120 minutes. The digested insert and vector bands were excised from the agarose gel under low energy UV light and cleaned with Wizard® PCR clean-up system as per manufacturer's protocol. The cleaned digested insert and vector DNA were used for cloning.

The mass of insert required for the ligation reaction was calculated as per the following formula.

$$Mass\ of\ insert = \frac{Insert\ to\ vector\ molar\ ratio \times Mass\ of\ vector \times Size\ of\ insert}{Size\ of\ vector}$$

$$= \frac{3 \times 100ng \times 0.45Kb}{5.5Kb}$$

$$\approx 25ng$$

A total of six ligation reactions were performed, one for each NGB mutant insert, wildtype NGB, vector without insert control and vector without DNA ligase control. Each test reaction contained 25ng of insert, 100ng of vector, 2µL of 10X ligase buffer (NEB, Massachusetts, USA), 1µL of 400U/µL T4 DNA ligase (NEB, Massachusetts, USA) and Milli-Q water in a total reaction volume of 20µL. Ligation was performed at 4°C for at least 16 hours.

All ligation reactions were transferred to clean 1.5mL Eppendorf tubes and 80µL of Milli-Q water added to each reaction. For precipitation of DNA 11µL of 3M pH5.2 sodium acetate, 2µL of glycogen carrier (Thermo Scientific, Massachusetts, USA) and 300µL of analytical grade ethanol was added to each reaction and tubes chilled at -80°C for at least 1 hour. All tubes were spun at >13,000g at 4°C for 15 minutes to pellet the DNA. The supernatant were removed and the pellets rinsed 3 times each with 1mL of 70% ethanol. Each DNA pellet was partially air-dried for 1 minute and resuspended in 10µL of Milli-Q water.

20µL of freshly thawed and chilled ElectroMAX DH5α-E E. Coli cells (Thermo Fisher, Massachusetts, USA) was added to chilled electroporation cuvettes (Bio-Rad Laboratories, California, USA) along with 2µL of the ligation mix. Electroporation was performed using the Biorad electroporator (Bio-Rad Laboratories, California, USA) set to the pre-set program Ec1 (V=1.8kV). Following electroporation, 500µL of SOC medium was added and the bacterial cells transferred to a clean Eppendorf tube. The

transformation mix was incubated at 37°C with shaking for 45 minutes. 165µL of 10X dilution of each transformation was plated on LB agar plates containing 100µg/mL of ampicillin and the plates incubated at 37°C for 16 hours to allow colony formation. Four colonies from each transformation were selected for culture in 2mL of LB medium containing 100µg/mL of ampicillin at 37°C for 16 hours.

From cultured bacterial colonies, plasmid DNA were extracted using QIAprep Spin Mini prep Kit (QIAgen, Hilden, Germany) as per the manufacturer's protocol. Briefly, 1.5mL of each culture was transferred to clean 1.5mL Eppendorf tubes and spun at >13000g for 2 minutes to pellet cells. The supernatants were removed by suction trap and the bacterial pellets resuspended in 100µL of P1 solution with vortexing at room temperature for 1-2 minutes. Following addition of 200µL of P2 solution, the tubes were gently inverted 2-3 times to allow contents to mix evenly and placed on ice for 5 minutes to allow cell lysis. 150µL of P3 solution was then added, and the tubes inverted gently twice to prevent shearing of bacterial chromosomal DNA. The tubes were spun for 10 minutes at >13000g to pellet bacterial chromosomal DNA. Approximately 420µL of the clear supernatant were transferred to clean Eppendorf tubes containing 900µL of analytical grade ethanol. The tubes were gently inverted for mixing and spun at >13000g for 10 mins to pellet the plasmid DNA. The pellets were washed 3 times with 70% ethanol and partially air-dried before resuspension in 20µL of Milli-Q water each.

For screening of positive clones, each ligated plasmid DNA was double digested with restriction enzymes that cut the pcDNA 3.1 myc-His(-) A vector on either side of the insert without cutting the insert itself. These digestion reactions contained 1µL of 10x NEB buffer 4 buffer (NEB, Massachusetts, USA), 0.1µL of 100X bovine serum albumin (NEB, Massachusetts, USA), 0.5µL of 20000U/mL Afl II (NEB, Massachusetts, USA), 0.5µL of 20000U/mL Xho I (NEB, Massachusetts, USA),

0.1µL of RNase cocktail (Invitrogen, California, USA), 1µL of plasmid DNA and 6.8µL of Milli-Q water in a total reaction volume of 10µL. All digestion reactions were incubated at 37°C for 90 minutes and then size separated on a 3-4µL of gel loading buffer 0.8% agarose gel at 80V for 120 minutes. The positive clones showed the presences of two bands, of approximately 5353bp and 614bp, the estimated sizes of the vector and insert, respectively, confirming the success of recombinant DNA cloning. The remaining plasmid DNA suspension were sent for sanger sequencing by capillary electrophoresis (IMVS Sequencing Facility, Flinders Medical Centre, SA) using T7 pcDNA3 forward primer and BGH reverse primer (Thermo Scientific, Massachusetts, USA) and confirmed the success of 2 out of 4 colonies for each NGB insert sequence. Glycerol stock of each positive clone was prepared in 30% glycerol and stored at -80°C. The positive colonies were cultured from their glycerol stock in 50mL LB medium with 100µg/mL of ampicillin with the plasmids extracted using HiSpeed Plasmid Midi Kit as per manufacturer's protocol, for transfection.

2.6.7 Differentiation of experimental human neurons

The SH-SY5Y human neuroblastoma cell line was selected for the transfection experiments. These cells are a robust source of human neuronal precursor cells and have been used extensively as a model for human neurons in the literature (Bell et al., 2013, Dwane et al., 2013, da Rocha et al., 2015). A frozen vial of SH-SY5Y cells (available in our laboratory) were thawed at 37°C and transferred to a tube containing 2mL of Dulbecco's Modified Eagle's Medium (DMEM) (Gibco, Thermo Scientific, Massachusetts, USA) containing 50% fetal bovine serum (FBS). The cells were incubated at room temperature for 15 minutes before pelleting of the cells by centrifugation at 200g for 5 minutes at room temperature. The cell pellet was washed twice with 2mL of fresh DMEM supplemented with 10% FBS and centrifuged as before. Then, the cells were resuspended in 5mL of, 45% Ham's F12 medium (Gibco, Thermo Scientific, Massachusetts, USA), 45% DMEM and 1:1000 GlutaMAX supplemented with 10% FBS (Gibco, Thermo Scientific, Massachusetts, USA) henceforth

referred to as culture medium. The cells were incubated to confluence in a T25 flask at 37°C in a humidified atmosphere with 5% CO_2 for 5 days and transferred to T75 flask. Prior to transfer, the cells were washed 3 times with 37°C phosphate buffered saline (PBS), and trypsinised with 0.05% trypsin for approximately 1 minute. 2 mL of culture medium was added to inactivate the trypsin. The cell suspection was homogenized and spun down at 200g for 5 minutes. The supernatant was removed and the cells were resuspended in 10mL of culture medium in a T75 flask and incubated at 37°C in a humidified atmosphere with 5% CO_2.

Differentiation of SH-SY5Y cells into human neuronal cells was facilitated with 9-cis retinoic acid (RA), which is a well-documented differentiation agent for this cell line (Bell et al., 2013, Dwane et al., 2013). Culturing conditions to stimulate optimal differentiation of SH-SY5Y was carried out by altering the concentration and duration of RA administration as well as the number of cells per well and coating the culture surface with laminin. All experiments were conduct in 6-well plates (Corning, Missouri, USA) with 2mL of culture medium per well. All cell cultures were incubated at 37°C in 5% CO_2 in a humidified environment with the culture medium replaced every two days. Morphological differentiation was assessed by examining differentiated cells by light microscopy. The cells differentiated with 10µM 9-cis retinoic acid and grown on laminin coated coverslips grew the longest dendrites in our experiments, in concordance with previous studies (Dwane et al., 2013, da Rocha et al., 2015) (Figure 6).

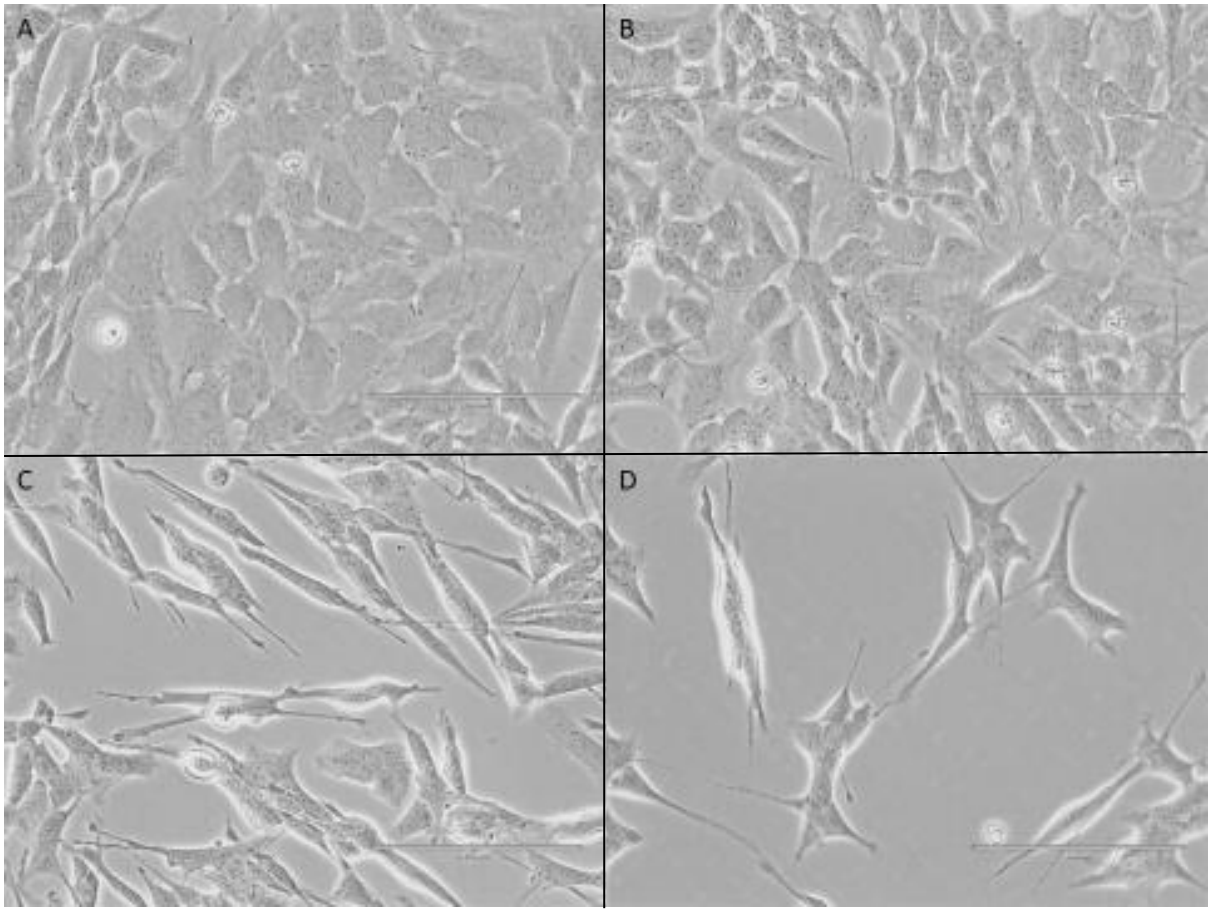

Figure 6: Differentiation of SHSY-5Y human neuroblastoma cells in culture. Light microscopy images of 40,000 cells cultured on: A) No coating, no retinoic acid; B) Laminin coating, no retinoic acid; C) No coating, 10µM retinoic acid; D) Laminin coating, 10µM retinoic acid, for 8 days. The cells in panle D are the most differentiated. All images are at 40X magnification.

Biochemical differentiation of cells grown in these conditions was assessed by the quantification of microtubule-associated protein 2 (MAP2) in the cell extract via western blotting to determine the optimal duration of differentiation. The protein extraction buffer used in our experiment was derived from a previous study (Bell et al., 2013) and was composed of 1mM pH 8 EDTA, 1mM pH 8 EGTA, 1.28mM sucrose, 2mM pH 7.6 Tris, 10% Triton X-100 and protease inhibitor cocktail (Promega, Wisconsin, USA). The culture medium was removed from each well prior to the addition of 200µL of protein extraction buffer. Contents of the wells were scraped into clean Eppendorf tubes

and pipetted to lyse cells. Cell debris was spun down at >13,000g at 4°C for 15 minutes and the supernatant containing the proteins was collected for western blotting. The protein concentrations were estimated using Pierce BCA protein assay kit (Thermo Scientific, Massachusetts, USA) as per manufacturer's protocol. The proteins in each extract were precipitated with 800µL of pre-chilled 100% acetone at -80°C for 16 hours. Each tube was then spun down at >13,000g for 15 minutes at 4°C to pellet the protein. The amount of protein used for western blotting was 11µg per sample as determined by the differentiation condition which produced the least amount of cells (10µM RA on laminin coating for 8 days).

A total of twelve experimental conditions were tested to find the optimal culture parameters (Figure 7). The conditions tested included seeding 40000 cells with no RA differentiation cultured on laminin coated and non-coated surfaces, 40000 seeding cells with 10µM RA differentiation on laminin coated and non-coated surfaces and 50000 seeding cells with 10µM RA differentiation on laminin coated and non-coated surfaces cultured for 8 and 14 days. Protein extracts from the twelve experimental conditions were size separated on an 18-well Biorad TGX stain-free precast gel (Biorad, California, USA) following reduction with 5µL of loading buffer containing 40µg/µL of dithiothreitol (DTT) per sample at 95°C for 2 minutes. The gels were ran at 300V for 30 minutes and transferred to Polyvinylidene difluoride (PVDF) membrane using the Trans-Blot® Turbo transfer system (Biorad, California, USA) for western blotting. The PVDF membrane was blocked with 1 X TBS with 5% skim milk protein and probed with 1:1000 anti-MAP2 antibody raised in mouse (catalog# M4403, Sigma-Aldrich, Missouri, USA) for 1 hour and then with 1:1000 anti-mouse antibody (catalog# 115-035-003, Jackson ImmunoResearch, Pennsylvania, USA) for 1 hour. The membrane was developed with ECL Pierce reagents A and B at 1:1 ratio for 3-4 minutes prior to imaging. The MAP2 protein was present in both day 8 and day 14 cultures. Given that cellular morphology appeared more optimal at the

shorter differentiation duration, optimal experimental differentiation time used was at around 1 week (Figure 8).

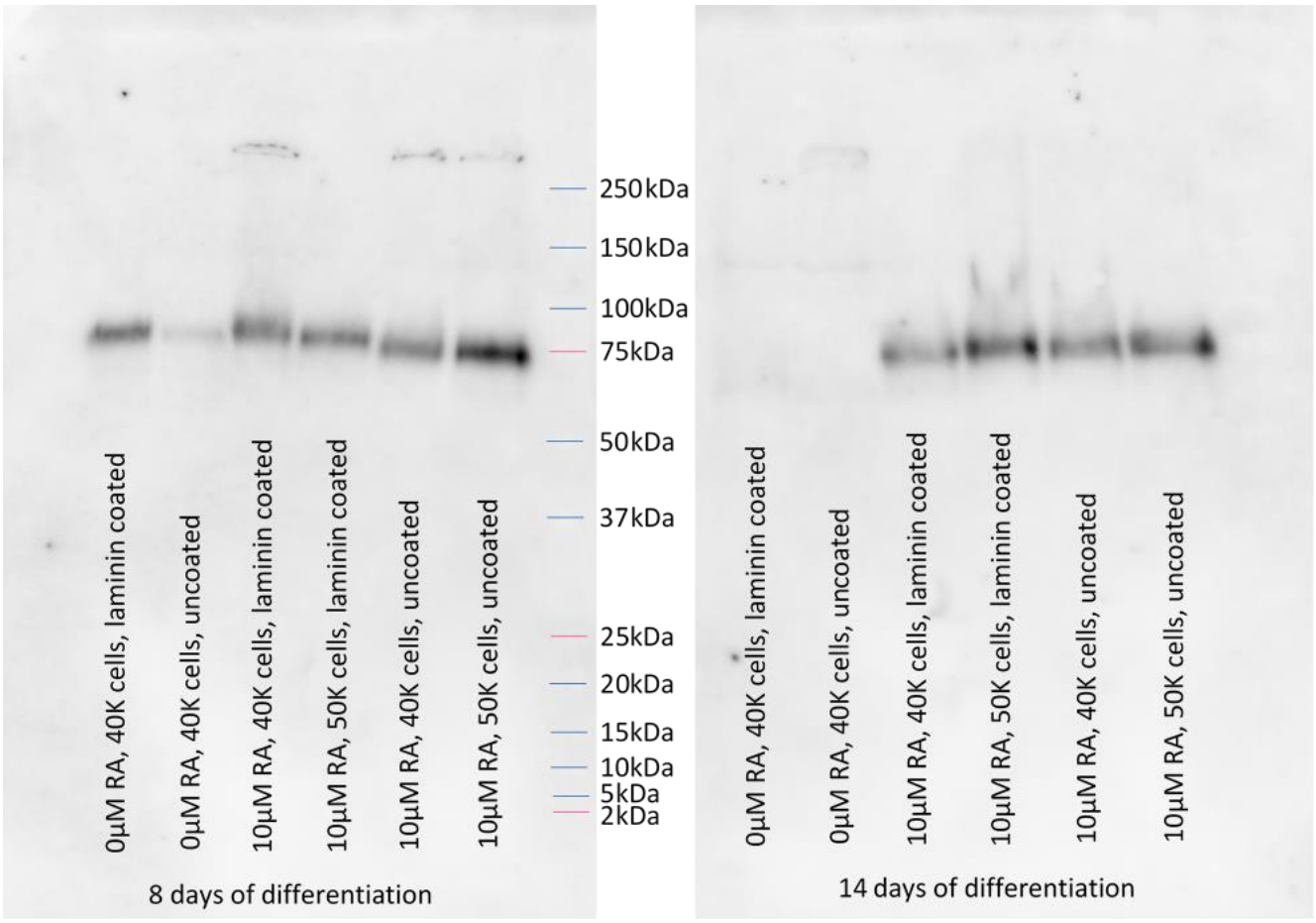

Figure 7: Western blot of protein extracts from SH-SY5Y differentiation optimization with retinoic acid (RA). The detected band is around 75kDA, which is the predicted size of MAP2 protein isoform C.

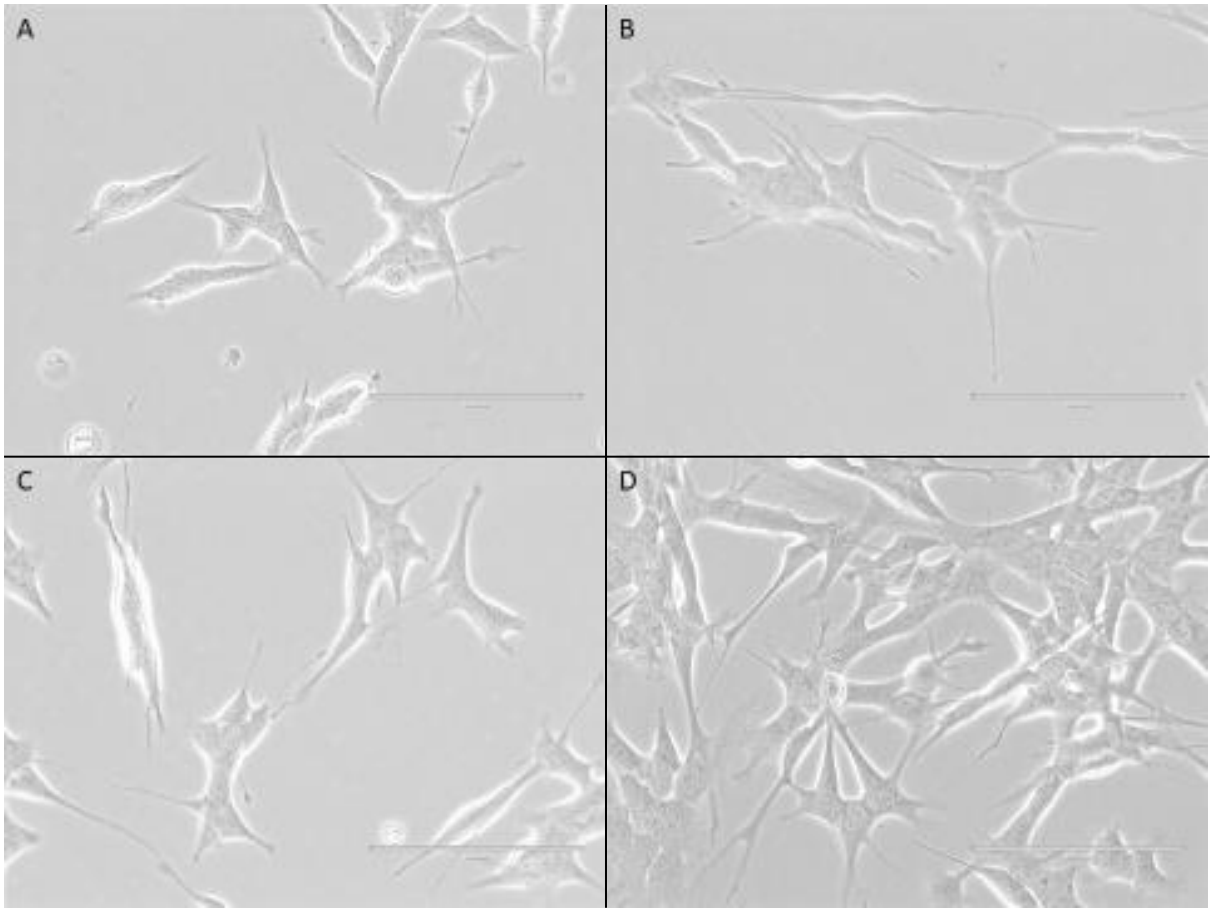

Figure 8: Differentiation of SHSY-5Y human neuroblastoma cells in culture. Light microscopy images of 40000 cells grown on laminin coated plates differentiated in 10µM retinoic acid for: A) 2 days; B) 6 days; C) 8 days; D) 14 days.

2.6.8 Transfection of NGB overexpressing plasmids

Transfection of NGB mutant plasmids was achieved using Lipofectamine 2000 (Invitrogen, California, USA). Transfection efficacy was determined using green fluorescent protein (GFP). Single transfection was only able to achieve approximately 22% transfection efficacy while double transfection achieved approximately 50% efficacy (Figure 9A & 9B). To account for the extra cell loss due to double transfection, a total of 160000 SH-SY5Y cells were seeded in 6-well. For all transfection experiments, cells were cultured in antibiotic free medium. On day 1, NGB mutants (C55R, S58W, exon 3 deletion), NGB wildtype and eGFP plasmid were independently transfected into

cells. 4µg of each plasmid DNA was diluted in Opti-MEM I (Gibco, Massachusetts, USA) in 250µL volume, in sterile Eppendorf tube, and incubated at room temperature for 5 minutes. 10µL of Lipofectamine 2000 was added to 240µL of Opti-MEM I for each transfection reaction (six in total) in a master mix and incubated at room temperature for 5 minutes. After incubation, 250µL of transfection master mix was added to the 250 µL diluted; the resulting 500µL of transfection mixture was incubated at room temperature for 20 minutes. Another 250µL of master mix was added to 250µL of Opti-MEM I and incubated at room temperature for 20 minutes as mock transfection control. The 500µL transfection mixtures were added dropwise to the culture well and cells incubated at 37°C in 5% CO_2 for 1 hour. Following that, the transfection medium was removed from cells and replaced with fresh culture medium. The transfection was repeated on day 2 of the experiment and culture medium supplemented with 10µM of RA was added to cells at the completion of the transfection. The cells were refed with culture medium containing 10µM RA on day 4, 6 and 8. On day 8, transfection efficacy of NGB constructs was confirmed with confocal microscopy following immunofluorescence labelling with rabbit anti-Myc tag antibody (71D10; Catalog# 2278, Cell Signalling) and fluorephore AlexaFluor488 conjugated goat anti-rabbit antibody (Catalog# A11034, Molecular Probes) (Figure 10).

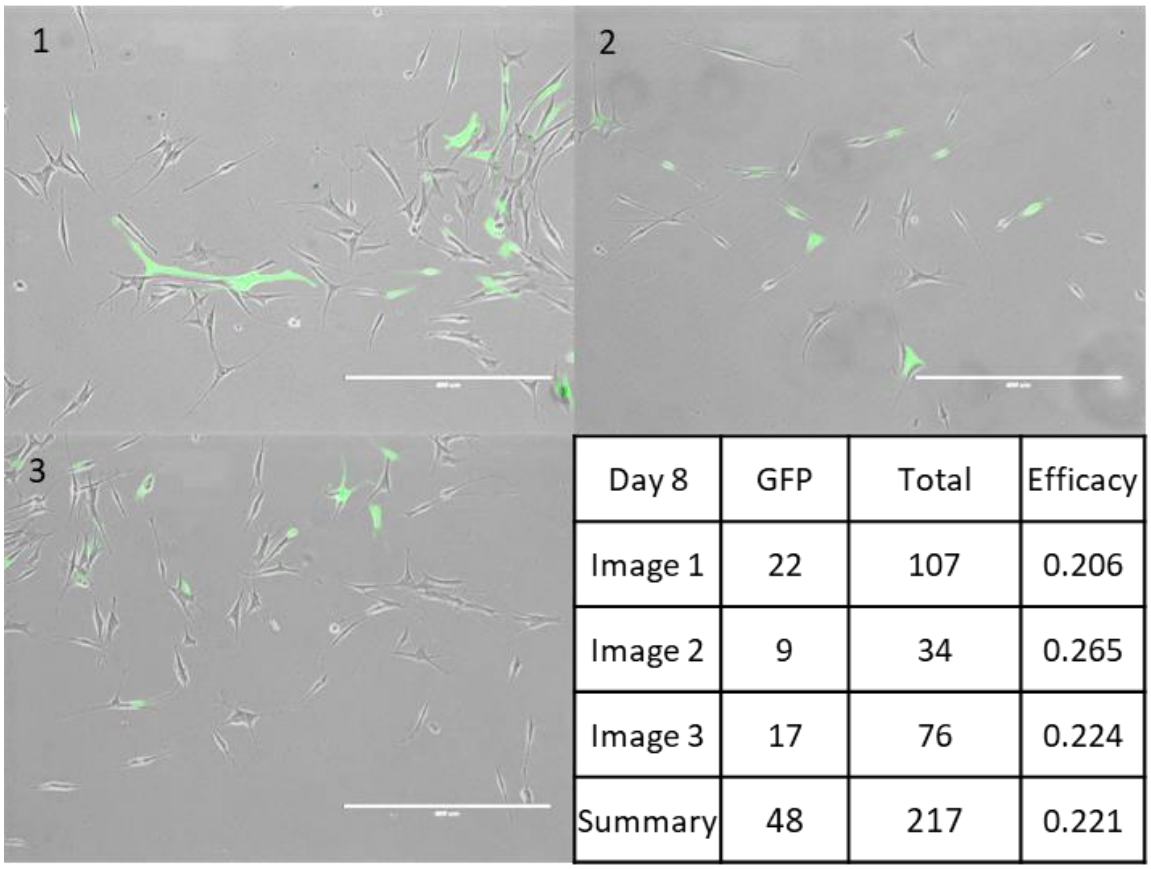

Day 8	GFP	Total	Efficacy
Image 1	22	107	0.206
Image 2	9	34	0.265
Image 3	17	76	0.224
Summary	48	217	0.221

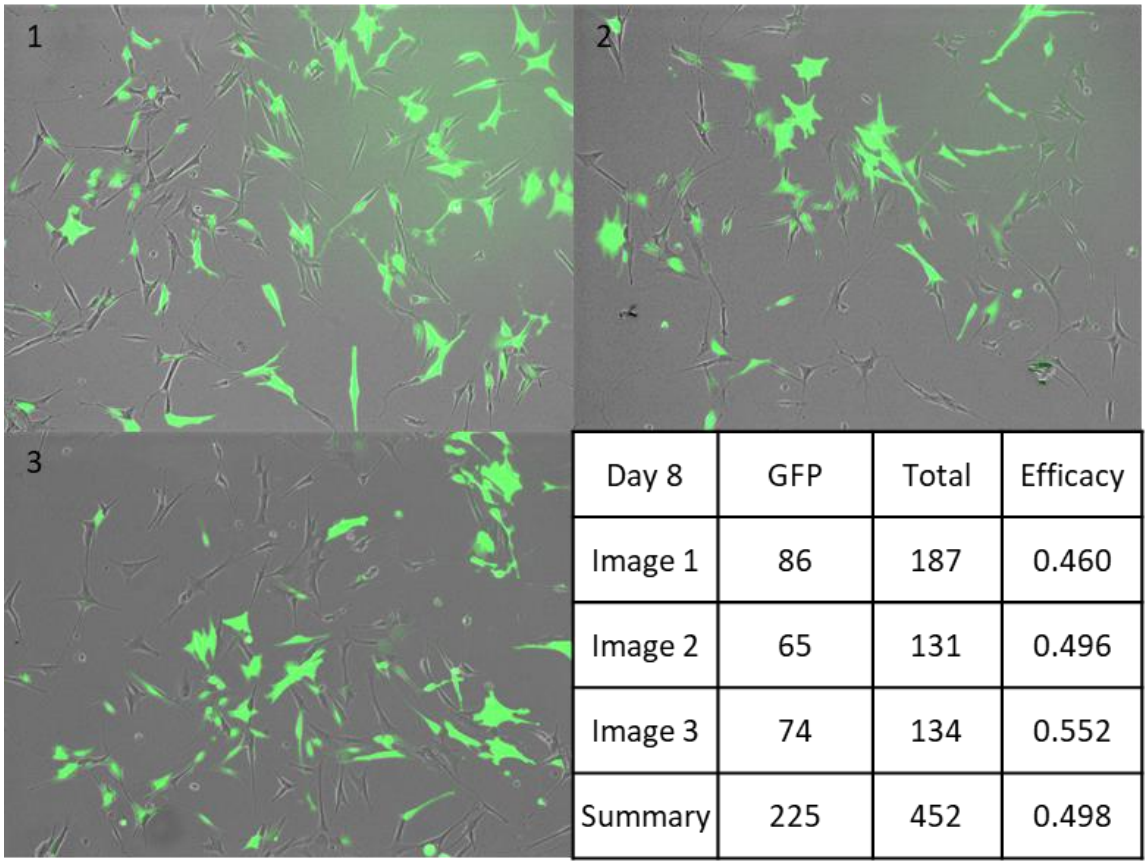

Day 8	GFP	Total	Efficacy
Image 1	86	187	0.460
Image 2	65	131	0.496
Image 3	74	134	0.552
Summary	225	452	0.498

Figure 9A& 9B: Single and double transfection of the GFP constructs in differentiated SH-SH5Y cells. All images are at 10X magnification.

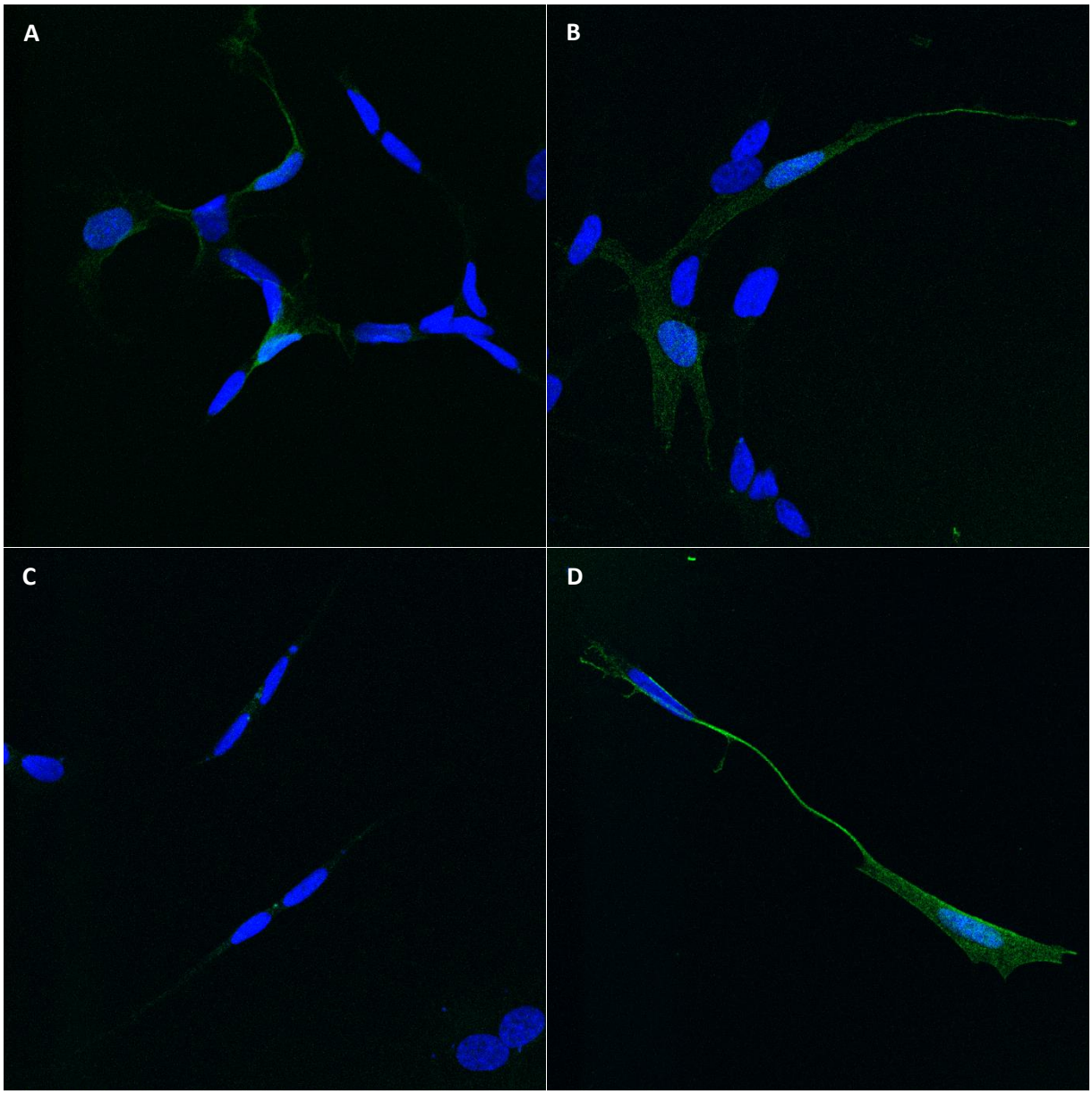

Figure 10: Confocal microscopy images showing immunofluorescence labelling of Myc-tagged transfected mutant or wildtype protein in (green) in differentiated SH-SY5Y cells. Cell nuclei were stained with DAPI (blue). Cells transfected with, A = *NGB* C55R, B = *NGB* S58W, C = *NGB* exon 3 deletion, and D = wildtype *NGB* constructs are shown. All images are at 40X magnification.

On the tenth day of the experiment, after 8 days of RA differentiation, H_2O_2 was added to the culture medium and the cells incubated at 37°C for 24 hours. H_2O_2 has been used in previous studies as a pro-apoptotic stressor in SH-SY5Y neuronal cells model (Jaworska-Feil et al., 2010, Suematsu et al.,

2011, Ramalingam and Kim, 2015, Mishra et al., 2017).The optimum concentration of H_2O_2 was 290µM as that was the highest tolerated concentration prior to total cell loss in SH-SY5Y cells . Following H_2O_2 stress test, cell viability of each well was tested using AQueous One solution cell proliferation assay (Promega, Wisconsin, USA). 400µL of AQueous One reagent was added to each well and incubated at 37°C in 5% CO_2 for 4 hours. 100µL of the media from each well was placed in triplicate in a 96-well plate with the absorbance measured on SpectraMax absorbance microplate reader (Molecular Devices, California, USA). The final cell viability testing was conducted in four replicates to account for biological variability.

No differences in mean absorbance was found between any mutant constructs, wildtype *NGB* and control SH-SY5Y cells (Figure 11). Differentiated SH-SY5Y cells without any transfected vectors were used as the transfection control and untransfected unstressed differentiated SH-SY5Y cells were used as positive control for cell viability. The viability assay control demonstrated significantly higher absorbance implying the greatest cell viability as per expectation due to the lack of H_2O_2 induced stress.

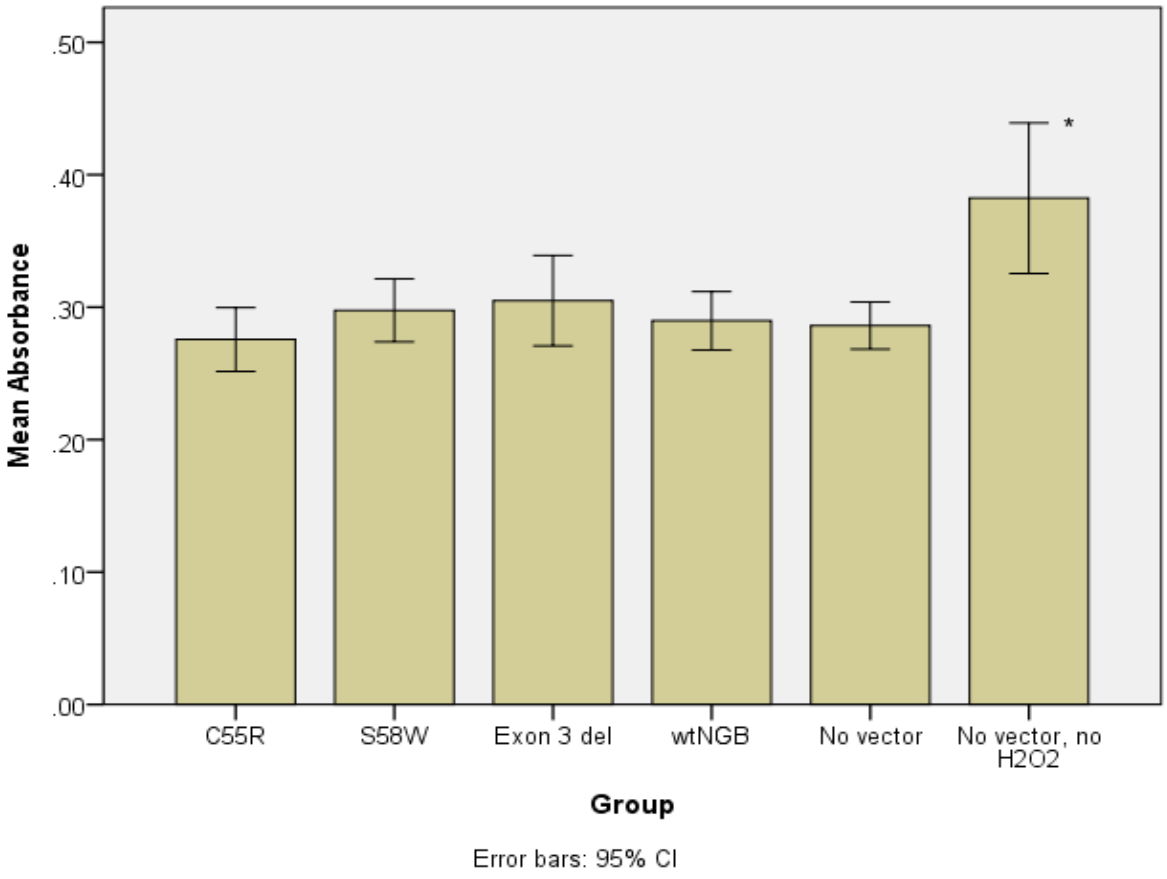

Figure 11: Cell viability of H2O2 stressed differentiated SH-SY5Y cells expressing mutant and wildtype NGB proteins. Mean absorbance values of all AQueous One cell viability assays performed using SH-SY5Y differentiated neurons with different vectors transfected. * denotes that the viability assay control demonstrated significantly higher absorbance value than all other test conditions.

2.7 Discussion

The primary hypothesis for this experiment was that wildtype *NGB* overexpression in neuronal differentiated SH-SY5Y cells would be protective against pro-apoptotic stresses. Secondly, the protein changing mutations identified in our advanced glaucoma cohort would negate the neuroprotective effects of wildtype *NGB*. There was insufficient evidence from the *NGB* overexpression experiment to support the hypothesis of NGB neuroprotection in this model.

Our cell transfection techniques were adapted from previous studies using SH-SY5Y as a human experimental neuronal cell model. We were able to demonstrate good morphological and biochemical neuronal differentiation of SH-SY5Y using retinoic acid as demonstrated by light microscopy and expression of the neuronal marker, MAP2. The transfection efficacy using a double transfection protocol was reasonably successful at around 50%. However the ability of this study to identify the effects of NGB on cell under H_2O_2 stress was limited by the significant loss of cells following transfection and stress with H_2O_2, only moderate transfection efficacy and potential heterogeneous expression in transfected cells.

If overexpression of mutant NGB is deleterious to cell survival, the results of our experiment should have demonstrated a reduction in the viability of cells transfected with mutant NGB. However if mutant NGB are not cytotoxic in any way, then no difference would be present between any of the experimentally transfected cells and controls. Therefore, the results of this study suggest that NGB mutation do not cause pathology via a dominant gain of function model. If NGB mutations were truly pathogenic, they are likely to act through a loss of function mechanism. In such a disease model, it is likely that when cells lose the normal neuroprotective function of wildtype NGB, they are more susceptible to oxidative cellular stresses.

One possible cause of the lack of difference between the transfected neuronal cells may have been the presence of normal endogenous NGB protein in SH-SY5Y cells. The outcome of our study showed that endogenous level of NGB in SY-SY5Y cells was insufficient to offset an oxidative stress from exposure to 290µM H_2O_2 for 24 hours *in vitro* as the mock transfected controls that were not exposed to H_2O_2 showed greater viability than the mock transfected controls exposed to H_2O_2.

Another experimental cause of the lack of difference in cell viability could be due to the cell stress model. Hydrogen peroxide exposure was the most robust and readily available oxidative stressor in our laboratory and has been utilized in previous studies as a pro-apoptotic stress in retinoic acid differentiated SH-SY5Y cells (Jaworska-Feil et al., 2010, Ramalingam and Kim, 2015). Through experimentation, the optimal H_2O_2 concentration was between 200 and 400µM. Incubation at 24 hours in 400µM of H_2O_2 caused complete cell death in all conditions. Therefore the final experimental H_2O_2 concentration was chosen at 290µM. However, as the H_2O_2 stressed cells did demonstrate reduced viability compared to the non-stressed controls, further optimization of the concentration of H_2O_2 would be unlikely to result in a difference in viability between the mutant and wildtype protein expressing cells. Other oxidative stress conditions that could be explored include hypoxia and or glucose deprivation stress conditions.

A previous study has already demonstrated that *NGB* knockdown causes retinal ganglion cell loss in a rat model (Lechauve et al., 2012). One way to test the pathogenicity of our NGB mutations would be to use NGB minus neuronal cells as a null expression control to eliminate the effect of endogenous NGB. Stable transfected cells will also be an improvement on the current transient expression cell model. Another method would change the native NGB from a neuronal cell line into our mutant NGB of interest using the CRISPR-Cas9 system, thereby eliminating potential issues associated with transient overexpression of supra-physiologic levels of NGB. Gene expression knockdown with small inhibitory RNAs would not be an appropriate model to test this hypothesis as they could also affect the overexpressed mutant NGB and mask any differences between the variants. Another loss of function model could involve using iPSC derived neuronal cells from participants with the NGB mutations and generating the controls using CRISPR-cas9 to change the mutant nucleotide back to the wildtype NGB. Both these methods would require significantly more time resources and are beyond the scope of this study.

Chapter 3: Contributions of known monogenic glaucoma genes to primary open-angle glaucoma

The contents of this chapter are published in the peer-reviewed journal Investigative Ophthalmology and Visual Science (Zhou et al., 2017b). Autosomal dominant mode of inheritance is present in a proportion of individuals with POAG. Estimates place the percentage of Mendelian inherited POAG explained by known causative genes at around 5% (Fingert, 2011). The Online Mendelian Inheritance in Man (OMIM) database (www.omim.org - accessed on 17/10/2016) documents seven genes (*MYOC* - *601652, *OPTN* - *602432, *CYP1B1* - *601771, *WDR36* - *609669, *ASB10* - *615054, *NTF4* - *162662 and *TBK1* - *604834) with potentially disease-causing variants in POAG and two (*CYP1B1*- *601771 and *LTBP2* - *602091) in PCG. Additionally, the GLC1C locus has since been linked to the gene *IL20RB* (Interleukin 20 Receptor Subunit Beta) via Sanger sequencing (Keller et al., 2014). Myocilin is the only known Mendelian disease gene with common variants that are significantly associated with POAG (Ramdas et al., 2011b). However, independently or combined with *MYOC* variants, optineurin and *WDR36* failed to show any significant enrichment of common variants in POAG (Ramdas et al., 2011b).

Family-based linkage studies on large affected pedigrees have revealed a number of genes linked to POAG with Mendelian inheritance. Only three genes (*MYOC*, *OPTN*, *CYP1B1*) with disease-causing single nucleotide variants (SNV) and one with copy number variants (*TBK1*) have been unequivocally replicated in discrete glaucoma cohorts. The first and the most prevalent gene discovered in familial POAG is myocilin (*MYOC*) (Sheffield et al., 1993, Stone et al., 1997). The prevalence of heterozygous *MYOC* disease-causing variants is around 4% in Caucasian POAG populations overall (Sheffield et al., 1993, Souzeau et al., 2013). It accounts for a greater proportion in the juvenile-onset POAG (JOAG) subset, with a prevalence of 17% in Australia (Souzeau et al., 2013) and up to 36% in the USA (Shimizu et al., 2000). Disease-causing variants are predominantly located within the third exon and

are likely a result of founder effects within European Caucasian populations (Faucher et al., 2002, Baird et al., 2003, Hewitt et al., 2007). The *MYOC* glaucoma phenotype is characterized by a young age of onset with high IOP (Shimizu et al., 2000, Souzeau et al., 2013). Optineurin (*OPTN*) was the second gene to be linked to Mendelian POAG (Rezaie et al., 2002). In contrast to *MYOC*, disease-causing *OPTN* variants impart a glaucoma phenotype with normal IOP and are rarer, with percentages ranging from 1.5% to 3.5% of the NTG population (Alward et al., 2003, Hauser et al., 2006b). In multiple study cohorts only the heterozygous p.Glu50Lys variant in *OPTN* has been definitively proven to be disease-causing (Rezaie et al., 2002, Alward et al., 2003, Hauser et al., 2006b, Ayala-Lugo et al., 2007) via a gain-of-function mechanism, thereby explaining the low frequency and lack of variant diversity seen in *OPTN*-related glaucoma. Both *MYOC* and *OPTN* variants are transmitted in an autosomal dominant manner. *TBK1* (TANK-binding kinase 1) has been linked to POAG in the form of autosomal dominant copy number duplication or triplication, with replication in multiple Caucasian POAG cohorts (Fingert et al., 2011, Awadalla et al., 2015). However, the incidence of *TBK1* copy number variant in glaucoma is very rare, accounting for only 0.8% (10 out of 1222 NTG cases) of individuals with NTG in Caucasian and Asian populations (Fingert et al., 2011, Kawase et al., 2012, Minegishi et al., 2013, Ritch et al., 2014, Awadalla et al., 2015, Kaurani et al., 2016). *CYP1B1* (cytochrome P450, family 1, subfamily B, polypeptide 1) disease-causing variants have been linked to both PCG and juvenile-onset POAG (Sarfarazi et al., 1995, Melki et al., 2004, Souzeau et al., 2015). Biallelic *CYP1B1* variants transmitted in an autosomal recessive manner are involved in PCG whereas both biallelic and heterozygous variants have been involved in POAG with a lower frequency rate. Deleterious *CYP1B1* variant frequency is highly variable between ethnicities: prevalence rates of *CYP1B1* variants have been reported as 4.6% in a French POAG case cohort (Melki et al., 2004), 4.62% in a Taiwanese Chinese JOAG case cohort (Su et al., 2012), 6.8% in an Australian JOAG case cohort (Souzeau et al., 2015), and 11.1% in an Iranian POAG case cohort (Suri et al., 2008). Like *CYP1B1*, variants in *LTBP2* (latent transforming growth factor beta binding protein

2) transmitted in an autosomal recessive manner were originally linked to PCG (Firasat et al., 2008a, Ali et al., 2009), with heterozygous variants later suggested in POAG (Jelodari-Mamaghani et al., 2013). Other genes linked to POAG but with less certainty include *ASB10*, *NTF4,* and *WDR36* (Wirtz et al., 1999, Monemi et al., 2005, Pasutto et al., 2009). *ASB10* (ankyrin repeat and SOCS box containing 10) and *WDR36* (WD repeat domain 36) have shown variability in their replication with subsequent studies reporting no statistically significant difference in the frequency of potentially pathogenic variants between POAG cases and controls within cohorts of similar ethnicities (Hauser et al., 2006a, Hewitt et al., 2006b, Fingert et al., 2007, Fingert et al., 2012). Heterozygous variants in *NTF4* (neurotrophin 4) have been suggested to be a rare cause of POAG, ranging from 0.3% in Chinese cohorts (Chen et al., 2012) to 2.26% in German cohorts (Pasutto et al., 2009), but were not associated with POAG in the USA (Liu et al., 2010) and Indian cohorts (Rao et al., 2010).

This analysis used whole exome sequencing (WES) to examine the disease burden of the nine known monogenic Mendelian POAG genes in a cohort of participants with the most severe glaucoma from a population based database - the Australian and New Zealand Registry of Advanced Glaucoma (ANZRAG) in order to highlight the relative disease burden of each of the known monogenic Mendelian POAG causing genes

3.1 Methods

3.1.1 Participants

The individuals comprising the study cohort were Caucasian participants from the ANZRAG database, which were collected in a prospective unselected manner and previously analyzed for common disease-associated variants in genome-wide association studies (GWAS) (Burdon et al., 2011, Gharahkhani et al., 2014, Hysi et al., 2014, Springelkamp et al., 2015). Participants with advanced glaucoma and the youngest age at diagnosis but older than 18 years of age were included in this

study. Participants with this study were selected from the ANZRAG database with inclusion criteria previously stated in the participant recruitment section chapter 2. Participants with HTG or NTG were included. HTG was defined as having a maximum recorded untreated IOP of greater than 21 mmHg. Individuals with secondary glaucoma were excluded from this study. Individuals with disease-causing *MYOC* variants detected on capillary sequencing were not analyzed by whole exome sequencing (Souzeau et al., 2013) (Appendix Table 1), but were included for analysis to enable relative proportions of POAG cases potentially explained by each individual gene to be assessed.

All local control participants were interviewed to exclude a family history of glaucoma and further examined to exclude glaucoma or phenotypic traits including cupping of the optic disc, deficit on Humphrey visual field testing and elevation of IOP that could be related to glaucoma. A total of 150 HTG, 68 NTG, 103 examined controls and 993 unexamined controls were analysed. A larger unexamined control cohort from the Australian Osteoporosis Genetics Consortium (AOGC) (Estrada et al., 2012) was included for *in-silico* analysis as outlined in Chapter 2.

3.1.2 Data analysis

Sequencing protocol was previously detailed in the whole exome sequencing section in chapter 2, but will be briefly summarized herein. DNA were prepared with SureSelect Human All Exon V4 enrichment kit (Agilent, Santa Clara, USA) as per manufacturer's protocol for whole exome capture and sequenced on a HiSeq2000 (Illumina, San Diego, USA) with 100bp paired end reads (Macrogen Next Generation Sequencing Services). Experimental data was joint-called with previously sequenced AOGC exomes, sequenced on the HiSeq2000 (Illumina),and annotated using ANNOVAR (Wang et al., 2010b).

Whole exomes from all glaucoma cases not carrying pathogenic *MYOC* variants (n = 189) and controls (n = 1096) were analysed concurrently. Only protein coding exonic and splicing site variants were selected for analysis following filtering with in house UNIX codes. The quality control threshold was set at a Genotype Quality (GQ) score of 20. In order to include only potentially disease-causing variants, all variants with a minor allele frequency (MAF) of greater than 0.01 in dbSNP, NHLBI GO Exome Sequencing Project (ESP), 1000 Genomes Project and ExAC were excluded. Pathogenicity filtering further removed all synonymous variants, and missense variants considered "tolerated" or "possibly damaging" by both SIFT and PolyPhen2 HVAR, respectively. The qualifying variants for analysis consisted of all protein-truncating variants in the canonical gene transcript, including nonsense, frameshift and essential splice site variants, as well as missense variants predicted to be deleterious by either SIFT or PolyPhen2 HVAR. Variants in nine monogenic POAG causing genes: *ASB10*, *CYP1B1*, *IL20RB*, *LTBP2*, *MYOC*, *NTF4*, *OPTN*, *TBK1* and *WDR36,* were selected. Of these genes, *LTBP2* has been linked to PCG, *CYP1B1* to both PCG and POAG, and the rest to POAG only. Variant loads per gene were calculated for the glaucoma case and control cohorts by summing the minor allele counts of all qualifying variants in the same gene and dividing by the average number of captured alleles for those variants to adjust for capture rate. Odds ratios were generated by comparing the glaucoma variant load with the control using Fisher's exact test to calculate *p*-values. Individual gene sequence validation by Sanger sequencing was not performed for this analysis due to the high quality scores and depth of coverage of all identified variants.

3.2 Results

This study included 218 participants with advanced POAG from the ANZRAG and 1096 controls (103 without clinical features of glaucoma and 993 unexamined Australian controls). There were 150 HTG and 68 NTG participants. The mean maximum recorded IOPs of each group were 32.9 ± 8.9 mmHg and 18.1 ± 2.9 mmHg, respectively. The mean age at diagnosis for the POAG cohort was 44.4 ± 10.4

years. Twenty-six HTG participants and 3 NTG participants were found to carry *MYOC* disease-causing variants upon capillary sequencing and were excluded from WES. WES was performed on the remaining 189 cases and 103 examined controls. The mean percentage of mappable reads was 99.4%, with an average total of 4.12×10^{9} on-target reads per sample, and an average depth of 73 reads per target base. Coverage of at least 10-fold was achieved at an average of 97.9% of all targeted exonic regions. AOGC controls had an average depth of 24 reads per target base and ≥10-fold coverage of 75.1%.

Qualifying variants in known primary glaucoma genes (all nine genes) were identified in 58 cases (58/218, 26.6%) and 128 controls (128/1096, 11.7%) generating an odds ratio of 2.74 (1.93 - 3.90, p = 1.01×10^{-7}) (Appendix Table 2 shows all variants found in glaucoma cases). Only one participant with POAG carried qualifying variants in more than one gene with qualifying variants both in *CYP1B1* and *WDR36*. Variants (heterozygous) for *MYOC* accounted for most carriers of qualifying variants in all the nine genes (26 or 17.3% of HTG, 3 or 4.4% of NTG, 29 or 13.3% of all POAG); and demonstrated significant enrichment within the POAG cohort (OR = 16.62, Fisher's p = 6.31×10^{-16}) (Table 5). All other genes except *TBK1* and *WDR36* exhibited nominal enrichment in POAG; however, the difference was not statistically significant (Table 5). No *TBK1* SNV or indels were detected in the POAG cohort and only one SNV was detected in 1096 controls.

Table 5: Numbers and percentages of POAG cases or controls carrying one or more qualifying variants in nine monogenic POAG genes. The data from 218 cases and 1096 controls is presented. Odds ratios are calculated using POAG case vs all controls with Fisher's exact test for *p*-value. POAG = primary open-angle glaucoma, HTG = high-tension glaucoma, NTG = normal-tension glaucoma, Ctrl = control, OR = odds ratio, CI = confidence interval.

Gene	Number of individuals (%)				OR (95% CI)			*p*-value
	POAG	HTG	NTG	Ctrl	POAG	HTG	NTG	POAG
ASB10	4 (1.83)	1 (0.67)	3 (4.41)	7 (0.72)	2.59 (0.75-8.93)	0.93 (0.11-7.62)	6.4 (1.62-25.33)	0.124
IL20RB	1 (0.46)	1 (0.67)	0	0	NA	NA	NA	0.120
CYP1B1	6 (2.75)	4 (2.67)	2 (2.94)	18 (2.00)	1.39 (0.54-3.53)	1.34 (0.45-4.02)	1.48 (0.34-6.53)	0.142
LTBP2	6 (2.75)	4 (2.67)	2 (2.94)	14 (1.29)	2.17 (0.82-5.71)	2.1 (0.68-6.47)	2.32 (0.52-10.43)	0.069
MYOC	29 (13.30)	26 (17.33)	3 (4.41)	10 (0.91)	16.62 (7.97-34.67)	22.72 (10.7-48.22)	5 (1.34-18.61)	**6.31×10^{-16}**
NTF4	3 (1.38)	3 (2.00)	0	11 (1.13)	1.22 (0.34-4.39)	1.78 (0.49-6.45)	NA	0.731
OPTN	1 (0.46)	0	1 (1.47)	1 (0.09)	5.04 (0.31-80.91)	NA	16.33 (1.01-263.94)	0.305
TBK1	0	0	0	1 (0.09)	NA	NA	NA	1
WDR36	8 (3.67)	6 (4.00)	2 (2.94)	75 (6.86)	0.52 (0.25-1.09)	0.57 (0.24-1.32)	0.41 (0.1-1.71)	0.098

PCG caused by mutations in both *CYP1B1* and *LTBP2* genes has an autosomal recessive pattern of disease inheritance, although both heterozygous and compound heterozygous variants have previously been reported in POAG cohorts (Jelodari-Mamaghani et al., 2013, Souzeau et al., 2015). Four cases carried two qualifying variants each in these genes. One participant was compound heterozygous and two were homozygous for *CYP1B1* qualifying variants. Another participant was compound heterozygous for *LTBP2* qualifying variants. Another three and five participants were heterozygotes for qualifying variants in *CYP1B1* and *LTBP2*, respectively. No control was homozygous or compound heterozygous for qualifying variants in *CYP1B1* (Fisher's p = 0.0047) or *LTBP2* (Fisher's p = 0.17). Carrier rates for *CYP1B1* and *LTBP2* in the control cohort are shown in Table 5.

WDR36 was the only gene to harbour more qualifying variants in the control cohort than in cases (OR = 0.52, 0.25-1.09). For the remaining eight monogenic POAG genes, a total of 50 POAG cases (22.9%) carried qualifying variants. The carrier rate for qualifying variants in each gene excluding *WDR36* and *TBK1* in cases versus controls is shown in Figure 12. With *WDR36* excluded, no cases carried qualifying variants in multiple monogenic POAG genes. The proportion of cases carrying qualifying variants in each monogenic POAG gene is presented in Figure 13.

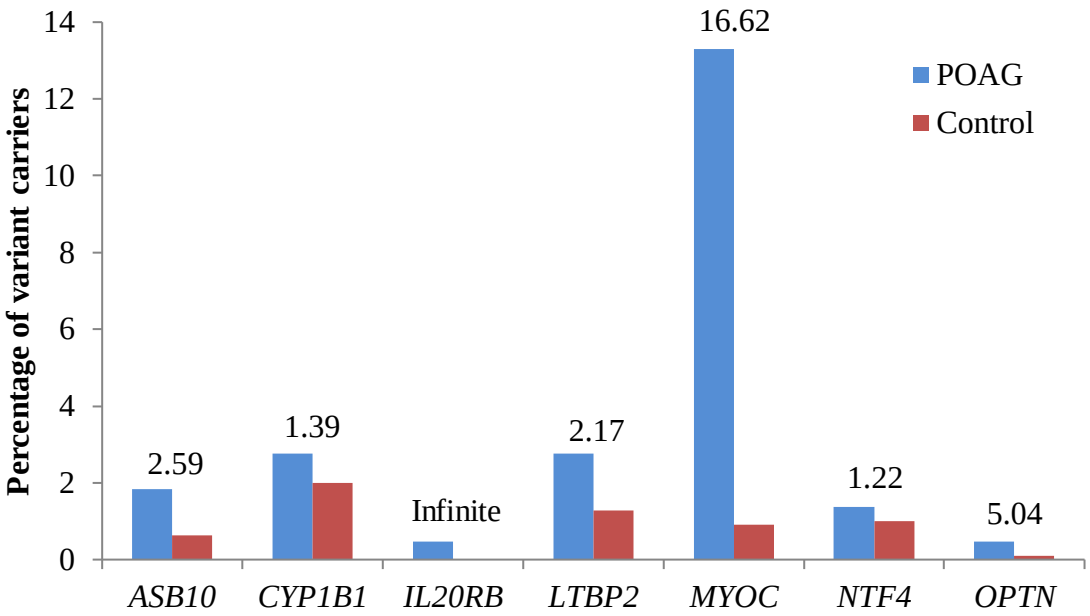

Figure 12: Carrier percentages of one or more qualifying variants in known glaucoma genes. The odds ratios of POAG cases versus controls are shown above each column pair.

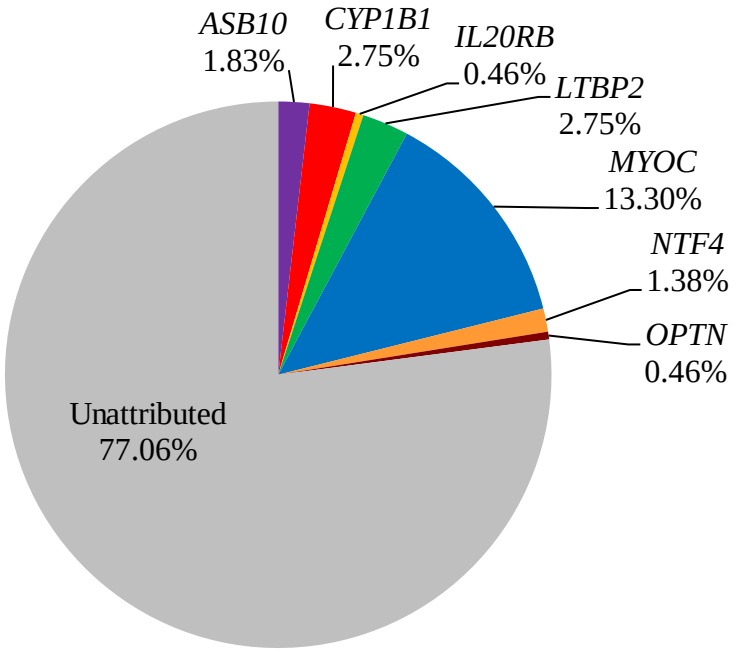

Figure 13: Comparative percentages of advanced POAG cases with one or more qualifying variants in monogenic glaucoma genes.

3.3 Discussion

This part of the study explored the genetic contribution of the nine known primary glaucoma genes in 218 Caucasian POAG participants from the ANZRAG with advanced disease and young age at diagnosis. We examined odds ratios associated with each gene to determine their relative contributions to POAG cases and controls. Our results highlight the overwhelming influence of *MYOC* amongst the known monogenic Mendelian POAG genes, but emphasize that the majority of POAG cases are not accounted for by mutations in the known monogenic glaucoma genes. These unexplained cases are likely to be accounted for by a combination of common GWAS alleles, rare variants in glaucoma risk genes, non-coding variants not found by WES, copy number variations and large structural variations that are difficult to detect by WES.

The proportions of our POAG cases explained by individual genes were largely in accord with previous publications, despite differences in cohorts, sequencing methods and qualifying variant definitions. The prevalence of *MYOC* disease-causing variants in advanced juvenile-onset POAG (JOAG) patients was reported to be 17% in our previous study (Souzeau et al., 2013) with an age at diagnosis cut-off of 40 years. The current study includes all *MYOC* JOAG participants (age at diagnosis less than 40 years) from our previous study as well as more recently identified *MYOC* participants up to 55 years old at diagnosis. In another study where the inclusion criteria for age at diagnosis was even younger, at 35 years (Shimizu et al., 2000), up to 36% of all JOAG was accounted for by disease-causing variants in *MYOC*. Although there was no strict limit to age at diagnosis in this study, the mean age of our POAG cohort was older than the thresholds for both previous studies but still relatively young for POAG at 44.4 ± 10.4 years. Therefore, our finding of 13.30% prevalence for *MYOC* glaucoma is consistent with previous data.

In our POAG cohort, there was one NTG participant out of 68 (1.5%) who carried the *OPTN* p.Glu50Lys disease-causing variant. This rate is comparable with other replication studies on *OPTN* (Alward et al., 2003, Hauser et al., 2006b, Ayala-Lugo et al., 2007) albeit much less than in the initial discovery cohort (13.5%) (Rezaie et al., 2002). Our data also demonstrates the highly conserved nature of the *OPTN* gene with only 1 person in the control cohort (0.1%) carrying a qualifying variant. This generated a highly skewed odds ratio towards NTG cases for this gene (OR = 16.33 (1.01 – 263.94)). However, this was not statistically significant due to the rarity of qualifying variants in cases. It should also be noted that the p.Glu50Lys variant is suspected to be a gain-of-function variant (Minegishi et al., 2013). Similar to copy number gains in *TBK1*, this may represent a pathogenic mechanism that our filtering criteria are not adequate to detect.

Although *CYP1B1* and *LTBP2* were initially linked to autosomal recessive PCG, there is evidence that heterozygous variants in these two genes may contribute to POAG (Pasutto et al., 2010, Jelodari-Mamaghani et al., 2013). In *CYP1B1*, the proportion of POAG cases with qualifying variants was 2.75% and was lower than previous reports in Caucasian populations in France (4.6%) (Melki et al., 2004) and New Zealand (6.1%) (Patel et al., 2012). This difference may be in part due to the younger age at diagnosis in the French JOAG study (median = 40, range 13-52) as our previous study examining the prevalence of *CYP1B1* variants in JOAG found a 6.8% rate (Souzeau et al., 2015). Additionally, the 3 cases in the French study harboured a known polymorphic variant, p.(Ala443Val), which brought their prevalence of the true mutations to 3.4%. The case cohort in the New Zealand study included pseudoexfoliative glaucoma, ocular hypertension and POAG suspect patients, which makes any direct comparison less meaningful. The biallelic rate (compound heterozygous or homozygous) in this study was 1.4%, which is similar to the 0.85% in the French study (Melki et al., 2004) and 1.8% in the New Zealand study (Patel et al., 2012).

LTBP2 was originally discovered as the gene responsible for PCG linked to the GLC3D locus(Firasat et al., 2008a). Since then, it has also been implicated in POAG in a study of 42 Iranian individuals. The prevalence of deleterious *LTBP2* coding variants was found to be 11.9% (5 out of 42) in the Iranian study (Jelodari-Mamaghani et al., 2013). However, a WES study failed to detect any deleterious *LTBP2* variants in Chinese POAG, JOAG and PCG patients (Huang et al., 2014). The prevalence of *LTBP2* predicted pathogenic variants in our Australian cohort (2.8%) was lower than the rate reported in the Iranian population. Taken with the evidence from the Chinese study, the prevalence rate of *LTBP2* in POAG appears to be heavily dependent on ethnicity like the prevalence rate of *CYP1B1* (Jelodari-Mamaghani et al., 2013, Huang et al., 2014).

The relevance of *ASB10* in POAG pathogenesis has been debated. Rare nonsynonymous variants in *ASB10* have been reported in 6.0% of Caucasian POAG cases compared with 2.8% of controls in a mixed cohort from the USA and Germany (Pasutto et al., 2012). A later study of a smaller US cohort (n = 158) (Fingert et al., 2012) found a 7.0% rare nonsynonymous variant rate in POAG cases, which was not significantly higher than the 3.7% in controls (n = 82). Within the Japanese population, one study reported significant association of microsatellite polymorphisms in the GLC1F/ASB10 locus with NTG (Murakami et al., 2010). A more recent Pakistani study of 238 cases found a significant association of *ASB10* rare nonsynonymous variants in POAG with 9.7% prevalence in cases compared to 1.3% in controls (Micheal et al., 2015). However, the variants did not segregate in their familial cases and one variant identified in cases but not in their controls (p.(Arg453Cys)) has an allelic frequency of 2.2% in the ExAC population database, emphasizing the importance of large control cohorts to avoid selection bias. The *ASB10* variant p.(Arg304Cys) found in 0.23% of our cases was previously reported in 0.4% of cases in the Pakistani study (Micheal et al., 2015). The other three variants found in our study have not been previously reported. Rates of our variants in cases and controls were lower than both previous studies due to the additional qualifying condition of

predicted pathogenicity via software prediction prior to analysis. In our cohort, there was skewing of *ASB10* variants towards NTG cases, which is supportive of the findings from the Pakistani study and the study of microsatellite polymorphisms in the Japanese NTG cohort. Given the rarity of predicted pathogenic variants in *ASB10*, larger case cohorts will be required to definitively examine its role in POAG pathogenesis.

The prevalence of *NTF4* variants in our cases was comparable, albeit slightly lower than the 1.7% reported in the discovery cohort of European Caucasians (Pasutto et al., 2009). Multiple groups have attempted to replicate these results with mixed success. Case-control studies of European Caucasians (Liu et al., 2010) and Indians (Rao et al., 2010) found a higher rate of *NTF4* mutation carriers in controls compared with POAG participants. The control cohort used in the European study (Liu et al., 2010) was significantly younger than the original discovery cohort and may include cases which develop glaucoma later in life. The mean age of our cases was even younger than the discovery cohort used in the European study. Our slightly lower prevalence rate may be attributable to the stringent filtering with pathogenicity prediction software and a possible "winner's curse" in the original discovery cohort. Meanwhile, two separate studies in Chinese populations have identified low rates of nonsynonymous variation in *NTF4* from 0.3-0.6% in POAG cases and none in controls suggesting that it may be a rare cause of POAG in Chinese people (Vithana et al., 2010, Chen et al., 2012).

In a Chinese WES study, the prevalence of *WDR36* variants was high and similar to *MYOC*, however no controls were sequenced (Huang et al., 2014). Our study found that *WDR36* variants were the second most frequently identified after *MYOC,* by a large margin. However, it is highly unlikely that *WDR36* variants are causative for POAG in our cohort of advanced glaucoma participants given the higher prevalence of *WDR36* variants in our age-matched local controls and AOGC controls than in

cases. Our findings are similar to several previous studies which also reported no significant association between *WDR36* and glaucoma pathogenesis owing to the high prevalence of coding variants in controls (Hauser et al., 2006a, Hewitt et al., 2006b, Fingert et al., 2007).

Glaucoma locus GLC1C was originally mapped to 3q21-q24 between markers D3S3637 and D3S1744(Wirtz et al., 1997). It was not until 2014 that the causative variant for the original linkage signal was identified in *IL20RB,* p.(Thr104Met), via Sanger sequencing (Keller et al., 2014). The variant was reported to reduce receptor function in primary dermal fibroblasts from patients. Human trabecular meshwork cells expressed the IL20RB protein and demonstrated its upregulation in response to cytokine treatment, indicating its role in aqueous outflow resistance in POAG. However, *IL20RB* diseasing-causing variants are exceedingly rare with none identified in the 230 random POAG cases screened in the American study (Keller et al., 2014). In this study, we report the presence of one novel nonsynonymous variant, p.(Arg140Ter) in 1 HTG case and no rare nonsynonymous variants in 1096 controls. This result supports the role of IL20RB in human trabecular meshwork cells found in the previous study (Keller et al., 2014) .

No qualifying variants were found in *TBK1* in our POAG cohort and only 0.1% of the control population carried any qualifying variants in this gene. Published work on *TBK1* implicates copy number gain in glaucoma pathogenesis (Fingert et al., 2011, Awadalla et al., 2015). Our data complements this evidence by showing an absence of potential disease-causing *TBK1* SNVs in our POAG cohort. However, one could not exclude entirely the possibility that *TBK1* SNVs or indels may be responsible for POAG in some cases given the rarity of disease-causing copy-number variation in *TBK1*.

The estimate of monogenic burden in POAG is traditionally reported at around 5% (Fingert, 2011). Another WES study similar to this study also found *MYOC* to be the gene with the largest genetic contribution to POAG in a Chinese cohort (Huang et al., 2014). The Chinese WES study (Huang et al., 2014) of predominantly POAG cases (n = 125 for whole exome sequences) stated that 8.9% of their cohort harboured a known monogenic cause of which 5.6% carried *WDR36* variants. The percentage of our POAG cohort carrying variants in known glaucoma genes (26.6%) was significantly higher than previous estimates of 5% (Fingert, 2011) and 8.9% from the Chinese WES study (Huang et al., 2014). This finding may be largely due to the result of our extreme disease phenotype selection, skewed towards a younger age of disease onset, as is seen in comparison of JOAG vs POAG cohorts (Rezaie et al., 2002, Souzeau et al., 2013). By selecting for only the most severe POAG disease phenotype, our case cohort is enriched for genetic causes of POAG with higher penetrance. This strategy maximises our ability to identify disease-causing variants, and has been valuable for discovering common disease alleles with modest cohort sizes (Burdon et al., 2011). However, given the rarity of disease-causing variants in most POAG-causing genes, our sample size was insufficiently powered to detect statistically significant association in genes other than *MYOC*.

The strength of this study lies in the study cohort and experimental design. This disease cohort is strongly enriched with well-selected extreme disease phenotypes, and it is the largest study to examine whole exomes of a well matched case control cohort of this nature in the glaucoma field to date. All the glaucoma cases have had detailed clinical examinations to ascertain their phenotypes. Our large control cohort is matched to our cases on ethnicity, with a local subset also having been clinically examined to ensure absence of glaucoma phenotype. Whole exome sequencing was performed contemporaneously on both cases and screened controls thereby minimizing technical variability.

This study has some limitations which were largely technical. Whole exome sequencing has enabled the rapid examination of large numbers of genes at a reasonable cost. Its advantage over microarray technology for genetic studies lies in its ability to capture rare coding variants. However this also introduces the challenge of variable capture. AOGC samples were sequenced on a different platform with a different capture probe set to the case cohort. Joint-calling of the two datasets was used to limit the amount of artefact generated *in silico*. However, capture- and sequencing platform-specific differences remained. Some difference in capture rate at specific locations was evident and translated to incomplete capture of some variants in the AOGC cohort. Adjustment for the capture rate was performed in the calculation of odds ratios and p-values. ExAC samples are more heterogeneous in data acquisition compared with the current study cohort. Inability to joint-call our data with ExAC may have overestimated the actual mutation burden in this public domain control cohort. Hence the odds ratio between case and controls falls considerably when ExAC data is included and may represent an underestimation. Alternatively, incomplete coverage of AOGC controls may have contributed to an overestimation of the discovery odds ratio.

The drawback of this study design is the potential under reporting of non-*MYOC* variants in cases carrying *MYOC* variants. As *MYOC* positive cases were excluded from exome sequencing, the co-occurrence of variants in the other POAG genes cannot be excluded. This scenario is likely to be rare, as the frequency of cases potentially explained by genes other than *MYOC* in this advanced POAG cohort is 9.2%, which equates to an underestimation of non-*MYOC* variants by 2 to 3 participants (9.6% of 29, assuming no excessive enrichment of these variants in the *MYOC* cohort). Moreover, JOAG participants in ANZRAG with *MYOC* disease-causing variants have been previously sequenced at the *CYP1B1* locus, and none carried disease-causing variants in the latter gene (Souzeau et al., 2015). Other limitations of this study relate to WES previously discussed and briefly stated herein. The ANZRAG cases and controls were captured with a different enrichment protocol to the AOGC

controls. Although sequencing was performed on the same platform, batch effects in addition to capture differences could confound our data. We attempted to minimize this systematic error by employing joint-calling of both datasets using the same bioinformatic pipeline. Additionally, although our local 103 controls were clinically screened to exclude glaucoma or its related endophenotypes, but no ophthalmic clinical examination was performed on the 993 AOGC controls. Therefore, it is likely the AOGC control cohort harbours the background population rate of POAG in the Caucasian population at around 2.37%. This reduces the power of this study to detect significant differences between our cases and the AOGC controls.

Overall, the majority of genetic causes for POAG remain unidentified. In our selective cohort of participants with early-onset advanced disease, *MYOC* had the single greatest influence on POAG, accounting for up to 13.3% of all cases. A role for *WDR36* variants in POAG was not supported in our cohort. The other eight monogenic Mendelian POAG genes did not show a significant enrichment of qualifying variants in POAG cases, although they may additively account for up to 9.6% of the POAG burden, providing an overall prevalence of up to 22.9% for known glaucoma genes in advanced early-onset POAG.

Chapter 4: Rare variants in known genome wide association genes

The contents of this chapter were published in the peer reviewed journal Molecular Genetics and Genomic Medicine (Zhou et al., 2016). The majority of POAG disease burden cannot be explained by the monogenic Mendelian inheritance model as collectively the known genes account for less than 5% of total disease burden in POAG (Fingert, 2011). The common disease, common variant hypothesis has been tested in POAG. Genome wide association studies (GWAS) suggest at least part of the disease burden is attributable to common variants near or within a number of genes including *ABCA1* (Chen et al., 2014b, Gharahkhani et al., 2014, Hysi et al., 2014), *AFAP1* (Gharahkhani et al., 2014), *ATOH7* (Ramdas et al., 2011c), *CAV1-CAV2* (Thorleifsson et al., 2010, Wiggs et al., 2011, Hysi et al., 2014), *CDKN2B-AS1* (Burdon et al., 2011, Osman et al., 2012, Nakano et al., 2012), *GAS7* (Hysi et al., 2014), *GMDS* (Gharahkhani et al., 2014), *PMM2* (Chen et al., 2014b), *SIX1-SIX6* (Ramdas et al., 2011c, Wiggs et al., 2012, Osman et al., 2012), and *TMCO1* (Burdon et al., 2011, van Koolwijk et al., 2012, Hysi et al., 2014). Some POAG risk loci have shown significant associations with quantitative traits related to the disease such as IOP, optic disc morphology and central corneal thickness (Lu et al., 2013, Hysi et al., 2014, Springelkamp et al., 2014). However the magnitude of odds ratios for all genome-wide associated disease polymorphisms are less than two, even for the strongest loci including *TMCO1* (Burdon et al., 2011) and *CDKN2B-AS1* (Burdon et al., 2011, Wiggs et al., 2012), with a significant proportion of normal controls also carrying the risk alleles at associated polymorphisms (Mackey and Hewitt, 2014). Furthermore, the majority of the GWAS signals are located in the non-coding regions of the genome. There is as yet no clear understanding of the mechanism of association of these non-coding polymorphisms with disease aetiology (Manolio et al., 2009).

The exact contribution of rare variants to glaucoma is not known. Common tagged single-nucleotide polymorphism (SNP) analysis at the genome level using SNP microarray technology cannot ascertain

the burden of rare variants due to the poor linkage disequilibrium between common and rare variants (Manolio et al., 2009, Siu et al., 2011). This case-control study utilized whole exome sequencing (WES) to investigate the degree of enrichment and proportion of disease burden accounted for by rare pathogenic variants in genes near common variants known to be associated with POAG and related quantitative traits from GWAS as this has not been adequately addressed in the literature.

This case-control study utilized whole exome sequencing (WES) to investigate the degree of enrichment and proportion of disease burden accounted for by rare pathogenic variants in genes near common variants known to be associated with POAG and related quantitative traits from GWAS as this has not been adequately addressed in the literature.

4.1 Methods

4.1.1 Participants

Unrelated Caucasian participants with advanced glaucoma and non-glaucoma Caucasian controls were included for the study as detailed in chapter 2. Participants were recruited from the ANZRAG database with inclusion criteria previously detailed in thesis chapter 2. Individuals with known *MYOC* mutations were excluded from this study as the genetic cause for their POAG has already been identified. For the local control cohort, all participants were examined to exclude glaucoma or glaucoma related phenotypes. 187 cases with advanced glaucoma and 103 local non-glaucomatous controls were analysed. Furthermore, *in-silico* analysis included a larger unexamined control cohort (n = 993) from the Australian Osteoporosis Genetics Consortium (Estrada et al., 2012) (AOGC).

4.1.2 Data acquisition and analysis

The whole exome sequencing protocol was previously stated in detail in the thesis methodology chapter. To summarize, DNA samples were prepared with the SureSelect Human All Exon V4 enrichment kit (Agilent, Santa Clara, USA) as per manufacturer's protocol and sequenced on a HiSeq2000 (Illumina, San Diego, USA) with 100bp paired end reads (Macrogen Next Generation Sequencing Services). Experimental data was joint-called with previously sequenced AOGC exomes, which were also sequenced on the HiSeq2000 (Illumina). Using in-house UNIX scripts, only protein coding exonic and splicing site variants were selected for analysis. Genes were included in the list if they were reported by any published GWAS or meta-analysis paper to be the closest to SNPs associated with POAG or a disease endophenotype at $p < 5\times10^{-8}$ in any ethnicity. Mutation loads per gene were calculated for the glaucoma cases, local control, AOGC control and ExAC control cohorts by summing the minor allele counts of all qualifying variants in the same gene and dividing by the average number of captured alleles for those variants, thereby adjusting for capture rate. Odds ratios were generated between cases and each control cohort separately, and Fisher's exact test used to calculate p-values, and Bonferroni correction applied for multiple testing of all analysed genes (n = 86, threshold $p = 5.81\times10^{-4}$). Five sets of randomly chosen independent groups of 86 WES captured genes were selected using a random number generator and analysed using the same protocol to act as control gene sets. This step further strengthens the positive results by examining the likelihood of false positive findings.

4.1.3 Validation of variants

All variants within significantly associated genes were independently validated by capillary sequencing (primers listed in Table 6). PCRs were conducted on carrier samples using 40ng of DNA, 10 µmol of each corresponding forward and reverse primers, 0.5 units of HotStar Taq DNA polymerase (Qiagen), 2 µmol of dNTP and PCR buffer in a 20 µL volume per reaction. Thirty cycles of

PCR were performed with denaturing temperature of 95°C, annealing temperature of 62°C and extension temperature of 72°C. Five µL of each PCR product was incubated with 2 µL of Shrimp Alkaline Phosphatase (Affymetrix) and 0.5 µL of *E. coli* exonuclease I (New England BioLabs) at 37 °C for 60 minutes to degrade primers and unused dNTP. Sequencing was carried out on the fluorescence-based capillary electrophoresis system 3130xl Genetic Analyzer (Life Technologies) using BigDye Terminator V3.1 (Life Technologies) according to manufacturer's protocol.

Table 6: PCR primers for validation of *CARD10* variants by direct sequencing. Optimal annealing temperature for PCR was at 62-64°C.

Position	Exon	cDNA change	Residue change	Forward Primer (5'>3')	Reverse Primer (5'>3')
chr22:37912044	3	c.635G>A	p.Arg212His	tccagaatttccctctagtgttt	ttatccacgtcaaagagccag
chr22:37904616	5	c.983C>T	p.Ala328Val	tgtccccttccttcccacac	gtgcctccgtcaacatctga
chr22:37904575	5	c.1024G>A	p.Val342Met	tgtccccttccttcccacac	gtgcctccgtcaacatctga
chr22:37902372	7	c.1210C>T	p.Arg404Trp	agctgccattctccttactgt	ttcaagttcccgcccctaac
chr22:37888801	17	c.2485C>T	p.Arg829Trp	gttttggggtatcgacgagc	acaggagggaaaggacttgg

4.2 Results

At the time of this study in 2017, 101 genes had been reported by GWAS studies as being near SNPs that are statistically associated with POAG or its endophenotypes, central corneal thickness, IOP or optic disc morphology. Of these 101 genes, 86 had qualifying (MAF < 0.01 and predicted pathogenic) variants captured in glaucoma and control cohorts in this study (Table 7).

Table 7: List of genes found on GWAS to be associated with POAG or endophenotypes. Bold = Genes analysed in this study. CCT = Central corneal thickness, ODA = Optic disc area, CA = Cup area, IOP = Intraocular pressure, NRR = Neuroretinal rim, VCDR = Vertical cup-to-disc ratio, NTG = Normal-tension glaucoma.

Locus	Genes	Top SNP	Phenotype	Populations	Publication
1p22	***CDC7, TGFBR3***	rs1192419	ODA	Dutch	(Axenovich et al., 2011)
		-	ODA	Asian	(Khor et al., 2011)
		rs1192415	ODA	Caucasian	(Ramdas et al., 2010)
		rs1192415	POAG	Asian, Caucasian, African	(Li et al., 2015)
		rs4658101	VCDR	Asian, Caucasian	(Springelkamp et al., 2014)
1p34.2	***COL8A2***	rs96067	CCT	Caucasian	(Lu et al., 2013)
		rs96067	CCT	Malay, Indian	(Vithana et al., 2011)
1p36	***RERE***	rs2252865	NRR	Dutch	(Axenovich et al., 2011)
		rs2252865	VCDR	Dutch	(Axenovich et al., 2011)
		rs301801	VCDR	Asian, Caucasian	(Springelkamp et al., 2014)
1p36.1	***DHRS3***	rs3924048	CA	Asian, Caucasian	(Springelkamp et al., 2015)
1q23	***F5***	rs12406092	ODA	Asian, Caucasian	(Springelkamp et al., 2015)
1q24.1	***TMCO1***	rs7555523	IOP	Asian, Caucasian	(Hysi et al., 2014)
		rs7518099	IOP	Caucasian	(Ozel et al., 2014)
		rs7555523	IOP	Caucasian	(van Koolwijk et al., 2012)
		rs4656461	POAG	Caucasian	(Burdon et al., 2011)
		rs7555523	POAG	Asian, Caucasian	(Hysi et al., 2014)
		rs7555523	POAG	Caucasian	(van Koolwijk et al., 2012)
1q42.11	***CDC42BPA***	rs6671926	ODA	Asian, Caucasian	(Springelkamp et al., 2015)
2p16	***EFEMP1***	rs1346786	CA	Asian, Caucasian	(Springelkamp et al., 2015)
2p21	***SRBD1***	rs3213787	NTG	Japanese	(Meguro et al., 2010)
2p24.3	***TRIB2***	rs2113818	CA	Asian, Caucasian	(Springelkamp et al., 2015)
2q35	***USP37***	rs10189064	CCT	Caucasian	(Lu et al., 2013)
2q35	***DIRC3***	rs1549733	ODA	Asian, Caucasian	(Springelkamp et al., 2015)
2q36	***COL4A3***	rs7606754	CCT	Asian, Caucasian	(Lu et al., 2013)
3p14.3	***FLNB***	rs6764184	CA	Asian, Caucasian	(Springelkamp et al., 2015)

3p24.2	***RARB***	rs11129176	ODA	Asian, Caucasian	(Springelkamp et al., 2015)
3q11.2	***GPR15***	rs3749260	CCT	Caucasian	(Lu et al., 2013)
3q12	***COL8A1***	rs2623325	VCDR	Asian, Caucasian	(Springelkamp et al., 2014)
3q12.2	***ABI3BP***	rs9860250	ODA	Asian, Caucasian	(Springelkamp et al., 2015)
3q25.31	***TIPARP***	rs9822953	CCT	Caucasian	(Lu et al., 2013)
3q26.31	***FNDC3B***	rs4894535	CCT	Asian, Caucasian	(Lu et al., 2013)
		rs6445055	IOP	Asian, Caucasian	(Hysi et al., 2014)
		rs4894535	POAG	Asian, Caucasian	(Lu et al., 2013)
3q26.32	***KCNMB2, TBL1XR1***	rs7620503	CCT	Asian, Caucasian	(Lu et al., 2013)
4p16.1	***AFAP1***	rs4619890	POAG	Caucasian	(Gharahkhani et al., 2014)
4q31	*NR3C2*	rs3931397	CCT	Asian, Caucasian	(Lu et al., 2013)
5q12	***ADAMTS6, CWC27***	rs1117707	CCT	Caucasian	(Lu et al., 2013)
5q35.1	***DUSP1***	rs17658229	VCDR	Asian, Caucasian	(Springelkamp et al., 2014)
6p12.1	***ELOVL5***	rs735860	NTG	Japanese	(Meguro et al., 2010)
6p25.3	***GMDS***	rs11969985	POAG	Caucasian	(Gharahkhani et al., 2014)
6p25.3	***FOXC1***	rs2745572	POAG	Asian, Caucasian	(Bailey et al., 2016)
6p25.3	***EXOC2***	rs17756712	VCDR	Asian, Caucasian	(Springelkamp et al., 2014)
6q14	***FAM46A***	rs1538138	CCT	Caucasian	(Lu et al., 2013)
6q14.1	***IBTK***	rs1538138	CCT	Caucasian	(Lu et al., 2013)
6q22.31	***HSF2***	rs868153	VCDR	Asian, Caucasian	(Springelkamp et al., 2014)
7p21	***GLCCI1***, ***ICA1***	rs59072263	IOP	Caucasian	(Strange et al., 2013)
7q11.21	***C7orf42***	rs4718428	CCT	Caucasian	(Lu et al., 2013)
7q11.21	***VKORC1L1***	rs11763147	CCT	Asian, Caucasian	(Lu et al., 2013)
7q31	***CAV1, CAV2***	rs10258482	IOP	Asian, Caucasian	(Hysi et al., 2014)
		rs10258482	POAG	Asian, Caucasian	(Hysi et al., 2014)
		rs4236601	POAG	Caucasian	(Thorleifsson et al., 2010)
		rs1052990	POAG	Caucasian	(Wiggs et al., 2011)
8q21.3	***DCAF4L2***	rs9969524	ODA	Asian, Caucasian	(Springelkamp et al., 2015)
9p22.3	***NFIB***	rs1324183	CCT	Caucasian	(Lu et al., 2013)
9p23	***MPDZ***	rs1324183	CCT	Caucasian	(Lu et al., 2013)
9q21	***CDKN2A, CDKN2B, CDKN2B-AS1***	rs523096	NTG	Japanese	(Takamoto et al., 2012)
		rs2157719	NTG	Caucasian	(Wiggs et al., 2012)
		rs4977756	POAG	Caucasian	(Burdon et al., 2011)
		rs2157719	POAG	Asian, Caucasian, African	(Li et al., 2015)
		rs7865618	POAG	Japanese	(Nakano et al., 2012)
		rs1063192	POAG	Japanese	(Osman et al., 2012)
		rs1063192	POAG	Caucasian	(Ramdas et al., 2011c)
		rs2157719	POAG	Caucasian	(Wiggs et al., 2012)
		rs1063192	VCDR	Caucasian	(Ramdas et al., 2010)
		rs7865618	VCDR	Asian, Caucasian	(Springelkamp et al., 2014)
9q31.1	***ABCA1***	rs2472493	IOP	Asian, Caucasian	(Hysi et al., 2014)
		rs2487032	POAG	Chinese	(Chen et al., 2014b)
		rs2472493	POAG	Caucasian	(Gharahkhani et al., 2014)
		rs2472493	POAG	Asian, Caucasian	(Hysi et al., 2014)

9q31.3	***LPAR1***	rs1007000	CCT	Asian, Caucasian	(Lu et al., 2013)
9q33.3	***FAM125B***	rs2286885	IOP	Caucasian	(Nag et al., 2014)
9q34.2	***ABO***	rs8176743	IOP	Asian, Caucasian	(Hysi et al., 2014)
9q34.2	***COL5A1***	rs3118515	CCT	Latino	(Gao et al., 2013)
	RXRA	rs1536482	CCT	Croatian, Scottish	(Vitart et al., 2010)
		rs4842044	CCT	Malay, Indian	(Vithana et al., 2011)
		rs3132306	CCT	Caucasian	(Hoehn et al., 2012)
		rs3118520	CCT	Caucasian	(Lu et al., 2013)
9q34.3	***LCN12, PTGDS***	rs11145951	CCT	Caucasian	(Lu et al., 2013)
10q21	***ATOH7***	rs1900005	ODA	Dutch	(Axenovich et al., 2011)
		-	ODA	Asian	(Khor et al., 2011)
		rs3858145	ODA	Caucasian	(Macgregor et al., 2010)
		rs1900004	ODA	Caucasian	(Ramdas et al., 2010)
		rs1900004	POAG	Caucasian	(Ramdas et al., 2011c)
		rs1900005	VCDR	Asian, Caucasian	(Springelkamp et al., 2014)
10q21.2	***ARID5B***	rs7090871	CCT	Asian, Caucasian	(Lu et al., 2013)
10q23	***PLCE1***	rs7072574	VCDR	Asian, Caucasian	(Springelkamp et al., 2014)
11p11.2	***RAPSN***	rs12419342	IOP	Asian, Caucasian	(Hysi et al., 2014)
	NUP160	rs747782	IOP	Asian, Caucasian	(Hysi et al., 2014)
	PTPRJ	rs1681630	IOP	Asian, Caucasian	(Hysi et al., 2014)
11p13	***ELP4***	rs11031436	ODA	Asian, Caucasian	(Springelkamp et al., 2015)
11q13.1	***SSSCA1***	rs1346	VCDR	Asian, Caucasian	(Springelkamp et al., 2014)
11q23.1	***ARHGAP20, POU2AF1***	rs4938174	CCT	Asian, Caucasian	(Lu et al., 2013)
11q25	***ADAMTS8***	rs4936099	VCDR	Asian, Caucasian	(Springelkamp et al., 2014)
12q13.11	***RPAP3***	rs11168187	VCDR	Asian, Caucasian	(Springelkamp et al., 2014)
12q21.31	***TMTC2***	rs10862688	VCDR	Asian, Caucasian	(Springelkamp et al., 2014)
		rs1511589	ODA	Asian, Caucasian	(Springelkamp et al., 2015)
12q23.3	***GLT8D2***	rs1564892	CCT	Asian, Caucasian	(Lu et al., 2013)
12q24.1	***ATXN2***	rs7137828	POAG	Asian, Caucasian	(Bailey et al., 2016)
12q24.31	***FAM101A***	rs10846617	CA	Asian, Caucasian	(Springelkamp et al., 2015)
13q11	***FGF9, SGCG***	rs1034200	CCT	Caucasian	(Lu et al., 2013)
13q12.11	***AVGR8***	rs1034200	CCT	Croatian, Scottish	(Vitart et al., 2010)
13q14.11	***FOXO1***	rs2755237	CCT	Croatian, Scottish	(Vitart et al., 2010)
		rs2721051	CCT	Latino	(Gao et al., 2013)
		rs2755237	CCT	Caucasian	(Lu et al., 2013)
		rs2721051	CCT	Caucasian	(Lu et al., 2013)
14q22	***SIX1***, ***SIX6***	rs10483727	POAG	Japanese	(Osman et al., 2012)
		rs10483727	POAG	Caucasian	(Ramdas et al., 2011c)
		rs10483727	POAG	Caucasian	(Wiggs et al., 2012)
		rs10483727	VCDR	Caucasian	(Ramdas et al., 2010)
		rs4901977	VCDR	Asian, Caucasian	(Springelkamp et al., 2014)
14q22.2	***DDHD1, BMP4***	rs10130556	CA	Asian, Caucasian	(Springelkamp et al., 2015)
15q13	***TJP1***	rs785422	CCT	Caucasian	(Lu et al., 2013)
15q22.33	***SMAD3***	rs12913547	CCT	Asian, Caucasian	(Lu et al., 2013)
15q25.3	***AKAP13***	rs6496932	CCT	Caucasian	(Lu et al., 2013)
		rs6496932	CCT	Croatian, Scottish	(Vitart et al., 2010)

15q26	***NR2F2***	rs8034595	ODA	Asian, Caucasian	(Springelkamp et al., 2015)
15q26.3	***CHSY1***	rs752092	CCT	Caucasian	(Lu et al., 2013)
15q26.3	***LRRK1***	rs2034809	CCT	Caucasian	(Lu et al., 2013)
15q26.3	***ASB7***	rs11247230	CA	Asian, Caucasian	(Springelkamp et al., 2015)
16p13.2	***PMM2***	rs3785176	POAG	Chinese	(Chen et al., 2014b)
16q12.1	***SALL1***	rs1362756	ODA	Caucasian	(Ramdas et al., 2010)
		rs1345467	VCDR	Asian, Caucasian	(Springelkamp et al., 2014)
16q24.2	***BANP***	rs9938149	CCT	Latino	(Gao et al., 2013)
	ZNF469	rs9938149	CCT	Caucasian	(Hoehn et al., 2012)
		rs12447690	CCT	Caucasian	(Lu et al., 2013)
		rs6540223	CCT	Caucasian	(Lu et al., 2013)
		rs12447690	CCT	Caucasian	(Ulmer et al., 2012)
		rs12447690	CCT	Croatian, Scottish	(Vitart et al., 2010)
		rs9938149	CCT	Malay, Indian	(Vithana et al., 2011)
17p12	***HS3ST3B1, PMP22***	rs2323457	CCT	Caucasian	(Lu et al., 2013)
17p13.1	***GAS7***	rs9913911	IOP	Asian, Caucasian	(Hysi et al., 2014)
		rs11656696	IOP	Caucasian	(van Koolwijk et al., 2012)
		rs9913911	POAG	Asian, Caucasian	(Hysi et al., 2014)
		rs11656696	POAG	Caucasian	(van Koolwijk et al., 2012)
17q21.32	***KPNB1***	rs11870935	CA	Asian, Caucasian	(Springelkamp et al., 2015)
17q23.2	***BCAS3***	rs11651885	CA	Asian, Caucasian	(Springelkamp et al., 2015)
20p12	***BMP2***	rs6054374	VCDR	Asian, Caucasian	(Springelkamp et al., 2014)
22q11.21	***TXNRD2***	rs35934224	POAG	Asian, Caucasian	(Bailey et al., 2016)
22q12.2	***HORMAD2***	rs2412970	ODA	Asian, Caucasian	(Springelkamp et al., 2015)
22q13.1	***CARD10***	rs9607469	ODA	Asian, Caucasian	(Khor et al., 2011)
		rs5756813	VCDR	Asian, Caucasian	(Springelkamp et al., 2014)
22q13.1	***TRIOBP***	rs5756813	CA	Asian, Caucasian	(Springelkamp et al., 2015)
22q21.1	***CHEK2***	rs1547014	VCDR	Asian, Caucasian	(Springelkamp et al., 2014)

A total of 1159 qualifying variants were within the 86 included genes in case, local or AOGC control cohorts. There was no significant enrichment (OR = 1.12, p = 0.51) in the total carrier rate of qualifying variants in this gene set in glaucoma cases (64.2%, 120 individuals) compared with local and AOGC controls combined (61.5%, 648 individuals) although there was a trend towards increased mutation load in POAG cases (Table 8).

Table 8: Summary of disease burden in genes near GWAS associated SNPs with POAG.

Gene	POAG count	Control count	Odds ratio	Fisher's p value	Bonferroni corrected p
ABCA1	2	16	0.731785	1	1
ABI3BP	0	2	0	1	1
ADAMTS6	1	3	1.951277	0.4685225	1
ADAMTS8	6	41	0.846902	0.8371469	1
AFAP1	1	15	0.38574	0.4935098	1
AKAP13	12	42	1.637602	0.1739341	1
ARHGAP20	1	4	1.463904	0.5459818	1
ARID5B	1	8	0.731856	1	1
ASB7	0	2	0	1	1
ATOH7	0	1	0	1	1
ATXN2	3	14	1.142475	0.7419943	1
BANP	3	3	5.353832	0.0542457	1
BCAS3	1	7	0.836516	1	1
BMP4	0	10	0	0.3748709	1
CARD10	8	3	13.19481	6.942E-05	0.006038
CAV1	1	3	1.948307	0.4689484	1
CAV2	0	1	0	1	1
CDC42BPA	2	10	1.169251	0.6913335	1
CDC7	2	8	1.461676	0.6471773	1
CDKN2A	3	4	4.379679	0.0698255	1
CDKN2B	0	0	NA	1	1
CHEK2	1	2	2.927807	0.3774745	1
CHSY1	0	4	0	1	1
COL4A3	2	33	0.354859	0.221211	1
COL5A1	3	10	1.752807	0.4216144	1
COL8A1	1	4	1.459447	0.5470427	1
COL8A2	2	8	1.24893	0.6771928	1
CWC27	5	3	6.893048	0.0094737	0.824212
DCAF4L2	1	5	1.170053	1	1
DDHD1	1	12	0.426025	0.7065254	1
DHRS3	1	7	0.835498	1	1
DUSP1	1	1	3.716578	0.3796932	1
EFEMP1	0	2	0	1	1
ELOVL5	6	3	3.240642	0.0942742	1
ELP4	4	28	0.836516	1	1
EXOC2	0	3	0	1	1
F5	3	13	1.350185	0.7187271	1
FAM101A	0	3	0	1	1
FAM46A	0	4	0	1	1
FGF9	1	0	NA	0.1461988	1

FLNB	6	40	0.876423	1	1
FNDC3B	0	3	0	1	1
FOXC1	1	1	3.195187	0.4205403	1
FOXO1	0	5	0	1	1
GLCCI1	0	3	0	1	1
GLT8D2	0	1	0	1	1
GMDS	0	2	0	1	1
GPR15	1	9	0.650624	1	1
HORMAD2	3	16	1.096257	0.750556	1
HS3ST3B1	3	1	4.235294	0.3134333	1
HSF2	1	2	2.927807	0.3774745	1
IBTK	0	5	0	1	1
ICA1	2	3	3.765894	0.1662715	1
KCNMB2	0	2	0	1	1
KPNB1	1	0	NA	0.1461988	1
LCN12	0	1	0	1	1
LPAR1	0	1	0	1	1
LRRK1	3	13	1.226381	0.7302581	1
MPDZ	15	83	1.058208	0.8839215	1
MVB12B	0	1	0	1	1
NFIB	2	3	3.329055	0.1973911	1
NUP160	1	11	0.532329	1	1
PLCE1	2	20	0.585495	0.7598727	1
PMM2	1	6	0.975936	1	1
PTPRJ	5	15	1.951515	0.1995138	1
RAPSN	2	9	1.258467	0.6752564	1
RARB	0	2	0	1	1
RERE	5	5	5.49052	0.0113591	0.988242
RPAP3	2	12	0.975267	1	1
RXRA	3	3	5.106952	0.0600931	1
SALL1	2	10	1.154724	0.6943531	1
SGCG	1	7	0.835943	1	1
SIX6	3	20	0.878075	1	1
SRBD1	6	27	1.300772	0.6173824	1
SSSCA1	0	1	0	1	1
TGFBR3	0	1	0	1	1
TIPARP	0	4	0	1	1
TJP1	0	19	0	0.0963562	1
TMCO1	0	2	0	1	1
TMTC2	0	3	0	1	1
TMTC2	0	3	0	1	1
TRIB2	0	3	0	1	1
TRIOBP	18	84	1.211585	0.4803774	1

TXNRD2	3	12	1.448243	0.4755275	1
USP37	5	4	7.319519	0.0051064	0.444257
VKORC1L1	1	4	1.460561	0.5467392	1
ZNF469	20	138	0.733251	0.2215127	1

Four genes (*CARD10*, *CWC27*, *RERE* and *USP37*) were nominally enriched (uncorrected $p < 0.05$) in the glaucoma cohort (Table 8). Only *CARD10* (caspase recruitment domain containing protein 10) remained statistically significant after Bonferroni correction for 86 tested genes ($p = 6.94\times10^{-5}$, corrected $p = 5.97\times10^{-3}$) with an odds ratio of 13.2 (3.5 - 50.2). Eight out of 187 POAG cases (4.28%) carried a rare predicted pathogenic variant in *CARD10* (NM_014550.3) that were confirmed by Sanger sequencing (Appendix Figure 1). Comparatively, qualifying variants in *CARD10* were carried by 0.27% (3/1096) of the joint-called controls. A total of five nonsynonymous variants in this gene were identified in the POAG cohort with all but one absent in the controls (Table 9). These variants were predicted to be pathogenic by SIFT or PolyPhen2 as per the filtering criteria. Additionally, the variants were located in highly conserved regions, all having GERP (Genomic Evolutionary Rate Profiling) scores of greater than 2 (mean GERP score = 4.8). When tested against qualifying variants in the unscreened public domain ExAC non-Finnish European cohort (n = 33370) filtered with our pipeline, *CARD10* remained significantly enriched in the glaucoma cohort, albeit with a lower odds ratio (OR = 3.3, $p = 3.9\times10^{-3}$). All eight *CARD10* qualifying variants were successfully validated in the carrier cases using capillary sequencing (Appendix Figure 1) and submitted to ClinVar database (http://www.ncbi.nlm.nih.gov/clinvar/) with accessions SCV000266585 - SCV000266589. Sub-analyses of the HTG and NTG cohorts with local and AOGC controls showed significant association of *CARD10* variants with HTG subgroup (OR = 15.2, corrected p = 0.01). Five control gene sets of 86 randomly selected genes were examined and none contained any gene that was significantly associated with POAG after Bonferroni correction (Appendix Table 3 - 7).

Table 9: Qualifying *CARD10* (NM_014550.3) variants captured in glaucoma cohort and controls. SIFT score < 0.05 is predicted damaging. PolyPhen2 HVAR score > 0.909 is predicted damaging.

cDNA change	Residue change	SIFT	PolyPhen2	POAG cases	POAG freq	Control freq	ExAC freq
c.635G>A	p.Arg212His	0.10	0.987	1	2.7×10^{-3}	0	0
c.983C>T	p.Ala328Val	0.02	0.944	3	8.0×10^{-3}	9.1×10^{-4}	3.6×10^{-3}
c.1024G>A	p.Val342Met	0.04	0.025	1	2.7×10^{-3}	0	2×10^{-4}
c.1210C>T	p.Arg404Trp	0.01	0.764	1	2.7×10^{-3}	0	1.5×10^{-5}
c.2485C>T	p.Arg829Trp	0.02	0.01	2	5.3×10^{-3}	0	4.0×10^{-4}
c.3081delC	p.Pro1027fs	NA	NA	0	0	4.6×10^{-4}	0

4.3 Discussion

Genome-wide association studies have been examined for common variants linked to POAG, NTG and various associated endophenotypes; IOP, vertical cup-to-disc ratio (VCDR), neuroretinal rim area, optic disc area and central corneal thickness. Poor linkage disequilibrium exists between common and rare variants; this has been demonstrated experimentally (Siu et al., 2011). For this reason, previous GWAS designs have reduced power to detect signals at single nucleotide variants (SNVs) with MAF of less than 1%. This study employed WES to patch the "gap" left by GWAS and to explore whether rare variants (MAF < 1%) within 86 putative POAG risk loci were also enriched within a severe POAG cohort. Although the majority of rare variants from the 86 POAG risk loci do not show significant enrichment in cases, the plausibility that GWAS candidates may contribute to disease via a common disease rare variant hypothesis has been demonstrated by our study.

A previous candidate gene study of *SIX6* reported an enrichment of rare variants in POAG in that gene (Carnes et al., 2014). The most prevalent variant, with a carrier frequency of 1.6% in cases, identified by Carnes and colleagues (rs146737847:G>A) was found in 1.6% of our POAG cases, but also in 1.9% of local screened controls and 1.6% of AOGC controls with an overall OR of 0.98. The other three rare variants found in that study at a carrier frequency of 0.4% were not detected in our

cases or controls. In summary, our study found no enrichment of rare variants in *SIX6* in our POAG cases versus controls.

Genome-wide association of *CARD10*

SNPs near *CARD10* were first found to be significantly associated with optic disc area by GWAS in Singaporean Asians, a result replicated in a Dutch Caucasian cohort (Khor et al., 2011). Optic disc area is relevant in POAG as a large optic disc is correlated with increased susceptibility to glaucoma in Caucasian populations (Healey and Mitchell, 1999). Meta-analysis of optic disc morphology further implicated common variants in *CARD10* in VCDR but not POAG after adjustment for optic disc area (Springelkamp et al., 2014). This result has since been replicated in a separate case-control study in an Indian population (Philomenadin et al., 2015). Cup-to-disc ratio is fundamental in POAG as it is often used as a diagnostic criterion due to its strong positive correlation with disease incidence (Miglior et al., 2007, Hollands et al., 2013). The SNPs from the original GWAS linking *CARD10* to optic disc area were situated between 3262 bp and 7204 bp upstream of *CARD10* (Khor et al., 2011). These SNPs are in strong linkage disequilibrium with all common SNPs up to and including rs9610775, which is a missense coding variant, p.R289Q in the *CARD10* gene with a population MAF of 13% (Figure 14). The signal identified in the GWAS of optic disc area may possibly relate to *CARD10* coding mutations. The SNPs found to be significantly associated with VCDR on meta-analysis were 260 kb upstream of *CARD10* with no linkage disequilibrium to the gene (Springelkamp et al., 2014). More likely, these variants are involved in gene expression and regulation. Therefore the published GWAS data suggests that both coding variants in *CARD10* and its expression level may contribute to optic disc pathology.

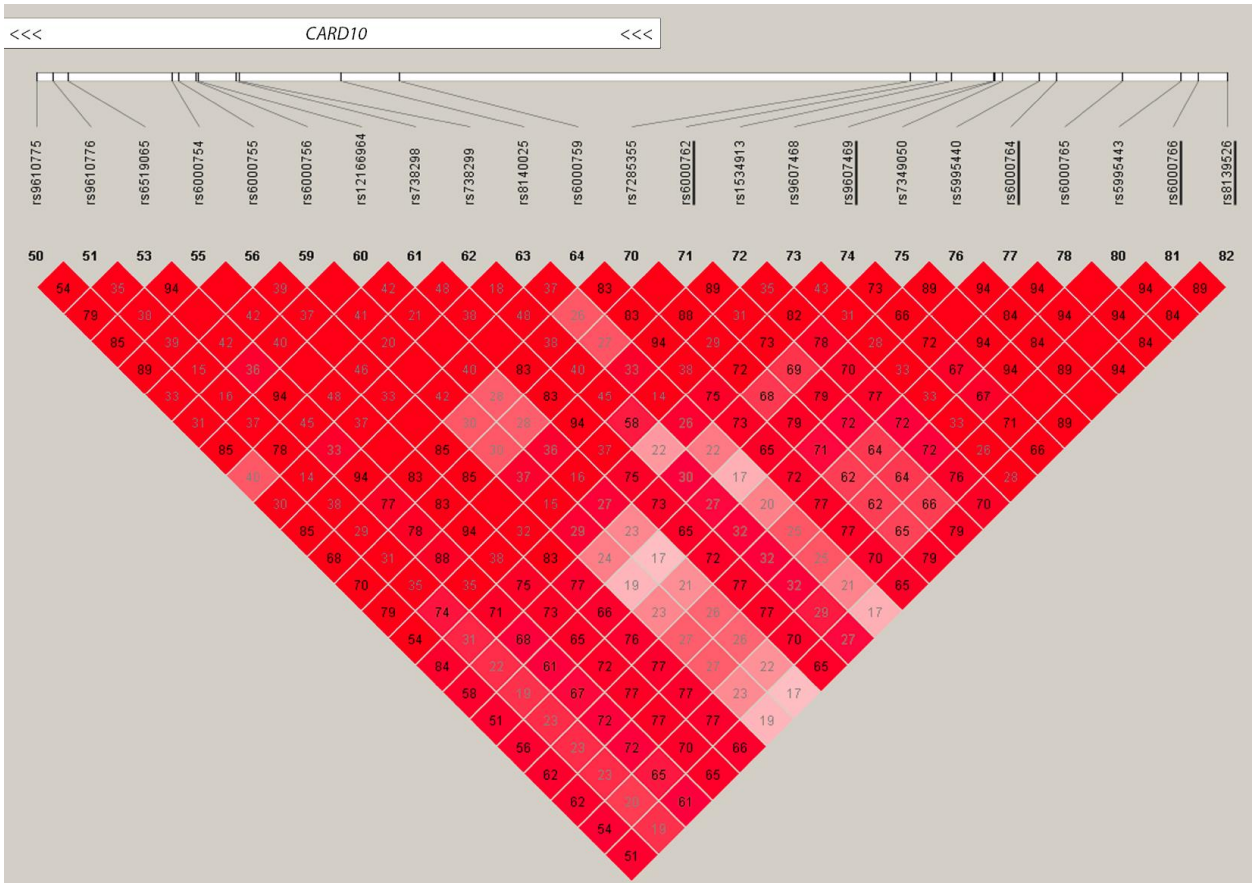

Figure 14. Linkage disequilibrium between GWAS SNPs and common SNPs in *CARD10* from HapMap CEU data showing D' values. GWAS SNPs are all underlined and upstream of *CARD10*. *CARD10* gene location is represented by rectangle at the top. The left-most SNP rs9610775 (p.Arg289Gln) represents the boundary of overlap between the GWAS significant LD block and the *CARD10* gene.

GWAS was able to highlight the association between regulatory and common coding SNPs in *CARD10* with crucial optic disc parameters for the development of POAG (Khor et al., 2011, Springelkamp et al., 2014, Philomenadin et al., 2015). This study complements the GWAS findings by implicating rare coding *CARD10* variants that likely disrupt gene function, and are associated with increased POAG risk within our cohort of advanced glaucoma participants. Both common and rare variants concurrently contribute to disease risk via differing mechanisms affecting the same gene - *CARD10*. Although more participants with HTG harboured rare *CARD10* variants than NTG participants, the

presence of *CARD10* variant carriers in NTG suggests that IOP elevation may not be required for *CARD10* mutations to cause glaucoma. No definitive inference can be made from this discrepancy due to the small sample size of the sub-cohorts. A plausible hypothesis would be that the increased susceptibility to retinal ganglion cell apoptosis in the *CARD10* mutation carrying individuals is compounded by elevated IOP to cause glaucoma at an earlier age and of greater severity. The participant inclusion criteria of this study selected exclusively for advanced glaucoma phenotype and young age of diagnosis, thus resulting in an enrichment of *CARD10* variant carriers who also had elevated IOP for other reasons.

***CARD10* function**

Discovered in 2001, *CARD10* functions as a signalling protein in the regulation of the NFκB (nuclear factor kappa B) pathway via activation of membrane-bound G protein-coupled receptors (McAllister-Lucas et al., 2001, Wang et al., 2001). This cascade is initiated through interactions between the N-terminal CARD domains of *CARD10*, *BCL10* and *MALT1*, which forms the CBM complex (Scudiero et al., 2014). Overexpression of *CARD10* has been demonstrated in multiple human neoplasias including bladder (Man et al., 2014), breast (Zhao et al., 2013), colon (Miao et al., 2012), lung (Li et al., 2012), ovarian (Xie et al., 2014), pancreatic (Du et al., 2014) and renal cancers (Wu et al., 2013). In all cases, the overexpression of *CARD10* is associated with increased cell survival, proliferation and therefore poor prognosis of cancer. The underlying physiology appears to involve enhanced cell cycling via NFκB facilitated up regulation of cyclin D1, cyclin E, Bcl-2 and phosphorylated IκB (Miao et al., 2012, Zhao et al., 2013, Xie et al., 2014). Other documented consequences of *CARD10* upregulation include leukocyte activation (Cowan et al., 2014) and inhibition of angiogenesis (Rau et al., 2014). Homozygous knockout of *Card10* in mice causes non-viability through neural tube defects (Grabiner et al., 2007). Grabiner and colleagues (2007) further demonstrated that *CARD10* may be

required for neural crest cell survival through G protein-coupled receptor induction of NFκB activation.

Primary open-angle glaucoma is a disease of enhanced retinal ganglion cell apoptosis (Foster et al., 2002). The NFκB pathway is profoundly involved in regulation of cellular apoptosis. Traditionally, it was only thought to be a promoter of cell survival and proliferation via downstream transcription of anti-apoptotic proteins. As such, overexpression of NFκB leads to enhanced growth of cancerous cells (Escarcega et al., 2007). However more recent evidence in the central nervous system suggests NFκB may also play a pro-apoptotic role depending on the nature of the noxious stimuli (Kaltschmidt et al., 2005). In certain situations such as neuronal ischemia and Parkinson's disease, upregulation of NFκB led to neuronal death via p53 signalling. Evidence in tumour cells indicates that *CARD10* promotes the anti-apoptotic effect of NFκB signalling. Therefore loss of function or downregulation of *CARD10* leads to increased apoptosis, especially in mouse neural crest cells (Grabiner et al., 2007). Conversely, pro-apoptotic activity of NFκB signalling has been recognized in the rat retina. NMDA (N-methyl-d-aspartate) induced expression of NFκB p65 led to retinal ganglion cell death which was ameliorated with knockdown of p65 by antisense oligonucleotides (Kitaoka et al., 2007). Retinal ganglion cell damage from NFκB is likely due to glial cell activation and interleukin (IL)-1β secretion (Kitaoka et al., 2007). Given the intimate and complex relationship between *CARD10*, NFκB and apoptosis, pathogenic coding mutations in *CARD10* are likely to affect apoptosis signalling. The coding mutations identified within the glaucoma cohort in this study have not been previously characterized, however they may augment retinal ganglion cell death via up or down-regulation of NFκB. This distinction is important to ascertain in order to translate these findings toward therapeutic strategies in glaucoma management.

Chapter 5: Systems analysis of rare variants in primary open-angle glaucoma

The contents of this chapter have been published in the peer reviewed journal PLoS One (Zhou et al., 2017a). Next-generation sequencing offers new ways to identify rare disease-associated variants with fewer restrictions than traditional linkage studies. Some rare variants are likely to have larger effect sizes than common variants (Bansal et al., 2010) and thus are more likely to initiate disease. In terms of clinical application, rare variants may have much greater positive predictive values than associated SNPs from GWAS. The drawback to rare variant analysis is the need for large sample sizes potentially in the magnitude of thousands to achieve statistical significance at a genome-wide level for the discovery a single rare causative gene (Gorlov et al., 2008). Using even the economical next-generation sequencing technique of whole exome sequencing (WES), the current costs and bioinformatics challenges of this venture are not trivial. However, genes do not act in isolation but form a complex network of interactions with other genes in various biological pathways.

Systems-medicine approaches, which employ methods to analyze biological networks and pathways, are an emerging tool to identify signatures of rare variant-disease associations that would not be identifiable in gene-by-gene based analyses. Recent successes have been achieved combining whole exome sequencing and pathway analysis in schizophrenia (Purcell et al., 2014) and amyotrophic lateral sclerosis (Cirulli et al., 2015). In the field of glaucoma research, no such WES studies have been published. In this chapter, I investigate the hypothesis that genes involved in POAG pathogenesis will be linked by functional biological pathways, and aims to identify these underlying biological pathways in POAG pathogenesis and its subtypes by examining genes enriched for pathogenic variants in POAG identified via whole exome sequencing.

5.1 Methods

5.1.1 Participants

Participant recruitment and inclusion criteria were detailed in chapter 2. Study participants were divided by IOP into HTG and NTG for analysis (Figure 15). NTG was defined as having a maximum recorded untreated IOP of less than 22 mmHg with the remainder of participants designated as HTG. Participants in ANZRAG with known disease-causing mutations in *MYOC,* identified by direct sequencing prior to the current study (Souzeau et al., 2012), were excluded from whole exome sequencing. Local controls were examined to ensure absence of clinically evident glaucoma or glaucoma associated phenotypes including vertical optic nerve cup to disc ratio and elevated IOP. A larger unscreened control cohort from the Australian Osteoporosis Genetics Consortium (AOGC) was also included for analysis. These controls were female participants with high or low bone mass who were otherwise self-reported to be healthy.

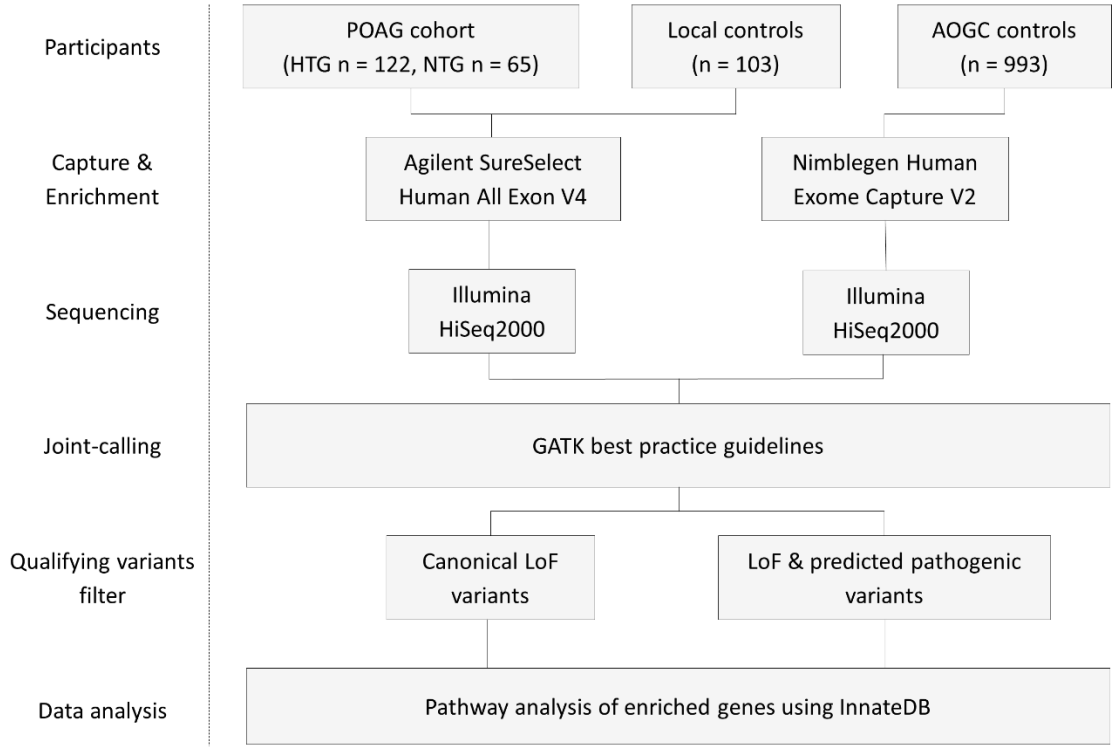

Figure 15: Experimental flowchart. POAG = primary open-angle glaucoma, HTG = high-tension glaucoma, NTG = normal-tension glaucoma, LoF = loss of function.

5.1.2 Data acquisition

Exome sequencing protocols were described in detail in the whole exome sequencing section of chapter 2. In order to focus on the influence of rare coding mutations, multi-stage variant filtering was performed to remove all non-coding variants, followed by all common variants and variants predicted not to be damaging by both the SIFT (Kumar et al., 2009) and PolyPhen-2 HumVAR (Adzhubei et al., 2010) software. The HumVAR version of PolyPhen-2 has a lower false positive rate and was chosen for the high sensitivity of its predictions. Variants with minor allele frequency (MAF) greater than or equal to 0.1 % in dbSNP v142 (www.ncbi.nlm.nih.gov/SNP/), NHLBI GO Exome Sequencing Project (ESP) v2 (evs.gs.washington.edu/), 1000 genomes v2014 (http://www.1000genomes.org/) or ExAC v3 (http://exac.broadinstitute.org/) public domain databases were defined as common. Rare canonical LoF variants in exonic regions (i.e. nonsense, splice site and frameshift mutations) were not subjected to pathogenicity filtering. The stringent control MAF cut-off of 0.1% within reference public domain databases was used in this study to limit the findings to truly rare and high penetrant variants. Typically, more common variant would have been detectable by previous GWAS (Burdon et al., 2011). PLINK (Purcell et al., 2007) was used to calculate allele frequencies and perform the final quality control filtering based on Hardy Weinberg Equilibrium ($p > 0.05$) and internal MAF (< 0.01).

Publicly available Exome Aggregation Consortium (ExAC) (Lek et al., 2016) v3 data were annotated using the ANNOVAR pipeline and filtered using the in-house UNIX scripts. The non-Finnish European subgroup in ExAC was used for MAF filtering as the closest approximation of the population ethnicity in the current study cohort. The study cohort was divided into HTG, NTG and all POAG for analysis. Mutation burden was calculated per gene for each cohort by dividing the sum of minor allele counts for all qualifying variants by the average number of captured alleles for those variants, thus adjusting for capture rate. Furthermore, two hierarchies of variant analysis were applied, the first using only

canonical LoF variants and the second utilizing both canonical LoF and predicted pathogenic variants, henceforth referred to as the LoF and predicted pathogenic models respectively. Odds ratios (OR) of the mutation burden between the case cohorts and each control cohort (local only, local plus AOGC and public ExAC data) were calculated. Genes that contained any qualifying variant in the 103 screened controls were excluded from the analysis to account for the unscreened nature of AOGC controls and variable capture between local and AOGC participants. Genes showing enrichment of rare variants based on OR of mutation burden were selected for Gene Ontology, pathway and network analysis using InnateDB (Lynn et al., 2008) (www.innatedb.com) for each comparison between case cohorts (HTG, NTG and all POAG) and all control groups. InnateDB is a publicly available platform incorporating major public domain pathway databases (including KEGG, Reactome, PID, Netpath and INOH). The database contains all human and mouse genes with their associated pathways and interactions. There is also improved annotation of the innate immunity interactome via manual curation. Hypergeometric distribution tests implemented in InnateDB were used to identify statistically enriched pathways among genes enriched for rare variants in POAG, and in the HTG and NTG sub-groups independently. P-values were adjusted using the Benjamini and Hochberg method (Lynn et al., 2008).

Network biology is a rapidly developing area of research, which recognises that biological processes are not chiefly controlled by individual proteins or discrete, unconnected linear pathways but rather by a complex system-level network of molecular interactions (Charitou et al., 2016). InnateDB (Lynn et al., 2008) was used to construct two different networks of the experimentally validated molecular interactions that are annotated to occur between genes enriched in HTG or NTG (or the encoded products of those genes) and their first neighbour interactors. Redundant edges (interactions), self-interactions and interactions involving the highly promiscuous interactor ubiquitin C (UBC) were removed from the network. The resulting network was visualized using Cytoscape v3.4.0. (Shannon

et al., 2003) The networks were analyzed using the jActiveModules plugin (Ideker et al., 2002) to identify high-scoring sub-networks in the larger networks that were both densely connected and enriched in either NTG or HTG associated genes (Figure 16). The parameters for the analysis were: the number of modules = 5; overlap threshold = 0.3 and search depth = 2. This type of analysis can aid in the identification of functionally relevant groups of enriched genes that may be acting in concert. High-scoring enriched sub-networks were identified and analyzed using the InnateDB ontology and pathway analysis tools to investigate whether these sub-networks were enriched in particular pathway components or functional gene categories.

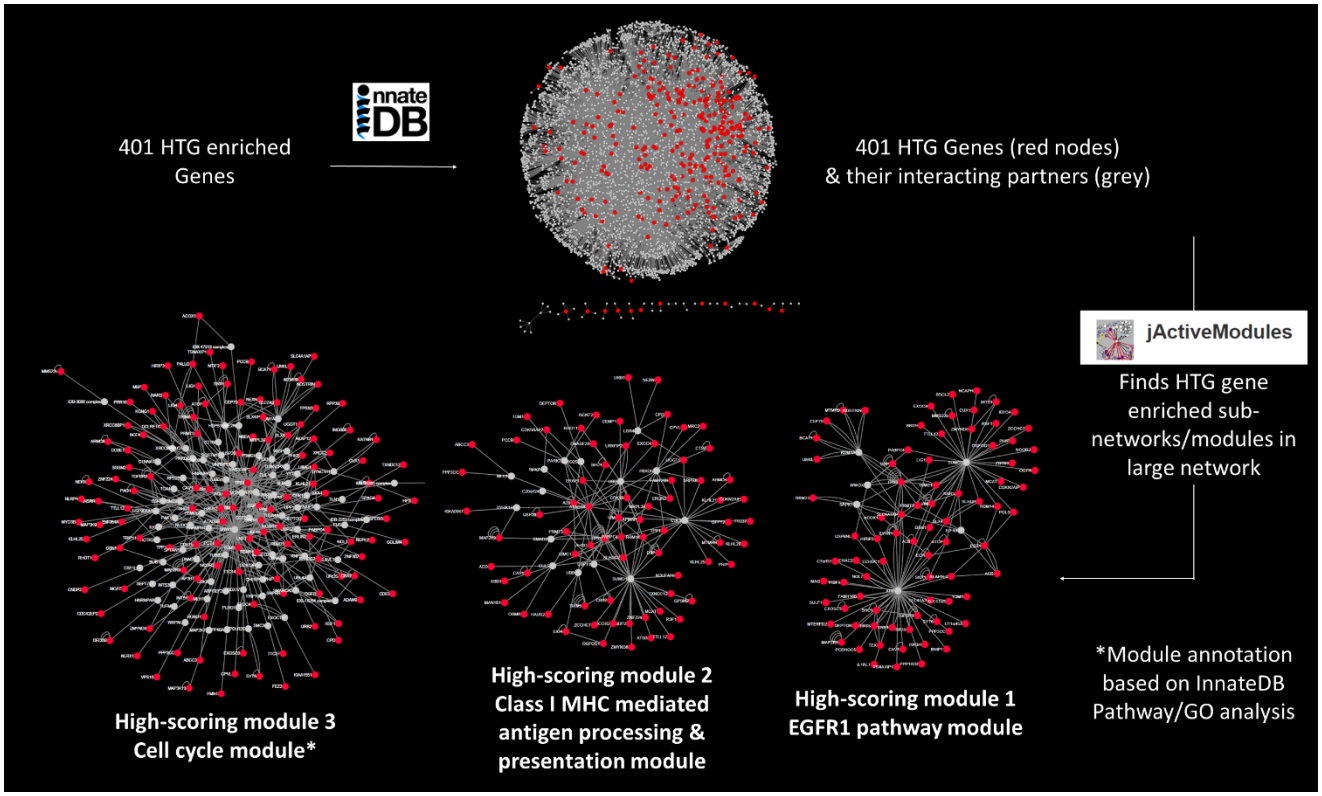

Figure 16: Flowchart showing network analysis using InnateDB using high-tension glaucoma (HTG) enriched genes as an example.

5.2 Results

Age of diagnosis in the HTG group was significantly younger ($p < 0.001$) than in the NTG group (Table 10). Otherwise there were no significant clinical differences between the two POAG subgroups. A total of 14,783 genes contained predicted pathogenic variants and 6087 of these genes contained canonical LoF variants in either case or control cohorts. The average variant per sample for each filtering step is shown in table 11.

Table 10: Clinical detail of POAG participants. The Mann-Whitney U test was used to assess statistical significance. HTG = high-tension glaucoma, NTG = normal-tension glaucoma, IOP = intraocular pressure, MD = mean deviation, CDR = cup-to-disc ratio, CCT = central corneal thickness

Group	HTG		NTG		P-value
	Mean	SD	Mean	SD	
IOP (mmHg)	31.5	0.74	18.1	0.35	-
MD (dB)	-18.16	0.84	-16.35	1.05	0.183
CDR	0.901	0.009	0.894	0.014	0.631
CCT (micron)	525.0	4.15	516.5	4.97	0.088
Age at diagnosis (Years)	42.5	0.89	47.9	1.29	<0.001

Table 11: Mean number of variants remaining at each stage of post-sequencing filtering.

All called variants per participant		
	Cases	**Controls**
Single nucleotide variants	66318	66181
Indels	6057	6017
Filtered coding variants		
Single nucleotide variants	19591	19632
Indels	466	462
Filtered qualifying variants		
Predicted pathogenic model	75.3	75.7
Canonical loss of function model	9.0	8.9

For the predicted pathogenic model, the mean number of qualifying variants (mutational burden) was not different between cases and controls (local and AOGC) at 75.3 per participant in the case cohort and 75.7 per participant in the control cohort ($p > 0.05$). Similarly, for the canonical LoF only model, the mean number of qualifying variants (mutational burden) was not different between cases and controls at 9.0 per participant in the case cohort compared to 8.9 per participant in the control cohort ($p > 0.05$). Genes were designated as enriched if the ORs between the case cohort and control cohort (local and AOGC) as well as the case cohort and public domain non-Finnish European ExAC cohort were greater than 5 for the LoF Model and OR greater than 4 for the predicted pathogenic model. These OR thresholds for variant enrichment were selected for the pathways analysis, because they generated an optimal number of genes for inclusion in the pathway analysis. The Venn diagram in Figure 17 illustrates the number of enriched genes included in pathway analysis from HTG, NTG and combined POAG cases, and the degree of overlap between these gene lists. The detailed gene lists are presented in Appendix Tables 8 to 13.

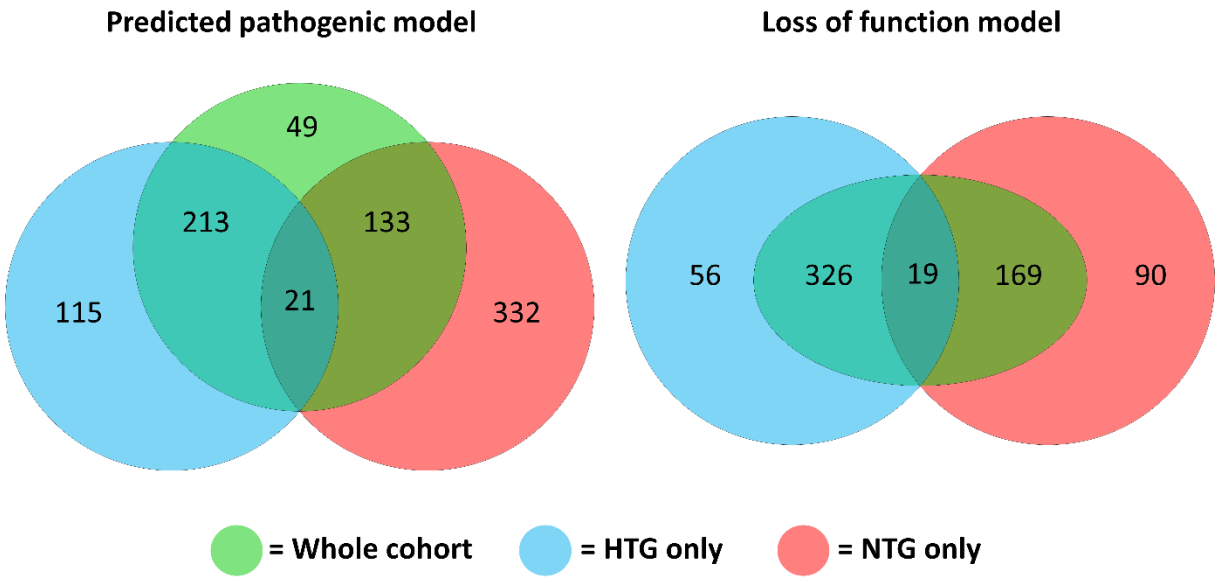

Figure 17: Venn diagram showing number of genes enriched in high-tension glaucoma, normal-tension glaucoma and all primary open-angle glaucoma cohorts compared with each of the control cohorts (local, AOGC and ExAC).

Gene Ontology analysis under a predicted pathogenic model showed significant over-representation of rare variants in camera-type eye development genes in all POAG cases combined - Gene Ontology Accession GO:0043010 ($p = 5.36\times10^{-7}$, corrected $p = 1.1\times10^{-3}$). Eleven enriched genes were included in this category (Table 12), with predicted pathogenic mutations in these genes present in 10.16% (19/187) of all POAG cases and 0.73% (12/1096) of all controls (OR = 10.22 (4.87-21.43), $p = 1.59\times10^{-9}$). Negative regulation of cardiac muscle cell apoptotic process - GO:0010667 ($p = 1.27\times10^{-5}$, corrected p = 0.015) was the other significantly enriched Gene Ontology term. This category contained only four enriched genes - *HAND2*, *NKX2-5*, *PDPK1* and *SFRP2*. A similar Gene Ontology analysis using the LoF model in all POAG cases combined failed to highlight any significantly over-represented terms.

Table 12: Significantly enriched Gene Ontology and biological pathways in POAG and its sub-types. LoF= Loss of function, OR = Odds ratio, CI = confidence interval.

Biological mechanism	P-value	Corrected p-value	Total genes in pathway	OR (95% CI)	Enriched genes (cases vs controls)
POAG (predicted pathogenic) gene ontology					
Camera-type eye development	1.40×10^{-7}	3.28×10^{-4}	67	10.22 (4.87-21.43)	*CRYBA4; GAS1; GJA8; HES5; MAB21L2; NEUROD4; NR2E1; PAX6; RXRA; SLC25A25; VAX1*
Negative regulation of cardiac muscle cell apoptotic process	1.27×10^{-7}	0.015	8	15.03 (2.89-78.04)	*HAND2; NKX2-5; PDPK1; SFRP2*
HTG (LoF) pathway analysis					
IRE1alpha activates chaperones	7.72×10^{-5}	0.013	50	76.84 (9.53-619.91)	*ACADVL; KDELR3; SHC1; SRPRB; SYVN1; TATDN2; TPP1*
XBP1(S) activates chaperone genes	5.90×10^{-5}	0.019	48	76.84 (9.53-619.91)	*ACADVL; KDELR3; SHC1; SRPRB; SYVN1; TATDN2; TPP1*
Unfolded Protein Response (UPR)	2.92×10^{-4}	0.032	81	87.21 (10.95-694.66)	*ACADVL; EXOSC3; KDELR3; SHC1; SRPRB; SYVN1; TATDN2; TPP1*
NTG (LoF) pathway analysis					
Ion channel transport	1.05×10^{-4}	0.027	169	17.93 (7.30-44.03)	*ATP2C2; ATP8B4; ATP9A; ATP9B; BEST3; CLCN1; GABRR2; TRPC3; TRPM8; TRPV1*

No established biological pathway or gene ontology term was significantly enriched under the predicted pathogenic model for HTG and NTG. However, in the HTG dataset, LoF mutations were significantly enriched in key regulators in the unfolded protein response (UPR) pathway - Reactome Accession R-HSA-381119 ($p = 2.92\times10^{-4}$, corrected p = 0.032) (Table 12). The other significant pathways were “IRE1alpha activates chaperones” (Reactome:R-HSA-381070) and “XBP1(S) activates chaperone genes” (Reactome:R-HSA-381038). The XBP1(S) pathway is a subgroup of the IRE1alpha

signalling pathway, which itself is a main component of the UPR. LoF mutations in the eight identified UPR genes were present in 7.37% (9/122) of all HTG cases compared to 0.82% (1/1096) of all controls (OR = 87.21 (10.95-694.66), $p = 7.08\times10^{-9}$).

The only significantly over-represented pathway in the NTG cohort was ion channel transport - Reactome: R-HSA-983712 ($p = 1.05\times10^{-4}$, corrected p = 0.027) (Table 12). Several classes of transporters were included in this classification including calcium, chloride and phospholipid transporters involved in transmembrane potential maintenance and homeostasis. LoF mutations in the ten identified ion channel transport genes were present in 15.38% (10/65) of the NTG cohort and 0.91% (11/1096) of local controls (OR = 17.93 (7.30-44.03), $p = 3.28\times10^{-8}$). Mutations in genes of all three significantly enriched pathways were carried by 19.25% (36/187) of POAG cases as well as 2.19% (24/1096) of all controls (OR = 10.65 (6.18-18.34), $p = 6.01\times10^{-17}$) (Table 12).

InnateDB.com (Lynn et al., 2008) was used to construct the HTG and NTG networks representing the annotated molecular interactions between HTG or NTG enriched genes (or the encoded products of those genes) and their first neighbour interactors (i.e. those genes, proteins or RNAs that are annotated by InnateDB to interact directly with the enriched genes). The HTG network consisted of 5196 nodes and 10524 edges and the NTG network consisted of 3748 nodes and 7134 edges. Sub-network analysis of the HTG network identified 3 high-scoring modules (Figure 18): HTG module 1 consisted of 87 nodes and 178 edges; HTG module 2 consisted of 88 nodes and 161 edges and HTG module 3 consisted of 210 nodes and 488 edges. Pathway analysis revealed that the top ranked pathways associated with genes in HTG module 1, 2 and 3 were the *EGFR1* pathway (FDR < 0.01), the Class I major histocompatibility complex (MHC) mediated antigen processing & presentation pathway (FDR < 0.01), and the cell cycle pathway ($FDR = 4.2\times10^{-9}$), respectively. Sub-network analysis of the NTG network identified two major high-scoring modules (Figure 19): NTG module 1 (78 nodes

and 123 edges) and NTG module 2 (94 nodes and 163 edges). No specific pathways were identified as being statistically enriched among genes in NTG module 1. Module 2 was identified, however, as being enriched in genes in the *EGFR1* pathway and in cell cycle related genes (FDR < 0.01) suggesting that similar processes may be involved in both NTG and HTG.

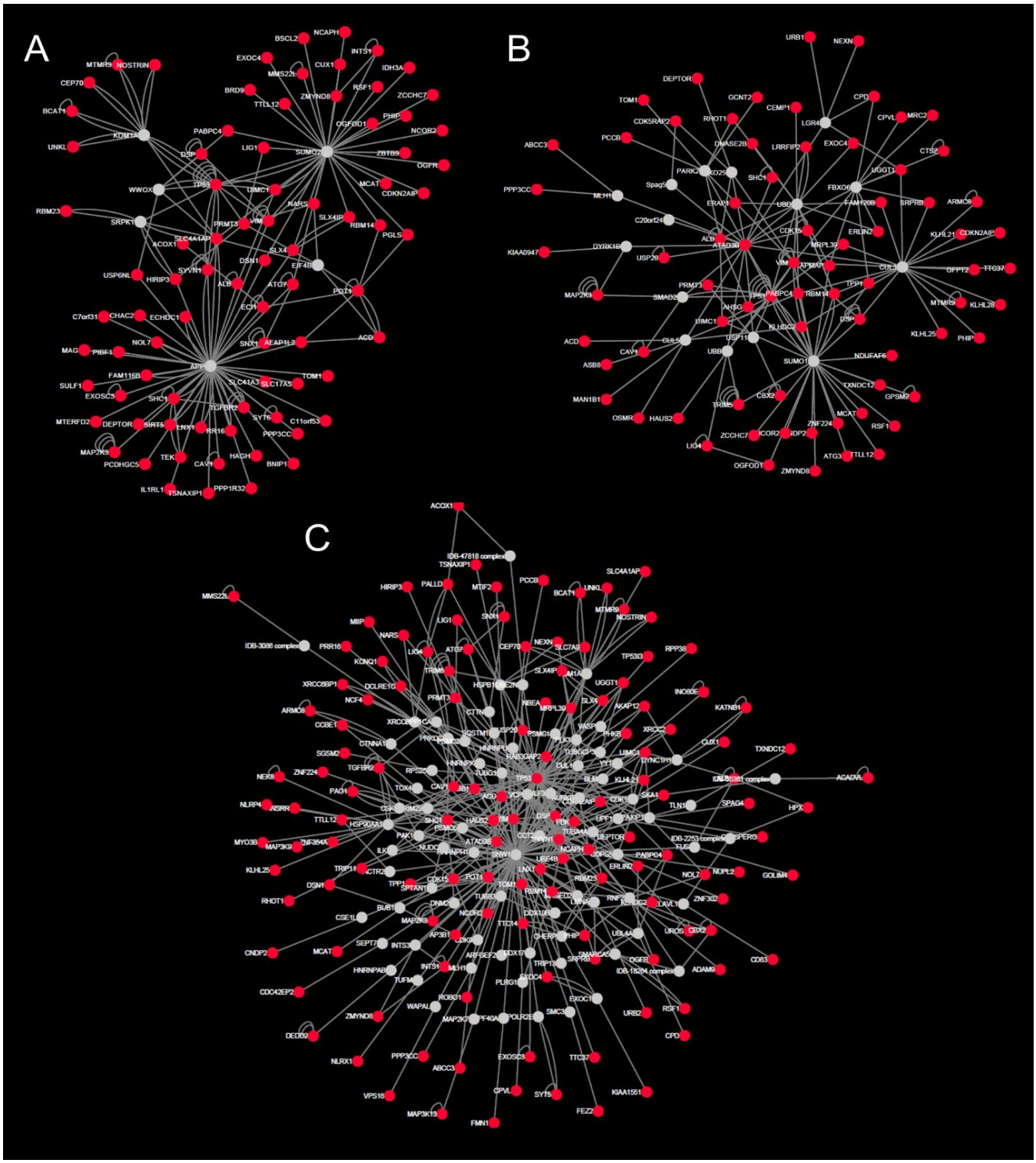

Figure 18: Major sub-networks/modules enriched in the high-tension glaucoma cohort. A: module 1 genes were significantly enriched for the *EGFR1* pathway. B: module 2 genes were significantly enriched for the Class I MHC mediated antigen processing & presentation pathway. C: module 3 genes were significantly enriched for the cell cycle pathway.

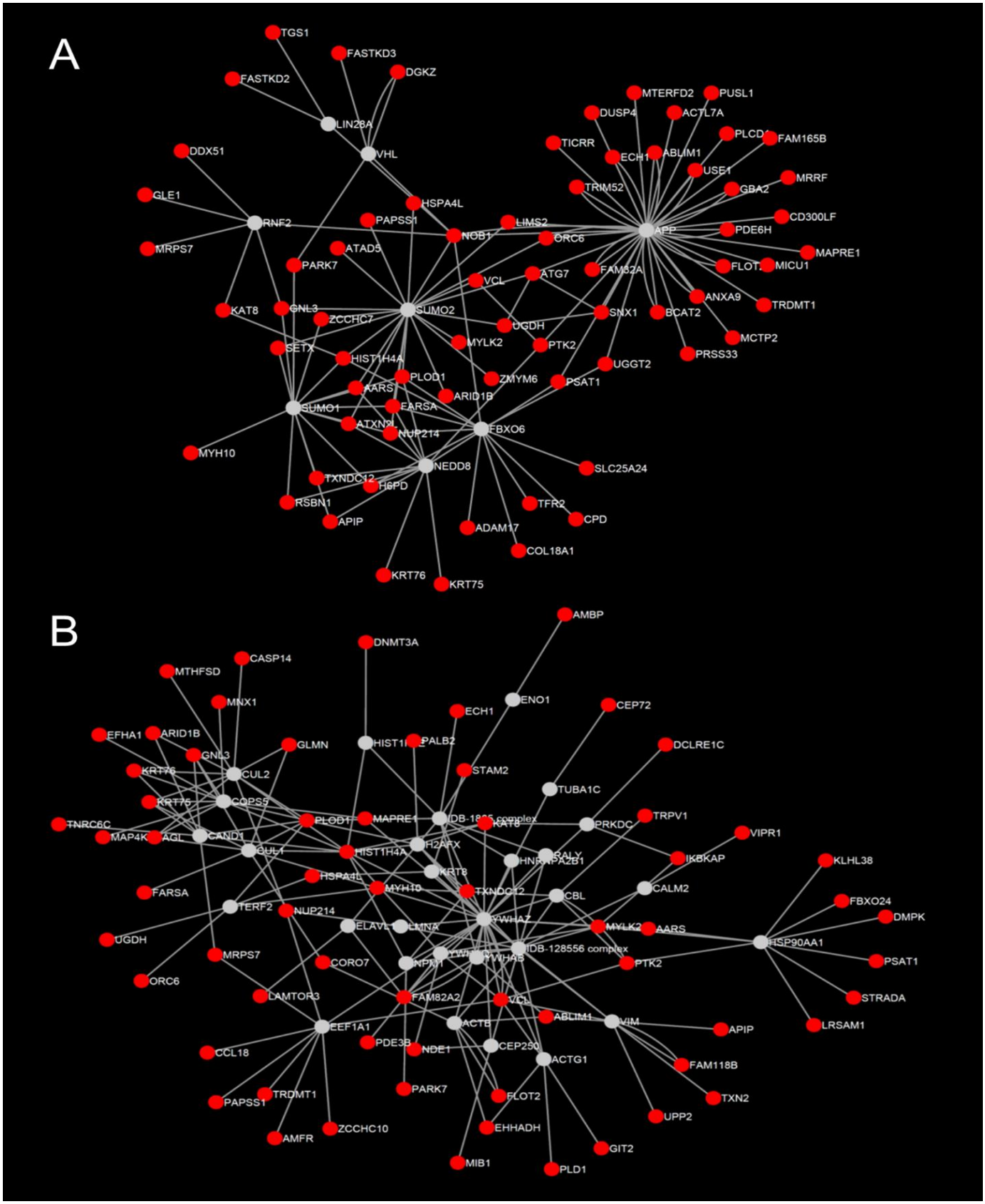

Figure 19: Major sub-networks/modules enriched in normal-tension glaucoma cohort. A: module 1 genes were not significantly enriched for any known biological pathways. B: module 2 genes were significantly enriched for the *EGFR1* and cell cycle pathways.

5.3 Discussion

Using a rare variant approach, this study identified several biological processes which likely contribute to pathogenesis of POAG. IOP data from the ANZRAG database allowed for sub-analysis to further distinguish its role in POAG. NTG was distinguished from HTG purely on the basis of an arbitrary IOP cut-off often used in the literature (<22mmHg) without consideration of other potential phenotypic discriminators. More participants with HTG satisfied the inclusion criteria of advanced glaucoma. The two POAG subgroups had similar clinical parameters with the exception of IOP and age at diagnosis. HTG was diagnosed earlier than NTG in participants included in this study. This may be a reflection of a more rapid disease progression seen in HTG and therefore an earlier age of onset. However, the difference may be due to recruitment bias as IOP is the most accessible ocular parameter in glaucoma diagnosis. As such, it is likely that HTG is detected and diagnosed earlier in the disease course than NTG, resulting in a difference in the age at diagnosis.

Primary open-angle glaucoma enriched genes

Previous studies have verified the contribution of *CYP1B1*, a gene that causes congenital glaucoma with high IOP, to juvenile and adult-onset POAG in various populations including Asian (Su et al., 2012), Australian (Souzeau et al., 2015) and Middle Eastern (Abu-Amero et al., 2013) ethnicities. Here we report that genes involved in camera-type eye development that are significantly enriched for rare variants in POAG, a condition which is intimately linked to congenital glaucoma. *GJA8* and *CRYBA4* are both crystalline lens-associated genes implicated in the formation of cataract. While it is well known that cataracts can contribute to the pathogenesis of angle-closure glaucoma, pathway analyses of GWAS SNPs (Hu et al., 2015) have identified associated SNPs in genes *CDK4PS* , *NFYAP1*, and *LGMNP1* shared between the POAG and cataract phenotypes, suggesting a potential genetic connection between these conditions. *GJA8* has been linked to the ocular developmental abnormalities of microcornea (Hu et al., 2010) and microphthalmia (Xia et al., 2012), both of which

may be related to glaucoma. The qualifying variants found in our study were different to the variants associated with microcornea and microphthalmia and unsurprisingly so, as our participants were screened to ensure the absence of any other ocular co-morbidity. Furthermore, one *GJA8* variant (p.(Asn190Ser)) has been reported in POAG cases and two *CRYBA4* variants (p.(Ser128Phe) and p.(Glu138Gly)) reported in primary angle-closure glaucoma in a Chinese cohort of 257 participants (Huang et al., 2015). Other identified eye development genes have roles in neuronal and/or anterior segment development. Certain genes in eye development ontology such as *PAX6* (Peter's anomaly), *VAX1* (microphthalmia) and *MAB21L2* (syndromic microphthalmia) are linked to glaucoma-associated congenital ocular pathologies (www.omim.org). GWAS have shown that common variants near *RXRA* (Lu et al., 2013) are associated with central corneal thickness and *PAX6* (Springelkamp et al., 2015) with optic disc area in various ethnicities including Caucasians. *PAX6* mutations cause aniridia which has a strong association with glaucoma development (Jordan et al., 1992). All mutations highlighted by the predicted pathogenic model are heterozygous and may represent a subtle form of congenital disease that only becomes observable in adulthood. The current results suggest that congenital glaucoma, whether *CYP1B1* related or not, and early adult-onset POAG may be different manifestations of the same disease continuum albeit with differing severity.

High-tension glaucoma enriched genes

The UPR and sub-classifications of this pathway were the only group of significantly enriched genes detected in the HTG cohort. A previous candidate gene study of common SNPs within UPR genes also revealed an association with POAG in general (Carbone et al., 2011). This pathway is involved in the pathogenesis of *myocilin* glaucoma (Yam et al., 2007a, Carbone et al., 2009), a form of POAG with very high IOP. Under normal physiological conditions, Myocilin protein is cleaved within the endoplasmic reticulum (ER) of trabecular meshwork (TM) cells and secreted into the aqueous humor to mediate cell adhesion and migration (Anholt and Carbone, 2013). *MYOC* mutants form

heterodimers with the wildtype protein that are less soluble and therefore retained within the ER (Gobeil et al., 2004). The biological cascade that follows from such an accumulation of misfolded proteins activates the UPR and has been established in *in vitro* human TM cells (Yam et al., 2007a) and an *in vivo* transgenic *Drosophila* model overexpressing mutant *Myoc* (Carbone et al., 2009). When invoked, the effects of UPR can be summarized into three main actions that counter ER stress via three sensor proteins - IRE1, ATF6 and PERK (Anholt and Carbone, 2013). One compensatory response is to lessen protein production via PERK-mediated inhibition of all mRNA translation. Concurrently, molecular chaperone transcription is stimulated via IRE1 and ATF6 signalling, which leads to increased solubility of misfolded proteins. IRE1 activation also induces translation of proteins involved in ER-associated protein degradation to lower the mutant protein load. If all compensatory mechanisms are overwhelmed by the accumulation of misfolded proteins, as in the case of *MYOC* mutants, then apoptosis is triggered via ATF6 and PERK signalling amongst others. Apoptosis of TM cells is recognized to contribute to IOP elevation and leads to the development of POAG (Sacca et al., 2015).

All but one of the UPR LoF mutations found in the HTG cohort are in genes involved in the IRE1 signalling pathway. The *EXOSC3* gene, while not a component of the IRE1 signalling, has a complementary role and is involved in ribonucleic acid degradation. The potential consequences of these mutations include a reduced rate of chaperone production and ER-associated protein degradation that are crucial to curtailing ER stress. Suppression of IRE1 signalling would lead to an unchecked accumulation of misfolded proteins, driving upregulation of ATF6 and PERK signalling, both of which initiate apoptosis. Molecular chaperones provide a feasible targeted therapy for managing HTG due to the ease of application. Two such substances, phenylbutyrate (PBA) (Yam et al., 2007b, Zode et al., 2011) and trimethylamine *N*-oxide (TMAO) (Jia et al., 2009) have been examined and found to be efficacious in treating *MYOC* mutants *in vitro* and in animal models. Both

PBA (Yam et al., 2007b) and TMAO (Jia et al., 2009) were successful in improving *MYOC* mutant protein folding, solubility and in turn cell survival in transfected human TM cells. Despite having normally functioning UPR pathways, *Myoc* mutant transgenic mice develop POAG like their human counterparts due to an overwhelming misfolded protein load. PBA has displayed *in vivo* efficacy in lowering IOP and increasing TM cell survival when administered orally (Zode et al., 2011) and topically (Zode et al., 2012) in these transgenic mice.

We have shown that rare LoF mutations in UPR genes are enriched in glaucoma within a cohort of advanced HTG patients. These findings suggest that functional deficiencies in the UPR mechanism would render it incapable of clearing misfolded proteins that are generated in normal cellular metabolism even in the absence of any extraneous load such as that from *MYOC* mutants. Our findings extend the relevance of the UPR pathway and the therapeutic potential of topical molecular chaperones to include non-*MYOC*-related HTG given that all cases with pathogenic *MYOC* mutations were excluded from this study. When excluded *MYOC* positive participants are taken into account, a total of 22.6% (33 out of 146) of all HTG may be related to protein misfolding, and hence potentially amenable to molecular chaperone therapy.

Normal-tension glaucoma enriched genes

The maintenance of transmembrane ion gradient is essential for the health and functioning of neurons such as retinal ganglion cells (RGC). Neuronal cell death can be triggered by large disruptions to this electrochemical balance as seen in the example of glutamate-associated excitotoxicity (Almasieh et al., 2012). Previous experimental studies have demonstrated that administration of glutamate to retina in animal models triggers apoptosis via an intracellular calcium surge (Almasieh et al., 2012). Furthermore, intracellular calcium itself can trigger neuronal apoptosis via calcineurin activation, endonuclease-mediated DNA degradation, reactive oxygen species

generation by phospholipases and loss of phospholipid asymmetry via inhibition of aminophospholipid translocase (Orrenius et al., 2003). Therefore, inadequate maintenance of calcium concentration and transmembrane ion balance could be a cause of RGC apoptosis in glaucoma.

The ten genes with LoF mutations in the NTG cohort consisted of transporters of a range of substrates including chloride, phospholipid, calcium and other cations. *ATP2C2*, *TRPC3*, *TRPM8* and *TRPV1* are calcium and cation channels. *TRPV1* knockout mice exhibit increased RGC susceptibility and enhanced axonal degeneration following IOP elevation (Ward et al., 2014). Conversely, activation of *TRPV1* may protect against NMDA-induced calcium-mediated RGC apoptosis (Sakamoto et al., 2014). *BEST3*, *CLCN1* and *GABRR2* are chloride channels. Their involvement in the homeostasis of transmembrane electrochemical potential may contribute to suppression of voltage-gated calcium channels thereby increasing resistance to intracellular calcium surge. *ATP8B4*, *ATP9A* and *ATP9B* are active transporters of phospholipid molecules. These three genes belong to the family of aminophospholipid translocases responsible for internalizing aminophospholipid phosphatidylserine (Takatsu et al., 2011). In normal cells, phospholipid asymmetry is maintained by aminophospholipid translocases such that phosphatidylserine is almost exclusively on the intracellular side of the phospholipid bilayer. Physiologic externalization of phosphatidylserine occurs in the neural retina and the process of phosphatidylserine-mediated phagocytosis has recently been shown to be the key mechanism for the diurnal recycling of photoreceptor outer segments in the retina in a mouse model (Ruggiero et al., 2012). Dysfunction of these translocases or their suppression by abundant intracellular calcium disrupts the phospholipid asymmetry and may incorrectly mark the affected cell for phagocytosis (Orrenius et al., 2003). Knockout of an aminophospholipid translocase in the same family as the transporters identified in this study (*ATP8A2*) causes increased phagocytosis and reduced viability of photoreceptor cells in the mouse (Coleman et al., 2014). The findings of the

current study suggest ion gradient and plasma membrane asymmetry homeostasis plays a role in regulating retinal ganglion cell survival in glaucoma.

Sub-network analysis enriched pathways

Network analysis of HTG and NTG enriched genes revealed three significantly associated pathways: HTG with MHC Class I antigen processing and presentation; both HTG and NTG with *EGFR1* and cell cycle pathways. It is worth noting that these pathways were not identified as statistically significant in the pathway analysis of all HTG or NTG genes, highlighting the power of the network biology approach to uncover signatures in the data that otherwise would be overlooked. Various immune response pathways have been implicated in the pathogenesis of POAG (Rieck, 2013). MHC Class I antigen presentation on the surface of a cell triggers its apoptosis via activation of cytotoxic T lymphocytes. However, MHC class I molecules are only expressed on the plasma membrane of neurons in the ONH under inflammatory conditions and not under normal physiological conditions (Rieck, 2013). This mechanism may be important in HTG as elevated IOP may subject the ONH ganglion cell axons to inflammation and the expression of MHC class I molecules. Therefore any abnormalities in MHC class I presentation in HTG patients may be a crucial trigger of their RGC apoptosis. Cell cycle pathways are often regarded as central to the cascade of RGC death in POAG (Jakobs, 2014). The glaucoma associated genes *TMCO1* and *CDKN2B-AS1* are both genes related to cell cycling (Burdon et al., 2011). Additionally, functional experimental studies have demonstrated that cell cycle genes are among the most up-regulated genes in animal models of ONH damage via elevated IOP and ON crush injury (Jakobs, 2014). These findings suggest that cell cycle pathways are involved in both HTG and NTG as supported by the outcomes of our network analysis. The role of *EGFR1* in glaucoma is as yet unknown, but it is well studied in human cancers and linked to cell cycle, proliferation and survival (Fromm et al., 2008). Based on our results in both HTG and NTG, *EGFR1* may be implicated in glaucoma pathogenesis via its influence on RGC survival.

The main limitation of this study design is the relatively small sample size. While this sample is underpowered to detect significant single gene effects, phenotypic enrichment for severe disease and precise endophenotype characterization in this study allowed for significant findings using a system-based analysis approach. Extreme phenotypic enrichment is a great advantage of the ANZRAG database and this study, which has served well in past GWAS discoveries with relatively few samples (Burdon et al., 2011, Gharahkhani et al., 2014). A technical limitation of this study is the variable capture between our experimental data, jointly called AOGC and public domain ExAC data. Joint-calling of local and AOGC data removed much experimental artefact that may contribute to false positives. Sequencing-related inconsistencies persisted due to incomplete coverage at some regions in the AOGC cohort that were covered well in the cases and local controls. The analysis took this into consideration by correcting for capture rate. Public domain ExAC controls were utilized as a secondary check to further limit false discoveries. Moreover, the conservative step of requiring consensus of odds ratios between cases and all controls for pathway analysis was implemented to minimize type-I errors. All measures aimed at reducing type-I error likely resulted in reduced power in the analysis. However, the robustness of system-levels analysis was able to overcome this limitation and achieve sufficient power for the detection of three biologically plausible pathways of importance in POAG. Our findings warrant further functional investigation and replication in an independent cohort of POAG cases.

In this study, rare variant investigation using whole exome sequencing has highlighted key mechanisms that contribute to glaucoma pathogenesis, complementing many decades of linkage and candidate functional work. Differing biologic mechanisms may underlie POAG with varying IOP characteristics although considerable overlap also exists. POAG may arise from abnormalities in ocular development that increase susceptibility to disease later in life with cell cycle pathways likely playing a major role. HTG is significantly associated with putative mutations in the UPR pathway that

neutralize protein misfolding, and abnormal MHC Class I antigen presentation. Potential therapeutic chaperones targeting the UPR pathway have shown promising results in *in vitro* and animal *in vivo* experiments. Mutations in ion channel transport genes significantly predispose to the development of NTG. Both pathways warrant replication in subsequent studies and ultimately further functional investigation in human POAG cohorts. Future studies with a larger whole exome sequenced cohort may be able to isolate single genes that contain rare variants associated with POAG.

Chapter 6: Ocular tissue gene expression profiling

Publicly archived ocular tissue expression data emerged during the era of expressed sequence tag (EST) technology. As such the longest available ocular expression database is kept by the NEIBank (https://neibank.nei.nih.gov/index.shtml) in the form of EST libraries (Tomarev et al., 2003, Wistow, 2006). However as the data contained within the NEIBank are stored as individual entries separated by tissue type without any systematic merging, no meaningful comparisons can be drawn between tissues. Moreover, the data is plagued by inherent problems with EST technology, which includes the inability to quantify transcript levels (Wang et al., 2009) and an overall transcript detection rate of only 60% (Morozova et al., 2009). An EST-based web tool of human ocular expression is available in the form of Tissue-specific Gene Expression and Regulation (TiGER) database (http://bioinfo.wilmer.jhu.edu/tiger/)(Liu et al., 2008). This tool presents the EST data stored within the dbEST (Boguski et al., 1993) of GenBank in a graphical format. All tissues within the eye are clustered into one entry and compared to the EST profiles of other tissues in the body. Again, the quantification limitation of EST technology makes these inter-tissue comparisons imprecise.

Microarray-based expression databases containing information on ocular tissue are also available online. The Gene Expression Omnibus (GEO) database (http://www.ncbi.nlm.nih.gov/gds/)(Edgar et al., 2002) is an open-access repository of high-throughput gene expression data from many tissues and species comprising predominantly microarray outputs with some next-generation sequencing outputs. There is no overarching guiding protocol for the data stored within the GEO database and every entry is an independent study with potentially vastly different experimental procedure. As such no systematic comparisons can be made between individual ocular tissues using the GEO database. The Glaucoma Discovery Platform from the Simon John Laboratory website (http://glaucomadb.jax.org/glaucoma) (Howell et al., 2011) provides microarray data from the retina and optic nerve head generated from the DBA/2J mouse model of glaucoma and matched control

mice. While this resource offers high quality expression data in a mouse model of glaucoma in two glaucoma-related tissues, the generalizability to humans is limited by the specific pathogenesis of glaucoma via iris pigment dispersion in the DBA/2J mouse (Libby et al., 2005, Steele et al., 2006).

The most complete human ocular tissue expression database to date is the Ocular Tissue Database (OTDB) (https://genome.uiowa.edu/otdb/) (Wagner et al., 2013). The OTDB contains microarray expression data from ten human ocular tissues presented in a searchable web tool by gene or tissue type. The main advantage of the OTDB over the GEO database is its ability to offer meaningful between-tissue expression comparisons for a range of ocular tissues. However, the OTDB is limited by the microarray technology in its coverage, accuracy, sensitivity and dynamic range. The coverage of hybridisation-based microarray technology is determinant on the probe set, therefore novel transcripts and genetic polymorphisms are not well captured. RNAseq technology has been available more recently, therefore ocular tissue expression data generated using this technology is limited. Sequence Read Archive (SRA) (http://www.ncbi.nlm.nih.gov/sra) is the largest public domain repository of RNAseq data. However, there is poor coverage of ocular tissues with a lack of standardisation of experimental conditions and protocols. All entries within the SRA are stored in the form of raw unprocessed reads, which require mapping, alignment and bioinformatic analysis before any comparisons can be made.

Pathway analyses of tissue RNA expression have been performed on microarray data from human and animal experimental glaucoma models (Wang et al., 2010a, Liu et al., 2013b). Tissues from these models used for analysis include human blood leukocytes (Colak et al., 2012) and POAG related ocular tissues such as human trabecular meshwork (Liu et al., 2013b), optic nerve astrocytes (Dong et al., 2014, Yan et al., 2015), lamina cribrosa (Dong et al., 2014) and rat retinal ganglion cells (Wang et al., 2010a). In the rat ganglion cell glaucoma model, hypertonic saline was injected into the

episcleral veins to induce ocular hypertension (Wang et al., 2010a). Retinal ganglion cells from the rat eyes exposed to ocular hypertension showed higher expression of apoptosis and complement component genes.

The leukocyte RNA expression in patients with glaucoma showed more varied enrichment in pathways including ephrin receptor, hypoxia, neuregulin, and G-protein coupled receptor signalling with significant enrichment of DNA replication, recombination, repair, protein synthesis and nervous system function and cell cycling genes (Colak et al., 2012). In a microarray expression comparison of trabecular meshwork cells from glaucoma patients and controls, *MYOC* glaucoma and non-*MYOC* glaucoma exhibited similar profiles (Liu et al., 2013b). The North Carolina study identified differential RNA expression in known glaucoma related genes such as *PAX6*, associated with anterior segment dysgenesis, and endocytic related genes such as *SPARC* and *TIMP2* (Liu et al., 2013b). Unfortunately, no systems approach analysis was performed on the human glaucoma trabecular meshwork microarray data.

Meta-analysis of previously archived human lamina cribrosa and optic nerve head astrocyte cultured cell lines combined from the GEO database highlighted significant enrichment of cancer related pathways including toll-like receptor signalling, glioma-related, and ErbB signalling pathways (Dong et al., 2014). A similar meta-analysis using optic nerve astrocytes expression data from the GEO database found enrichment in complement and coagulation cascades, arrhythmogenic right ventricular cardiomyopathy, extracellular matrix-receptor interaction, cancer related and focal adhesion pathways (Yan et al., 2015). Another meta-analysis using combined trabecular meshwork and lamina cribrosa cell lines from the GEO database highlighted the significance of Wnt and Akt pathways in both tissues in relation to glaucoma pathogenesis (Zhavoronkov et al., 2016).

The current study proposed the hypothesis that tissue gene expression is a reflection of its function. Under this model, genes that are highly expressed in a given tissue are more likely to be important in biological processes that the tissue is involved in. This study aimed to utilize RNAseq to provide the most comprehensive and accurate expression profiling of ten normal ocular tissues to date, including tissues involved in glaucoma with an emphasis for glaucoma gene discovery.

6.1 Methods

6.1.1 Tissue preparation

Experimental samples were obtained from the EyeBank of South Australia with the inclusion criteria of cadaveric human eyes that had no known ocular disease and were either unsuitable or unused for corneal transplantation. Ethical approval for the study was granted by the Southern Adelaide Clinical Human Research Ethics Committee, SA, Australia. Tissue dissection was performed under a surgical microscope within 24 hours post-mortem (mean = 9.5 ± 5.1 hours) to isolate ocular tissues including the corneal epithelium, corneal stroma, corneal endothelium (Figure 20A), trabecular meshwork (TM) (Figure 20B), peripheral iris, pars plicata of the ciliary body, neural retina, sclera, optic nerve head (ONH) (Figure 20C) and optic nerve (ON).

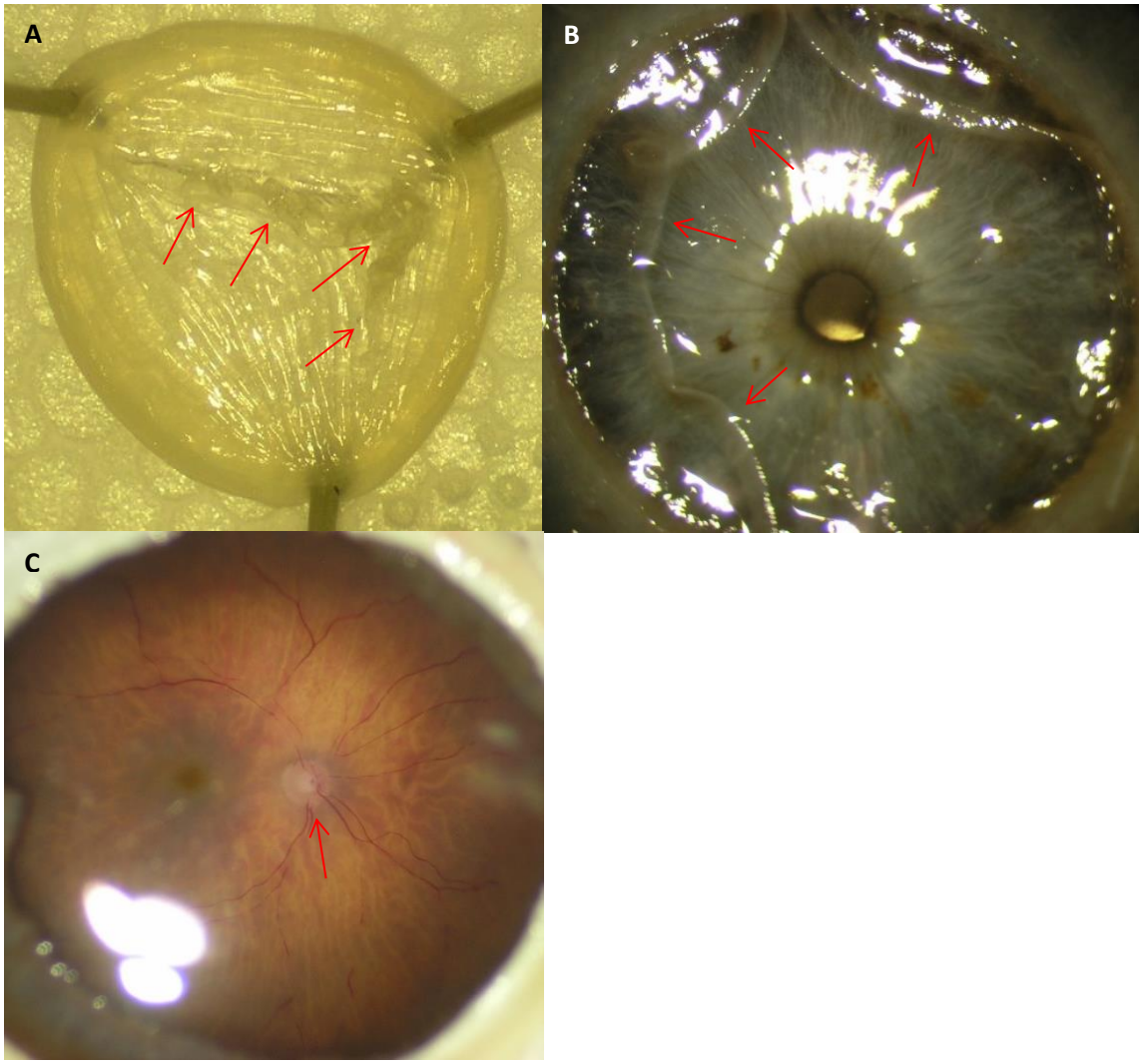

Figure 20: Tissue dissection for collection of A) Corneal endothelium being separated from corneal stromal button; B) Trabecular meshwork being dissected from the ciliary body and C) optic nerve head prior to collection with 3 mm biopsy punch. Red arrows indicate the tissue of interest.

The same dissection protocol was followed for each cadaveric specimen with omission of ocular samples that were collected for corneal transplantation where applicable. The following protocol describes the dissection procedure for a complete eye globe. Firstly, the optic nerve was transected by scalpel at its insertion at the posterior scleral aperture and collected after stripping of the meninges. The ocular specimen was then loosely secured by encirclement with wet gauze strip and

immobilized within an overturned 50mL conical tube lid. Using a spatula, the corneal epithelium is scraped from the anterior surface with only the non-limbal epithelium collected. The limbal epithelium was not collected for this experiment. Once the entire corneal epithelium had been removed, an incision was made at the surgical limbus with a 15 degree straight blade. The incision was extended with the blade to allow curved scissors to cut circumferentially in order to free the remaining cornea. The Descemet's membrane was separated from the corneal stroma with a blunt tipped needle and both tissues were collected separately. A longitudinal cut was made into the limbal cornea and sclera, followed by cutting of the sclera parallel to the limbus at the level of the insertion of the medial rectus tendon approximately 5.5cm from the limbus. The freed strip of sclera was attached at the iridocorneal angle by the trabecular meshwork and separated from the underlying choroid by the suprachoroidal space. The trabecular meshwork was carefully separated from the scleral strip and collected. With the scleral strip removed, the iris and anterior choroid was exposed. Peripheral iris samples were collected with scissors at the root of the iris insertion into the ciliary body and the rest of the iris was removed. A stab incision was made at the level of the pars plana followed by a circumferential cut along the pars plana with the curved scissors freeing the intermediate uvea from the posterior segment of the eye. The zonules and the lens were removed from the intermediate uvea. The pars plicata of the ciliary body was collected by separating it from the pars plana with the curved scissors. The optic nerve head and macula fovea samples were collected using a 3 mm biopsy punch trephine. A retinal break was created using scissors at the peripheral retina approximately 1 cm posterior to the ora serrata. The break was extended 360 degrees using the scissors followed by cutting the vitreous off the inner retinal surface to isolate the retina for collection. With the retina removed, the exposed choroid was collected. Finally, the sclera was collected. Collected tissues were immediately fixed in RNAlater for approximately 5 days prior to storage at -80°C after removal of RNAlater.

6.1.2 RNA extraction and sequencing

Total RNA extraction from each tissue was performed using the TRIzol® (Invitrogen, Carlsbad, CA, USA) extraction protocol as per manufacturer's instructions and stored at -80°C. Only RNase-free reagents and disposables were used to minimize RNA degradation. Each frozen preserved tissue was transferred to a separate 2mL round bottom tube containing 1 mL of TRIzol® reagent. A stainless steel bead was added to the tube for tissue homogenization with the Tissuelyser (QIAGEN, Hilden, Germany). Homogenization was performed in 4 cycles of 2 minutes each at 30 hertz with chilling on ice for 30 seconds between cycles. The homogenized samples were incubated at room temperature for 30 minutes, following which the liquid phase were transferred to 1.5mL Eppendorf tubes. 200µL of chloroform (BDH Chemicals, Kilsyth, VIC, Australia) was added to each tube. The tubes were vortexed vigorously for 15 seconds and incubated at room temperature for 2.5 minutes. The samples were centrifuged at >13000g for 15 minutes at 4°C. Following centrifugation, the sample separated into a pink lower phase, a white fluffy interphase and a clear upper phase. The clear upper phase of each sample containing the total RNA and was pipetted into fresh 1.5mL Eppendorf tubes. RNA was precipitated with 500µL of isopropanol (Sigma Aldrich, St. Louis, Missouri, USA) for 15 minutes at room temperature. Preciptated RNA was pelleted by centrifugation at >13000g at 4°C for 10 minutes. The supernatant was removed and the pellet washed with 1mL of cold 75% ethanol prepared with RNase-free MilliQ water. Final centrifugation was performed at 10000g at 4°C for 5 minutes to re-pellet RNA. After the removal of the supernatant, the RNA was air dried for 10 minutes and dissolved in 15 to 20 µL of RNase-free MilliQ water and stored frozen at -80°C until use.

For pars plicata of the ciliary body, a tissue with high melanin content, the extracted RNA was passed through QIAGEN Genomic-tip 20/G (Catalog #10223, Hilden, Germany) as per manufacturer's instruction for removing the melanin pigment. RNA concentrations were measured by fluorometric quantification on the Qubit® 2.0 Fluorometer (Catalog #Q32866, Carlsbad, USA) using Qubit™ RNA

Assay Kits (Catalog #Q32852, Carlsbad, USA). RNA quality was assessed using Agilent Bioanalyzer 2100 RNA 6000 Nano Assay (Catalog #G2938C, Santa Clara, USA). Samples were included for sequencing only if the RNA integrity number (RIN) scores were greater than or equal to 3.8 and both 28S and 18S ribosomal RNA intensity peaks were prominent (mean RIN = 6.6 ± 1.8).

Library preparation was performed using Bioo Scientific® NEXTflex™ Rapid Directional mRNA-Seq Kit Bundle with RNA-Seq Barcodes and poly(A) beads (Catalog #5138-10, Austin, Texas). 250 nanograms of total RNA from each tissue sample was used for sequencing without pooling of any samples. Sixteen cycles of PCR was completed for the final library. Sequencing was conducted on the Illumina NextSeq® 500 using High Output v2 Kit (75 cycles) (Catalog #FC-404-2005, San Diego, USA). Samples were sequenced contemporaneously to minimize batch effects over a total of three runs at the South Australian Health and Medical Research Institute. A low level of internal sequencing control PhiX (Illumina) was spiked into every run pool for monitoring and troubleshooting.

6.1.3 Post-sequencing data analysis

The quality and number of the reads for each sample was assessed using FASTQC v0.11.3 (http://www.bioinformatics.babraham.ac.uk/projects/fastqc/). Trimgalore v0.4.0 (http://www.bioinformatics.babraham.ac.uk/projects/trim_galore/) was used to trim adaptors from reads where necessary and to trim low quality bases, with a Phred score of less than 28, from the ends of reads. Reads shorter than 20 bases after trimming were discarded. All reads which passed every quality control step were then aligned to the human genome (GRCh38 assembly) using TopHat v2.1.1 (Trapnell et al., 2009, Kim et al., 2013) allowing for 2 mismatches per read. Reads that did not uniquely align to the genomic template were discarded. Uniquely aligned reads were assigned an Ensembl version 84 annotated human gene ID using the union model in HTSeq-count v0.6.0 (Anders et al., 2015). Count data was normalised across libraries using the trimmed mean of M-values (TMM)

normalisation method (Bullard et al., 2010) in Bioconductor R package EdgeR v3.10.2 (Robinson et al., 2010). Comparison with previously available public domain data (Wagner et al., 2013) was conducted using scatterplot and linear regression modelling with the PLIER score for microarray data used as the surrogate for read counts. Correlation analysis was performed using SPSS statistics software v20 (IBM, NY, USA). Gene differential expression was analysed using EdgeR software with Benjamini Hochberg adjustment (Benjamini and Hochberg, 1995) applied for false discovery rate correction. Differential expression was calculated between each tissue and all other tissues combined. Scatterplots and linear regression modelling was performed in R statistics using variations of the following code.

```
plot(log10(d$OTDB+10e-10), log10(d$RNAseq+10e-10), xlab="OTDB tissue", ylab="RNAseq tissue",
xlim = c(-0.5,4), ylim = c(-3,4.5), cex=0.2, abline(lm(log10(d$OTDB+10e-10)~ log10(d$RNAseq+10e-
10)), col="red"))
```

EdgeR package was downloaded from Bioconductor website within R statistic software.

```
source("http://bioconductor.org/biocLite.R")
biocLite("edgeR")
```

Raw counts data was loaded into R statistics software for analysis with EdgeR.

```
library(edgeR)
setwd("working directory")
D <- as.matrix(read.table("Counts.txt", header=TRUE, row.names = 1))
g.all <-
factor(c(0,0,0,0,0,0,1,1,1,1,1,2,2,2,2,2,2,2,3,3,3,3,3,3,4,4,4,4,4,4,5,5,5,5,5,5,6,6,6,6,6,6,7,7,7,7,7,7,8,8
```

```
,8,8,8,9,9,9,9,9,9,9,0,0,0)) ## corneal epithelium (CE) = 0, corneal stroma (CS) = 1, corneal endothelium/Descemet's membrane (DM) = 2, trabecular meshwork (TM) = 3, ciliary body/pars plicata (PP) = 4, retina (R) = 5, optic nerve head (ONH) = 6, optic nerve (ON) = 7, peripheral iris (PI) = 8, sclera (S) = 9
```

Count data normalization and capture quality filtering was performed with EdgeR.

```
d.all <- DGEList(counts = D, group = g.all)
cpm.d.all <- cpm(d.all)
d.all <- d.all[rowSums(cpm.d.all > 1) >=3, ] ## filter for genes with at least counts per million of 1 in 3 samples
d.all <- calcNormFactors(d.all, method=c("TMM"))
d.all <- estimateTagwiseDisp(d.all)
```

Each sample was labelled with a different colour for the multidimensional scaling analysis plot.

```
lab.tissue <- c("CE", "CE", "CE", "CE", "CE", "CE", "CS", "CS", "CS", "CS", "CS", "DM", "DM", "DM", "DM", "DM", "DM", "DM", "DM", "DM", "DM", "TM", "TM", "TM", "TM", "TM", "TM", "CB", "CB", "CB", "CB", "CB", "CB", "Retina", "Retina", "Retina", "Retina", "Retina", "Retina", "ONH", "ONH", "ONH", "ONH", "ONH", "ONH", "ON", "ON", "ON", "ON", "ON", "ON", "PI", "PI", "PI", "PI", "PI", "S", "S", "S", "S", "S", "S", "S", "CE", "CE", "CE")
cols <- c("blue1", "blue1", "blue1", "blue1", "blue1", "blue1", "cyan1", "cyan1", "cyan1", "cyan1", "cyan1", "green1", "green1", "green1", "green1", "green1", "green1", "green1", "purple2", "purple2", "purple2", "purple2", "purple2", "purple2", "tan4", "tan4", "tan4", "tan4", "tan4", "tan4", "red1", "red1", "red1", "red1", "red1", "red1", "gold", "gold", "gold", "gold", "gold", "gold", "orange1", "orange1", "orange1", "orange1", "orange1", "orange1", "steelblue2", "steelblue2",
```

```
"steelblue2", "steelblue2", "steelblue2", "black", "black", "black", "black", "black", "black", "black",
"blue1", "blue1", "blue1")
pdf(file="MDS_tissue.pdf", height=8, width=8 )
plotMDS(d.all, xlim=c(-5,4), labels=lab.tissue, cex=1, col = cols, top = 2000)
dev.off()
```

Data dispersion plot was also generated to assess the relative variance of expression between biological replicates.

```
pdf(file="Disp.pdf", height=6, width=6 )
plotBCV(d.all, col.trend= "blue")
dev.off()
```

P values for differential expression per gene was calculated with EdgeR comparing each tissue to the others combined as the control.

```
D <- as.matrix(read.table("Counts.txt", header=TRUE, row.names = 1))
g.CE <-
factor(c(0,0,0,0,0,0,1,1,1,1,1,1,1,1,1,1,1,1,1,1,1,1,1,1,1,1,1,1,1,1,1,1,1,1,1,1,1,1,1,1,1,1,1,1,1,1,1,1,1,1,1
,1,1,1,1,1,1,1,1,1,1,0,0,0)) ## CE = 0, others = 1
d.CE <- DGEList(counts = D, group = g.CE)
cpm.d.CE <- cpm(d.CE)
d.CE <- d.CE[rowSums(cpm.d.CE > 1) >=3, ] ## filter for genes with at least counts per million of 1 in 3
samples
d.CE <- calcNormFactors(d.CE, method=c("TMM"))
d.CE <- estimateTagwiseDisp(d.CE)
CE_others <- exactTest(d.CE, pair=c("1","0"))
```

```
write.table(CE_others$table, file="CE_others.txt", sep="\t", col.names=TRUE, row.names=TRUE)
```

```
g.CS <-
factor(c(1,1,1,1,1,1,0,0,0,0,0,1,1,1,1,1,1,1,1,1,1,1,1,1,1,1,1,1,1,1,1,1,1,1,1,1,1,1,1,1,1,1,1,1,1,1,1,1,1,1
,1,1,1,1,1,1,1,1,1,1,0,0,0)) ## CS = 0, others = 1
d.CS <- DGEList(counts = D, group = g.CS)
cpm.d.CS <- cpm(d.CS)
d.CS <- d.CS[rowSums(cpm.d.CS > 1) >=3, ] ## filter for genes with at least counts per million of 1 in 3
samples
d.CS <- calcNormFactors(d.CS, method=c("TMM"))
d.CS <- estimateTagwiseDisp(d.CS)
CS_others <- exactTest(d.CS, pair=c("1","0"))
write.table(CS_others$table, file="CS_others.txt", sep="\t", col.names=TRUE, row.names=TRUE)
```

```
g.DM <-
factor(c(1,1,1,1,1,1,1,1,1,1,1,0,0,0,0,0,0,0,1,1,1,1,1,1,1,1,1,1,1,1,1,1,1,1,1,1,1,1,1,1,1,1,1,1,1,1,1,1,1,1
,1,1,1,1,1,1,1,1,1,1,1,1,1)) ## DM = 0, others = 1
d.DM <- DGEList(counts = D, group = g.DM)
cpm.d.DM <- cpm(d.DM)
d.DM <- d.DM[rowSums(cpm.d.DM > 1) >=3, ] ## filter for genes with at least counts per million of 1
in 3 samples
d.DM <- calcNormFactors(d.DM, method=c("TMM"))
d.DM <- estimateTagwiseDisp(d.DM)
DM_others <- exactTest(d.DM, pair=c("1","0"))
write.table(DM_others$table, file="DM_others.txt", sep="\t", col.names=TRUE, row.names=TRUE)
```

```
g.TM <-
factor(c(1,1,1,1,1,1,1,1,1,1,1,1,1,1,1,1,1,0,0,0,0,0,0,1,1,1,1,1,1,1,1,1,1,1,1,1,1,1,1,1,1,1,1,1,1,1,1,1
,1,1,1,1,1,1,1,1,1,1,1,1,1)) ## TM = 0, other = 1
d.TM <- DGEList(counts = D, group = g.TM)
cpm.d.TM <- cpm(d.TM)
d.TM <- d.TM[rowSums(cpm.d.TM > 1) >=3, ] ## filter for genes with at least counts per million of 1
in 3 samples
d.TM <- calcNormFactors(d.TM, method=c("TMM"))
d.TM <- estimateTagwiseDisp(d.TM)
TM_others <- exactTest(d.TM, pair=c("1","0"))
write.table(TM_others$table, file="TM_others.txt", sep="\t", col.names=TRUE, row.names=TRUE)
```

```
g.PP <-
factor(c(1,1,1,1,1,1,1,1,1,1,1,1,1,1,1,1,1,1,1,1,1,1,1,0,0,0,0,0,0,1,1,1,1,1,1,1,1,1,1,1,1,1,1,1,1,1,1,1
,1,1,1,1,1,1,1,1,1,1,1,1,1)) ## PP = 0, others = 1
d.PP <- DGEList(counts = D, group = g.PP)
cpm.d.PP <- cpm(d.PP)
d.PP <- d.PP[rowSums(cpm.d.PP > 1) >=3, ] ## filter for genes with at least counts per million of 1 in 3
samples
d.PP <- calcNormFactors(d.PP, method=c("TMM"))
d.PP <- estimateTagwiseDisp(d.PP)
PP_others <- exactTest(d.PP, pair=c("1","0"))
write.table(PP_others$table, file="PP_others.txt", sep="\t", col.names=TRUE, row.names=TRUE)
```

```
g.R <-
factor(c(1,1,1,1,1,1,1,1,1,1,1,1,1,1,1,1,1,1,1,1,1,1,1,1,1,1,1,0,0,0,0,0,0,1,1,1,1,1,1,1,1,1,1,1,1,1
,1,1,1,1,1,1,1,1,1,1,1,1,1,1,1,1,1,1,1)) ## Retina = 0, other = 1
d.R <- DGEList(counts = D, group = g.R)
cpm.d.R <- cpm(d.R)
d.R <- d.R[rowSums(cpm.d.R > 1) >=3, ] ## filter for genes with at least counts per million of 1 in 3
samples
d.R <- calcNormFactors(d.R, method=c("TMM"))
d.R <- estimateTagwiseDisp(d.R)
R_others <- exactTest(d.R, pair=c("1","0"))
write.table(R_others$table, file="R_others.txt", sep="\t", col.names=TRUE, row.names=TRUE)
```

```
g.ONH <-
factor(c(1,1,1,1,1,1,1,1,1,1,1,1,1,1,1,1,1,1,1,1,1,1,1,1,1,1,1,1,1,1,1,0,0,0,0,0,0,1,1,1,1,1,1,1,1
,1,1,1,1,1,1,1,1,1,1,1,1,1,1,1,1,1,1,1)) ## ONH = 0, other = 1
d.ONH <- DGEList(counts = D, group = g.ONH)
cpm.d.ONH <- cpm(d.ONH)
d.ONH <- d.ONH[rowSums(cpm.d.ONH > 1) >=3, ] ## filter for genes with at least counts per million
of 1 in 3 samples
d.ONH <- calcNormFactors(d.ONH, method=c("TMM"))
d.ONH <- estimateTagwiseDisp(d.ONH)
ONH_others <- exactTest(d.ONH, pair=c("1","0"))
write.table(ONH_others$table, file="ONH_others.txt", sep="\t", col.names=TRUE, row.names=TRUE)
```

```
g.ON <-
factor(c(1,1,1,1,1,1,1,1,1,1,1,1,1,1,1,1,1,1,1,1,1,1,1,1,1,1,1,1,1,1,1,1,1,1,1,1,1,1,1,1,1,1,1,1,1,0,0,0,0,0,0,1,1
,1,1,1,1,1,1,1,1,1,1,1,1,1)) ## ON = 0, other = 1
d.ON <- DGEList(counts = D, group = g.ON)
cpm.d.ON <- cpm(d.ON)
d.ON <- d.ON[rowSums(cpm.d.ON > 1) >=3, ] ## filter for genes with at least counts per million of 1
in 3 samples
d.ON <- calcNormFactors(d.ON, method=c("TMM"))
d.ON <- estimateTagwiseDisp(d.ON)
ON_others <- exactTest(d.ON, pair=c("1","0"))
write.table(ON_others$table, file="ON_others.txt", sep="\t", col.names=TRUE, row.names=TRUE)
```

```
g.PI <-
factor(c(1,1,1,1,1,1,1,1,1,1,1,1,1,1,1,1,1,1,1,1,1,1,1,1,1,1,1,1,1,1,1,1,1,1,1,1,1,1,1,1,1,1,1,1,1,1,1,1,1,1,1,0,0
,0,0,0,1,1,1,1,1,1,1,1,1,1)) ## PI = 0, other = 1
d.PI <- DGEList(counts = D, group = g.PI)
cpm.d.PI <- cpm(d.PI)
d.PI <- d.PI[rowSums(cpm.d.PI > 1) >=3, ] ## filter for genes with at least counts per million of 1 in 3
samples
d.PI <- calcNormFactors(d.PI, method=c("TMM"))
d.PI <- estimateTagwiseDisp(d.PI)
PI_others <- exactTest(d.PI, pair=c("1","0"))
write.table(PI_others$table, file="PI_others.txt", sep="\t", col.names=TRUE, row.names=TRUE)
```

```
g.S <-
factor(c(1,1,1,1,1,1,1,1,1,1,1,1,1,1,1,1,1,1,1,1,1,1,1,1,1,1,1,1,1,1,1,1,1,1,1,1,1,1,1,1,1,1,1,1,1,1,1,1,1,1
,1,1,1,0,0,0,0,0,0,0,1,1,1)) ## S = 0, other = 1
d.S <- DGEList(counts = D, group = g.S)
cpm.d.S <- cpm(d.S)
d.S <- d.S[rowSums(cpm.d.S > 1) >=3, ] ## filter for genes with at least counts per million of 1 in 3
samples
d.S <- calcNormFactors(d.S, method=c("TMM"))
d.S <- estimateTagwiseDisp(d.S)
S_others <- exactTest(d.S, pair=c("1","0"))
write.table(S_others$table, file="S_others.txt", sep="\t", col.names=TRUE, row.names=TRUE)
```

The resulting EdgeR output files do not have any identifying labels within the files denoting the comparisons. Therefore, it was necessary to add filename labels inside all files for easy identification prior to merging the data within one common datasheet for convenient analysis. The quickest method to achieve this involved placing all EdgeR output files in the same folder and inserting the filename as the first cell of the file using the following UNIX command.

```
$ for filename in *; do replacement=$(echo $filename | sed -e 's|^.*/||' -e 's|\.[^\.]*$||'); [ -f
"$filename" ] && sed -i "1s/^/$replacement\t/" "$filename"; done
```

P-value adjustment with Benjamini-Hochberg and Bonferroni corrections were performed in R statistics with the results appended onto the output files from EdgeR.

```
files <- list.files(pattern="*.txt")
lapply(files, function(i) {
x <- read.table(i, sep = "\t", header=TRUE)
```

```
BH <- p.adjust(x$PValue, 'BH')
Bon <- p.adjust(x$PValue, 'bonferroni')
y <- cbind(x,BH, Bon)
write.table(y, file = i, sep="\t", quote=F, row.names=F, col.names=T)
})
```

All newline delimiters in output files were replaced with tab delimiters for data manipulation in UNIX with the following command.

```
$ find ./ -type f -exec sed -i "s/\n/\t/g" {} \;
```

The output of EdgeR labels all genes using ENSEMBL identifiers. Therefore HGNC gene identifiers for each ENSEMBL transcript ID were downloaded from the ENSEMBL BioMart webtool (https://www.ensembl.org/biomart/martview) for annotation purposes. A tab-delimited file (i.e. ENSEMBL_cpm1x3.txt) was made using the equivalent HGNC identifier for each captured transcript extracted from the ENSEMBL file. All EdgeR output files were merged together and with the constructed annotation file to produce an annotated final output using UNIX.

```
$ paste *.txt > All.txt
$ paste ENSEMBL_cpm1x3.txt All.txt > Final.txt
```

Heat maps were plotted in R statistics using ggplot2 to visualize counts per million metric for genes of interest. To accommodate the wide dynamic range of the expression data, log transformation was performed prior to data visualization. The “melt” function in R statistics transformed any table in the form of variable x by variable y into a 3-column table with variable x in column 1, variable y in column 2 and the value in column 3.

```
Library(ggplot2, reshape2)
```

```
x <- read.table("Input_logcpm.txt", header=TRUE, sep="\t")
melt <- melt(x)
names(melt) <- c("Genename", "Tissue", "logCPM")
cpm <- read.table("Input_cpm.txt", header=TRUE, sep="\t")
cpm <- round(cpm, 0)
cpm <- melt(cpm)
names(cpm) <- c("Genename", "Tissue", "CPM")
melt$Tissue <- factor(melt$Tissue, levels = unique(melt$Tissue))
melt$Genename <- factor(melt$Genename, levels = unique(rev(melt$Genename)))
cpm$Tissue <- factor(cpm$Tissue, levels = unique(cpm$Tissue))
cpm$Genename <- factor(cpm$Genename, levels = unique(rev(cpm$Genename)))
ggplot(melt, aes(x=Tissue, y=Genename, fill = logCPM)) + geom_tile(color = "white") +
geom_text(aes(x=Tissue, y=Genename, label = logCPM), color = "black", size = 3) +
scale_fill_gradient2(low = "white", mid = "deepskyblue2",  high = "red", midpoint = 4) + ylab("Gene
name") + theme(axis.title.x = element_text(size = 14, face = "bold"), axis.title.y = element_text(size =
14, face = "bold"), axis.text.y = element_text(face = "italic"), axis.ticks = element_blank(),
panel.border = element_rect(fill=NA, size = 2, color = "gray90"), panel.background =
element_blank(), panel.grid = element_blank())
ggsave("Output.png")
```

6.1.4 Pathway analysis of differentially expressed genes

The top 500 differentially expressed genes in each tissue were assessed with pathway and network analysis using InnateDB (Lynn et al., 2008). Pathway over-representation was calculated in InnateDB using hypergeometric distribution tests for the top 500 differentially expressed genes in each tissue. P-values were adjusted using the Benjamini and Hochberg method (Lynn et al., 2008). Network

analysis is based on the observation that biological processes are driven by complex, interwoven networks of molecular interactions and not by discrete macromolecules or disconnected linear pathways (Charitou et al., 2016). A network of experimentally validated molecular interactions that occur between input genes and their first order interactors was constructed for each tissue using the top 500 differentially expressed genes using InnateDB (Lynn et al., 2008). Cytoscape v3.4.0. (Shannon et al., 2003) was used to visualize the constructed networks and remove duplicated interactions, self-interactions and interactions involving the pervasive molecular interactor ubiquitin C (UBC). The jActiveModules plugin (Ideker et al., 2002) was implemented to identify sub-networks that were both densely connected and enriched in each tissue-specific network with the following parameters: number of modules = 5; overlap threshold = 0.3 and search depth = 2. Top biological processes in each sub-network with at least 20 genes were annotated using InnateDB gene ontology and pathway analysis tools. Sub-network analysis increases the power of detection for key underlying biological mechanisms within each tissue by further reducing the background expression signals.

6.2 Results

6.2.1 Sequencing metrics

63 samples from a total of 21 different donors were sequenced for 10 ocular tissues of interest. The goal was to include 6 samples of every examined tissue for sequencing, however some samples did not produce sufficient good quality RNA and were replaced with additional samples of another tissue. At least six samples per tissue were sequenced except the corneal stroma and peripheral iris, for which five samples of each were sequenced. The mean RNA integrity number of sequenced samples was 6.6 ± 1.8 (Table 13). A total of 58,302 gene transcripts were captured in the ten ocular tissues with an average capture depth of 48.1 million mapped reads per sample. After filtering for sequencing noise to retain only transcripts with ≥1 count per million reads or more expression in at

least 3 samples, a total of 22,701 transcripts representing 22,670 genes were retained. The multidimensional scaling analysis of all samples demonstrated consistent clustering of expression signatures within each tissue type (Figure 21). There was some degree of overlap of expression between the corneal tissues (corneal epithelium, stroma and endothelium) and the uveal tissues (trabecular meshwork, peripheral iris and ciliary body), as would be expected.

Table 13: Characteristics of the 63 human cadaveric ocular tissue samples used for RNA sequencing. RIN = RNA integrity number

Sample No.	Donor No.	Tissue	Age	Sex	Hours post-mortem	RIN
1	8	Corneal epithelium	58	Male	11	8.5
2	9	Corneal epithelium	92	Male	12	9
3	10	Corneal epithelium	79	Male	5	6.5
4	11	Corneal epithelium	58	Male	5.5	8.9
5	12	Corneal epithelium	74	Male	6.5	10
6	13	Corneal epithelium	80	Male	10	9.6
7	6	Corneal epithelium	90	Male	3	8.1
8	8	Corneal epithelium	55	Female	19	8.9
9	9	Corneal epithelium	50	Male	6	8.8
10	15	Corneal stroma	58	Male	11	7.6
11	17	Corneal stroma	92	Male	12	6.1
12	6	Corneal stroma	79	Male	5	6.7
13	7	Corneal stroma	79	Male	13	4.3
14	9	Corneal stroma	82	Male	24	4.9
15	11	Corneal endothelium	58	Male	11	4.8
16	14	Corneal endothelium	66	Male	14	5.3
17	16	Corneal endothelium	79	Male	5	6.8
18	17	Corneal endothelium	74	Male	6.5	6.2
19	9	Corneal endothelium	72	Male	11.5	6.8
20	10	Corneal endothelium	55	Female	19	3

21	11	Corneal endothelium	82	Male	24	2.9
22	12	Trabecular meshwork	79	Male	5	7
23	13	Trabecular meshwork	58	Male	5.5	7
24	15	Trabecular meshwork	74	Male	6.5	7.2
25	6	Trabecular meshwork	80	Male	10	6.8
26	9	Trabecular meshwork	90	Male	3	7.3
27	10	Trabecular meshwork	79	Male	13	7.7
28	11	Ciliary body	58	Male	11	8.4
29	13	Ciliary body	79	Male	5	8.2
30	14	Ciliary body	58	Male	5.5	9.5
31	3	Ciliary body	74	Male	6.5	8.9
32	4	Ciliary body	90	Male	3	8.7
33	9	Ciliary body	72	Male	11.5	7.9
34	11	Neural retina	76	Female	21	7.1
35	14	Neural retina	76	Male	15	4.3
36	15	Neural retina	79	Male	5	7
37	2	Neural retina	74	Male	6.5	6.9
38	7	Neural retina	72	Male	11.5	5.5
39	9	Neural retina	79	Male	13	6.8
40	11	Optic nerve head	70	Female	11	6
41	13	Optic nerve head	66	Male	14	5.6
42	15	Optic nerve head	79	Male	5	6.6
43	1	Optic nerve head	74	Male	6.5	6.2
44	4	Optic nerve head	90	Male	3	6.2
45	7	Optic nerve head	79	Male	13	6.1
46	9	Optic nerve	61	Male	5	3.9
47	11	Optic nerve	76	Male	15	4.4
48	15	Optic nerve	66	Male	14	3.8
49	5	Optic nerve	79	Male	5	4.5
50	6	Optic nerve	74	Male	6.5	4.2
51	9	Optic nerve	79	Male	13	4.3
52	12	Peripheral iris	70	Female	3	8

53	13	Peripheral iris	58	Male	11	8.6
54	7	Peripheral iris	79	Male	5	8
55	10	Peripheral iris	80	Male	10	8.6
56	15	Peripheral iris	90	Male	3	7.5
57	18	Sclera	66	Male	14	5.2
58	19	Sclera	58	Male	5.5	5.7
59	20	Sclera	79	Male	13	4
60	21	Sclera	45	Male	12	5.7
61	6	Sclera	50	Male	6	NA
62	16	Sclera	80	Male	12.5	4.8
63	19	Sclera	88	Male	4	4.5

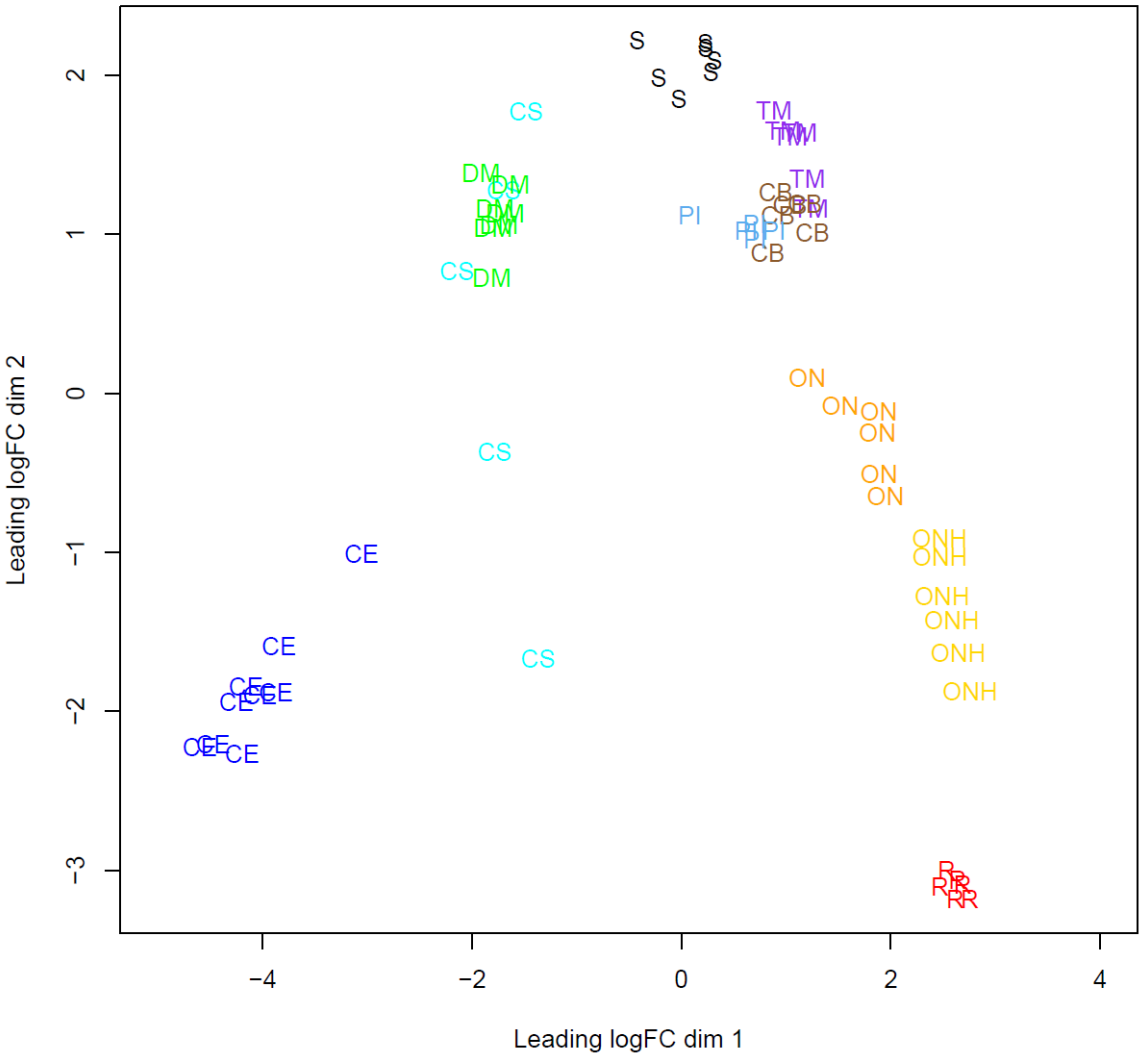

Figure 21: The multidimensional scaling analysis shows clustering of the expression profiles of each tissue. CE = corneal epithelium, CS = corneal stroma, DM = corneal endothelium (Descemet's membrane), TM = trabecular meshwork, PI = peripheral iris, CB = ciliary body (pars plicata), R = retina, ONH = optic nerve head, ON = optic nerve, S = sclera.

6.2.2 Comparison with microarray data

To examine the concordance of our RNAseq data with published microarray gene expression data in the OTDB, PLIER scores from four equivalent tissues (trabecular meshwork, Retina, optic nerve and

optic nerve head) (Wagner et al., 2013) was compared between the two data sets. Figures 22 to 25 show scatter plots of gene expression values with log converted scales and associated spearman rho tests for each tissue comparison. There was significant correlation between the current RNA-seq results and previously published array based expression data (Wagner et al., 2013) with spearman rho coefficients ranging between 0.514 and 0.591.

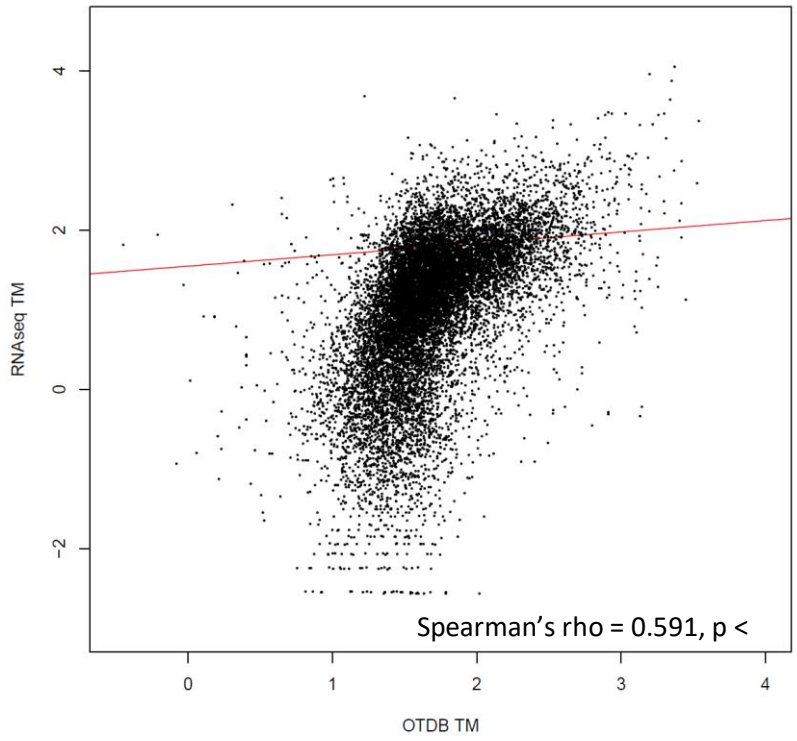

Figure 22: Comparison of gene expression in the trabecular meshwork (TM) between the present RNAseq and previously published microarray gene expression (OTDB) data. Spearman's rho correlation is statistically significant (p <0.01).

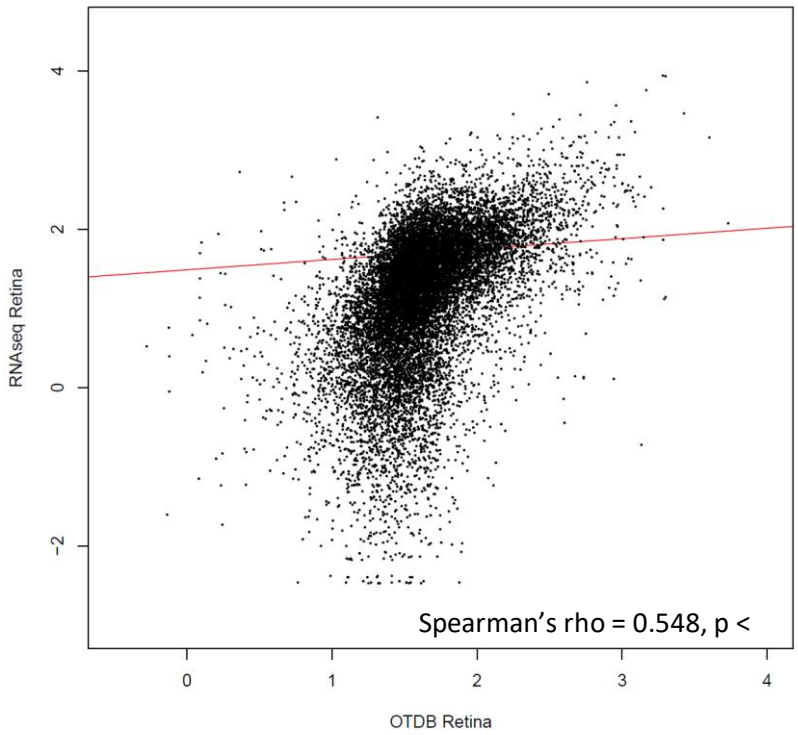

Figure 23: Comparison of gene expression in the retina between the present RNAseq and previously published microarray gene expression (OTDB) data. Spearman's rho correlation is statistically significant (p <0.01)

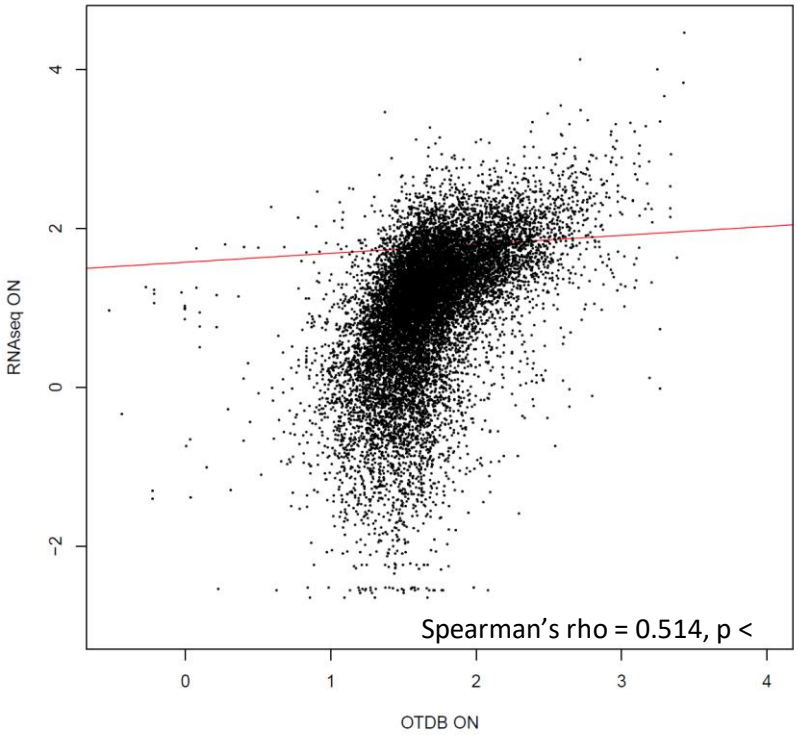

Figure 24: Comparison of gene expression in the optic nerve (ON) between the present RNAseq and previously published microarray gene expression (OTDB) data. Correlation table shows statistically significant correlation.

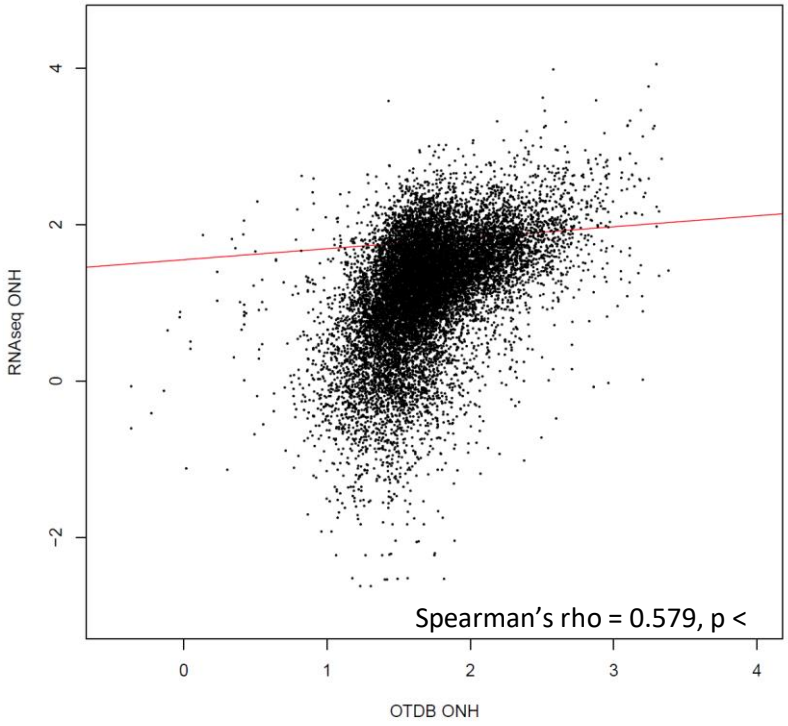

Figure 25: Comparison of gene expression in the optic nerve head (ONH) between the present RNAseq and previously published microarray gene expression (OTDB) data. Correlation table shows statistically significant correlation.

6.2.3 Signature genes

Certain genes are known to be highly and specifically expressed in particular ocular tissues. The validity of our RNAseq expression database was checked against these known signature genes. The genes listed in table 14 are eight such genes with strong experimental evidence for being good tissue marker genes - *KRT12* for corneal epithelium (Nishida et al., 1996), *KERA* for corneal stroma (Diehn et al., 2005), *SLC4A11* for corneal endothelium (Chng et al., 2013), *MYOC* for trabecular meshwork (Tomarev et al., 2003), *OPTC* for ciliary body (Takanosu et al., 2001), *RHO* for retina (Wistow, 2006), *GFAP* for optic nerve (Turkmen et al., 2008) and *CRYBA1* for crystalline lens (Diehn et al., 2005). The crystalline lens was not collected in the present study, but expression of *CRYBA1* was examined to act as a negative control for cross contamination during tissue preparation. The results of our RNAseq expression database concur well with known experimental data.

Table 14: RNAseq tissue expression profile of eight genes with well-known expression signature. The numbers represent mean counts per million. CE = corneal epithelium, CS = corneal stroma, DM = corneal endothelium, TM = trabecular meshwork, PI = peripheral iris, CB = ciliary body, R = retina, ONH = optic nerve head, ON = optic nerve, S = sclera.

Symbol	Name	Signature tissue	CE	CS	DM	TM	PI	CB	R	ONH	ON	S
KRT12	Keratin 12	Corneal epithelium	**19296**	5060	6	0	32	6	0	0	0	12
KERA	Keratocan	Corneal stroma	5	**5765**	2	0	0	1	0	0	0	19
SLC4A11	Solute carrier family 4 member 11	Corneal endothelium	143	229	**3154**	109	3	14	2	351	575	12
MYOC	Myocilin	Trabecular meshwork	49	390	3727	**9118**	1656	924	2	90	3	5235
OPTC	Opticin	Ciliary body	6	0	4	0	1758	**4403**	0	0	0	1
RHO	Rhodopsin	Retina	0	54	0	5	0	0	**5696**	995	4	0
GFAP	Glial fibrillary acidic protein	Optic nerve	0	4	11	19	9	3	592	**9703**	13325	1
CRYBA1	Crystallin beta A1	Crystalline lens	0	0	0	0	0	0	0	0	0	0

6.2.4 Top genes by tissue

The top 20 differentially expressed genes with the highest expression in each target tissue are listed in the tables below (Tables 15 – 24). CPM denotes counts per million, which a normalized measure of gene expression. Comparisons were performed with each individual tissue of interest against the combined expression of all other tissues as control. These comparisons highlighted genes that were highly and selectively expressed in each ocular tissue. The top 500 selectively expressed genes from

each tissue were analyzed with pathway analysis and gene ontology to test the hypothesis that gene expression reflects tissue function (Appendix tables 14 to 23).

In the corneal epithelium, the top expressed genes belonged to the keratin family, which are abundant in most stratified epithelium (Table 15). Transforming growth factor beta induced (*TGFBI*), a gene associated with various corneal dystrophies, was also highly expressed in the corneal epithelium. Other highly expressed genes in the corneal epithelium included collagen genes and desmoplakin (*DSP*), a gene associated with formation of desmosomes that link adjacent epithelial cells. Enriched biological pathways and gene ontology included cell junction organization, cell-cell communication and cornification (Appendix tables 14A and 14B).

Table 15: Top 20 differentially expressed genes in the corneal epithelium ranked by normalized counts. CPM = counts per million.

Gene name	ENSEMBL	CPM	Fold change	P value	Corrected p value
KRT5	ENSG00000186081	19894	28.56	1.37E-05	6.01E-05
KRT12	ENSG00000187242	19297	39.24	1.32E-05	5.8E-05
TGFBI	ENSG00000120708	17269	19.20	1.41E-12	2.65E-11
CLU	ENSG00000120885	15269	2.90	0.000272	0.000862
FTH1	ENSG00000167996	5903	2.41	5.98E-07	3.65E-06
DSP	ENSG00000096696	3760	37.05	7.09E-22	5.88E-20
COL17A1	ENSG00000065618	3525	34.59	4.18E-09	4.11E-08
KRT3	ENSG00000186442	3413	60.17	2.95E-07	1.94E-06
TRIM29	ENSG00000137699	3029	34.70	3.8E-11	5.63E-10
TKT	ENSG00000163931	2803	10.39	1.62E-30	4.9E-28
CRTAC1	ENSG00000095713	2534	21.30	7.22E-16	2.29E-14
PERP	ENSG00000112378	2410	27.35	1.09E-21	8.72E-20
NQO1	ENSG00000181019	2319	16.39	9.41E-18	4.17E-16
SDC1	ENSG00000115884	2236	11.49	2.43E-07	1.64E-06
H19	ENSG00000130600	1916	10.70	3.44E-08	2.81E-07
KRT14	ENSG00000186847	1860	20.50	3.67E-05	0.000146
CXCL14	ENSG00000145824	1860	8.60	2.07E-10	2.69E-09
TACSTD2	ENSG00000184292	1704	34.87	1.13E-09	1.27E-08
PAX6	ENSG00000007372	1638	11.49	3.53E-09	3.52E-08
MYH14	ENSG00000105357	1627	13.90	7.14E-18	3.2E-16

In the corneal stroma, the most abundantly expressed genes belonged to extracellular matrix structural proteins such as collagen and proteoglycans including decorin (*DCN*), lumican (*LUM*) and keratocan (*KERA*) (Table 16). Keratocan expression is known to be associated with the corneal stromal ectatic condition keratoconus. Enriched pathways and gene ontology in the corneal stroma included collagen formation and organization, proteoglycan synthesis, positive regulation of fibroblasts and negative regulation of T cell migration, which emphasize the immune privilege of the cornea (Appendix table 15A and 15B).

Table 16: Top 20 differentially expressed genes in the corneal stroma ranked by normalized counts. CPM = counts per million.

Gene name	ENSEMBL	CPM	Fold change	P value	Corrected p value
DCN	ENSG00000011465	38878	17.42	4.11E-10	2.28E-07
APOD	ENSG00000189058	21178	7.10	1.19E-05	0.000633
ALDH3A1	ENSG00000108602	21063	18.37	1.25E-05	0.000662
ENO1	ENSG00000074800	6093	2.19	0.021478	0.090237
KERA	ENSG00000139330	5766	890.32	9.06E-23	2.94E-19
COL12A1	ENSG00000111799	4361	8.40	2.32E-05	0.001005
COL6A2	ENSG00000142173	4096	7.47	1.38E-06	0.000147
LUM	ENSG00000139329	3628	41.12	6.66E-22	1.51E-18
HTRA1	ENSG00000166033	2861	9.60	7.36E-22	1.52E-18
LDHA	ENSG00000134333	2842	2.22	0.00156	0.016545
COL6A1	ENSG00000142156	2557	5.15	6.41E-07	8.17E-05
ITGBL1	ENSG00000198542	2474	12.90	8.25E-08	1.72E-05
THBS4	ENSG00000113296	2393	4.78	0.005432	0.036875
LRP1	ENSG00000123384	2309	1.95	0.000411	0.007073
CST3	ENSG00000101439	1929	2.16	0.003439	0.027441
COL6A3	ENSG00000163359	1918	17.03	2.78E-14	2.87E-11
AQP1	ENSG00000240583	1736	3.35	0.007176	0.043875
SOD3	ENSG00000109610	1685	4.76	0.000252	0.005111
ITGB4	ENSG00000132470	1585	3.12	1.92E-05	0.00087
STEAP4	ENSG00000127954	1429	13.87	3.82E-12	2.71E-09

The most highly expressed genes in the corneal endothelial belonged to mitochondrially encoded oxidative phosphorylation related genes (Table 17). This result is in concordance with the knowledge that the corneal endothelium contains an abundance of mitochondria and its dysfunction leads to Fuch's endothelial dystrophy, a disease of mitochondrial damage (Miyai, 2018). Pathway and gene ontology analysis of the genes showing selectively expression in the corneal endothelium highlighted mitochondrial oxidative phosphorylation related processes as the key biological processes involved (Appendix table 16A and 16B).

Table 17: Top 20 differentially expressed genes in the corneal endothelium ranked by normalized counts. CPM = counts per million.

Gene name	ENSEMBL	CPM	Fold change	P value	Corrected p value
MT-ND4	ENSG00000198886	120339	12.22	6.33E-35	4.43E-32
MT-CO1	ENSG00000198804	112628	12.67	5.34E-39	5.51E-36
MT-ND5	ENSG00000198786	54823	20.84	5.17E-59	2.35E-55
MT-CYB	ENSG00000198727	42902	9.64	2.3E-32	1.09E-29
MT-CO3	ENSG00000198938	42716	10.86	3.59E-33	1.94E-30
MT-CO2	ENSG00000198712	41174	11.44	3.28E-30	1.29E-27
MT-ATP6	ENSG00000198899	36424	7.89	2.98E-22	5.99E-20
MT-ND1	ENSG00000198888	31005	6.70	1.93E-14	1.75E-12
MTCO1P12	ENSG00000237973	29391	12.86	2.94E-40	3.71E-37
MTATP6P1	ENSG00000248527	12850	7.82	1.78E-22	3.74E-20
MT-ND4L	ENSG00000212907	7438	15.20	8.26E-46	1.7E-42
MTND2P28	ENSG00000225630	5824	5.57	3.89E-11	1.99E-09
MTCO3P12	ENSG00000198744	5023	11.51	1.48E-35	1.09E-32
MT-ND3	ENSG00000198840	4653	7.29	4.25E-16	4.98E-14
GAPDH	ENSG00000111640	4010	3.59	3.16E-15	3.4E-13
MTND1P23	ENSG00000225972	3829	6.83	4.03E-14	3.42E-12
APP	ENSG00000142192	3159	8.44	2.57E-53	9.73E-50
SLC4A11	ENSG00000088836	3154	43.66	5.75E-21	1E-18
MT-ATP8	ENSG00000228253	2364	12.06	3.34E-33	1.85E-30
MTCO2P12	ENSG00000229344	2277	11.81	6.56E-30	2.48E-27

The genes showing highest selective expression in the trabecular meshwork included myocilin and contractile filaments such as myosin heavy chain 11 (*MYH11*), filamin A (*FLNA*) and actin alpha 2 (*ACTA2*) (Table 18). Myocilin was extensively discussed in this thesis as the most common monogenic cause of POAG. The most enriched biological processes in the trabecular meshwork included smooth muscle contraction, extracellular matrix interactions and focal adhesion (Appendix table 17A and 17B).

Table 18: Top 20 differentially expressed genes in the trabecular meshwork ranked by normalized counts. CPM = counts per million.

Gene name	ENSEMBL	CPM	Fold change	P value	Corrected p value
MYH11	ENSG00000133392	11090	20.58	6.82E-09	2.28E-06
MYOC	ENSG00000034971	9118	5.03	0.005735	0.078138
FLNA	ENSG00000196924	4474	5.05	5.48E-11	3.55E-08
MYLK	ENSG00000065534	2905	8.96	4.2E-06	0.000456
A2M	ENSG00000175899	2896	7.26	8.47E-06	0.000801
TNS1	ENSG00000079308	2830	4.65	2.86E-05	0.002081
MYL9	ENSG00000101335	2786	8.41	1.55E-06	0.000219
ACTA2	ENSG00000107796	2314	8.38	1.12E-05	0.001002
ATP2A1	ENSG00000196296	2111	15.56	3.1E-06	0.000375
TPM2	ENSG00000198467	2101	14.68	3.14E-16	1.19E-12
ATP2A2	ENSG00000174437	2080	6.76	1.26E-14	1.79E-11
PPP1R12B	ENSG00000077157	1449	8.07	1.23E-08	3.63E-06
TAGLN	ENSG00000149591	1423	6.11	1.97E-05	0.001555
TPM1	ENSG00000140416	1420	8.99	6.03E-16	1.52E-12
DES	ENSG00000175084	1331	18.19	1.2E-06	0.000177
HSPG2	ENSG00000142798	1179	4.24	4.34E-06	0.000461
FLNC	ENSG00000128591	1171	11.21	7.46E-07	0.000118
TLN1	ENSG00000137076	1107	2.71	1.51E-05	0.001284
ITPKB	ENSG00000143772	1088	5.20	7.9E-05	0.004483
MRVI1	ENSG00000072952	1005	9.67	3.84E-06	0.000428

The top differentially expressed genes in the peripheral iris the were related to the immune system, such as immunoglobins *IGHG1*, *IGKC* and *IGHG2*, and melanin pigment formation, such as dopachrome tautomerase (*DCT*) and premelanosome protein (*PMEL*) (Table 18). Cytochrome P450 family 1 subfamily B member 1 (*CYP1B1*), the most common monogenic cause of primary congenital glaucoma was also abundantly expressed in the peripheral iris. Biological processes showing the greatest enrichment included complement activation and immune responses (Appendix table 18A and 18B).

Table 19: Top 20 differentially expressed genes in the peripheral iris ranked by normalized counts. CPM = counts per million.

Gene name	ENSEMBL	CPM	Fold change	P value	Corrected p value
IGHG1	ENSG00000211896	6967	139.67	1.06E-10	4.08E-08
IGKC	ENSG00000211592	3504	64.56	3.98E-09	1.04E-06
DCT	ENSG00000080166	3113	25.47	8.62E-09	2.08E-06
PMEL	ENSG00000185664	2817	23.25	5.93E-10	1.95E-07
GPNMB	ENSG00000136235	1610	6.52	3.96E-07	6.03E-05
TYRP1	ENSG00000107165	1552	7.11	0.001481	0.049506
SLC7A5	ENSG00000103257	1052	7.67	5.82E-09	1.45E-06
CYP1B1	ENSG00000138061	1050	5.70	0.000659	0.027845
MT2A	ENSG00000125148	899	3.71	0.001453	0.048875
KANK2	ENSG00000197256	827	3.63	0.000312	0.015665
ZFAND5	ENSG00000107372	826	2.79	0.000143	0.008347
IGHG2	ENSG00000211893	692	63.67	3.12E-08	6.1E-06
RELN	ENSG00000189056	678	18.78	1.46E-10	5.33E-08
STC1	ENSG00000159167	629	9.64	5.81E-07	7.99E-05
VAT1	ENSG00000108828	611	3.69	2.98E-07	4.59E-05
HHATL	ENSG00000010282	606	12.39	2.31E-05	0.001788
IGHG4	ENSG00000211892	563	87.03	2.1E-09	6.11E-07
IGLC2	ENSG00000211677	561	36.72	3.16E-06	0.000321
GRINA	ENSG00000178719	549	2.11	0.00035	0.017343
EDNRB	ENSG00000136160	539	11.41	1.69E-16	2.73E-13

The genes with the greatest expression in the pars plicata of the ciliary body included glutathione peroxidase 3 (*GPX3*), a gene that detoxifies hydrogen peroxide, opticin (*OPTC*), previously identified as a ciliary body marker gene and *CPAMD8* (C3 and PZP like, alpha-2-macroglobulin domain containing 8), a gene associated with anterior segment dysgenesis and congenital glaucoma (Siggs et al., 2020) (Table 20). The top enriched biological processes in the ciliary body involved transport of small molecules and ions, which alluded to its role in aqueous humour production (Appendix table 19A and 19B).

Table 20: Top 20 differentially expressed genes in the pars plicata of the ciliary body ranked by normalized counts. CPM = counts per million.

Gene name	ENSEMBL	CPM	Fold change	P value	Corrected p value
GPX3	ENSG00000211445	13553	7.64	1.68E-05	0.000449
OPTC	ENSG00000188770	4403	35.72	3.14E-06	0.000115
CPAMD8	ENSG00000160111	3294	6.34	8.14E-07	3.77E-05
C4B	ENSG00000224389	1964	11.66	6.2E-10	8.33E-08
SERPINF1	ENSG00000132386	1902	3.22	0.005715	0.036118
ALDOA	ENSG00000149925	1898	2.21	8.63E-05	0.001676
C4A	ENSG00000244731	1844	11.50	4.98E-10	6.82E-08
ATP1A2	ENSG00000018625	1699	7.89	4.69E-05	0.001012
B2M	ENSG00000166710	1501	3.02	2.85E-05	0.000692
TFPI2	ENSG00000105825	1480	30.48	1.57E-10	2.45E-08
IFITM3	ENSG00000142089	1297	2.93	0.003751	0.026924
FRZB	ENSG00000162998	1280	9.16	2.43E-06	9.3E-05
CD74	ENSG00000019582	1167	2.89	0.002478	0.020449
SLC23A2	ENSG00000089057	1147	6.75	9.62E-16	4.75E-13
IGFBP7	ENSG00000163453	1117	4.10	2.27E-05	0.000579
PARM1	ENSG00000169116	1065	13.18	5.56E-09	5.51E-07
SLC13A4	ENSG00000164707	1042	33.86	3.26E-10	4.57E-08
AOC3	ENSG00000131471	1037	25.19	1.53E-13	4.66E-11
EFEMP1	ENSG00000115380	1018	4.18	9.81E-07	4.42E-05
AOC2	ENSG00000131480	798	113.04	1.44E-42	1.09E-38

The cells of the retina have a high level of organization and specialization, which was reflected in its expression profile (Table 21). The top differentially expressed genes were associated with photoreceptor cells, found only in the retina, and included rhodopsin (*RHO*), phosphodiesterase 6A (*PDE6A*) and retinol binding protein 3 (*RBP3*). *ABCA4*, another highly and selectively expressed gene in the retina, is the most common cause of the retinal disease known as Stargardt's disease. The majority of enriched biological processes in the retina were related to visual transduction and photoreceptor metabolism (Appendix table 20A and 20B).

Table 21: Top 20 differentially expressed genes in the neural retina ranked by normalized counts. CPM = counts per million.

Gene name	ENSEMBL	CPM	Fold change	P value	Corrected p value
TF	ENSG00000091513	8436	12.83	1.48E-05	0.000131
RHO	ENSG00000163914	5696	42.73	9.63E-07	1.28E-05
GLUL	ENSG00000135821	5015	1.69	0.008032	0.02391
PDE6A	ENSG00000132915	3608	57.72	1.24E-13	1.15E-11
SAG	ENSG00000130561	2888	53.23	1.15E-12	8.14E-11
LENG8	ENSG00000167615	2839	4.84	1.25E-15	1.9E-13
ENO2	ENSG00000111674	2787	8.30	3.38E-10	1.28E-08
GNB1	ENSG00000078369	2245	5.46	6.56E-25	6.77E-22
GNAT1	ENSG00000114349	2090	36.40	6.03E-07	8.64E-06
RBP3	ENSG00000265203	1843	41.62	5.45E-08	1.07E-06
HSP90AA1	ENSG00000080824	1680	2.19	0.000238	0.00135
UNC119	ENSG00000109103	1667	20.32	1.92E-23	1.32E-20
AIPL1	ENSG00000129221	1659	43.92	7.91E-09	2.02E-07
ABCA4	ENSG00000198691	1598	15.46	3.68E-07	5.66E-06
PDE6G	ENSG00000185527	1562	39.30	1.49E-09	4.67E-08
CNGB1	ENSG00000070729	1530	53.52	4.7E-12	2.92E-10
DDX17	ENSG00000100201	1505	1.80	0.000198	0.001165
VEGFA	ENSG00000112715	1492	3.27	0.000293	0.001603
ATP1A3	ENSG00000105409	1466	16.26	9.32E-07	1.25E-05
ATP1B2	ENSG00000129244	1442	5.49	0.000112	0.000723

The genes with the highest expression in the optic nerve head included Wnt inhibitor factor 1 (*WIF1*), kinesin family member 5A (*KIF5A*), a gene involved in axonal transport in neurons, and nerve growth factor receptor (*NGFR*) (Table 22). The optic nerve head contains a mixture of neuronal tissue and fibrous connective tissue, which was echoed in the enriched biological pathways. Top enriched pathways and gene ontology included axonal guidance, extracellular matrix proteoglycans and transmission across synapses (Appendix table 21A and 21B).

Table 22: Top 20 differentially expressed genes in the optic nerve head ranked by normalized counts. CPM = counts per million.

Gene name	ENSEMBL	CPM	Fold change	P value	Corrected p value
WIF1	ENSG00000156076	2035	21.95	4.5E-07	0.000238
CDC42EP4	ENSG00000179604	742	3.09	0.00012	0.020966
KIF5A	ENSG00000155980	704	11.19	1.18E-06	0.000517
PRDX6	ENSG00000117592	532	3.07	1.91E-07	0.000111
NGFR	ENSG00000064300	408	8.86	4.9E-07	0.000247
ECE1	ENSG00000117298	371	2.66	7.5E-06	0.002403
NEFL	ENSG00000277586	338	10.82	0.000162	0.025088
FAM168A	ENSG00000054965	325	2.89	6.35E-05	0.012761
TUBB2B	ENSG00000137285	307	4.46	0.00015	0.023597
ABLIM3	ENSG00000173210	292	4.75	0.000133	0.022223
UNC13C	ENSG00000137766	273	20.74	3.09E-11	2.92E-08
FGFRL1	ENSG00000127418	271	3.10	2.49E-06	0.000993
RASSF4	ENSG00000107551	263	3.03	0.000151	0.023676
NEFM	ENSG00000104722	247	15.05	1.54E-05	0.004376
SPTBN4	ENSG00000160460	218	5.68	2.3E-08	1.58E-05
PAX2	ENSG00000075891	218	33.07	1.02E-07	6.28E-05
TUBB2A	ENSG00000137267	215	3.32	0.000415	0.044163
KLHDC8A	ENSG00000162873	212	8.12	2.41E-05	0.00607
PAX8	ENSG00000125618	203	9.29	3.72E-06	0.001406
ABCC3	ENSG00000108846	192	5.86	9.54E-08	6.01E-05

Top differentially expressed genes in the optic nerve exhibit its neuronal disposition and included myelin basic protein (*MBP*), glial fibrillary acidic protein (*GFAP*) and myelin proteolipid protein 1 (*PLP1*) (Table 23). Top enriched biological processes in the optic nerve included molecular transportation, central nervous system myelination and cytoskeleton organization (Appendix table 22A and 22B). This result was within expectation as the optic nerve contains predominantly the axons and myelin of retinal ganglion cells.

Table 23: Top 20 differentially expressed genes in the optic nerve ranked by normalized counts. CPM = counts per million.

Gene name	ENSEMBL	CPM	Fold change	P value	Corrected p value
MT-RNR2	ENSG00000210082	63155	2.63	0.00468	0.028298
MBP	ENSG00000197971	29090	177.07	1.26E-42	1.91E-39
MT-ND2	ENSG00000198763	25600	2.65	0.003573	0.023353
GFAP	ENSG00000131095	13325	16.16	4.29E-05	0.000733
PLP1	ENSG00000123560	6776	77.80	2.93E-19	5.74E-17
MTURN	ENSG00000180354	3526	52.53	4.1E-80	9.3E-76
PLEKHB1	ENSG00000021300	2799	14.78	4.26E-09	1.86E-07
MOBP	ENSG00000168314	2478	304.82	5.12E-23	1.88E-20
CRYAB	ENSG00000109846	2210	4.72	4.86E-09	2.11E-07
MAP4	ENSG00000047849	2177	5.95	1.07E-22	3.55E-20
SCD	ENSG00000099194	2138	4.04	0.001231	0.010617
TP53INP2	ENSG00000078804	2035	19.54	4.15E-30	2.85E-27
CNP	ENSG00000173786	1844	22.38	8.14E-60	6.16E-56
BCAS1	ENSG00000064787	1521	82.46	3.7E-20	8.15E-18
TUBA1A	ENSG00000167552	1502	7.38	1.87E-13	1.62E-11
HIPK2	ENSG00000064393	1481	12.91	1.85E-27	9.79E-25
TUBB4A	ENSG00000104833	1382	24.52	9.56E-12	6.44E-10
ABCA2	ENSG00000107331	1301	12.52	3.11E-31	2.35E-28
NDRG2	ENSG00000165795	1252	7.13	1.05E-19	2.18E-17
PAQR6	ENSG00000160781	1221	98.27	1.86E-55	8.45E-52

Sclera is comprised largely of fibrous connective tissue. The top differentially expressed genes prolargin (*PRELP*) and metalloproteinase inhibitor 3 (*TIMP3*) are both integral to connective tissue extracellular matrix metabolism (Table 24). The enriched pathways and gene ontology from scleral gene expression were related to protein translation and nonsense mediated decay, the significance of which were not apparent (Appendix table 23A and 23B). The gene *LTBP2* is of particular interest, as null mutation in this genes leads to an ocular syndrome with megalocornea, spherophakia and congenital glaucoma (Désir et al., 2010).

Table 24: Top 20 differentially expressed genes in the sclera ranked by normalized counts. CPM = counts per million.

Gene name	ENSEMBL	CPM	Fold change	P value	Corrected p value
PRELP	ENSG00000188783	12496	18.55	9.72E-15	3.56E-12
ANGPTL7	ENSG00000171819	12243	8.78	0.000163	0.002395
TIMP3	ENSG00000100234	11049	6.88	2.52E-08	1.83E-06
EEF1A1	ENSG00000156508	10522	2.61	1.2E-07	7.14E-06
PLA2G2A	ENSG00000188257	8884	276.78	2.43E-30	7.88E-27
GSN	ENSG00000148180	6321	6.04	3E-17	1.84E-14
IGFBP5	ENSG00000115461	4988	4.45	8.42E-05	0.001446
TPT1	ENSG00000133112	4074	3.47	3.6E-11	6.14E-09
AD000090.1	ENSG00000283907	3963	8.02	1.27E-16	6.72E-14
FTL	ENSG00000087086	3823	3.98	9.71E-09	8.11E-07
CHI3L1	ENSG00000133048	3802	6.12	0.00098	0.008945
AHNAK	ENSG00000124942	3137	3.63	2.56E-07	1.36E-05
EEF2	ENSG00000167658	3090	2.31	7.94E-06	0.000229
ACTG1	ENSG00000184009	2543	1.88	0.000277	0.003524
FMOD	ENSG00000122176	2438	9.52	9.89E-10	1.11E-07
TIMP2	ENSG00000035862	2346	5.11	9.14E-08	5.73E-06
BGN	ENSG00000182492	2328	13.21	7.95E-15	2.96E-12
LTBP2	ENSG00000119681	2296	7.71	1.37E-07	7.89E-06
RPL3	ENSG00000100316	2159	2.09	1.94E-05	0.000472
EEF1A1P5	ENSG00000196205	2110	2.83	5.06E-09	4.63E-07

6.2.5 Expression profile of known glaucoma genes

In order to better understand the genetic profile of POAG, the expression profiles of genes associated with known Mendelian inherited open angle glaucoma were examined from the RNAseq data and are graphically represented in the heat map below (Figure 26). Genetic defects in these genes are the only known monogenic causes to date to be associated with POAG, primary congenital glaucoma or anterior segment dysgenesis as listed by OMIM database (www.omim.org accessed 04/08/2018). This analysis demonstrates higher expression of genes involved in high pressure glaucoma (*CYP1B1*, *FOXC1*, *LTBP2*, *MYOC*, *PITX2*) within the trabecular meshwork, peripheral iris and ciliary body, the tissues critical for IOP regulation. This finding supports the hypothesis that gene expression mirrors tissue function.

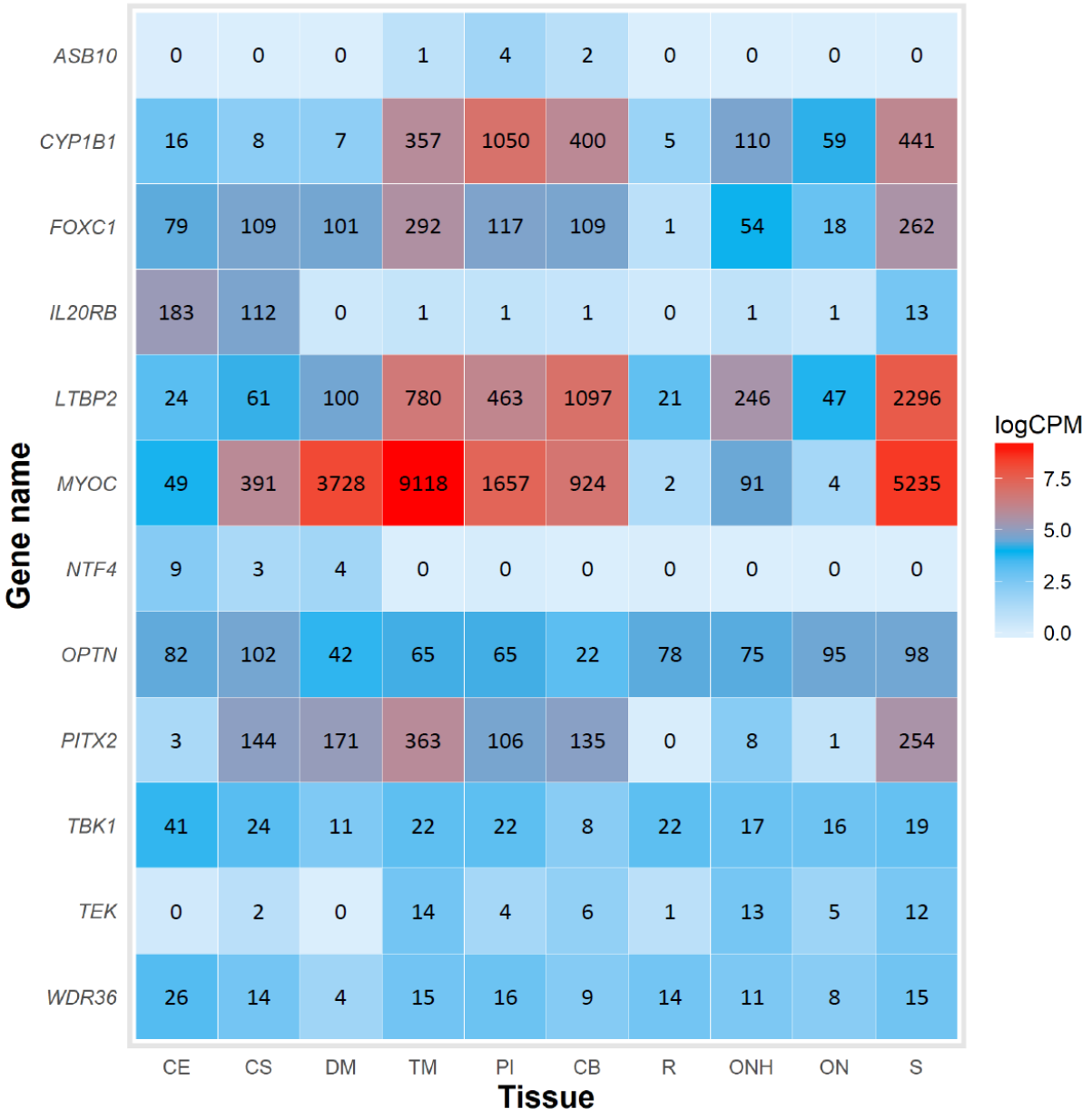

Figure 26: Heat map showing expression profile of known monogenic glaucoma causing genes.

6.2.6 Pathway and ontology analysis

To better understand the biological mechanisms underlying high pressure glaucoma, a comparison between tissues involved in production and regulation of IOP (trabecular meshwork and ciliary body combined) was made against non-pressure related neural tissues. The rationale for this comparison was based on the trend noticed in the expression profile of the known HTG causing genes noted

above, that is mRNA expression of HTG causing genes was significantly higher in the trabecular meshwork and ciliary body than the retina and optic nerve. A total of 2283 genes were expressed significantly higher in the trabecular meshwork and ciliary body. *OPTC* had the highest fold change of 769.67 in the IOP regulating tissues. The top 20 significantly enriched pathways in trabecular meshwork and ciliary body are listed below (Table 25). The most enriched pathways were involved in focal adhesion, extracellular matrix organization and smooth muscle contractility. Network analysis was performed using the top 500 differentially expressed genes in the trabecular meshwork and ciliary body combined compared to retina and optic nerve combined (Figure 27). The top network in tissues associated with IOP regulation represented biological processes involved in focal adhesion and extracellular matrix organization and interactions. The purpose of the network analysis was to distill the key interactions between genes that are selectively expressed in IOP regulating tissues. As such, the result of the network analysis mirrors the results of the top enriched pathways in the pathway analysis of the entire differentially expressed dataset. Top 20 significantly enriched pathways and gene ontology terms were also analysed for all ten tissues sequenced (Appendix Tables 14 – 23).

Table 25: Top 20 enriched biological pathways in intraocular pressure regulating tissues (trabecular meshwork and ciliary body)

Pathway Name	Source Name	ID	P-value (corrected)
Focal adhesion	KEGG	546	1.01E-09
Extracellular matrix organization	REACTOME	17095	1.52E-08
Smooth Muscle Contraction	REACTOME	13919	3.79E-08
Beta1 integrin cell surface interactions	PID NCI	14944	2.75E-07
Integrin signalling pathway	PID BIOCARTA	4024	1.33E-06
Vascular smooth muscle contraction	KEGG	4376	6.11E-06
Rho cell motility signalling pathway	PID BIOCARTA	4044	1.32E-05
Muscle contraction	REACTOME	19261	1.89E-05
PDGFR-beta signalling pathway	PID NCI	15816	2.11E-05
Laminin interactions	REACTOME	18928	4.51E-05
Erk and pi-3 kinase are necessary for collagen binding in corneal epithelia	PID BIOCARTA	4125	5.60E-05
Antigen processing and presentation	KEGG	493	6.03E-05
Cell-extracellular matrix interactions	REACTOME	13836	9.18E-05
Integrin signalling pathway	INOH	16138	9.86E-05
Regulation of actin cytoskeleton	KEGG	404	1.05E-04
Degradation of the extracellular matrix	REACTOME	17498	1.31E-04
EGFR1	NETPATH	15908	1.38E-04
Integrin cell surface interactions	REACTOME	13303	2.38E-04
Non-integrin membrane-ECM interactions	REACTOME	18527	2.38E-04
Hemostasis	REACTOME	19856	2.59E-04

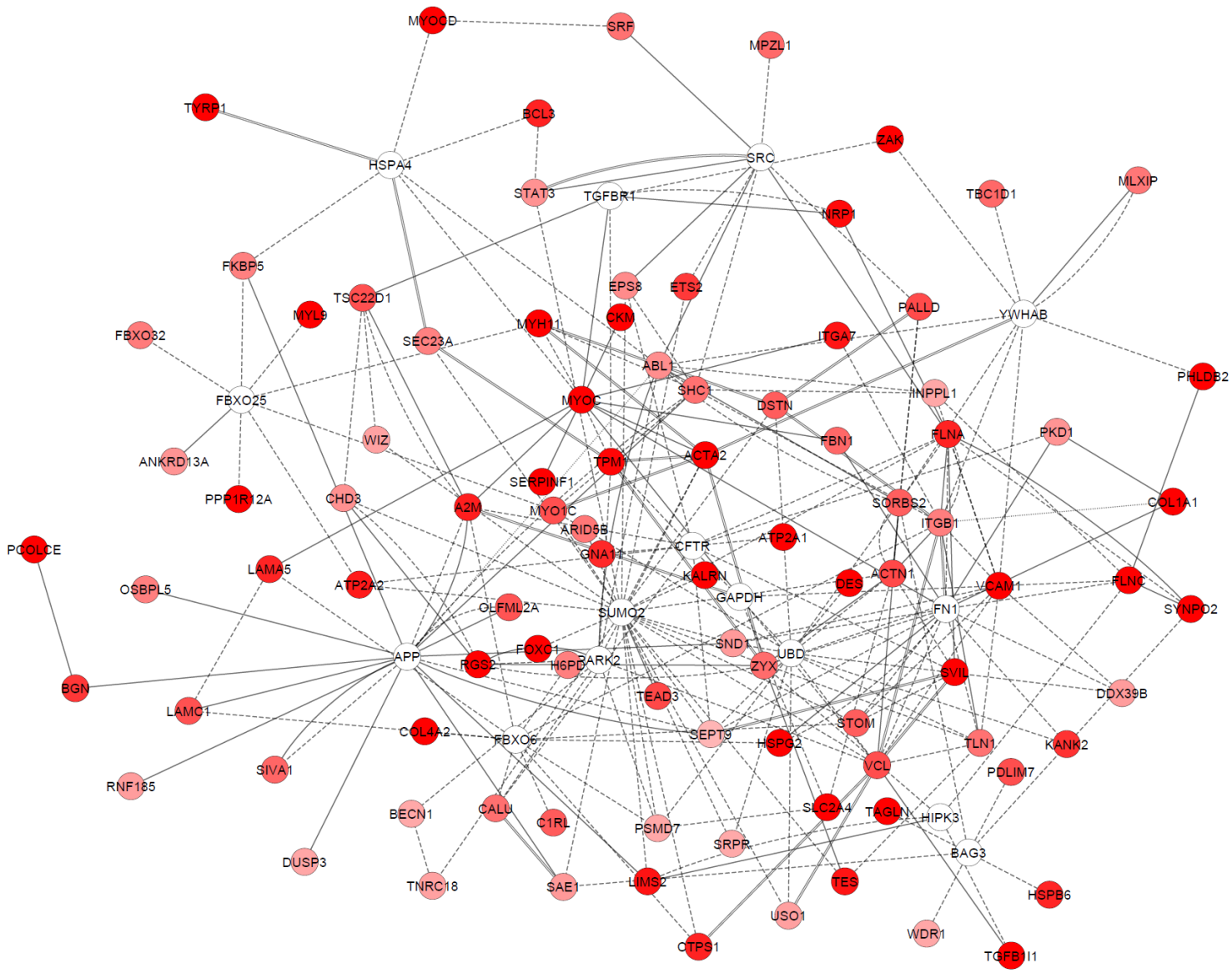

Figure 27: Top network generated using the top 500 differentially expressed genes in the trabecular meshwork and ciliary body combined when compared with non-pressure related neural tissues. This network represented biological processes involved in focal adhesion and extracellular matrix organization and interactions.

6.3 Discussion

Sensitivity and specificity of our expression data was examined using known signature markers of various ocular tissues. Eight marker genes were examined in total – *KRT12*, *KERA*, *SLC4A11*, *MYOC*,

OPTC, *RHO*, *GFAP*, *CRYBA1*. Keratin 12 (*KRT12*) is one of six types of collagen constituents of corneal epithelial intermediate filaments, and one of two genes highly specific to the corneal epithelium, the other being keratin 3 (Nishida et al., 1996). *KRT12* was the gene with second highest expression level in the list of differentially expressed genes for the corneal epithelium. Keratocan (*KERA*) is a hydrophilic proteoglycan that forms the extracellular matrix of the corneal stroma and maintains corneal shape via hydration. Alterations in its expression leads to the corneal ectasia known as keratoconus (Diehn et al., 2005). *KERA* was the 5th most prevalent differentially expressed gene in the corneal stroma. *SLC4A11* is a cation transport molecule that was previously found to be highly and specifically expressed in corneal endothelial cells from RNAseq analysis of human cadaveric specimens (Chng et al., 2013). Myocilin (*MYOC*) is well known to cause high pressure POAG and was shown to be the third most abundantly expressed gene in the human trabecular meshwork using expressed sequence tag methods as a part of the NEIBank database (Tomarev et al., 2003). It was the second most abundant differentially expressed gene in our RNAseq expression analysis of human trabecular meshwork. Opticin (*OPTC*) has been localised to the non-pigmented ciliary epithelium in the mouse model (Takanosu et al., 2001). In humans *OPTC* has also been localized to the iris (Hobby et al., 2000). Non-pigmented ciliary epithelium is located almost exclusively in the pars plicata and to a lesser degree the pars plana of the ciliary body. Our RNAseq expression analysis utilized pars plicata specimens which provides a high concentration of non-pigmented ciliary epithelium. *OPTC* was the second highest differentially expressed gene in the pars plicata of the ciliary body in our data as well as having a strong expression in the iris. These findings concur with the known literature. Rhodopsin (*RHO*) has long been known as the photo-pigment of the human retina located in the retinal outer segments. It has the highest cDNA concentration of any gene in the retina in the NEIBank (Wistow, 2006). In our dataset, *RHO* was the second most abundantly expressed mRNA in the retina after transferrin (*TF*). It is more specifically expressed in the retina than transferrin. Glial fibrillary acidic protein (*GFAP*) is an intermediate filament protein found in the central nervous

system glial cells, especially the astrocytes. In healthy human eyes, its expression is restricted predominantly to the optic nerve and to the ganglion cells of the inner retina (Tuccari et al., 1986). The expression profile of *GFAP* in our RNAseq dataset is in concordance with previous knowledge with the highest expression in the optic nerve, followed by the optic nerve head, the retina and hardly any expression in the other ocular tissues. The Crystallin Beta A1 (CRYBA1) gene was used as a negative control as it is a specific constituent of human lens fibres (Diehn et al., 2005). As the human lens tissue was not included in our study, no tissues in our study exhibited any significant *CRYBA1* expression.

The high levels of expression of the aforementioned marker genes in the signature tissues and very low to no expression in unrelated tissues demonstrates a high specificity of our RNAseq expression data with little to no cross-contamination of the tissue samples, which is a major potential confounder to this experimental design. The other major confounder is the degree of RNA degradation of the ocular tissue post-mortem which would affect the sensitivity of RNAseq capture. The RNAseq capture protocol utilized poly-A tail enrichment selection using Bioo Scientific® NEXTflex™ Rapid Directional mRNA-Seq Kit Bundle with poly(A) beads. In eukaryotes, polyadenylation is one of the final steps in mRNA maturation whereby consecutive adenine bases are added to the 3' end of the gene transcript to form the poly-A tail of the mature mRNA sequence prior to its translation. mRNA degradation causes gradual loss of the poly-A tail which is the target for capture of our RNAseq protocol. The 5' cap of mRNA protects the actual transcript from being altered prior to the loss of the poly-A tail. Therefore RNA degradation is highly unlikely to generate spurious results. The net result of RNA degradation in the context of the present RNAseq study would be a reduction in the detection of genes with low expression thereby reducing the sensitivity. Unfortunately, the time to tissue fixation post-mortem hence the potential loss of sensitivity at the

lower threshold of expression, particularly for unstable RNAs is beyond the control of this experimental design.

Prior to detailed analysis, the quality of our RNAseq expression data was assessed using the best available public domain data. Previous studies (Marioni et al., 2008, Zhao et al., 2014) have shown comparable expression patterns between RNAseq and microarray data, demonstrating some degree of generalizability despite differences between the two techniques. The performance of our RNAseq data was compared with the best available public domain ocular expression database – OTDB (Wagner et al., 2013). The PLIER score from the OTDB microarray data was used as the surrogate of expression level. Our data showed greater sensitivity at lower expression levels as evident in the vertically elongated lower threshold of all comparison scatterplots (Figures 22-25) which gives all four correlation plots the appearance of kidney beans. This implies that for the proportion of genes at the lowest threshold of detection on microarray where minimal difference in gene expression was identified (between PLIER scores of 10 and 10^1.5 = 32), RNAseq profiling was able to ascertain significant differential expression to the order of 100 fold magnitude. Therefore from our results, a PLIER score of 30 appears to be the lower limit of discrimination for the OTDB microarray expression data. Our RNAseq expression data also exhibited greater dynamic range overall in comparison to OTDB microarray data with dynamic range of 10^5 and 10^2 respectively. The findings of superior lower limit of detection and greater dynamic range of RNAseq have been previously reported (Zhao et al., 2014).

Having established the accuracy and specificity of our RNAseq expression against previously available data, the ocular expression profile of previously identified glaucoma causing genes was examined and the biological mechanisms that defined each sequenced human ocular tissue was explored using systems-approach pathway analysis with a special focus on the pathophysiology of

POAG. A proportion of the known monogenic glaucoma genes did not exhibit considerable differential expression in our ocular tissue expression dataset and these included *ASB10*, *NTF4*, WDR36 and the NTG associated genes *OPTN* and *TBK1*. Out of these genes, ASB10 and NTF4 had low expression levels across all tissues sequenced, whereas the others were essentially evenly expressed across all tissues.

There was a strong trend in the expression profile of six glaucoma genes (*CYP1B1*, *FOXC1*, *LTBP2*, *MYOC*, *PITX2*, *TEK*). These genes all demonstrated significantly higher expression in the anterior uveal tissues relating to IOP regulation (trabecular meshwork, peripheral iris and ciliary body) than the neural tissues (retina and optic nerve). Also of note, was the expression in the optic nerve head which was significantly higher than that of the adjacent neural tissues of retina and optic nerve. These six genes are the most well-known and replicated monogenic causes of primary congenital glaucoma, anterior segment dysgenesis and HTG, which are all characterised by a very high IOP disease phenotype. The results of our RNAseq ocular tissue expression parallels the disease mechanism of HTG. As these genes potentially have important IOP regulating functions, their elevated expression in the tissues of IOP regulation follows the initial hypothesis of this chapter. Extrapolating from this result, any HTG causing genes discovered in future may also exhibit similar tissue expression profiles, and this requires further evaluation as the knowledge of HTG causation increases.

Interleukin 20 receptor beta (*IL20RB*) showed selective expression in the anterior cornea (corneal epithelium and stroma) and to a lesser extent the sclera with trace expressions in the other ocular tissues except the retina. Our results differed from a previous study (Keller et al., 2014) where the expression of *IL20RB* was identified in primary cultures of human trabecular meshwork cells via immunohistochemistry and western blotting. One explanation for the difference may be a gain of

expression of *IL20RB* in cell culture conditions. Immunohistochemistry and western blotting required cell culturing post tissue dissection in the experimental design of the previous study, which may have altered gene expression. RNAseq allowed our experiment to be conducted with minimal amounts of tissue, thus avoiding potential expression variations which may arise due to cell culturing. A second explanation may be that the level of *IL20RB* protein expression may not mirror its mRNA level and a trace level of *IL20RB* mRNA in the trabecular meshwork could have resulted in a significant concentration of protein that was detectable on immunohistochemistry and western blotting. Finally, there is a possibility as previously stated that mRNA degradation post-mortem reduced the signal of *IL20RB* on RNAseq. This justification is the least likely, as high expression of *IL20RB* was detected in the anterior cornea and any degradation of mRNA would have occurred in all tissues examined.

The tissue expression signature for the monogenic Mendelian glaucoma genes discovered in this experiment suggested that genes important in the pathogenesis of high pressure POAG are selectively expressed at higher levels in the trabecular meshwork and ciliary body than the retina and optic nerve head. It follows that a comparison between the expression profile of trabecular meshwork plus ciliary body and retina plus optic nerve may highlight important pathways involved in IOP regulation and therefore POAG aetiology. The most significantly enriched pathways from this analysis belonged to the focal adhesion family (KEGG ID: 546) (Figure 28 from KEGG database, https://www.genome.jp/dbget-bin/www_bget?map04510). Focal adhesion describes the interaction between the extracellular matrix and the cells within that matrix, which can trigger a series of signalling events leading to cell motility, proliferation, differentiation and survival. The sites for these interactions are at the plasma membrane between integrin receptors and their associated actin filaments.

The link between trabecular meshwork and optic nerve head gene expression and glaucoma pathogenesis has been previously examined by two meta-analyses of GEO database trabecular meshwork and lamina cribrosa cultured cell expression. Comparison between glaucoma patients and controls (Yan et al., 2015, Zhavoronkov et al., 2016) suggested that in glaucoma pathogenesis, similar biologic dysfunction may be occurring at the trabecular meshwork and the lamina cribrosa. The optic nerve astrocyte expression meta-analysis identified focal adhesion and extracellular matrix-receptor interaction as two of five significantly enriched canonical pathways (Yan et al., 2015). The meta-analysis of combined GEO database trabecular meshwork and lamina cribrosa expression identified pro-fibrotic pathways related to TGFβ as the common pathogenic link in both the trabecular meshwork and lamina cribrosa of glaucoma patients (Zhavoronkov et al., 2016).

In the context of glaucoma, activation of focal adhesion causes contraction of cytoskeletal actin and of tight junctions through RhoA kinase activation resulting in increased aqueous outflow resistance (Figure 28) (Inoue and Tanihara, 2013). Rho kinase (ROCK) inhibitors are a novel glaucoma treatment with proposed benefits of reducing IOP and offering neuroprotection by improving optic nerve head blood flow (Abbhi and Piplani, 2018). Ripasudil is the only available ROCK inhibitor on the market with 5 other ROCK inhibitors currently in trial (AMA0076, K115, PG324, Y39983 and RKI-983). The other downstream targets of focal adhesion are less well studied in glaucoma and include phosphatidyl inositol-Akt, Wnt, and MAPK signalling pathways (Figure 28). The classical Wnt signalling pathway has been previously found to play a role in IOP regulation (Mao et al., 2012). Blocking the classical Wnt signalling pathway in mouse eyes, the IOP rose by an average of 8 mmHg in 1 week lasting for at least one week duration. The same study also confirmed the presence of Wnt pathway genes in primary cultured human trabecular meshwork cells by immunofluorescence (Mao et al., 2012). Our finding of significant enrichment of genes related to the Wnt pathway concurs with the previous study in suggesting the importance of Wnt signalling in IOP regulation. Phosphatidyl

inositol inhibitors have been shown in rats to induce retinal ganglion cell loss in IOP stressed retinas but not normal retinas at (Huang et al., 2008). This finding implied that the phosphatidyl inositol pathway may confer protection against pressure related stress on retinal ganglion cell metabolism. Our finding that genes in this pathway are enriched in the trabecular meshwork infers that phosphatidyl inositol plays a role in the trabecular meshwork as well as the retinal ganglion cell in glaucoma pathogenesis.

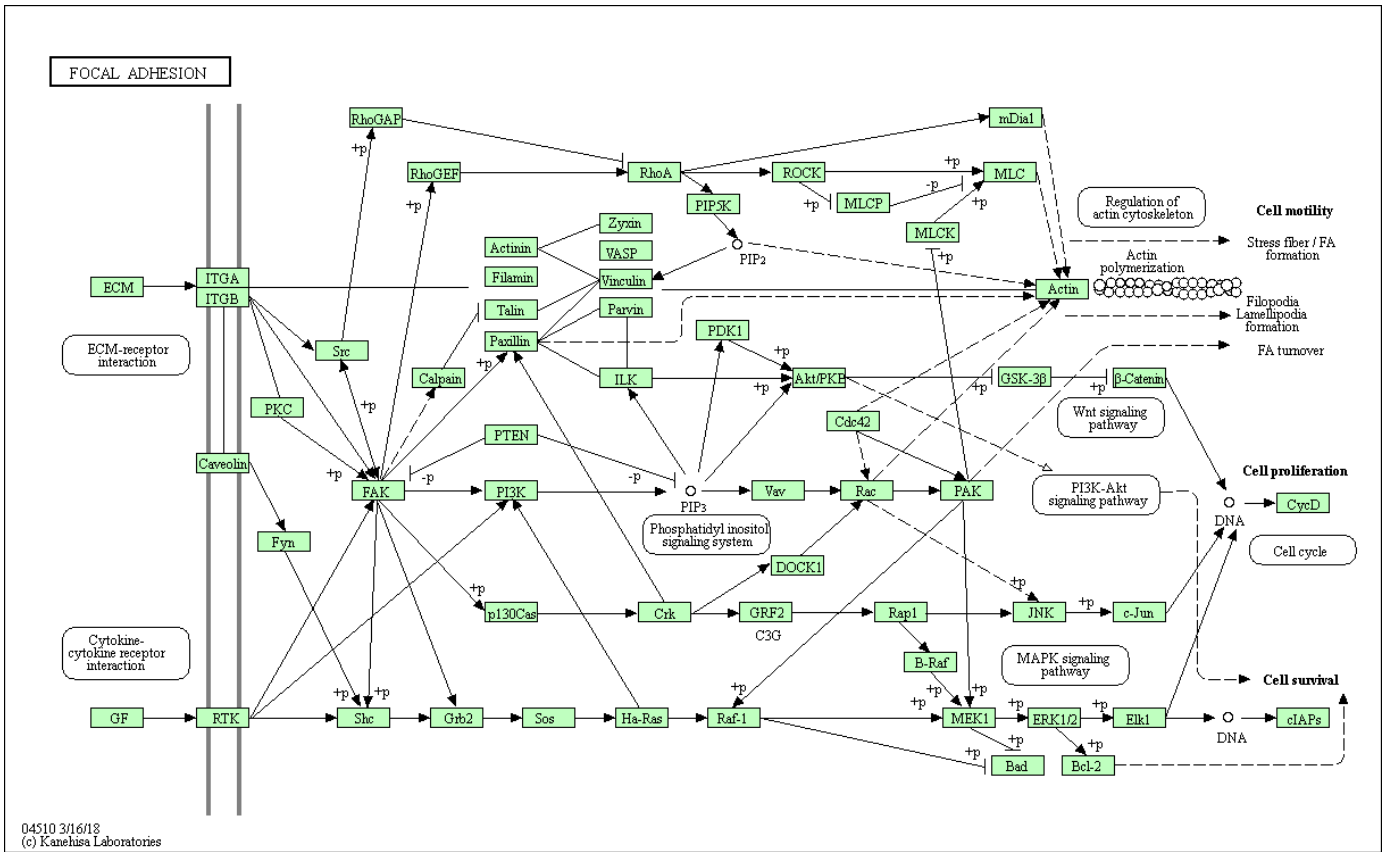

Figure 28: Schematic diagram of focal adhesion biological process as identified by the Kyoto Encyclopedia of Genes and Genomes (KEGG ID: 546). Many pathways within this process have been implicated in glaucoma pathogenesis including RhoA activation of ROCK and canonical Wnt signalling pathway.

In summary, RNAseq is one of the most sensitive and informative analyses of gene expression currently available. The findings of the present ocular tissue gene expression study strongly support

the hypothesis that ocular tissue gene expression profile is a reflection of its function. By examining the expression profile of each of the ten ocular tissues of interest, this study identified some key biological processes occurring at each tissue as well as the most common disease genes affecting certain tissues. Gene expression of IOP regulating tissues revealed the importance of focal adhesion and extracellular matrix interactions in IOP homeostasis and suggests a possible role of these pathways in glaucoma pathogenesis.

Chapter 7: Summary of findings

The primary impetus of this thesis is to build upon current knowledge of the genetic composition of primary open-angle glaucoma using next-generation sequencing techniques. Secondary aims included using next generation RNAseq methods to identify important functional genes in tissues implicated in POAG pathogenesis to identify potential disease candidates and pathways. Finally, the ocular tissue expression dataset established from this thesis will provide a basis for tissue expression analysis, which forms a platform for understanding of various ocular diseases and disease gene discovery.

7.1 High effect rare variant hypothesis

With the initial expectation of the potential of NGS comes the realization of the new hurdles this technology brings. On the logistics level, the colossal volume of data generated with each run of sequencing poses a new challenge in data management and storage. Analysing the vast data output requires expert bioinformatics input and intensive computing power. On the technical level, exome sequencing is capture based and therefore prone to variability in capture efficiency, sequencing depths and probe design. Although whole genome sequencing eliminates the capture-based issues of whole exome sequencing, it generates significantly more data and is more expensive. As the majority of rare genetic mutations are non-pathogenic, new statistical challenges arise in extracting useful information from the confusing tangle that is the sequencing output.

Sample size for non-hypothesis driven gene discovery has always been an issue since the early years of the GWAS era. Non-hypothesis driven genetic association testing is firmly rooted in a purely statistical argument. Due to the scarce number of rare mutations and correction for copious multiple testing, large number of participants are required to achieve adequate statistical power to detect truly pathogenic variants amongst the random noise. In our study, it became apparent that the rarity

of pathogenic gene variants prevented the discovery of high effect size monogenic disease genes using a cohort of 218 cases. However *MYOC* was an exception to the rule, being a monogenic cause of POAG that was frequent enough to be detected on our previous GWAS data (Gharahkhani et al., 2014). This study has demonstrated the lack of another monogenic gene with disease burden close to that of *MYOC*. This lack of another significant rare genetic 'hit' represents the result of the disease burden of POAG with potential rare monogenic causes at prevalence below the threshold of detection for our small WES cohort. For single gene discovery of rare variants, the number of required genetic sequences (exome or whole genome) may exceed 1000. A WES study of autism spectrum disorder (Liu et al., 2013a) with 1039 participants and another WES study of schizophrenia (Purcell et al., 2014) with 2536 participants both failed to identify any single genetic cause of disease. Although both these disorders are physiologically more heterogeneous than POAG, the challenge of single gene rare variant discovery in POAG is not trivial. Successful single rare variant analysis is achievable as demonstrated by the 2015 study linking TBK1 to amyotrophic lateral sclerosis (ALS) (Cirulli et al., 2015) where a cohort of 2874 cases with ALS and 6405 controls was used.

One way to improve power with a small cohort is select extreme phenotype enriched cases for sequencing (Cirulli and Goldstein, 2010). The studies detailed within this thesis utilized the strategy of phenotypic enrichment by selecting the participants with advanced disease and earliest age of onset for sequencing. Combining phenotypic enrichment with co-segregation analysis of available family members may also improve the potential for gene discovery with a limited sample size (Johar et al., 2015). Large population-based controls are also required in rare variant analysis to increase precision of the population minor allele frequency. The largest current population database is the Exome Aggregation Consortium (ExAC) which is a publically available repository of whole exome sequences from 60706 unrelated individuals (Lek et al., 2016). The 100,000 Genomes Project

currently in progress will further assist the search for rare disease-causing genes in complex diseases.

Various analytical methods to improve the power of rare variant discovery have been attempted. The most commonly used methods involve grouping rare variants by gene and are collectively known as gene burden testing (Dering et al., 2011). These methods have sound theoretical validity as genes encode for proteins, which are the biological functional units. The earliest of these methods involve assigning a binomial value for the presence or lack thereof of variants in every gene for each participant to form the 'cohort allelic sums test' or CAST statistic (Morgenthaler and Thilly, 2007). While intuitive, this test oversimplifies the data and fails to account for the potential difference in pathogenicity between common and rare variants. The combined multivariate and collapsing method (CMC) was developed to address that issue and clustered the common and rare variants within each gene separately to isolate their effects (Li and Leal, 2008). The weighted sum statistic (WSS) method was developed to further improve the power of the gene burden test by assigning graded weighting to clusters of SNVs based on variant frequency, conservation and gene characteristics (Madsen and Browning, 2009). These traditional gene burden tests all assume the direction and magnitude of effect for each cluster of SNVs are homogenous, that is all rare variants within a gene are equally deleterious.

Reality is more complex with each rare SNV offering distinct pathogenicity, evident in the many pathogenic mutations of *MYOC*. Some SNV may even provide protection against disease while the majority likely have no effect on disease phenotype. Currently, the sequence kernel association test (SKAT) is one of the analyses that most comprehensively addresses the issues of gene burden testing using regression of SNVs within gene regions while correcting using principles components to mitigate effects such as population stratification (Wu et al., 2011). In our study, the application of

SKAT also failed to highlight any single significantly enriched rare disease-causing gene. Despite this, several candidate genes were identified by the analysis, among which neuroglobin was the standout.

Neuroglobin (*NGB*) is a well conserved gene across numerous species (Droge et al., 2012) with highly selective expression in retinal tissue (Schmidt et al., 2003). Its normal function confers neuroprotective properties via increasing tissue resistance to ischaemia (Greenberg et al., 2008, Li et al., 2010). In experimental animal models of glaucoma, overexpression of neuroglobin prevented IOP induced ganglion cell death (Wei et al., 2011, Chan et al., 2012) and prevented glaucoma in the harlequin rat (Lechauve et al., 2014) and DBA/2J mice (Cwerman-Thibault et al., 2017) models.

Using site directed mutagenesis, cDNA with mutations in neuroglobin found in 3 participants in our study cohort (C55R, S58W and exon 3 deletion) were generated and transfected into human neuronal cells differentiated from SH-SY5Y cell lineage. The resistance to oxidative stress of neuronal cells overexpressing mutant neuroglobin was compared to those overexpressing wildtype neuroglobin and non-transfected controls. These experiments were unable to show a significant difference in the viability of neuronal cells overexpressing different types of neuroglobin. As discussed in Chapter 2, these results show that mutant neuroglobin is not cytotoxic and any pathogenicity that may occur will be due to a loss of wildtype function. The presence of wildtype neuroglobin in all neuronal-differentiated cells used in the experiments may have contributed to the lack of difference in the viability of the transfected groups. This issue could be overcome by several methods including targeting the wildtype neuroglobin in the experimental neuronal cells with siRNA knockdown or CRISPR-Cas9 system. Induced pluripotent stem cells from the affected individuals could be generated and differentiated into retinal ganglion cells for use as the experimental cell model. Hydrogen peroxide exposure was selected as the oxidative stress as it is well studied and readily available (Jaworska-Feil et al., 2010, Ramalingam and Kim, 2015). However, other oxidative

stress conditions such as hypoxia and glucose deprivation may reflect the physiologic stressors experienced by retinal ganglion cells more closely.

7.2 The genetic architecture of monogenic POAG

One aim of this thesis was to examine the contributions of known monogenic causes of POAG in our cohort of participants with severe POAG phenotype. The results reaffirm the knowledge that *MYOC* is the single most prevalent cause of monogenic POAG by far, accounting for 13.3% of all POAG in our cohort with advanced disease. Our study failed to identify another monogenic cause of POAG in our cohort of 218 participants with advanced POAG that came close to MYOC in terms of prevalence. All other known monogenic causes of POAG combined accounted for the same prevalence of *MYOC* alone (13.3%). Our advanced disease cohort carries a relative high monogenic disease burden, in comparison to other studies (Stone et al., 1997, Fingert et al., 1999), due to the effects of phenotypic enrichment (Johar et al., 2015). The results provide valuable insight into the disease contribution of monogenic POAG as no previous study had examined the relative contributions of monogenic causes in POAG to our knowledge. In our study, WDR36 failed to show any sign of enrichment for rare potentially pathogenic variants when compared to controls (3.67% to 6.86%). Our findings were in concordance with a previous Australian and US study in cohorts of similar ethnicity (Hewitt et al., 2006b, Fingert et al., 2007). Many previous studies of WDR36 gene prevalence in POAG either did not sequence any controls (Miyazawa et al., 2007, Huang et al., 2014) or sequenced only very few controls (<100) (Fan et al., 2009). WDR36 was initially discovered through familial linkage study of two large US POAG families. The result of our study highlights the value of contemporary sequencing of ethnically matched controls in rare gene prevalence studies in limiting false positive discoveries.

7.3 Comparisons between common and rare variants

Genome wide association studies have identified numerous POAG associated loci and the list is growing every year (Burdon et al., 2011, Springelkamp et al., 2017). Each of these loci typically carry low effect sizes, which may have an additive consequence on an individual's POAG risk (Cuellar-Partida et al., 2016). The overall heritability of POAG as calculated using common GWAS associated loci was found to be $h^2_g = 0.42 \pm 0.09$ (Cuellar-Partida et al., 2016), which still leaves a significant portion of POAG unaccounted for. The signal from genome-wide association loci identified via GWAS are thought to be the result of linkage between the common variants with the putative disease causing variants as the associated loci are seldom deleterious in nature (Bodmer and Bonilla, 2008, Hemminki et al., 2008). The hypothesis of the GWAS relies on the notion that linkage disequilibrium of genetic loci may highlight regions on the genome that warrant closer attention. However as common variants do not exhibit robust linkage disequilibrium with rare variants (Siu et al., 2011), GWAS findings typically shed no light on the relationship between common and rare disease association variants.

To explore the genetic architecture of POAG, the exomes of our participants were screened for enrichment of rare potential disease-causing variants when compared to a large control cohort. Only the GWAS associated locus near *CARD10* (caspase recruitment domain containing protein 10) was statistically significantly enriched for rare potentially disease causing variants after Bonferroni correction for a total of 86 tested genes ($p = 6.94\times10^{-5}$, corrected $p = 5.97\times10^{-3}$) with an odds ratio of 13.2 (3.5 - 50.2). Our results demonstrated the poor linkage between common SNPs and rare variants in a real-life experimental cohort with advanced POAG, a common polygenic disease. However, as demonstrated by the case of *CARD10*, having a significant common variant association to disease does not preclude a possible rare disease causing variant association in the same gene.

7.4 Pathway analysis of genes enriched for rare variants

With the advent of next generation sequencing, ever enlarging lists of genes of interest are being generated for all researched diseases. As previously noted, proving causality of disease from a single gene with rare variants may be difficult to achieve due to low variant frequency leading to lack of robust statistical significance. For novel rare disease causing variants, the large sample cohorts that require sequencing in order to achieve adequate power have not yet been sequenced. One improvisation takes the clustering of variants to the next hierarchy.

Clustering variant signals at a gene and transcript level is an arbitrary cut-off based on an over-simplification of our understanding of molecular genetics. Biological processes do not exist in isolation driven by lone genes. At the most fundamental level, a large number of protein machinery components are comprised of multiple gene products; human haemoglobin for instance is made up of α-globin transcribed from *HBA1* and *HBA2* genes and β-globin transcribed from the *HBB* gene (Hardison, 2012). Collections of closely interacting genes and gene products function together to drive biological functions. Systems approach network analysis is an emerging tool that utilizes the interaction between interconnected genes and gene products to analyse clusters of pathways, which provide a better understanding of their underlying biological function (Charitou et al., 2016). This form of analysis allows for detection of enrichment in biological pathways from even small sample cohorts, where using a single gene approach may have yielded no significant result.

In our pathway analysis of whole exome data from participants with advanced POAG, we identified enrichment in rare variants in genes involved in camera-type eye development ($p = 3.28\times10^{-4}$, OR = 10.22 (4.87-21.43)). This may come as no surprise, given that POAG is an eye disease. However, the implication of this finding is that even adult onset POAG may be a result of developmental ocular abnormalities. Furthermore, each enriched gene within the pathway (*CRYBA4*, *GAS1*, *GJA8*, *HES5*,

MAB21L2, *NEUROD4*, *NR2E1*, *PAX6*, *RXRA*, *SLC25A25*, *VAX1*) warrants further investigation as a potential POAG causing gene. Some genes such as *CRYBA4* (Hu et al., 2015, Huang et al., 2015), *GJA8* (Hu et al., 2010, Xia et al., 2012), *MAB21L2*, *PAX6* (Springelkamp et al., 2015), *RXRA* (Lu et al., 2013), and *VAX1* are already linked to glaucoma or glaucoma related phenotypes, while the association of the other genes with POAG are yet to be elucidated.

In the sub-analysis separating hypertensive POAG (HTG) and normotensive POAG (NTG) cohorts, we have demonstrated that different pathophysiologies are involved in causing the two disease subtypes. The defining characteristic of HTG is the elevation of intraocular pressure that is thought to cause or at least significantly contribute towards POAG development. The enriched unfolded protein response (UPR) pathway functions to increase protein solubility via molecular chaperones and misfolded protein degradation and have been implicated previously in candidate gene studies of POAG (Carbone et al., 2011). Our approach is more robust than candidate gene studies as we started without any *a priori* assumptions using a non-hypothesis driven analysis. Nonetheless, our results are in concordance with the findings of the previous candidate gene studies linking the importance of UPR to pathogenesis of POAG (Anholt and Carbone, 2013, Carbone et al., 2011). In brief, a defective UPR pathway may become overwhelmed at the trabecular meshwork cells, a region with a high potential load of misfolded protein due to UV denaturing and accumulation in the aqueous humour, leading to apoptosis of trabeculocytes, increasing aqueous outflow resistance, increasing intraocular pressure, and eventually glaucoma.

Normal tension glaucoma (NTG) may have different pathogenesis to HTG according to the findings of our pathway sub-analysis. Abnormal maintenance of transmembrane ion potential was highlighted in NTG cases from our study. Patients with NTG lack the high intraocular pressures of their HTG counterparts, yet their ganglion cells undergo degeneration. Therefore the disease aetiology seems

to suggest one of increased susceptibility to ganglion cell neuronal apoptosis. Our findings implicating defects in transmembrane ion gradient maintenance fits well with this hypothesis. Inability to maintain a stable transmembrane potential leads to neuro-excitotoxicity, increased intracellular calcium levels and ultimately apoptosis (Orrenius et al., 2003, Dong et al., 2009). Furthermore, three genes identified in the transmembrane potential maintenance pathway belong to a family of enzymes known as the aminophospholipid translocases. These enzymes ensure the outer surface of the cell plasma membrane is low in aminophospholipid phosphatidylserine, which is an activator of phagocytosis (Takatsu et al., 2011). Defects in this pathway further increase the rate of apoptosis of the afflicted cell. These enriched rare variants in NTG participants conspire to increase ganglion cell susceptibility to apoptosis, leading to disease.

7.5 Transcriptomics with RNAseq analysis

Next generation RNAseq has been a major breakthrough in the study of transcriptomics. Our results confirm the superior sensitivity at lower detection threshold and greater dynamic range of RNAseq in comparison to microarray technology. One major confounder in any expression profiling study is the signal to noise ratio. Our experimental results were concordant with previous studies in regards to the expression profiles of tissue marker genes. The specificity of these tissue marker genes demonstrated a minimal noise signal from our RNAseq and tissue dissection protocol, which was further substantiated by the absence of lens specific *CRYBA1* in any of our ocular tissues. By examining the expression profiles of well-known glaucoma genes, we ascertained that high pressure POAG genes displayed a signature whereby their tissue expression is significantly higher in the trabecular meshwork and ciliary body when compared to the retina and optic nerve. Pathway analysis of genes highly differentially expressed in the trabecular meshwork and ciliary body revealed that the canonical focal adhesion pathway played a major role in the function of the pressure regulating tissues of the eye and therefore contribute substantially to IOP regulation and

possible pathogenesis of POAG. This finding was concordant with previous meta-analyses on GEO database expression data (Yan et al., 2015, Zhavoronkov et al., 2016), where focal adhesion and its sub-pathway extracellular matrix-receptor interaction were found to be differentially expressed in the trabecular meshwork and lamina cribrosa of patients with glaucoma. Our results and the results of the GEO database meta-analyses (Yan et al., 2015, Zhavoronkov et al., 2016) suggest a common link in the pathophysiologic mechanisms occurring at the trabecular meshwork and the optic nerve head, two non-adjacent tissues with seemingly distinct functions, which coalesce to produce the disease of POAG.

Finally, I would like to conclude by summarizing the improved understanding of primary open-angle glaucoma achieved via non-hypothesis driven genomic and transcriptomic exploration using next generation sequencing techniques. Genomic sequencing has revealed that high pressure glaucoma and normal tension glaucoma may have distinct underlying pathophysiologies. High pressure glaucoma may arise from inadequate aqueous outflow resulting from defects in the clearance of misfolded proteins. Normal tension glaucoma may arise from increased ganglion cell susceptibility to apoptosis resulting from impairment in transmembrane ion homeostasis. Transcriptomic investigation has revealed that the biologic functions of both the pressure regulating ocular tissues and the damaged tissue in glaucoma interconnect significantly via the canonical focal adhesion pathway. Therefore boundaries of high pressure and normal tension glaucoma are as expected not clear, and are likely to exist on a continual spectrum, directed by abnormalities in extracellular matrix and cell receptor interactions. In clinical terms, this implies that the development of glaucoma may occur at varied IOP for individual patients. For patients with neuronal susceptibility, a low IOP will lead to glaucoma, and these patients we designate as NTG patients. For patients without neuronal susceptibility, then a high IOP is required to cause glaucoma, and we designate these patients as HTG patients. This finding is certainly supported by the existence of overlapping clinical

phenotypes of glaucoma patients in the ANZRAG database, the largest genetic repository of patients with advanced glaucoma.

Appendix

Exons	Primer sequence (forward/reverse)	Size (bp)
1.1	5’-CACCTCTCAGCACAGCAGAG-3’ 5’-GTAGGCAGTCTCCAACTCTCTG-3’	478
1.2	5’-CCATGTCAGTCATCCATAACTTAC-3’ 5’-TAGGAGAAAGGGCAGGCAG-3’	505
2	5’-CAACATAGTCAATCCTTGGGC-3’ 5’-ATACTGATTCTCTGAACACAGCAC-3’	269
3.1	5’-GGGCTGTCACATCTACTGGC-3’ 5’-GCTGTAAATGACCCAGAGGC-3’	555
3.2	5’-GCTGAATACCGAGACAGTGAAG-3’ 5’-AACTTGGAAAGCAGTCAAAGC-3’	590

Appendix Table 1: Primers used for PCR and direct sequencing of the Myocilin gene.

Appendix Table 2: All pathogenic variants in known monogenic Mendelian glaucoma genes found on whole exome sequencing. MAF = minor allele frequency, N = number of cases

Gene	Exon	cDNA change	Amino acid change	SIFT	Polyphen2 HVAR	ExAC MAF	Glaucoma N (MAF)	Control N (MAF)
ASB10 (NM_001142459)	exon 3	c.667G>A	p.Arg223Thr	D	D	9.37E-05	1 (0.0023)	0 (0)
ASB10 (NM_001142459)	exon 3	c.910C>T	p.Arg304Cys	T	D	0.0037	1 (0.0023)	1 (0.0005)
ASB10 (NM_001142459)	exon 3	c.986C>T	p.Thr329Met	D	D	0.0015	1 (0.0023)	0 (0)
ASB10 (NM_001142459)	exon 4	c.1141G>C	p.Glu381Gln	T	D	0.0001	1 (0.0023)	2 (0.0009)
CYP1B1 (NM_000104)	exon 2	c.241T>A	p.Tyr81Asn	D	D	0.007	1 (0.0023)	0 (0)
CYP1B1 (NM_000104)	exon 2	c.535delG	p.Ala179ArgfsTer18	.	.	0.0001134	1 (0.0023)	0 (0)
CYP1B1 (NM_000104)	exon 2	c.710C>A	p.Ala237Glu	D	D	.	2 (0.0046)	0 (0)
CYP1B1 (NM_000104)	exon 2	c.868dupC	p.Arg290ProfsTer37	.	.	7.73E-05	2 (0.0046)	0 (0)
CYP1B1 (NM_000104)	exon 3	c.1103G>A	p.Arg368His	D	D	0.0029	1 (0.0023)	3 (0.0014)
CYP1B1 (NM_000104)	exon 3	c.1159G>A	p.Glu387Lys	D	D	0.00056	1 (0.0023)	0 (0)
CYP1B1 (NM_000104)	exon 3	c.1586T>G	p.Leu529Arg	D	P	.	1 (0.0023)	0 (0)
IL20RB (NM_144717)	exon 4	c.418C>T	p.Arg140Ter	.	.	.	1 (0.0023)	0 (0)
LTBP2 (NM_000428)	exon 5	c.1096C>T	p.Arg366Cys	D	B	4.59E-05	1 (0.0023)	0 (0)
LTBP2 (NM_000428)	exon 7	c.1612C>T	p.Arg538Trp	D	P	0.0002	1 (0.0023)	0 (0)
LTBP2 (NM_000428)	exon 16	c.2612dupT	p.Cys872LeufsTer17	.	.	.	1 (0.0023)	0 (0)
LTBP2 (NM_000428)	exon 21	c.3262G>A	p.Gly1088Ser	D	B	0.0045	2 (0.0046)	9 (0.0041)
LTBP2 (NM_000428)	exon 31	c.4498G>T	p.Gly1500Cys	D	D	.	1 (0.0023)	0 (0)
LTBP2 (NM_000428)	exon 34	c.4964A>G	p.Tyr1655Cys	T	D	0.0005	1 (0.0023)	1 (0.0005)
MYOC (NM_000261)	exon 3	c.754G>A	p.Gly252Arg	D	D	.	1 (0.0023)	0 (0)
MYOC (NM_000261)	exon 3	c.856T>C	p.Trp286Arg	D	D	.	1 (0.0023)	0 (0)
MYOC (NM_000261)	exon 3	c.1099G>A	p.Gly367Arg	D	D	.	2 (0.0046)	0 (0)
MYOC (NM_000261)	exon 3	c.1102C>T	p.Gln368Ter	D	D	0.003629	19 (0.0436)	5 (0.0023)
MYOC (NM_000261)	exon 3	c.1109C>T	p.Pro370Leu	D	D	.	1 (0.0023)	0 (0)
MYOC (NM_000261)	exon 3	c.1130C>T	p.Thr377Met	D	D	9.61E-05	2 (0.0046)	0 (0)
MYOC (NM_000261)	exon 3	c.1138G>C	p.Asp380His	D	D	.	1 (0.0023)	0 (0)
MYOC (NM_000261)	exon 3	c.1313C>T	p.Thr438Ile	T	D	.	1 (0.0023)	0 (0)
MYOC (NM_000261)	exon 3	c.1441C>T	p.Pro481Ser	T	P	0.0001156	1 (0.0023)	0 (0)
NTF4 (NM_006179)	exon 2	c.263C>T	p.Arg88Val	D	P	0.0041	1 (0.0023)	4 (0.0018)

NTF4 (NM_006179)	exon 2	c.320G>C	p.Arg107Pro	D	P	.	1 (0.0023)	1 (0.0005)
NTF4 (NM_006179)	exon 2	c.419G>A	p.Arg140His	D	D	4.60E-05	1 (0.0023)	0 (0)
OPTN (NM_021980)	exon 2	c.148G>A	p.Glu50Lys	T	D	.	1 (0.0023)	0 (0)
WDR36 (NM_139281)	exon 1	c.98A>G	p.Asp33Gly	D	B	.	1 (0.0023)	0 (0)
WDR36 (NM_139281)	exon 1	c.99C>G	p.Asp33Glu	D	B	0.006	3 (0.0069)	7 (0.0032)
WDR36 (NM_139281)	exon 3	c.376G>A	p.Asp126Asn	D	B	0.0009	1 (0.0023)	3 (0.0014)
WDR36 (NM_139281)	exon 11	c.1345G>A	p.Arg449Thr	D	B	0.0049	1 (0.0023)	6 (0.0027)
WDR36 (NM_139281)	exon 17	c.1973A>G	p.Asp658Gly	D	D	0.0065	2 (0.0046)	22 (0.01)

Sample with chr22:37912044, c.G635A, p.R212H:

AG0168

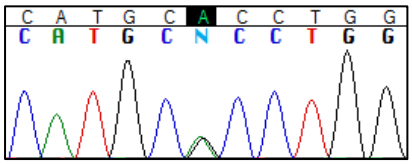

Samples with chr22:37904616, c.C983T, p.A328V:

AG0197 AG0679 AG1478

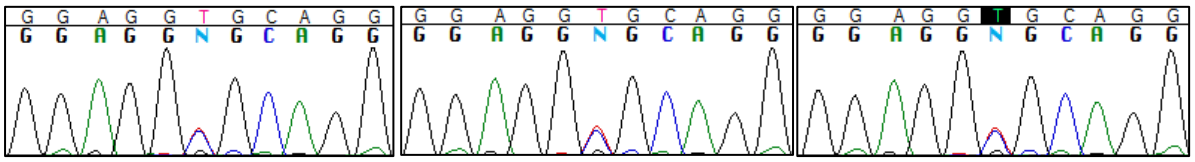

Sample with chr22:37904575, c.G1024A, p.V342M:

AG0605

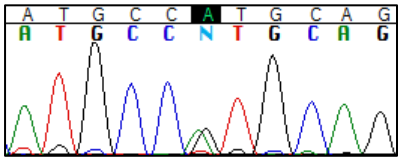

Sample with chr22:37902372, c.C1210T, p.R404W:

AG1733

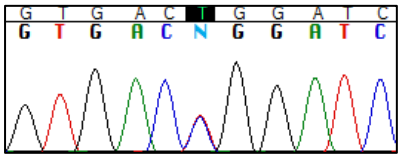

Samples with chr22:37888801, c.C2485T, p.R829W:

AG1739 AG1751

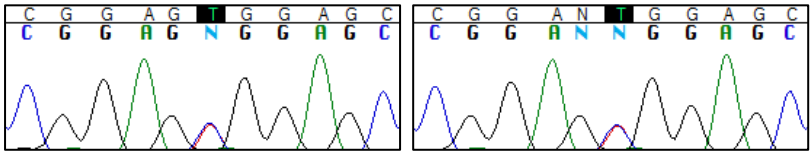

Appendix Figure 1: Chromatograms of all eight *CARD10* mutation carriers in the POAG cohort. Mutations in all carriers found on WES were successfully validated using direct sequencing. The sixth base from the left displays the mutation of interest.

Appendix Table 3: 86 randomly selected genes (Set 1 of 5).

Gene	POAG count	Control count	Odds ratio	Fisher's p value	Bonferroni corrected p
A1CF	2	2	5.85205	0.1048289	1
ADAMTS13	7	35	1.124465	0.8272367	1
AHCTF1	4	4	5.826453	0.0200615	1
ANKMY1	12	40	1.742435	0.1118611	1
ANO8	0	6	0	0.6013381	1
ARL14	1	2	2.927807	0.3774745	1
ATAD5	4	15	1.561477	0.5084975	1
ATR	1	6	0.970945	1	1
BEST3	2	4	2.927139	0.2147428	1
BTNL9	1	1	3.240642	0.4166409	1
C16orf58	1	11	0.53305	1	1
C1orf112	1	4	1.462121	0.546436	1
CADPS2	3	35	0.501416	0.3518734	1
CBR3	1	2	2.927807	0.3774745	1
CCDC18	2	23	0.507944	0.5666427	1
CCKBR	1	11	0.510938	1	1
CCL5	2	6	1.951872	0.3307526	1
CEMP1	3	5	3.192513	0.1203588	1
COG3	1	0	NA	1	1
DAB1	1	0	NA	0.1463129	1
EFCC1	6	4	3.63	0.0730326	1
EHMT2	1	5	1.147594	1	1
ENAM	2	9	1.301099	0.6683562	1
ERP27	0	2	0	1	1
ERVV-2	0	2	0	0.2193723	1
FAM134A	0	5	0	1	1
FAM186B	3	16	1.097594	0.7503793	1
FBXO3	0	2	0	1	1
FDX1	0	1	0	1	1
FRAS1	16	104	0.900741	0.7916693	1
FUT10	2	25	0.468327	0.4136134	1
GBE1	2	17	0.688756	1	1
GSTA1	0	2	0	1	1
HFM1	3	7	2.503329	0.1710959	1
HHIP	2	4	2.926916	0.2148756	1
HRNR	1	3	1.950535	0.4685225	1
IFI30	1	4	1.158088	1	1
ITGAE	1	18	0.32518	0.3429425	1
KDELR1	0	1	0	1	1
KDM3B	2	5	2.342674	0.2728739	1

L3MBTL1	3	18	0.975579	1	1
LDLRAP1	0	2	0	1	1
LOC100505841	3	0	NA	0.2626683	1
LPO	2	16	0.730318	1	1
LRRC1	2	7	1.604889	0.6330924	1
MAPK9	0	1	0	1	1
METTL21A	0	2	0	1	1
MRPL19	1	3	1.950535	0.4685225	1
MSMB	0	3	0	1	1
MTMR10	2	7	1.598167	0.6336662	1
MX1	6	21	1.665393	0.2722551	1
NIP7	0	2	0	1	1
NOP14	9	37	1.421323	0.3974909	1
NOTCH1	2	35	0.29892	0.1084715	1
NR2E1	1	0	NA	0.1461988	1
OPLAH	4	60	0.348289	0.0354409	1
OPN3	2	26	0.449404	0.4163838	1
OR10A5	0	5	0	1	1
OR6C4	3	8	2.195856	0.2100524	1
OVGP1	4	13	1.797844	0.2980062	1
PAQR4	0	9	0	0.3701724	1
PARP12	0	1	0	1	1
PARP8	1	4	1.464349	0.5458305	1
PMPCB	3	8	2.164773	0.2154121	1
PRR14	0	3	0	1	1
RBFA	0	4	0	1	1
RNF26	0	4	0	1	1
RPS6KB2	6	14	2.413579	0.1066764	1
SCN8A	2	8	1.446357	0.6489218	1
SGCB	0	2	0	1	1
SGPL1	0	6	0	0.6017614	1
SLA2	1	6	0.971658	1	1
SLC15A5	2	1	1.786096	1	1
SLC34A2	5	22	1.323286	0.5821436	1
SYCE2	5	14	2.091291	0.1824342	1
TAF1D	0	2	0	1	1
TCF3	4	28	0.787406	0.8080159	1
TMEM198	2	16	0.715775	1	1
TRAF7	1	1	4.5	0.3311565	1
TST	2	1	11.66845	0.0583192	1
WDR31	1	5	1.171658	1	1
WDR91	0	6	0	0.6016694	1
ZCRB1	0	1	0	1	1

ZNF296	0	2	0	1	1
ZNF649	0	7	0	0.6029747	1
ZPBP2	6	16	2.195053	0.1214391	1

Appendix Table 4: 86 randomly selected genes (Set 2 of 5).

Gene	POAG count	Control count	Odds ratio	Fisher's p value	Bonferroni corrected p
AATK	3	3	3.88057	0.1059226	1
ACOT4	3	4	4.393048	0.069347	1
ADCK2	6	21	1.66794	0.2718428	1
ADTRP	1	1	5.855615	0.2709749	1
ALPPL2	2	4	2.901515	0.2174225	1
AOC2	1	8	0.727189	1	1
APOL1	5	12	2.43984	0.0911279	1
ARHGAP25	6	17	2.066688	0.1345317	1
ATAT1	0	1	0	1	1
ATRNL1	1	13	0.391032	0.4896112	1
BMP5	1	2	2.926916	0.3775991	1
BNIPL	2	3	3.900178	0.1581839	1
BRD1	1	3	1.942246	0.4699452	1
C15orf48	1	1	5.850267	0.2711696	1
C16orf96	4	27	0.852106	1	1
C4orf26	0	3	0	1	1
C9orf89	2	4	2.876114	0.2200136	1
CABIN1	7	51	0.791505	0.7082924	1
CCDC113	1	2	2.927807	0.3774745	1
CCDC159	0	7	0	0.6029715	1
CCIN	1	14	0.418204	0.7113386	1
CCNL1	2	2	5.855615	0.104756	1
CDCA8	0	5	0	1	1
CDK20	2	4	2.927807	0.2147428	1
CES4A	0	5	0	1	1
CFAP61	2	18	0.64099	0.7563381	1
CHL1	2	24	0.487857	0.5718871	1
CHP1	1	0	NA	0.1504212	1
COLEC12	0	2	0	1	1
DAZAP2	0	6	0	0.6017614	1
DEFB132	0	16	0	0.1504114	1
EHD3	1	4	1.463636	0.5459818	1
EPS15L1	1	0	NA	0.1461988	1
FAM117A	0	5	0	1	1
FAM193B	4	17	1.349733	0.539973	1
FAM196B	1	8	0.729412	1	1
FAXC	1	7	0.831169	1	1
FBXL14	3	16	1.044786	1	1
GTF2H1	0	1	0	1	1
HAT1	1	3	1.951872	0.4683807	1

HEATR5A	8	54	0.835446	0.8566907	1
HM13	0	1	0	1	1
HOXC8	0	1	0	1	1
IKBKE	3	18	0.973262	1	1
ING2	0	1	0	1	1
ITGBL1	1	12	0.487879	0.7063688	1
KARS	3	29	0.605854	0.6121912	1
KRT71	1	26	0.223673	0.1647471	1
LIG3	1	5	1.171123	1	1
NEK10	1	6	0.699049	1	1
NHP2	0	2	0	1	1
NIPSNAP3A	3	10	1.755615	0.4211953	1
NISCH	4	13	1.518268	0.5111687	1
NUCB2	1	0	NA	0.1467136	1
NUP88	0	6	0	0.6014656	1
OR10H2	2	4	2.927807	0.2147428	1
PDCD11	7	53	0.773336	0.7100059	1
PINX1	1	11	0.532268	1	1
PPP1R16A	2	9	1.003367	1	1
PRMT3	1	10	0.584492	1	1
PRR14	0	3	0	1	1
PRSS41	1	30	0.194831	0.0750453	1
RECQL4	16	89	0.966543	1	1
RHCE	0	1	0	1	1
RPL7A	3	17	1.033344	1	1
SORBS1	7	20	1.764643	0.1947405	1
SPHK2	1	5	1.039572	1	1
SPON2	3	2	7.692513	0.0338768	1
STK33	0	3	0	1	1
TARSL2	1	4	1.13135	1	1
TCAIM	0	7	0	0.602978	1
TCHH	0	20	0	0.0602135	1
TGFB2	2	7	1.647059	0.6297847	1
TRAF7	1	1	4.5	0.3311565	1
TRAPPC9	4	17	1.372968	0.535401	1
TRIM63	1	13	0.44626	0.7073792	1
TSPAN1	0	2	0	1	1
TXNRD3NB	1	5	1.168984	1	1
ZBTB8OS	1	3	1.950089	0.4686644	1
ZFR2	3	11	1.391763	0.7141015	1
ZNF286A	0	8	0	0.6121791	1
ZNF560	2	8	1.463755	0.646954	1
ZNF664	0	1	0	1	1

ZNF786	2	7	1.504966	0.6424142	1
ZNF829	0	2	0	1	1
ZNHIT3	0	3	0	1	1

Appendix Table 5: 86 randomly selected genes (Set 3 of 5).

Gene	POAG count	Control count	Odds ratio	Fisher's p value	Bonferroni corrected p
AARSD1	0	3	0	1	1
ABCA1	2	19	0.61624	0.7573342	1
ACSL1	0	2	0	1	1
ADGRB3	2	11	1.064268	1	1
ADGRF2	7	36	1.136902	0.6680412	1
AHSG	1	25	0.233497	0.1618712	1
ARHGAP29	2	8	1.459626	0.6474015	1
ARPC4-TTLL3	1	12	0.485406	0.7062143	1
BRINP3	3	10	1.755258	0.4212998	1
C2	1	30	0.191711	0.0745187	1
C2CD4B	1	0	NA	1	1
CDH16	2	19	0.615649	0.7573527	1
CDH18	0	4	0	1	1
CFHR2	0	1	0	1	1
CLASP1	4	17	1.377233	0.5345755	1
CTNNA3	2	16	0.731746	1	1
CTNNBL1	0	2	0	1	1
DPYSL5	0	3	0	1	1
EARS2	0	5	0	1	1
EIF3B	3	9	1.951872	0.400524	1
FAM126A	3	16	1.096257	0.750556	1
FKBP3	1	2	2.77139	0.3926209	1
FLCN	2	7	1.668755	0.6282273	1
FSD1	1	1	5.762032	0.2744232	1
FZD6	3	4	4.392513	0.0694151	1
GALNT18	0	9	0	0.3734094	1
GDF6	1	2	2.894385	0.3806141	1
GJB7	0	9	0	0.3734094	1
GNB1L	1	6	0.863458	1	1
GPC5	0	12	0	0.2347457	1
GPR3	0	4	0	1	1
GSTP1	0	6	0	0.6017614	1
GUSB	0	8	0	0.6122945	1
GZMH	0	6	0	0.6017614	1
HINFP	3	17	1.033344	1	1
HMMR	0	3	0	1	1
IGSF5	1	9	0.650178	1	1
IL17RD	2	7	1.66864	0.6282273	1
KIF3B	0	1	0	1	1

KIT	0	3	0	1	1
KPRP	5	15	1.949279	0.1999143	1
KRTCAP2	0	6	0	0.6013985	1
LRRFIP2	4	7	3.346066	0.0645457	1
LUC7L	0	1	0	1	1
MAP4K2	4	28	0.832018	1	1
MAPK3	0	3	0	1	1
MED10	0	0	NA	1	1
MINOS1	1	1	3.160428	0.4235706	1
MORC2	0	7	0	0.6029747	1
MUS81	1	8	0.731618	1	1
N4BP1	0	1	0	1	1
NDRG3	1	1	5.855615	0.2709749	1
NDUFB6	1	11	0.506563	1	1
NEFH	1	7	0.752568	1	1
NEXN	2	13	0.89963	1	1
OR4Q3	0	8	0	0.6122366	1
OTUD3	1	23	0.181134	0.0669601	1
P4HA2	0	6	0	0.6017614	1
PDP2	0	1	0	1	1
PPAP2A	0	3	0	1	1
PRLHR	0	5	0	0.5900972	1
PTF1A	1	0	NA	0.1461988	1
PYGO2	1	2	2.925134	0.3777238	1
PZP	8	28	1.673033	0.2307263	1
RAD54L	6	29	1.210098	0.6311035	1
RHBDD1	2	7	1.673033	0.6279043	1
RYR3	18	79	1.332262	0.3056558	1
SCUBE1	3	16	1.085561	0.7525348	1
SLC34A3	3	9	1.394162	0.7114481	1
SLC41A1	0	2	0	1	1
SLC7A4	6	47	0.73708	0.6937788	1
SLFN12L	4	15	1.561497	0.508433	1
SMYD1	9	34	1.548196	0.2738271	1
SRL	1	2	2.910873	0.3791007	1
SYT10	1	3	1.951872	0.4683807	1
TALDO1	2	20	0.581952	0.7601671	1
TARBP2	1	8	0.727941	1	1
TAS2R16	0	1	0	1	1
TBC1D32	9	17	3.076096	0.0097235	0.836218
TBXA2R	3	24	0.665274	0.7892756	1
TCTN2	1	4	1.437166	0.5520959	1
TLCD2	1	25	0.233155	0.1618711	1

TOMM20L	0	1	0	1	1
TPRN	2	17	0.451068	0.3960126	1
TRIL	0	0	NA	1	1
UTP14C	4	15	1.561497	0.508433	1

Appendix Table 6: 86 randomly selected genes (Set 4 of 5).

Gene	POAG count	Control count	Odds ratio	Fisher's p value	Bonferroni corrected p
ABCC9	0	11	0	0.3838643	1
ACOT6	0	2	0	1	1
ADD2	1	8	0.718416	1	1
ADORA3	1	3	1.793672	0.4948261	1
AFF1	8	26	1.791855	0.1464416	1
ANAPC16	1	4	1.463904	0.5459818	1
ANKRD46	1	0	NA	1	1
APOBEC3G	0	5	0	1	1
ARRDC5	0	5	0	1	1
ATP5SL	2	5	2.219608	0.2920291	1
ATP6V1D	3	6	2.927807	0.1331597	1
BMP3	2	11	1.015881	1	1
C21orf62	1	3	1.951872	0.4683807	1
C6orf25	1	1	5.631016	0.2793998	1
C7orf65	0	3	0	1	1
CAPRIN2	3	17	1.033134	1	1
CBS	3	21	0.807257	1	1
CCDC168	38	314	0.708517	0.0602607	1
CCDC183	0	4	0	1	1
CD200R1L	3	5	3.508556	0.0995173	1
CD27	1	4	1.443405	0.5507093	1
CFHR1	0	4	0	1	1
CLN6	0	2	0	1	1
COBL	3	19	0.856389	1	1
CRYZ	2	11	1.063685	1	1
DAB2IP	3	22	0.78541	1	1
DES	1	2	2.609626	0.4095845	1
DHRS1	3	4	4.392284	0.0694151	1
DIEXF	2	12	0.975045	1	1
DLGAP4	1	12	0.463012	0.7053515	1
DRAXIN	0	2	0	1	1
ELF3	1	4	1.461898	0.546436	1
ENDOD1	0	2	0	1	1
FAM189B	4	27	0.835443	1	1
FLG2	2	17	0.688162	1	1
GFI1	0	21	0	0.0604393	1
GNB1L	1	6	0.863458	1	1
GPR21	0	1	0	1	1
HEATR6	1	39	0.150075	0.0230659	1
HIF3A	1	11	0.476746	0.7037453	1

HIST1H4C	1	0	NA	0.1461419	1
IKZF2	3	4	4.391711	0.0694151	1
KCTD18	1	9	0.650386	1	1
KIF22	0	2	0	1	1
LCN10	0	3	0	1	1
LINGO2	0	1	0	1	1
MIDN	1	1	3.187166	0.4212358	1
MMP11	0	13	0	0.2379489	1
MROH9	1	5	1.170053	1	1
MSRB2	2	2	5.855615	0.104756	1
N4BP2L1	0	2	0	1	1
NAT14	1	1	4.566845	0.3275764	1
NINJ1	0	3	0	1	1
OR4S1	0	4	0	1	1
OR5D18	2	9	1.301446	0.6683562	1
PDE9A	2	4	2.927807	0.2147428	1
PGK2	2	9	1.301464	0.6683562	1
PIGM	2	7	1.67085	0.6280654	1
PLAC9	1	2	2.914439	0.3787242	1
PLXNA2	8	44	1.059796	0.8433038	1
PRKACG	0	4	0	1	1
PTH2R	1	8	0.731952	1	1
RARB	0	2	0	1	1
REM2	2	0	NA	0.0214227	1
RETNLB	0	2	0	1	1
RHOU	0	3	0	1	1
SDR42E1	0	8	0	0.6122366	1
SERPINI2	1	5	1.170053	1	1
SGK494	3	14	1.25234	0.7279438	1
SIGLEC15	0	1	0	1	1
SIT1	0	4	0	1	1
SLC13A4	1	2	2.890374	0.3809943	1
SLC5A7	1	20	0.292914	0.3467883	1
SLFNL1	6	22	1.504063	0.4250656	1
SNX33	2	8	1.460784	0.6473266	1
TARS2	1	11	0.531704	1	1
TCEB3B	0	4	0	1	1
TDRD5	5	25	1.170053	0.7934176	1
TRPA1	6	28	1.254393	0.6234452	1
TSKU	0	8	0	0.6151802	1
TTC39C	0	2	0	1	1
WDR83	1	5	1.158075	1	1
XPC	3	10	1.635963	0.4390256	1

ZC3H12A	0	21	0	0.0604527	1
ZFYVE16	1	6	0.975045	1	1
ZNF836	1	6	0.975936	1	1

Appendix Table 7: 86 randomly selected genes (Set 5 of 5).

Gene	POAG count	Control count	Odds ratio	Fisher's p value	Bonferroni corrected p
ABCC1	3	24	0.731618	0.787467	1
ABCC5	0	6	0	0.6017614	1
ADAMTS15	1	9	0.635175	1	1
ALDH18A1	1	3	1.951426	0.4683807	1
ARHGAP9	6	23	1.441758	0.4347851	1
ARL6IP6	0	1	0	1	1
ASB3	3	1	2.679144	0.6265628	1
BAGE2	1	1	1.390374	1	1
BIVM-ERCC5	2	12	0.975681	1	1
C1orf115	1	18	0.321351	0.3421671	1
C1orf159	3	10	1.683957	0.4314019	1
C2CD3	5	17	1.646579	0.3645786	1
C6	6	32	1.097928	0.8166957	1
CACNA2D2	6	9	3.744652	0.0179085	1
CAMSAP3	1	7	0.745034	1	1
CCDC173	2	6	1.951872	0.3307526	1
CDK4	1	4	1.464238	0.5458305	1
CHRNA2	1	0	NA	0.1461988	1
COL27A1	6	26	1.328906	0.4607456	1
COL6A5	7	67	0.611723	0.2443287	1
DHX37	1	5	1.154439	1	1
EEF2	2	7	1.640183	0.630303	1
ENDOU	2	2	4.142602	0.1731901	1
EPHB2	4	13	1.799484	0.2977954	1
ERICH3	1	15	0.389967	0.4941027	1
FAM107A	0	8	0	0.6135303	1
FAM3B	1	7	0.777438	1	1
FBXL13	1	16	0.365642	0.4945189	1
FBXL6	0	4	0	1	1
FBXO24	2	8	1.394003	0.655376	1
FPGT	4	9	2.594573	0.1110443	1
FRY	4	10	2.342246	0.1371047	1
GABBR1	1	6	0.962567	1	1
GPSM3	0	3	0	1	1
H2AFZ	1	1	5.839572	0.2715599	1
HSPA4	0	3	0	1	1
IFNAR2	1	11	0.532329	1	1
IL17A	2	9	1.296257	0.6690938	1
INVS	2	15	0.780749	1	1
ITGB3BP	0	5	0	1	1

KBTBD13	3	4	1.707219	0.443393	1
KRTAP26-1	0	2	0	1	1
KRTAP5-9	1	11	0.529169	1	1
LAMA2	13	83	0.908738	0.8832301	1
LAPTM4B	1	3	1.3041	1	1
LIPJ	1	6	0.974153	1	1
LOC81691	0	7	0	0.6029747	1
LRCOL1	2	1	1.574332	1	1
MEIS2	1	3	1.950089	0.4686644	1
MTA1	1	1	3.468806	0.3981581	1
MYBPC2	2	18	0.632997	0.7562212	1
NOL12	1	0	NA	0.1511487	1
NUB1	2	3	3.881759	0.1592283	1
OR1C1	1	2	2.925134	0.3777238	1
OR1S1	2	11	1.064657	1	1
OTX2	1	0	NA	0.1463129	1
PFKFB4	0	3	0	1	1
PLA2G10	0	1	0	1	1
POLR2I	0	1	0	1	1
RCBTB2	0	5	0	1	1
RHOB	0	10	0	0.3769304	1
RPAIN	0	3	0	1	1
RSG1	1	6	0.962567	1	1
RTCA	0	2	0	1	1
SAP30L	1	1	5.855615	0.2709749	1
SCN11A	2	10	1.170945	0.6910151	1
SCN7A	14	60	1.363815	0.3167056	1
SERPINI2	1	5	1.170053	1	1
SETMAR	3	6	2.917494	0.1341161	1
SIGLEC6	1	5	1.168128	1	1
SIN3B	1	2	2.818182	0.3879669	1
SIX4	1	5	1.117005	1	1
SLC25A23	1	8	0.729278	1	1
SMYD4	1	13	0.450144	0.7072659	1
SULT4A1	0	1	0	1	1
SYCN	1	1	3.86631	0.3693644	1
TBC1D2	4	30	0.756726	0.8089525	1
TEP1	11	74	0.86684	0.756227	1
TTC37	3	9	1.951223	0.4005981	1
TTC39C	0	2	0	1	1
UGT2A1	2	6	1.897802	0.3420271	1
VPS33B	0	1	0	1	1
YWHAQ	0	3	0	1	1

ZBTB8B	0	6	0	0.6017153	1
ZFYVE19	2	24	0.487701	0.5719418	1
ZNF846	2	27	0.433749	0.4214984	1

Appendix Table 8: List of enriched genes for POAG cohort under a predicted pathogenic model

Headings:

Gene: HGNC gene name

POAG: Number of cases in POAG cohort

CTRL: Number of cases in local and AOGC controls

POAG CTRL OR (95%CI): Odds ratio of POAG cohort compared to controls

POAG NFE OR (95% CI): Odds ratio of POAG cohort compared to non-Finnish European ExAC public domain data

Gene	POAG	CTRL	POAG CTRL OR (95%CI)	POAG NFE OR (95% CI)
ABHD6	1	0	Inf	4.16 (0.57-30.34)
ACBD5	2	2	5.86 (0.82-41.89)	4.76 (1.16-19.55)
ACD	5	2	13.31 (2.56-69.11)	4 (1.63-9.82)
ACTA1	1	0	Inf	8 (1.07-59.64)
AES	1	0	Inf	8.21 (1.07-62.79)
AGO1	1	1	5.88 (0.37-94.36)	5.07 (0.69-37.21)
AGPAT3	1	1	5.55 (0.35-89.06)	5.01 (0.68-36.76)
AGPAT6	1	1	5.88 (0.37-94.45)	4.15 (0.57-30.29)
AKTIP	1	1	5.88 (0.37-94.45)	4.69 (0.64-34.36)
ALDOC	3	4	4.44 (0.99-20.01)	5.51 (1.73-17.55)
AMMECR1L	1	0	Inf	11.12 (1.47-84.26)
ANAPC10	1	0	Inf	13.78 (1.79-105.87)
ANGPT2	3	2	8.91 (1.48-53.7)	7.43 (2.32-23.78)
ANKRD34A	1	0	Inf	5.27 (0.72-38.81)
ANKRD46	1	0	Inf	9.76 (1.29-73.74)
AP1AR	3	4	4.44 (0.99-20.02)	6.32 (1.98-20.19)
AP1S3	1	1	5.88 (0.37-94.45)	5.19 (0.71-38.11)
APOH	2	2	5.91 (0.83-42.19)	5.34 (1.3-21.95)
APOM	1	0	Inf	6.41 (0.87-47.41)
ARHGAP25	2	2	5.91 (0.83-42.2)	5.69 (1.38-23.44)
ARL14EPL	3	0	Inf	5.83 (1.38-24.58)
ARL5B	1	1	5.88 (0.37-94.45)	6.59 (0.89-48.79)
ATF2	1	1	5.88 (0.37-94.41)	5.01 (0.68-36.77)
ATG3	2	0	Inf	7.6 (1.83-31.53)
ATP5I	1	1	5.27 (0.33-84.7)	4.44 (0.61-32.51)
ATP6AP1L	1	0	Inf	5.11 (0.7-37.52)
ATP6V1G1	1	1	5.88 (0.37-94.36)	5.23 (0.7-39.31)
B3GNT7	1	0	Inf	4.65 (0.63-34.07)
BAD	3	1	13.73 (1.42-132.73)	4.14 (1.3-13.14)
BHLHA9	1	0	Inf	Inf
BLOC1S4	1	0	Inf	7.42 (0.98-56.49)

BMPR1A	2	1	11.83 (1.07-131.1)	5.06 (1.23-20.78)
BPIFA1	1	0	Inf	3.94 (0.54-28.77)
BTBD3	1	1	5.11 (0.32-82.11)	4.13 (0.57-30.16)
BZW2	1	0	Inf	6.3 (0.85-46.64)
C10orf95	2	0	Inf	25.25 (5.56-114.73)
C11orf86	1	1	5.46 (0.34-87.72)	17.98 (1.12-288.68)
C11orf91	1	0	Inf	3.89 (0.35-43.14)
C15orf48	1	1	5.88 (0.37-94.36)	12.48 (1.63-95.4)
C17orf105	1	1	5.88 (0.37-94.45)	7.51 (0.78-72.51)
C1orf226	1	1	5.84 (0.36-93.8)	4.03 (0.55-29.73)
C1orf52	1	1	5.15 (0.32-82.63)	6.66 (0.9-49.49)
C20orf62	3	0	Inf	8 (1.9-33.74)
C3orf14	2	1	11.82 (1.07-131.04)	18.77 (4.34-81.17)
C4A	2	0	Inf	25.18 (5.68-111.56)
C4orf32	2	0	Inf	8.97 (2.13-37.79)
C6orf120	2	0	Inf	6.7 (1.61-27.86)
C6orf52	1	0	Inf	7.89 (0.82-76.2)
C8orf37	1	0	Inf	5.1 (0.7-37.45)
CA13	2	2	5.89 (0.82-42.09)	4.33 (1.06-17.74)
CACNG4	1	1	5.74 (0.36-92.25)	5.58 (0.76-41.1)
CADM2	1	0	Inf	8.08 (1.08-60.28)
CALU	1	1	5.88 (0.37-94.45)	5.08 (0.69-37.38)
CAMK1	3	2	8.91 (1.48-53.68)	4.22 (1.33-13.38)
CATSPER3	3	3	5.93 (1.19-29.63)	4.61 (1.45-14.64)
CBFB	1	0	Inf	9.44 (1.26-70.85)
CBLL1	2	1	11.83 (1.07-131.1)	10.87 (2.59-45.65)
CCDC179	1	0	Inf	Inf
CCDC6	1	1	5.88 (0.37-94.45)	5.27 (0.72-38.75)
CCDC94	1	1	5.85 (0.36-93.93)	5.31 (0.72-39.2)
CCRN4L	1	0	Inf	5.59 (0.76-41.14)
CCSAP	1	0	Inf	7.23 (0.97-54.05)
CDC23	1	1	5.88 (0.37-94.45)	7.11 (0.96-52.78)
CDKN2AIP	3	1	17.84 (1.85-172.41)	9.5 (2.94-30.65)
CEBPD	1	0	Inf	8.96 (1.18-68.19)
CHAMP1	2	2	5.91 (0.83-42.2)	13.83 (3.26-58.69)
CHMP1B	1	0	Inf	5.9 (0.79-43.75)
CHP1	1	0	Inf	19.88 (2.51-157.71)
CHRAC1	1	0	Inf	16.68 (2.1-132.36)
CHST2	2	1	8.55 (0.77-94.81)	10.5 (2.48-44.47)
CLCN3	2	1	11.83 (1.07-131.1)	4.54 (1.11-18.62)
CLEC4D	2	2	5.91 (0.83-42.19)	9.49 (2.27-39.65)
CLPSL2	2	1	10.52 (0.95-116.57)	11.72 (2.68-51.34)
CLVS1	1	0	Inf	7.74 (1.04-57.6)
COQ10B	1	0	Inf	6.79 (0.92-50.29)
COQ5	2	1	11.82 (1.07-130.98)	4.25 (1.04-17.42)
COX17	1	0	Inf	42.21 (4.7-379.45)

COX5A	2	0	Inf	5.62 (1.37-23.14)
COX6A1	1	1	5.31 (0.33-85.3)	5.19 (0.71-38.15)
CPLX2	1	1	5.32 (0.33-85.39)	7.28 (0.97-54.65)
CPOX	2	1	4.68 (0.42-51.91)	4.83 (1.18-19.84)
CREG1	1	1	5.88 (0.37-94.36)	4.73 (0.64-34.67)
CRIPT	1	1	5.88 (0.37-94.45)	5.22 (0.71-38.3)
CRYBA4	3	2	8.9 (1.48-53.66)	7.39 (2.31-23.66)
CST3	1	0	Inf	12.24 (1.52-98.35)
CST6	2	2	4.16 (0.58-29.7)	60.24 (11.61-312.48)
CST7	2	2	5.53 (0.77-39.51)	10.9 (2.6-45.75)
CTDSP1	2	0	Inf	12.96 (3.05-55.1)
CTXN3	1	1	5.88 (0.37-94.45)	13.79 (1.79-105.95)
CYP46A1	1	1	5.88 (0.37-94.45)	6.33 (0.85-47.06)
DCAF5	4	2	11.95 (2.17-65.69)	6.08 (2.22-16.66)
DCD	1	1	5.88 (0.37-94.45)	4.57 (0.62-33.66)
DCK	1	0	Inf	7.4 (1-54.96)
DCTN3	1	0	Inf	5.27 (0.72-38.8)
DCTN5	1	0	Inf	9.23 (1.22-69.69)
DDRGK1	3	0	Inf	4.22 (1.33-13.41)
DEFB135	3	2	8.91 (1.48-53.69)	8.43 (2.63-27.09)
DESI2	1	0	Inf	19.13 (2.41-151.74)
DGCR6L	3	3	4.12 (0.82-20.58)	5.16 (1.62-16.45)
DNAJA2	1	1	5.88 (0.37-94.36)	4.44 (0.61-32.43)
DNAJC11	2	1	11.82 (1.07-131.01)	4.75 (1.16-19.49)
DPF2	1	1	5.88 (0.37-94.45)	5.66 (0.77-41.64)
DPM1	1	1	5.88 (0.37-94.36)	5.59 (0.76-41.12)
DRG1	1	0	Inf	8.94 (1.19-66.97)
DYDC1	2	1	11.83 (1.07-131.1)	14.29 (3.36-60.77)
DYNC1I1	2	2	5.91 (0.83-42.2)	5.06 (1.23-20.81)
DYNLRB1	1	0	Inf	16.33 (2.08-128.25)
EBF3	2	2	5.89 (0.82-42.05)	7.13 (1.72-29.56)
ECHDC3	3	1	11.69 (1.21-113.04)	4.4 (1.39-13.96)
EEF1E1	1	0	Inf	9.64 (1.28-72.81)
EGFL8	2	2	5.53 (0.77-39.53)	4.02 (0.98-16.47)
EID1	1	0	Inf	8.26 (1.11-61.74)
EIF2S1	1	0	Inf	6.37 (0.86-47.08)
EIF4H	1	0	Inf	4.38 (0.6-32)
EMID1	2	0	Inf	5.16 (1.25-21.28)
ERICH2	3	0	Inf	13.84 (2.77-69.03)
ERLIN2	2	0	Inf	12.85 (3.04-54.32)
EVI2A	1	0	Inf	3.96 (0.54-28.86)
FAM110A	2	0	Inf	5.32 (1.28-22.06)
FAM131A	2	2	5.64 (0.79-40.27)	4.44 (1.08-18.23)
FAM181B	1	0	Inf	5.23 (0.69-39.47)
FAM32A	2	2	5.91 (0.83-42.19)	9.61 (2.24-41.18)
FAM89B	1	0	Inf	9.04 (1.2-67.89)

FBXO21	2	1	4.71 (0.42-52.26)	6.34 (1.53-26.27)
FBXO22	2	1	10.54 (0.95-116.79)	6.03 (1.46-24.96)
FBXW12	3	3	5.93 (1.19-29.62)	4.73 (1.49-15.03)
FGF9	1	0	Inf	16.26 (2.09-126.62)
FGL2	3	4	4.44 (0.99-20)	5.79 (1.82-18.45)
FNTA	1	1	5.88 (0.37-94.41)	5.5 (0.75-40.61)
FOXD2	1	0	Inf	7.29 (0.96-55.24)
FOXG1	1	0	Inf	13.11 (1.67-102.9)
FOXH1	2	2	5.42 (0.76-38.7)	4.57 (1.11-18.82)
FOXO6	1	0	Inf	5.96 (0.54-66.06)
FRAT1	1	1	5.63 (0.35-90.39)	6.6 (0.85-51.04)
FST	1	0	Inf	6.18 (0.84-45.59)
FXYD4	1	0	Inf	5.43 (0.74-39.9)
FXYD7	1	0	Inf	25.6 (3.13-209.09)
GAS1	2	0	Inf	15.01 (3.27-68.98)
GATAD1	1	0	Inf	5.27 (0.72-38.74)
GDF1	2	0	Inf	4.93 (1.08-22.39)
GDF10	2	2	5.88 (0.82-42.04)	4.62 (1.12-19.01)
GDNF	1	1	5.88 (0.37-94.41)	4.5 (0.61-33)
GEMIN2	1	0	Inf	5.06 (0.69-37.13)
GFPT1	2	1	11.83 (1.07-131.1)	9.75 (2.33-40.79)
GGACT	1	0	Inf	12.47 (0.78-200.19)
GJA8	3	4	4.43 (0.98-19.95)	6.03 (1.89-19.21)
GLYR1	2	0	Inf	6.35 (1.54-26.23)
GPN2	2	1	11.56 (1.04-128.16)	4.73 (1.15-19.42)
GPR183	1	0	Inf	11.89 (1.56-90.48)
GRAMD4	2	1	11.46 (1.03-127.03)	4.51 (1.1-18.49)
GTF2B	1	1	5.88 (0.37-94.36)	4.7 (0.64-34.42)
H2AFZ	1	1	5.87 (0.37-94.19)	178.89 (11.15-2870.92)
HAND2	1	0	Inf	30.36 (3.53-261.17)
HAUS2	1	1	5.87 (0.37-94.32)	5.4 (0.73-39.73)
HBEGF	1	0	Inf	14.96 (1.92-116.44)
HCN1	1	1	5.76 (0.36-92.46)	4.03 (0.55-29.43)
HDAC3	1	0	Inf	8.53 (1.14-63.73)
HDGFL1	1	0	Inf	4.23 (0.57-31.23)
HES3	3	0	Inf	25.53 (7.46-87.42)
HES5	1	0	Inf	12.39 (1.58-97.28)
HIGD1B	1	0	Inf	7.09 (0.96-52.57)
HIST1H2AG	1	0	Inf	4.55 (0.62-33.31)
HIST1H3B	1	1	5.77 (0.36-92.59)	7.72 (1.04-57.48)
HIST1H3F	1	0	Inf	7.46 (1-55.45)
HIST1H4I	1	1	5.65 (0.35-90.74)	4.32 (0.59-31.6)
HIST2H2AB	2	0	Inf	14.78 (3.47-62.99)
HLA-DMB	1	1	5.88 (0.37-94.45)	5.39 (0.73-39.71)
HNRNPA3	1	0	Inf	24.99 (2.99-208.59)
HPGDS	2	1	11.82 (1.07-131.04)	4.49 (1.1-18.4)

HS3ST3B1	1	0	Inf	5.99 (0.8-44.68)
HSBP1	1	0	Inf	18.01 (2.16-150.33)
HTR1A	1	1	5.86 (0.36-94.1)	6.14 (0.83-45.29)
IFFO2	2	1	7.82 (0.71-86.71)	4.66 (1.1-19.82)
IGF2BP1	1	0	Inf	4.5 (0.61-32.91)
IL20RB	1	0	Inf	5.1 (0.7-37.42)
IL36A	1	0	Inf	6.64 (0.9-49.1)
IL5	1	0	Inf	6.88 (0.93-50.99)
IMMP2L	1	0	Inf	4.81 (0.66-35.24)
IMPAD1	1	1	5.88 (0.37-94.49)	5.58 (0.76-41.17)
INSL3	2	0	Inf	5.84 (1.4-24.38)
ITPA	3	1	17.83 (1.84-172.37)	11.18 (3.45-36.21)
ITPK1	3	2	7.84 (1.3-47.25)	6.86 (2.14-22.03)
JUNB	1	0	Inf	6.59 (0.88-49.35)
KAT8	1	0	Inf	7.73 (1.04-57.65)
KATNAL1	1	0	Inf	4.56 (0.62-33.33)
KBTBD4	3	3	4.27 (0.86-21.34)	5.77 (1.81-18.37)
KCNH1	3	0	Inf	7.28 (2.27-23.29)
KCNMA1	4	2	5.86 (1.07-32.28)	7.17 (2.6-19.76)
KCTD4	1	0	Inf	8.52 (1.14-63.69)
KLF13	1	0	Inf	8.31 (1.1-62.74)
KNG1	3	1	17.83 (1.84-172.36)	4.11 (1.3-13.02)
KPNB1	1	0	Inf	13.6 (1.77-104.48)
KRTAP20-1	1	0	Inf	3.97 (0.54-28.92)
KRTAP29-1	2	0	Inf	7.24 (1.32-39.79)
LAMTOR3	1	0	Inf	13.67 (1.77-105.65)
LBX1	1	1	5.78 (0.36-92.9)	4.27 (0.58-31.23)
LCN6	2	1	11.78 (1.06-130.56)	5.35 (1.3-22.03)
LEMD1	1	0	Inf	5.29 (0.72-38.91)
LGI4	4	3	4.21 (0.93-18.98)	5.46 (1.97-15.07)
LHX9	1	0	Inf	4.81 (0.66-35.25)
LMO2	1	0	Inf	6.68 (0.9-49.64)
LMO7DN	1	0	Inf	Inf
LOC730159	1	0	Inf	9.42 (0.59-151.28)
LPCAT4	3	4	4.44 (0.99-20.01)	6.45 (2.02-20.6)
LST1	2	0	Inf	5.37 (1.3-22.26)
LYPD2	2	2	5.81 (0.81-41.48)	4.3 (1.04-17.73)
MAB21L2	1	1	5.85 (0.36-93.89)	6.1 (0.83-45.02)
MAGEF1	3	2	6.25 (1.04-37.69)	11.83 (3.64-38.43)
MAP2K7	2	2	5.67 (0.79-40.49)	5.35 (1.3-22.08)
MAPKAPK2	1	1	5.62 (0.35-90.22)	6.37 (0.86-47.06)
MAPRE1	1	0	Inf	8.13 (1.09-60.62)
MB21D1	4	5	4.72 (1.26-17.76)	4.76 (1.74-12.99)
MBTD1	1	1	5.88 (0.37-94.49)	8.14 (1.09-60.82)
MEA1	1	0	Inf	5.86 (0.8-43.21)
MED19	1	0	Inf	4.83 (0.66-35.42)

MLLT3	1	0	Inf	4.95 (0.67-36.27)
MMD	1	1	5.88 (0.37-94.45)	8.01 (1.07-59.74)
MNX1	1	0	Inf	4.14 (0.56-30.84)
MORN3	2	2	5.89 (0.82-42.05)	5.62 (1.36-23.2)
MRPL12	1	0	Inf	4.33 (0.59-31.74)
MRPL17	2	2	5.86 (0.82-41.88)	11.31 (2.69-47.62)
MRPS10	3	1	17.84 (1.85-172.41)	6.57 (2.06-21)
MRPS12	1	0	Inf	7.55 (1.01-56.22)
MRPS26	2	0	Inf	6.82 (1.64-28.35)
MS4A3	1	0	Inf	4.68 (0.64-34.24)
MS4A6E	1	1	5.88 (0.37-94.49)	9.96 (1.32-74.99)
MYLK2	3	3	5.92 (1.19-29.55)	6.93 (2.16-22.2)
NACC1	2	1	10.1 (0.91-112)	12.31 (2.91-52.13)
NAPB	1	0	Inf	6.36 (0.86-47.06)
NAT14	1	1	4.59 (0.29-73.66)	10.91 (1.27-93.84)
NBL1	1	0	Inf	4.78 (0.5-46.22)
NBPF3	3	1	17.82 (1.84-172.25)	4.32 (1.36-13.7)
NDFIP2	1	1	5.5 (0.34-88.28)	10.57 (1.4-80.15)
NDNL2	2	1	11.82 (1.07-130.98)	9.2 (2.2-38.55)
NDRG3	1	1	5.88 (0.37-94.45)	4.59 (0.63-33.58)
NDUFA12	2	1	11.82 (1.07-131.06)	8.77 (2.11-36.54)
NDUFB2	1	1	5.88 (0.37-94.45)	4.61 (0.63-33.91)
NDUFC2-KCTD14	1	0	Inf	Inf
NECAP2	2	0	Inf	7.45 (1.8-30.92)
NEUROD4	2	2	5.91 (0.83-42.2)	5.89 (1.43-24.25)
NFKBIL1	2	0	Inf	6.89 (1.66-28.67)
NGB	3	0	Inf	21.8 (6.3-75.46)
NKX2-5	1	0	Inf	6.48 (0.87-48.55)
NKX6-2	3	0	Inf	11.01 (3.39-35.81)
NOL7	2	2	5.27 (0.74-37.64)	8.71 (2.07-36.56)
NOVA1	1	0	Inf	4.77 (0.65-35.02)
NOXRED1	2	0	Inf	5.23 (1.27-21.49)
NPAS3	3	4	4.06 (0.9-18.28)	4.35 (1.36-13.84)
NPW	1	0	Inf	4.11 (0.55-30.52)
NR2E1	1	0	Inf	12.05 (1.57-92.55)
NRL	1	0	Inf	6.82 (0.91-50.96)
NTMT1	1	0	Inf	4.23 (0.58-30.91)
NUP54	2	1	11.83 (1.07-131.1)	10.72 (2.55-45.07)
NUSAP1	4	3	7.95 (1.76-35.8)	4.95 (1.81-13.56)
ONECUT1	2	2	5.13 (0.72-36.66)	4.35 (1.06-17.82)
OR2J2	4	1	23.92 (2.66-215.2)	6.59 (2.41-18.06)
OR5R1	4	3	7.96 (1.77-35.84)	5.64 (2.06-15.42)
OSR2	1	1	5.82 (0.36-93.5)	4.1 (0.56-30.04)
OTX1	1	0	Inf	5.19 (0.71-38.11)
OTX2	1	0	Inf	6.85 (0.92-50.75)
PARL	1	0	Inf	4.05 (0.55-29.59)

PAX6	1	0	Inf	4.61 (0.63-33.78)
PBK	2	2	5.9 (0.83-42.18)	4.68 (1.14-19.18)
PDCD7	2	1	5.93 (0.53-65.78)	4.77 (1.16-19.63)
PDHB	1	1	5.88 (0.37-94.45)	4.66 (0.64-34.12)
PDPK1	2	2	5.37 (0.75-38.37)	13.22 (3.12-55.99)
PDX1	1	0	Inf	6.4 (0.85-47.91)
PDZD9	1	0	Inf	10.09 (1.34-76.22)
PELO	1	1	5.87 (0.37-94.28)	9.86 (1.31-74.25)
PEX11B	3	1	15.86 (1.64-153.32)	5.41 (1.7-17.24)
PEX3	1	0	Inf	6.34 (0.86-46.82)
PF4	2	2	5.91 (0.83-42.2)	25.79 (5.78-115.09)
PGF	3	4	4.39 (0.97-19.78)	13.84 (4.23-45.28)
PHIP	2	1	11.82 (1.07-131.06)	4.22 (1.03-17.29)
PIGC	1	0	Inf	3.96 (0.54-28.91)
PNPLA8	3	4	4.44 (0.99-20.02)	6.07 (1.9-19.36)
POLR3A	3	1	17.84 (1.85-172.41)	4.04 (1.28-12.82)
POLR3D	2	1	6.62 (0.6-73.44)	6.64 (1.61-27.47)
PPIH	2	2	5.9 (0.83-42.17)	8.97 (2.15-37.4)
PPM1L	2	1	11.83 (1.07-131.1)	10.55 (2.52-44.23)
PPP2R5A	2	1	11.82 (1.07-130.98)	8.14 (1.95-33.95)
PRLR	2	2	4.2 (0.59-30)	5.61 (1.36-23.09)
PRPSAP2	1	0	Inf	4.65 (0.63-34.04)
PRR23C	1	0	Inf	4.88 (0.65-36.29)
PSMB1	1	1	5.88 (0.37-94.45)	6.15 (0.83-45.44)
RAB13	1	1	5.88 (0.37-94.36)	5.56 (0.76-40.87)
RAB29	1	1	5.88 (0.37-94.36)	4.84 (0.66-35.5)
RAB2A	1	0	Inf	36.42 (4.05-327.43)
RAB6A	1	0	Inf	11 (1.45-83.4)
RAD21L1	3	0	Inf	23.75 (4.76-118.49)
RARRES2	1	0	Inf	6.04 (0.81-45.14)
RASL10B	1	1	5.71 (0.36-91.69)	24.57 (3.01-200.68)
RCHY1	1	1	5.71 (0.36-91.65)	4.21 (0.58-30.76)
RCN2	1	0	Inf	9.16 (1.22-68.97)
REEP3	1	1	5.88 (0.37-94.41)	9.14 (1.2-69.56)
RFX6	3	0	Inf	4.35 (1.37-13.79)
RGS17	1	0	Inf	5.17 (0.7-38)
RGS2	2	2	5.9 (0.83-42.17)	6.65 (1.61-27.47)
RLBP1	3	3	5.85 (1.17-29.2)	5.75 (1.8-18.33)
RND3	2	1	11.82 (1.07-131.06)	7.33 (1.77-30.36)
RNF141	4	4	5.96 (1.48-24.05)	38.28 (12.9-113.62)
RPL15	1	0	Inf	11.02 (1.42-85.81)
RPL18A	1	0	Inf	4.21 (0.58-30.79)
RPL5	1	1	5.88 (0.37-94.36)	5.22 (0.71-38.33)
RPL8	1	0	Inf	6.24 (0.85-46.13)
RPP38	1	1	5.88 (0.37-94.45)	4.23 (0.58-30.88)
RPRM	1	1	5.76 (0.36-92.55)	12.23 (1.6-93.45)

RRAGA	1	0	Inf	14.93 (1.93-115.4)
RSPO3	1	1	5.88 (0.37-94.45)	5.66 (0.77-41.68)
RXRA	2	0	Inf	12.15 (2.88-51.29)
SAC3D1	3	1	9.74 (1.01-94.22)	11.94 (3.65-39.08)
SAP30L	1	1	5.88 (0.37-94.45)	5.26 (0.71-38.79)
SERPINB2	2	2	5.91 (0.83-42.2)	4.18 (1.02-17.12)
SERPINF2	1	0	Inf	5.28 (0.72-38.79)
SFRP2	1	0	Inf	6.83 (0.92-50.66)
SGCZ	1	1	5.88 (0.37-94.45)	4.43 (0.61-32.43)
SHISA7	1	0	Inf	Inf
SIRT7	1	0	Inf	4.46 (0.61-32.7)
SLBP	3	0	Inf	22.61 (6.75-75.75)
SLC25A25	2	2	5.85 (0.82-41.79)	4.89 (1.19-20.09)
SLC25A48	3	2	8.91 (1.48-53.69)	11.43 (3.52-37.19)
SLC35F6	2	0	Inf	7.42 (1.79-30.83)
SLC39A14	2	1	6.6 (0.6-73.2)	4.49 (1.09-18.41)
SLC40A1	1	1	5.88 (0.37-94.45)	5.11 (0.7-37.48)
SLC48A1	1	0	Inf	5.31 (0.72-39.16)
SLX4IP	2	1	11.83 (1.07-131.1)	8.51 (2.05-35.43)
SMARCA4	4	3	6.39 (1.42-28.78)	5.02 (1.83-13.72)
SMEK2	2	2	5.87 (0.82-41.91)	4.46 (1.09-18.3)
SMIM11	1	0	Inf	19.63 (2.47-155.7)
SMIM14	2	1	11.83 (1.07-131.1)	15.63 (3.66-66.79)
SMIM18	1	0	Inf	Inf
SMR3A	1	1	5.88 (0.37-94.45)	5.96 (0.81-43.94)
SMR3B	2	2	5.91 (0.83-42.2)	4.22 (1.03-17.27)
SNAP25	1	0	Inf	16.63 (2.12-130.6)
SNN	1	0	Inf	10.4 (1.38-78.52)
SNX27	2	1	11.82 (1.07-130.98)	5.8 (1.4-23.98)
SNX8	3	2	8.63 (1.43-52.01)	12 (3.67-39.17)
SOWAHA	1	0	Inf	10.32 (1.33-80.32)
SP9	1	0	Inf	3.91 (0.48-31.97)
SPINK1	1	0	Inf	8.57 (1.14-64.22)
SPINK4	1	1	5.88 (0.37-94.45)	10.86 (1.43-82.3)
SPTY2D1	3	3	5.93 (1.19-29.61)	8.19 (2.55-26.29)
SRR	1	0	Inf	4.71 (0.64-34.48)
SRSF11	1	0	Inf	4.05 (0.56-29.57)
SRSF5	3	1	17.84 (1.85-172.41)	4.79 (1.51-15.22)
ST8SIA2	1	0	Inf	4.96 (0.68-36.46)
STAG1	1	0	Inf	4.31 (0.59-31.52)
STAM2	2	0	Inf	4.92 (1.2-20.21)
STIP1	1	0	Inf	3.89 (0.53-28.43)
STK24	1	0	Inf	5.24 (0.71-38.46)
STK4	2	1	11.83 (1.07-131.1)	7.8 (1.88-32.36)
SUPT16H	1	0	Inf	4.58 (0.63-33.54)
SVIP	1	0	Inf	4.94 (0.67-36.4)

TAC3	1	0	Inf	7.31 (0.98-54.35)
TADA2B	1	1	5.89 (0.37-94.54)	8.31 (1.11-62.24)
TAGLN3	1	0	Inf	16.25 (2.09-126.49)
TAPT1	3	3	5.93 (1.19-29.63)	8.25 (2.55-26.76)
TBC1D22A	3	4	4.17 (0.92-18.77)	4.86 (1.53-15.48)
TCTN3	5	4	7.45 (1.98-28.01)	9.88 (3.96-24.64)
TDP2	1	0	Inf	4.81 (0.66-35.27)
TGFBR2	3	1	14.18 (1.47-137.1)	6.95 (2.17-22.24)
TIRAP	2	2	5.85 (0.82-41.81)	5.6 (1.36-23.07)
TLX1	1	0	Inf	4.01 (0.54-29.46)
TMBIM1	3	2	8.91 (1.48-53.68)	5.45 (1.71-17.38)
TMEM116	2	1	11.82 (1.07-131.02)	5.88 (1.43-24.23)
TMEM14E	1	0	Inf	5.36 (0.73-39.43)
TMEM223	1	0	Inf	4.07 (0.55-30.1)
TMEM256	1	0	Inf	5.42 (0.73-40.11)
TMEM65	1	1	5.88 (0.37-94.45)	15.22 (1.94-119.5)
TMEM69	1	0	Inf	4.23 (0.58-30.91)
TMEM86A	2	2	5.88 (0.82-41.99)	6.31 (1.53-26.08)
TMEM8B	6	5	6.9 (2.09-22.86)	8.05 (3.51-18.49)
TMEM92	2	0	Inf	14.75 (3.46-62.87)
TNFRSF11B	1	1	5.88 (0.37-94.45)	6.63 (0.9-49.03)
TNFRSF25	2	1	10.57 (0.95-117.15)	6.43 (1.55-26.78)
TNFSF14	1	1	5.88 (0.37-94.41)	6.31 (0.85-46.76)
TNFSF15	1	0	Inf	5.24 (0.71-38.55)
TNFSF18	2	2	5.9 (0.83-42.16)	6.06 (1.47-24.98)
TNIP2	2	1	11.68 (1.05-129.42)	5.56 (1.35-22.93)
TPH2	2	2	5.91 (0.83-42.19)	3.99 (0.98-16.33)
TRIB1	2	1	11.83 (1.07-131.1)	4.58 (1.12-18.79)
TRIM44	1	0	Inf	4.35 (0.59-31.82)
TRMT12	2	1	11.83 (1.07-131.14)	4.91 (1.2-20.18)
TRMT5	1	0	Inf	4.13 (0.57-30.17)
TSPAN18	2	0	Inf	5.98 (1.45-24.63)
TSPAN3	1	1	5.88 (0.37-94.36)	8.78 (1.17-66.08)
TTLL1	2	0	Inf	4.41 (1.08-18.09)
TXNDC12	3	0	Inf	18.09 (5.46-59.92)
TYROBP	1	0	Inf	6.03 (0.82-44.61)
UBIAD1	1	0	Inf	9.43 (1.26-70.78)
UBP1	3	2	8.91 (1.48-53.69)	5.74 (1.8-18.3)
UBXN7	1	1	5.88 (0.37-94.45)	7.73 (1.04-57.57)
UCHL5	2	0	Inf	18.67 (4.28-81.4)
UFC1	2	0	Inf	5.28 (1.28-21.71)
UNC5D	4	2	8.45 (1.54-46.48)	4.37 (1.6-11.92)
USE1	1	0	Inf	5.03 (0.68-37.1)
UTP18	4	0	Inf	7.2 (2.62-19.8)
VAX1	1	1	5.63 (0.35-90.48)	8.2 (1.09-61.58)
VDAC3	1	1	5.88 (0.37-94.45)	4.44 (0.61-32.49)

WDYHV1	1	1	5.88 (0.37-94.45)	5.32 (0.72-39.16)
XRCC2	2	0	Inf	6.27 (1.52-25.88)
YBEY	1	0	Inf	5.71 (0.77-42.12)
YRDC	1	0	Inf	6.81 (0.91-50.9)
YWHAB	1	0	Inf	4.05 (0.55-29.53)
YWHAE	1	1	5.48 (0.34-88.06)	17.8 (2.27-139.78)
ZBED2	3	0	Inf	6.39 (2-20.4)
ZBTB34	1	0	Inf	7.68 (1.03-57.14)
ZBTB44	3	2	8.91 (1.48-53.67)	4.56 (1.43-14.49)
ZIC2	1	0	Inf	6.74 (0.9-50.39)
ZMYND19	1	0	Inf	5.34 (0.73-39.26)
ZNF146	2	1	11.84 (1.07-131.22)	15.64 (3.66-66.8)
ZNF205	3	3	5.27 (1.06-26.33)	4.72 (1.49-15)
ZNF511	2	1	11.23 (1.01-124.51)	4.24 (1.03-17.38)
ZNF716	6	0	Inf	5.04 (2.21-11.5)
ZNF768	2	1	11.38 (1.03-126.13)	7.48 (1.8-31.01)
ZPBP2	2	1	11.82 (1.07-131.02)	5.41 (1.32-22.27)

Appendix Table 9: List of enriched genes for POAG cohort under a loss of function model

Headings:

Gene: HGNC gene name

POAG: Number of cases in POAG cohort

CTRL: Number of cases in local and AOGC controls

POAG CTRL OR (95% CI): Odds ratio of POAG cohort compared to controls

POAG NFE OR (95% CI): Odds ratio of POAG cohort compared to non-Finnish European ExAC public domain data

Gene	POAG	CTRL	POAG CTRL OR (95% CI)	POAG NFE OR (95%CI)
AARS	1	0	Inf	14.47 (1.87-111.82)
ABCA2	1	0	Inf	12.35 (1.57-97.01)
ABCC3	1	0	Inf	5.08 (0.69-37.3)
ABLIM1	1	1	5.87 (0.37-94.32)	18.57 (2.34-147.34)
ACADVL	2	0	Inf	20.06 (4.6-87.45)
ACD	1	0	Inf	6.54 (0.88-48.41)
ACOX1	1	0	Inf	29.84 (3.57-249.09)
ADAM17	1	0	Inf	18.41 (2.32-146.05)
ADAM9	2	0	Inf	72.04 (13.89-373.69)
ADD1	1	0	Inf	6.77 (0.91-50.3)
ADPRHL1	1	1	5.87 (0.37-94.32)	5.19 (0.71-38.14)
ADTRP	1	0	Inf	14.12 (1.78-112.03)
AFAP1L2	1	0	Inf	8.49 (1.12-64.15)
AGL	2	2	5.9 (0.83-42.16)	5.03 (1.23-20.68)
AGPAT2	1	0	Inf	16.73 (2.11-132.73)
AHSG	1	0	Inf	11.06 (1.46-83.84)
AKAP12	1	1	5.88 (0.37-94.45)	15.8 (2.03-122.97)
ALB	1	0	Inf	16.14 (2.07-125.68)
ALKBH1	1	1	5.88 (0.37-94.49)	9.43 (1.26-70.77)
AMBP	1	0	Inf	11.08 (1.46-83.95)
AMFR	1	0	Inf	35.09 (4.08-301.84)
ANKDD1A	1	0	Inf	7.13 (0.96-52.97)
ANO3	1	1	5.88 (0.37-94.45)	9.79 (1.3-73.68)
ANXA9	1	1	5.88 (0.37-94.36)	5.86 (0.8-43.21)
AP3B1	1	0	Inf	85.31 (7.7-944.96)
APIP	1	0	Inf	12.42 (1.62-94.92)
APMAP	1	1	5.88 (0.37-94.45)	16.9 (2.15-132.7)
APOBEC1	1	0	Inf	58.31 (6.04-563.14)
APOBR	1	1	5.85 (0.36-93.93)	5.01 (0.68-37.19)
APOH	1	0	Inf	17.73 (2.26-139.25)
ARHGEF25	1	0	Inf	9.42 (1.25-70.9)

ARHGEF26	1	0	Inf	4.98 (0.68-36.69)
ARID1B	1	0	Inf	21.1 (2.63-169.57)
ARMC8	1	0	Inf	79.92 (7.22-885.21)
ARRDC2	1	0	Inf	10.09 (1.33-76.46)
ARSK	1	0	Inf	18.73 (2.36-148.62)
ATAD3B	1	0	Inf	5.18 (0.71-38.09)
ATAD5	1	1	5.88 (0.37-94.45)	19.69 (2.48-156.24)
ATG3	1	0	Inf	44.34 (4.93-398.58)
ATG4D	1	0	Inf	7.03 (0.94-52.42)
ATG7	2	0	Inf	15.56 (3.64-66.46)
ATP5G2	1	0	Inf	25.42 (3.11-207.66)
ATP6V0A2	2	0	Inf	23.65 (5.37-104.14)
ATP6V1E2	1	0	Inf	13.76 (1.79-105.7)
ATP9A	1	0	Inf	35.06 (4.08-301.53)
ATXN2L	1	0	Inf	7.54 (1.01-56.26)
AVPR1A	1	1	5.67 (0.35-91.04)	25.14 (3.08-205.36)
BAAT	1	0	Inf	19.79 (2.49-157)
BCAT1	1	0	Inf	18.78 (2.37-148.99)
BCAT2	1	0	Inf	15.3 (1.97-119.11)
BDH2	1	1	5.88 (0.37-94.45)	6.42 (0.87-47.57)
BIN3	1	0	Inf	17.86 (2.25-141.67)
BRD9	1	0	Inf	35.71 (4.15-307.13)
BRF2	1	0	Inf	6.84 (0.92-50.67)
BSCL2	1	1	5.88 (0.37-94.49)	10.3 (1.36-77.79)
C11orf1	1	0	Inf	5.46 (0.74-40.23)
C11orf53	1	0	Inf	12.74 (1.67-97.35)
C12orf40	1	1	5.88 (0.37-94.45)	8.89 (1.18-66.79)
C17orf67	1	0	Inf	19.8 (2.5-157.11)
C1orf109	1	0	Inf	15.44 (1.98-120.24)
C3orf30	2	1	11.82 (1.07-131.04)	21.04 (4.83-91.73)
C7orf31	2	1	11.82 (1.07-131.06)	9.43 (2.26-39.39)
CABS1	1	0	Inf	12.69 (1.66-96.99)
CACNA1S	1	0	Inf	5.46 (0.74-40.19)
CAPRIN2	1	0	Inf	8.91 (1.19-66.76)
CASP14	1	0	Inf	8.11 (1.09-60.5)
CATSPER2	1	0	Inf	8.47 (1.13-63.26)
CATSPERG	3	1	17.8 (1.84-172.09)	5.68 (1.78-18.14)
CAV1	1	0	Inf	19.89 (2.51-157.82)
CBX2	1	0	Inf	15.86 (2.04-123.47)
CCBE1	1	0	Inf	9.91 (1.32-74.61)
CCDC57	3	1	17.74 (1.84-171.46)	13.59 (4.14-44.59)
CCL18	1	0	Inf	35.82 (4.16-308.11)
CCR5	4	3	7.96 (1.77-35.84)	9.31 (3.37-25.72)
CD200R1L	2	0	Inf	44.08 (9.3-208.97)
CD300LF	1	0	Inf	14.72 (1.9-113.81)
CD83	1	0	Inf	54.01 (5.59-521.66)

CDC42EP2	1	0	Inf	Inf
CDCP1	1	0	Inf	34.83 (4.05-299.61)
CDK15	1	0	Inf	6.83 (0.92-50.58)
CDKN2AIP	1	0	Inf	Inf
CEACAM18	1	0	Inf	11.02 (1.45-83.5)
CEMP1	1	0	Inf	58.84 (6.09-568.32)
CEP128	1	1	5.88 (0.37-94.45)	5.99 (0.81-44.28)
CEP72	1	0	Inf	5.05 (0.69-37.08)
CES3	1	0	Inf	13.55 (1.76-104.08)
CH25H	1	1	5.88 (0.37-94.49)	27.17 (3.26-226.82)
CHAC2	1	1	5.88 (0.37-94.41)	5.43 (0.74-39.93)
CHRNB2	1	0	Inf	41.94 (4.67-377.04)
CIB1	1	0	Inf	25.57 (3.13-208.87)
CLEC4D	2	0	Inf	28.82 (6.41-129.69)
CLEC4M	1	0	Inf	25.45 (3.12-207.92)
CLPSL2	1	0	Inf	48.45 (4.37-536.7)
CNBD1	1	1	5.88 (0.37-94.36)	8.78 (1.16-66.33)
CNDP2	1	0	Inf	19.82 (2.5-157.24)
COG2	1	0	Inf	28.02 (3.36-233.87)
CPD	2	0	Inf	40.02 (8.59-186.49)
CRYBB1	1	0	Inf	29.82 (3.57-248.88)
CTSH	1	0	Inf	7.08 (0.95-52.58)
CTSZ	1	0	Inf	7.74 (1.04-57.69)
CUX1	1	0	Inf	13.46 (1.75-103.46)
CYP21A2	1	0	Inf	36.69 (3.8-354.41)
CYP2E1	1	0	Inf	9.8 (1.3-73.82)
CYP46A1	1	0	Inf	89.65 (8.09-993.03)
DCLRE1C	4	1	23.92 (2.66-215.2)	15.3 (5.46-42.91)
DEDD2	1	0	Inf	4.9 (0.65-36.86)
DEFB135	1	0	Inf	8.88 (1.19-66.5)
DENND6B	1	1	5.85 (0.36-93.97)	37.32 (4.15-335.48)
DEPTOR	1	0	Inf	19.7 (2.48-156.29)
DERL3	1	0	Inf	8.92 (1.17-67.87)
DGKZ	1	0	Inf	26.36 (2.93-237)
DHX32	1	1	5.88 (0.37-94.45)	8.36 (1.12-62.51)
DKK4	1	0	Inf	22.17 (2.76-178.17)
DMRT3	1	1	5.88 (0.37-94.45)	14.91 (1.93-115.23)
DNAJC16	1	0	Inf	5.4 (0.74-39.71)
DNAJC27	1	0	Inf	35.28 (4.1-303.47)
DNASE1L3	1	0	Inf	16.2 (2.08-126.12)
DNASE2B	1	0	Inf	6.14 (0.83-45.43)
DPP6	1	1	5.88 (0.37-94.49)	23.65 (2.83-197.42)
DSN1	1	0	Inf	5.53 (0.75-40.65)
DSP	1	0	Inf	9.4 (1.25-70.59)
DUSP16	1	0	Inf	44.71 (4.97-401.89)
DUSP4	1	0	Inf	40.37 (4.49-362.93)

ECH1	1	1	5.88 (0.37-94.41)	7.81 (1.04-58.61)
ECHDC1	1	1	5.88 (0.37-94.45)	5.96 (0.81-43.92)
ECI1	1	0	Inf	8.47 (1.13-63.61)
EGFL8	1	0	Inf	21.6 (2.69-173.6)
EPG5	1	0	Inf	6.13 (0.83-45.21)
ERLIN2	1	0	Inf	89.4 (8.07-990.25)
EXOC4	1	1	5.88 (0.37-94.45)	11.85 (1.56-90.15)
EXOG	1	0	Inf	7.76 (1.04-57.74)
EXOSC3	1	0	Inf	84.82 (7.66-939.5)
FAM118B	1	0	Inf	29.78 (3.57-248.55)
FAM120B	2	0	Inf	8.65 (2.07-36.12)
FAM124A	1	1	5.88 (0.37-94.36)	18.64 (2.35-147.84)
FAM178A	1	0	Inf	10.74 (1.42-81.41)
FAM32A	1	0	Inf	132.27 (8.24-2122.7)
FAM46B	1	0	Inf	8.43 (1.13-63.16)
FAM69C	2	1	11.47 (1.03-127.15)	72.02 (13.88-373.59)
FAM71C	1	0	Inf	8.05 (1.08-60.05)
FAM71E2	1	0	Inf	Inf
FAM83B	1	0	Inf	16.25 (2.09-126.5)
FAM84B	1	0	Inf	37.89 (4.21-340.62)
FAR2	1	0	Inf	89.44 (8.07-990.67)
FARSA	1	0	Inf	28.41 (3.4-237.12)
FASTKD2	1	0	Inf	12.57 (1.64-96.09)
FBLN2	1	0	Inf	15.56 (1.96-123.47)
FBXO24	1	0	Inf	12.21 (1.59-93.84)
FBXO39	1	0	Inf	16.27 (2.09-126.64)
FCN1	2	1	11.81 (1.07-130.86)	5.17 (1.26-21.27)
FLOT2	1	0	Inf	20.95 (2.61-168.33)
FMN1	1	1	5.87 (0.37-94.32)	7.65 (1.02-57.15)
FMO5	1	0	Inf	5.23 (0.71-38.43)
FNDC9	1	0	Inf	17.66 (2.25-138.66)
FREM1	1	1	5.88 (0.37-94.41)	5.01 (0.68-36.88)
FXYD7	1	0	Inf	179.4 (11.18-2879.12)
FZD2	1	0	Inf	89.27 (8.06-988.8)
FZD6	1	0	Inf	9.32 (1.24-70)
GAL3ST3	1	0	Inf	18.15 (2.22-148.24)
GALNS	1	0	Inf	14.13 (1.82-110.04)
GALNT14	2	2	5.91 (0.83-42.2)	14.94 (3.5-63.84)
GALNT3	1	0	Inf	11.63 (1.53-88.51)
GAS2L2	1	1	5.88 (0.37-94.49)	7.88 (1.05-58.85)
GBA2	1	0	Inf	10.98 (1.45-83.21)
GCNT2	2	0	Inf	13.33 (3.15-56.45)
GFPT2	1	0	Inf	5.31 (0.72-39.06)
GIT2	1	0	Inf	42.77 (4.76-384.51)
GJA8	1	0	Inf	19.43 (2.45-154.13)
GLE1	1	1	5.88 (0.37-94.45)	10.41 (1.38-78.66)

GLIPR2	1	0	Inf	5.45 (0.74-40.1)
GML	2	0	Inf	35.93 (7.82-165.12)
GOLIM4	1	0	Inf	6.55 (0.89-48.48)
GPBAR1	1	0	Inf	7.59 (1.02-56.71)
GPR149	1	0	Inf	8.43 (1.13-63)
GPR37L1	1	0	Inf	21.81 (2.71-175.25)
GPX5	1	0	Inf	44.77 (4.98-402.51)
GRAMD2	1	0	Inf	16.27 (2.09-126.64)
GRIN2C	1	0	Inf	11.5 (1.49-88.9)
GUCA1C	1	0	Inf	19.59 (2.47-155.44)
HAGH	1	1	5.48 (0.34-88.06)	9.84 (1.31-74.13)
HAUS2	1	0	Inf	24.72 (3.03-201.96)
HCN1	1	0	Inf	35.02 (4.07-301.24)
HECW1	1	0	Inf	29.48 (3.53-246.06)
HIRIP3	1	1	5.88 (0.37-94.45)	19.68 (2.48-156.09)
HIST1H4A	1	0	Inf	7.7 (1.04-57.35)
HMGCLL1	1	0	Inf	13.26 (1.73-101.92)
HPS4	1	1	5.88 (0.37-94.45)	6.75 (0.91-50.03)
HPX	1	0	Inf	12.66 (1.66-96.8)
HSPA4L	1	1	5.88 (0.37-94.41)	15.73 (2.02-122.42)
ICE1	1	0	Inf	23.91 (2.93-195.32)
IDH3A	1	0	Inf	89.64 (8.09-992.89)
IFI44L	1	0	Inf	10.86 (1.43-82.33)
IFT88	1	0	Inf	5.66 (0.77-41.7)
IGFBP6	1	0	Inf	11.17 (1.47-84.69)
IL1RL1	1	1	5.88 (0.37-94.49)	17.75 (2.26-139.4)
IL20RB	1	0	Inf	13.69 (1.78-105.17)
IMPG2	2	0	Inf	13.58 (3.2-57.64)
INO80E	1	0	Inf	9.27 (1.18-72.8)
INSM2	1	0	Inf	29.14 (3.39-250.67)
INSRR	2	1	11.82 (1.07-130.98)	10.33 (2.46-43.36)
INTS1	1	1	5.78 (0.36-92.81)	6.8 (0.91-50.62)
INTU	1	1	5.88 (0.37-94.45)	7.41 (1-55.06)
IRGM	1	0	Inf	22.86 (1.42-366.92)
KAT8	1	0	Inf	43 (4.78-386.52)
KATNB1	1	0	Inf	14.68 (1.9-113.49)
KCNH1	1	0	Inf	25.36 (3.11-207.19)
KCNH5	2	1	11.82 (1.07-131.04)	11.07 (2.63-46.55)
KCNJ1	1	0	Inf	6.59 (0.89-48.72)
KCNJ14	2	1	11.64 (1.05-129)	53.23 (10.67-265.45)
KCNQ1	1	1	5.88 (0.37-94.41)	5.43 (0.74-39.91)
KCTD19	1	1	5.88 (0.37-94.45)	7.45 (1-55.38)
KHDC1L	1	0	Inf	7.08 (0.92-54.39)
KIAA1549	1	1	5.88 (0.37-94.45)	41.57 (4.62-373.72)
KIAA1551	1	0	Inf	5.72 (0.78-42.12)
KIF12	1	0	Inf	13.16 (1.71-101.09)

KLHDC2	1	0	Inf	12.76 (1.66-98.07)
KLHL21	1	0	Inf	32.04 (3.56-287.99)
KLHL25	1	0	Inf	7.08 (0.95-52.53)
KLHL28	1	0	Inf	171.61 (10.69-2754.1)
KLK1	1	0	Inf	9.38 (1.25-70.42)
KNG1	1	0	Inf	11.15 (1.47-84.48)
KRT75	2	2	5.91 (0.83-42.18)	5.53 (1.34-22.75)
KRT76	1	0	Inf	10.88 (1.43-82.43)
KY	1	0	Inf	10.38 (1.36-79.01)
LAMTOR3	1	0	Inf	172.6 (10.76-2770.02)
LDHAL6A	1	0	Inf	16.27 (2.09-126.67)
LDLRAD2	1	0	Inf	26.33 (3.06-226.5)
LEMD1	1	0	Inf	25.94 (3.11-216.56)
LHX4	1	0	Inf	44.78 (4.98-402.53)
LIG1	1	0	Inf	7.43 (1-55.32)
LIPI	1	0	Inf	11.56 (1.52-87.96)
LMBRD2	1	0	Inf	15.76 (2.02-122.72)
LMOD2	1	0	Inf	12.54 (1.58-99.51)
LNX1	1	1	5.88 (0.37-94.45)	5.47 (0.74-40.26)
LPIN3	3	3	5.93 (1.19-29.63)	5.89 (1.85-18.77)
LRRC23	1	0	Inf	6.83 (0.92-50.62)
LRRC66	2	0	Inf	5.41 (1.32-22.25)
LRRFIP2	1	1	5.88 (0.37-94.45)	6.62 (0.89-48.97)
LRSAM1	1	0	Inf	10.24 (1.36-77.37)
LTBP2	1	0	Inf	9.7 (1.28-73.25)
MAG	1	0	Inf	21.29 (2.65-171.1)
MAP3K13	2	0	Inf	25.41 (5.74-112.61)
MAP3K9	1	1	5.86 (0.36-94.06)	35.3 (4.1-303.65)
MAP4K3	1	0	Inf	11.56 (1.52-87.97)
MAPRE1	1	0	Inf	179.39 (11.18-2878.86)
MATN3	1	0	Inf	15.25 (1.96-118.74)
MB21D1	1	0	Inf	8.07 (1.07-60.96)
MBOAT1	1	0	Inf	9.13 (1.22-68.56)
MCAT	1	0	Inf	9.98 (1.32-75.4)
METTL4	1	0	Inf	8.8 (1.17-65.9)
MICU1	1	0	Inf	6.68 (0.9-49.83)
MICU2	1	0	Inf	12.43 (1.62-95.53)
MMS22L	1	0	Inf	14.46 (1.87-111.81)
MNX1	1	0	Inf	Inf
MOV10L1	2	2	5.91 (0.83-42.2)	8.62 (2.07-35.92)
MRC2	1	0	Inf	28.22 (3.28-242.73)
MRPL39	1	1	5.88 (0.37-94.45)	11.17 (1.47-84.63)
MRPS7	1	0	Inf	43.86 (4.88-394.27)
MRRF	1	0	Inf	12.78 (1.67-97.67)
MS4A7	1	0	Inf	44.75 (4.98-402.25)
MSR1	1	0	Inf	5.32 (0.72-39.12)

MT1F	1	0	Inf	35.83 (4.17-308.16)
MTERF4	2	0	Inf	13.3 (3.14-56.34)
MTHFS	1	0	Inf	25.62 (3.14-209.31)
MTHFSD	1	1	5.88 (0.37-94.45)	5.07 (0.69-37.37)
MTIF2	1	0	Inf	6.38 (0.86-47.12)
MTMR9	1	0	Inf	44.71 (4.97-401.89)
MUC15	1	1	5.88 (0.37-94.45)	11.02 (1.45-83.55)
MYCBPAP	1	0	Inf	12.35 (1.61-94.91)
MYH10	1	1	5.88 (0.37-94.45)	10.44 (1.38-79.17)
MYLK2	1	0	Inf	Inf
MYO16	1	0	Inf	11.68 (1.53-89.26)
NAA38	1	0	Inf	10.71 (1.41-81.14)
NARS	1	0	Inf	13.26 (1.73-101.89)
NARS2	1	0	Inf	22.31 (2.78-179.24)
NBEA	1	0	Inf	15.74 (2.02-122.54)
NCAPH	1	0	Inf	30.95 (3.6-266.17)
NCF4	2	0	Inf	5.32 (1.29-21.89)
NCOR2	1	0	Inf	6.58 (0.88-49.04)
NDE1	1	0	Inf	25.51 (3.12-208.41)
NDST4	1	1	5.88 (0.37-94.41)	29.29 (3.51-244.5)
NDUFAF6	1	0	Inf	6.72 (0.91-49.87)
NEK8	1	0	Inf	9.93 (1.32-74.74)
NEU2	1	1	5.7 (0.35-91.47)	21.68 (2.7-174.21)
NEXN	1	0	Inf	6.04 (0.82-44.58)
NGB	1	0	Inf	Inf
NLRP11	1	0	Inf	10.51 (1.39-79.36)
NLRP4	1	1	5.87 (0.37-94.28)	13.63 (1.77-104.72)
NLRX1	2	1	11.64 (1.05-129.06)	7.42 (1.79-30.73)
NMNAT3	1	0	Inf	5.09 (0.69-37.4)
NOB1	1	0	Inf	17.3 (2.2-135.82)
NOL7	1	1	5.84 (0.36-93.8)	12.83 (1.66-99.19)
NOSTRIN	1	1	5.88 (0.37-94.41)	7.4 (1-54.97)
NPBWR1	1	0	Inf	5.68 (0.77-42.14)
NPHS2	1	0	Inf	12.67 (1.66-96.85)
NPR1	1	0	Inf	13.59 (1.76-105.02)
NPTX2	1	0	Inf	171.79 (10.7-2756.94)
NRL	1	0	Inf	21.52 (2.68-172.93)
NSUN7	1	0	Inf	10.04 (1.31-77.18)
NUP214	1	0	Inf	5.39 (0.73-39.63)
NXPE1	1	0	Inf	25.36 (3.1-207.13)
OGFOD1	1	1	5.88 (0.37-94.45)	10.51 (1.39-79.41)
OGFR	1	0	Inf	14.2 (1.77-114.11)
OR10AD1	1	0	Inf	13.73 (1.79-105.53)
OR11H6	1	0	Inf	5.56 (0.76-40.92)
OR12D3	1	0	Inf	12.97 (1.69-99.62)
OR13A1	1	0	Inf	59.29 (6.14-572.64)

OR2AE1	1	0	Inf	22.09 (2.75-177.53)
OR51Q1	1	0	Inf	16.3 (2.09-126.86)
OR52E4	1	0	Inf	25.58 (3.13-208.92)
OR6Q1	1	0	Inf	16.15 (2.07-125.71)
OR6T1	1	0	Inf	16.3 (2.09-126.89)
OR9I1	1	0	Inf	12.77 (1.67-97.59)
ORC6	1	0	Inf	13.95 (1.81-107.86)
OSBPL1A	1	1	5.88 (0.37-94.45)	9.4 (1.25-70.55)
OSMR	1	0	Inf	5.56 (0.76-40.88)
OTOP3	1	0	Inf	21.69 (2.7-174.32)
OVGP1	2	0	Inf	8.42 (2.02-35.05)
OVOL1	1	0	Inf	125.31 (7.81-2011.1)
P2RX1	1	0	Inf	13.87 (1.79-107.24)
PAG1	1	0	Inf	29.66 (3.55-247.6)
PARK7	1	0	Inf	5.04 (0.69-37)
PAX4	1	0	Inf	7.09 (0.95-53.12)
PBK	1	0	Inf	9.2 (1.22-69.07)
PCCB	1	0	Inf	8.84 (1.18-66.21)
PCDHB10	1	1	5.88 (0.37-94.45)	8.01 (1.07-59.73)
PCDHGA8	1	0	Inf	10.44 (1.38-78.86)
PCDHGC5	1	1	5.88 (0.37-94.49)	12.31 (1.61-94.09)
PCNX	1	0	Inf	12.71 (1.66-97.17)
PCSK7	1	0	Inf	18.6 (2.34-147.52)
PDE6H	1	0	Inf	24.83 (3.04-202.82)
PDK4	1	0	Inf	8 (1.07-59.77)
PDZD8	1	0	Inf	178.15 (11.1-2859.01)
PGLS	1	0	Inf	31.44 (3.5-282.61)
PHIP	1	0	Inf	24.27 (2.97-198.26)
PHKB	2	0	Inf	9.09 (2.18-37.92)
PIBF1	1	0	Inf	5.36 (0.73-39.4)
PIGC	1	0	Inf	16.23 (2.08-126.37)
PIGL	1	1	5.88 (0.37-94.45)	17.92 (2.28-140.71)
PLCB4	1	0	Inf	21.83 (2.72-175.43)
PLCH1	2	0	Inf	22.23 (5.08-97.37)
PLOD1	1	0	Inf	9.17 (1.22-68.87)
PLVAP	1	1	5.88 (0.37-94.45)	59.23 (6.13-572.08)
PODN	1	0	Inf	7.31 (0.98-54.65)
POT1	1	0	Inf	9.12 (1.21-68.5)
PPP3CC	1	0	Inf	11.74 (1.54-89.37)
PRMT3	1	1	5.88 (0.37-94.49)	7.13 (0.96-52.96)
PRR16	1	0	Inf	60.79 (5.49-673.39)
PRR30	1	0	Inf	13.45 (1.75-103.34)
PRSS36	2	0	Inf	4.87 (1.18-20.02)
PSAT1	1	0	Inf	16.29 (2.09-126.78)
PTDSS2	1	0	Inf	25.39 (3.11-207.43)
PTK2	1	0	Inf	89.44 (8.07-990.64)

PUSL1	2	0	Inf	6.9 (1.64-28.98)
PYGM	1	0	Inf	6.8 (0.92-50.38)
RAB3GAP2	1	0	Inf	14.64 (1.89-113.13)
RBM14	1	0	Inf	Inf
RBM23	1	0	Inf	7.14 (0.96-53.03)
RCN3	1	1	5.79 (0.36-92.98)	10.26 (1.35-78.07)
RFX6	1	0	Inf	13.78 (1.79-105.88)
RHOT1	1	0	Inf	12.67 (1.66-96.83)
RMDN3	2	2	5.9 (0.83-42.17)	38.38 (8.24-178.84)
RNASE12	1	0	Inf	6.39 (0.87-47.24)
RNF112	1	0	Inf	50.76 (5.26-490.2)
RNF141	1	0	Inf	35.8 (4.16-307.93)
RNLS	1	0	Inf	7.44 (1-55.3)
ROBO1	1	0	Inf	8.81 (1.17-66.16)
RPP38	1	1	5.88 (0.37-94.45)	17.84 (2.27-140.07)
RRH	1	0	Inf	6.58 (0.89-48.67)
RSF1	1	0	Inf	Inf
RTN4IP1	2	0	Inf	8.92 (2.14-37.17)
SCN9A	1	0	Inf	4.98 (0.68-36.62)
SDR39U1	1	0	Inf	8.31 (1.11-62.28)
SEC22C	1	0	Inf	8 (1.07-59.66)
SELL	1	0	Inf	39.41 (4.08-380.63)
SEMA3D	1	0	Inf	17.38 (2.21-136.49)
SETD6	1	0	Inf	7.2 (0.97-53.48)
SETX	1	1	5.88 (0.37-94.45)	7.64 (1.03-56.89)
SFRP4	1	0	Inf	16.24 (2.09-126.42)
SGCZ	1	0	Inf	14.58 (1.87-113.49)
SGSM2	1	1	5.68 (0.35-91.26)	8.46 (1.13-63.35)
SH3TC2	1	1	5.88 (0.37-94.41)	6.39 (0.87-47.24)
SHB	1	0	Inf	82.82 (5.16-1329.08)
SHC1	1	0	Inf	25.44 (3.11-207.82)
SIAH3	1	0	Inf	88.92 (8.03-984.95)
SIRT5	1	1	5.88 (0.37-94.45)	9.81 (1.3-73.88)
SKA1	1	1	5.87 (0.37-94.23)	5.39 (0.73-39.65)
SLC12A9	2	1	11.59 (1.05-128.52)	15.75 (3.67-67.66)
SLC15A3	2	0	Inf	10.88 (2.59-45.75)
SLC17A5	1	0	Inf	5.23 (0.71-38.47)
SLC22A15	1	1	5.88 (0.37-94.36)	14.67 (1.88-114.19)
SLC25A26	1	1	5.88 (0.37-94.45)	6.31 (0.84-47.23)
SLC26A7	1	0	Inf	11.7 (1.54-89.02)
SLC28A3	1	0	Inf	9.36 (1.25-70.3)
SLC36A2	2	1	11.83 (1.07-131.1)	12.78 (3.02-54.05)
SLC41A3	1	0	Inf	12.54 (1.64-95.88)
SLC47A1	1	0	Inf	8.86 (1.18-66.38)
SLC4A1AP	1	0	Inf	6.62 (0.89-48.95)
SLC5A9	2	2	5.9 (0.83-42.15)	6.63 (1.6-27.38)

SLC6A5	1	0	Inf	11.2 (1.47-85.2)
SLC7A9	1	0	Inf	5.59 (0.76-41.09)
SLC9A5	1	0	Inf	5.57 (0.76-40.98)
SLX4IP	1	0	Inf	12.7 (1.66-97.11)
SMIM11	1	0	Inf	87.35 (7.89-967.57)
SMOC2	2	0	Inf	31 (6.82-140.85)
SMPD2	1	0	Inf	4.96 (0.68-36.38)
SNAPC1	1	0	Inf	19.76 (2.49-156.76)
SNX1	2	1	11.82 (1.07-130.98)	88.28 (16.07-484.98)
SPAG4	2	0	Inf	21.78 (4.95-95.93)
SPHKAP	1	0	Inf	25.51 (3.12-208.35)
SPINK1	1	0	Inf	17.61 (2.22-139.74)
SPINK4	1	0	Inf	178.81 (11.14-2869.54)
SRMS	1	0	Inf	10.96 (1.43-84.22)
SRPRB	1	0	Inf	17.77 (2.26-139.54)
ST6GALNAC2	1	0	Inf	4.89 (0.67-35.92)
STAM2	2	0	Inf	27.55 (6.17-122.93)
STEAP4	1	0	Inf	7.07 (0.95-52.49)
STRADA	1	1	5.88 (0.37-94.45)	12.47 (1.63-95.31)
STRN3	1	1	5.88 (0.37-94.36)	22.19 (2.76-178.3)
SULF1	1	0	Inf	35.68 (4.15-306.93)
SULT1B1	1	0	Inf	10.26 (1.36-77.49)
SULT1C3	1	1	5.89 (0.37-94.54)	6.83 (0.92-50.58)
SULT2A1	1	0	Inf	13.74 (1.79-105.6)
SYT5	1	1	5.88 (0.37-94.45)	5.88 (0.79-43.65)
SYT6	1	0	Inf	59 (6.11-569.8)
SYVN1	1	0	Inf	Inf
TACC3	1	0	Inf	12.59 (1.65-96.26)
TATDN2	1	0	Inf	13.56 (1.76-104.18)
TBX19	1	1	5.88 (0.37-94.36)	7.77 (1.04-57.81)
TCF12	1	0	Inf	35.78 (4.16-307.79)
TEDDM1	1	0	Inf	17.9 (2.28-140.52)
TEK	1	0	Inf	89.42 (8.07-990.48)
TFR2	2	0	Inf	26.32 (5.85-118.45)
TGFBR2	1	0	Inf	59.49 (6.16-574.6)
TGS1	1	0	Inf	8.77 (1.17-65.86)
TM4SF1	1	1	5.88 (0.37-94.45)	22.36 (2.78-179.7)
TMBIM1	1	1	5.88 (0.37-94.41)	9.73 (1.28-73.74)
TMED3	1	0	Inf	6.19 (0.84-45.74)
TMEM116	1	0	Inf	12.68 (1.66-96.94)
TMEM132B	1	0	Inf	31.04 (3.61-267)
TMEM144	2	1	11.83 (1.07-131.1)	10.88 (2.59-45.69)
TMEM161A	1	0	Inf	25.67 (3.08-214.27)
TMEM256	1	0	Inf	19.85 (2.5-157.48)
TMEM5	1	0	Inf	19.12 (2.38-153.62)
TMEM70	1	0	Inf	6.16 (0.84-45.48)

TMEM86A	1	0	Inf	22.18 (2.76-178.22)
TMEM8C	1	0	Inf	44.59 (4.96-400.84)
TNFAIP6	1	1	5.88 (0.37-94.36)	5.26 (0.72-38.6)
TNFRSF18	1	0	Inf	4.9 (0.66-36.26)
TNRC6C	1	0	Inf	27.42 (3.19-235.87)
TOM1	1	0	Inf	8.54 (1.14-64.14)
TP53	1	0	Inf	65.67 (5.93-727.42)
TP53I3	1	0	Inf	5.27 (0.72-38.7)
TPP1	1	0	Inf	6.64 (0.9-49.09)
TRDMT1	1	0	Inf	16.85 (2.15-132.27)
TREML1	1	1	5.88 (0.37-94.45)	14.77 (1.91-114.17)
TRIM52	1	0	Inf	19.69 (2.48-156.24)
TRIP11	4	3	7.93 (1.76-35.7)	15.91 (5.66-44.7)
TRPC3	1	0	Inf	11.86 (1.55-90.63)
TRPM8	1	0	Inf	7.67 (1.03-57.12)
TSNAXIP1	4	1	23.92 (2.66-215.19)	12.28 (4.41-34.25)
TSSK4	1	0	Inf	5.95 (0.81-43.87)
TTC14	1	1	5.87 (0.37-94.28)	6.71 (0.9-49.75)
TTLL1	1	0	Inf	7.13 (0.96-52.92)
TTLL12	1	0	Inf	8.73 (1.17-65.39)
TULP3	2	1	11.83 (1.07-131.1)	7.35 (1.76-30.65)
TXN2	1	0	Inf	25.5 (3.12-208.29)
TXNDC12	2	0	Inf	110.6 (18.37-665.77)
UBE4B	1	0	Inf	35.42 (4.12-304.61)
UCP2	1	0	Inf	6.54 (0.88-48.44)
UFC1	1	0	Inf	44.83 (4.99-403.01)
UGDH	1	0	Inf	6.77 (0.91-50.14)
UGGT1	1	0	Inf	10.11 (1.34-76.35)
UIMC1	2	2	5.91 (0.83-42.22)	45.02 (9.5-213.44)
UNKL	1	1	5.69 (0.35-91.3)	5.93 (0.76-46.15)
UPP2	1	0	Inf	6.12 (0.83-45.19)
URB1	2	1	11.55 (1.04-128.02)	14.23 (2.36-85.66)
UROS	1	0	Inf	12.54 (1.64-95.83)
USE1	1	0	Inf	42.6 (4.74-382.97)
USP20	1	0	Inf	9.53 (1.27-71.78)
USP44	2	0	Inf	13.25 (3.13-56.12)
USP6NL	1	0	Inf	13.06 (1.68-101.71)
UTS2	1	0	Inf	8.14 (1.09-60.67)
VCL	1	1	5.88 (0.37-94.49)	16.13 (2.07-125.54)
VIM	1	0	Inf	Inf
VIPR1	2	2	5.9 (0.83-42.15)	27.5 (6.11-123.72)
VNN1	1	1	5.88 (0.37-94.45)	14.8 (1.92-114.44)
VPREB1	1	0	Inf	29.35 (3.52-244.97)
VPS16	1	0	Inf	16.23 (2.08-126.37)
VPS9D1	1	0	Inf	18.19 (2.26-146.2)
VSTM2B	1	0	Inf	9.73 (0.88-107.85)

WBSCR27	1	0	Inf	11.62 (1.52-88.82)
WDR38	3	3	5.88 (1.18-29.36)	14.59 (4.46-47.73)
XRCC2	1	0	Inf	8.43 (1.13-62.97)
XRCC6BP1	1	0	Inf	13.66 (1.78-104.93)
ZBTB9	1	0	Inf	19.57 (2.47-155.29)
ZCCHC10	1	0	Inf	58.32 (6.04-563.23)
ZCCHC7	2	0	Inf	32.61 (7.18-148.16)
ZIM2	1	0	Inf	16.29 (2.09-126.83)
ZKSCAN8	1	1	5.88 (0.37-94.45)	19.79 (2.49-156.96)
ZMYM6	1	0	Inf	7.19 (0.96-53.73)
ZMYND8	1	0	Inf	177.47 (11.06-2848.16)
ZNF146	1	0	Inf	Inf
ZNF177	1	0	Inf	7.55 (1.01-56.57)
ZNF234	1	1	5.88 (0.37-94.49)	5.58 (0.76-41.02)
ZNF256	1	0	Inf	4.96 (0.68-36.4)
ZNF300	1	0	Inf	10.65 (1.4-80.72)
ZNF354A	1	1	5.88 (0.37-94.45)	25.44 (3.11-207.77)
ZNF391	1	1	5.88 (0.37-94.45)	9.94 (1.32-74.88)
ZNF484	1	0	Inf	11.9 (1.56-90.57)
ZNF500	1	0	Inf	21.54 (2.68-173.05)
ZNF567	1	0	Inf	17.62 (2.24-138.34)
ZNF607	2	2	5.91 (0.83-42.2)	6.42 (1.56-26.5)
ZNF716	2	0	Inf	12.12 (2.86-51.35)

Appendix Table 10: List of enriched genes for high-tension glaucoma cohort under a predicted pathogenic model

Headings:

Gene: HGNC gene name

HTG: Number of cases in high-tension glaucoma cohort

CTRL: Number of cases in local and AOGC controls

HTG CTRL OR (95%CI): Odds ratio of high-tension glaucoma cohort compared to controls

HTG NFE OR (95% CI): Odds ratio of high-tension glaucoma cohort compared to non-Finnish European ExAC public domain data

Gene	HTG	CTRL	HTG CTRL OR (95% CI)	HTG NFE OR (95% CI)
ACD	5	2	20.7 (3.97-107.89)	6.22 (2.52-15.38)
ACP1	1	2	4.52 (0.41-50.18)	9.01 (1.22-66.61)
ACTA1	1	0	Inf	12.29 (1.64-91.93)
ADPRHL2	2	3	6.06 (1-36.64)	4.36 (1.07-17.85)
AES	1	0	Inf	12.63 (1.65-96.78)
AGO1	1	1	9.03 (0.56-145.34)	7.79 (1.06-57.36)
AGPAT3	1	1	8.52 (0.53-137.17)	7.7 (1.05-56.66)
AGPAT6	1	1	9.04 (0.56-145.48)	6.38 (0.87-46.69)
AKTIP	1	1	9.04 (0.56-145.48)	7.21 (0.98-52.97)
ALDOC	3	4	6.87 (1.52-31.06)	8.53 (2.66-27.27)
AMMECR1L	1	0	Inf	17.09 (2.25-129.88)
ANAPC10	1	0	Inf	21.18 (2.75-163.19)
ANKRD13C	1	2	4.35 (0.39-48.37)	6.14 (0.84-44.9)
AP1M1	1	0	Inf	4.75 (0.65-34.67)
APOM	1	0	Inf	9.85 (1.33-73.08)
ARIH1	1	1	5.69 (0.35-91.52)	18.13 (2.32-141.52)
ARL5B	1	1	9.04 (0.56-145.48)	10.14 (1.37-75.2)
ARL6IP5	1	0	Inf	5.94 (0.81-43.45)
ARMC1	2	4	4.55 (0.82-25.08)	9.16 (2.21-37.9)
ARMC8	1	1	9.04 (0.56-145.48)	4.85 (0.67-35.39)
ASB8	2	3	6.07 (1-36.67)	6.68 (1.62-27.46)
ATAD2	2	3	5.85 (0.97-35.38)	6.17 (1.5-25.36)
ATF2	1	1	9.04 (0.56-145.41)	7.7 (1.05-56.68)
ATG3	2	0	Inf	11.72 (2.82-48.8)
ATP5I	1	1	8.11 (0.5-130.46)	6.82 (0.93-50.12)
ATP6V1G1	1	1	9.03 (0.56-145.34)	8.05 (1.07-60.59)
ATXN10	1	0	Inf	5.43 (0.74-39.69)
AVPR1A	2	3	5.92 (0.98-35.79)	5.96 (1.45-24.49)
B3GNT7	1	0	Inf	7.14 (0.97-52.52)

BAD	2	1	14.03 (1.26-155.95)	4.23 (1.03-17.31)
BPIFA1	1	0	Inf	6.06 (0.83-44.35)
BTBD3	1	1	7.86 (0.49-126.47)	6.35 (0.87-46.5)
BZW2	1	0	Inf	9.69 (1.31-71.89)
C10orf95	1	0	Inf	19.31 (2.47-150.71)
C11orf86	1	1	8.4 (0.52-135.11)	27.65 (1.72-444.64)
C15orf48	1	1	9.03 (0.56-145.34)	19.18 (2.5-147.04)
C1orf226	1	1	8.98 (0.56-144.48)	6.2 (0.84-45.83)
C1orf52	1	1	7.91 (0.49-127.27)	10.24 (1.37-76.28)
C4A	2	0	Inf	38.81 (8.73-172.64)
C4orf32	1	0	Inf	6.85 (0.93-50.67)
C6orf120	2	0	Inf	10.34 (2.48-43.12)
C6orf52	1	0	Inf	12.13 (1.25-117.42)
C7orf25	1	1	6.33 (0.39-101.93)	5.84 (0.8-42.75)
C8orf37	1	0	Inf	7.85 (1.07-57.73)
C8orf59	1	1	9.04 (0.56-145.41)	5.8 (0.79-42.56)
CACNG4	1	1	8.83 (0.55-142.09)	8.57 (1.16-63.35)
CALU	1	1	9.04 (0.56-145.48)	7.81 (1.06-57.62)
CAMK1	3	2	13.77 (2.28-83.27)	6.53 (2.05-20.79)
CBFB	1	0	Inf	14.5 (1.93-109.21)
CBLL1	1	1	9.04 (0.56-145.48)	8.31 (1.13-61.27)
CCL7	1	2	4.51 (0.41-50.13)	8.87 (1.2-65.48)
CCRN4L	1	0	Inf	8.6 (1.17-63.41)
CDC23	1	1	9.04 (0.56-145.48)	10.94 (1.47-81.36)
CDC42EP2	1	2	4.48 (0.4-49.83)	9.63 (1.3-71.36)
CDKN2AIP	2	1	18.23 (1.64-202.58)	9.71 (2.34-40.28)
CDYL	1	1	9.04 (0.56-145.48)	6.05 (0.83-44.3)
CEACAM18	2	0	Inf	5.54 (1.35-22.73)
CEBPD	1	0	Inf	13.78 (1.81-105.11)
CELF2	1	2	4.51 (0.41-50.11)	8.53 (1.16-62.9)
CEP76	2	4	4.48 (0.81-24.73)	10.6 (2.55-44.02)
CHAMP1	2	2	9.11 (1.27-65.25)	21.32 (5-90.83)
CHMP1B	1	0	Inf	9.06 (1.22-67.44)
CHP1	1	0	Inf	30.56 (3.84-243.09)
CHRAC1	1	0	Inf	25.65 (3.22-204.01)
CHST2	2	1	13.18 (1.19-146.51)	16.19 (3.81-68.83)
CIART	2	3	6.06 (1-36.64)	4.58 (1.12-18.74)
CLCN3	2	1	18.23 (1.64-202.58)	7 (1.7-28.82)
CLEC4D	2	2	9.11 (1.27-65.23)	14.63 (3.49-61.37)
CLVS1	1	0	Inf	11.9 (1.59-88.79)
CNNM4	2	4	4.47 (0.81-24.64)	4.09 (1-16.72)
CNOT3	2	0	Inf	4.65 (1.14-19.06)
COQ10B	1	0	Inf	10.43 (1.4-77.51)
COX19	1	0	Inf	5.23 (0.72-38.2)
COX5A	1	0	Inf	4.3 (0.59-31.24)
COX6A1	1	1	8.17 (0.51-131.39)	7.99 (1.08-58.8)

CPLX2	1	1	8.17 (0.51-131.52)	11.19 (1.49-84.25)
CPOX	2	1	7.21 (0.65-80.21)	7.45 (1.81-30.71)
CST7	2	2	8.53 (1.19-61.09)	16.8 (3.99-70.81)
CTDSP1	1	0	Inf	9.9 (1.33-73.68)
CYP46A1	1	1	9.04 (0.56-145.48)	9.73 (1.31-72.54)
DCAF5	3	2	13.78 (2.28-83.28)	7.01 (2.2-22.38)
DEFB135	2	2	9.11 (1.27-65.25)	8.62 (2.09-35.62)
DEFB136	1	0	Inf	4.06 (0.56-29.5)
DESI2	1	0	Inf	29.4 (3.7-233.88)
DGCR6L	2	3	4.21 (0.7-25.46)	5.27 (1.28-21.66)
DHX40	1	2	4.52 (0.41-50.18)	5.45 (0.75-39.77)
DIRC2	1	1	9.04 (0.56-145.48)	4.64 (0.64-33.8)
DNAJC11	2	1	18.22 (1.64-202.44)	7.32 (1.78-30.16)
DPF2	1	1	9.04 (0.56-145.48)	8.69 (1.18-64.19)
DRGX	1	1	8.86 (0.55-142.62)	5.45 (0.74-39.91)
DUSP19	1	2	4.51 (0.41-50.12)	6.85 (0.93-50.2)
DYDC1	2	1	18.23 (1.64-202.58)	22.03 (5.16-94.06)
EBF3	1	2	4.5 (0.41-49.99)	5.45 (0.75-39.82)
EEF1E1	1	0	Inf	14.82 (1.96-112.22)
EFCAB1	1	1	9.04 (0.56-145.41)	5.48 (0.75-39.98)
EIF5A	1	2	4.52 (0.41-50.18)	13.24 (1.72-101.98)
ENTPD8	3	6	4.49 (1.11-18.2)	4.46 (1.4-14.16)
ERICH2	3	0	Inf	21.39 (4.27-107.12)
ERLIN2	2	0	Inf	19.8 (4.67-84.07)
EVA1B	1	0	Inf	4.89 (0.66-36.02)
FAM110A	2	0	Inf	8.2 (1.97-34.14)
FAM181B	1	0	Inf	8.03 (1.06-60.84)
FAM89B	1	0	Inf	13.9 (1.85-104.65)
FBXW12	3	3	9.17 (1.83-45.97)	7.32 (2.29-23.36)
FGF19	1	1	4.48 (0.28-72.12)	37.19 (4.54-304.61)
FGF9	1	0	Inf	25 (3.2-195.17)
FGL2	3	4	6.87 (1.52-31.05)	8.96 (2.8-28.67)
FKBP3	1	2	4.27 (0.38-47.49)	16.94 (2.23-128.76)
FLVCR1	2	3	5.99 (0.99-36.21)	9.29 (2.24-38.49)
FLVCR2	1	1	8.9 (0.55-143.22)	3.99 (0.55-28.94)
FOXD2	1	0	Inf	11.2 (1.47-85.15)
FRAT1	1	1	8.65 (0.54-139.23)	10.15 (1.31-78.68)
FXYD4	1	0	Inf	8.34 (1.13-61.5)
FXYD7	1	0	Inf	39.35 (4.8-322.26)
GAS1	2	0	Inf	23.14 (5.02-106.73)
GATA3	2	2	6.18 (0.86-44.28)	13.5 (3.22-56.56)
GATAD1	1	0	Inf	8.09 (1.1-59.72)
GCHFR	1	1	9.02 (0.56-145.08)	6.02 (0.82-44.26)
GDF1	2	0	Inf	7.6 (1.67-34.65)
GEMIN2	1	0	Inf	7.78 (1.06-57.24)
GFPT1	2	1	18.23 (1.64-202.58)	15.03 (3.58-63.13)

GGACT	1	0	Inf	19.17 (1.19-308.35)
GLTP	1	0	Inf	4.75 (0.65-34.6)
GLYR1	1	0	Inf	4.85 (0.67-35.36)
GPN2	2	1	17.83 (1.6-198.05)	7.29 (1.77-30.05)
GPR183	1	0	Inf	18.28 (2.4-139.46)
GPR20	3	3	8.54 (1.7-42.78)	5.51 (1.72-17.59)
GSPT1	1	1	4.94 (0.31-79.56)	8.28 (1.11-61.79)
GTF2B	1	1	9.03 (0.56-145.34)	7.23 (0.98-53.06)
H2AFZ	1	1	9.02 (0.56-145.08)	274.99 (17.1-4421.97)
HAND2	1	0	Inf	46.68 (5.41-402.5)
HAUS2	1	1	9.03 (0.56-145.28)	8.3 (1.13-61.24)
HBEGF	1	0	Inf	22.99 (2.95-179.47)
HDGFL1	1	0	Inf	6.5 (0.88-48.13)
HECA	1	2	4.52 (0.41-50.19)	5.77 (0.79-42.22)
HES5	1	0	Inf	19.04 (2.42-149.93)
HIGD1B	1	0	Inf	10.89 (1.46-81.04)
HIST1H2AG	1	0	Inf	7 (0.95-51.34)
HIST1H3F	1	0	Inf	11.47 (1.54-85.48)
HIST1H4I	1	1	8.69 (0.54-139.76)	6.65 (0.91-48.71)
HIST2H2AB	1	0	Inf	11.3 (1.52-84.19)
HNRNPA3	1	0	Inf	38.41 (4.59-321.48)
HPGDS	2	1	18.23 (1.64-202.49)	6.92 (1.68-28.48)
HS3ST3B1	1	0	Inf	9.21 (1.23-68.88)
HSDL1	1	0	Inf	5.85 (0.8-42.75)
HTR1A	1	1	9.01 (0.56-144.95)	9.43 (1.27-69.81)
IDH3A	1	1	9.03 (0.56-145.34)	4.91 (0.67-35.75)
IL1RN	1	1	9.04 (0.56-145.41)	5.17 (0.71-37.72)
IL5	1	0	Inf	10.58 (1.42-78.6)
IMPAD1	1	1	9.05 (0.56-145.54)	8.58 (1.16-63.46)
INSL3	2	0	Inf	9.01 (2.15-37.73)
INSM2	2	0	Inf	5.57 (1.36-22.86)
IPO13	1	1	9.03 (0.56-145.34)	4.69 (0.64-34.13)
IRF2BP2	1	0	Inf	5.63 (0.77-41.21)
JPH4	2	3	5.94 (0.98-35.93)	5.25 (1.28-21.57)
JUNB	1	0	Inf	10.13 (1.35-76.07)
KCTD4	1	0	Inf	13.1 (1.75-98.17)
KLF13	1	0	Inf	12.77 (1.69-96.72)
KRTAP29-1	2	0	Inf	11.16 (2.02-61.55)
LBX1	1	1	8.89 (0.55-143.08)	6.56 (0.89-48.14)
LCE6A	1	2	4.51 (0.41-50.11)	5.62 (0.67-47.07)
LCN6	2	1	18.16 (1.63-201.75)	8.24 (1.99-34.09)
LEMD1	1	0	Inf	8.14 (1.1-59.98)
LHX9	1	0	Inf	7.4 (1.01-54.34)
LMO2	1	0	Inf	10.27 (1.38-76.51)
LMO7DN	1	0	Inf	Inf
LOC730159	1	0	Inf	14.48 (0.9-233.01)

LPCAT4	3	4	6.87 (1.52-31.06)	9.97 (3.1-32.01)
LRP2BP	3	6	4.57 (1.13-18.53)	5.93 (1.86-18.88)
LYPD2	2	2	8.95 (1.25-64.14)	6.63 (1.6-27.44)
LYPD8	1	2	4.51 (0.41-50.13)	7.02 (0.81-60.51)
MAB21L2	1	1	8.99 (0.56-144.61)	9.38 (1.27-69.4)
MBNL2	1	2	4.5 (0.4-49.97)	7.21 (0.98-52.92)
MBTD1	1	1	9.05 (0.56-145.54)	12.51 (1.67-93.75)
METTL7A	2	1	18.21 (1.64-202.3)	5.31 (1.3-21.78)
MGAT2	1	0	Inf	4.43 (0.61-32.2)
MLLT3	1	0	Inf	7.6 (1.03-55.9)
MMP16	1	0	Inf	5.71 (0.78-41.74)
MOB3C	2	1	16.86 (1.52-187.32)	4.5 (1.1-18.41)
MRPL12	1	0	Inf	6.66 (0.91-48.92)
MRPL17	2	2	9.04 (1.26-64.75)	17.44 (4.13-73.7)
MRPL33	1	2	4.52 (0.41-50.18)	6.07 (0.83-44.39)
MRPS10	3	1	27.58 (2.85-267.25)	10.16 (3.16-32.63)
MRPS12	1	0	Inf	11.61 (1.56-86.66)
MS4A6E	1	1	9.05 (0.56-145.54)	15.31 (2.03-115.59)
MTA2	1	2	4.52 (0.41-50.18)	4.25 (0.58-30.88)
MYOT	3	5	5.49 (1.3-23.26)	7.42 (2.32-23.69)
N6AMT2	1	1	9.04 (0.56-145.48)	4.59 (0.63-33.42)
NACC1	2	1	15.58 (1.4-173.07)	18.97 (4.46-80.68)
NAPB	1	0	Inf	9.78 (1.32-72.54)
NAT14	1	1	7.05 (0.44-113.45)	16.77 (1.94-144.63)
NBL1	1	0	Inf	7.35 (0.76-71.22)
NDFIP2	1	1	8.45 (0.53-135.98)	16.25 (2.14-123.54)
NDRG3	1	1	9.04 (0.56-145.48)	7.05 (0.96-51.76)
NDUFA12	2	1	18.23 (1.64-202.52)	13.53 (3.23-56.56)
NFE2L2	2	2	9.11 (1.27-65.27)	5.94 (1.45-24.39)
NFKBIL1	2	0	Inf	10.63 (2.55-44.37)
NGB	3	0	Inf	33.71 (9.69-117.22)
NKX2-5	1	0	Inf	9.96 (1.33-74.83)
NKX6-2	1	0	Inf	5.58 (0.76-40.85)
NMI	2	1	18.23 (1.64-202.58)	4.84 (1.18-19.82)
NOL7	2	2	8.12 (1.13-58.2)	13.43 (3.19-56.59)
NOXRED1	2	0	Inf	8.06 (1.95-33.26)
NPW	1	0	Inf	6.32 (0.85-47.04)
NR2E1	1	0	Inf	18.52 (2.4-142.66)
NRGN	1	2	4.05 (0.36-44.95)	63.42 (6.55-614.03)
NRL	1	0	Inf	10.48 (1.4-78.55)
NUP54	2	1	18.23 (1.64-202.58)	16.53 (3.92-69.76)
NUSAP1	4	3	12.33 (2.73-55.74)	7.68 (2.79-21.15)
OTX1	1	0	Inf	7.98 (1.08-58.74)
OTX2	1	0	Inf	10.53 (1.42-78.23)
PAQR8	1	2	4.52 (0.41-50.18)	8.04 (1.09-59.18)
PBK	2	2	9.1 (1.27-65.21)	7.21 (1.75-29.69)

PDCD7	2	1	9.14 (0.82-101.64)	7.36 (1.78-30.38)
PDHB	1	1	9.04 (0.56-145.48)	7.16 (0.98-52.6)
PEBP1	1	0	Inf	4.21 (0.58-30.6)
PELO	1	1	9.02 (0.56-145.21)	15.16 (2.01-114.45)
PEX11B	2	1	16.21 (1.46-180.14)	5.53 (1.35-22.71)
PEX3	1	0	Inf	9.74 (1.31-72.16)
PF4	2	2	9.11 (1.27-65.25)	39.76 (8.88-178.1)
PGF	3	4	6.79 (1.5-30.69)	21.39 (6.51-70.35)
PIGC	1	0	Inf	6.09 (0.83-44.56)
PLSCR2	2	2	6.4 (0.89-45.85)	5.07 (1.24-20.76)
PNPLA8	3	4	6.87 (1.52-31.08)	9.39 (2.93-30.09)
POPDC2	3	5	5.49 (1.3-23.27)	5.1 (1.6-16.2)
PPARD	1	1	9.03 (0.56-145.34)	6.08 (0.83-44.48)
PPBP	1	2	4.52 (0.41-50.18)	13.12 (1.75-98.32)
PPIH	2	2	9.1 (1.27-65.19)	13.83 (3.31-57.88)
PPM1L	1	1	9.04 (0.56-145.48)	8.06 (1.1-59.39)
PPP2R5A	1	1	9.03 (0.56-145.34)	6.23 (0.85-45.65)
PPP3CA	1	2	4.47 (0.4-49.63)	7.95 (1.08-58.57)
PRIMA1	1	0	Inf	5.67 (0.77-41.59)
PRPSAP2	1	0	Inf	7.15 (0.97-52.47)
PSEN1	1	2	4.52 (0.41-50.18)	10.93 (1.47-81.29)
PSMB1	1	1	9.04 (0.56-145.48)	9.45 (1.28-70.05)
PSMD11	1	1	9.03 (0.56-145.34)	5.5 (0.75-40.15)
PTCHD4	4	3	12.34 (2.73-55.8)	5.64 (2.06-15.42)
RAB13	1	1	9.03 (0.56-145.34)	8.54 (1.16-63)
RAB15	1	1	6.37 (0.4-102.55)	4.1 (0.56-29.78)
RAB27A	2	2	9.1 (1.27-65.19)	4.71 (1.15-19.28)
RAB6A	1	0	Inf	16.91 (2.23-128.55)
RAD21L1	3	0	Inf	36.73 (7.34-183.86)
RARRES2	1	0	Inf	9.28 (1.24-69.57)
RCBTB1	2	4	4.54 (0.82-25.07)	4.6 (1.12-18.84)
RCN2	1	0	Inf	14.08 (1.86-106.31)
REEP3	1	1	9.04 (0.56-145.41)	14.05 (1.84-107.22)
RGS17	1	0	Inf	7.95 (1.08-58.58)
RGS2	2	2	9.1 (1.27-65.19)	10.25 (2.47-42.52)
RIC8B	1	1	9.04 (0.56-145.48)	5.84 (0.8-42.67)
RIPPLY2	1	0	Inf	4.51 (0.62-32.83)
RLBP1	2	3	5.98 (0.99-36.14)	5.88 (1.43-24.14)
RNF141	3	4	6.88 (1.52-31.09)	44.15 (12.89-151.17)
RNF144A	1	2	4.52 (0.41-50.18)	4.1 (0.56-29.76)
RNF166	1	0	Inf	5.7 (0.77-41.94)
RPL15	1	0	Inf	16.94 (2.17-132.26)
RPL18A	1	0	Inf	6.48 (0.88-47.46)
RPL39L	1	0	Inf	5.16 (0.71-37.6)
RPL5	1	1	9.03 (0.56-145.34)	8.02 (1.09-59.09)
RPP38	1	1	9.04 (0.56-145.48)	6.5 (0.89-47.59)

RPRM	1	1	8.86 (0.55-142.55)	18.79 (2.45-144.04)
RRAGA	1	0	Inf	22.95 (2.96-177.88)
RSPO3	1	1	9.04 (0.56-145.48)	8.7 (1.18-64.25)
RUVBL2	3	5	5.39 (1.27-22.86)	5.66 (1.78-18.01)
RXRA	2	0	Inf	18.73 (4.42-79.38)
S100A2	1	1	9.03 (0.56-145.34)	5.72 (0.78-41.78)
SERPINF2	1	0	Inf	8.11 (1.1-59.79)
SGCZ	1	1	9.04 (0.56-145.48)	6.81 (0.93-49.99)
SGMS2	1	0	Inf	5.08 (0.7-37)
SIK2	2	3	6.07 (1-36.67)	4.68 (1.14-19.14)
SIN3A	2	3	6.06 (1-36.62)	8.52 (2.06-35.21)
SIRT6	2	3	5.68 (0.94-34.35)	6.57 (1.58-27.3)
SIRT7	1	0	Inf	6.86 (0.93-50.4)
SLBP	2	0	Inf	23.11 (5.4-98.89)
SLC25A25	2	2	9.02 (1.26-64.61)	7.54 (1.83-31.09)
SLC35F6	2	0	Inf	11.44 (2.75-47.71)
SLC48A1	1	0	Inf	8.17 (1.1-60.36)
SLC6A3	2	2	9.05 (1.26-64.86)	4.74 (1.16-19.43)
SLX4IP	2	1	18.23 (1.64-202.58)	13.13 (3.14-54.84)
SMIM14	2	1	18.23 (1.64-202.58)	24.1 (5.62-103.37)
SMIM18	1	0	Inf	Inf
SMPD2	2	3	6.01 (1-36.36)	5.88 (1.43-24.14)
SMR3A	1	1	9.04 (0.56-145.48)	9.16 (1.24-67.73)
SNAP25	1	0	Inf	25.57 (3.25-201.3)
SNN	1	0	Inf	15.98 (2.11-121.03)
SNX27	2	1	18.22 (1.64-202.4)	8.94 (2.15-37.12)
SNX33	1	2	4.5 (0.41-50.04)	4.23 (0.58-30.74)
SNX7	1	0	Inf	4.05 (0.56-29.44)
SPINK1	1	0	Inf	13.18 (1.75-98.99)
SPINK4	1	1	9.04 (0.56-145.48)	16.69 (2.2-126.86)
SPTY2D1	2	3	6.06 (1-36.64)	8.38 (2.03-34.58)
SRF	1	1	4.94 (0.31-79.56)	4.05 (0.56-29.44)
SRR	1	0	Inf	7.24 (0.99-53.15)
SRSF11	1	0	Inf	6.23 (0.85-45.58)
STAG1	1	0	Inf	6.63 (0.9-48.59)
STK24	1	0	Inf	8.05 (1.09-59.29)
STK4	2	1	18.23 (1.64-202.58)	12.02 (2.89-50.08)
SUPT16H	1	0	Inf	7.05 (0.96-51.7)
SVIP	1	0	Inf	7.6 (1.03-56.11)
SYT9	2	3	6.07 (1-36.67)	6.85 (1.67-28.21)
TAC3	1	0	Inf	11.24 (1.51-83.77)
TBC1D22A	3	4	6.44 (1.42-29.13)	7.52 (2.35-24.06)
TCTN3	4	4	9.19 (2.27-37.25)	12.19 (4.4-33.78)
TFAP2C	1	0	Inf	5.67 (0.78-41.44)
TGFB1	2	2	9.1 (1.27-65.16)	5.42 (1.32-22.29)
TLX1	1	0	Inf	6.16 (0.83-45.42)

TMBIM1	2	2	9.11 (1.27-65.24)	5.57 (1.36-22.88)
TMEM106A	2	4	4.55 (0.82-25.09)	7.5 (1.82-30.88)
TMEM116	2	1	18.22 (1.64-202.46)	9.06 (2.19-37.51)
TMEM14E	1	0	Inf	8.25 (1.12-60.78)
TMEM63B	1	0	Inf	4.02 (0.55-29.21)
TMEM65	1	1	9.04 (0.56-145.48)	23.4 (2.97-184.19)
TMEM70	1	2	4.52 (0.41-50.21)	4.46 (0.61-32.4)
TMEM8B	5	5	8.9 (2.54-31.2)	10.38 (4.17-25.83)
TMEM92	1	0	Inf	11.28 (1.51-84.03)
TNFSF14	1	1	9.04 (0.56-145.41)	9.7 (1.31-72.08)
TNFSF18	2	2	9.1 (1.27-65.18)	9.33 (2.25-38.66)
TOX	1	2	4.52 (0.41-50.18)	14.41 (1.91-108.48)
TSLP	2	3	6.06 (1-36.65)	9.74 (2.35-40.33)
TSPAN18	2	0	Inf	9.21 (2.23-38.12)
TSPAN3	1	1	9.03 (0.56-145.34)	13.49 (1.79-101.86)
TTC9	1	2	4.52 (0.41-50.18)	15.56 (2.05-118.26)
UBA3	1	1	9.04 (0.56-145.48)	5.99 (0.82-43.79)
UBIAD1	1	0	Inf	14.49 (1.92-109.1)
UBP1	2	2	9.11 (1.27-65.25)	5.87 (1.43-24.1)
UBXN7	1	1	9.04 (0.56-145.48)	11.89 (1.59-88.73)
UCHL5	2	0	Inf	28.79 (6.58-125.97)
UCK1	1	2	4.49 (0.4-49.93)	5.05 (0.69-36.83)
UNC5D	3	2	9.74 (1.61-58.92)	5.04 (1.59-16.02)
USP30	1	0	Inf	4.45 (0.61-32.4)
VDAC3	1	1	9.04 (0.56-145.48)	6.83 (0.93-50.08)
WBSCR16	1	2	4.52 (0.41-50.18)	9.14 (1.22-68.46)
WDR45B	1	2	4.52 (0.41-50.18)	6.44 (0.88-47.14)
WDR61	1	1	9.03 (0.56-145.34)	5.48 (0.75-40.01)
WIPI2	1	1	9.04 (0.56-145.48)	5.85 (0.8-42.78)
YRDC	1	0	Inf	10.47 (1.4-78.46)
YWHAB	1	0	Inf	6.22 (0.85-45.52)
YWHAE	1	1	8.43 (0.52-135.64)	27.37 (3.48-215.45)
ZBTB34	1	0	Inf	11.8 (1.58-88.09)
ZBTB44	3	2	13.77 (2.28-83.26)	7.05 (2.21-22.51)
ZCCHC9	1	2	4.52 (0.41-50.18)	5.08 (0.7-36.99)
ZDHHC17	1	2	4.43 (0.4-49.19)	5 (0.68-36.67)
ZIC2	1	0	Inf	10.36 (1.38-77.67)
ZMYND19	1	0	Inf	8.21 (1.11-60.52)
ZNF131	1	1	9.04 (0.56-145.48)	5.22 (0.72-38.06)
ZNF146	2	1	18.25 (1.64-202.77)	24.11 (5.62-103.39)
ZNF605	1	2	4.52 (0.41-50.18)	13.72 (1.83-103.05)
ZNF716	6	0	Inf	7.86 (3.42-18.07)
ZNF768	2	1	17.54 (1.58-194.9)	11.53 (2.77-47.99)
ZPBP2	2	1	18.22 (1.64-202.46)	8.35 (2.02-34.46)

Appendix Table 11: List of enriched genes for high-tension glaucoma cohort under a loss of function model

Headings:

Gene: HGNC gene name

HTG: Number of cases in high-tension glaucoma cohort

CTRL: Number of cases in local and AOGC controls

HTG CTRL OR (95% CI): Odds ratio of high-tension glaucoma cohort compared to controls

HTG NFE OR (95% CI): Odds ratio of high-tension glaucoma cohort compared to non-Finnish European ExAC public domain data

Gene	HTG	CTRL	HTG CTRL OR (95% CI)	HTG NFE OR (95% CI)
ABCA2	1	0	Inf	18.99 (2.41-149.52)
ABCC3	1	0	Inf	7.81 (1.06-57.5)
ACADVL	2	0	Inf	30.93 (7.07-135.34)
ACD	1	0	Inf	10.05 (1.35-74.63)
ACOX1	1	0	Inf	45.87 (5.48-383.9)
ADAM9	2	0	Inf	111.06 (21.34-578.07)
ADPRHL1	1	1	9.03 (0.56-145.28)	7.98 (1.08-58.79)
ADTRP	1	0	Inf	21.71 (2.73-172.67)
AFAP1L2	1	0	Inf	13.06 (1.72-98.88)
AGPAT2	1	0	Inf	25.72 (3.23-204.58)
AHSG	1	0	Inf	17 (2.24-129.24)
AKAP12	1	1	9.04 (0.56-145.48)	24.28 (3.11-189.55)
ALB	1	0	Inf	24.82 (3.18-193.71)
ANKDD1A	1	0	Inf	10.96 (1.47-81.64)
ANKRD27	1	1	9.04 (0.56-145.48)	5.74 (0.79-41.99)
ANO3	1	1	9.04 (0.56-145.48)	15.04 (1.99-113.58)
AP3B1	1	0	Inf	131.14 (11.81-1455.94)
APMAP	1	1	9.04 (0.56-145.48)	25.98 (3.3-204.53)
APOBR	1	1	8.99 (0.56-144.68)	7.71 (1.04-57.32)
ARMC8	1	0	Inf	122.85 (11.07-1363.87)
ARRDC2	1	0	Inf	15.51 (2.04-117.85)
ARSK	1	0	Inf	28.8 (3.62-229.07)
ASB8	1	0	Inf	5.73 (0.78-41.86)
ATAD3B	1	0	Inf	7.97 (1.08-58.71)
ATG3	1	0	Inf	68.15 (7.56-614.24)
ATG4D	1	0	Inf	10.8 (1.44-80.8)
ATG7	1	0	Inf	11.89 (1.59-88.76)

ATP6V0A2	1	0	Inf	18.08 (2.37-137.93)
ATP6V1E2	1	0	Inf	21.15 (2.74-162.92)
AVPR1A	1	1	8.71 (0.54-140.23)	38.65 (4.72-316.51)
BAAT	1	0	Inf	30.42 (3.82-241.98)
BCAT1	1	0	Inf	28.87 (3.63-229.64)
BDH2	1	1	9.04 (0.56-145.48)	9.87 (1.33-73.33)
BIN3	1	0	Inf	27.45 (3.45-218.36)
BNIP1	1	1	9.05 (0.56-145.54)	5.17 (0.71-37.68)
BRD9	1	0	Inf	54.89 (6.37-473.33)
BSCL2	1	1	9.05 (0.56-145.54)	15.83 (2.09-119.9)
C11orf53	1	0	Inf	19.58 (2.55-150.06)
C12orf56	1	0	Inf	7.09 (0.96-52.61)
C14orf177	1	1	9.03 (0.56-145.34)	24.11 (3.09-188.23)
C1orf109	1	0	Inf	23.74 (3.04-185.33)
C3orf30	1	1	9.04 (0.56-145.41)	16.09 (2.12-121.84)
C7orf31	2	1	18.23 (1.64-202.52)	14.53 (3.46-60.97)
CABS1	1	0	Inf	19.51 (2.54-149.5)
CACNA1S	1	0	Inf	8.4 (1.14-61.95)
CAPN13	1	1	9.05 (0.56-145.54)	5.68 (0.77-41.6)
CAPS2	1	0	Inf	6.14 (0.84-45.09)
CATSPER2	1	0	Inf	13.01 (1.74-97.51)
CATSPERG	3	1	27.53 (2.84-266.76)	8.78 (2.74-28.18)
CAV1	1	0	Inf	30.58 (3.84-243.24)
CBX2	1	0	Inf	24.38 (3.12-190.32)
CCBE1	1	0	Inf	15.23 (2.02-115.01)
CCDC57	2	1	18.13 (1.63-201.47)	13.9 (3.3-58.43)
CCR5	3	3	9.18 (1.83-45.98)	10.74 (3.34-34.53)
CCT8L2	1	0	Inf	19.67 (2.57-150.77)
CD200R1L	1	0	Inf	33.7 (4.18-271.49)
CD83	1	0	Inf	83.03 (8.58-803.85)
CDC42EP2	1	0	Inf	Inf
CDK15	1	0	Inf	10.5 (1.41-77.96)
CDK5RAP2	1	0	Inf	5.81 (0.79-42.44)
CDKN2AIP	1	0	Inf	Inf
CEACAM18	1	0	Inf	16.94 (2.23-128.71)
CEMP1	1	0	Inf	90.45 (9.34-875.76)
CEP70	1	0	Inf	7.26 (0.99-53.33)
CES3	1	0	Inf	20.82 (2.7-160.43)
CHAC2	1	1	9.04 (0.56-145.41)	8.34 (1.13-61.55)
CHRNB2	1	0	Inf	64.47 (7.15-581.05)
CIB1	1	0	Inf	39.31 (4.8-321.93)
CLEC4D	2	0	Inf	44.44 (9.84-200.68)
CLPSL2	1	0	Inf	74.48 (6.71-826.91)
CLUL1	1	1	9.04 (0.56-145.52)	6.88 (0.94-50.5)
CNBD1	1	1	9.03 (0.56-145.34)	13.5 (1.78-102.24)
CNDP2	1	0	Inf	30.47 (3.83-242.35)

COL22A1	2	3	6.05 (1-36.56)	7.98 (1.93-32.98)
CPD	1	0	Inf	30.59 (3.85-243.36)
CPVL	1	1	9.04 (0.56-145.48)	7.39 (1.01-54.28)
CRYBB1	1	0	Inf	45.83 (5.48-383.58)
CTSE	1	1	9.03 (0.56-145.34)	13.73 (1.83-103.15)
CTSH	1	0	Inf	10.88 (1.46-81.05)
CTSZ	1	0	Inf	11.89 (1.59-88.92)
CUX1	1	0	Inf	20.7 (2.69-159.47)
CYP21A2	1	0	Inf	56.41 (5.83-546.12)
CYP46A1	1	0	Inf	137.81 (12.41-1530)
DCLRE1C	2	1	18.24 (1.64-202.63)	11.67 (2.8-48.58)
DEDD2	1	0	Inf	7.53 (1-56.82)
DEFB135	1	0	Inf	13.65 (1.82-102.5)
DENND6B	1	1	9 (0.56-144.75)	57.37 (6.37-517.01)
DEPTOR	1	0	Inf	30.28 (3.81-240.89)
DERL3	1	0	Inf	13.71 (1.8-104.62)
DNAJC27	1	0	Inf	54.24 (6.29-467.7)
DNASE1L3	1	0	Inf	24.9 (3.19-194.4)
DNASE2B	1	0	Inf	9.44 (1.27-70.03)
DPP6	1	1	9.05 (0.56-145.54)	36.36 (4.34-304.27)
DSN1	1	0	Inf	8.49 (1.15-62.66)
DSP	1	0	Inf	14.45 (1.92-108.81)
DUSP16	1	0	Inf	68.72 (7.63-619.34)
ECHDC1	1	1	9.04 (0.56-145.48)	9.16 (1.24-67.7)
ECI1	1	0	Inf	13.02 (1.73-98.06)
EPG5	1	0	Inf	9.42 (1.27-69.69)
ERAP1	1	1	9.04 (0.56-145.48)	5.24 (0.72-38.24)
ERLIN2	1	0	Inf	137.43 (12.38-1525.71)
EXOC4	1	1	9.04 (0.56-145.48)	18.21 (2.39-138.95)
EXOG	1	0	Inf	11.92 (1.6-89)
EXOSC3	1	0	Inf	130.38 (11.74-1447.52)
FAM120B	1	0	Inf	6.61 (0.9-48.55)
FAM186B	1	1	9.03 (0.56-145.34)	8.4 (1.14-61.96)
FAM198A	1	1	8.87 (0.55-142.69)	6.68 (0.77-57.64)
FAM46B	1	0	Inf	12.96 (1.73-97.36)
FAM69C	1	1	8.77 (0.54-141.09)	55.06 (6.38-474.78)
FAM71C	1	0	Inf	12.38 (1.66-92.56)
FAM83B	1	0	Inf	24.98 (3.2-194.98)
FBLN2	1	0	Inf	23.92 (3.01-190.3)
FBXO39	1	0	Inf	25 (3.2-195.19)
FEZ2	1	0	Inf	16.92 (2.22-129.12)
FMN1	1	1	9.03 (0.56-145.28)	11.76 (1.57-88.1)
FNDC9	1	0	Inf	27.15 (3.45-213.73)
FOXRED1	1	0	Inf	5.92 (0.81-43.26)
FREM1	1	1	9.04 (0.56-145.41)	7.71 (1.04-56.84)

FXYD7	1	0	Inf	275.78 (17.15-4434.6)
FZD2	1	0	Inf	137.23 (12.36-1523.48)
FZD6	1	0	Inf	14.33 (1.9-107.9)
GALNT3	1	0	Inf	17.88 (2.34-136.42)
GAS2L2	1	1	9.05 (0.56-145.54)	12.11 (1.62-90.71)
GCC2	1	0	Inf	6.76 (0.92-49.55)
GCNT2	1	0	Inf	10.19 (1.37-75.57)
GFPT2	1	0	Inf	8.16 (1.11-60.21)
GLIPR1L2	1	0	Inf	5.11 (0.7-37.27)
GLIPR2	1	0	Inf	8.38 (1.14-61.81)
GOLIM4	1	0	Inf	10.07 (1.36-74.73)
GPR149	1	0	Inf	12.96 (1.73-97.1)
GPR37L1	1	0	Inf	33.52 (4.16-270.1)
GPSM2	1	1	9.03 (0.56-145.34)	5.72 (0.78-41.81)
GRAMD2	1	0	Inf	25 (3.2-195.19)
GRIN2C	1	0	Inf	17.68 (2.28-137.03)
GSTA5	1	0	Inf	6.4 (0.87-46.87)
GUCA1C	1	0	Inf	30.12 (3.79-239.59)
HAGH	1	1	8.43 (0.52-135.64)	15.13 (2-114.27)
HAUS2	1	0	Inf	38.01 (4.64-311.28)
HECW1	1	0	Inf	45.31 (5.41-379.23)
HIRIP3	1	1	9.04 (0.56-145.48)	30.24 (3.8-240.58)
HMGCLL1	1	0	Inf	20.39 (2.65-157.09)
HPS4	1	1	9.04 (0.56-145.48)	10.38 (1.4-77.11)
HPX	1	0	Inf	19.47 (2.54-149.21)
ICE1	1	0	Inf	36.76 (4.49-301.04)
IDH3A	1	0	Inf	137.79 (12.41-1529.79)
IFT88	1	0	Inf	8.7 (1.18-64.28)
IL1RL1	1	1	9.05 (0.56-145.54)	27.29 (3.47-214.87)
IL20RB	1	0	Inf	21.04 (2.73-162.11)
IMPG2	2	0	Inf	20.94 (4.91-89.21)
INO80E	1	0	Inf	14.25 (1.81-112.22)
INSM2	1	0	Inf	44.8 (5.19-386.31)
INSRR	2	1	18.22 (1.64-202.4)	15.93 (3.78-67.12)
INTS1	1	1	8.88 (0.55-142.95)	10.45 (1.4-78.02)
INTU	1	1	9.04 (0.56-145.48)	11.39 (1.53-84.87)
IQUB	1	1	9.05 (0.56-145.54)	5.84 (0.8-42.71)
IRGM	1	0	Inf	35.14 (2.18-565.15)
KATNB1	1	0	Inf	22.57 (2.91-174.93)
KCNH1	1	0	Inf	38.99 (4.76-319.33)
KCNH5	1	1	9.04 (0.56-145.41)	8.47 (1.15-62.45)
KCNJ1	1	0	Inf	10.12 (1.36-75.1)
KCNJ14	1	1	8.9 (0.55-143.15)	40.69 (4.86-340.55)
KCNQ1	1	1	9.04 (0.56-145.41)	8.34 (1.13-61.52)
KCTD19	1	1	9.04 (0.56-145.48)	11.46 (1.54-85.36)

KDELR3	1	1	8.62 (0.54-138.7)	5 (0.69-36.4)
KIAA1551	1	0	Inf	8.79 (1.19-64.93)
KLHDC2	1	0	Inf	19.62 (2.55-151.16)
KLHL21	1	0	Inf	49.24 (5.46-443.81)
KLHL25	1	0	Inf	10.88 (1.46-80.97)
KLHL28	1	0	Inf	263.8 (16.41-4242.04)
KLK1	1	0	Inf	14.42 (1.91-108.55)
KY	1	0	Inf	15.96 (2.09-121.79)
LDHAL6A	1	0	Inf	25.01 (3.2-195.25)
LDLRAD2	1	0	Inf	40.48 (4.69-349.06)
LEMD1	1	0	Inf	39.88 (4.77-333.77)
LIG1	1	0	Inf	11.42 (1.53-85.27)
LIG4	1	1	9.04 (0.56-145.48)	5.37 (0.74-39.18)
LIPI	1	0	Inf	17.77 (2.33-135.59)
LMOD2	1	0	Inf	19.28 (2.42-153.38)
LNX1	1	1	9.04 (0.56-145.48)	8.41 (1.14-62.07)
LRRFIP2	1	1	9.04 (0.56-145.48)	10.18 (1.37-75.49)
LTBP2	1	0	Inf	14.91 (1.97-112.9)
MAG	1	0	Inf	32.73 (4.06-263.72)
MAN1B1	1	1	9.05 (0.56-145.54)	6.05 (0.83-44.31)
MAP2K3	1	0	Inf	6.65 (0.91-48.75)
MAP3K13	2	0	Inf	39.18 (8.81-174.27)
MAP3K9	1	1	9 (0.56-144.88)	54.27 (6.29-467.97)
MATN3	1	0	Inf	23.45 (3-183.02)
MBOAT1	1	0	Inf	14.03 (1.86-105.68)
MCAT	1	0	Inf	15.34 (2.03-116.22)
MCMDC2	1	0	Inf	6.91 (0.94-50.79)
MEI1	1	0	Inf	5.19 (0.71-37.93)
METTL4	1	0	Inf	13.53 (1.8-101.59)
MIIP	1	1	8.35 (0.52-134.38)	5.48 (0.75-40.06)
MMS22L	1	0	Inf	22.23 (2.87-172.34)
MOV10L1	2	2	9.11 (1.27-65.25)	13.29 (3.18-55.6)
MRC2	1	0	Inf	43.38 (5.03-374.08)
MRPL39	1	1	9.04 (0.56-145.48)	17.16 (2.26-130.45)
MS4A14	1	0	Inf	5.33 (0.73-38.89)
MS4A7	1	0	Inf	68.78 (7.63-619.9)
MSH5	1	1	9.04 (0.56-145.48)	6.11 (0.83-44.68)
MSR1	1	0	Inf	8.18 (1.11-60.31)
MT1F	1	0	Inf	55.07 (6.39-474.93)
MTERF4	1	0	Inf	10.17 (1.37-75.43)
MTIF2	1	0	Inf	9.8 (1.32-72.63)
MTMR9	1	0	Inf	68.72 (7.63-619.34)
MUC15	1	1	9.04 (0.56-145.48)	16.95 (2.23-128.79)
MYCBPAP	1	0	Inf	18.99 (2.46-146.3)
MYO16	1	0	Inf	17.95 (2.34-137.59)
MYO3B	2	2	9.11 (1.27-65.25)	7.15 (1.74-29.45)

NAA38	1	0	Inf	16.46 (2.17-125.07)
NARS	1	0	Inf	20.38 (2.65-157.05)
NARS2	1	0	Inf	34.29 (4.26-276.25)
NBEA	1	0	Inf	24.2 (3.1-188.88)
NCAPH	1	0	Inf	47.57 (5.52-410.2)
NCF4	2	0	Inf	8.21 (1.99-33.88)
NCOR2	1	0	Inf	10.11 (1.35-75.6)
NDST4	1	1	9.04 (0.56-145.41)	45.03 (5.38-376.83)
NDUFAF6	1	0	Inf	10.33 (1.39-76.88)
NEK8	1	0	Inf	15.26 (2.02-115.2)
NEU2	1	1	8.76 (0.54-140.89)	33.33 (4.14-268.51)
NEXN	1	0	Inf	9.29 (1.25-68.71)
NGB	1	0	Inf	Inf
NLRP11	1	0	Inf	16.15 (2.13-122.33)
NLRP4	1	1	9.02 (0.56-145.21)	20.95 (2.72-161.41)
NLRX1	2	1	17.95 (1.62-199.44)	11.43 (2.75-47.57)
NMNAT3	1	0	Inf	7.83 (1.06-57.65)
NOL7	1	1	8.98 (0.56-144.48)	19.72 (2.54-152.88)
NOSTRIN	1	1	9.04 (0.56-145.41)	11.37 (1.53-84.73)
NPBWR1	1	0	Inf	8.73 (1.17-64.96)
NPR1	1	0	Inf	20.88 (2.69-161.88)
NRL	1	0	Inf	33.08 (4.11-266.54)
NUPL2	1	0	Inf	7.25 (0.98-53.31)
NXPE1	1	0	Inf	38.98 (4.76-319.24)
OGFOD1	1	1	9.04 (0.56-145.48)	16.16 (2.13-122.41)
OGFR	1	0	Inf	21.83 (2.71-175.88)
OR11H6	1	0	Inf	8.55 (1.16-63.08)
OR12D3	1	0	Inf	19.93 (2.59-153.55)
OR13A1	1	0	Inf	91.14 (9.41-882.41)
OR2AE1	1	0	Inf	33.96 (4.22-273.62)
OR51Q1	1	0	Inf	25.05 (3.21-195.54)
OR52E4	1	0	Inf	39.32 (4.8-322.01)
OR52E6	1	0	Inf	22.93 (2.96-177.7)
OR6Q1	1	0	Inf	24.82 (3.18-193.77)
OR9I1	1	0	Inf	19.63 (2.56-150.43)
OSBPL1A	1	1	9.04 (0.56-145.48)	14.44 (1.92-108.74)
OSMR	1	0	Inf	8.54 (1.16-63.01)
PABPC4	1	0	Inf	5.95 (0.81-43.47)
PAG1	1	0	Inf	45.6 (5.45-381.61)
PALLD	1	1	9.04 (0.56-145.48)	7.28 (0.99-53.54)
PAX4	1	0	Inf	10.9 (1.45-81.88)
PBK	1	0	Inf	14.14 (1.88-106.46)
PCCB	1	0	Inf	13.59 (1.81-102.05)
PCDHB10	1	1	9.04 (0.56-145.48)	12.31 (1.65-92.08)
PCDHGB6	1	0	Inf	7.04 (0.96-51.71)
PCDHGC5	1	1	9.05 (0.56-145.54)	18.92 (2.47-145.03)

PCNX	1	0	Inf	19.54 (2.55-149.77)
PDK4	1	0	Inf	12.29 (1.64-92.13)
PDZD8	1	0	Inf	273.85 (17.03-4403.63)
PGLS	1	0	Inf	48.32 (5.36-435.52)
PHIP	1	0	Inf	37.31 (4.56-305.57)
PHKB	2	0	Inf	14.01 (3.35-58.69)
PIBF1	1	0	Inf	8.24 (1.12-60.73)
PIGC	1	0	Inf	24.95 (3.2-194.78)
PIGL	1	1	9.04 (0.56-145.48)	27.55 (3.5-216.89)
PLCH1	2	0	Inf	34.27 (7.79-150.68)
PLVAP	1	1	9.04 (0.56-145.48)	91.05 (9.4-881.55)
POT1	1	0	Inf	14.02 (1.86-105.59)
PPP1R32	1	1	9.05 (0.56-145.54)	5.7 (0.78-41.74)
PPP3CC	1	0	Inf	18.05 (2.37-137.75)
PRMT3	1	1	9.05 (0.56-145.54)	10.96 (1.47-81.64)
PRR16	1	0	Inf	93.45 (8.42-1037.52)
PRR30	1	0	Inf	20.68 (2.68-159.29)
PYGM	1	0	Inf	10.45 (1.41-77.66)
RAB3GAP2	1	0	Inf	22.5 (2.9-174.38)
RBM14	1	0	Inf	Inf
RBM23	1	0	Inf	10.97 (1.47-81.74)
RFX6	1	0	Inf	21.18 (2.75-163.21)
RGS12	1	0	Inf	5.09 (0.7-37.09)
RHOT1	1	0	Inf	19.47 (2.54-149.26)
RNASE12	1	0	Inf	9.83 (1.33-72.82)
RNF141	1	0	Inf	55.03 (6.38-474.57)
RNLS	1	0	Inf	11.44 (1.54-85.25)
ROBO1	1	0	Inf	13.54 (1.8-101.97)
RPP38	1	1	9.04 (0.56-145.48)	27.42 (3.48-215.9)
RRH	1	0	Inf	10.11 (1.36-75.02)
RSF1	1	0	Inf	Inf
SCN9A	1	0	Inf	7.65 (1.04-56.45)
SDR39U1	1	0	Inf	12.78 (1.7-95.99)
SEC31B	2	2	9.11 (1.27-65.25)	5.16 (1.26-21.13)
SELL	1	0	Inf	60.58 (6.26-586.53)
SEMA3D	1	0	Inf	26.72 (3.39-210.38)
SETD6	1	0	Inf	11.06 (1.48-82.44)
SFRP4	1	0	Inf	24.96 (3.2-194.85)
SGCZ	1	0	Inf	22.41 (2.87-174.92)
SGSM2	1	1	8.74 (0.54-140.56)	13 (1.73-97.65)
SHB	1	0	Inf	127.3 (7.92-2047.13)
SHC1	1	0	Inf	39.11 (4.78-320.3)
SIRT5	1	1	9.04 (0.56-145.48)	15.08 (2-113.88)
SKA1	1	1	9.02 (0.56-145.14)	8.29 (1.13-61.12)
SLC12A9	1	1	8.86 (0.55-142.62)	12.04 (1.61-90.22)
SLC15A3	1	0	Inf	8.32 (1.13-61.38)

SLC17A5	1	0	Inf	8.05 (1.09-59.3)
SLC22A15	1	1	9.03 (0.56-145.34)	22.55 (2.89-176)
SLC25A26	1	1	9.04 (0.56-145.48)	9.69 (1.29-72.8)
SLC26A7	1	0	Inf	17.98 (2.36-137.22)
SLC28A3	1	0	Inf	14.39 (1.91-108.36)
SLC36A2	2	1	18.23 (1.64-202.58)	19.71 (4.64-83.65)
SLC41A3	1	0	Inf	19.28 (2.52-147.79)
SLC4A1AP	1	0	Inf	10.17 (1.37-75.46)
SLC6A16	1	1	9.04 (0.56-145.41)	6.52 (0.89-47.72)
SLC6A5	1	0	Inf	17.21 (2.26-131.32)
SLC7A9	1	0	Inf	8.59 (1.16-63.34)
SLC9A5	1	0	Inf	8.56 (1.16-63.17)
SLX4	1	1	9.02 (0.56-145.21)	7.27 (0.99-53.4)
SLX4IP	1	0	Inf	19.53 (2.55-149.69)
SMOC2	2	0	Inf	47.8 (10.48-217.96)
SMPD2	1	0	Inf	7.63 (1.04-56.08)
SNAPC1	1	0	Inf	30.38 (3.82-241.62)
SNX1	1	1	9.03 (0.56-145.34)	67.49 (7.49-608.25)
SPAG4	2	0	Inf	33.58 (7.6-148.46)
SPHKAP	1	0	Inf	39.21 (4.79-321.11)
SPINK1	1	0	Inf	27.08 (3.4-215.38)
SPINK4	1	0	Inf	274.86 (17.09-4419.85)
SRMS	1	0	Inf	16.85 (2.19-129.82)
SRPRB	1	0	Inf	27.32 (3.47-215.07)
ST6GALNAC2	1	0	Inf	7.52 (1.02-55.37)
STEAP2	1	1	9.04 (0.56-145.48)	6.19 (0.85-45.32)
STEAP4	1	0	Inf	10.88 (1.46-80.9)
SULF1	1	0	Inf	54.85 (6.36-473.02)
SULT1B1	1	0	Inf	15.77 (2.08-119.45)
SYT5	1	1	9.04 (0.56-145.48)	9.04 (1.22-67.28)
SYT6	1	0	Inf	90.69 (9.37-878.03)
SYVN1	1	0	Inf	Inf
SZT2	1	1	9.03 (0.56-145.34)	4.98 (0.68-36.3)
TATDN2	1	0	Inf	20.84 (2.71-160.58)
TBC1D32	1	1	9.03 (0.56-145.34)	5.57 (0.76-40.69)
TBX19	1	1	9.03 (0.56-145.34)	11.94 (1.6-89.1)
TEDDM1	1	0	Inf	27.51 (3.49-216.59)
TEK	1	0	Inf	137.46 (12.38-1526.07)
TEKT5	1	0	Inf	5.17 (0.71-37.67)
TGFBR2	1	0	Inf	91.45 (9.45-885.42)
TMC2	1	0	Inf	5.72 (0.78-41.8)
TMED3	1	0	Inf	9.52 (1.28-70.51)
TMEM116	1	0	Inf	19.49 (2.54-149.42)
TMEM132B	1	0	Inf	47.72 (5.53-411.49)
TMEM144	2	1	18.23 (1.64-202.58)	16.78 (3.98-70.71)

TMEM161A	1	0	Inf	39.46 (4.71-330.24)
TMEM5	1	0	Inf	29.39 (3.65-236.78)
TMEM70	1	0	Inf	9.47 (1.28-70.11)
TMEM8C	1	0	Inf	68.54 (7.61-617.72)
TNFAIP6	1	1	9.03 (0.56-145.34)	8.08 (1.1-59.5)
TOM1	1	0	Inf	13.13 (1.74-98.86)
TP53	1	0	Inf	100.95 (9.09-1120.76)
TP53I3	1	0	Inf	8.09 (1.1-59.66)
TPP1	1	0	Inf	10.2 (1.38-75.67)
TREML1	1	1	9.04 (0.56-145.48)	22.7 (2.93-175.98)
TRIM5	1	1	9.04 (0.56-145.48)	7 (0.95-51.34)
TRIP11	4	3	12.29 (2.72-55.58)	24.68 (8.74-69.71)
TRPA1	3	5	5.49 (1.3-23.27)	12.02 (3.73-38.74)
TSNAXIP1	4	1	37.09 (4.11-334.6)	19.05 (6.79-53.41)
TTC14	1	1	9.02 (0.56-145.21)	10.31 (1.39-76.68)
TTC37	1	1	9.04 (0.56-145.41)	7.15 (0.97-52.52)
TTLL1	1	0	Inf	10.97 (1.47-81.58)
TTLL12	1	0	Inf	13.42 (1.79-100.79)
TULP3	2	1	18.23 (1.64-202.58)	11.33 (2.71-47.43)
TXNDC12	1	0	Inf	84.55 (8.73-818.57)
UBE4B	1	0	Inf	54.44 (6.31-469.46)
UCP2	1	0	Inf	10.05 (1.35-74.67)
UGGT1	1	0	Inf	15.54 (2.05-117.68)
UIMC1	2	2	9.11 (1.27-65.27)	69.41 (14.59-330.25)
UNKL	1	1	8.74 (0.54-140.63)	9.11 (1.17-71.14)
URB1	2	1	17.81 (1.6-197.83)	21.93 (3.63-132.47)
URB2	1	1	9.03 (0.56-145.34)	5.6 (0.77-40.89)
UROS	1	0	Inf	19.27 (2.51-147.72)
USP20	1	0	Inf	14.65 (1.94-110.64)
USP6NL	1	0	Inf	20.08 (2.57-156.77)
UTS2	1	0	Inf	12.51 (1.67-93.52)
VIM	1	0	Inf	Inf
VNN1	1	1	9.04 (0.56-145.48)	22.76 (2.94-176.4)
VPS16	1	0	Inf	24.95 (3.2-194.78)
VSTM2B	1	0	Inf	14.96 (1.35-166.16)
XRCC2	1	0	Inf	12.95 (1.73-97.07)
XRCC6BP1	1	0	Inf	20.99 (2.72-161.73)
ZBTB9	1	0	Inf	30.09 (3.78-239.35)
ZCCHC7	1	0	Inf	24.93 (3.19-194.62)
ZIM2	1	0	Inf	25.04 (3.21-195.48)
ZKSCAN8	1	1	9.04 (0.56-145.48)	30.41 (3.82-241.92)
ZMYND8	1	0	Inf	272.81 (16.97-4386.92)
ZNF146	1	0	Inf	Inf
ZNF154	1	0	Inf	18.35 (2.4-140.01)
ZNF177	1	0	Inf	11.61 (1.55-87.19)
ZNF224	2	3	6.06 (1-36.66)	13.74 (3.28-57.48)

ZNF234	1	1	9.05 (0.56-145.54)	8.57 (1.16-63.23)
ZNF300	1	0	Inf	16.37 (2.15-124.42)
ZNF302	1	0	Inf	17.35 (2.27-132.42)
ZNF354A	1	1	9.04 (0.56-145.48)	39.1 (4.77-320.23)
ZNF391	1	1	9.04 (0.56-145.48)	15.29 (2.02-115.42)
ZNF484	1	0	Inf	18.3 (2.4-139.61)
ZNF567	1	0	Inf	27.08 (3.44-213.23)
ZNF607	2	2	9.11 (1.27-65.25)	9.9 (2.39-41.02)
ZNF716	2	0	Inf	18.69 (4.4-79.48)

Appendix Table 12: List of enriched genes for normal-tension glaucoma cohort under a predicted pathogenic model

Headings:

Gene: HGNC gene name

NTG: Number of cases in normal-tension glaucoma cohort

CTRL: Number of cases in local and AOGC controls

NTG CTRL OR (95% CI): Odds ratio of normal-tension glaucoma cohort compared to controls

NTG NFE OR (95% CI): Odds ratio of normal-tension glaucoma cohort compared to non-Finnish European ExAC public domain data

Gene	NTG	CTRL	NTG CTRL OR (95% CI)	NTG NFE OR (95% CI)
A1CF	1	1	17.08 (1.06-276.19)	5.96 (0.82-43.41)
ABHD6	1	0	Inf	12.08 (1.64-89.04)
ACKR1	1	4	4.25 (0.47-38.62)	6.66 (0.91-48.58)
ACOX1	2	7	4.93 (1-24.24)	4.93 (1.2-20.3)
ADAT2	1	1	17.09 (1.06-276.44)	8.25 (1.13-60.36)
AGGF1	2	2	12.39 (1.72-89.42)	8.05 (1.95-33.26)
AKT1S1	1	3	5.04 (0.52-49.16)	13.53 (1.8-101.49)
ALDOA	2	5	6.91 (1.31-36.31)	7.36 (1.78-30.41)
AMBP	2	3	11.35 (1.86-69.15)	7.07 (1.71-29.15)
AMFR	2	0	Inf	8.39 (2.03-34.68)
ANKRA2	1	4	4.17 (0.46-37.85)	6.44 (0.88-47)
ANKRD34A	1	0	Inf	15.32 (2.06-113.91)
ANKRD46	1	0	Inf	28.37 (3.72-216.4)
AP1B1	2	3	11.4 (1.87-69.44)	5.41 (1.31-22.28)
AP1G1	1	0	Inf	9.72 (1.32-71.38)
AP1S3	1	1	17.09 (1.06-276.44)	15.08 (2.03-111.85)
APOBEC3A	1	0	Inf	18.33 (2.45-136.93)
APOH	1	2	8.54 (0.76-95.4)	7.72 (1.06-56.44)
ARHGAP26	1	2	8.54 (0.76-95.43)	8.04 (1.1-58.84)
ARL14EPL	2	0	Inf	11.35 (2.16-59.62)
ARMC2	2	3	11.54 (1.89-70.32)	5.73 (1.39-23.62)
ATG9A	2	8	4.27 (0.89-20.54)	8.86 (2.14-36.64)
ATP5G2	1	0	Inf	11.01 (1.49-81.18)
ATP6AP1L	1	0	Inf	14.86 (2.01-110.13)
ATP6V1D	1	1	17.09 (1.06-276.44)	7.3 (1-53.38)
ATP9A	2	2	17.23 (2.39-124.38)	6.38 (1.55-26.29)
AURKAIP1	1	0	Inf	8.94 (1.22-65.59)
AURKB	1	3	5.68 (0.58-55.42)	4.56 (0.63-33.18)
AZIN1	1	2	8.38 (0.75-93.59)	12.34 (1.67-91.04)

BHLHA9	1	0	Inf	Inf
BLOC1S4	1	0	Inf	21.58 (2.81-165.78)
BMPR1A	2	1	35.01 (3.13-391.34)	14.98 (3.59-62.4)
BRD3	1	2	7.02 (0.63-78.5)	11.12 (1.51-81.88)
BTBD2	1	0	Inf	4.29 (0.59-31.19)
BTG4	1	0	Inf	9.73 (1.33-71.43)
C10orf95	1	0	Inf	36.5 (4.64-286.89)
C11orf91	1	0	Inf	13.16 (1.18-147.38)
C12orf4	2	5	6.92 (1.32-36.36)	7.67 (1.86-31.68)
C12orf43	1	0	Inf	7.82 (1.07-57.28)
C16orf45	2	1	33.54 (3-374.9)	11.16 (2.68-46.38)
C16orf70	1	3	5.69 (0.58-55.45)	9.13 (1.24-66.91)
C17orf105	1	1	17.09 (1.06-276.44)	21.82 (2.24-212.58)
C17orf49	1	1	17.09 (1.06-276.44)	7.13 (0.98-52.14)
C19orf52	1	2	5.63 (0.5-62.97)	6.63 (0.9-48.65)
C1orf186	1	2	8.54 (0.76-95.38)	8.52 (1.16-62.45)
C20orf197	1	3	5.66 (0.58-55.21)	6.4 (0.88-46.82)
C20orf62	2	0	Inf	15.58 (2.97-81.82)
C21orf59	1	1	17.09 (1.06-276.44)	5.16 (0.71-37.6)
C3orf14	2	1	34.71 (3.11-388.02)	55.12 (12.57-241.63)
C3orf18	1	0	Inf	8.7 (1.18-63.94)
C4orf32	1	0	Inf	12.96 (1.74-96.47)
CA11	1	2	8.52 (0.76-95.25)	7.48 (1.02-54.8)
CA13	2	2	17.3 (2.4-124.86)	12.72 (3.06-52.84)
CADM2	1	0	Inf	23.49 (3.12-176.91)
CAPZB	1	0	Inf	11.27 (1.53-83.17)
CARM1	1	2	8.33 (0.74-93.04)	20.51 (2.74-153.68)
CATSPER4	2	7	4.93 (1-24.21)	10.15 (2.45-42.04)
CBLL1	1	1	17.09 (1.06-276.44)	15.72 (2.12-116.65)
CBR4	1	1	17.05 (1.05-275.81)	5.25 (0.72-38.26)
CCDC127	1	0	Inf	9.44 (1.29-69.24)
CCDC179	1	0	Inf	Inf
CCDC6	1	1	17.09 (1.06-276.44)	15.31 (2.06-113.74)
CCDC94	1	1	17 (1.05-274.93)	15.42 (2.07-115.06)
CCL18	1	2	8.53 (0.76-95.37)	43.37 (5.56-338.52)
CCL5	2	6	5.76 (1.14-29.13)	10.97 (2.64-45.5)
CCNE1	1	2	8.54 (0.76-95.43)	10.52 (1.43-77.44)
CCNE2	1	0	Inf	6.55 (0.9-47.78)
CCSAP	1	0	Inf	21.02 (2.79-158.63)
CDKN2AIP	1	1	17.09 (1.06-276.44)	9.1 (1.24-66.81)
CDS1	1	4	4.26 (0.47-38.67)	5.2 (0.71-37.88)
CH25H	1	2	8.54 (0.76-95.45)	18.25 (2.44-136.55)
CHMP4A	2	2	17.33 (2.4-125.05)	8.74 (2.11-36.12)
CHRM4	1	4	4.26 (0.47-38.67)	7.97 (1.09-58.39)
CHST10	1	2	8.54 (0.76-95.43)	9.44 (1.29-69.26)
CHST13	1	0	Inf	10 (1.34-74.63)

CHSY3	1	0	Inf	6.21 (0.85-45.32)
CIAO1	1	2	8.54 (0.76-95.43)	5.93 (0.81-43.21)
CLEC4C	1	0	Inf	5.52 (0.76-40.2)
CLRN2	1	4	4.24 (0.47-38.51)	10.38 (1.41-76.28)
CNNM3	2	3	7 (1.15-42.81)	10.89 (2.62-45.2)
CNR1	1	2	8.54 (0.76-95.43)	8.48 (1.16-62.09)
CNRIP1	2	2	9.12 (1.26-65.86)	31.2 (7.24-134.53)
COG2	2	2	17.33 (2.4-125.09)	10.19 (2.46-42.21)
COMMD2	1	1	17.09 (1.06-276.44)	9.34 (1.27-68.53)
COQ10A	1	4	4.26 (0.47-38.69)	5.67 (0.78-41.34)
CORO1C	1	2	4.79 (0.43-53.59)	8.95 (1.22-65.7)
COX17	1	0	Inf	122.67 (13.52-1112.7)
COX5A	1	0	Inf	8.13 (1.11-59.48)
CPSF4L	1	4	4.26 (0.47-38.69)	4.14 (0.54-31.72)
CREG1	1	1	17.08 (1.06-276.19)	13.74 (1.86-101.76)
CRIPT	1	1	17.09 (1.06-276.44)	15.16 (2.04-112.42)
CRISPLD1	2	0	Inf	7.27 (1.76-30.02)
CRTC1	1	2	8.54 (0.76-95.43)	4.23 (0.58-30.74)
CRX	1	1	16.63 (1.03-268.99)	7.17 (0.98-52.37)
CST3	1	0	Inf	35.57 (4.38-288.54)
CST6	1	2	6.01 (0.54-67.16)	87.06 (10.03-755.73)
CTDSP1	1	0	Inf	18.73 (2.5-140.29)
CTSD	1	0	Inf	7.38 (1.01-53.98)
CTXN3	1	1	17.09 (1.06-276.44)	40.08 (5.17-310.9)
CXCR6	1	4	4.26 (0.47-38.69)	11.08 (1.51-81.51)
CYGB	1	0	Inf	5.88 (0.81-42.88)
CYP17A1	1	4	4.26 (0.47-38.68)	6.36 (0.87-46.43)
DAPK3	2	2	16.9 (2.34-121.94)	6.94 (1.68-28.69)
DBR1	2	7	4.93 (1-24.23)	8.28 (2-34.21)
DCD	1	1	17.09 (1.06-276.44)	13.28 (1.79-98.78)
DCK	1	0	Inf	21.5 (2.86-161.3)
DCTN3	1	0	Inf	15.31 (2.06-113.88)
DCTN5	1	0	Inf	26.81 (3.52-204.51)
DCTPP1	1	2	8.42 (0.75-94.09)	15.34 (2.07-113.83)
DEFB135	1	2	8.54 (0.76-95.43)	8.08 (1.1-59.15)
DGKA	1	4	4.26 (0.47-38.67)	5.46 (0.75-39.78)
DMRTA2	1	0	Inf	10.79 (1.44-80.94)
DNAJA2	1	1	17.08 (1.06-276.19)	12.89 (1.75-95.2)
DNAJB14	2	1	24.84 (2.22-277.68)	9.79 (2.36-40.53)
DNAJC5G	1	3	5.69 (0.58-55.45)	10.39 (1.41-76.37)
DPM1	1	1	17.08 (1.06-276.19)	16.24 (2.19-120.68)
DRG1	1	0	Inf	25.99 (3.44-196.54)
DUSP14	1	1	17.09 (1.06-276.44)	7.16 (0.98-52.29)
DUSP4	1	0	Inf	6.26 (0.86-45.77)
DYNC1I1	1	2	8.54 (0.76-95.43)	7.31 (1-53.51)
DYNLRB1	1	0	Inf	47.47 (5.99-376.29)

EBF3	1	2	8.51 (0.76-95.08)	10.31 (1.4-75.82)
ECH1	2	5	6.91 (1.31-36.32)	13.22 (3.17-55.05)
ECHDC3	2	1	22.76 (2.04-254.52)	8.56 (2.07-35.4)
EFR3B	1	1	17.1 (1.06-276.57)	4.81 (0.62-37.14)
EGFL8	2	2	16.25 (2.25-117.27)	11.82 (2.85-49.07)
EGLN1	1	0	Inf	25.86 (3.38-197.96)
EHD1	1	4	4.25 (0.47-38.6)	4.7 (0.65-34.2)
EHD4	2	6	5.72 (1.13-28.94)	8.77 (2.12-36.29)
EID1	1	0	Inf	24.01 (3.18-181.2)
EIF2S1	1	0	Inf	18.52 (2.48-138.16)
EIF4H	1	0	Inf	12.72 (1.72-93.92)
ELP6	1	4	4.26 (0.47-38.69)	6.56 (0.9-47.85)
EN1	1	4	4.1 (0.45-37.22)	9.08 (1.23-66.7)
ENTPD1	1	3	5.69 (0.58-55.45)	5.67 (0.78-41.31)
EVI2A	1	0	Inf	11.5 (1.56-84.7)
EZH2	1	2	8.54 (0.76-95.43)	13.52 (1.83-99.94)
F10	1	2	8.37 (0.75-93.54)	6.71 (0.92-48.95)
FAM118B	1	2	8.54 (0.76-95.4)	7.84 (1.07-57.33)
FAM131A	1	2	8.15 (0.73-91.06)	6.42 (0.88-46.89)
FAM132B	1	0	Inf	5.01 (0.59-42.21)
FAM219A	1	2	8.34 (0.75-93.16)	16.27 (2.19-120.99)
FAM32A	2	2	17.34 (2.4-125.16)	28.23 (6.5-122.6)
FAM91A1	1	2	8.53 (0.76-95.29)	4.61 (0.63-33.52)
FAR2	1	3	5.69 (0.58-55.45)	7.98 (1.09-58.4)
FARSA	3	4	13.18 (2.89-60.16)	7.99 (2.49-25.67)
FBL	1	4	4.2 (0.46-38.12)	4.9 (0.67-35.71)
FBXO21	1	1	6.81 (0.42-110.19)	9.17 (1.25-67.39)
FBXO22	1	1	15.23 (0.94-246.27)	8.72 (1.19-64.05)
FBXO46	1	0	Inf	6.14 (0.84-44.85)
FBXW7	1	1	17.08 (1.06-276.19)	13.22 (1.79-97.78)
FIS1	1	2	8.51 (0.76-95.05)	13.89 (1.88-102.84)
FKBP2	1	2	8.52 (0.76-95.16)	7.26 (0.99-53.02)
FKBP7	1	4	4.26 (0.47-38.69)	6.18 (0.85-45.09)
FLOT2	2	5	6.9 (1.31-36.28)	8.29 (2-34.24)
FLRT2	1	2	8.54 (0.76-95.45)	6.17 (0.85-45)
FNTA	1	1	17.09 (1.06-276.32)	15.99 (2.15-119.18)
FOXG1	1	0	Inf	38.09 (4.8-301.91)
FOXH1	1	2	7.83 (0.7-87.51)	6.6 (0.9-48.37)
FOXO6	1	0	Inf	17.33 (1.55-193.57)
FRG2C	1	2	8.54 (0.76-95.47)	Inf
FST	1	0	Inf	17.95 (2.41-133.8)
GAL3ST3	1	0	Inf	4.67 (0.64-34.04)
GAPVD1	3	12	4.37 (1.2-15.87)	6.24 (1.95-20)
GCLM	1	1	17.08 (1.06-276.19)	7.22 (0.99-52.81)
GCNT1	1	2	8.54 (0.76-95.43)	8.36 (1.14-61.21)
GDNF	1	1	17.09 (1.06-276.32)	13.07 (1.76-96.86)

GET4	1	3	5.54 (0.57-53.99)	6.84 (0.94-49.97)
GIT2	1	4	4.26 (0.47-38.66)	5.18 (0.71-37.69)
GJA5	1	4	4.26 (0.47-38.65)	16.25 (2.19-120.73)
GJA8	2	4	8.62 (1.55-47.99)	11.73 (2.83-48.69)
GLRA1	1	3	5.68 (0.58-55.42)	7.43 (1.02-54.29)
GLYR1	1	0	Inf	9.18 (1.25-67.34)
GM2A	1	3	5.67 (0.58-55.25)	10.17 (1.38-74.86)
GNL3	1	3	5.69 (0.58-55.45)	5.88 (0.81-42.84)
GP9	1	0	Inf	8.97 (1.22-66.03)
GPAT2	1	1	16.99 (1.05-274.8)	6.17 (0.85-45.03)
GPATCH11	1	2	8.45 (0.76-94.42)	6.97 (0.94-51.43)
GPR132	1	4	4.23 (0.47-38.37)	8.76 (1.2-64.23)
GRAMD4	1	1	16.56 (1.02-267.86)	6.52 (0.89-47.57)
GRHL2	1	4	4.26 (0.47-38.69)	5.22 (0.72-38.01)
GRM7	1	3	5.68 (0.58-55.42)	4.7 (0.65-34.19)
GRP	1	0	Inf	8.45 (1.15-62.28)
GRXCR2	2	6	5.76 (1.14-29.12)	11.3 (2.73-46.87)
GUCD1	1	2	8.25 (0.74-92.17)	7.24 (0.99-52.98)
HCAR1	2	7	4.93 (1-24.22)	6.99 (1.69-28.82)
HCN1	1	1	16.73 (1.03-270.64)	11.72 (1.59-86.38)
HCST	1	2	8.41 (0.75-93.97)	50.82 (6.41-402.87)
HDAC3	1	0	Inf	24.78 (3.28-187.03)
HDAC9	3	4	13.19 (2.89-60.25)	6.57 (2.05-21.1)
HES6	1	0	Inf	10.74 (1.44-79.93)
HEXIM1	1	0	Inf	9.07 (1.24-66.53)
HIST1H2AI	1	0	Inf	8.02 (1.09-58.69)
HIST1H3B	1	1	16.76 (1.04-271.01)	22.44 (2.99-168.7)
HIST1H4A	1	1	17.09 (1.06-276.44)	6.2 (0.85-45.22)
HIST2H2AB	1	0	Inf	21.36 (2.85-160.3)
HLA-DMB	1	1	17.09 (1.06-276.44)	15.67 (2.11-116.55)
HLX	1	3	4.49 (0.46-43.83)	6.18 (0.84-45.2)
HMBS	2	4	8.66 (1.56-48.18)	10.27 (2.48-42.58)
HNRNPR	1	1	17.08 (1.06-276.19)	7.85 (1.07-57.39)
HOPX	1	1	13.2 (0.82-213.56)	9.04 (1.23-66.61)
HPGD	1	0	Inf	6.32 (0.87-46.17)
HSBP1	1	0	Inf	52.34 (6.21-440.96)
HSD17B3	1	2	8.54 (0.76-95.43)	6.46 (0.89-47.12)
IGF2BP1	1	0	Inf	13.07 (1.77-96.6)
IL10RA	1	0	Inf	6.92 (0.95-50.5)
IL17B	1	0	Inf	6.2 (0.85-45.27)
IL17F	2	0	Inf	14.22 (3.42-59.21)
IL34	1	3	5.62 (0.58-54.81)	7.66 (1.05-56.07)
IL36A	1	0	Inf	19.29 (2.58-144.09)
IMMP2L	1	0	Inf	13.98 (1.89-103.44)
IMPDH2	1	2	8.54 (0.76-95.4)	5.8 (0.8-42.29)
INS-IGF2	2	3	10.54 (1.73-64.26)	35.81 (8.3-154.4)

INTS7	2	1	34.7 (3.1-387.84)	9.74 (2.35-40.3)
ISL1	1	2	8.49 (0.76-94.9)	17.92 (2.41-133.57)
ITPA	2	1	34.72 (3.11-388.1)	21.76 (5.18-91.48)
KAT8	1	0	Inf	22.47 (2.98-169.19)
KBTBD2	1	0	Inf	6.63 (0.91-48.4)
KBTBD4	2	3	8.32 (1.36-50.7)	11.23 (2.71-46.56)
KBTBD6	1	1	16.8 (1.04-271.65)	6.83 (0.94-49.89)
KCNH1	2	0	Inf	14.17 (3.4-58.97)
KCNMA1	3	2	12.98 (2.13-79.2)	15.88 (4.89-51.58)
KEAP1	1	1	16.73 (1.03-270.64)	3.99 (0.55-29)
KIAA0040	1	1	17.08 (1.06-276.19)	9.14 (1.11-75.4)
KISS1	1	1	8.05 (0.5-130.23)	15.69 (2.05-120.1)
KLHL2	1	1	17.09 (1.06-276.44)	23.37 (3.1-175.98)
KNG1	3	1	52.92 (5.43-516.15)	12.19 (3.78-39.34)
KPNB1	1	0	Inf	39.52 (5.09-306.58)
KRTAP10-12	1	2	7.91 (0.71-88.36)	7.17 (0.98-52.42)
KRTAP20-1	1	0	Inf	11.53 (1.56-84.89)
L3MBTL3	1	1	17.09 (1.06-276.44)	7.92 (1.08-57.92)
LAMTOR3	1	0	Inf	39.72 (5.09-310.01)
LEPROT	1	1	9.88 (0.61-159.9)	8.28 (1.13-60.66)
LKAAEAR1	1	0	Inf	10.51 (1.37-80.43)
LMAN2L	1	2	8.54 (0.76-95.38)	5.21 (0.72-37.91)
LMBRD2	1	3	5.68 (0.58-55.39)	5.62 (0.77-40.94)
LMX1B	1	0	Inf	9.75 (1.32-71.88)
LOX	1	0	Inf	11.19 (1.52-82.55)
LPAR5	1	4	4.18 (0.46-37.98)	7.18 (0.97-52.97)
LPCAT2	3	9	5.48 (1.45-20.74)	9.04 (2.81-29.09)
LPPR1	1	2	8.54 (0.76-95.43)	19.28 (2.58-144.01)
LRRC14	1	0	Inf	5.53 (0.76-40.31)
LRRC25	1	0	Inf	7.31 (1-53.4)
LSM11	1	0	Inf	8.4 (1.15-61.56)
MAP2K7	1	2	8.19 (0.73-91.56)	7.73 (1.05-56.7)
MAP4K3	1	2	7.26 (0.65-81.19)	6.05 (0.83-44.09)
MAPKAPK2	1	1	16.33 (1.01-264.07)	18.51 (2.48-138.12)
MAPRE1	1	0	Inf	23.63 (3.14-177.92)
MARCH9	1	1	16.91 (1.05-273.41)	10.87 (1.47-80.27)
MB21D1	2	5	6.86 (1.31-36.07)	6.91 (1.67-28.52)
MDM4	1	2	8.53 (0.76-95.34)	6.01 (0.82-43.85)
MEA1	1	0	Inf	17.04 (2.29-126.83)
MED19	1	0	Inf	14.05 (1.9-103.96)
MED27	1	1	17.1 (1.06-276.57)	10.33 (1.4-76.16)
MEF2D	1	3	5.31 (0.54-51.73)	6.21 (0.85-45.31)
MEPCE	1	3	5.67 (0.58-55.31)	9.8 (1.33-72.13)
METTL14	1	2	8.53 (0.76-95.37)	9.55 (1.3-70.11)
METTL6	2	3	11.53 (1.89-70.27)	12.33 (2.96-51.31)
MFAP3L	1	2	8.54 (0.76-95.45)	13.64 (1.84-100.83)

MGAT4D	1	0	Inf	5.33 (0.61-46.31)
MICU2	1	1	17.07 (1.06-276.07)	7.12 (0.97-52.07)
MITF	1	2	8.54 (0.76-95.43)	12.16 (1.65-89.66)
MMD	1	1	17.09 (1.06-276.44)	23.28 (3.09-175.34)
MNX1	1	0	Inf	12.04 (1.6-90.5)
MRAP2	1	4	4.26 (0.47-38.69)	8.79 (1.2-64.4)
MRPS25	1	3	5.69 (0.58-55.45)	25.05 (3.3-190.49)
MRPS26	2	0	Inf	20.02 (4.75-84.43)
MRPS7	1	1	17.1 (1.06-276.57)	9.71 (1.32-71.29)
MS4A8	1	2	8.54 (0.76-95.43)	15.2 (2.05-112.71)
MYF5	1	3	5.66 (0.58-55.23)	15.17 (2.05-112.54)
MYLK2	2	3	11.53 (1.89-70.23)	13.49 (3.24-56.2)
MZB1	1	0	Inf	5.08 (0.69-37.33)
NAIP	1	3	5.75 (0.59-56.04)	8.17 (1.12-59.79)
NAT1	1	3	5.69 (0.58-55.45)	7.5 (1.02-54.95)
NDE1	1	1	17.09 (1.06-276.36)	5.03 (0.69-36.62)
NDNL2	1	1	17.08 (1.06-276.19)	13.3 (1.8-98.57)
NDUFB2	1	1	17.09 (1.06-276.44)	13.41 (1.81-99.52)
NDUFB8	2	3	11.56 (1.9-70.41)	14.73 (3.53-61.37)
NDUFC2-KCTD14	1	0	Inf	Inf
NEK6	1	4	4.23 (0.47-38.37)	7.84 (1.07-57.47)
NEUROD4	1	2	8.54 (0.76-95.43)	8.51 (1.16-62.31)
NFXL1	1	1	17.09 (1.06-276.32)	6.5 (0.89-47.49)
NHLRC1	1	2	6.16 (0.55-68.85)	11.75 (1.59-86.81)
NIT2	1	3	5.69 (0.58-55.45)	6.54 (0.9-47.73)
NKX2-6	1	1	13.23 (0.82-213.94)	4.61 (0.59-35.76)
NKX6-2	2	0	Inf	21.44 (5.08-90.4)
NOB1	1	0	Inf	6.19 (0.85-45.17)
NOS1AP	1	2	8.52 (0.76-95.16)	8.38 (1.14-61.4)
NOV	1	3	5.69 (0.58-55.45)	7.95 (1.09-58.16)
NOVA1	1	0	Inf	13.87 (1.87-102.79)
NPFFR1	1	1	17.09 (1.06-276.44)	6.21 (0.85-45.58)
NPTX2	1	2	8.32 (0.74-92.95)	7.6 (1.04-55.65)
NT5DC1	1	1	17.09 (1.06-276.44)	8.15 (1.11-59.65)
NT5DC3	1	3	5.69 (0.58-55.45)	4.43 (0.61-32.22)
NTMT1	1	0	Inf	12.3 (1.67-90.72)
NUB1	1	3	5.66 (0.58-55.14)	5.3 (0.73-38.69)
NUDT1	1	3	5.69 (0.58-55.45)	4.43 (0.61-32.21)
NUDT9	1	1	17.09 (1.06-276.44)	8.27 (1.13-60.58)
ONECUT1	1	2	7.42 (0.66-82.89)	6.28 (0.86-45.85)
ORAOV1	1	2	8.54 (0.76-95.38)	17.35 (2.33-129.15)
OSGIN2	1	1	17.09 (1.06-276.44)	13.29 (1.8-98.24)
OSTF1	1	2	8.52 (0.76-95.25)	6.21 (0.85-45.32)
OTUD3	1	1	9.67 (0.6-156.49)	14.86 (2-110.21)
OVOL1	1	3	5.63 (0.58-54.89)	12.99 (1.75-96.16)
PAGR1	1	3	5.17 (0.53-50.43)	6.97 (0.95-51.28)

PARK7	1	1	17.08 (1.06-276.19)	8.24 (1.13-60.33)
PARL	1	0	Inf	11.77 (1.59-86.86)
PAX6	1	0	Inf	13.41 (1.81-99.16)
PCBP4	1	3	5.59 (0.57-54.47)	5.13 (0.7-37.32)
PDE6H	1	0	Inf	11.11 (1.51-81.78)
PDPK1	2	2	15.77 (2.19-113.81)	38.82 (9.04-166.72)
PDS5B	1	2	8.54 (0.76-95.43)	8.17 (1.12-59.82)
PDX1	1	0	Inf	18.59 (2.46-140.61)
PDZD9	1	0	Inf	29.33 (3.85-223.67)
PEX11B	1	1	15.2 (0.94-245.82)	5.18 (0.71-37.77)
PHF21A	1	3	5.66 (0.58-55.2)	6.47 (0.89-47.25)
PHIP	1	1	17.09 (1.06-276.36)	6.1 (0.84-44.51)
PHOSPHO2	1	1	17.09 (1.06-276.44)	7.27 (0.99-53.1)
PHYHIP	1	1	16.31 (1.01-263.82)	11.41 (1.54-84.26)
PI4KB	1	2	8.53 (0.76-95.34)	10.73 (1.46-78.89)
PIK3CB	1	4	4.26 (0.47-38.65)	5.5 (0.76-40.07)
PIP4K2C	2	6	5.76 (1.14-29.13)	7.5 (1.82-30.96)
PKNOX1	1	1	17.09 (1.06-276.44)	10.96 (1.49-80.65)
PLAGL1	1	3	5.69 (0.58-55.45)	10.09 (1.37-74.12)
PLEKHO1	1	2	8.32 (0.74-93.01)	6 (0.82-43.78)
PNN	1	2	8.54 (0.76-95.45)	5.47 (0.75-39.83)
POLR2B	1	1	17.1 (1.06-276.57)	14.71 (1.99-109.03)
POLR3D	1	1	9.57 (0.59-154.85)	9.6 (1.31-70.49)
POLR3H	1	1	15.4 (0.95-249.04)	8.11 (1.11-59.35)
POU1F1	1	3	5.69 (0.58-55.45)	5.61 (0.77-40.87)
PPDPF	1	3	4.31 (0.44-42)	8.28 (1.13-60.75)
PPM1L	1	1	17.09 (1.06-276.44)	15.25 (2.06-113.08)
PPP2R5A	1	1	17.08 (1.06-276.19)	11.77 (1.59-86.93)
PRKG2	1	0	Inf	8.45 (1.15-61.91)
PRLR	1	2	6.07 (0.54-67.83)	8.11 (1.11-59.35)
PROP1	1	1	16.56 (1.02-267.86)	6.47 (0.89-47.22)
PRPF6	1	0	Inf	8.77 (1.2-64.28)
PRR16	1	4	4.26 (0.47-38.69)	8.72 (1.19-63.95)
PRR23A	1	3	5.61 (0.58-54.69)	12.31 (1.65-91.75)
PRSS8	1	2	8.46 (0.76-94.51)	9.02 (1.23-66.19)
PSMD12	1	2	8.53 (0.76-95.37)	17.72 (2.38-132.08)
PSMG2	1	1	17.09 (1.06-276.44)	9.89 (1.35-72.66)
PTAR1	1	3	5.69 (0.58-55.45)	6.32 (0.87-46.23)
PTBP1	1	2	8.46 (0.76-94.51)	10.74 (1.46-79.13)
PTPN12	1	4	4.26 (0.47-38.69)	5.11 (0.7-37.23)
PTRH2	1	3	5.69 (0.58-55.45)	22.6 (3.01-169.85)
PUSL1	2	2	16.97 (2.35-122.46)	7.23 (1.74-29.99)
PWWP2A	1	2	8.54 (0.76-95.48)	11.19 (1.51-82.77)
RAB29	1	1	17.08 (1.06-276.19)	14.07 (1.9-104.2)
RAB2A	1	0	Inf	105.85 (11.67-960.14)
RAB4B	1	2	8.39 (0.75-93.77)	4.12 (0.57-29.95)

RASD1	1	1	16.53 (1.02-267.35)	6.78 (0.93-49.66)
RASL10B	1	1	16.59 (1.03-268.36)	71.4 (8.66-588.71)
RBBP6	3	8	6.07 (1.57-23.46)	7.5 (2.33-24.07)
RCHY1	1	1	16.59 (1.03-268.24)	12.23 (1.66-90.28)
REC8	1	2	8.53 (0.76-95.34)	5.3 (0.73-38.57)
RGS21	1	2	8.52 (0.76-95.25)	6.53 (0.89-47.66)
RGS5	1	3	5.66 (0.58-55.2)	7.59 (1.04-55.5)
RIPK4	3	5	9.13 (2.13-39.1)	6.89 (2.15-22.11)
RMND1	1	4	4.26 (0.47-38.64)	4.29 (0.59-31.16)
RNASEL	4	8	8.9 (2.61-30.39)	6.86 (2.48-18.99)
RND3	1	1	17.09 (1.06-276.36)	10.59 (1.44-77.87)
RNF126	1	1	15.19 (0.94-245.64)	5.02 (0.68-36.8)
RNF130	1	2	8.54 (0.76-95.43)	15.42 (2.07-114.81)
RNF141	1	4	4.26 (0.47-38.69)	27.36 (3.61-207.47)
RNF19B	1	3	5.68 (0.58-55.4)	9.02 (1.23-66.18)
RNF34	1	2	8.54 (0.76-95.43)	10.27 (1.4-75.5)
RPL13	1	2	8.53 (0.76-95.34)	6.55 (0.9-47.89)
RPL8	1	0	Inf	18.15 (2.43-135.39)
RPS19BP1	1	2	8.26 (0.74-92.29)	18.45 (2.46-138.23)
RTN4IP1	2	3	11.56 (1.9-70.41)	7.79 (1.89-32.17)
S1PR2	1	0	Inf	6.92 (0.95-50.56)
SAAL1	1	2	8.54 (0.76-95.43)	5.74 (0.79-41.84)
SAP30L	1	1	17.09 (1.06-276.44)	15.28 (2.05-113.84)
SATB1	1	3	5.69 (0.58-55.45)	14.56 (1.96-107.9)
SDF4	2	1	33.41 (2.99-373.42)	11 (2.65-45.64)
SDS	1	4	4.15 (0.46-37.69)	4.69 (0.64-34.11)
SEC22C	1	2	8.52 (0.76-95.25)	9.4 (1.28-68.95)
SEPT12	4	10	7.08 (2.16-23.23)	8.67 (3.13-24.05)
SF3A1	1	2	5.99 (0.54-66.96)	9.01 (1.23-66.11)
SFRP2	1	0	Inf	19.85 (2.65-148.69)
SFT2D2	1	3	5.68 (0.58-55.41)	15.25 (2.05-113.27)
SIAH3	1	0	Inf	9.75 (1.33-71.58)
SKAP1	1	1	17.09 (1.06-276.44)	10.07 (1.37-73.99)
SLBP	1	0	Inf	21.9 (2.92-164.33)
SLC23A2	1	3	5.69 (0.58-55.44)	6.01 (0.82-43.78)
SLC30A2	1	0	Inf	6.67 (0.91-48.71)
SLC35B4	1	4	4.26 (0.47-38.69)	6.27 (0.86-45.74)
SLC35F3	1	3	5.68 (0.58-55.4)	12.24 (1.66-90.32)
SLC39A14	1	1	9.54 (0.59-154.35)	6.49 (0.89-47.35)
SLC40A1	1	1	17.09 (1.06-276.44)	14.85 (2-110.01)
SLC51B	1	3	5.68 (0.58-55.4)	14.39 (1.94-106.9)
SLCO3A1	1	3	5.68 (0.58-55.35)	5.09 (0.7-37.1)
SMARCA4	3	3	14.14 (2.8-71.52)	11.11 (3.44-35.85)
SMCO3	1	1	17.09 (1.06-276.44)	5.56 (0.76-40.5)
SMIM11	1	0	Inf	57.04 (7.12-456.81)
SMR3B	2	2	17.35 (2.4-125.2)	12.39 (2.98-51.44)

SNCG	1	1	16.87 (1.04-272.82)	9.19 (1.25-67.46)
SNX17	1	4	4.26 (0.47-38.69)	9.96 (1.36-73.16)
SNX22	1	3	5.68 (0.58-55.35)	23.58 (3.13-177.58)
SNX8	2	2	16.8 (2.33-121.27)	23.36 (5.52-98.82)
SOAT1	2	2	17.33 (2.4-125.06)	7.55 (1.83-31.15)
SP9	1	0	Inf	11.37 (1.38-93.8)
SPTY2D1	1	3	5.68 (0.58-55.41)	7.85 (1.07-57.44)
SRRM4	1	2	8.54 (0.76-95.43)	7.11 (0.97-52.03)
SRSF5	2	1	34.73 (3.11-388.19)	9.33 (2.26-38.59)
ST6GALNAC3	1	2	8.53 (0.76-95.34)	10.76 (1.46-79.15)
ST8SIA2	1	0	Inf	14.43 (1.95-107.01)
STAM2	2	0	Inf	14.45 (3.47-60.2)
STIP1	1	0	Inf	11.32 (1.54-83.45)
STRADA	1	1	17.09 (1.06-276.44)	5.84 (0.8-42.55)
STX18	1	0	Inf	9.39 (1.28-69.01)
SUDS3	1	2	8.52 (0.76-95.25)	11.04 (1.49-81.82)
SULT2A1	1	3	5.69 (0.58-55.45)	6.33 (0.87-46.18)
SUMO4	1	2	8.54 (0.76-95.43)	32.42 (4.24-248.11)
SYCN	1	1	11.28 (0.7-182.5)	6.61 (0.9-48.35)
SYNGAP1	2	6	5.75 (1.14-29.05)	12.65 (3.04-52.57)
SYT4	1	3	5.67 (0.58-55.25)	6.18 (0.85-45.06)
TADA2B	1	1	17.11 (1.06-276.7)	24.15 (3.19-182.66)
TAF2	1	4	4.26 (0.47-38.69)	5.39 (0.74-39.24)
TAGLN3	1	0	Inf	47.22 (6.01-371.15)
TAS2R39	1	1	17.08 (1.06-276.19)	8.67 (1.18-63.51)
TBC1D10A	2	3	11.54 (1.89-70.3)	5.67 (1.38-23.35)
TBX1	1	0	Inf	8.52 (1.16-62.56)
TBX20	1	4	4.26 (0.47-38.69)	6.26 (0.86-45.71)
TCTN3	1	4	4.24 (0.47-38.47)	5.62 (0.77-40.98)
TDP2	1	0	Inf	13.99 (1.89-103.51)
TM6SF1	2	4	8.65 (1.55-48.13)	10.09 (2.44-41.8)
TMBIM1	1	2	8.54 (0.76-95.4)	5.22 (0.72-38.07)
TMED10	1	2	8.51 (0.76-95.12)	47.24 (6.01-371.33)
TMEM121	1	0	Inf	11.02 (1.48-82.11)
TMEM140	1	4	4.24 (0.47-38.46)	12.65 (1.71-93.4)
TMEM256	1	0	Inf	15.76 (2.11-117.72)
TMEM41A	1	1	17.09 (1.06-276.44)	6.48 (0.89-47.48)
TMEM86A	2	2	17.26 (2.39-124.57)	18.54 (4.43-77.66)
TMEM92	1	0	Inf	21.32 (2.84-159.98)
TMIGD1	1	1	17.09 (1.06-276.44)	4.81 (0.66-34.97)
TMOD2	1	2	8.53 (0.76-95.34)	4.28 (0.59-31.11)
TNFRSF11B	1	1	17.09 (1.06-276.44)	19.26 (2.58-143.89)
TNFRSF25	1	1	15.27 (0.94-247.02)	9.3 (1.26-68.6)
TNFSF15	1	0	Inf	15.24 (2.05-113.14)
TNIP2	1	1	16.88 (1.04-272.91)	8.04 (1.1-58.9)
TOP2A	2	5	6.92 (1.32-36.36)	8.18 (1.98-33.83)

TPH2	1	2	8.54 (0.76-95.4)	5.77 (0.79-42.04)
TRA2A	1	1	17.09 (1.06-276.44)	10.15 (1.38-74.56)
TRIB1	1	1	17.09 (1.06-276.44)	6.62 (0.91-48.33)
TRIM25	1	4	4.18 (0.46-37.94)	8.65 (1.18-63.54)
TRIM32	1	4	4.26 (0.47-38.67)	9.1 (1.24-66.73)
TRIM44	1	0	Inf	12.64 (1.71-93.38)
TRIM52	1	0	Inf	6.47 (0.89-47.21)
TRMT12	1	1	17.1 (1.06-276.53)	7.1 (0.97-51.89)
TRPC3	1	0	Inf	6.96 (0.95-50.83)
TSPO	1	1	16.4 (1.01-265.21)	7.28 (0.99-53.77)
TTC23	1	2	8.53 (0.76-95.34)	5.32 (0.73-38.73)
TTYH3	3	9	5.23 (1.38-19.81)	7.75 (2.41-24.95)
TUBG2	1	0	Inf	4.37 (0.6-31.77)
TXN2	1	3	5.56 (0.57-54.2)	16.71 (2.25-124.29)
UBASH3B	1	0	Inf	8.29 (1.13-60.7)
UBP1	1	2	8.54 (0.76-95.43)	5.5 (0.76-40.09)
UBQLN1	1	1	17.09 (1.06-276.44)	9.14 (1.25-67.11)
UFC1	1	0	Inf	7.63 (1.04-55.82)
USE1	1	0	Inf	14.63 (1.96-108.89)
UTP11L	2	5	6.91 (1.32-36.33)	7.63 (1.85-31.51)
VAX1	1	1	16.38 (1.01-264.83)	23.83 (3.14-180.72)
VEGFC	1	1	17.09 (1.06-276.44)	9.01 (1.23-66.11)
VIMP	1	1	17.08 (1.06-276.19)	6.06 (0.83-44.37)
VPS54	1	4	4.26 (0.47-38.66)	6.82 (0.93-49.79)
VWC2	1	1	9.44 (0.58-152.7)	12.12 (1.59-92.43)
WBP11	1	2	8.53 (0.76-95.28)	8.61 (1.17-63.09)
WDR88	1	1	17.09 (1.06-276.44)	6.41 (0.88-46.78)
WNT4	1	1	16.63 (1.03-268.99)	7.19 (0.98-52.53)
XRCC2	1	0	Inf	9.06 (1.24-66.45)
YBEY	1	0	Inf	16.59 (2.23-123.61)
ZBTB5	1	1	17.09 (1.06-276.36)	9.08 (1.24-66.57)
ZC2HC1A	1	1	17.09 (1.06-276.44)	8.39 (1.14-61.45)
ZCCHC3	1	2	7.11 (0.64-79.42)	16.69 (2.24-124.56)
ZDHHC14	1	0	Inf	7.25 (0.99-53.16)
ZIC1	1	2	6.9 (0.62-77.15)	5.82 (0.8-42.46)
ZNF213	1	2	8.13 (0.73-90.89)	5.59 (0.77-40.74)
ZNF326	1	1	17.05 (1.05-275.81)	7.16 (0.98-52.36)
ZNF34	1	2	8.54 (0.76-95.43)	8.15 (1.11-59.67)
ZNF362	1	1	10.96 (0.68-177.39)	5.3 (0.73-38.64)
ZNF511	1	1	16.23 (1-262.55)	6.12 (0.84-44.7)
ZNF547	1	3	5.69 (0.58-55.45)	7.64 (1.04-55.86)
ZNF624	1	1	17.09 (1.06-276.44)	6.24 (0.86-45.54)
ZNF641	1	2	8.54 (0.76-95.4)	5.16 (0.71-37.54)

Appendix Table 13: List of enriched genes for normal-tension glaucoma cohort under a loss of function model

Headings:

Gene: HGNC gene name

NTG: Number of cases in normal-tension glaucoma cohort

CTRL: Number of cases in local and AOGC controls

NTG CTRL OR (95% CI): Odds ratio of normal-tension glaucoma cohort compared to controls

NTG NFE OR (95% CI): Odds ratio of normal-tension glaucoma cohort compared to non-Finnish European ExAC public domain data

Gene	NTG	CTRL	NTG CTRL OR (95% CI)	NTG NFE OR (95% CI)
AARS	1	0	Inf	42.04 (5.39-328.12)
AASDH	1	1	17.09 (1.06-276.44)	12.25 (1.66-90.38)
ABCC6	1	0	Inf	9.54 (1.3-70.12)
ABLIM1	1	1	17.07 (1.06-276.07)	53.98 (6.74-432.28)
ACTL7A	1	2	8.54 (0.76-95.43)	47.18 (6-370.82)
ADAM17	1	0	Inf	53.5 (6.68-428.5)
ADD1	1	0	Inf	19.67 (2.62-147.63)
AGL	1	2	8.53 (0.76-95.32)	7.28 (1-53.17)
AKR1A1	1	0	Inf	10.4 (1.41-76.41)
ALKBH1	1	1	17.1 (1.06-276.57)	27.39 (3.61-207.7)
AMBP	1	0	Inf	32.19 (4.21-246.36)
AMFR	1	0	Inf	101.99 (11.75-885.28)
ANXA9	1	1	17.08 (1.06-276.19)	17.04 (2.29-126.82)
APIP	1	0	Inf	36.09 (4.68-278.54)
APOBEC1	1	0	Inf	169.46 (17.39-1650.88)
APOH	1	0	Inf	51.54 (6.5-408.56)
ARHGEF25	1	0	Inf	27.37 (3.6-208.07)
ARHGEF26	1	0	Inf	14.48 (1.95-107.69)
ARID1B	1	0	Inf	61.33 (7.56-497.47)
ARMC2	1	0	Inf	12.75 (1.72-94.26)
ATAD5	1	1	17.09 (1.06-276.44)	57.24 (7.15-458.39)
ATG7	1	0	Inf	22.48 (2.99-168.99)
ATP2C2	1	1	17.09 (1.06-276.44)	4.97 (0.68-36.16)
ATP5G2	1	0	Inf	73.88 (8.96-609.17)
ATP6V0A2	1	0	Inf	34.18 (4.45-262.6)
ATP8B4	1	1	17.09 (1.06-276.32)	7.3 (1-53.36)
ATP9A	1	0	Inf	101.88 (11.74-884.37)
ATP9B	1	2	8.54 (0.76-95.43)	19.74 (2.64-147.67)

ATXN2L	1	0	Inf	21.92 (2.91-165.11)
BCAT2	1	0	Inf	44.46 (5.66-349.49)
BEST3	1	2	8.54 (0.76-95.43)	6.35 (0.87-46.35)
BRF2	1	0	Inf	19.88 (2.66-148.73)
C11orf1	1	0	Inf	15.88 (2.13-118.07)
C12orf40	1	1	17.09 (1.06-276.44)	25.85 (3.41-196)
C17orf67	1	0	Inf	57.56 (7.19-460.96)
C3orf30	1	1	17.09 (1.06-276.32)	30.41 (3.99-231.97)
CAPRIN2	1	0	Inf	25.9 (3.42-195.92)
CARD6	1	3	5.65 (0.58-55.13)	5.31 (0.73-38.7)
CASP14	1	0	Inf	23.58 (3.13-177.56)
CASR	1	2	8.54 (0.76-95.38)	173.54 (17.81-1690.7)
CC2D2A	2	3	11.56 (1.9-70.41)	12.94 (3.1-54.01)
CCDC57	1	1	17 (1.05-274.93)	13.03 (1.76-96.54)
CCDC84	1	1	17.09 (1.06-276.44)	11.27 (1.53-83.12)
CCL18	1	0	Inf	104.11 (11.99-903.66)
CCR5	1	3	5.69 (0.58-55.45)	6.66 (0.91-48.61)
CD200R1L	1	0	Inf	63.71 (7.85-516.77)
CD300LF	1	0	Inf	42.79 (5.48-333.95)
CDAN1	1	2	8.34 (0.75-93.16)	20.47 (2.72-154.17)
CDCP1	1	0	Inf	101.23 (11.66-878.72)
CDON	1	1	17.09 (1.06-276.44)	13.24 (1.79-97.92)
CEP128	1	1	17.09 (1.06-276.44)	17.42 (2.33-129.96)
CEP72	1	0	Inf	14.68 (1.98-108.84)
CH25H	1	1	17.1 (1.06-276.57)	78.97 (9.37-665.32)
CLCN1	1	1	17.09 (1.06-276.44)	11.27 (1.53-83)
CLEC4C	1	0	Inf	6.48 (0.89-47.25)
CLEC4M	1	0	Inf	73.98 (8.97-609.96)
CLHC1	1	2	8.53 (0.76-95.31)	11.46 (1.56-84.41)
COG2	1	0	Inf	81.43 (9.66-686.01)
COL18A1	2	3	11.12 (1.82-67.75)	11.43 (2.74-47.66)
CORO7	1	1	15.98 (0.99-258.51)	12.52 (1.68-93)
CPD	1	0	Inf	57.84 (7.22-463.24)
CYP2E1	1	0	Inf	28.49 (3.75-216.63)
CYP2J2	1	1	16.84 (1.04-272.28)	14.41 (1.95-106.67)
DCLRE1C	2	1	34.74 (3.11-388.28)	22.22 (5.28-93.47)
DDX51	2	0	Inf	11.86 (2.86-49.25)
DGKZ	1	0	Inf	76.62 (8.45-694.98)
DHX32	1	1	17.09 (1.06-276.44)	24.31 (3.22-183.46)
DKK4	1	0	Inf	64.44 (7.94-522.7)
DMPK	1	1	15.76 (0.97-254.85)	8.42 (1.14-62.08)
DMRT3	1	1	17.09 (1.06-276.44)	43.32 (5.55-338.13)
DNAJC16	1	0	Inf	15.7 (2.12-116.55)
DNMT3A	1	3	5.69 (0.58-55.47)	5.8 (0.8-42.24)
DOPEY2	1	1	17.09 (1.06-276.36)	7.06 (0.97-51.6)
DUSP4	1	0	Inf	117.33 (12.94-1064.23)

ECH1	1	1	17.09 (1.06-276.32)	22.68 (2.99-172)
EGFL8	1	0	Inf	62.79 (7.74-509.31)
EHHADH	1	3	5.68 (0.58-55.37)	10.73 (1.46-78.95)
ELP2	1	2	8.54 (0.76-95.4)	18.54 (2.49-138.36)
FAM111A	1	2	8.54 (0.76-95.43)	17.78 (2.39-132.52)
FAM118B	1	0	Inf	86.53 (10.27-729.05)
FAM120B	1	0	Inf	12.5 (1.69-92.44)
FAM124A	1	1	17.08 (1.06-276.19)	54.16 (6.76-433.75)
FAM178A	1	0	Inf	31.21 (4.08-238.89)
FAM186A	1	1	17.09 (1.06-276.44)	5.32 (0.68-41.54)
FAM32A	1	0	Inf	384.41 (23.78-6212.96)
FAM69C	1	1	16.58 (1.03-268.11)	104.09 (11.99-903.54)
FAM71E2	1	0	Inf	Inf
FAM84B	1	0	Inf	110.12 (12.14-998.81)
FAR2	1	0	Inf	259.93 (23.28-2902.75)
FARSA	1	0	Inf	82.56 (9.8-695.53)
FASTKD2	1	0	Inf	36.54 (4.73-281.98)
FASTKD3	1	2	8.54 (0.76-95.43)	11.21 (1.52-82.56)
FBXO24	1	0	Inf	35.49 (4.58-275.37)
FCN1	1	1	17.06 (1.06-275.94)	7.48 (1.02-54.67)
FLOT2	1	0	Inf	60.88 (7.51-493.83)
FMO5	1	0	Inf	15.21 (2.05-112.78)
GABRR2	1	3	5.69 (0.58-55.45)	20.58 (2.74-154.44)
GAL3ST3	1	0	Inf	52.74 (6.4-434.88)
GALNS	1	0	Inf	41.08 (5.23-322.89)
GALNT14	1	2	8.54 (0.76-95.43)	21.6 (2.87-162.35)
GBA2	1	0	Inf	31.91 (4.17-244.19)
GCNT2	1	0	Inf	19.26 (2.58-143.89)
GIT2	1	0	Inf	124.31 (13.7-1127.54)
GJA8	1	0	Inf	56.47 (7.05-452.22)
GLE1	1	1	17.09 (1.06-276.44)	30.27 (3.97-230.84)
GLMN	1	2	8.49 (0.76-94.87)	22.98 (3.05-173.03)
GML	1	0	Inf	51.93 (6.55-411.65)
GNL3	1	0	Inf	12.57 (1.7-92.75)
GPBAR1	1	0	Inf	22.06 (2.92-166.44)
GPX5	1	0	Inf	130.13 (14.35-1180.3)
H6PD	1	2	8.53 (0.76-95.34)	18.59 (2.49-138.89)
HCN1	1	0	Inf	101.79 (11.73-883.51)
HEPHL1	2	5	6.92 (1.32-36.35)	14.96 (3.58-62.41)
HIST1H4A	1	0	Inf	22.39 (2.98-168.3)
HSPA4L	1	1	17.09 (1.06-276.32)	45.7 (5.81-359.21)
HYAL4	1	2	8.54 (0.76-95.43)	11.26 (1.53-82.87)
IFI44L	1	0	Inf	31.57 (4.12-241.6)
IGFBP6	1	0	Inf	32.47 (4.24-248.54)
IGFN1	2	4	8.65 (1.56-48.14)	13.37 (3.18-56.21)

IKBKAP	1	2	8.54 (0.76-95.47)	21.52 (2.87-161.47)
IQGAP2	1	3	5.69 (0.58-55.43)	6.74 (0.92-49.18)
KAT8	1	0	Inf	124.96 (13.78-1133.4)
KCNH5	1	1	17.09 (1.06-276.32)	16.01 (2.15-118.91)
KCNJ14	1	1	16.82 (1.04-272.02)	76.93 (9.13-648.14)
KCNU1	1	0	Inf	12.83 (1.74-94.89)
KHDC1L	1	0	Inf	20.57 (2.65-159.6)
KHNYN	1	1	16.87 (1.04-272.78)	6.13 (0.84-44.72)
KIAA1549	1	1	17.09 (1.06-276.44)	120.82 (13.32-1095.88)
KIAA1614	1	0	Inf	6.89 (0.94-50.36)
KIF12	1	0	Inf	38.24 (4.93-296.63)
KLHL38	1	3	5.69 (0.58-55.47)	12.05 (1.63-88.83)
KNG1	1	0	Inf	32.39 (4.23-247.9)
KRT75	1	2	8.54 (0.76-95.38)	7.99 (1.09-58.47)
KRT76	1	0	Inf	31.61 (4.13-241.89)
LAMTOR3	1	0	Inf	501.63 (31.04-8107.58)
LCE5A	1	0	Inf	64.35 (7.93-522.03)
LHX4	1	0	Inf	130.13 (14.35-1180.35)
LIMS2	1	2	8.47 (0.76-94.64)	17.22 (2.3-129.24)
LMBR1	1	1	17.09 (1.06-276.44)	8.94 (1.22-65.64)
LMBRD2	1	0	Inf	45.81 (5.83-360.09)
LPIN3	2	3	11.56 (1.9-70.41)	11.46 (2.76-47.57)
LRRC15	1	3	5.69 (0.58-55.45)	50.98 (6.43-404.13)
LRRC23	1	0	Inf	19.86 (2.65-148.58)
LRRC34	2	2	17.27 (2.39-124.63)	14.44 (3.47-60.13)
LRRC66	1	0	Inf	7.82 (1.07-57.21)
LRRC74A	1	0	Inf	12.67 (1.71-93.84)
LRRCC1	1	0	Inf	13.83 (1.87-102.52)
LRSAM1	1	0	Inf	29.77 (3.9-227.05)
MAP4K3	1	0	Inf	33.6 (4.37-258.14)
MAPRE1	1	0	Inf	521.34 (32.26-8426.15)
MB21D1	1	0	Inf	23.45 (3.08-178.88)
MCTP2	1	3	5.68 (0.58-55.38)	9.48 (1.29-69.57)
MIB1	1	3	5.69 (0.58-55.47)	5.79 (0.79-42.19)
MICALCL	1	1	17.09 (1.06-276.44)	5.05 (0.69-36.74)
MICU1	1	0	Inf	19.42 (2.58-146.24)
MICU2	1	0	Inf	36.13 (4.66-280.31)
MNX1	1	0	Inf	Inf
MRPS7	1	0	Inf	127.46 (14.05-1156.13)
MRRF	1	0	Inf	37.14 (4.81-286.61)
MTERF4	1	0	Inf	19.22 (2.57-143.61)
MTHFS	1	0	Inf	74.47 (9.03-614.01)

MTHFSD	1	1	17.09 (1.06-276.44)	14.75 (1.98-109.68)
MTNR1A	1	2	8.54 (0.76-95.43)	86.85 (10.31-731.74)
MUTYH	1	2	8.47 (0.76-94.64)	33.83 (4.4-259.9)
MYH10	1	1	17.09 (1.06-276.44)	30.35 (3.97-232.32)
MYLK2	1	0	Inf	Inf
NDE1	1	0	Inf	74.15 (8.99-611.37)
NOB1	1	0	Inf	50.27 (6.34-398.5)
NPHS2	1	0	Inf	36.82 (4.77-284.21)
NPTX2	1	0	Inf	499.27 (30.89-8069.32)
NSUN7	1	0	Inf	29.19 (3.76-226.47)
NUP214	1	0	Inf	15.66 (2.11-116.33)
OR10AD1	1	0	Inf	39.92 (5.15-309.67)
OR10G7	1	0	Inf	65.09 (8.02-528.01)
OR6T1	1	0	Inf	47.37 (6.03-372.33)
ORC6	1	0	Inf	40.55 (5.2-316.49)
OTOP3	1	0	Inf	63.05 (7.77-511.42)
OVGP1	2	0	Inf	24.71 (5.85-104.37)
OVOL1	1	0	Inf	364.2 (22.53-5886.31)
P2RX1	1	0	Inf	40.32 (5.17-314.67)
PALB2	1	1	17.09 (1.06-276.44)	12.02 (1.63-88.63)
PAPSS1	1	0	Inf	5.93 (0.81-43.24)
PARK7	1	0	Inf	14.65 (1.98-108.59)
PCDHGA5	1	1	17.09 (1.06-276.44)	7.11 (0.97-51.93)
PCDHGA8	1	0	Inf	30.34 (3.98-231.42)
PCSK7	1	0	Inf	54.04 (6.75-432.83)
PCSK9	1	0	Inf	18.36 (2.45-137.77)
PDE3B	1	2	8.18 (0.73-91.37)	6.53 (0.89-47.67)
PDE6H	1	0	Inf	72.16 (8.75-594.97)
PLA2G4E	1	2	8.53 (0.76-95.34)	16.03 (2.14-120.28)
PLCB4	1	0	Inf	63.45 (7.82-514.67)
PLCD1	1	3	5.68 (0.58-55.42)	12.11 (1.64-89.33)
PLD1	1	0	Inf	9.55 (1.3-70.11)
PLOD1	1	0	Inf	26.66 (3.52-202.12)
PODN	1	0	Inf	21.25 (2.82-160.38)
PROCA1	1	1	17.09 (1.06-276.44)	20.42 (2.73-152.95)
PRR23A	1	3	5.61 (0.58-54.69)	330.28 (20.43-5338.1)
PRSS33	1	2	8.18 (0.73-91.41)	29.57 (3.76-232.4)
PRSS36	1	0	Inf	7.04 (0.96-51.47)
PSAT1	1	0	Inf	47.33 (6.02-372.01)
PTDSS2	1	0	Inf	73.8 (8.95-608.5)
PTK2	1	0	Inf	259.93 (23.28-2902.68)
PUSL1	2	0	Inf	20.27 (4.76-86.29)
QRICH2	1	2	8.46 (0.76-94.5)	5.88 (0.81-42.85)
RAD51AP2	1	0	Inf	10.13 (1.38-74.58)
RCN3	1	1	16.83 (1.04-272.15)	29.82 (3.88-229.11)

RGL3	1	1	14.99 (0.93-242.48)	15.15 (2.03-112.76)
RMDN3	1	2	8.53 (0.76-95.34)	55.47 (6.93-444.23)
RNF112	1	0	Inf	147.51 (15.14-1437.05)
RSBN1	1	0	Inf	8.46 (1.15-62.03)
RTN4IP1	2	0	Inf	26.19 (6.2-110.7)
SAMD11	1	0	Inf	6.74 (0.92-49.38)
SAXO2	1	0	Inf	12.28 (1.66-90.66)
SCN7A	1	1	17.07 (1.06-276.02)	12.31 (1.66-91.34)
SEC22C	1	0	Inf	23.25 (3.09-175.09)
SETX	1	1	17.09 (1.06-276.44)	22.21 (2.95-166.95)
SH3TC2	1	1	17.09 (1.06-276.32)	18.58 (2.49-138.63)
SHPK	1	2	8.54 (0.76-95.38)	27.21 (3.58-206.91)
SIAH3	1	0	Inf	258.43 (23.14-2885.99)
SLC12A9	1	1	16.76 (1.04-271.01)	22.76 (3.02-171.78)
SLC15A3	1	0	Inf	15.73 (2.12-116.87)
SLC25A24	1	1	17.08 (1.06-276.19)	10.35 (1.41-76.13)
SLC26A8	1	1	17.09 (1.06-276.44)	6.53 (0.89-47.71)
SLC2A7	1	2	8.53 (0.76-95.34)	14.35 (1.94-106.45)
SLC47A1	1	0	Inf	25.76 (3.41-194.82)
SLC5A9	1	2	8.53 (0.76-95.29)	9.58 (1.3-70.28)
SMIM11	1	0	Inf	253.87 (22.73-2835.07)
SNX1	1	1	17.08 (1.06-276.19)	127.6 (14.07-1157.38)
STAM2	2	0	Inf	80.89 (17.89-365.85)
STKLD1	1	1	17.08 (1.06-276.19)	9.71 (1.32-71.46)
STRADA	1	1	17.09 (1.06-276.44)	36.24 (4.7-279.68)
STRN3	1	1	17.08 (1.06-276.19)	64.49 (7.95-523.1)
SULT1C3	1	1	17.11 (1.06-276.7)	19.85 (2.65-148.46)
SULT2A1	1	0	Inf	39.94 (5.15-309.87)
SYTL3	1	2	8.54 (0.76-95.43)	9.07 (1.24-66.6)
TACC3	1	0	Inf	36.6 (4.74-282.48)
TAS2R10	1	0	Inf	16.65 (2.24-123.81)
TCF12	1	0	Inf	104 (11.98-902.71)
TFR2	2	0	Inf	77.3 (16.95-352.48)
TGS1	1	0	Inf	25.49 (3.36-193.29)
TICRR	1	1	17.08 (1.06-276.19)	12.26 (1.66-90.53)
TLR10	1	2	8.54 (0.76-95.43)	9.53 (1.3-69.95)
TM4SF1	1	1	17.09 (1.06-276.44)	64.99 (8.01-527.19)
TMBIM1	1	1	17.09 (1.06-276.32)	28.28 (3.69-216.41)
TMEM256	1	0	Inf	57.69 (7.2-462.03)
TMEM86A	1	0	Inf	64.46 (7.95-522.87)
TMPRSS9	1	1	15.93 (0.98-257.63)	10.5 (1.42-77.47)
TNFRSF18	1	0	Inf	14.24 (1.91-106.41)
TNRC6C	1	0	Inf	79.7 (9.18-691.8)
TRDMT1	1	0	Inf	48.96 (6.18-388.1)

TRIM52	1	0	Inf	57.24 (7.15-458.4)
TRPC3	1	0	Inf	34.46 (4.46-265.94)
TRPM8	1	0	Inf	22.3 (2.97-167.64)
TRPV1	1	1	17.09 (1.06-276.44)	9.99 (1.36-73.63)
TSSK4	1	0	Inf	17.3 (2.32-128.75)
TXN2	1	0	Inf	74.11 (8.99-611.02)
TXNDC12	1	0	Inf	159.85 (16.41-1557.26)
UFC1	1	0	Inf	130.29 (14.36-1181.77)
UGDH	1	0	Inf	19.67 (2.63-147.15)
UGGT2	1	0	Inf	13.34 (1.8-98.67)
UPP2	1	0	Inf	17.8 (2.39-132.64)
USE1	1	0	Inf	123.81 (13.65-1123.01)
USP44	2	0	Inf	38.9 (9.06-167.09)
VARS2	1	0	Inf	6.59 (0.9-48.16)
VCL	1	1	17.1 (1.06-276.57)	46.86 (5.96-368.35)
VIPR1	1	2	8.53 (0.76-95.31)	39.74 (5.09-310.17)
VPREB1	1	0	Inf	85.29 (10.12-718.55)
VPS9D1	1	0	Inf	52.88 (6.52-428.93)
VWF	1	1	17.05 (1.05-275.69)	7.14 (0.98-52.21)
WBSCR27	1	0	Inf	33.77 (4.38-260.63)
WDR38	2	3	11.45 (1.88-69.77)	28.4 (6.7-120.38)
ZCCHC10	1	0	Inf	169.48 (17.4-1651.12)
ZCCHC7	1	0	Inf	47.14 (6-370.5)
ZMYM6	1	0	Inf	20.89 (2.77-157.67)
ZNF256	1	0	Inf	14.43 (1.95-106.84)
ZNF337	1	3	5.69 (0.58-55.45)	8 (1.09-58.56)
ZNF500	1	0	Inf	62.59 (7.72-507.69)
ZNF835	1	1	17.07 (1.06-276.07)	10.55 (1.43-77.66)

Appendix Table 14A: Top 20 enriched pathways in corneal epithelium.

Pathway name	Source Name	Id	P-value (corrected)
EGFR1	NETPATH	6101	7.15E-21
Cell junction organization	REACTOME	2071	1.70E-09
Formation of the cornified envelope	REACTOME	4980	2.96E-09
Cell-Cell communication	REACTOME	699	1.14E-08
Alpha6Beta4Integrin	NETPATH	6100	1.65E-08
Type I hemidesmosome assembly	REACTOME	5608	2.04E-08
Adherens junction	KEGG	477	7.21E-08
Signalling by Receptor Tyrosine Kinases	REACTOME	3266	4.07E-07
E-cadherin signalling in the nascent adherens junction	PID NCI	5981	4.38E-07
Stabilization and expansion of the E-cadherin adherens junction	PID NCI	5951	3.17E-06
Validated transcriptional targets of TAp63 isoforms	PID NCI	6020	6.78E-06
Pathogenic Escherichia coli infection	KEGG	575	7.13E-06
Neutrophil degranulation	REACTOME	1953	7.68E-06
Immune System	REACTOME	3147	9.18E-06
Regulation of actin cytoskeleton	KEGG	520	9.63E-06
Laminin interactions	REACTOME	5156	1.24E-05
Keratinization	REACTOME	1087	1.47E-05
a6b1 and a6b4 Integrin signalling	PID NCI	6070	1.54E-05
Validated targets of C-MYC transcriptional repression	PID NCI	5889	1.63E-05
Membrane Trafficking	REACTOME	5163	1.65E-05

Appendix Table 14B: Top 20 enriched gene ontology in corneal epithelium.

Gene ontology name	Id	P-value (corrected)
cornification	GO:0070268	2.51E-12
cell-cell adhesion	GO:0098609	6.68E-11
cell adhesion	GO:0007155	5.33E-09
neutrophil degranulation	GO:0043312	1.33E-07
epidermis development	GO:0008544	2.77E-07
hemidesmosome assembly	GO:0031581	3.91E-07
viral process	GO:0016032	3.04E-06
intermediate filament cytoskeleton organization	GO:0045104	1.16E-05
keratinization	GO:0031424	1.78E-05
viral entry into host cell	GO:0046718	2.39E-05
adherens junction organization	GO:0034332	2.53E-05
membrane organization	GO:0061024	2.67E-05
keratinocyte differentiation	GO:0030216	3.26E-05
wound healing	GO:0042060	3.48E-05
positive regulation of protein localization to plasma membrane	GO:1903078	3.49E-05
establishment or maintenance of cell polarity	GO:0007163	3.51E-05
apoptotic process	GO:0006915	1.81E-04
negative regulation of extrinsic apoptotic signalling pathway	GO:2001237	2.18E-04
extracellular matrix organization	GO:0030198	2.68E-04
regulation of cell proliferation	GO:0042127	3.70E-04

Appendix Table 15A: Top 20 enriched pathways in corneal stroma

Pathway name	Source Name	Id	P-value (corrected)
EGFR1	NETPATH	6101	2.91E-07
Extracellular matrix organization	REACTOME	5707	1.19E-06
Assembly of collagen fibrils and other multimeric structures	REACTOME	5691	3.60E-05
Collagen formation	REACTOME	1684	5.67E-05
Integrin.owl	INOH	6178	1.30E-04
Focal adhesion	KEGG	474	8.12E-04
Beta1 integrin cell surface interactions	PID NCI	5890	0.001001
Degradation of the extracellular matrix	REACTOME	2286	0.005836
Proteoglycans in cancer	KEGG	601	0.007006
Rap1 signalling pathway	KEGG	424	0.00879
Integrin cell surface interactions	REACTOME	653	0.008919
Keratan sulfate biosynthesis	REACTOME	1720	0.009056
Signalling by Receptor Tyrosine Kinases	REACTOME	3266	0.009185
Diseases associated with glycosaminoglycan metabolism	REACTOME	2542	0.009211
Stabilization and expansion of the E-cadherin adherens junction	PID NCI	5951	0.009389
ECM-receptor interaction	KEGG	475	0.00939
Signalling by PDGF	REACTOME	5446	0.009672
Alpha6 beta4 integrin-ligand interactions	PID NCI	5936	0.009679
Type I hemidesmosome assembly	REACTOME	5608	0.009679
Arf6 signalling events	PID NCI	6000	0.009721

Appendix Table 15B: Top 20 enriched gene ontology in corneal stroma

Gene ontology name	Id	P-value (corrected)
cell adhesion	GO:0007155	2.70E-05
extracellular matrix organization	GO:0030198	1.05E-04
positive regulation of fibroblast proliferation	GO:0048146	9.68E-04
negative regulation of T cell migration	GO:2000405	0.003105
cellular response to hydrogen peroxide	GO:0070301	0.003134
wound healing	GO:0042060	0.003278
positive regulation of angiogenesis	GO:0045766	0.00455
positive regulation of protein phosphorylation	GO:0001934	0.006913
keratan sulfate biosynthetic process	GO:0018146	0.007959
negative regulation of growth	GO:0045926	0.008605
lamellipodium assembly	GO:0030032	0.013036
hemidesmosome assembly	GO:0031581	0.013695
negative regulation of glucose import	GO:0046325	0.019467
odontogenesis	GO:0042476	0.02019
establishment of epithelial cell polarity	GO:0090162	0.025061
hematopoietic stem cell proliferation	GO:0071425	0.025061
endothelium development	GO:0003158	0.028564
response to oxidative stress	GO:0006979	0.029296
regulation of ERK1 and ERK2 cascade	GO:0070372	0.029303
cellular response to retinoic acid	GO:0071300	0.02952

Appendix Table 16A: Top 20 enriched pathways in corneal endothelium

Pathway name	Source Name	Id	P-value (corrected)
Parkinson's disease	KEGG	563	4.24E-34
The citric acid (TCA) cycle and respiratory electron transport	REACTOME	1776	2.48E-33
Respiratory electron transport, ATP synthesis by chemiosmotic coupling, and heat production by uncoupling proteins.	REACTOME	2559	9.19E-33
Oxidative phosphorylation	KEGG	331	5.89E-30
Respiratory electron transport	REACTOME	5154	2.73E-24
Thermogenesis	KEGG	505	1.74E-21
Huntington's disease	KEGG	565	6.55E-20
Alzheimer's disease	KEGG	562	4.58E-19
Metabolism	REACTOME	4798	3.68E-14
Non-alcoholic fatty liver disease (NAFLD)	KEGG	542	1.28E-12
Cardiac muscle contraction	KEGG	461	1.35E-12
TP53 Regulates Metabolic Genes	REACTOME	4148	5.33E-10
Formation of ATP by chemiosmotic coupling	REACTOME	2918	2.03E-09
Cristae formation	REACTOME	3928	7.91E-08
Glycolysis / Gluconeogenesis	KEGG	316	1.38E-06
HIF-1-alpha transcription factor network	PID NCI	6025	3.35E-06
Complex I biogenesis	REACTOME	3038	5.04E-06
Collagen formation	REACTOME	1684	5.26E-06
Collagen biosynthesis and modifying enzymes	REACTOME	4070	6.11E-06
Glycolysis Gluconeogenesis.owl	INOH	6122	1.77E-05

Appendix Table 16B: Top 20 enriched gene ontology in corneal endothelium

Gene ontology name	Id	P-value (corrected)
oxidation-reduction process	GO:0055114	2.13E-12
mitochondrial ATP synthesis coupled proton transport	GO:0042776	6.79E-12
mitochondrial electron transport, cytochrome c to oxygen	GO:0006123	1.28E-11
ATP biosynthetic process	GO:0006754	1.65E-09
glycolytic process	GO:0006096	1.60E-08
ATP synthesis coupled proton transport	GO:0015986	1.89E-08
mitochondrial electron transport, NADH to ubiquinone	GO:0006120	4.10E-08
hydrogen ion transmembrane transport	GO:1902600	4.17E-08
cristae formation	GO:0042407	4.60E-07
mitochondrial respiratory chain complex I assembly	GO:0032981	8.27E-07
canonical glycolysis	GO:0061621	1.16E-06
mitochondrial electron transport, ubiquinol to cytochrome c	GO:0006122	4.34E-06
aerobic respiration	GO:0009060	5.78E-06
ATP synthesis coupled electron transport	GO:0042773	7.23E-06
response to hypoxia	GO:0001666	7.29E-06
oxidative phosphorylation	GO:0006119	3.74E-05
gluconeogenesis	GO:0006094	1.69E-04
ATP hydrolysis coupled cation transmembrane transport	GO:0099132	5.67E-04
mitochondrion organization	GO:0007005	7.21E-04
extracellular matrix organization	GO:0030198	9.82E-04

Appendix Table 17A: Top 20 enriched pathways in trabecular meshwork

Pathway name	Source Name	Id	P-value (corrected)
Smooth Muscle Contraction	REACTOME	5517	9.06E-11
Vascular smooth muscle contraction	KEGG	463	2.03E-09
Muscle contraction	REACTOME	2538	2.96E-09
cGMP-PKG signalling pathway	KEGG	426	1.48E-08
Focal adhesion	KEGG	474	1.25E-07
Cell-extracellular matrix interactions	REACTOME	3172	6.41E-07
RHO GTPases Activate ROCKs	REACTOME	3570	1.63E-06
RHO GTPases activate PAKs	REACTOME	3459	3.66E-06
Dilated cardiomyopathy (DCM)	KEGG	632	8.79E-06
Hypertrophic cardiomyopathy (HCM)	KEGG	630	2.38E-05
RHO GTPases activate CIT	REACTOME	756	2.54E-05
Phosphatidylinositol signalling system	KEGG	433	2.91E-05
Oxytocin signalling pathway	KEGG	532	2.05E-04
Striated Muscle Contraction	REACTOME	3485	2.18E-04
Inositol phosphate metabolism.owl	INOH	6210	6.88E-04
Synthesis of IP2, IP, and Ins in the cytosol	REACTOME	4478	0.001052
Nitric oxide stimulates guanylate cyclase	REACTOME	1005	0.001107
Platelet activation	KEGG	482	0.001158
Cell junction organization	REACTOME	2071	0.001168
Inositol phosphate metabolism	REACTOME	1176	0.001431

Appendix Table 17B: Top 20 enriched gene ontology in trabecular meshwork

Gene ontology name	Id	P-value (corrected)
muscle contraction	GO:0006936	5.94E-14
sarcomere organization	GO:0045214	3.43E-07
cell-matrix adhesion	GO:0007160	2.06E-06
muscle organ development	GO:0007517	2.63E-05
muscle filament sliding	GO:0030049	3.67E-05
extracellular matrix organization	GO:0030198	6.15E-05
cell adhesion	GO:0007155	2.77E-04
cell junction assembly	GO:0034329	3.24E-04
smooth muscle contraction	GO:0006939	6.04E-04
integrin-mediated signalling pathway	GO:0007229	0.001156
inositol phosphate metabolic process	GO:0043647	0.001347
positive regulation of transcription from RNA polymerase II promoter involved in smooth muscle cell differentiation	GO:2000721	0.001376
positive regulation of transforming growth factor beta receptor signalling pathway	GO:0030511	0.002054
skeletal muscle tissue development	GO:0007519	0.002366
substrate adhesion-dependent cell spreading	GO:0034446	0.002519
adherens junction assembly	GO:0034333	0.003141
intracellular signal transduction	GO:0035556	0.003147
regulation of cell adhesion	GO:0030155	0.00541
positive regulation of GTPase activity	GO:0043547	0.006073
heart development	GO:0007507	0.006745

Appendix Table 18A: Top 20 enriched pathways in peripheral iris

Pathway name	Source Name	Id	P-value (corrected)
Classical antibody-mediated complement activation	REACTOME	876	1.03E-21
Initial triggering of complement	REACTOME	2317	1.10E-21
Role of phospholipids in phagocytosis	REACTOME	4512	1.11E-21
FCGR activation	REACTOME	2146	2.91E-21
Creation of C4 and C2 activators	REACTOME	1596	7.81E-21
CD22 mediated BCR regulation	REACTOME	5450	1.46E-19
Role of LAT2/NTAL/LAB on calcium mobilization	REACTOME	4036	2.73E-18
Complement cascade	REACTOME	1642	5.69E-18
Regulation of Complement cascade	REACTOME	3256	7.49E-18
FCERI mediated Ca+2 mobilization	REACTOME	5410	7.90E-18
Binding and Uptake of Ligands by Scavenger Receptors	REACTOME	4426	1.81E-17
Antigen activates B Cell Receptor (BCR) leading to generation of second messengers	REACTOME	3080	2.76E-17
Scavenging of heme from plasma	REACTOME	3662	3.56E-17
FCERI mediated MAPK activation	REACTOME	3297	1.49E-16
Fcgamma receptor (FCGR) dependent phagocytosis	REACTOME	2145	5.90E-16
Regulation of actin dynamics for phagocytic cup formation	REACTOME	2147	9.29E-16
FCERI mediated NF-kB activation	REACTOME	1357	4.72E-12
Immunoregulatory interactions between a Lymphoid and a non-Lymphoid cell	REACTOME	5114	1.09E-11
Signalling by the B Cell Receptor (BCR)	REACTOME	1991	3.68E-11
Cell surface interactions at the vascular wall	REACTOME	4168	5.83E-11

Appendix Table 18B: Top 20 enriched gene ontology in peripheral iris

Gene ontology name	Id	P-value (corrected)
complement activation	GO:0006956	2.08E-20
regulation of complement activation	GO:0030449	3.95E-17
complement activation, classical pathway	GO:0006958	7.83E-17
Fc-gamma receptor signalling pathway involved in phagocytosis	GO:0038096	3.09E-15
adaptive immune response	GO:0002250	2.51E-11
regulation of immune response	GO:0050776	4.13E-11
receptor-mediated endocytosis	GO:0006898	4.14E-11
Fc-epsilon receptor signalling pathway	GO:0038095	3.18E-10
leukocyte migration	GO:0050900	6.39E-10
immune system process	GO:0002376	2.83E-07
immune response	GO:0006955	2.17E-06
melanocyte differentiation	GO:0030318	2.28E-06
melanin biosynthetic process	GO:0042438	3.59E-06
proteolysis	GO:0006508	3.63E-05
pigmentation	GO:0043473	5.28E-05
developmental pigmentation	GO:0048066	2.08E-04
cell surface receptor signalling pathway	GO:0007166	8.91E-04
B cell receptor signalling pathway	GO:0050853	0.001691
melanin biosynthetic process from tyrosine	GO:0006583	0.023392
positive regulation of B cell activation	GO:0050871	0.044715

Appendix Table 19A: Top 20 enriched pathways in ciliary body

Pathway name	Source Name	Id	P-value (corrected)
Metabolism	REACTOME	4798	6.13E-05
Regulation of Insulin-like Growth Factor (IGF) transport and uptake by Insulin-like Growth Factor Binding Proteins (IGFBPs)	REACTOME	2798	1.40E-04
Post-translational protein phosphorylation	REACTOME	1272	1.40E-04
Transport of small molecules	REACTOME	3525	1.51E-04
Metabolism of proteins	REACTOME	2984	1.97E-04
Oxidative phosphorylation	KEGG	331	8.01E-04
Antigen Presentation: Folding, assembly and peptide loading of class I MHC	REACTOME	4661	0.001007
Lysosome	KEGG	447	0.00101
Antigen processing and presentation	KEGG	483	0.001154
The citric acid (TCA) cycle and respiratory electron transport	REACTOME	1776	0.00281
Vibrio cholerae infection	KEGG	573	0.002922
Citrate cycle (TCA cycle)	KEGG	317	0.002934
Formation of the ternary complex, and subsequently, the 43S complex	REACTOME	5425	0.003124
XBP1(S) activates chaperone genes	REACTOME	1989	0.003356
IRE1alpha activates chaperones	REACTOME	4864	0.003724
SRP-dependent cotranslational protein targeting to membrane	REACTOME	3189	0.003812
HTLV-I infection	KEGG	593	0.003828
Iron uptake and transport	REACTOME	4436	0.004676
Ribosomal scanning and start codon recognition	REACTOME	3307	0.00483
Translation initiation complex formation	REACTOME	4965	0.00483

Appendix Table 19B: Top 20 enriched gene ontology in ciliary body

Gene ontology name	Id	P-value (corrected)
cellular protein metabolic process	GO:0044267	2.31E-05
hydrogen ion transmembrane transport	GO:1902600	3.93E-05
ion transport	GO:0006811	1.42E-04
transferrin transport	GO:0033572	5.18E-04
antigen processing and presentation of peptide antigen via MHC class I	GO:0002474	5.25E-04
ATP hydrolysis coupled proton transport	GO:0015991	6.63E-04
lipid metabolic process	GO:0006629	9.38E-04
neutrophil degranulation	GO:0043312	9.62E-04
oxidation-reduction process	GO:0055114	0.001326
antigen processing and presentation of exogenous peptide antigen via MHC class I, TAP-independent	GO:0002480	0.001698
IRE1-mediated unfolded protein response	GO:0036498	0.001748
post-translational protein modification	GO:0043687	0.001799
SRP-dependent cotranslational protein targeting to membrane	GO:0006614	0.001846
extracellular matrix organization	GO:0030198	0.001883
insulin receptor signalling pathway	GO:0008286	0.002878
nuclear-transcribed mRNA catabolic process, nonsense-mediated decay	GO:0000184	0.004082
protein stabilization	GO:0050821	0.004092
positive regulation of cell cycle	GO:0045787	0.00462
viral process	GO:0016032	0.004692
regulation of vascular endothelial growth factor signalling pathway	GO:1900746	0.004718

Appendix Table 20A: Top 20 enriched pathways in retina

Pathway name	Source Name	Id	P-value (corrected)
The phototransduction cascade	REACTOME	4750	3.76E-16
Phototransduction	KEGG	518	8.30E-16
Activation of the phototransduction cascade	REACTOME	1130	1.74E-15
Inactivation, recovery and regulation of the phototransduction cascade	REACTOME	3986	1.88E-15
Visual signal transduction: Rods	PID NCI	5902	4.99E-14
Neuronal System	REACTOME	2969	1.39E-12
Visual phototransduction	REACTOME	2982	1.67E-11
Transmission across Chemical Synapses	REACTOME	5642	2.80E-11
Synaptic vesicle cycle	KEGG	507	7.04E-11
Glutamate Neurotransmitter Release Cycle	REACTOME	1736	1.57E-08
Glutamatergic synapse	KEGG	510	2.34E-08
GABAergic synapse	KEGG	513	1.45E-07
Neurotransmitter release cycle	REACTOME	2974	3.66E-07
Ca2+ pathway	REACTOME	915	3.72E-07
G alpha (i) signalling events	REACTOME	4048	7.08E-07
Insulin secretion	KEGG	522	4.06E-06
Transport of small molecules	REACTOME	3525	1.20E-05
Astrocytic Glutamate-Glutamine Uptake And Metabolism	REACTOME	4045	2.27E-05
Neurotransmitter uptake and metabolism In glial cells	REACTOME	2973	2.27E-05
Effects of Botulinum toxin	PID NCI	5894	6.89E-05

Appendix Table 20B: Top 20 enriched gene ontology in retina

Gene ontology name	Id	P-value (corrected)
visual perception	GO:0007601	1.11E-29
rhodopsin mediated signalling pathway	GO:0016056	1.29E-14
regulation of rhodopsin mediated signalling pathway	GO:0022400	2.99E-12
phototransduction	GO:0007602	1.68E-11
glutamate secretion	GO:0014047	5.91E-09
synaptic vesicle exocytosis	GO:0016079	7.70E-09
retina development in camera-type eye	GO:0060041	8.67E-09
photoreceptor cell maintenance	GO:0045494	5.44E-08
response to stimulus	GO:0050896	3.82E-07
eye photoreceptor cell development	GO:0042462	5.77E-07
chemical synaptic transmission	GO:0007268	1.78E-06
phototransduction, visible light	GO:0007603	1.92E-06
nervous system development	GO:0007399	4.86E-06
neurotransmitter secretion	GO:0007269	6.10E-06
detection of light stimulus involved in visual perception	GO:0050908	8.25E-06
exocytosis	GO:0006887	1.03E-05
Wnt signalling pathway, calcium modulating pathway	GO:0007223	2.00E-05
glycolytic process	GO:0006096	2.00E-05
presynaptic dense core vesicle exocytosis	GO:0099525	2.83E-05
synaptic vesicle maturation	GO:0016188	3.57E-05

Appendix Table 21A: Top 20 enriched pathways in optic nerve head

Pathway name	Source Name	Id	P-value (corrected)
Neuronal System	REACTOME	2969	1.11E-07
Transmission across Chemical Synapses	REACTOME	5642	2.16E-04
L1CAM interactions	REACTOME	4210	0.006307
S1P1 pathway	PID NCI	5952	0.007446
Cushing's syndrome	KEGG	544	0.007558
Basal cell carcinoma	KEGG	610	0.007693
ECM proteoglycans	REACTOME	744	0.007718
Circadian entrainment	KEGG	504	0.007774
CRMPs in Sema3A signalling	REACTOME	3093	0.007789
Potassium Channels	REACTOME	1739	0.007854
Axon guidance	KEGG	468	0.008172
Cardiac conduction	REACTOME	2143	0.008461
Ca2+ pathway	REACTOME	915	0.008561
Neurexins and neuroligins	REACTOME	5747	0.008795
Hippo signalling pathway	KEGG	472	0.008835
Dopamine Neurotransmitter Release Cycle	REACTOME	4794	0.008901
Voltage gated Potassium channels	REACTOME	2037	0.009138
Neurotransmitter receptors and postsynaptic signal transmission	REACTOME	2971	0.009471
Cell adhesion molecules (CAMs)	KEGG	476	0.009774
Protein-protein interactions at synapses	REACTOME	4586	0.01051

Appendix Table 21B: Top 20 enriched gene ontology in optic nerve head

Gene ontology name	Id	P-value (corrected)
nervous system development	GO:0007399	1.27E-13
multicellular organism development	GO:0007275	3.30E-05
metanephric nephron tubule formation	GO:0072289	8.86E-05
extracellular matrix organization	GO:0030198	5.12E-04
chemical synaptic transmission	GO:0007268	6.94E-04
cell adhesion	GO:0007155	7.14E-04
neurotransmitter secretion	GO:0007269	8.38E-04
branching involved in blood vessel morphogenesis	GO:0001569	9.63E-04
axon guidance	GO:0007411	0.001
angiogenesis	GO:0001525	0.001331
regulation of exocytosis	GO:0017157	0.001454
cell differentiation	GO:0030154	0.001485
neurofilament bundle assembly	GO:0033693	0.001541
synapse assembly	GO:0007416	0.001948
ion transport	GO:0006811	0.002162
central nervous system projection neuron axonogenesis	GO:0021952	0.002169
synapse maturation	GO:0060074	0.002169
retina development in camera-type eye	GO:0060041	0.002574
social behavior	GO:0035176	0.003053
calcium ion-regulated exocytosis of neurotransmitter	GO:0048791	0.004055

Appendix Table 22A: Top 20 enriched pathways in optic nerve

Pathway name	Source Name	Id	P-value (corrected)
COPI-independent Golgi-to-ER retrograde traffic	REACTOME	2849	6.33E-09
Membrane Trafficking	REACTOME	5163	9.06E-08
HSP90 chaperone cycle for steroid hormone receptors (SHR)	REACTOME	4597	1.29E-07
Vesicle-mediated transport	REACTOME	4919	7.10E-07
Cholesterol biosynthesis	REACTOME	2451	1.25E-06
Signalling by Rho GTPases	REACTOME	3524	2.79E-06
Golgi-to-ER retrograde transport	REACTOME	4448	3.45E-06
Intra-Golgi and retrograde Golgi-to-ER traffic	REACTOME	4679	2.17E-05
MHC class II antigen presentation	REACTOME	3593	2.23E-05
Vasopressin-regulated water reabsorption	KEGG	549	2.23E-05
Recycling pathway of L1	REACTOME	852	4.36E-05
COPI-mediated anterograde transport	REACTOME	5506	6.03E-05
RHO GTPases Activate Formins	REACTOME	3560	6.83E-05
Post-chaperonin tubulin folding pathway	REACTOME	3152	9.73E-05
RHO GTPases activate IQGAPs	REACTOME	5653	9.95E-05
RHO GTPase Effectors	REACTOME	1136	1.01E-04
Steroids metabolism.owl	INOH	6163	1.27E-04
Axon guidance	REACTOME	3431	1.65E-04
Translocation of SLC2A4 (GLUT4) to the plasma membrane	REACTOME	5528	1.77E-04
Gap junction	KEGG	479	2.10E-04

Appendix Table 22B: Top 20 enriched gene ontology in optic nerve

Gene ontology name	Id	P-value (corrected)
substantia nigra development	GO:0021762	1.13E-09
central nervous system myelination	GO:0022010	1.17E-08
cytoskeleton organization	GO:0007010	5.74E-07
cytoskeleton-dependent intracellular transport	GO:0030705	1.43E-06
oligodendrocyte differentiation	GO:0048709	8.49E-06
membrane organization	GO:0061024	8.95E-06
nervous system development	GO:0007399	9.08E-06
myelination	GO:0042552	5.39E-05
cholesterol biosynthetic process	GO:0006695	6.39E-05
sterol biosynthetic process	GO:0016126	6.56E-05
regulation of cholesterol biosynthetic process	GO:0045540	1.74E-04
steroid biosynthetic process	GO:0006694	2.26E-04
oligodendrocyte development	GO:0014003	2.50E-04
microtubule-based process	GO:0007017	4.00E-04
transport along microtubule	GO:0010970	4.74E-04
actin filament organization	GO:0007015	5.80E-04
negative regulation of axonogenesis	GO:0050771	7.67E-04
positive regulation of myelination	GO:0031643	7.82E-04
regulation of cell shape	GO:0008360	7.83E-04
microtubule cytoskeleton organization	GO:0000226	7.91E-04

Appendix Table 23A: Top 20 enriched pathways in sclera

Pathway name	Source Name	Id	P-value (corrected)
L13a-mediated translational silencing of Ceruloplasmin expression	REACTOME	3981	1.56E-103
GTP hydrolysis and joining of the 60S ribosomal subunit	REACTOME	3310	2.97E-103
Cap-dependent Translation Initiation	REACTOME	4421	7.34E-102
Eukaryotic Translation Initiation	REACTOME	2530	7.34E-102
Formation of a pool of free 40S subunits	REACTOME	5793	1.14E-101
Peptide chain elongation	REACTOME	2027	3.12E-99
Eukaryotic Translation Elongation	REACTOME	905	1.19E-98
Viral mRNA Translation	REACTOME	4585	7.60E-95
Nonsense Mediated Decay (NMD) independent of the Exon Junction Complex (EJC)	REACTOME	1026	4.18E-93
Eukaryotic Translation Termination	REACTOME	3602	2.55E-92
Selenocysteine synthesis	REACTOME	2603	2.55E-92
SRP-dependent cotranslational protein targeting to membrane	REACTOME	3189	5.00E-90
Selenoamino acid metabolism	REACTOME	751	2.57E-86
Nonsense Mediated Decay (NMD) enhanced by the Exon Junction Complex (EJC)	REACTOME	1025	4.21E-83
Nonsense-Mediated Decay (NMD)	REACTOME	3125	4.21E-83
Influenza Viral RNA Transcription and Replication	REACTOME	4006	1.20E-75
Ribosome	KEGG	404	5.11E-74
Influenza Life Cycle	REACTOME	3697	8.75E-73
Influenza Infection	REACTOME	4763	1.31E-69
Translation	REACTOME	5478	2.40E-68

Appendix Table 23B: Top 20 enriched gene ontology in sclera

Gene ontology name	Id	P-value (corrected)
SRP-dependent cotranslational protein targeting to membrane	GO:0006614	1.77E-102
translational initiation	GO:0006413	1.74E-99
viral transcription	GO:0019083	2.57E-88
nuclear-transcribed mRNA catabolic process, nonsense-mediated decay	GO:0000184	6.23E-88
translation	GO:0006412	2.50E-72
rRNA processing	GO:0006364	3.48E-63
cytoplasmic translation	GO:0002181	1.24E-43
osteoblast differentiation	GO:0001649	4.13E-09
extracellular matrix organization	GO:0030198	1.33E-08
ribosomal large subunit assembly	GO:0000027	5.35E-07
positive regulation of translation	GO:0045727	4.21E-06
ribosomal small subunit assembly	GO:0000028	5.71E-06
cellular protein metabolic process	GO:0044267	5.92E-06
skeletal system development	GO:0001501	1.85E-04
keratan sulfate catabolic process	GO:0042340	2.14E-04
intramembranous ossification	GO:0001957	3.03E-04
ribosomal small subunit biogenesis	GO:0042274	3.33E-04
supramolecular fiber organization	GO:0097435	5.09E-04
transforming growth factor beta receptor signalling pathway	GO:0007179	5.98E-04
cartilage development	GO:0051216	6.57E-04

References

ABBHI, V. & PIPLANI, P. 2018. Rho-kinase (ROCK) Inhibitors- A Neuroprotective Therapeutic Paradigm with a Focus on Ocular Utility. *Curr Med Chem*.

ABECASIS, G. R., AUTON, A., BROOKS, L. D., DEPRISTO, M. A., DURBIN, R. M., HANDSAKER, R. E., KANG, H. M., MARTH, G. T. & MCVEAN, G. A. 2012. An integrated map of genetic variation from 1,092 human genomes. *Nature,* 491**,** 56-65.

ABU-AMERO, K. K., AZAD, T. A., SPAETH, G. L., MYERS, J., KATZ, L. J., MOSTER, M. & BOSLEY, T. M. 2012. Unaltered myocilin expression in the blood of primary open angle glaucoma patients. *Mol Vis,* 18**,** 1004-9.

ABU-AMERO, K. K., MORALES, J., ALJASIM, L. A. & EDWARD, D. P. 2013. CYP1B1 Mutations are a Major Contributor to Juvenile-Onset Open Angle Glaucoma in Saudi Arabia. *Ophthalmic Genet*.

ABU-AMERO, K. K., MORALES, J. & BOSLEY, T. M. 2006. Mitochondrial abnormalities in patients with primary open-angle glaucoma. *Invest Ophthalmol Vis Sci,* 47**,** 2533-41.

ACHARYA, M., MOOKHERJEE, S., BHATTACHARJEE, A., BANDYOPADHYAY, A. K., DAULAT THAKUR, S. K., BHADURI, G., SEN, A. & RAY, K. 2006. Primary role of CYP1B1 in Indian juvenile-onset POAG patients. *Mol Vis,* 12**,** 399-404.

ADAM, M. F., BELMOUDEN, A., BINISTI, P., BREZIN, A. P., VALTOT, F., BECHETOILLE, A., DASCOTTE, J. C., COPIN, B., GOMEZ, L., CHAVENTRE, A., BACH, J. F. & GARCHON, H. J. 1997. Recurrent mutations in a single exon encoding the evolutionarily conserved olfactomedin-homology domain of TIGR in familial open-angle glaucoma. *Hum Mol Genet,* 6**,** 2091-7.

ADZHUBEI, I. A., SCHMIDT, S., PESHKIN, L., RAMENSKY, V. E., GERASIMOVA, A., BORK, P., KONDRASHOV, A. S. & SUNYAEV, S. R. 2010. A method and server for predicting damaging missense mutations. *Nat Methods,* 7**,** 248-9.

ALI, M., MCKIBBIN, M., BOOTH, A., PARRY, D. A., JAIN, P., RIAZUDDIN, S. A., HEJTMANCIK, J. F., KHAN, S. N., FIRASAT, S., SHIRES, M., GILMOUR, D. F., TOWNS, K., MURPHY, A. L., AZMANOV, D.,

TOURNEV, I., CHERNINKOVA, S., JAFRI, H., RAASHID, Y., TOOMES, C., CRAIG, J., MACKEY, D. A., KALAYDJIEVA, L., RIAZUDDIN, S. & INGLEHEARN, C. F. 2009. Null mutations in LTBP2 cause primary congenital glaucoma. *Am J Hum Genet,* 84**,** 664-71.

ALLINGHAM, R. R., WIGGS, J. L., DE LA PAZ, M. A., VOLLRATH, D., TALLETT, D. A., BROOMER, B., JONES, K. H., DEL BONO, E. A., KERN, J., PATTERSON, K., HAINES, J. L. & PERICAK-VANCE, M. A. 1998. Gln368STOP myocilin mutation in families with late-onset primary open-angle glaucoma. *Invest Ophthalmol Vis Sci,* 39**,** 2288-95.

ALLINGHAM, R. R., WIGGS, J. L., HAUSER, E. R., LAROCQUE-ABRAMSON, K. R., SANTIAGO-TURLA, C., BROOMER, B., DEL BONO, E. A., GRAHAM, F. L., HAINES, J. L., PERICAK-VANCE, M. A. & HAUSER, M. A. 2005. Early adult-onset POAG linked to 15q11-13 using ordered subset analysis. *Invest Ophthalmol Vis Sci,* 46**,** 2002-5.

ALMASIEH, M., WILSON, A. M., MORQUETTE, B., CUEVA VARGAS, J. L. & DI POLO, A. 2012. The molecular basis of retinal ganglion cell death in glaucoma. *Prog Retin Eye Res,* 31**,** 152-81.

ALWARD, W. L., KWON, Y. H., KAWASE, K., CRAIG, J. E., HAYREH, S. S., JOHNSON, A. T., KHANNA, C. L., YAMAMOTO, T., MACKEY, D. A., ROOS, B. R., AFFATIGATO, L. M., SHEFFIELD, V. C. & STONE, E. M. 2003. Evaluation of optineurin sequence variations in 1,048 patients with open-angle glaucoma. *Am J Ophthalmol,* 136**,** 904-10.

ANDERS, S., PYL, P. T. & HUBER, W. 2015. HTSeq--a Python framework to work with high-throughput sequencing data. *Bioinformatics,* 31**,** 166-9.

ANDERSON, D. R., DRANCE, S. M. & SCHULZER, M. 2001. Natural history of normal-tension glaucoma. *Ophthalmology,* 108**,** 247-53.

ANGIUS, A., SPINELLI, P., GHILOTTI, G., CASU, G., SOLE, G., LOI, A., TOTARO, A., ZELANTE, L., GASPARINI, P., ORZALESI, N., PIRASTU, M. & BONOMI, L. 2000. Myocilin Gln368stop mutation and advanced age as risk factors for late-onset primary open-angle glaucoma. *Arch Ophthalmol,* 118**,** 674-9.

ANHOLT, R. R. & CARBONE, M. A. 2013. A molecular mechanism for glaucoma: endoplasmic reticulum stress and the unfolded protein response. *Trends Mol Med,* 19**,** 586-93.

AWADALLA, M. S., FINGERT, J. H., ROOS, B. E., CHEN, S., HOLMES, R., GRAHAM, S. L., CHEHADE, M., GALANOPOLOUS, A., RIDGE, B., SOUZEAU, E., ZHOU, T., SIGGS, O. M., HEWITT, A. W., MACKEY, D. A., BURDON, K. P. & CRAIG, J. E. 2015. Copy number variations of TBK1 in Australian patients with primary open-angle glaucoma. *Am J Ophthalmol,* 159**,** 124-30 e1.

AXENOVICH, T., ZORKOLTSEVA, I., BELONOGOVA, N., VAN KOOLWIJK, L. M., BORODIN, P., KIRICHENKO, A., BABENKO, V., RAMDAS, W. D., AMIN, N., DESPRIET, D. D., VINGERLING, J. R., LEMIJ, H. G., OOSTRA, B. A., KLAVER, C. C., AULCHENKO, Y. & VAN DUIJN, C. M. 2011. Linkage and association analyses of glaucoma related traits in a large pedigree from a Dutch genetically isolated population. *J Med Genet,* 48**,** 802-9.

AYALA-LUGO, R. M., PAWAR, H., REED, D. M., LICHTER, P. R., MOROI, S. E., PAGE, M., EADIE, J., AZOCAR, V., MAUL, E., NTIM-AMPONSAH, C., BROMLEY, W., OBENG-NYARKOH, E., JOHNSON, A. T., KIJEK, T. G., DOWNS, C. A., JOHNSON, J. M., PEREZ-GROSSMANN, R. A., GUEVARA-FUJITA, M. L., FUJITA, R., WALLACE, M. R. & RICHARDS, J. E. 2007. Variation in optineurin (OPTN) allele frequencies between and within populations. *Mol Vis,* 13**,** 151-63.

AZMANOV, D. N., DIMITROVA, S., FLOREZ, L., CHERNINKOVA, S., DRAGANOV, D., MORAR, B., SAAT, R., JUAN, M., AROSTEGUI, J. I., GANGULY, S., SOODYALL, H., CHAKRABARTI, S., PADH, H., LOPEZ-NEVOT, M. A., CHERNODRINSKA, V., ANGUELOV, B., MAJUMDER, P., ANGELOVA, L., KANEVA, R., MACKEY, D. A., TOURNEV, I. & KALAYDJIEVA, L. 2011. LTBP2 and CYP1B1 mutations and associated ocular phenotypes in the Roma/Gypsy founder population. *Eur J Hum Genet,* 19**,** 326-33.

BAHRAMI, H. 2006. Causal inference in primary open angle glaucoma: specific discussion on intraocular pressure. *Ophthalmic Epidemiol,* 13**,** 283-9.

BAILEY, J. N., LOOMIS, S. J., KANG, J. H., ALLINGHAM, R. R., GHARAHKHANI, P., KHOR, C. C., BURDON, K. P., ASCHARD, H., CHASMAN, D. I., IGO, R. P., JR., HYSI, P. G., GLASTONBURY, C. A.,

ASHLEY-KOCH, A., BRILLIANT, M., BROWN, A. A., BUDENZ, D. L., BUIL, A., CHENG, C. Y., CHOI, H., CHRISTEN, W. G., CURHAN, G., DE VIVO, I., FINGERT, J. H., FOSTER, P. J., FUCHS, C., GAASTERLAND, D., GAASTERLAND, T., HEWITT, A. W., HU, F., HUNTER, D. J., KHAWAJA, A. P., LEE, R. K., LI, Z., LICHTER, P. R., MACKEY, D. A., MCGUFFIN, P., MITCHELL, P., MOROI, S. E., PERERA, S. A., PEPPER, K. W., QI, Q., REALINI, T., RICHARDS, J. E., RIDKER, P. M., RIMM, E., RITCH, R., RITCHIE, M., SCHUMAN, J. S., SCOTT, W. K., SINGH, K., SIT, A. J., SONG, Y. E., TAMIMI, R. M., TOPOUZIS, F., VISWANATHAN, A. C., VERMA, S. S., VOLLRATH, D., WANG, J. J., WEISSCHUH, N., WISSINGER, B., WOLLSTEIN, G., WONG, T. Y., YASPAN, B. L., ZACK, D. J., ZHANG, K., STUDY, E. N., WEINREB, R. N., PERICAK-VANCE, M. A., SMALL, K., HAMMOND, C. J., AUNG, T., LIU, Y., VITHANA, E. N., MACGREGOR, S., CRAIG, J. E., KRAFT, P., HOWELL, G., HAUSER, M. A., PASQUALE, L. R., HAINES, J. L. & WIGGS, J. L. 2016. Genome-wide association analysis identifies TXNRD2, ATXN2 and FOXC1 as susceptibility loci for primary open-angle glaucoma. *Nat Genet,* 48**,** 189-94.

BAIRD, P. N., CRAIG, J. E., RICHARDSON, A. J., RING, M. A., SIM, P., STANWIX, S., FOOTE, S. J. & MACKEY, D. A. 2003. Analysis of 15 primary open-angle glaucoma families from Australia identifies a founder effect for the Q368STOP mutation of myocilin. *Hum Genet,* 112**,** 110-6.

BAIRD, P. N., RICHARDSON, A. J., CRAIG, J. E., MACKEY, D. A., ROCHTCHINA, E. & MITCHELL, P. 2004. Analysis of optineurin (OPTN) gene mutations in subjects with and without glaucoma: the Blue Mountains Eye Study. *Clin Experiment Ophthalmol,* 32**,** 518-22.

BAIRD, P. N., RICHARDSON, A. J., MACKEY, D. A., CRAIG, J. E., FAUCHER, M. & RAYMOND, V. 2005. A common disease haplotype for the Q368STOP mutation of the myocilin gene in Australian and Canadian glaucoma families. *Am J Ophthalmol,* 140**,** 760-2.

BAMSHAD, M. J., NG, S. B., BIGHAM, A. W., TABOR, H. K., EMOND, M. J., NICKERSON, D. A. & SHENDURE, J. 2011. Exome sequencing as a tool for Mendelian disease gene discovery. *Nat Rev Genet,* 12**,** 745-55.

BANSAL, V., LIBIGER, O., TORKAMANI, A. & SCHORK, N. J. 2010. Statistical analysis strategies for association studies involving rare variants. *Nat Rev Genet,* 11**,** 773-85.

BASHIR, R., SANAI, M., AZEEM, A., ALTAF, I., SALEEM, F. & NAZ, S. 2014. Contribution of GLC3A locus to Primary Congenital Glaucoma in Pakistani population. *Pak J Med Sci,* 30**,** 1341-5.

BEJJANI, B. A., LEWIS, R. A., TOMEY, K. F., ANDERSON, K. L., DUEKER, D. K., JABAK, M., ASTLE, W. F., OTTERUD, B., LEPPERT, M. & LUPSKI, J. R. 1998. Mutations in CYP1B1, the gene for cytochrome P4501B1, are the predominant cause of primary congenital glaucoma in Saudi Arabia. *Am J Hum Genet,* 62**,** 325-33.

BEJJANI, B. A., STOCKTON, D. W., LEWIS, R. A., TOMEY, K. F., DUEKER, D. K., JABAK, M., ASTLE, W. F. & LUPSKI, J. R. 2000. Multiple CYP1B1 mutations and incomplete penetrance in an inbred population segregating primary congenital glaucoma suggest frequent de novo events and a dominant modifier locus. *Hum Mol Genet,* 9**,** 367-74.

BELL, N., HANN, V., REDFERN, C. P. & CHEEK, T. R. 2013. Store-operated Ca(2+) entry in proliferating and retinoic acid-differentiated N- and S-type neuroblastoma cells. *Biochim Biophys Acta,* 1833**,** 643-51.

BENGTSSON, B. 1981. The prevalence of glaucoma. *Br J Ophthalmol,* 65**,** 46-9.

BENGTSSON, B., LESKE, M. C., HYMAN, L. & HEIJL, A. 2007. Fluctuation of intraocular pressure and glaucoma progression in the early manifest glaucoma trial. *Ophthalmology,* 114**,** 205-9.

BENJAMINI, Y. & HOCHBERG, Y. 1995. Controlling the False Discovery Rate: A Practical and Powerful Approach to Multiple Testing. *Journal of the Royal Statistical Society. Series B (Methodological),* 57**,** 289-300.

BENTMANN, A., SCHMIDT, M., REUSS, S., WOLFRUM, U., HANKELN, T. & BURMESTER, T. 2005. Divergent distribution in vascular and avascular mammalian retinae links neuroglobin to cellular respiration. *J Biol Chem,* 280**,** 20660-5.

BODMER, W. & BONILLA, C. 2008. Common and rare variants in multifactorial susceptibility to common diseases. *Nat Genet,* 40**,** 695-701.

BOGUSKI, M. S., LOWE, T. M. & TOLSTOSHEV, C. M. 1993. dbEST--database for "expressed sequence tags". *Nat Genet,* 4**,** 332-3.

BOLAND, M. V. & QUIGLEY, H. A. 2007. Risk factors and open-angle glaucoma: classification and application. *J Glaucoma,* 16**,** 406-18.

BOURNE, R. R., STEVENS, G. A., WHITE, R. A., SMITH, J. L., FLAXMAN, S. R., PRICE, H., JONAS, J. B., KEEFFE, J., LEASHER, J., NAIDOO, K., PESUDOVS, K., RESNIKOFF, S. & TAYLOR, H. R. 2013. Causes of vision loss worldwide, 1990-2010: a systematic analysis. *Lancet Glob Health,* 1**,** e339-49.

BREZIN, A. P., ADAM, M. F., BELMOUDEN, A., LUREAU, M. A., CHAVENTRE, A., COPIN, B., GOMEZ, L., DE DINECHIN, S. D., BERKANI, M., VALTOT, F., ROULAND, J. F., DASCOTTE, J. C., BACH, J. F. & GARCHON, H. J. 1998. Founder effect in GLC1A-linked familial open-angle glaucoma in Northern France. *Am J Med Genet,* 76**,** 438-45.

BRITTAIN, T. 2012. The anti-apoptotic role of neuroglobin. *Cells,* 1**,** 1133-55.

BUDDE, W. M. & JONAS, J. B. 1999. Family history of glaucoma in the primary and secondary open-angle glaucomas. *Graefes Arch Clin Exp Ophthalmol,* 237**,** 554-7.

BULLARD, J. H., PURDOM, E., HANSEN, K. D. & DUDOIT, S. 2010. Evaluation of statistical methods for normalization and differential expression in mRNA-Seq experiments. *BMC Bioinformatics,* 11**,** 94.

BURDON, K. P. 2012. Genome-wide association studies in the hunt for genes causing primary open-angle glaucoma: a review. *Clin Experiment Ophthalmol,* 40**,** 358-63.

BURDON, K. P., MACGREGOR, S., HEWITT, A. W., SHARMA, S., CHIDLOW, G., MILLS, R. A., DANOY, P., CASSON, R., VISWANATHAN, A. C., LIU, J. Z., LANDERS, J., HENDERS, A. K., WOOD, J., SOUZEAU, E., CRAWFORD, A., LEO, P., WANG, J. J., ROCHTCHINA, E., NYHOLT, D. R., MARTIN, N. G., MONTGOMERY, G. W., MITCHELL, P., BROWN, M. A., MACKEY, D. A. & CRAIG, J. E. 2011. Genome-

wide association study identifies susceptibility loci for open angle glaucoma at TMCO1 and CDKN2B-AS1. *Nat Genet,* 43**,** 574-8.

BURDON, K. P., MITCHELL, P., LEE, A., HEALEY, P. R., WHITE, A. J., ROCHTCHINA, E., THOMAS, P. B., WANG, J. J. & CRAIG, J. E. 2015. Association of open-angle glaucoma loci with incident glaucoma in the Blue Mountains Eye Study. *Am J Ophthalmol,* 159**,** 31-6 e1.

BURMESTER, T., WEICH, B., REINHARDT, S. & HANKELN, T. 2000. A vertebrate globin expressed in the brain. *Nature,* 407**,** 520-3.

BURNS, J. N., TURNAGE, K. C., WALKER, C. A. & LIEBERMAN, R. L. 2011. The stability of myocilin olfactomedin domain variants provides new insight into glaucoma as a protein misfolding disorder. *Biochemistry,* 50**,** 5824-33.

CAIXETA-UMBELINO, C., DE VASCONCELLOS, J. P., COSTA, V. P., KASAHARA, N., DELLA PAOLERA, M., DE ALMEIDA, G. V., COHEN, R., MANDIA, C., JR., ROCHA, M. N., RICHETI, F., LONGUI, C. A. & DE MELO, M. B. 2009. Lack of association between optineurin gene variants T34T, E50K, M98K, 691_692insAG and R545Q and primary open angle glaucoma in Brazilian patients. *Ophthalmic Genet,* 30**,** 13-8.

CAO, K. Y., KAPASI, M., BETCHKAL, J. A. & BIRT, C. M. 2012. Relationship between central corneal thickness and progression of visual field loss in patients with open-angle glaucoma. *Can J Ophthalmol,* 47**,** 155-8.

CARBONARO, F., HYSI, P. G., FAHY, S. J., NAG, A. & HAMMOND, C. J. 2014. Optic disc planimetry, corneal hysteresis, central corneal thickness, and intraocular pressure as risk factors for glaucoma. *Am J Ophthalmol,* 157**,** 441-6.

CARBONE, M. A., AYROLES, J. F., YAMAMOTO, A., MOROZOVA, T. V., WEST, S. A., MAGWIRE, M. M., MACKAY, T. F. & ANHOLT, R. R. 2009. Overexpression of myocilin in the Drosophila eye activates the unfolded protein response: implications for glaucoma. *PLoS One,* 4**,** e4216.

CARBONE, M. A., CHEN, Y., HUGHES, G. A., WEINREB, R. N., ZABRISKIE, N. A., ZHANG, K. & ANHOLT, R. R. 2011. Genes of the unfolded protein response pathway harbor risk alleles for primary open angle glaucoma. *PLoS One,* 6**,** e20649.

CARNES, M. U., LIU, Y. P., ALLINGHAM, R. R., WHIGHAM, B. T., HAVENS, S., GARRETT, M. E., QIAO, C., KATSANIS, N., WIGGS, J. L., PASQUALE, L. R., ASHLEY-KOCH, A., OH, E. C. & HAUSER, M. A. 2014. Discovery and functional annotation of SIX6 variants in primary open-angle glaucoma. *PLoS Genet,* 10**,** e1004372.

CHAKRABARTI, S., DEVI, K. R., KOMATIREDDY, S., KAUR, K., PARIKH, R. S., MANDAL, A. K., CHANDRASEKHAR, G. & THOMAS, R. 2007. Glaucoma-associated CYP1B1 mutations share similar haplotype backgrounds in POAG and PACG phenotypes. *Invest Ophthalmol Vis Sci,* 48**,** 5439-44.

CHALASANI, M. L., RADHA, V., GUPTA, V., AGARWAL, N., BALASUBRAMANIAN, D. & SWARUP, G. 2007. A glaucoma-associated mutant of optineurin selectively induces death of retinal ganglion cells which is inhibited by antioxidants. *Invest Ophthalmol Vis Sci,* 48**,** 1607-14.

CHALASANI, M. L., SWARUP, G. & BALASUBRAMANIAN, D. 2009. Optineurin and its mutants: molecules associated with some forms of glaucoma. *Ophthalmic Res,* 42**,** 176-84.

CHAN, A. S., SARASWATHY, S., REHAK, M., UEKI, M. & RAO, N. A. 2012. Neuroglobin protection in retinal ischemia. *Invest Ophthalmol Vis Sci,* 53**,** 704-11.

CHARITOU, T., BRYAN, K. & LYNN, D. J. 2016. Using biological networks to integrate, visualize and analyze genomics data. *Genet Sel Evol,* 48**,** 27.

CHARLESWORTH, J., KRAMER, P. L., DYER, T., DIEGO, V., SAMPLES, J. R., CRAIG, J. E., MACKEY, D. A., HEWITT, A. W., BLANGERO, J. & WIRTZ, M. K. 2010. The path to open-angle glaucoma gene discovery: endophenotypic status of intraocular pressure, cup-to-disc ratio, and central corneal thickness. *Invest Ophthalmol Vis Sci,* 51**,** 3509-14.

CHARLIAT, G., JOLLY, D. & BLANCHARD, F. 1994. Genetic risk factor in primary open-angle glaucoma: a case-control study. *Ophthalmic Epidemiol,* 1**,** 131-8.

CHAUHAN, B. C., HUTCHISON, D. M., LEBLANC, R. P., ARTES, P. H. & NICOLELA, M. T. 2005. Central corneal thickness and progression of the visual field and optic disc in glaucoma. *Br J Ophthalmol,* 89**,** 1008-12.

CHEN, L. J., NG, T. K., FAN, A. H., LEUNG, D. Y., ZHANG, M., WANG, N., ZHENG, Y., LIANG, X. Y., CHIANG, S. W., TAM, P. O. & PANG, C. P. 2012. Evaluation of NTF4 as a causative gene for primary open-angle glaucoma. *Mol Vis,* 18**,** 1763-72.

CHEN, X., CHEN, Y., WANG, L., JIANG, D., WANG, W., XIA, M., YU, L. & SUN, X. 2014a. CYP1B1 genotype influences the phenotype in primary congenital glaucoma and surgical treatment. *Br J Ophthalmol,* 98**,** 246-51.

CHEN, Y., LIN, Y., VITHANA, E. N., JIA, L., ZUO, X., WONG, T. Y., CHEN, L. J., ZHU, X., TAM, P. O., GONG, B., QIAN, S., LI, Z., LIU, X., MANI, B., LUO, Q., GUZMAN, C., LEUNG, C. K., LI, X., CAO, W., YANG, Q., THAM, C. C., CHENG, Y., ZHANG, X., WANG, N., AUNG, T., KHOR, C. C., PANG, C. P., SUN, X. & YANG, Z. 2014b. Common variants near ABCA1 and in PMM2 are associated with primary open-angle glaucoma. *Nat Genet,* 46**,** 1115-9.

CHI, Z. L., AKAHORI, M., OBAZAWA, M., MINAMI, M., NODA, T., NAKAYA, N., TOMAREV, S., KAWASE, K., YAMAMOTO, T., NODA, S., SASAOKA, M., SHIMAZAKI, A., TAKADA, Y. & IWATA, T. 2010. Overexpression of optineurin E50K disrupts Rab8 interaction and leads to a progressive retinal degeneration in mice. *Hum Mol Genet,* 19**,** 2606-15.

CHIANG, P. W., WANG, J., CHEN, Y., FU, Q., ZHONG, J., YI, X., WU, R., GAN, H., SHI, Y., BARNETT, C., WHEATON, D., DAY, M., SUTHERLAND, J., HEON, E., WELEBER, R. G., GABRIEL, L. A., CONG, P., CHUANG, K., YE, S., SALLUM, J. M. & QI, M. 2012. Exome sequencing identifies NMNAT1 mutations as a cause of Leber congenital amaurosis. *Nat Genet,* 44**,** 972-4.

CHITSAZIAN, F., TUSI, B. K., ELAHI, E., SAROEI, H. A., SANATI, M. H., YAZDANI, S., PAKRAVAN, M., NILFOROOSHAN, N., ESLAMI, Y., MEHRJERDI, M. A., ZAREEI, R., JABBARVAND, M., ABDOLAHI, A., LASHEYEE, A. R., ETEMADI, A., BAYAT, B., SADEGHI, M., BANOEI, M. M., GHAFARZADEH, B., ROHANI,

M. R., RISMANCHIAN, A., THORSTENSON, Y. & SARFARAZI, M. 2007. CYP1B1 mutation profile of Iranian primary congenital glaucoma patients and associated haplotypes. *J Mol Diagn,* 9**,** 382-93.

CHNG, Z., PEH, G. S., HERATH, W. B., CHENG, T. Y., ANG, H. P., TOH, K. P., ROBSON, P., MEHTA, J. S. & COLMAN, A. 2013. High throughput gene expression analysis identifies reliable expression markers of human corneal endothelial cells. *PLoS One,* 8**,** e67546.

CHO, H. K. & KEE, C. 2014. Population-based glaucoma prevalence studies in Asians. *Surv Ophthalmol,* 59**,** 434-47.

CIRULLI, E. T. & GOLDSTEIN, D. B. 2010. Uncovering the roles of rare variants in common disease through whole-genome sequencing. *Nat Rev Genet,* 11**,** 415-25.

CIRULLI, E. T., LASSEIGNE, B. N., PETROVSKI, S., SAPP, P. C., DION, P. A., LEBLOND, C. S., COUTHOUIS, J., LU, Y. F., WANG, Q., KRUEGER, B. J., REN, Z., KEEBLER, J., HAN, Y., LEVY, S. E., BOONE, B. E., WIMBISH, J. R., WAITE, L. L., JONES, A. L., CARULLI, J. P., DAY-WILLIAMS, A. G., STAROPOLI, J. F., XIN, W. W., CHESI, A., RAPHAEL, A. R., MCKENNA-YASEK, D., CADY, J., VIANNEY DE JONG, J. M., KENNA, K. P., SMITH, B. N., TOPP, S., MILLER, J., GKAZI, A., AL-CHALABI, A., VAN DEN BERG, L. H., VELDINK, J., SILANI, V., TICOZZI, N., SHAW, C. E., BALOH, R. H., APPEL, S., SIMPSON, E., LAGIER-TOURENNE, C., PULST, S. M., GIBSON, S., TROJANOWSKI, J. Q., ELMAN, L., MCCLUSKEY, L., GROSSMAN, M., SHNEIDER, N. A., CHUNG, W. K., RAVITS, J. M., GLASS, J. D., SIMS, K. B., VAN DEERLIN, V. M., MANIATIS, T., HAYES, S. D., ORDUREAU, A., SWARUP, S., LANDERS, J., BAAS, F., ALLEN, A. S., BEDLACK, R. S., HARPER, J. W., GITLER, A. D., ROULEAU, G. A., BROWN, R., HARMS, M. B., COOPER, G. M., HARRIS, T., MYERS, R. M. & GOLDSTEIN, D. B. 2015. Exome sequencing in amyotrophic lateral sclerosis identifies risk genes and pathways. *Science*.

COLAK, D., MORALES, J., BOSLEY, T. M., AL-BAKHEET, A., ALYOUNES, B., KAYA, N. & ABU-AMERO, K. K. 2012. Genome-wide expression profiling of patients with primary open angle glaucoma. *Invest Ophthalmol Vis Sci,* 53**,** 5899-904.

COLEMAN, J. A., ZHU, X., DJAJADI, H. R., MOLDAY, L. L., SMITH, R. S., LIBBY, R. T., JOHN, S. W. & MOLDAY, R. S. 2014. Phospholipid flippase ATP8A2 is required for normal visual and auditory function and photoreceptor and spiral ganglion cell survival. *J Cell Sci,* 127**,** 1138-49.

COWAN, C., MURALEEDHARAN, C. K., O'DONNELL, J. J., 3RD, SINGH, P. K., LUM, H., KUMAR, A. & XU, S. 2014. MicroRNA-146 inhibits thrombin-induced NF-kappaB activation and subsequent inflammatory responses in human retinal endothelial cells. *Invest Ophthalmol Vis Sci,* 55**,** 4944-51.

CRAIG, J. E., BAIRD, P. N., HEALEY, D. L., MCNAUGHT, A. I., MCCARTNEY, P. J., RAIT, J. L., DICKINSON, J. L., ROE, L., FINGERT, J. H., STONE, E. M. & MACKEY, D. A. 2001. Evidence for genetic heterogeneity within eight glaucoma families, with the GLC1A Gln368STOP mutation being an important phenotypic modifier. *Ophthalmology,* 108**,** 1607-20.

CUELLAR-PARTIDA, G., CRAIG, J. E., BURDON, K. P., WANG, J. J., VOTE, B. J., SOUZEAU, E., MCALLISTER, I. L., ISAACS, T., LAKE, S., MACKEY, D. A., CONSTABLE, I. J., MITCHELL, P., HEWITT, A. W. & MACGREGOR, S. 2016. Assessment of polygenic effects links primary open-angle glaucoma and age-related macular degeneration. *Sci Rep,* 6**,** 26885.

CWERMAN-THIBAULT, H., LECHAUVE, C., AUGUSTIN, S., ROUSSEL, D., REBOUSSIN, E., MOHAMMAD, A., DEGARDIN-CHICAUD, J., SIMONUTTI, M., LIANG, H., BRIGNOLE-BAUDOUIN, F., MARON, A., DEBEIR, T. & CORRAL-DEBRINSKI, M. 2017. Neuroglobin Can Prevent or Reverse Glaucomatous Progression in DBA/2J Mice. *Mol Ther Methods Clin Dev,* 5**,** 200-220.

DA ROCHA, J. F., DA CRUZ E SILVA, O. A. & VIEIRA, S. I. 2015. Analysis of the amyloid precursor protein role in neuritogenesis reveals a biphasic SH-SY5Y neuronal cell differentiation model. *J Neurochem,* 134**,** 288-301.

DANECEK, P., AUTON, A., ABECASIS, G., ALBERS, C. A., BANKS, E., DEPRISTO, M. A., HANDSAKER, R. E., LUNTER, G., MARTH, G. T., SHERRY, S. T., MCVEAN, G. & DURBIN, R. 2011. The variant call format and VCFtools. *Bioinformatics,* 27**,** 2156-8.

DAWN TEARE, M. & BARRETT, J. H. 2005. Genetic linkage studies. *Lancet,* 366**,** 1036-44.

DAY, A. C., MACHIN, D., AUNG, T., GAZZARD, G., HUSAIN, R., CHEW, P. T., KHAW, P. T., SEAH, S. K. & FOSTER, P. J. 2011. Central corneal thickness and glaucoma in East Asian people. *Invest Ophthalmol Vis Sci,* 52**,** 8407-12.

DE MARCO, N., BUONO, M., TROISE, F. & DIEZ-ROUX, G. 2006. Optineurin increases cell survival and translocates to the nucleus in a Rab8-dependent manner upon an apoptotic stimulus. *J Biol Chem,* 281**,** 16147-56.

DE MORAES, C. G., LIEBMANN, J. M., PARK, S. C., TENG, C. C., NEMIROFF, J., TELLO, C. & RITCH, R. 2013. Optic disc progression and rates of visual field change in treated glaucoma. *Acta Ophthalmol,* 91**,** e86-91.

DE VASCONCELLOS, J. P., DE MELO, M. B., SCHIMITI, R., COSTA, F. F. & COSTA, V. P. 2003. Penetrance and phenotype of the Cys433Arg myocilin mutation in a family pedigree with primary open-angle glaucoma. *J Glaucoma,* 12**,** 104-7.

DE VOOGD, S., IKRAM, M. K., WOLFS, R. C., JANSONIUS, N. M., WITTEMAN, J. C., HOFMAN, A. & DE JONG, P. T. 2006. Is diabetes mellitus a risk factor for open-angle glaucoma? The Rotterdam Study. *Ophthalmology,* 113**,** 1827-31.

DEOL, M., TAYLOR, D. A. & RADCLIFFE, N. M. 2015. Corneal hysteresis and its relevance to glaucoma. *Curr Opin Ophthalmol,* 26**,** 96-102.

DEPRISTO, M. A., BANKS, E., POPLIN, R., GARIMELLA, K. V., MAGUIRE, J. R., HARTL, C., PHILIPPAKIS, A. A., DEL ANGEL, G., RIVAS, M. A., HANNA, M., MCKENNA, A., FENNELL, T. J., KERNYTSKY, A. M., SIVACHENKO, A. Y., CIBULSKIS, K., GABRIEL, S. B., ALTSHULER, D. & DALY, M. J. 2011. A framework for variation discovery and genotyping using next-generation DNA sequencing data. *Nat Genet,* 43**,** 491-8.

DERING, C., HEMMELMANN, C., PUGH, E. & ZIEGLER, A. 2011. Statistical analysis of rare sequence variants: an overview of collapsing methods. *Genet Epidemiol,* 35 Suppl 1**,** S12-7.

DÉSIR, J., SZNAJER, Y., DEPASSE, F., ROULEZ, F., SCHROOYEN, M., MEIRE, F. & ABRAMOWICZ, M. 2010. LTBP2 null mutations in an autosomal recessive ocular syndrome with megalocornea, spherophakia, and secondary glaucoma. *Eur J Hum Genet,* 18**,** 761-7.

DEVA, N. C., INSULL, E., GAMBLE, G. & DANESH-MEYER, H. V. 2008. Risk factors for first presentation of glaucoma with significant visual field loss. *Clin Experiment Ophthalmol,* 36**,** 217-21.

DIEHN, J. J., DIEHN, M., MARMOR, M. F. & BROWN, P. O. 2005. Differential gene expression in anatomical compartments of the human eye. *Genome Biol,* 6**,** R74.

DIMASI, D. P., BURDON, K. P., HEWITT, A. W., FITZGERALD, J., WANG, J. J., HEALEY, P. R., MITCHELL, P., MACKEY, D. A. & CRAIG, J. E. 2012. Genetic investigation into the endophenotypic status of central corneal thickness and optic disc parameters in relation to open-angle glaucoma. *Am J Ophthalmol,* 154**,** 833-842 e2.

DIMASI, D. P., HEWITT, A. W., STRAGA, T., PATER, J., MACKINNON, J. R., ELDER, J. E., CASEY, T., MACKEY, D. A. & CRAIG, J. E. 2007. Prevalence of CYP1B1 mutations in Australian patients with primary congenital glaucoma. *Clin Genet,* 72**,** 255-60.

DONG, L. Y., YIN, M. & KANG, X. L. 2014. Bibliometric network analysis of glaucoma. *Genet Mol Res,* 13**,** 3577-85.

DONG, X. X., WANG, Y. & QIN, Z. H. 2009. Molecular mechanisms of excitotoxicity and their relevance to pathogenesis of neurodegenerative diseases. *Acta Pharmacol Sin,* 30**,** 379-87.

DOSHI, V., YING-LAI, M., AZEN, S. P. & VARMA, R. 2008. Sociodemographic, family history, and lifestyle risk factors for open-angle glaucoma and ocular hypertension. The Los Angeles Latino Eye Study. *Ophthalmology,* 115**,** 639-647 e2.

DOSS, E. L., DOSS, L., HAN, Y., HUANG, S., PORCO, T., PEKMEZCI, M. & LIN, S. 2014. Risk factors for glaucoma suspicion in healthy young asian and caucasian americans. *J Ophthalmol,* 2014**,** 726760.

DRANCE, S., ANDERSON, D. R. & SCHULZER, M. 2001. Risk factors for progression of visual field abnormalities in normal-tension glaucoma. *Am J Ophthalmol,* 131**,** 699-708.

DROGE, J., PANDE, A., ENGLANDER, E. W. & MAKALOWSKI, W. 2012. Comparative genomics of neuroglobin reveals its early origins. *PLoS One,* 7**,** e47972.

DU, S., JIA, L., ZHANG, Y., FANG, L., ZHANG, X. & FAN, Y. 2014. CARMA3 is upregulated in human pancreatic carcinoma, and its depletion inhibits tumor proliferation, migration, and invasion. *Tumour Biol,* 35**,** 5965-70.

DUEKER, D. K., SINGH, K., LIN, S. C., FECHTNER, R. D., MINCKLER, D. S., SAMPLES, J. R. & SCHUMAN, J. S. 2007. Corneal thickness measurement in the management of primary open-angle glaucoma: a report by the American Academy of Ophthalmology. *Ophthalmology,* 114**,** 1779-87.

DUGGAN, D. J., BITTNER, M., CHEN, Y., MELTZER, P. & TRENT, J. M. 1999. Expression profiling using cDNA microarrays. *Nat Genet,* 21**,** 10-4.

DWANE, S., DURACK, E. & KIELY, P. A. 2013. Optimising parameters for the differentiation of SH-SY5Y cells to study cell adhesion and cell migration. *BMC Res Notes,* 6**,** 366.

EDGAR, R., DOMRACHEV, M. & LASH, A. E. 2002. Gene Expression Omnibus: NCBI gene expression and hybridization array data repository. *Nucleic Acids Res,* 30**,** 207-10.

EID, T. M., SPAETH, G. L., BITTERMAN, A. & STEINMANN, W. C. 2003. Rate and amount of visual loss in 102 patients with open-angle glaucoma followed up for at least 15 years. *Ophthalmology,* 110**,** 900-7.

ENNIS, S., GIBSON, J., GRIFFITHS, H., BUNYAN, D., CREE, A. J., ROBINSON, D., SELF, J., MACLEOD, A. & LOTERY, A. 2010. Prevalence of myocilin gene mutations in a novel UK cohort of POAG patients. *Eye (Lond),* 24**,** 328-33.

ESCARCEGA, R. O., FUENTES-ALEXANDRO, S., GARCIA-CARRASCO, M., GATICA, A. & ZAMORA, A. 2007. The transcription factor nuclear factor-kappa B and cancer. *Clin Oncol (R Coll Radiol),* 19**,** 154-61.

ESTRADA, K., STYRKARSDOTTIR, U., EVANGELOU, E., HSU, Y. H., DUNCAN, E. L., NTZANI, E. E., OEI, L., ALBAGHA, O. M., AMIN, N., KEMP, J. P., KOLLER, D. L., LI, G., LIU, C. T., MINSTER, R. L., MOAYYERI, A., VANDENPUT, L., WILLNER, D., XIAO, S. M., YERGES-ARMSTRONG, L. M., ZHENG, H. F., ALONSO, N., ERIKSSON, J., KAMMERER, C. M., KAPTOGE, S. K., LEO, P. J., THORLEIFSSON, G., WILSON, S. G., WILSON, J. F., AALTO, V., ALEN, M., ARAGAKI, A. K., ASPELUND, T., CENTER, J. R., DAILIANA, Z., DUGGAN, D. J., GARCIA, M., GARCIA-GIRALT, N., GIROUX, S., HALLMANS, G., HOCKING, L. J., HUSTED, L. B., JAMESON, K. A., KHUSAINOVA, R., KIM, G. S., KOOPERBERG, C., KOROMILA, T., KRUK, M., LAAKSONEN, M., LACROIX, A. Z., LEE, S. H., LEUNG, P. C., LEWIS, J. R., MASI, L., MENCEJ-BEDRAC, S., NGUYEN, T. V., NOGUES, X., PATEL, M. S., PREZELJ, J., ROSE, L. M., SCOLLEN, S., SIGGEIRSDOTTIR, K., SMITH, A. V., SVENSSON, O., TROMPET, S., TRUMMER, O., VAN SCHOOR, N. M., WOO, J., ZHU, K., BALCELLS, S., BRANDI, M. L., BUCKLEY, B. M., CHENG, S., CHRISTIANSEN, C., COOPER, C., DEDOUSSIS, G., FORD, I., FROST, M., GOLTZMAN, D., GONZALEZ-MACIAS, J., KAHONEN, M., KARLSSON, M., KHUSNUTDINOVA, E., KOH, J. M., KOLLIA, P., LANGDAHL, B. L., LESLIE, W. D., LIPS, P., LJUNGGREN, O., LORENC, R. S., MARC, J., MELLSTROM, D., OBERMAYER-PIETSCH, B., OLMOS, J. M., PETTERSSON-KYMMER, U., REID, D. M., RIANCHO, J. A., RIDKER, P. M., ROUSSEAU, F., SLAGBOOM, P. E., TANG, N. L., et al. 2012. Genome-wide meta-analysis identifies 56 bone mineral density loci and reveals 14 loci associated with risk of fracture. *Nat Genet,* 44**,** 491-501.

FAN, B. J., LEUNG, Y. F., WANG, N., LAM, S. C., LIU, Y., TAM, O. S. & PANG, C. P. 2004. Genetic and environmental risk factors for primary open-angle glaucoma. *Chin Med J (Engl),* 117**,** 706-10.

FAN, B. J., WANG, D. Y., CHENG, C. Y., KO, W. C., LAM, S. C. & PANG, C. P. 2009. Different WDR36 mutation pattern in Chinese patients with primary open-angle glaucoma. *Mol Vis,* 15**,** 646-53.

FAUCHER, M., ANCTIL, J. L., RODRIGUE, M. A., DUCHESNE, A., BERGERON, D., BLONDEAU, P., COTE, G., DUBOIS, S., BERGERON, J., ARSENEAULT, R., MORISSETTE, J. & RAYMOND, V. 2002.

Founder TIGR/myocilin mutations for glaucoma in the Quebec population. *Hum Mol Genet,* 11**,** 2077-90.

FAUTSCH, M. P., BAHLER, C. K., JEWISON, D. J. & JOHNSON, D. H. 2000. Recombinant TIGR/MYOC increases outflow resistance in the human anterior segment. *Invest Ophthalmol Vis Sci,* 41**,** 4163-8.

FERNANDEZ-BAHAMONDE, J. L., ROMAN-RODRIGUEZ, C. & FERNANDEZ-RUIZ, M. C. 2011. Central corneal thickness as a predictor of visual field loss in primary open angle glaucoma for a Hispanic population. *Semin Ophthalmol,* 26**,** 28-32.

FINGERT, J. H. 2011. Primary open-angle glaucoma genes. *Eye (Lond),* 25**,** 587-95.

FINGERT, J. H., ALWARD, W. L., KWON, Y. H., SHANKAR, S. P., ANDORF, J. L., MACKEY, D. A., SHEFFIELD, V. C. & STONE, E. M. 2007. No association between variations in the WDR36 gene and primary open-angle glaucoma. *Arch Ophthalmol,* 125**,** 434-6.

FINGERT, J. H., HEON, E., LIEBMANN, J. M., YAMAMOTO, T., CRAIG, J. E., RAIT, J., KAWASE, K., HOH, S. T., BUYS, Y. M., DICKINSON, J., HOCKEY, R. R., WILLIAMS-LYN, D., TROPE, G., KITAZAWA, Y., RITCH, R., MACKEY, D. A., ALWARD, W. L., SHEFFIELD, V. C. & STONE, E. M. 1999. Analysis of myocilin mutations in 1703 glaucoma patients from five different populations. *Hum Mol Genet,* 8**,** 899-905.

FINGERT, J. H., ROBIN, A. L., STONE, J. L., ROOS, B. R., DAVIS, L. K., SCHEETZ, T. E., BENNETT, S. R., WASSINK, T. H., KWON, Y. H., ALWARD, W. L., MULLINS, R. F., SHEFFIELD, V. C. & STONE, E. M. 2011. Copy number variations on chromosome 12q14 in patients with normal tension glaucoma. *Hum Mol Genet,* 20**,** 2482-94.

FINGERT, J. H., ROOS, B. R., SOLIVAN-TIMPE, F., MILLER, K. A., OETTING, T. A., WANG, K., KWON, Y. H., SCHEETZ, T. E., STONE, E. M. & ALWARD, W. L. 2012. Analysis of ASB10 variants in open angle glaucoma. *Hum Mol Genet,* 21**,** 4543-8.

FINGERT, J. H., STONE, E. M., SHEFFIELD, V. C. & ALWARD, W. L. 2002. Myocilin glaucoma. *Surv Ophthalmol,* 47**,** 547-61.

FIRASAT, S., RIAZUDDIN, S. A., HEJTMANCIK, J. F. & RIAZUDDIN, S. 2008a. Primary congenital glaucoma localizes to chromosome 14q24.2-24.3 in two consanguineous Pakistani families. *Mol Vis,* 14**,** 1659-65.

FIRASAT, S., RIAZUDDIN, S. A., KHAN, S. N. & RIAZUDDIN, S. 2008b. Novel CYP1B1 mutations in consanguineous Pakistani families with primary congenital glaucoma. *Mol Vis,* 14**,** 2002-9.

FONSECA, N. A., RUNG, J., BRAZMA, A. & MARIONI, J. C. 2012. Tools for mapping high-throughput sequencing data. *Bioinformatics,* 28**,** 3169-77.

FORDEL, E., THIJS, L., MARTINET, W., SCHRIJVERS, D., MOENS, L. & DEWILDE, S. 2007. Anoxia or oxygen and glucose deprivation in SH-SY5Y cells: a step closer to the unraveling of neuroglobin and cytoglobin functions. *Gene,* 398**,** 114-22.

FOSTER, P. J., BUHRMANN, R., QUIGLEY, H. A. & JOHNSON, G. J. 2002. The definition and classification of glaucoma in prevalence surveys. *Br J Ophthalmol,* 86**,** 238-42.

FRANCIS, B. A., VARMA, R., CHOPRA, V., LAI, M. Y., SHTIR, C. & AZEN, S. P. 2008. Intraocular pressure, central corneal thickness, and prevalence of open-angle glaucoma: the Los Angeles Latino Eye Study. *Am J Ophthalmol,* 146**,** 741-6.

FRASER, S., BUNCE, C. & WORMALD, R. 1999. Risk factors for late presentation in chronic glaucoma. *Invest Ophthalmol Vis Sci,* 40**,** 2251-7.

FROMM, J. A., JOHNSON, S. A. & JOHNSON, D. L. 2008. Epidermal growth factor receptor 1 (EGFR1) and its variant EGFRvIII regulate TATA-binding protein expression through distinct pathways. *Mol Cell Biol,* 28**,** 6483-95.

FU, X., FU, N., GUO, S., YAN, Z., XU, Y., HU, H., MENZEL, C., CHEN, W., LI, Y., ZENG, R. & KHAITOVICH, P. 2009. Estimating accuracy of RNA-Seq and microarrays with proteomics. *BMC Genomics,* 10**,** 161.

GAO, J., OHTSUBO, M., HOTTA, Y. & MINOSHIMA, S. 2014. Oligomerization of optineurin and its oxidative stress- or E50K mutation-driven covalent cross-linking: possible relationship with glaucoma pathology. *PLoS One,* 9**,** e101206.

GAO, X., GAUDERMAN, W. J., LIU, Y., MARJORAM, P., TORRES, M., HARITUNIANS, T., KUO, J. Z., CHEN, Y. D., ALLINGHAM, R. R., HAUSER, M. A., TAYLOR, K. D., ROTTER, J. I. & VARMA, R. 2013. A genome-wide association study of central corneal thickness in Latinos. *Invest Ophthalmol Vis Sci,* 54**,** 2435-43.

GARWAY-HEATH, D. F., CRABB, D. P., BUNCE, C., LASCARATOS, G., AMALFITANO, F., ANAND, N., AZUARA-BLANCO, A., BOURNE, R. R., BROADWAY, D. C., CUNLIFFE, I. A., DIAMOND, J. P., FRASER, S. G., HO, T. A., MARTIN, K. R., MCNAUGHT, A. I., NEGI, A., PATEL, K., RUSSELL, R. A., SHAH, A., SPRY, P. G., SUZUKI, K., WHITE, E. T., WORMALD, R. P., XING, W. & ZEYEN, T. G. 2015. Latanoprost for open-angle glaucoma (UKGTS): a randomised, multicentre, placebo-controlled trial. *Lancet,* 385**,** 1295-304.

GAZZARD, G., KONSTANTAKOPOULOU, E., GARWAY-HEATH, D., GARG, A., VICKERSTAFF, V., HUNTER, R., AMBLER, G., BUNCE, C., WORMALD, R., NATHWANI, N., BARTON, K., RUBIN, G. & BUSZEWICZ, M. 2019. Selective laser trabeculoplasty versus eye drops for first-line treatment of ocular hypertension and glaucoma (LiGHT): a multicentre randomised controlled trial. *Lancet,* 393**,** 1505-1516.

GEMENETZI, M., YANG, Y. & LOTERY, A. J. 2012. Current concepts on primary open-angle glaucoma genetics: a contribution to disease pathophysiology and future treatment. *Eye (Lond),* 26**,** 355-69.

GHARAHKHANI, P., BURDON, K. P., FOGARTY, R., SHARMA, S., HEWITT, A. W., MARTIN, S., LAW, M. H., CREMIN, K., BAILEY, J. N., LOOMIS, S. J., PASQUALE, L. R., HAINES, J. L., HAUSER, M. A., VISWANATHAN, A. C., MCGUFFIN, P., TOPOUZIS, F., FOSTER, P. J., GRAHAM, S. L., CASSON, R. J., CHEHADE, M., WHITE, A. J., ZHOU, T., SOUZEAU, E., LANDERS, J., FITZGERALD, J. T., KLEBE, S.,

RUDDLE, J. B., GOLDBERG, I., HEALEY, P. R., MILLS, R. A., WANG, J. J., MONTGOMERY, G. W., MARTIN, N. G., RADFORD-SMITH, G., WHITEMAN, D. C., BROWN, M. A., WIGGS, J. L., MACKEY, D. A., MITCHELL, P., MACGREGOR, S. & CRAIG, J. E. 2014. Common variants near ABCA1, AFAP1 and GMDS confer risk of primary open-angle glaucoma. *Nat Genet,* 46**,** 1120-5.

GOBEIL, S., RODRIGUE, M. A., MOISAN, S., NGUYEN, T. D., POLANSKY, J. R., MORISSETTE, J. & RAYMOND, V. 2004. Intracellular sequestration of hetero-oligomers formed by wild-type and glaucoma-causing myocilin mutants. *Invest Ophthalmol Vis Sci,* 45**,** 3560-7.

GOEL, M., PICCIANI, R. G., LEE, R. K. & BHATTACHARYA, S. K. 2010. Aqueous humor dynamics: a review. *Open Ophthalmol J,* 4**,** 52-9.

GONG, G., KOSOKO-LASAKI, O., HAYNATZKI, G. R. & WILSON, M. R. 2004. Genetic dissection of myocilin glaucoma. *Hum Mol Genet,* 13 Spec No 1**,** R91-102.

GONG, G., KOSOKO-LASAKI, S., HAYNATZKI, G., LYNCH, H. T., LYNCH, J. A. & WILSON, M. R. 2007. Inherited, familial and sporadic primary open-angle glaucoma. *J Natl Med Assoc,* 99**,** 559-63.

GORDON, M. O., BEISER, J. A., BRANDT, J. D., HEUER, D. K., HIGGINBOTHAM, E. J., JOHNSON, C. A., KELTNER, J. L., MILLER, J. P., PARRISH, R. K., 2ND, WILSON, M. R. & KASS, M. A. 2002. The Ocular Hypertension Treatment Study: baseline factors that predict the onset of primary open-angle glaucoma. *Arch Ophthalmol,* 120**,** 714-20; discussion 829-30.

GORLOV, I. P., GORLOVA, O. Y., SUNYAEV, S. R., SPITZ, M. R. & AMOS, C. I. 2008. Shifting paradigm of association studies: value of rare single-nucleotide polymorphisms. *Am J Hum Genet,* 82**,** 100-12.

GRABINER, B. C., BLONSKA, M., LIN, P. C., YOU, Y., WANG, D., SUN, J., DARNAY, B. G., DONG, C. & LIN, X. 2007. CARMA3 deficiency abrogates G protein-coupled receptor-induced NF-{kappa}B activation. *Genes Dev,* 21**,** 984-96.

GRAFF, C., URBAK, S. F., JERNDAL, T. & WADELIUS, C. 1995. Confirmation of linkage to 1q21-31 in a Danish autosomal dominant juvenile-onset glaucoma family and evidence of genetic heterogeneity. *Hum Genet,* 96**,** 285-9.

GRAMER, G., WEBER, B. H. & GRAMER, E. 2014. Results of a patient-directed survey on frequency of family history of glaucoma in 2170 patients. *Invest Ophthalmol Vis Sci,* 55**,** 259-64.

GRAUL, T. A., KWON, Y. H., ZIMMERMAN, M. B., KIM, C. S., SHEFFIELD, V. C., STONE, E. M. & ALWARD, W. L. 2002. A case-control comparison of the clinical characteristics of glaucoma and ocular hypertensive patients with and without the myocilin Gln368Stop mutation. *Am J Ophthalmol,* 134**,** 884-90.

GREEN, C. M., KEARNS, L. S., WU, J., BARBOUR, J. M., WILKINSON, R. M., RING, M. A., CRAIG, J. E., WONG, T. L., HEWITT, A. W. & MACKEY, D. A. 2007. How significant is a family history of glaucoma? Experience from the Glaucoma Inheritance Study in Tasmania. *Clin Experiment Ophthalmol,* 35**,** 793-9.

GREENBERG, D. A., JIN, K. & KHAN, A. A. 2008. Neuroglobin: an endogenous neuroprotectant. *Curr Opin Pharmacol,* 8**,** 20-4.

GRODUM, K., HEIJL, A. & BENGTSSON, B. 2001. Refractive error and glaucoma. *Acta Ophthalmol Scand,* 79**,** 560-6.

GUNVANT, P., PORSIA, L., WATKINS, R. J., BAYLISS-BROWN, H. & BROADWAY, D. C. 2008. Relationships between central corneal thickness and optic disc topography in eyes with glaucoma, suspicion of glaucoma, or ocular hypertension. *Clin Ophthalmol,* 2**,** 591-9.

HARDISON, R. C. 2012. Evolution of hemoglobin and its genes. *Cold Spring Harb Perspect Med,* 2**,** a011627.

HARDY, K. M., HOFFMAN, E. A., GONZALEZ, P., MCKAY, B. S. & STAMER, W. D. 2005. Extracellular trafficking of myocilin in human trabecular meshwork cells. *J Biol Chem,* 280**,** 28917-26.

HAUSER, M. A., ALLINGHAM, R. R., LINKROUM, K., WANG, J., LAROCQUE-ABRAMSON, K., FIGUEIREDO, D., SANTIAGO-TURLA, C., DEL BONO, E. A., HAINES, J. L., PERICAK-VANCE, M. A. & WIGGS, J. L. 2006a. Distribution of WDR36 DNA sequence variants in patients with primary open-angle glaucoma. *Invest Ophthalmol Vis Sci,* 47**,** 2542-6.

HAUSER, M. A., SENA, D. F., FLOR, J., WALTER, J., AUGUSTE, J., LAROCQUE-ABRAMSON, K., GRAHAM, F., DELBONO, E., HAINES, J. L., PERICAK-VANCE, M. A., RAND ALLINGHAM, R. & WIGGS, J. L. 2006b. Distribution of optineurin sequence variations in an ethnically diverse population of low-tension glaucoma patients from the United States. *J Glaucoma,* 15**,** 358-63.

HEALEY, P. R. & MITCHELL, P. 1999. Optic disk size in open-angle glaucoma: the Blue Mountains Eye Study. *Am J Ophthalmol,* 128**,** 515-7.

HEIJL, A., BENGTSSON, B., HYMAN, L. & LESKE, M. C. 2009. Natural history of open-angle glaucoma. *Ophthalmology,* 116**,** 2271-6.

HEIJL, A., BENGTSSON, B. & OSKARSDOTTIR, S. E. 2013. Prevalence and severity of undetected manifest glaucoma: results from the early manifest glaucoma trial screening. *Ophthalmology,* 120**,** 1541-5.

HEMMINKI, K., FORSTI, A. & BERMEJO, J. L. 2008. The 'common disease-common variant' hypothesis and familial risks. *PLoS One,* 3**,** e2504.

HERNDON, L. W., WEIZER, J. S. & STINNETT, S. S. 2004. Central corneal thickness as a risk factor for advanced glaucoma damage. *Arch Ophthalmol,* 122**,** 17-21.

HEWITT, A. W., BENNETT, S. L., DIMASI, D. P., CRAIG, J. E. & MACKEY, D. A. 2006a. A myocilin Gln368STOP homozygote does not exhibit a more severe glaucoma phenotype than heterozygous cases. *Am J Ophthalmol,* 141**,** 402-3.

HEWITT, A. W., DIMASI, D. P., MACKEY, D. A. & CRAIG, J. E. 2006b. A Glaucoma Case-control Study of the WDR36 Gene D658G sequence variant. *Am J Ophthalmol,* 142**,** 324-5.

HEWITT, A. W., MACKEY, D. A. & CRAIG, J. E. 2008. Myocilin allele-specific glaucoma phenotype database. *Hum Mutat,* 29**,** 207-11.

HEWITT, A. W., SAMPLES, J. R., ALLINGHAM, R. R., JARVELA, I., KITSOS, G., KRISHNADAS, S. R., RICHARDS, J. E., LICHTER, P. R., PETERSEN, M. B., SUNDARESAN, P., WIGGS, J. L., MACKEY, D. A. & WIRTZ, M. K. 2007. Investigation of founder effects for the Thr377Met Myocilin mutation in glaucoma families from differing ethnic backgrounds. *Mol Vis,* 13**,** 487-92.

HIRSCHHORN, J. N. & DALY, M. J. 2005. Genome-wide association studies for common diseases and complex traits. *Nat Rev Genet,* 6**,** 95-108.

HITZEMANN, R., BOTTOMLY, D., DARAKJIAN, P., WALTER, N., IANCU, O., SEARLES, R., WILMOT, B. & MCWEENEY, S. 2013. Genes, behavior and next-generation RNA sequencing. *Genes Brain Behav,* 12**,** 1-12.

HOBBY, P., WYATT, M. K., GAN, W., BERNSTEIN, S., TOMAREV, S., SLINGSBY, C. & WISTOW, G. 2000. Cloning, modeling, and chromosomal localization for a small leucine-rich repeat proteoglycan (SLRP) family member expressed in human eye. *Mol Vis,* 6**,** 72-8.

HODGES, E., XUAN, Z., BALIJA, V., KRAMER, M., MOLLA, M. N., SMITH, S. W., MIDDLE, C. M., RODESCH, M. J., ALBERT, T. J., HANNON, G. J. & MCCOMBIE, W. R. 2007. Genome-wide in situ exon capture for selective resequencing. *Nat Genet,* 39**,** 1522-7.

HOEHN, R., ZELLER, T., VERHOEVEN, V. J., GRUS, F., ADLER, M., WOLFS, R. C., UITTERLINDEN, A. G., CASTAGNE, R., SCHILLERT, A., KLAVER, C. C., PFEIFFER, N. & MIRSHAHI, A. 2012. Population-based meta-analysis in Caucasians confirms association with COL5A1 and ZNF469 but not COL8A2 with central corneal thickness. *Hum Genet,* 131**,** 1783-93.

HOGEWIND, B. F., MUKHOPADHYAY, A., THEELEN, T., HOLLANDER, A. I. & HOYNG, C. B. 2010. Variable clinical spectrum of the myocilin Gln368X mutation in a Dutch family with primary open angle glaucoma. *Curr Eye Res,* 35**,** 31-6.

HOLLANDS, H., JOHNSON, D., HOLLANDS, S., SIMEL, D. L., JINAPRIYA, D. & SHARMA, S. 2013. Do findings on routine examination identify patients at risk for primary open-angle glaucoma? The rational clinical examination systematic review. *Jama,* 309**,** 2035-42.

HOWELL, G. R., WALTON, D. O., KING, B. L., LIBBY, R. T. & JOHN, S. W. 2011. Datgan, a reusable software system for facile interrogation and visualization of complex transcription profiling data. *BMC Genomics,* 12**,** 429.

HSU, C. H., CHEN, R. I. & LIN, S. C. 2015. Myopia and glaucoma: sorting out the difference. *Curr Opin Ophthalmol,* 26**,** 90-5.

HU, S., WANG, B., ZHOU, Z., ZHOU, G., WANG, J., MA, X. & QI, Y. 2010. A novel mutation in GJA8 causing congenital cataract-microcornea syndrome in a Chinese pedigree. *Mol Vis,* 16**,** 1585-92.

HU, T., DARABOS, C., CRICCO, M. E., KONG, E. & MOORE, J. H. 2015. Genome-wide genetic interaction analysis of glaucoma using expert knowledge derived from human phenotype networks. *Pac Symp Biocomput***,** 207-18.

HUANG, L., ZHANG, H., CHENG, C. Y., WEN, F., TAM, P. O., ZHAO, P., CHEN, H., LI, Z., CHEN, L., TAI, Z., YAMASHIRO, K., DENG, S., ZHU, X., CHEN, W., CAI, L., LU, F., LI, Y., CHEUNG, C. M., SHI, Y., MIYAKE, M., LIN, Y., GONG, B., LIU, X., SIM, K. S., YANG, J., MORI, K., ZHANG, X., CACKETT, P. D., TSUJIKAWA, M., NISHIDA, K., HAO, F., MA, S., LIN, H., CHENG, J., FEI, P., LAI, T. Y., TANG, S., LAUDE, A., INOUE, S., YEO, I. Y., SAKURADA, Y., ZHOU, Y., IIJIMA, H., HONDA, S., LEI, C., ZHANG, L., ZHENG, H., JIANG, D., ZHU, X., WONG, T. Y., KHOR, C. C., PANG, C. P., YOSHIMURA, N. & YANG, Z. 2016. A missense variant in FGD6 confers increased risk of polypoidal choroidal vasculopathy. *Nat Genet,* 48**,** 640-7.

HUANG, X., LI, M., GUO, X., LI, S., XIAO, X., JIA, X., LIU, X. & ZHANG, Q. 2014. Mutation analysis of seven known glaucoma-associated genes in Chinese patients with glaucoma. *Invest Ophthalmol Vis Sci,* 55**,** 3594-602.

HUANG, X., XIAO, X., JIA, X., LI, S., LI, M., GUO, X., LIU, X. & ZHANG, Q. 2015. Mutation analysis of the genes associated with anterior segment dysgenesis, microcornea and microphthalmia in 257 patients with glaucoma. *Int J Mol Med,* 36**,** 1111-7.

HUANG, Y., CEN, L. P., LUO, J. M., WANG, N., ZHANG, M. Z., VAN ROOIJEN, N., PANG, C. P. & CUI, Q. 2008. Differential roles of phosphatidylinositol 3-kinase/akt pathway in retinal ganglion cell survival in rats with or without acute ocular hypertension. *Neuroscience,* 153**,** 214-25.

HYSI, P. G., CHENG, C. Y., SPRINGELKAMP, H., MACGREGOR, S., BAILEY, J. N., WOJCIECHOWSKI, R., VITART, V., NAG, A., HEWITT, A. W., HOHN, R., VENTURINI, C., MIRSHAHI, A., RAMDAS, W. D., THORLEIFSSON, G., VITHANA, E., KHOR, C. C., STEFANSSON, A. B., LIAO, J., HAINES, J. L., AMIN, N., WANG, Y. X., WILD, P. S., OZEL, A. B., LI, J. Z., FLECK, B. W., ZELLER, T., STAFFIERI, S. E., TEO, Y. Y., CUELLAR-PARTIDA, G., LUO, X., ALLINGHAM, R. R., RICHARDS, J. E., SENFT, A., KARSSEN, L. C., ZHENG, Y., BELLENGUEZ, C., XU, L., IGLESIAS, A. I., WILSON, J. F., KANG, J. H., VAN LEEUWEN, E. M., JONSSON, V., THORSTEINSDOTTIR, U., DESPRIET, D. D., ENNIS, S., MOROI, S. E., MARTIN, N. G., JANSONIUS, N. M., YAZAR, S., TAI, E. S., AMOUYEL, P., KIRWAN, J., VAN KOOLWIJK, L. M., HAUSER, M. A., JONASSON, F., LEO, P., LOOMIS, S. J., FOGARTY, R., RIVADENEIRA, F., KEARNS, L., LACKNER, K. J., DE JONG, P. T., SIMPSON, C. L., PENNELL, C. E., OOSTRA, B. A., UITTERLINDEN, A. G., SAW, S. M., LOTERY, A. J., BAILEY-WILSON, J. E., HOFMAN, A., VINGERLING, J. R., MAUBARET, C., PFEIFFER, N., WOLFS, R. C., LEMIJ, H. G., YOUNG, T. L., PASQUALE, L. R., DELCOURT, C., SPECTOR, T. D., KLAVER, C. C., SMALL, K. S., BURDON, K. P., STEFANSSON, K., WONG, T. Y., VISWANATHAN, A., MACKEY, D. A., CRAIG, J. E., WIGGS, J. L., VAN DUIJN, C. M., HAMMOND, C. J. & AUNG, T. 2014. Genome-wide analysis of multi-ancestry cohorts identifies new loci influencing intraocular pressure and susceptibility to glaucoma. *Nat Genet,* 46**,** 1126-30.

IDEKER, T., OZIER, O., SCHWIKOWSKI, B. & SIEGEL, A. F. 2002. Discovering regulatory and signalling circuits in molecular interaction networks. *Bioinformatics,* 18 Suppl 1**,** S233-40.

ILIEV, M. E., BODMER, S., GALLATI, S., LANZ, R., STURMER, J., KATSOULIS, K., WOLF, S., TRITTIBACH, P. & SARRA, G. M. 2008. Glaucoma phenotype in a large Swiss pedigree with the myocilin Gly367Arg mutation. *Eye (Lond),* 22**,** 880-8.

INOUE, T. & TANIHARA, H. 2013. Rho-associated kinase inhibitors: a novel glaucoma therapy. *Prog Retin Eye Res,* 37**,** 1-12.

INSULL, E., NICHOLAS, S., ANG, G. S., POOSTCHI, A., CHAN, K. & WELLS, A. 2010. Optic disc area and correlation with central corneal thickness, corneal hysteresis and ocular pulse amplitude in glaucoma patients and controls. *Clin Experiment Ophthalmol,* 38**,** 839-44.

JAKOBS, T. C. 2014. Differential gene expression in glaucoma. *Cold Spring Harb Perspect Med,* 4**,** a020636.

JANSSEN, S. F., GORGELS, T. G., RAMDAS, W. D., KLAVER, C. C., VAN DUIJN, C. M., JANSONIUS, N. M. & BERGEN, A. A. 2013. The vast complexity of primary open angle glaucoma: disease genes, risks, molecular mechanisms and pathobiology. *Prog Retin Eye Res,* 37**,** 31-67.

JAWORSKA-FEIL, L., JANTAS, D., LESKIEWICZ, M., BUDZISZEWSKA, B., KUBERA, M., BASTA-KAIM, A., LIPKOWSKI, A. W. & LASON, W. 2010. Protective effects of TRH and its analogues against various cytotoxic agents in retinoic acid (RA)-differentiated human neuroblastoma SH-SY5Y cells. *Neuropeptides,* 44**,** 495-508.

JELODARI-MAMAGHANI, S., HAJI-SEYED-JAVADI, R., SURI, F., NILFORUSHAN, N., YAZDANI, S., KAMYAB, K. & ELAHI, E. 2013. Contribution of the latent transforming growth factor-beta binding protein 2 gene to etiology of primary open angle glaucoma and pseudoexfoliation syndrome. *Mol Vis,* 19**,** 333-47.

JIA, L. Y., GONG, B., PANG, C. P., HUANG, Y., LAM, D. S., WANG, N. & YAM, G. H. 2009. Correction of the disease phenotype of myocilin-causing glaucoma by a natural osmolyte. *Invest Ophthalmol Vis Sci,* 50**,** 3743-9.

JIANG, X., VARMA, R., WU, S., TORRES, M., AZEN, S. P., FRANCIS, B. A., CHOPRA, V. & NGUYEN, B. B. 2012. Baseline risk factors that predict the development of open-angle glaucoma in a population: the Los Angeles Latino Eye Study. *Ophthalmology,* 119**,** 2245-53.

JOE, M. K., KWON, H. S., COJOCARU, R. & TOMAREV, S. I. 2014. Myocilin regulates cell proliferation and survival. *J Biol Chem,* 289**,** 10155-67.

JOE, M. K., SOHN, S., HUR, W., MOON, Y., CHOI, Y. R. & KEE, C. 2003. Accumulation of mutant myocilins in ER leads to ER stress and potential cytotoxicity in human trabecular meshwork cells. *Biochem Biophys Res Commun,* 312**,** 592-600.

JOE, M. K. & TOMAREV, S. I. 2010. Expression of myocilin mutants sensitizes cells to oxidative stress-induced apoptosis: implication for glaucoma pathogenesis. *Am J Pathol,* 176**,** 2880-90.

JOHAR, A. S., ANAYA, J. M., ANDREWS, D., PATEL, H. R., FIELD, M., GOODNOW, C. & ARCOS-BURGOS, M. 2015. Candidate gene discovery in autoimmunity by using extreme phenotypes, next generation sequencing and whole exome capture. *Autoimmun Rev,* 14**,** 204-209.

JONAS, J. B., STROUX, A., VELTEN, I., JUENEMANN, A., MARTUS, P. & BUDDE, W. M. 2005. Central corneal thickness correlated with glaucoma damage and rate of progression. *Invest Ophthalmol Vis Sci,* 46**,** 1269-74.

JORDAN, T., HANSON, I., ZALETAYEV, D., HODGSON, S., PROSSER, J., SEAWRIGHT, A., HASTIE, N. & VAN HEYNINGEN, V. 1992. The human PAX6 gene is mutated in two patients with aniridia. *Nat Genet,* 1**,** 328-32.

KACHANER, D., GENIN, P., LAPLANTINE, E. & WEIL, R. 2012. Toward an integrative view of Optineurin functions. *Cell Cycle,* 11**,** 2808-18.

KALTSCHMIDT, B., WIDERA, D. & KALTSCHMIDT, C. 2005. Signaling via NF-kappaB in the nervous system. *Biochim Biophys Acta,* 1745**,** 287-99.

KASS, M. A., HEUER, D. K., HIGGINBOTHAM, E. J., JOHNSON, C. A., KELTNER, J. L., MILLER, J. P., PARRISH, R. K., 2ND, WILSON, M. R. & GORDON, M. O. 2002. The Ocular Hypertension Treatment

Study: a randomized trial determines that topical ocular hypotensive medication delays or prevents the onset of primary open-angle glaucoma. *Arch Ophthalmol,* 120**,** 701-13; discussion 829-30.

KAURANI, L., VISHAL, M., RAY, J., SEN, A., RAY, K. & MUKHOPADHYAY, A. 2016. TBK1 duplication is found in normal tension and not in high tension glaucoma patients of Indian origin. *J Genet,* 95**,** 459-61.

KAWASE, K., ALLINGHAM, R. R., MEGURO, A., MIZUKI, N., ROOS, B., SOLIVAN-TIMPE, F. M., ROBIN, A. L., RITCH, R. & FINGERT, J. H. 2012. Confirmation of TBK1 duplication in normal tension glaucoma. *Exp Eye Res,* 96**,** 178-80.

KELLER, K. E., YANG, Y. F., SUN, Y. Y., SYKES, R., ACOTT, T. S. & WIRTZ, M. K. 2013. Ankyrin repeat and suppressor of cytokine signaling box containing protein-10 is associated with ubiquitin-mediated degradation pathways in trabecular meshwork cells. *Mol Vis,* 19**,** 1639-55.

KELLER, K. E., YANG, Y. F., SUN, Y. Y., SYKES, R., GAUDETTE, N. D., SAMPLES, J. R., ACOTT, T. S. & WIRTZ, M. K. 2014. Interleukin-20 receptor expression in the trabecular meshwork and its implication in glaucoma. *J Ocul Pharmacol Ther,* 30**,** 267-76.

KHOR, C. C., RAMDAS, W. D., VITHANA, E. N., CORNES, B. K., SIM, X., TAY, W. T., SAW, S. M., ZHENG, Y., LAVANYA, R., WU, R., WANG, J. J., MITCHELL, P., UITTERLINDEN, A. G., RIVADENEIRA, F., TEO, Y. Y., CHIA, K. S., SEIELSTAD, M., HIBBERD, M., VINGERLING, J. R., KLAVER, C. C., JANSONIUS, N. M., TAI, E. S., WONG, T. Y., VAN DUIJN, C. M. & AUNG, T. 2011. Genome-wide association studies in Asians confirm the involvement of ATOH7 and TGFBR3, and further identify CARD10 as a novel locus influencing optic disc area. *Hum Mol Genet,* 20**,** 1864-72.

KIM, B. S., SAVINOVA, O. V., REEDY, M. V., MARTIN, J., LUN, Y., GAN, L., SMITH, R. S., TOMAREV, S. I., JOHN, S. W. & JOHNSON, R. L. 2001. Targeted Disruption of the Myocilin Gene (Myoc) Suggests that Human Glaucoma-Causing Mutations Are Gain of Function. *Mol Cell Biol,* 21**,** 7707-13.

KIM, D., PERTEA, G., TRAPNELL, C., PIMENTEL, H., KELLEY, R. & SALZBERG, S. L. 2013. TopHat2: accurate alignment of transcriptomes in the presence of insertions, deletions and gene fusions. *Genome Biol,* 14**,** R36.

KIM, H. J., SUH, W., PARK, S. C., KIM, C. Y., PARK, K. H., KOOK, M. S., KIM, Y. Y., KIM, C. S., PARK, C. K., KI, C. S. & KEE, C. 2011. Mutation spectrum of CYP1B1 and MYOC genes in Korean patients with primary congenital glaucoma. *Mol Vis,* 17**,** 2093-101.

KIM, J. W. & CHEN, P. P. 2004. Central corneal pachymetry and visual field progression in patients with open-angle glaucoma. *Ophthalmology,* 111**,** 2126-32.

KIM, M. J., KIM, H. S., JEOUNG, J. W. & PARK, K. H. 2014. Risk factors for open-angle glaucoma with normal baseline intraocular pressure in a young population: the Korea National Health and Nutrition Examination Survey. *Clin Experiment Ophthalmol,* 42**,** 825-32.

KITAOKA, Y., MUNEMASA, Y., NAKAZAWA, T. & UENO, S. 2007. NMDA-induced interleukin-1beta expression is mediated by nuclear factor-kappa B p65 in the retina. *Brain Res,* 1142**,** 247-55.

KOCH, L. 2020. Exploring human genomic diversity with gnomAD. *Nat Rev Genet*.

KONG, X., CHEN, Y., CHEN, X. & SUN, X. 2011. Influence of family history as a risk factor on primary angle closure and primary open angle glaucoma in a Chinese population. *Ophthalmic Epidemiol,* 18**,** 226-32.

KONG, X., ZHU, W., CHEN, X., CHEN, Y. & SUN, X. 2013. Familial aggregation of primary open angle glaucoma in Shanghai, China. *Mol Vis,* 19**,** 1859-65.

KRISHNAMOORTHY, R. R., CLARK, A. F., DAUDT, D., VISHWANATHA, J. K. & YORIO, T. 2013. A forensic path to RGC-5 cell line identification: lessons learned. *Invest Ophthalmol Vis Sci,* 54**,** 5712-9.

KROEBER, M., OHLMANN, A., RUSSELL, P. & TAMM, E. R. 2006. Transgenic studies on the role of optineurin in the mouse eye. *Exp Eye Res,* 82**,** 1075-85.

KUMAR, A., BASAVARAJ, M. G., GUPTA, S. K., QAMAR, I., ALI, A. M., BAJAJ, V., RAMESH, T. K., PRAKASH, D. R., SHETTY, J. S. & DORAIRAJ, S. K. 2007. Role of CYP1B1, MYOC, OPTN, and OPTC genes

in adult-onset primary open-angle glaucoma: predominance of CYP1B1 mutations in Indian patients. *Mol Vis,* 13**,** 667-76.

KUMAR, P., HENIKOFF, S. & NG, P. C. 2009. Predicting the effects of coding non-synonymous variants on protein function using the SIFT algorithm. *Nat Protoc,* 4**,** 1073-81.

KWON, Y. H., FINGERT, J. H., KUEHN, M. H. & ALWARD, W. L. 2009. Primary open-angle glaucoma. *N Engl J Med,* 360**,** 1113-24.

KWON, Y. H., KIM, C. S., ZIMMERMAN, M. B., ALWARD, W. L. & HAYREH, S. S. 2001. Rate of visual field loss and long-term visual outcome in primary open-angle glaucoma. *Am J Ophthalmol,* 132**,** 47-56.

LAM, D. S., LEUNG, Y. F., CHUA, J. K., BAUM, L., FAN, D. S., CHOY, K. W. & PANG, C. P. 2000. Truncations in the TIGR gene in individuals with and without primary open-angle glaucoma. *Invest Ophthalmol Vis Sci,* 41**,** 1386-91.

LANDER, E. S., LINTON, L. M., BIRREN, B., NUSBAUM, C., ZODY, M. C., BALDWIN, J., DEVON, K., DEWAR, K., DOYLE, M., FITZHUGH, W., FUNKE, R., GAGE, D., HARRIS, K., HEAFORD, A., HOWLAND, J., KANN, L., LEHOCZKY, J., LEVINE, R., MCEWAN, P., MCKERNAN, K., MELDRIM, J., MESIROV, J. P., MIRANDA, C., MORRIS, W., NAYLOR, J., RAYMOND, C., ROSETTI, M., SANTOS, R., SHERIDAN, A., SOUGNEZ, C., STANGE-THOMANN, N., STOJANOVIC, N., SUBRAMANIAN, A., WYMAN, D., ROGERS, J., SULSTON, J., AINSCOUGH, R., BECK, S., BENTLEY, D., BURTON, J., CLEE, C., CARTER, N., COULSON, A., DEADMAN, R., DELOUKAS, P., DUNHAM, A., DUNHAM, I., DURBIN, R., FRENCH, L., GRAFHAM, D., GREGORY, S., HUBBARD, T., HUMPHRAY, S., HUNT, A., JONES, M., LLOYD, C., MCMURRAY, A., MATTHEWS, L., MERCER, S., MILNE, S., MULLIKIN, J. C., MUNGALL, A., PLUMB, R., ROSS, M., SHOWNKEEN, R., SIMS, S., WATERSTON, R. H., WILSON, R. K., HILLIER, L. W., MCPHERSON, J. D., MARRA, M. A., MARDIS, E. R., FULTON, L. A., CHINWALLA, A. T., PEPIN, K. H., GISH, W. R., CHISSOE, S. L., WENDL, M. C., DELEHAUNTY, K. D., MINER, T. L., DELEHAUNTY, A., KRAMER, J. B., COOK, L. L., FULTON, R. S., JOHNSON, D. L., MINX, P. J., CLIFTON, S. W., HAWKINS, T., BRANSCOMB, E., PREDKI,

P., RICHARDSON, P., WENNING, S., SLEZAK, T., DOGGETT, N., CHENG, J. F., OLSEN, A., LUCAS, S., ELKIN, C., UBERBACHER, E., FRAZIER, M., et al. 2001. Initial sequencing and analysis of the human genome. *Nature,* 409**,** 860-921.

LANDERS, J., GOLDBERG, I. & GRAHAM, S. 2003. Does a family history of glaucoma affect disease severity at the time of diagnosis? *J Glaucoma,* 12**,** 31-5.

LASCARATOS, G., GARWAY-HEATH, D. F., WILLOUGHBY, C. E., CHAU, K. Y. & SCHAPIRA, A. H. 2012. Mitochondrial dysfunction in glaucoma: understanding genetic influences. *Mitochondrion,* 12**,** 202-12.

LE, A., MUKESH, B. N., MCCARTY, C. A. & TAYLOR, H. R. 2003. Risk factors associated with the incidence of open-angle glaucoma: the visual impairment project. *Invest Ophthalmol Vis Sci,* 44**,** 3783-9.

LECHAUVE, C., AUGUSTIN, S., CWERMAN-THIBAULT, H., BOUAITA, A., FORSTER, V., CELIER, C., RUSTIN, P., MARDEN, M. C., SAHEL, J. A. & CORRAL-DEBRINSKI, M. 2012. Neuroglobin involvement in respiratory chain function and retinal ganglion cell integrity. *Biochim Biophys Acta,* 1823**,** 2261-73.

LECHAUVE, C., AUGUSTIN, S., CWERMAN-THIBAULT, H., REBOUSSIN, E., ROUSSEL, D., LAI-KUEN, R., SAUBAMEA, B., SAHEL, J. A., DEBEIR, T. & CORRAL-DEBRINSKI, M. 2014. Neuroglobin gene therapy prevents optic atrophy and preserves durably visual function in Harlequin mice. *Mol Ther,* 22**,** 1096-109.

LECHAUVE, C., AUGUSTIN, S., ROUSSEL, D., SAHEL, J. A. & CORRAL-DEBRINSKI, M. 2013. Neuroglobin involvement in visual pathways through the optic nerve. *Biochim Biophys Acta,* 1834**,** 1772-8.

LEE, M. K., WOO, S. J., KIM, J. I., CHO, S. I., KIM, H., SUNG, J., SEO, J. S. & KIM, D. M. 2010. Replication of a glaucoma candidate gene on 5q22.1 for intraocular pressure in mongolian populations: the GENDISCAN Project. *Invest Ophthalmol Vis Sci,* 51**,** 1335-40.

LEE, S., VAN BERGEN, N. J., KONG, G. Y., CHRYSOSTOMOU, V., WAUGH, H. S., O'NEILL, E. C., CROWSTON, J. G. & TROUNCE, I. A. 2011. Mitochondrial dysfunction in glaucoma and emerging bioenergetic therapies. *Exp Eye Res,* 93**,** 204-12.

LEK, M., KARCZEWSKI, K. J., MINIKEL, E. V., SAMOCHA, K. E., BANKS, E., FENNELL, T., O'DONNELL-LURIA, A. H., WARE, J. S., HILL, A. J., CUMMINGS, B. B., TUKIAINEN, T., BIRNBAUM, D. P., KOSMICKI, J. A., DUNCAN, L. E., ESTRADA, K., ZHAO, F., ZOU, J., PIERCE-HOFFMAN, E., BERGHOUT, J., COOPER, D. N., DEFLAUX, N., DEPRISTO, M., DO, R., FLANNICK, J., FROMER, M., GAUTHIER, L., GOLDSTEIN, J., GUPTA, N., HOWRIGAN, D., KIEZUN, A., KURKI, M. I., MOONSHINE, A. L., NATARAJAN, P., OROZCO, L., PELOSO, G. M., POPLIN, R., RIVAS, M. A., RUANO-RUBIO, V., ROSE, S. A., RUDERFER, D. M., SHAKIR, K., STENSON, P. D., STEVENS, C., THOMAS, B. P., TIAO, G., TUSIE-LUNA, M. T., WEISBURD, B., WON, H. H., YU, D., ALTSHULER, D. M., ARDISSINO, D., BOEHNKE, M., DANESH, J., DONNELLY, S., ELOSUA, R., FLOREZ, J. C., GABRIEL, S. B., GETZ, G., GLATT, S. J., HULTMAN, C. M., KATHIRESAN, S., LAAKSO, M., MCCARROLL, S., MCCARTHY, M. I., MCGOVERN, D., MCPHERSON, R., NEALE, B. M., PALOTIE, A., PURCELL, S. M., SALEHEEN, D., SCHARF, J. M., SKLAR, P., SULLIVAN, P. F., TUOMILEHTO, J., TSUANG, M. T., WATKINS, H. C., WILSON, J. G., DALY, M. J. & MACARTHUR, D. G. 2016. Analysis of protein-coding genetic variation in 60,706 humans. *Nature,* 536**,** 285-91.

LESKE, M. C., HEIJL, A., HUSSEIN, M., BENGTSSON, B., HYMAN, L. & KOMAROFF, E. 2003. Factors for glaucoma progression and the effect of treatment: the early manifest glaucoma trial. *Arch Ophthalmol,* 121**,** 48-56.

LESKE, M. C., HEIJL, A., HYMAN, L., BENGTSSON, B., DONG, L. & YANG, Z. 2007a. Predictors of long-term progression in the early manifest glaucoma trial. *Ophthalmology,* 114**,** 1965-72.

LESKE, M. C., HYMAN, L., HUSSEIN, M., HEIJL, A. & BENGTSSON, B. 1999. Comparison of glaucomatous progression between untreated patients with normal-tension glaucoma and patients with therapeutically reduced intraocular pressures. The effectiveness of intraocular pressure reduction in the treatment of normal-tension glaucoma. *Am J Ophthalmol,* 127**,** 625-6.

LESKE, M. C., WU, S. Y., HONKANEN, R., NEMESURE, B., SCHACHAT, A., HYMAN, L. & HENNIS, A. 2007b. Nine-year incidence of open-angle glaucoma in the Barbados Eye Studies. *Ophthalmology,* 114**,** 1058-64.

LEVY, S., SUTTON, G., NG, P. C., FEUK, L., HALPERN, A. L., WALENZ, B. P., AXELROD, N., HUANG, J., KIRKNESS, E. F., DENISOV, G., LIN, Y., MACDONALD, J. R., PANG, A. W., SHAGO, M., STOCKWELL, T. B., TSIAMOURI, A., BAFNA, V., BANSAL, V., KRAVITZ, S. A., BUSAM, D. A., BEESON, K. Y., MCINTOSH, T. C., REMINGTON, K. A., ABRIL, J. F., GILL, J., BORMAN, J., ROGERS, Y. H., FRAZIER, M. E., SCHERER, S. W., STRAUSBERG, R. L. & VENTER, J. C. 2007. The diploid genome sequence of an individual human. *PLoS Biol,* 5**,** e254.

LI, B. & LEAL, S. M. 2008. Methods for detecting associations with rare variants for common diseases: application to analysis of sequence data. *Am J Hum Genet,* 83**,** 311-21.

LI, H. 2011. Tabix: fast retrieval of sequence features from generic TAB-delimited files. *Bioinformatics,* 27**,** 718-719.

LI, H., AO, X., JIA, J., WANG, Q. & ZHANG, Z. 2011. Effects of optineurin siRNA on apoptotic genes and apoptosis in RGC-5 cells. *Mol Vis,* 17**,** 3314-25.

LI, R. C., GUO, S. Z., LEE, S. K. & GOZAL, D. 2010. Neuroglobin protects neurons against oxidative stress in global ischemia. *J Cereb Blood Flow Metab,* 30**,** 1874-82.

LI, R. C., LEE, S. K., POURANFAR, F., BRITTIAN, K. R., CLAIR, H. B., ROW, B. W., WANG, Y. & GOZAL, D. 2006. Hypoxia differentially regulates the expression of neuroglobin and cytoglobin in rat brain. *Brain Res,* 1096**,** 173-9.

LI, Z., ALLINGHAM, R. R., NAKANO, M., JIA, L., CHEN, Y., IKEDA, Y., MANI, B., CHEN, L. J., KEE, C., GARWAY-HEATH, D. F., SRIPRIYA, S., FUSE, N., ABU-AMERO, K. K., HUANG, C., NAMBURI, P., BURDON, K., PERERA, S. A., GHARAHKHANI, P., LIN, Y., UENO, M., OZAKI, M., MIZOGUCHI, T., KRISHNADAS, S. R., OSMAN, E. A., LEE, M. C., CHAN, A. S., TAJUDIN, L. S., DO, T., GONCALVES, A., REYNIER, P., ZHANG, H., BOURNE, R., GOH, D., BROADWAY, D., HUSAIN, R., NEGI, A. K., SU, D. H., HO,

C. L., BLANCO, A. A., LEUNG, C. K., WONG, T. T., YAKUB, A., LIU, Y., NONGPIUR, M. E., HAN, J. C., HON, D. N., SHANTHA, B., ZHAO, B., SANG, J., ZHANG, N., SATO, R., YOSHII, K., PANDA-JONAS, S., ASHLEY KOCH, A. E., HERNDON, L. W., MOROI, S. E., CHALLA, P., FOO, J. N., BEI, J. X., ZENG, Y. X., SIMMONS, C. P., BICH CHAU, T. N., SHARMILA, P. F., CHEW, M., LIM, B., TAM, P. O., CHUA, E., NG, X. Y., YONG, V. H., CHONG, Y. F., MEAH, W. Y., VIJAYAN, S., SEONGSOO, S., XU, W., TEO, Y. Y., COOKE BAILEY, J. N., KANG, J. H., HAINES, J. L., CHENG, C. Y., SAW, S. M., TAI, E. S., RICHARDS, J. E., RITCH, R., GAASTERLAND, D. E., PASQUALE, L. R., LIU, J., JONAS, J. B., MILEA, D., GEORGE, R., AL-OBEIDAN, S. A., MORI, K., MACGREGOR, S., HEWITT, A. W., GIRKIN, C. A., ZHANG, M., SUNDARESAN, P., VIJAYA, L., MACKEY, D. A., WONG, T. Y., CRAIG, J. E., et al. 2015. A common variant near TGFBR3 is associated with primary open angle glaucoma. *Hum Mol Genet,* 24**,** 3880-3892.

LI, Z., QU, L., DONG, Q., HUANG, B., LI, H., TANG, Z., XU, Y., LUO, W., LIU, L., QIU, X. & WANG, E. 2012. Overexpression of CARMA3 in non-small-cell lung cancer is linked for tumor progression. *PLoS One,* 7**,** e36903.

LIBBY, R. T., ANDERSON, M. G., PANG, I. H., ROBINSON, Z. H., SAVINOVA, O. V., COSMA, I. M., SNOW, A., WILSON, L. A., SMITH, R. S., CLARK, A. F. & JOHN, S. W. 2005. Inherited glaucoma in DBA/2J mice: pertinent disease features for studying the neurodegeneration. *Vis Neurosci,* 22**,** 637-48.

LIN, W., AOYAMA, Y., KAWASE, K. & YAMAMOTO, T. 2009. Relationship between central corneal thickness and visual field defect in open-angle glaucoma. *Jpn J Ophthalmol,* 53**,** 477-81.

LIU, L., SABO, A., NEALE, B. M., NAGASWAMY, U., STEVENS, C., LIM, E., BODEA, C. A., MUZNY, D., REID, J. G., BANKS, E., COON, H., DEPRISTO, M., DINH, H., FENNEL, T., FLANNICK, J., GABRIEL, S., GARIMELLA, K., GROSS, S., HAWES, A., LEWIS, L., MAKAROV, V., MAGUIRE, J., NEWSHAM, I., POPLIN, R., RIPKE, S., SHAKIR, K., SAMOCHA, K. E., WU, Y., BOERWINKLE, E., BUXBAUM, J. D., COOK, E. H., JR., DEVLIN, B., SCHELLENBERG, G. D., SUTCLIFFE, J. S., DALY, M. J., GIBBS, R. A. & ROEDER, K. 2013a.

Analysis of rare, exonic variation amongst subjects with autism spectrum disorders and population controls. *PLoS Genet,* 9**,** e1003443.

LIU, X., YU, X., ZACK, D. J., ZHU, H. & QIAN, J. 2008. TiGER: a database for tissue-specific gene expression and regulation. *BMC Bioinformatics,* 9**,** 271.

LIU, Y., ALLINGHAM, R. R., QIN, X., LAYFIELD, D., DELLINGER, A. E., GIBSON, J., WHEELER, J., ASHLEY-KOCH, A. E., STAMER, W. D. & HAUSER, M. A. 2013b. Gene expression profile in human trabecular meshwork from patients with primary open-angle glaucoma. *Invest Ophthalmol Vis Sci,* 54**,** 6382-9.

LIU, Y., LIU, W., CROOKS, K., SCHMIDT, S., ALLINGHAM, R. R. & HAUSER, M. A. 2010. No evidence of association of heterozygous NTF4 mutations in patients with primary open-angle glaucoma. *Am J Hum Genet,* 86**,** 498-9; author reply 500.

LIU, Y. & VOLLRATH, D. 2004. Reversal of mutant myocilin non-secretion and cell killing: implications for glaucoma. *Hum Mol Genet,* 13**,** 1193-204.

LOPEZ-GARRIDO, M. P., BLANCO-MARCHITE, C., SANCHEZ-SANCHEZ, F., LOPEZ-SANCHEZ, E., CHAQUES-ALEPUZ, V., CAMPOS-MOLLO, E., SALINAS-SANCHEZ, A. S. & ESCRIBANO, J. 2010. Functional analysis of CYP1B1 mutations and association of heterozygous hypomorphic alleles with primary open-angle glaucoma. *Clin Genet,* 77**,** 70-8.

LOPEZ-MARTINEZ, F., LOPEZ-GARRIDO, M. P., SANCHEZ-SANCHEZ, F., CAMPOS-MOLLO, E., COCA-PRADOS, M. & ESCRIBANO, J. 2007. Role of MYOC and OPTN sequence variations in Spanish patients with primary open-angle glaucoma. *Mol Vis,* 13**,** 862-72.

LU, Y., VITART, V., BURDON, K. P., KHOR, C. C., BYKHOVSKAYA, Y., MIRSHAHI, A., HEWITT, A. W., KOEHN, D., HYSI, P. G., RAMDAS, W. D., ZELLER, T., VITHANA, E. N., CORNES, B. K., TAY, W. T., TAI, E. S., CHENG, C. Y., LIU, J., FOO, J. N., SAW, S. M., THORLEIFSSON, G., STEFANSSON, K., DIMASI, D. P., MILLS, R. A., MOUNTAIN, J., ANG, W., HOEHN, R., VERHOEVEN, V. J., GRUS, F., WOLFS, R., CASTAGNE, R., LACKNER, K. J., SPRINGELKAMP, H., YANG, J., JONASSON, F., LEUNG, D. Y., CHEN, L. J.,

THAM, C. C., RUDAN, I., VATAVUK, Z., HAYWARD, C., GIBSON, J., CREE, A. J., MACLEOD, A., ENNIS, S., POLASEK, O., CAMPBELL, H., WILSON, J. F., VISWANATHAN, A. C., FLECK, B., LI, X., SISCOVICK, D., TAYLOR, K. D., ROTTER, J. I., YAZAR, S., ULMER, M., LI, J., YASPAN, B. L., OZEL, A. B., RICHARDS, J. E., MOROI, S. E., HAINES, J. L., KANG, J. H., PASQUALE, L. R., ALLINGHAM, R. R., ASHLEY-KOCH, A., MITCHELL, P., WANG, J. J., WRIGHT, A. F., PENNELL, C., SPECTOR, T. D., YOUNG, T. L., KLAVER, C. C., MARTIN, N. G., MONTGOMERY, G. W., ANDERSON, M. G., AUNG, T., WILLOUGHBY, C. E., WIGGS, J. L., PANG, C. P., THORSTEINSDOTTIR, U., LOTERY, A. J., HAMMOND, C. J., VAN DUIJN, C. M., HAUSER, M. A., RABINOWITZ, Y. S., PFEIFFER, N., MACKEY, D. A., CRAIG, J. E., MACGREGOR, S. & WONG, T. Y. 2013. Genome-wide association analyses identify multiple loci associated with central corneal thickness and keratoconus. *Nat Genet,* 45**,** 155-63.

LYNN, D. J., WINSOR, G. L., CHAN, C., RICHARD, N., LAIRD, M. R., BARSKY, A., GARDY, J. L., ROCHE, F. M., CHAN, T. H., SHAH, N., LO, R., NASEER, M., QUE, J., YAU, M., ACAB, M., TULPAN, D., WHITESIDE, M. D., CHIKATAMARLA, A., MAH, B., MUNZNER, T., HOKAMP, K., HANCOCK, R. E. & BRINKMAN, F. S. 2008. InnateDB: facilitating systems-level analyses of the mammalian innate immune response. *Mol Syst Biol,* 4**,** 218.

MABUCHI, F., SAKURADA, Y., KASHIWAGI, K., YAMAGATA, Z., IIJIMA, H. & TSUKAHARA, S. 2015. Involvement of genetic variants associated with primary open-angle glaucoma in pathogenic mechanisms and family history of glaucoma. *Am J Ophthalmol,* 159**,** 437-44 e2.

MACGREGOR, S., HEWITT, A. W., HYSI, P. G., RUDDLE, J. B., MEDLAND, S. E., HENDERS, A. K., GORDON, S. D., ANDREW, T., MCEVOY, B., SANFILIPPO, P. G., CARBONARO, F., TAH, V., LI, Y. J., BENNETT, S. L., CRAIG, J. E., MONTGOMERY, G. W., TRAN-VIET, K. N., BROWN, N. L., SPECTOR, T. D., MARTIN, N. G., YOUNG, T. L., HAMMOND, C. J. & MACKEY, D. A. 2010. Genome-wide association identifies ATOH7 as a major gene determining human optic disc size. *Hum Mol Genet,* 19**,** 2716-24.

MACKEY, D. A., HEALEY, D. L., FINGERT, J. H., COOTE, M. A., WONG, T. L., WILKINSON, C. H., MCCARTNEY, P. J., RAIT, J. L., DE GRAAF, A. P., STONE, E. M. & CRAIG, J. E. 2003. Glaucoma phenotype in pedigrees with the myocilin Thr377Met mutation. *Arch Ophthalmol,* 121**,** 1172-80.

MACKEY, D. A. & HEWITT, A. W. 2014. Genome-wide association study success in ophthalmology. *Curr Opin Ophthalmol,* 25**,** 386-93.

MADSEN, B. E. & BROWNING, S. R. 2009. A groupwise association test for rare mutations using a weighted sum statistic. *PLoS Genet,* 5**,** e1000384.

MAN, X., HE, J., KONG, C., ZHU, Y. & ZHANG, Z. 2014. Clinical significance and biological roles of CARMA3 in human bladder carcinoma. *Tumour Biol,* 35**,** 4131-6.

MANGOURITSAS, G., MORPHIS, G., MOURTZOUKOS, S. & FERETIS, E. 2009. Association between corneal hysteresis and central corneal thickness in glaucomatous and non-glaucomatous eyes. *Acta Ophthalmol,* 87**,** 901-5.

MANNI, G., ODDONE, F., PARISI, V., TOSTO, A. & CENTOFANTI, M. 2008. Intraocular pressure and central corneal thickness. *Prog Brain Res,* 173**,** 25-30.

MANOLIO, T. A., COLLINS, F. S., COX, N. J., GOLDSTEIN, D. B., HINDORFF, L. A., HUNTER, D. J., MCCARTHY, M. I., RAMOS, E. M., CARDON, L. R., CHAKRAVARTI, A., CHO, J. H., GUTTMACHER, A. E., KONG, A., KRUGLYAK, L., MARDIS, E., ROTIMI, C. N., SLATKIN, M., VALLE, D., WHITTEMORE, A. S., BOEHNKE, M., CLARK, A. G., EICHLER, E. E., GIBSON, G., HAINES, J. L., MACKAY, T. F., MCCARROLL, S. A. & VISSCHER, P. M. 2009. Finding the missing heritability of complex diseases. *Nature,* 461**,** 747-53.

MANTIONE, K. J., KREAM, R. M., KUZELOVA, H., PTACEK, R., RABOCH, J., SAMUEL, J. M. & STEFANO, G. B. 2014. Comparing bioinformatic gene expression profiling methods: microarray and RNA-Seq. *Med Sci Monit Basic Res,* 20**,** 138-42.

MAO, W., MILLAR, J. C., WANG, W. H., SILVERMAN, S. M., LIU, Y., WORDINGER, R. J., RUBIN, J. S., PANG, I. H. & CLARK, A. F. 2012. Existence of the canonical Wnt signaling pathway in the human trabecular meshwork. *Invest Ophthalmol Vis Sci,* 53**,** 7043-51.

MARCUS, M. W., DE VRIES, M. M., JUNOY MONTOLIO, F. G. & JANSONIUS, N. M. 2011. Myopia as a risk factor for open-angle glaucoma: a systematic review and meta-analysis. *Ophthalmology,* 118**,** 1989-1994 e2.

MARDIS, E. R. 2008. Next-generation DNA sequencing methods. *Annu Rev Genomics Hum Genet,* 9**,** 387-402.

MARIONI, J. C., MASON, C. E., MANE, S. M., STEPHENS, M. & GILAD, Y. 2008. RNA-seq: an assessment of technical reproducibility and comparison with gene expression arrays. *Genome Res,* 18**,** 1509-17.

MASHIMA, Y., SUZUKI, Y., SERGEEV, Y., OHTAKE, Y., TANINO, T., KIMURA, I., MIYATA, H., AIHARA, M., TANIHARA, H., INATANI, M., AZUMA, N., IWATA, T. & ARAIE, M. 2001. Novel cytochrome P4501B1 (CYP1B1) gene mutations in Japanese patients with primary congenital glaucoma. *Invest Ophthalmol Vis Sci,* 42**,** 2211-6.

MATAFTSI, A., ACHACHE, F., HEON, E., MERMOUD, A., COUSIN, P., METTHEZ, G., SCHORDERET, D. F. & MUNIER, F. L. 2001. MYOC mutation frequency in primary open-angle glaucoma patients from Western Switzerland. *Ophthalmic Genet,* 22**,** 225-31.

MCALLISTER-LUCAS, L. M., INOHARA, N., LUCAS, P. C., RULAND, J., BENITO, A., LI, Q., CHEN, S., CHEN, F. F., YAMAOKA, S., VERMA, I. M., MAK, T. W. & NUNEZ, G. 2001. Bimp1, a MAGUK family member linking protein kinase C activation to Bcl10-mediated NF-kappaB induction. *J Biol Chem,* 276**,** 30589-97.

MCCALL, C. M., MOSIER, S., THIESS, M., DEBELJAK, M., PALLAVAJJALA, A., BEIERL, K., DEAK, K. L., DATTO, M. B., GOCKE, C. D., LIN, M. T. & ESHLEMAN, J. R. 2014. False positives in multiplex PCR-based next-generation sequencing have unique signatures. *J Mol Diagn,* 16**,** 541-9.

MCKENNA, A., HANNA, M., BANKS, E., SIVACHENKO, A., CIBULSKIS, K., KERNYTSKY, A., GARIMELLA, K., ALTSHULER, D., GABRIEL, S., DALY, M. & DEPRISTO, M. A. 2010. The Genome Analysis

Toolkit: a MapReduce framework for analyzing next-generation DNA sequencing data. *Genome Res,* 20**,** 1297-303.

MCNAUGHT, A. I., ALLEN, J. G., HEALEY, D. L., MCCARTNEY, P. J., COOTE, M. A., WONG, T. L., CRAIG, J. E., GREEN, C. M., RAIT, J. L. & MACKEY, D. A. 2000. Accuracy and implications of a reported family history of glaucoma: experience from the Glaucoma Inheritance Study in Tasmania. *Arch Ophthalmol,* 118**,** 900-4.

MEDEIROS, F. A., ALENCAR, L. M., ZANGWILL, L. M., SAMPLE, P. A. & WEINREB, R. N. 2009. The Relationship between intraocular pressure and progressive retinal nerve fiber layer loss in glaucoma. *Ophthalmology,* 116**,** 1125-33 e1-3.

MEGURO, A., INOKO, H., OTA, M., MIZUKI, N. & BAHRAM, S. 2010. Genome-wide association study of normal tension glaucoma: common variants in SRBD1 and ELOVL5 contribute to disease susceptibility. *Ophthalmology,* 117**,** 1331-8.e5.

MELKI, R., COLOMB, E., LEFORT, N., BREZIN, A. P. & GARCHON, H. J. 2004. CYP1B1 mutations in French patients with early-onset primary open-angle glaucoma. *J Med Genet,* 41**,** 647-51.

MELKI, R., IDHAJJI, A., DRIOUICHE, S., HASSANI, M., BOUKABBOUCHA, A., AKHAYAT, O., GARCHON, H. & BELMOUDEN, A. 2003. Mutational analysis of the Myocilin gene in patients with primary open-angle glaucoma in Morocco. *Ophthalmic Genet,* 24**,** 153-60.

MENAA, F., BRAGHINI, C. A., VASCONCELLOS, J. P., MENAA, B., COSTA, V. P., FIGUEIREDO, E. S. & MELO, M. B. 2011. Keeping an eye on myocilin: a complex molecule associated with primary open-angle glaucoma susceptibility. *Molecules,* 16**,** 5402-21.

MEYER, A., VALTOT, F., BECHETOILLE, A., ROULAND, J. F., DASCOTTE, J. C., FEREC, C., BACH, J. F., CHAVENTRE, A. & GARCHON, H. J. 1994. [Linkage between juvenile glaucoma and chromosome 1q in 2 French families]. *C R Acad Sci III,* 317**,** 565-70.

MI, X. S., YUAN, T. F. & SO, K. F. 2014. The current research status of normal tension glaucoma. *Clin Interv Aging,* 9**,** 1563-71.

MIAO, Z., ZHAO, T., WANG, Z., XU, Y., SONG, Y., WU, J. & XU, H. 2012. CARMA3 is overexpressed in colon cancer and regulates NF-kappaB activity and cyclin D1 expression. *Biochem Biophys Res Commun,* 425**,** 781-7.

MICHEAL, S., AYUB, H., ISLAM, F., SIDDIQUI, S. N., KHAN, W. A., AKHTAR, F., QAMAR, R., KHAN, M. I. & DEN HOLLANDER, A. I. 2015. Variants in the ASB10 Gene Are Associated with Primary Open Angle Glaucoma. *PLoS One,* 10**,** e0145005.

MIGLIOR, S., PFEIFFER, N., TORRI, V., ZEYEN, T., CUNHA-VAZ, J. & ADAMSONS, I. 2007. Predictive factors for open-angle glaucoma among patients with ocular hypertension in the European Glaucoma Prevention Study. *Ophthalmology,* 114**,** 3-9.

MIN JOU, W., HAEGEMAN, G., YSEBAERT, M. & FIERS, W. 1972. Nucleotide sequence of the gene coding for the bacteriophage MS2 coat protein. *Nature,* 237**,** 82-8.

MINEGISHI, Y., IEJIMA, D., KOBAYASHI, H., CHI, Z. L., KAWASE, K., YAMAMOTO, T., SEKI, T., YUASA, S., FUKUDA, K. & IWATA, T. 2013. Enhanced optineurin E50K-TBK1 interaction evokes protein insolubility and initiates familial primary open-angle glaucoma. *Hum Mol Genet,* 22**,** 3559-67.

MISHRA, C. B., KUMARI, S., MANRAL, A., PRAKASH, A., SAINI, V., LYNN, A. M. & TIWARI, M. 2017. Design, synthesis, in-silico and biological evaluation of novel donepezil derivatives as multi-target-directed ligands for the treatment of Alzheimer's disease. *Eur J Med Chem,* 125**,** 736-750.

MITCHELL, P., HOURIHAN, F., SANDBACH, J. & WANG, J. J. 1999. The relationship between glaucoma and myopia: the Blue Mountains Eye Study. *Ophthalmology,* 106**,** 2010-5.

MITCHELL, P., ROCHTCHINA, E., LEE, A. J. & WANG, J. J. 2002. Bias in self-reported family history and relationship to glaucoma: the Blue Mountains Eye Study. *Ophthalmic Epidemiol,* 9**,** 333-45.

MITCHELL, P., SMITH, W., ATTEBO, K. & HEALEY, P. R. 1996. Prevalence of open-angle glaucoma in Australia. The Blue Mountains Eye Study. *Ophthalmology,* 103**,** 1661-9.

MIYAI, T. 2018. Fuchs Endothelial Corneal Dystrophy and Mitochondria. *Cornea,* 37 Suppl 1**,** S74-s77.

MIYAZAWA, A., FUSE, N., MENGKEGALE, M., RYU, M., SEIMIYA, M., WADA, Y. & NISHIDA, K. 2007. Association between primary open-angle glaucoma and WDR36 DNA sequence variants in Japanese. *Mol Vis,* 13**,** 1912-9.

MONEMI, S., SPAETH, G., DASILVA, A., POPINCHALK, S., ILITCHEV, E., LIEBMANN, J., RITCH, R., HEON, E., CRICK, R. P., CHILD, A. & SARFARAZI, M. 2005. Identification of a novel adult-onset primary open-angle glaucoma (POAG) gene on 5q22.1. *Hum Mol Genet,* 14**,** 725-33.

MOOKHERJEE, S., CHAKRABORTY, S., VISHAL, M., BANERJEE, D., SEN, A. & RAY, K. 2011. WDR36 variants in East Indian primary open-angle glaucoma patients. *Mol Vis,* 17**,** 2618-27.

MORGENTHALER, S. & THILLY, W. G. 2007. A strategy to discover genes that carry multi-allelic or mono-allelic risk for common diseases: a cohort allelic sums test (CAST). *Mutat Res,* 615**,** 28-56.

MORISSETTE, J., CLEPET, C., MOISAN, S., DUBOIS, S., WINSTALL, E., VERMEEREN, D., NGUYEN, T. D., POLANSKY, J. R., COTE, G., ANCTIL, J. L., AMYOT, M., PLANTE, M., FALARDEAU, P. & RAYMOND, V. 1998. Homozygotes carrying an autosomal dominant TIGR mutation do not manifest glaucoma. *Nat Genet,* 19**,** 319-21.

MOROZOVA, O., HIRST, M. & MARRA, M. A. 2009. Applications of new sequencing technologies for transcriptome analysis. *Annu Rev Genomics Hum Genet,* 10**,** 135-51.

MURAKAMI, K., MEGURO, A., OTA, M., SHIOTA, T., NOMURA, N., KASHIWAGI, K., MABUCHI, F., IIJIMA, H., KAWASE, K., YAMAMOTO, T., NAKAMURA, M., NEGI, A., SAGARA, T., NISHIDA, T., INATANI, M., TANIHARA, H., AIHARA, M., ARAIE, M., FUKUCHI, T., ABE, H., HIGASHIDE, T., SUGIYAMA, K., KANAMOTO, T., KIUCHI, Y., IWASE, A., OHNO, S., INOKO, H. & MIZUKI, N. 2010. Analysis of microsatellite polymorphisms within the GLC1F locus in Japanese patients with normal tension glaucoma. *Mol Vis,* 16**,** 462-6.

MUSCH, D. C., GILLESPIE, B. W., NIZIOL, L. M., CASHWELL, L. F. & LICHTER, P. R. 2008. Factors associated with intraocular pressure before and during 9 years of treatment in the Collaborative Initial Glaucoma Treatment Study. *Ophthalmology,* 115**,** 927-33.

MUSCH, D. C., SHIMIZU, T., NIZIOL, L. M., GILLESPIE, B. W., CASHWELL, L. F. & LICHTER, P. R. 2012. Clinical characteristics of newly diagnosed primary, pigmentary and pseudoexfoliative open-angle glaucoma in the Collaborative Initial Glaucoma Treatment Study. *Br J Ophthalmol,* 96**,** 1180-4.

NAG, A., VENTURINI, C., SMALL, K. S., YOUNG, T. L., VISWANATHAN, A. C., MACKEY, D. A., HYSI, P. G. & HAMMOND, C. 2014. A genome-wide association study of intra-ocular pressure suggests a novel association in the gene FAM125B in the TwinsUK cohort. *Hum Mol Genet,* 23**,** 3343-8.

NAGABHUSHANA, A., CHALASANI, M. L., JAIN, N., RADHA, V., RANGARAJ, N., BALASUBRAMANIAN, D. & SWARUP, G. 2010. Regulation of endocytic trafficking of transferrin receptor by optineurin and its impairment by a glaucoma-associated mutant. *BMC Cell Biol,* 11**,** 4.

NAKANO, M., IKEDA, Y., TOKUDA, Y., FUWA, M., OMI, N., UENO, M., IMAI, K., ADACHI, H., KAGEYAMA, M., MORI, K., KINOSHITA, S. & TASHIRO, K. 2012. Common variants in CDKN2B-AS1 associated with optic-nerve vulnerability of glaucoma identified by genome-wide association studies in Japanese. *PLoS One,* 7**,** e33389.

NAROOIE-NEJAD, M., PAYLAKHI, S. H., SHOJAEE, S., FAZLALI, Z., REZAEI KANAVI, M., NILFORUSHAN, N., YAZDANI, S., BABRZADEH, F., SURI, F., RONAGHI, M., ELAHI, E. & PAISAN-RUIZ, C. 2009. Loss of function mutations in the gene encoding latent transforming growth factor beta binding protein 2, LTBP2, cause primary congenital glaucoma. *Hum Mol Genet,* 18**,** 3969-77.

NATARAJAN, M., DAS, K. & JEGANATHAN, J. 2013. Comparison of central corneal thickness of primary open angle glaucoma patients with normal controls in South India. *Oman J Ophthalmol,* 6**,** 33-6.

NEMESURE, B., HE, Q., MENDELL, N., WU, S. Y., HEJTMANCIK, J. F., HENNIS, A. & LESKE, M. C. 2001. Inheritance of open-angle glaucoma in the Barbados family study. *Am J Med Genet,* 103**,** 36-43.

NEMESURE, B., HONKANEN, R., HENNIS, A., WU, S. Y. & LESKE, M. C. 2007. Incident open-angle glaucoma and intraocular pressure. *Ophthalmology,* 114**,** 1810-5.

NG, P. C., LEVY, S., HUANG, J., STOCKWELL, T. B., WALENZ, B. P., LI, K., AXELROD, N., BUSAM, D. A., STRAUSBERG, R. L. & VENTER, J. C. 2008. Genetic variation in an individual human exome. *PLoS Genet,* 4**,** e1000160.

NG, S. K., CASSON, R. J., BURDON, K. P. & CRAIG, J. E. 2014. Chromosome 9p21 primary open-angle glaucoma susceptibility locus: a review. *Clin Experiment Ophthalmol,* 42**,** 25-32.

NGUYEN, R. L., RAJA, S. C. & TRABOULSI, E. I. 2000. Screening relatives of patients with familial chronic open angle glaucoma. *Ophthalmology,* 107**,** 1294-7.

NGUYEN, T. D., CHEN, P., HUANG, W. D., CHEN, H., JOHNSON, D. & POLANSKY, J. R. 1998. Gene structure and properties of TIGR, an olfactomedin-related glycoprotein cloned from glucocorticoid-induced trabecular meshwork cells. *J Biol Chem,* 273**,** 6341-50.

NISHIDA, K., ADACHI, W., SHIMIZU-MATSUMOTO, A., KINOSHITA, S., MIZUNO, K., MATSUBARA, K. & OKUBO, K. 1996. A gene expression profile of human corneal epithelium and the isolation of human keratin 12 cDNA. *Invest Ophthalmol Vis Sci,* 37**,** 1800-9.

OLIVER, J. E., HATTENHAUER, M. G., HERMAN, D., HODGE, D. O., KENNEDY, R., FANG-YEN, M. & JOHNSON, D. H. 2002. Blindness and glaucoma: a comparison of patients progressing to blindness from glaucoma with patients maintaining vision. *Am J Ophthalmol,* 133**,** 764-72.

ORRENIUS, S., ZHIVOTOVSKY, B. & NICOTERA, P. 2003. Regulation of cell death: the calcium-apoptosis link. *Nat Rev Mol Cell Biol,* 4**,** 552-65.

OSBORNE, N. N. 2008. Pathogenesis of ganglion "cell death" in glaucoma and neuroprotection: focus on ganglion cell axonal mitochondria. *Prog Brain Res,* 173**,** 339-52.

OSMAN, W., LOW, S. K., TAKAHASHI, A., KUBO, M. & NAKAMURA, Y. 2012. A genome-wide association study in the Japanese population confirms 9p21 and 14q23 as susceptibility loci for primary open angle glaucoma. *Hum Mol Genet,* 21**,** 2836-42.

OZEL, A. B., MOROI, S. E., REED, D. M., NIKA, M., SCHMIDT, C. M., AKBARI, S., SCOTT, K., ROZSA, F., PAWAR, H., MUSCH, D. C., LICHTER, P. R., GAASTERLAND, D., BRANHAM, K., GILBERT, J., GARNAI, S. J., CHEN, W., OTHMAN, M., HECKENLIVELY, J., SWAROOP, A., ABECASIS, G., FRIEDMAN, D. S., ZACK, D., ASHLEY-KOCH, A., ULMER, M., KANG, J. H., LIU, Y., YASPAN, B. L., HAINES, J., ALLINGHAM, R. R., HAUSER, M. A., PASQUALE, L., WIGGS, J., RICHARDS, J. E. & LI, J. Z. 2014. Genome-wide association study and meta-analysis of intraocular pressure. *Hum Genet,* 133**,** 41-57.

OZSOLAK, F. & MILOS, P. M. 2011. RNA sequencing: advances, challenges and opportunities. *Nat Rev Genet,* 12**,** 87-98.

PAKRAVAN, M., PARSA, A., SANAGOU, M. & PARSA, C. F. 2007. Central corneal thickness and correlation to optic disc size: a potential link for susceptibility to glaucoma. *Br J Ophthalmol,* 91**,** 26-8.

PANG, C. P., FAN, B. J., CANLAS, O., WANG, D. Y., DUBOIS, S., TAM, P. O., LAM, D. S., RAYMOND, V. & RITCH, R. 2006. A genome-wide scan maps a novel juvenile-onset primary open angle glaucoma locus to chromosome 5q. *Mol Vis,* 12**,** 85-92.

PARK, B., YING, H., SHEN, X., PARK, J. S., QIU, Y., SHYAM, R. & YUE, B. Y. 2010. Impairment of protein trafficking upon overexpression and mutation of optineurin. *PLoS One,* 5**,** e11547.

PARK, B. C., SHEN, X., SAMARAWEERA, M. & YUE, B. Y. 2006. Studies of optineurin, a glaucoma gene: Golgi fragmentation and cell death from overexpression of wild-type and mutant optineurin in two ocular cell types. *Am J Pathol,* 169**,** 1976-89.

PARK, B. C., TIBUDAN, M., SAMARAWEERA, M., SHEN, X. & YUE, B. Y. 2007. Interaction between two glaucoma genes, optineurin and myocilin. *Genes Cells,* 12**,** 969-79.

PASCOLINI, D. & MARIOTTI, S. P. 2012. Global estimates of visual impairment: 2010. *Br J Ophthalmol,* 96**,** 614-8.

PASUTTO, F., CHAVARRIA-SOLEY, G., MARDIN, C. Y., MICHELS-RAUTENSTRAUSS, K., INGELMAN-SUNDBERG, M., FERNANDEZ-MARTINEZ, L., WEBER, B. H., RAUTENSTRAUSS, B. & REIS, A. 2010. Heterozygous loss-of-function variants in CYP1B1 predispose to primary open-angle glaucoma. *Invest Ophthalmol Vis Sci,* 51**,** 249-54.

PASUTTO, F., KELLER, K. E., WEISSCHUH, N., STICHT, H., SAMPLES, J. R., YANG, Y. F., ZENKEL, M., SCHLOTZER-SCHREHARDT, U., MARDIN, C. Y., FREZZOTTI, P., EDMUNDS, B., KRAMER, P. L., GRAMER, E., REIS, A., ACOTT, T. S. & WIRTZ, M. K. 2012. Variants in ASB10 are associated with open-angle glaucoma. *Hum Mol Genet,* 21**,** 1336-49.

PASUTTO, F., MARDIN, C. Y., MICHELS-RAUTENSTRAUSS, K., WEBER, B. H., STICHT, H., CHAVARRIA-SOLEY, G., RAUTENSTRAUSS, B., KRUSE, F. & REIS, A. 2008. Profiling of WDR36 missense variants in German patients with glaucoma. *Invest Ophthalmol Vis Sci,* 49**,** 270-4.

PASUTTO, F., MATSUMOTO, T., MARDIN, C. Y., STICHT, H., BRANDSTATTER, J. H., MICHELS-RAUTENSTRAUSS, K., WEISSCHUH, N., GRAMER, E., RAMDAS, W. D., VAN KOOLWIJK, L. M., KLAVER, C. C., VINGERLING, J. R., WEBER, B. H., KRUSE, F. E., RAUTENSTRAUSS, B., BARDE, Y. A. & REIS, A. 2009. Heterozygous NTF4 mutations impairing neurotrophin-4 signaling in patients with primary open-angle glaucoma. *Am J Hum Genet,* 85**,** 447-56.

PATEL, H. Y., RICHARDS, A. J., DE KAROLYI, B., BEST, S. J., DANESH-MEYER, H. V. & VINCENT, A. L. 2012. Screening glaucoma genes in adult glaucoma suggests a multiallelic contribution of CYP1B1 to open-angle glaucoma phenotypes. *Clin Experiment Ophthalmol,* 40**,** e208-17.

PENGELLY, R. J., TAPPER, W., GIBSON, J., KNUT, M., TEARLE, R., COLLINS, A. & ENNIS, S. 2015. Whole genome sequences are required to fully resolve the linkage disequilibrium structure of human populations. *BMC Genomics,* 16**,** 666.

PERERA, S. A., WONG, T. Y., TAY, W. T., FOSTER, P. J., SAW, S. M. & AUNG, T. 2010. Refractive error, axial dimensions, and primary open-angle glaucoma: the Singapore Malay Eye Study. *Arch Ophthalmol,* 128**,** 900-5.

PHILOMENADIN, F. S., ASOKAN, R., N, V., GEORGE, R., LINGAM, V. & SARANGAPANI, S. 2015. Genetic association of SNPs near ATOH7, CARD10, CDKN2B, CDC7 and SIX1/SIX6 with the endophenotypes of primary open angle glaucoma in Indian population. *PLoS One,* 10**,** e0119703.

PLASILOVA, M., STOILOV, I., SARFARAZI, M., KADASI, L., FERAKOVA, E. & FERAK, V. 1999. Identification of a single ancestral CYP1B1 mutation in Slovak Gypsies (Roms) affected with primary congenital glaucoma. *J Med Genet,* 36**,** 290-4.

POVOA, C. A., MALTA, R. F., REZENDE MDE, M., DE MELO, K. F. & GIANNELLA-NETO, D. 2006. Correlation between genotype and phenotype in primary open angle glaucoma of Brazilian families with mutations in exon 3 of the TIGR/MYOC gene. *Arq Bras Oftalmol,* 69**,** 289-97.

PURCELL, S., NEALE, B., TODD-BROWN, K., THOMAS, L., FERREIRA, M. A., BENDER, D., MALLER, J., SKLAR, P., DE BAKKER, P. I., DALY, M. J. & SHAM, P. C. 2007. PLINK: a tool set for whole-genome association and population-based linkage analyses. *Am J Hum Genet,* 81**,** 559-75.

PURCELL, S. M., MORAN, J. L., FROMER, M., RUDERFER, D., SOLOVIEFF, N., ROUSSOS, P., O'DUSHLAINE, C., CHAMBERT, K., BERGEN, S. E., KAHLER, A., DUNCAN, L., STAHL, E., GENOVESE, G., FERNANDEZ, E., COLLINS, M. O., KOMIYAMA, N. H., CHOUDHARY, J. S., MAGNUSSON, P. K., BANKS, E., SHAKIR, K., GARIMELLA, K., FENNELL, T., DEPRISTO, M., GRANT, S. G., HAGGARTY, S. J., GABRIEL, S., SCOLNICK, E. M., LANDER, E. S., HULTMAN, C. M., SULLIVAN, P. F., MCCARROLL, S. A. & SKLAR, P. 2014. A polygenic burden of rare disruptive mutations in schizophrenia. *Nature,* 506**,** 185-90.

QIU, M., WANG, S. Y., SINGH, K. & LIN, S. C. 2013. Association between myopia and glaucoma in the United States population. *Invest Ophthalmol Vis Sci,* 54**,** 830-5.

QUIGLEY, H. A. 2011. Glaucoma. *Lancet,* 377**,** 1367-77.

QUIGLEY, H. A. & BROMAN, A. T. 2006. The number of people with glaucoma worldwide in 2010 and 2020. *Br J Ophthalmol,* 90**,** 262-7.

QUIGLEY, H. A., ENGER, C., KATZ, J., SOMMER, A., SCOTT, R. & GILBERT, D. 1994. Risk factors for the development of glaucomatous visual field loss in ocular hypertension. *Arch Ophthalmol,* 112**,** 644-9.

QUIGLEY, H. A., MCKINNON, S. J., ZACK, D. J., PEASE, M. E., KERRIGAN-BAUMRIND, L. A., KERRIGAN, D. F. & MITCHELL, R. S. 2000. Retrograde axonal transport of BDNF in retinal ganglion cells is blocked by acute IOP elevation in rats. *Invest Ophthalmol Vis Sci,* 41**,** 3460-6.

QUIGLEY, H. A., VARMA, R., TIELSCH, J. M., KATZ, J., SOMMER, A. & GILBERT, D. L. 1999. The relationship between optic disc area and open-angle glaucoma: the Baltimore Eye Survey. *J Glaucoma,* 8**,** 347-52.

RAIDA, Z., HUNDAHL, C. A., NYENGAARD, J. R. & HAY-SCHMIDT, A. 2013. Neuroglobin over expressing mice: expression pattern and effect on brain ischemic infarct size. *PLoS One,* 8**,** e76565.

RAMALINGAM, M. & KIM, S. J. 2015. Insulin exerts neuroprotective effects via Akt/Bcl-2 signaling pathways in differentiated SH-SY5Y cells. *J Recept Signal Transduct Res,* 35**,** 1-7.

RAMDAS, W. D., AMIN, N., VAN KOOLWIJK, L. M., JANSSENS, A. C., DEMIRKAN, A., DE JONG, P. T., AULCHENKO, Y. S., WOLFS, R. C., HOFMAN, A., RIVADENEIRA, F., UITTERLINDEN, A. G., OOSTRA, B. A., LEMIJ, H. G., KLAVER, C. C., VINGERLING, J. R., JANSONIUS, N. M. & VAN DUIJN, C. M. 2011a. Genetic architecture of open angle glaucoma and related determinants. *J Med Genet,* 48**,** 190-6.

RAMDAS, W. D., VAN KOOLWIJK, L. M., CREE, A. J., JANSSENS, A. C., AMIN, N., DE JONG, P. T., WOLFS, R. C., GIBSON, J., KIRWAN, J. F., HOFMAN, A., RIVADENEIRA, F., OOSTRA, B. A., UITTERLINDEN, A. G., ENNIS, S., LOTERY, A. J., LEMIJ, H. G., KLAVER, C. C., VINGERLING, J. R., JANSONIUS, N. M. & VAN DUIJN, C. M. 2011b. Clinical implications of old and new genes for open-angle glaucoma. *Ophthalmology,* 118**,** 2389-97.

RAMDAS, W. D., VAN KOOLWIJK, L. M., IKRAM, M. K., JANSONIUS, N. M., DE JONG, P. T., BERGEN, A. A., ISAACS, A., AMIN, N., AULCHENKO, Y. S., WOLFS, R. C., HOFMAN, A., RIVADENEIRA, F., OOSTRA, B. A., UITTERLINDEN, A. G., HYSI, P., HAMMOND, C. J., LEMIJ, H. G., VINGERLING, J. R., KLAVER, C. C. & VAN DUIJN, C. M. 2010. A genome-wide association study of optic disc parameters. *PLoS Genet,* 6**,** e1000978.

RAMDAS, W. D., VAN KOOLWIJK, L. M., LEMIJ, H. G., PASUTTO, F., CREE, A. J., THORLEIFSSON, G., JANSSEN, S. F., JACOLINE, T. B., AMIN, N., RIVADENEIRA, F., WOLFS, R. C., WALTERS, G. B., JONASSON, F., WEISSCHUH, N., MARDIN, C. Y., GIBSON, J., ZEGERS, R. H., HOFMAN, A., DE JONG, P. T., UITTERLINDEN, A. G., OOSTRA, B. A., THORSTEINSDOTTIR, U., GRAMER, E., WELGEN-LUSSEN, U. C., KIRWAN, J. F., BERGEN, A. A., REIS, A., STEFANSSON, K., LOTERY, A. J., VINGERLING, J. R., JANSONIUS, N. M., KLAVER, C. C. & VAN DUIJN, C. M. 2011c. Common genetic variants associated with open-angle glaucoma. *Hum Mol Genet,* 20**,** 2464-71.

RAO, K. N., KAUR, I., PARIKH, R. S., MANDAL, A. K., CHANDRASEKHAR, G., THOMAS, R. & CHAKRABARTI, S. 2010. Variations in NTF4, VAV2, and VAV3 genes are not involved with primary open-angle and primary angle-closure glaucomas in an indian population. *Invest Ophthalmol Vis Sci,* 51**,** 4937-41.

RATAN, A., MILLER, W., GUILLORY, J., STINSON, J., SESHAGIRI, S. & SCHUSTER, S. C. 2013. Comparison of sequencing platforms for single nucleotide variant calls in a human sample. *PLoS One,* 8**,** e55089.

RAU, C. S., YANG, J. C., CHEN, Y. C., WU, C. J., LU, T. H., TZENG, S. L., WU, Y. C. & HSIEH, C. H. 2014. Lipopolysaccharide-induced microRNA-146a targets CARD10 and regulates angiogenesis in human umbilical vein endothelial cells. *Toxicol Sci,* 140**,** 315-26.

RESCH, Z. T. & FAUTSCH, M. P. 2009. Glaucoma-associated myocilin: a better understanding but much more to learn. *Exp Eye Res,* 88**,** 704-12.

REZAIE, T., CHILD, A., HITCHINGS, R., BRICE, G., MILLER, L., COCA-PRADOS, M., HEON, E., KRUPIN, T., RITCH, R., KREUTZER, D., CRICK, R. P. & SARFARAZI, M. 2002. Adult-onset primary open-angle glaucoma caused by mutations in optineurin. *Science,* 295**,** 1077-9.

RICHARDS, J. E., LICHTER, P. R., BOEHNKE, M., URO, J. L., TORREZ, D., WONG, D. & JOHNSON, A. T. 1994. Mapping of a gene for autosomal dominant juvenile-onset open-angle glaucoma to chromosome Iq. *Am J Hum Genet,* 54**,** 62-70.

RIECK, J. 2013. The pathogenesis of glaucoma in the interplay with the immune system. *Invest Ophthalmol Vis Sci,* 54**,** 2393-409.

RITCH, R., DARBRO, B., MENON, G., KHANNA, C. L., SOLIVAN-TIMPE, F., ROOS, B. R., SARFARZI, M., KAWASE, K., YAMAMOTO, T., ROBIN, A. L., LOTERY, A. J. & FINGERT, J. H. 2014. TBK1 gene duplication and normal-tension glaucoma. *JAMA Ophthalmol,* 132**,** 544-8.

ROBINSON, M. D., MCCARTHY, D. J. & SMYTH, G. K. 2010. edgeR: a Bioconductor package for differential expression analysis of digital gene expression data. *Bioinformatics,* 26**,** 139-40.

ROGERS, D. L., CANTOR, R. N., CATOIRA, Y., CANTOR, L. B. & WUDUNN, D. 2007. Central corneal thickness and visual field loss in fellow eyes of patients with open-angle glaucoma. *Am J Ophthalmol,* 143**,** 159-61.

ROZSA, F. W., SHIMIZU, S., LICHTER, P. R., JOHNSON, A. T., OTHMAN, M. I., SCOTT, K., DOWNS, C. A., NGUYEN, T. D., POLANSKY, J. & RICHARDS, J. E. 1998. GLC1A mutations point to regions of potential functional importance on the TIGR/MYOC protein. *Mol Vis,* 4**,** 20.

RUDNICKA, A. R., MT-ISA, S., OWEN, C. G., COOK, D. G. & ASHBY, D. 2006. Variations in primary open-angle glaucoma prevalence by age, gender, and race: a Bayesian meta-analysis. *Invest Ophthalmol Vis Sci,* 47**,** 4254-61.

RUGGIERO, L., CONNOR, M. P., CHEN, J., LANGEN, R. & FINNEMANN, S. C. 2012. Diurnal, localized exposure of phosphatidylserine by rod outer segment tips in wild-type but not Itgb5-/- or Mfge8-/- mouse retina. *Proc Natl Acad Sci U S A,* 109**,** 8145-8.

RUSSELL, P., TAMM, E. R., GREHN, F. J., PICHT, G. & JOHNSON, M. 2001. The presence and properties of myocilin in the aqueous humor. *Invest Ophthalmol Vis Sci,* 42**,** 983-6.

SACCA, S. C., PULLIERO, A. & IZZOTTI, A. 2015. The dysfunction of the trabecular meshwork during glaucoma course. *J Cell Physiol,* 230**,** 510-25.

SAHLENDER, D. A., ROBERTS, R. C., ARDEN, S. D., SPUDICH, G., TAYLOR, M. J., LUZIO, J. P., KENDRICK-JONES, J. & BUSS, F. 2005. Optineurin links myosin VI to the Golgi complex and is involved in Golgi organization and exocytosis. *J Cell Biol,* 169**,** 285-95.

SAKAMOTO, K., KUROKI, T., OKUNO, Y., SEKIYA, H., WATANABE, A., SAGAWA, T., ITO, H., MIZUTA, A., MORI, A., NAKAHARA, T. & ISHII, K. 2014. Activation of the TRPV1 channel attenuates N-methyl-D-aspartic acid-induced neuronal injury in the rat retina. *Eur J Pharmacol,* 733**,** 13-22.

SALE, M. M., FITZGERALD, L. M., KAGAME, K., ERDMANN, I., CRAIG, J. E., DICKINSON, J. L. & COOPER, R. L. 2002. Investigation of the prevalence of the myocilin Q368STOP mutation in Ugandan glaucoma patients. *Ophthalmic Genet,* 23**,** 67-9.

SANGER, F. & COULSON, A. R. 1975. A rapid method for determining sequences in DNA by primed synthesis with DNA polymerase. *J Mol Biol,* 94**,** 441-8.

SANGER, F., NICKLEN, S. & COULSON, A. R. 1977. DNA sequencing with chain-terminating inhibitors. *Proc Natl Acad Sci U S A,* 74**,** 5463-7.

SARFARAZI, M., AKARSU, A. N., HOSSAIN, A., TURACLI, M. E., AKTAN, S. G., BARSOUM-HOMSY, M., CHEVRETTE, L. & SAYLI, B. S. 1995. Assignment of a locus (GLC3A) for primary congenital glaucoma (Buphthalmos) to 2p21 and evidence for genetic heterogeneity. *Genomics,* 30**,** 171-7.

SARFARAZI, M., CHILD, A., STOILOVA, D., BRICE, G., DESAI, T., TRIFAN, O. C., POINOOSAWMY, D. & CRICK, R. P. 1998. Localization of the fourth locus (GLC1E) for adult-onset primary open-angle glaucoma to the 10p15-p14 region. *Am J Hum Genet,* 62**,** 641-52.

SCHMIDT-KASTNER, R., HABERKAMP, M., SCHMITZ, C., HANKELN, T. & BURMESTER, T. 2006. Neuroglobin mRNA expression after transient global brain ischemia and prolonged hypoxia in cell culture. *Brain Res,* 1103**,** 173-80.

SCHMIDT, M., GIESSL, A., LAUFS, T., HANKELN, T., WOLFRUM, U. & BURMESTER, T. 2003. How does the eye breathe? Evidence for neuroglobin-mediated oxygen supply in the mammalian retina. *J Biol Chem,* 278**,** 1932-5.

SCUDIERO, I., VITO, P. & STILO, R. 2014. The three CARMA sisters: so different, so similar: a portrait of the three CARMA proteins and their involvement in human disorders. *J Cell Physiol,* 229**,** 990-7.

SENA, D. F. & LINDSLEY, K. 2013. Neuroprotection for treatment of glaucoma in adults. *Cochrane Database Syst Rev,* 2**,** Cd006539.

SENATOROV, V., MALYUKOVA, I., FARISS, R., WAWROUSEK, E. F., SWAMINATHAN, S., SHARAN, S. K. & TOMAREV, S. 2006. Expression of mutated mouse myocilin induces open-angle glaucoma in transgenic mice. *J Neurosci,* 26**,** 11903-14.

SHANNON, P., MARKIEL, A., OZIER, O., BALIGA, N. S., WANG, J. T., RAMAGE, D., AMIN, N., SCHWIKOWSKI, B. & IDEKER, T. 2003. Cytoscape: a software environment for integrated models of biomolecular interaction networks. *Genome Res,* 13**,** 2498-504.

SHEFFIELD, V. C., STONE, E. M., ALWARD, W. L., DRACK, A. V., JOHNSON, A. T., STREB, L. M. & NICHOLS, B. E. 1993. Genetic linkage of familial open angle glaucoma to chromosome 1q21-q31. *Nat Genet,* 4**,** 47-50.

SHEN, X., YING, H., QIU, Y., PARK, J. S., SHYAM, R., CHI, Z. L., IWATA, T. & YUE, B. Y. 2011. Processing of optineurin in neuronal cells. *J Biol Chem,* 286**,** 3618-29.

SHEN, X., YING, H. & YUE, B. Y. 2012. Wnt activation by wild type and mutant myocilin in cultured human trabecular meshwork cells. *PLoS One,* 7**,** e44902.

SHIGEEDA, T., TOMIDOKORO, A., ARAIE, M., KOSEKI, N. & YAMAMOTO, S. 2002. Long-term follow-up of visual field progression after trabeculectomy in progressive normal-tension glaucoma. *Ophthalmology,* 109**,** 766-70.

SHIMIZU, S., LICHTER, P. R., JOHNSON, A. T., ZHOU, Z., HIGASHI, M., GOTTFREDSDOTTIR, M., OTHMAN, M., MOROI, S. E., ROZSA, F. W., SCHERTZER, R. M., CLARKE, M. S., SCHWARTZ, A. L., DOWNS, C. A., VOLLRATH, D. & RICHARDS, J. E. 2000. Age-dependent prevalence of mutations at the GLC1A locus in primary open-angle glaucoma. *Am J Ophthalmol,* 130**,** 165-77.

SIGGS, O. M., SOUZEAU, E., TARANATH, D. A., DUBOWSKY, A., CHAPPELL, A., ZHOU, T., JAVADIYAN, S., NICHOLL, J., KEARNS, L. S., STAFFIERI, S. E., NARITA, A., SMITH, J. E. H., PATER, J., HEWITT, A. W., RUDDLE, J. B., ELDER, J. E., MACKEY, D. A., BURDON, K. P. & CRAIG, J. E. 2020. Biallelic CPAMD8 Variants Are a Frequent Cause of Childhood and Juvenile Open-Angle Glaucoma. *Ophthalmology,* 127**,** 758-766.

SIPPL, C., BOSSERHOFF, A. K., FISCHER, D. & TAMM, E. R. 2011. Depletion of optineurin in RGC-5 cells derived from retinal neurons causes apoptosis and reduces the secretion of neurotrophins. *Exp Eye Res,* 93**,** 669-80.

SIPPL, C., ZEILBECK, L. F., FUCHSHOFER, R. & TAMM, E. R. 2014. Optineurin associates with the podocyte Golgi complex to maintain its structure. *Cell Tissue Res,* 358**,** 567-83.

SIRBU, A., KERR, G., CRANE, M. & RUSKIN, H. J. 2012. RNA-Seq vs dual- and single-channel microarray data: sensitivity analysis for differential expression and clustering. *PLoS One,* 7**,** e50986.

SIROHI, K., CHALASANI, M. L., SUDHAKAR, C., KUMARI, A., RADHA, V. & SWARUP, G. 2013. M98K-OPTN induces transferrin receptor degradation and RAB12-mediated autophagic death in retinal ganglion cells. *Autophagy,* 9**,** 510-27.

SIU, H., ZHU, Y., JIN, L. & XIONG, M. 2011. Implication of next-generation sequencing on association studies. *BMC Genomics,* 12**,** 322.

SOHN, S., HUR, W., CHOI, Y. R., CHUNG, Y. S., KI, C. S. & KEE, C. 2010. Little evidence for association of the glaucoma gene MYOC with open-angle glaucoma. *Br J Ophthalmol,* 94**,** 639-42.

SOMMER, A. 1996. Glaucoma risk factors observed in the Baltimore Eye Survey. *Curr Opin Ophthalmol,* 7**,** 93-8.

SOUZEAU, E., BURDON, K. P., DUBOWSKY, A., GRIST, S., USHER, B., FITZGERALD, J. T., CRAWFORD, A., HEWITT, A. W., GOLDBERG, I., MILLS, R. A., RUDDLE, J. B., LANDERS, J., MACKEY, D. A. & CRAIG, J. E. 2013. Higher prevalence of myocilin mutations in advanced glaucoma in comparison with less advanced disease in an Australasian disease registry. *Ophthalmology,* 120**,** 1135-43.

SOUZEAU, E., GOLDBERG, I., HEALEY, P. R., MILLS, R. A., LANDERS, J., GRAHAM, S. L., GRIGG, J. R., USHER, B., STRAGA, T., CRAWFORD, A., CASSON, R. J., MORGAN, W. H., RUDDLE, J. B., COOTE, M. A., WHITE, A., STEWART, J., HEWITT, A. W., MACKEY, D. A., BURDON, K. P. & CRAIG, J. E. 2012. Australian and New Zealand Registry of Advanced Glaucoma: methodology and recruitment. *Clin Experiment Ophthalmol,* 40**,** 569-75.

SOUZEAU, E., HAYES, M., ZHOU, T., SIGGS, O. M., RIDGE, B., AWADALLA, M. S., SMITH, J. E., RUDDLE, J. B., ELDER, J. E., MACKEY, D. A., HEWITT, A. W., HEALEY, P. R., GOLDBERG, I., MORGAN, W. H., LANDERS, J., DUBOWSKY, A., BURDON, K. P. & CRAIG, J. E. 2015. Occurrence of CYP1B1 Mutations in Juvenile Open-Angle Glaucoma With Advanced Visual Field Loss. *JAMA Ophthalmol,* 133**,** 826-33.

SPRINGELKAMP, H., HOHN, R., MISHRA, A., HYSI, P. G., KHOR, C. C., LOOMIS, S. J., BAILEY, J. N., GIBSON, J., THORLEIFSSON, G., JANSSEN, S. F., LUO, X., RAMDAS, W. D., VITHANA, E., NONGPIUR, M. E., MONTGOMERY, G. W., XU, L., MOUNTAIN, J. E., GHARAHKHANI, P., LU, Y., AMIN, N., KARSSEN, L. C., SIM, K. S., VAN LEEUWEN, E. M., IGLESIAS, A. I., VERHOEVEN, V. J., HAUSER, M. A., LOON, S. C., DESPRIET, D. D., NAG, A., VENTURINI, C., SANFILIPPO, P. G., SCHILLERT, A., KANG, J. H., LANDERS, J., JONASSON, F., CREE, A. J., VAN KOOLWIJK, L. M., RIVADENEIRA, F., SOUZEAU, E., JONSSON, V., MENON, G., WEINREB, R. N., DE JONG, P. T., OOSTRA, B. A., UITTERLINDEN, A. G., HOFMAN, A., ENNIS, S., THORSTEINSDOTTIR, U., BURDON, K. P., SPECTOR, T. D., MIRSHAHI, A., SAW, S. M.,

VINGERLING, J. R., TEO, Y. Y., HAINES, J. L., WOLFS, R. C., LEMIJ, H. G., TAI, E. S., JANSONIUS, N. M., JONAS, J. B., CHENG, C. Y., AUNG, T., VISWANATHAN, A. C., KLAVER, C. C., CRAIG, J. E., MACGREGOR, S., MACKEY, D. A., LOTERY, A. J., STEFANSSON, K., BERGEN, A. A., YOUNG, T. L., WIGGS, J. L., PFEIFFER, N., WONG, T. Y., PASQUALE, L. R., HEWITT, A. W., VAN DUIJN, C. M. & HAMMOND, C. J. 2014. Meta-analysis of genome-wide association studies identifies novel loci that influence cupping and the glaucomatous process. *Nat Commun,* 5**,** 4883.

SPRINGELKAMP, H., IGLESIAS, A. I., MISHRA, A., HOHN, R., WOJCIECHOWSKI, R., KHAWAJA, A. P., NAG, A., WANG, Y. X., WANG, J. J., CUELLAR-PARTIDA, G., GIBSON, J., BAILEY, J. N., VITHANA, E. N., GHARAHKHANI, P., BOUTIN, T., RAMDAS, W. D., ZELLER, T., LUBEN, R. N., YONOVA-DOING, E., VISWANATHAN, A. C., YAZAR, S., CREE, A. J., HAINES, J. L., KOH, J. Y., SOUZEAU, E., WILSON, J. F., AMIN, N., MULLER, C., VENTURINI, C., KEARNS, L. S., KANG, J. H., THAM, Y. C., ZHOU, T., VAN LEEUWEN, E. M., NICKELS, S., SANFILIPPO, P., LIAO, J., VAN DER LINDE, H., ZHAO, W., VAN KOOLWIJK, L. M., ZHENG, L., RIVADENEIRA, F., BASKARAN, M., VAN DER LEE, S. J., PERERA, S., DE JONG, P. T., OOSTRA, B. A., UITTERLINDEN, A. G., FAN, Q., HOFMAN, A., TAI, E. S., VINGERLING, J. R., SIM, X., WOLFS, R. C., TEO, Y. Y., LEMIJ, H. G., KHOR, C. C., WILLEMSEN, R., LACKNER, K. J., AUNG, T., JANSONIUS, N. M., MONTGOMERY, G., WILD, P. S., YOUNG, T. L., BURDON, K. P., HYSI, P. G., PASQUALE, L. R., WONG, T. Y., KLAVER, C. C., HEWITT, A. W., JONAS, J. B., MITCHELL, P., LOTERY, A. J., FOSTER, P. J., VITART, V., PFEIFFER, N., CRAIG, J. E., MACKEY, D. A., HAMMOND, C. J., WIGGS, J. L., CHENG, C. Y., VAN DUIJN, C. M. & MACGREGOR, S. 2017. New insights into the genetics of primary open-angle glaucoma based on meta-analyses of intraocular pressure and optic disc characteristics. *Hum Mol Genet,* 26**,** 438-453.

SPRINGELKAMP, H., MISHRA, A., HYSI, P. G., GHARAHKHANI, P., HOHN, R., KHOR, C. C., COOKE BAILEY, J. N., LUO, X., RAMDAS, W. D., VITHANA, E., KOH, V., YAZAR, S., XU, L., FORWARD, H., KEARNS, L. S., AMIN, N., IGLESIAS, A. I., SIM, K. S., VAN LEEUWEN, E. M., DEMIRKAN, A., VAN DER LEE, S., LOON, S. C., RIVADENEIRA, F., NAG, A., SANFILIPPO, P. G., SCHILLERT, A., DE JONG, P. T.,

OOSTRA, B. A., UITTERLINDEN, A. G., HOFMAN, A., ZHOU, T., BURDON, K. P., SPECTOR, T. D., LACKNER, K. J., SAW, S. M., VINGERLING, J. R., TEO, Y. Y., PASQUALE, L. R., WOLFS, R. C., LEMIJ, H. G., TAI, E. S., JONAS, J. B., CHENG, C. Y., AUNG, T., JANSONIUS, N. M., KLAVER, C. C., CRAIG, J. E., YOUNG, T. L., HAINES, J. L., MACGREGOR, S., MACKEY, D. A., PFEIFFER, N., WONG, T. Y., WIGGS, J. L., HEWITT, A. W., VAN DUIJN, C. M. & HAMMOND, C. J. 2015. Meta-analysis of Genome-Wide Association Studies Identifies Novel Loci Associated With Optic Disc Morphology. *Genet Epidemiol,* 39**,** 207-16.

SPRY, P. G., SPARROW, J. M., DIAMOND, J. P. & HARRIS, H. S. 2005. Risk factors for progressive visual field loss in primary open angle glaucoma. *Eye (Lond),* 19**,** 643-51.

STEELE, M. R., INMAN, D. M., CALKINS, D. J., HORNER, P. J. & VETTER, M. L. 2006. Microarray analysis of retinal gene expression in the DBA/2J model of glaucoma. *Invest Ophthalmol Vis Sci,* 47**,** 977-85.

STOILOV, I., AKARSU, A. N. & SARFARAZI, M. 1997. Identification of three different truncating mutations in cytochrome P4501B1 (CYP1B1) as the principal cause of primary congenital glaucoma (Buphthalmos) in families linked to the GLC3A locus on chromosome 2p21. *Hum Mol Genet,* 6**,** 641-7.

STOILOVA, D., CHILD, A., BRICE, G., CRICK, R. P., FLECK, B. W. & SARFARAZI, M. 1997. Identification of a new 'TIGR' mutation in a family with juvenile-onset primary open angle glaucoma. *Ophthalmic Genet,* 18**,** 109-18.

STOILOVA, D., CHILD, A., TRIFAN, O. C., CRICK, R. P., COAKES, R. L. & SARFARAZI, M. 1996. Localization of a locus (GLC1B) for adult-onset primary open angle glaucoma to the 2cen-q13 region. *Genomics,* 36**,** 142-50.

STONE, E. M., FINGERT, J. H., ALWARD, W. L., NGUYEN, T. D., POLANSKY, J. R., SUNDEN, S. L., NISHIMURA, D., CLARK, A. F., NYSTUEN, A., NICHOLS, B. E., MACKEY, D. A., RITCH, R., KALENAK, J. W., CRAVEN, E. R. & SHEFFIELD, V. C. 1997. Identification of a gene that causes primary open angle glaucoma. *Science,* 275**,** 668-70.

STRANGE, A., BELLENGUEZ, C., SIM, X., LUBEN, R., HYSI, P. G., RAMDAS, W. D., VAN KOOLWIJK, L. M., FREEMAN, C., PIRINEN, M., SU, Z., BAND, G., PEARSON, R., VUKCEVIC, D., LANGFORD, C., DELOUKAS, P., HUNT, S., GRAY, E., DRONOV, S., POTTER, S. C., TASHAKKORI-GHANBARIA, A., EDKINS, S., BUMPSTEAD, S. J., BLACKWELL, J. M., BRAMON, E., BROWN, M. A., CASAS, J. P., CORVIN, A., DUNCANSON, A., JANKOWSKI, J. A., MARKUS, H. S., MATHEW, C. G., PALMER, C. N., PLOMIN, R., RAUTANEN, A., SAWCER, S. J., TREMBATH, R. C., WOOD, N. W., BARROSO, I., PELTONEN, L., HEALEY, P., MCGUFFIN, P., TOPOUZIS, F., KLAVER, C. C., VAN DUIJN, C. M., MACKEY, D. A., YOUNG, T. L., HAMMOND, C. J., KHAW, K. T., WAREHAM, N., WANG, J. J., WONG, T. Y., FOSTER, P. J., MITCHELL, P., SPENCER, C. C., DONNELLY, P. & VISWANATHAN, A. C. 2013. Genome-wide association study of intraocular pressure identifies the GLCCI1/ICA1 region as a glaucoma susceptibility locus. *Hum Mol Genet,* 22**,** 4653-60.

STRINGER, C. 2003. Human evolution: Out of Ethiopia. *Nature,* 423**,** 692-3, 695.

SU, C. C., LIU, Y. F., LI, S. Y., YANG, J. J. & YEN, Y. C. 2012. Mutations in the CYP1B1 gene may contribute to juvenile-onset open-angle glaucoma. *Eye (Lond),* 26**,** 1369-77.

SUEMATSU, N., HOSODA, M. & FUJIMORI, K. 2011. Protective effects of quercetin against hydrogen peroxide-induced apoptosis in human neuronal SH-SY5Y cells. *Neurosci Lett,* 504**,** 223-7.

SULLIVAN-MEE, M., HALVERSON, K. D., SAXON, G. B., SAXON, M. C. & QUALLS, C. 2006. Relationship between central corneal thickness and severity of glaucomatous visual field loss in a primary care population. *Optometry,* 77**,** 40-6.

SUN, J., ZHOU, X., KANG, Y., YAN, L., SUN, X., SUI, H., QIN, D. & YUAN, H. 2012. Prevalence and risk factors for primary open-angle glaucoma in a rural northeast China population: a population-based survey in Bin County, Harbin. *Eye (Lond),* 26**,** 283-91.

SUN, Y., JIN, K., MAO, X. O., ZHU, Y. & GREENBERG, D. A. 2001. Neuroglobin is up-regulated by and protects neurons from hypoxic-ischemic injury. *Proc Natl Acad Sci U S A,* 98**,** 15306-11.

SUNG, V. C., KOPPENS, J. M., VERNON, S. A., PAWSON, P., RUBINSTEIN, M., KING, A. J. & TATTERSALL, C. L. 2006. Longitudinal glaucoma screening for siblings of patients with primary open angle glaucoma: the Nottingham Family Glaucoma Screening Study. *Br J Ophthalmol,* 90**,** 59-63.

SURI, F., KALHOR, R., ZARGAR, S. J., NILFOROOSHAN, N., YAZDANI, S., NEZARI, H., PAYLAKHI, S. H., NAROOIE-NEJHAD, M., BAYAT, B., SEDAGHATI, T., AHMADIAN, A. & ELAHI, E. 2008. Screening of common CYP1B1 mutations in Iranian POAG patients using a microarray-based PrASE protocol. *Mol Vis,* 14**,** 2349-56.

SURIYAPPERUMA, S. P., CHILD, A., DESAI, T., BRICE, G., KERR, A., CRICK, R. P. & SARFARAZI, M. 2007. A new locus (GLC1H) for adult-onset primary open-angle glaucoma maps to the 2p15-p16 region. *Arch Ophthalmol,* 125**,** 86-92.

SUZUKI, Y., IWASE, A., ARAIE, M., YAMAMOTO, T., ABE, H., SHIRATO, S., KUWAYAMA, Y., MISHIMA, H. K., SHIMIZU, H., TOMITA, G., INOUE, Y. & KITAZAWA, Y. 2006. Risk factors for open-angle glaucoma in a Japanese population: the Tajimi Study. *Ophthalmology,* 113**,** 1613-7.

TACHMAZIDOU, I., MORRIS, A. & ZEGGINI, E. 2012. Rare variant association testing for next-generation sequencing data via hierarchical clustering. *Hum Hered,* 74**,** 165-71.

TAKAMOTO, M., KABURAKI, T., MABUCHI, A., ARAIE, M., AMANO, S., AIHARA, M., TOMIDOKORO, A., IWASE, A., MABUCHI, F., KASHIWAGI, K., SHIRATO, S., YASUDA, N., KAWASHIMA, H., NAKAJIMA, F., NUMAGA, J., KAWAMURA, Y., SASAKI, T. & TOKUNAGA, K. 2012. Common variants on chromosome 9p21 are associated with normal tension glaucoma. *PLoS One,* 7**,** e40107.

TAKANOSU, M., BOYD, T. C., LE GOFF, M., HENRY, S. P., ZHANG, Y., BISHOP, P. N. & MAYNE, R. 2001. Structure, chromosomal location, and tissue-specific expression of the mouse opticin gene. *Invest Ophthalmol Vis Sci,* 42**,** 2202-10.

TAKATSU, H., BABA, K., SHIMA, T., UMINO, H., KATO, U., UMEDA, M., NAKAYAMA, K. & SHIN, H. W. 2011. ATP9B, a P4-ATPase (a putative aminophospholipid translocase), localizes to the trans-Golgi network in a CDC50 protein-independent manner. *J Biol Chem,* 286**,** 38159-67.

TANWAR, M., DADA, T., SIHOTA, R., DAS, T. K., YADAV, U. & DADA, R. 2009. Mutation spectrum of CYP1B1 in North Indian congenital glaucoma patients. *Mol Vis,* 15**,** 1200-9.

TENNESSEN, J. A., BIGHAM, A. W., O'CONNOR, T. D., FU, W., KENNY, E. E., GRAVEL, S., MCGEE, S., DO, R., LIU, X., JUN, G., KANG, H. M., JORDAN, D., LEAL, S. M., GABRIEL, S., RIEDER, M. J., ABECASIS, G., ALTSHULER, D., NICKERSON, D. A., BOERWINKLE, E., SUNYAEV, S., BUSTAMANTE, C. D., BAMSHAD, M. J. & AKEY, J. M. 2012. Evolution and functional impact of rare coding variation from deep sequencing of human exomes. *Science,* 337**,** 64-9.

TEZEL, G. 2006. Oxidative stress in glaucomatous neurodegeneration: mechanisms and consequences. *Prog Retin Eye Res,* 25**,** 490-513.

THAM, Y. C., LI, X., WONG, T. Y., QUIGLEY, H. A., AUNG, T. & CHENG, C. Y. 2014. Global prevalence of glaucoma and projections of glaucoma burden through 2040: a systematic review and meta-analysis. *Ophthalmology,* 121**,** 2081-90.

THORLEIFSSON, G., WALTERS, G. B., HEWITT, A. W., MASSON, G., HELGASON, A., DEWAN, A., SIGURDSSON, A., JONASDOTTIR, A., GUDJONSSON, S. A., MAGNUSSON, K. P., STEFANSSON, H., LAM, D. S., TAM, P. O., GUDMUNDSDOTTIR, G. J., SOUTHGATE, L., BURDON, K. P., GOTTFREDSDOTTIR, M. S., ALDRED, M. A., MITCHELL, P., ST CLAIR, D., COLLIER, D. A., TANG, N., SVEINSSON, O., MACGREGOR, S., MARTIN, N. G., CREE, A. J., GIBSON, J., MACLEOD, A., JACOB, A., ENNIS, S., YOUNG, T. L., CHAN, J. C., KARWATOWSKI, W. S., HAMMOND, C. J., THORDARSON, K., ZHANG, M., WADELIUS, C., LOTERY, A. J., TREMBATH, R. C., PANG, C. P., HOH, J., CRAIG, J. E., KONG, A., MACKEY, D. A., JONASSON, F., THORSTEINSDOTTIR, U. & STEFANSSON, K. 2010. Common variants near CAV1 and CAV2 are associated with primary open-angle glaucoma. *Nat Genet,* 42**,** 906-9.

TIELSCH, J. M., KATZ, J., SOMMER, A., QUIGLEY, H. A. & JAVITT, J. C. 1994. Family history and risk of primary open angle glaucoma. The Baltimore Eye Survey. *Arch Ophthalmol,* 112**,** 69-73.

TOMAREV, S. I., WISTOW, G., RAYMOND, V., DUBOIS, S. & MALYUKOVA, I. 2003. Gene expression profile of the human trabecular meshwork: NEIBank sequence tag analysis. *Invest Ophthalmol Vis Sci,* 44**,** 2588-96.

TRAPNELL, C., PACHTER, L. & SALZBERG, S. L. 2009. TopHat: discovering splice junctions with RNA-Seq. *Bioinformatics,* 25**,** 1105-11.

TRIFAN, O. C., TRABOULSI, E. I., STOILOVA, D., ALOZIE, I., NGUYEN, R., RAJA, S. & SARFARAZI, M. 1998. A third locus (GLC1D) for adult-onset primary open-angle glaucoma maps to the 8q23 region. *Am J Ophthalmol,* 126**,** 17-28.

TUCCARI, G., TROMBETTA, C., GIARDINELLI, M. M., ARENA, F. & BARRESI, G. 1986. Distribution of glial fibrillary acidic protein in normal and gliotic human retina. *Basic Appl Histochem,* 30**,** 425-32.

TURKMEN, N., EREN, B., FEDAKAR, R., AKGOZ, S. & COMUNOGLU, N. 2008. Glial fibrillary acidic protein (GFAP) and CD34 expression in the human optic nerve and brain in methanol toxicity. *Adv Ther,* 25**,** 123-32.

TURTURRO, S., SHEN, X., SHYAM, R., YUE, B. Y. & YING, H. 2014. Effects of mutations and deletions in the human optineurin gene. *Springerplus,* 3**,** 99.

UHLER, T. A. & PILTZ-SEYMOUR, J. 2008. Optic disc hemorrhages in glaucoma and ocular hypertension: implications and recommendations. *Curr Opin Ophthalmol,* 19**,** 89-94.

ULMER, M., LI, J., YASPAN, B. L., OZEL, A. B., RICHARDS, J. E., MOROI, S. E., HAWTHORNE, F., BUDENZ, D. L., FRIEDMAN, D. S., GAASTERLAND, D., HAINES, J., KANG, J. H., LEE, R., LICHTER, P., LIU, Y., PASQUALE, L. R., PERICAK-VANCE, M., REALINI, A., SCHUMAN, J. S., SINGH, K., VOLLRATH, D., WEINREB, R., WOLLSTEIN, G., ZACK, D. J., ZHANG, K., YOUNG, T., ALLINGHAM, R. R., WIGGS, J. L., ASHLEY-KOCH, A. & HAUSER, M. A. 2012. Genome-wide analysis of central corneal thickness in primary open-angle glaucoma cases in the NEIGHBOR and GLAUGEN consortia. *Invest Ophthalmol Vis Sci,* 53**,** 4468-74.

VAJARANANT, T. S., NAYAK, S., WILENSKY, J. T. & JOSLIN, C. E. 2010. Gender and glaucoma: what we know and what we need to know. *Curr Opin Ophthalmol,* 21**,** 91-9.

VAN BERGEN, N. J., WOOD, J. P., CHIDLOW, G., TROUNCE, I. A., CASSON, R. J., JU, W. K., WEINREB, R. N. & CROWSTON, J. G. 2009. Recharacterization of the RGC-5 retinal ganglion cell line. *Invest Ophthalmol Vis Sci,* 50**,** 4267-72.

VAN DER AUWERA, G. A., CARNEIRO, M. O., HARTL, C., POPLIN, R., DEL ANGEL, G., LEVY-MOONSHINE, A., JORDAN, T., SHAKIR, K., ROAZEN, D., THIBAULT, J., BANKS, E., GARIMELLA, K. V., ALTSHULER, D., GABRIEL, S. & DEPRISTO, M. A. 2013. From FastQ data to high confidence variant calls: the Genome Analysis Toolkit best practices pipeline. *Curr Protoc Bioinformatics,* 11**,** 11.10.1-11.10.33.

VAN DER VALK, R., WEBERS, C. A., SCHOUTEN, J. S., ZEEGERS, M. P., HENDRIKSE, F. & PRINS, M. H. 2005. Intraocular pressure-lowering effects of all commonly used glaucoma drugs: a meta-analysis of randomized clinical trials. *Ophthalmology,* 112**,** 1177-85.

VAN DIJK, E. L., AUGER, H., JASZCZYSZYN, Y. & THERMES, C. 2014. Ten years of next-generation sequencing technology. *Trends Genet,* 30**,** 418-26.

VAN KOOLWIJK, L. M., BUNCE, C. & VISWANATHAN, A. C. 2013. Gene finding in primary open-angle glaucoma. *J Glaucoma,* 22**,** 473-86.

VAN KOOLWIJK, L. M., RAMDAS, W. D., IKRAM, M. K., JANSONIUS, N. M., PASUTTO, F., HYSI, P. G., MACGREGOR, S., JANSSEN, S. F., HEWITT, A. W., VISWANATHAN, A. C., TEN BRINK, J. B., HOSSEINI, S. M., AMIN, N., DESPRIET, D. D., WILLEMSE-ASSINK, J. J., KRAMER, R., RIVADENEIRA, F., STRUCHALIN, M., AULCHENKO, Y. S., WEISSCHUH, N., ZENKEL, M., MARDIN, C. Y., GRAMER, E., WELGE-LUSSEN, U., MONTGOMERY, G. W., CARBONARO, F., YOUNG, T. L., BELLENGUEZ, C., MCGUFFIN, P., FOSTER, P. J., TOPOUZIS, F., MITCHELL, P., WANG, J. J., WONG, T. Y., CZUDOWSKA, M. A., HOFMAN, A., UITTERLINDEN, A. G., WOLFS, R. C., DE JONG, P. T., OOSTRA, B. A., PATERSON, A. D., MACKEY, D. A., BERGEN, A. A., REIS, A., HAMMOND, C. J., VINGERLING, J. R., LEMIJ, H. G., KLAVER, C.

C. & VAN DUIJN, C. M. 2012. Common genetic determinants of intraocular pressure and primary open-angle glaucoma. *PLoS Genet,* 8**,** e1002611.

VASS, C., HIRN, C., SYCHA, T., FINDL, O., BAUER, P. & SCHMETTERER, L. 2007. Medical interventions for primary open angle glaucoma and ocular hypertension. *Cochrane Database Syst Rev***,** CD003167.

VENTER, J. C., ADAMS, M. D., MYERS, E. W., LI, P. W., MURAL, R. J., SUTTON, G. G., SMITH, H. O., YANDELL, M., EVANS, C. A., HOLT, R. A., GOCAYNE, J. D., AMANATIDES, P., BALLEW, R. M., HUSON, D. H., WORTMAN, J. R., ZHANG, Q., KODIRA, C. D., ZHENG, X. H., CHEN, L., SKUPSKI, M., SUBRAMANIAN, G., THOMAS, P. D., ZHANG, J., GABOR MIKLOS, G. L., NELSON, C., BRODER, S., CLARK, A. G., NADEAU, J., MCKUSICK, V. A., ZINDER, N., LEVINE, A. J., ROBERTS, R. J., SIMON, M., SLAYMAN, C., HUNKAPILLER, M., BOLANOS, R., DELCHER, A., DEW, I., FASULO, D., FLANIGAN, M., FLOREA, L., HALPERN, A., HANNENHALLI, S., KRAVITZ, S., LEVY, S., MOBARRY, C., REINERT, K., REMINGTON, K., ABU-THREIDEH, J., BEASLEY, E., BIDDICK, K., BONAZZI, V., BRANDON, R., CARGILL, M., CHANDRAMOULISWARAN, I., CHARLAB, R., CHATURVEDI, K., DENG, Z., DI FRANCESCO, V., DUNN, P., EILBECK, K., EVANGELISTA, C., GABRIELIAN, A. E., GAN, W., GE, W., GONG, F., GU, Z., GUAN, P., HEIMAN, T. J., HIGGINS, M. E., JI, R. R., KE, Z., KETCHUM, K. A., LAI, Z., LEI, Y., LI, Z., LI, J., LIANG, Y., LIN, X., LU, F., MERKULOV, G. V., MILSHINA, N., MOORE, H. M., NAIK, A. K., NARAYAN, V. A., NEELAM, B., NUSSKERN, D., RUSCH, D. B., SALZBERG, S., SHAO, W., SHUE, B., SUN, J., WANG, Z., WANG, A., WANG, X., WANG, J., WEI, M., WIDES, R., XIAO, C., YAN, C., et al. 2001. The sequence of the human genome. *Science,* 291**,** 1304-51.

VISWANATHAN, D., GOLDBERG, I. & GRAHAM, S. L. 2013. Relationship of change in central corneal thickness to visual field progression in eyes with glaucoma. *Graefes Arch Clin Exp Ophthalmol,* 251**,** 1593-9.

VITART, V., BENCIC, G., HAYWARD, C., SKUNCA HERMAN, J., HUFFMAN, J., CAMPBELL, S., BUCAN, K., NAVARRO, P., GUNJACA, G., MARIN, J., ZGAGA, L., KOLCIC, I., POLASEK, O., KIRIN, M.,

HASTIE, N. D., WILSON, J. F., RUDAN, I., CAMPBELL, H., VATAVUK, Z., FLECK, B. & WRIGHT, A. 2010. New loci associated with central cornea thickness include COL5A1, AKAP13 and AVGR8. *Hum Mol Genet,* 19**,** 4304-11.

VITHANA, E. N., AUNG, T., KHOR, C. C., CORNES, B. K., TAY, W. T., SIM, X., LAVANYA, R., WU, R., ZHENG, Y., HIBBERD, M. L., CHIA, K. S., SEIELSTAD, M., GOH, L. K., SAW, S. M., TAI, E. S. & WONG, T. Y. 2011. Collagen-related genes influence the glaucoma risk factor, central corneal thickness. *Hum Mol Genet,* 20**,** 649-58.

VITHANA, E. N., NONGPIUR, M. E., VENKATARAMAN, D., CHAN, S. H., MAVINAHALLI, J. & AUNG, T. 2010. Identification of a novel mutation in the NTF4 gene that causes primary open-angle glaucoma in a Chinese population. *Mol Vis,* 16**,** 1640-5.

WAGNER, A. H., ANAND, V. N., WANG, W. H., CHATTERTON, J. E., SUN, D., SHEPARD, A. R., JACOBSON, N., PANG, I. H., DELUCA, A. P., CASAVANT, T. L., SCHEETZ, T. E., MULLINS, R. F., BRAUN, T. A. & CLARK, A. F. 2013. Exon-level expression profiling of ocular tissues. *Exp Eye Res,* 111**,** 105-11.

WANG, D., HUANG, W., LI, Y., ZHENG, Y., FOSTER, P. J., CONGDON, N. & HE, M. 2011. Intraocular pressure, central corneal thickness, and glaucoma in chinese adults: the liwan eye study. *Am J Ophthalmol,* 152**,** 454-462 e1.

WANG, D. Y., FAN, B. J., CHUA, J. K., TAM, P. O., LEUNG, C. K., LAM, D. S. & PANG, C. P. 2006. A genome-wide scan maps a novel juvenile-onset primary open-angle glaucoma locus to 15q. *Invest Ophthalmol Vis Sci,* 47**,** 5315-21.

WANG, D. Y., RAY, A., RODGERS, K., ERGORUL, C., HYMAN, B. T., HUANG, W. & GROSSKREUTZ, C. L. 2010a. Global gene expression changes in rat retinal ganglion cells in experimental glaucoma. *Invest Ophthalmol Vis Sci,* 51**,** 4084-95.

WANG, K., LI, M. & HAKONARSON, H. 2010b. ANNOVAR: functional annotation of genetic variants from high-throughput sequencing data. *Nucleic Acids Res,* 38**,** e164.

WANG, L., DAMJI, K. F., MUNGER, R., JONASSON, F., ARNARSSON, A., SASAKI, H. & SASAKI, K. 2003. Increased disk size in glaucomatous eyes vs normal eyes in the Reykjavik eye study. *Am J Ophthalmol,* 135**,** 226-8.

WANG, L., GUO, Y., HUANG, W. J., KE, X., POYET, J. L., MANJI, G. A., MERRIAM, S., GLUCKSMANN, M. A., DISTEFANO, P. S., ALNEMRI, E. S. & BERTIN, J. 2001. Card10 is a novel caspase recruitment domain/membrane-associated guanylate kinase family member that interacts with BCL10 and activates NF-kappa B. *J Biol Chem,* 276**,** 21405-9.

WANG, S. Y., MELLES, R. & LIN, S. C. 2014. The impact of central corneal thickness on the risk for glaucoma in a large multiethnic population. *J Glaucoma,* 23**,** 606-12.

WANG, W. Y., BARRATT, B. J., CLAYTON, D. G. & TODD, J. A. 2005. Genome-wide association studies: theoretical and practical concerns. *Nat Rev Genet,* 6**,** 109-18.

WANG, X., HARMON, J., ZABRIESKIE, N., CHEN, Y., GROB, S., WILLIAMS, B., LEE, C., KASUGA, D., SHAW, P. X., BUEHLER, J., WANG, N. & ZHANG, K. 2010c. Using the Utah Population Database to assess familial risk of primary open angle glaucoma. *Vision Res,* 50**,** 2391-5.

WANG, Z., GERSTEIN, M. & SNYDER, M. 2009. RNA-Seq: a revolutionary tool for transcriptomics. *Nat Rev Genet,* 10**,** 57-63.

WARD, N. J., HO, K. W., LAMBERT, W. S., WEITLAUF, C. & CALKINS, D. J. 2014. Absence of transient receptor potential vanilloid-1 accelerates stress-induced axonopathy in the optic projection. *J Neurosci,* 34**,** 3161-70.

WEI, X., YU, Z., CHO, K. S., CHEN, H., MALIK, M. T., CHEN, X., LO, E. H., WANG, X. & CHEN, D. F. 2011. Neuroglobin is an endogenous neuroprotectant for retinal ganglion cells against glaucomatous damage. *Am J Pathol,* 179**,** 2788-97.

WEIH, L. M., NANJAN, M., MCCARTY, C. A. & TAYLOR, H. R. 2001. Prevalence and predictors of open-angle glaucoma: results from the visual impairment project. *Ophthalmology,* 108**,** 1966-72.

WEINREB, R. N., AUNG, T. & MEDEIROS, F. A. 2014. The pathophysiology and treatment of glaucoma: a review. *Jama,* 311**,** 1901-11.

WEINREB, R. N., LIEBMANN, J. M., CIOFFI, G. A., GOLDBERG, I., BRANDT, J. D., JOHNSON, C. A., ZANGWILL, L. M., SCHNEIDER, S., BADGER, H. & BEJANIAN, M. 2018. Oral Memantine for the Treatment of Glaucoma: Design and Results of 2 Randomized, Placebo-Controlled, Phase 3 Studies. *Ophthalmology,* 125**,** 1874-1885.

WEISSCHUH, N., WOLF, C., WISSINGER, B. & GRAMER, E. 2009. A clinical and molecular genetic study of German patients with primary congenital glaucoma. *Am J Ophthalmol,* 147**,** 744-53.

WENSOR, M. D., MCCARTY, C. A., STANISLAVSKY, Y. L., LIVINGSTON, P. M. & TAYLOR, H. R. 1998. The prevalence of glaucoma in the Melbourne Visual Impairment Project. *Ophthalmology,* 105**,** 733-9.

WENTZ-HUNTER, K., SHEN, X., OKAZAKI, K., TANIHARA, H. & YUE, B. Y. 2004. Overexpression of myocilin in cultured human trabecular meshwork cells. *Exp Cell Res,* 297**,** 39-48.

WENTZ-HUNTER, K., UEDA, J., SHIMIZU, N. & YUE, B. Y. 2002. Myocilin is associated with mitochondria in human trabecular meshwork cells. *J Cell Physiol,* 190**,** 46-53.

WIGGS, J. L., HAINES, J. L., PAGLINAUAN, C., FINE, A., SPORN, C. & LOU, D. 1994. Genetic linkage of autosomal dominant juvenile glaucoma to 1q21-q31 in three affected pedigrees. *Genomics,* 21**,** 299-303.

WIGGS, J. L., KANG, J. H., YASPAN, B. L., MIREL, D. B., LAURIE, C., CRENSHAW, A., BRODEUR, W., GOGARTEN, S., OLSON, L. M., ABDRABOU, W., DELBONO, E., LOOMIS, S., HAINES, J. L. & PASQUALE, L. R. 2011. Common variants near CAV1 and CAV2 are associated with primary open-angle glaucoma in Caucasians from the USA. *Hum Mol Genet,* 20**,** 4707-13.

WIGGS, J. L., LYNCH, S., YNAGI, G., MASELLI, M., AUGUSTE, J., DEL BONO, E. A., OLSON, L. M. & HAINES, J. L. 2004. A genomewide scan identifies novel early-onset primary open-angle glaucoma loci on 9q22 and 20p12. *Am J Hum Genet,* 74**,** 1314-20.

WIGGS, J. L. & VOLLRATH, D. 2001. Molecular and clinical evaluation of a patient hemizygous for TIGR/MYOC. *Arch Ophthalmol,* 119**,** 1674-8.

WIGGS, J. L., YASPAN, B. L., HAUSER, M. A., KANG, J. H., ALLINGHAM, R. R., OLSON, L. M., ABDRABOU, W., FAN, B. J., WANG, D. Y., BRODEUR, W., BUDENZ, D. L., CAPRIOLI, J., CRENSHAW, A., CROOKS, K., DELBONO, E., DOHENY, K. F., FRIEDMAN, D. S., GAASTERLAND, D., GAASTERLAND, T., LAURIE, C., LEE, R. K., LICHTER, P. R., LOOMIS, S., LIU, Y., MEDEIROS, F. A., MCCARTY, C., MIREL, D., MOROI, S. E., MUSCH, D. C., REALINI, A., ROZSA, F. W., SCHUMAN, J. S., SCOTT, K., SINGH, K., STEIN, J. D., TRAGER, E. H., VANVELDHUISEN, P., VOLLRATH, D., WOLLSTEIN, G., YONEYAMA, S., ZHANG, K., WEINREB, R. N., ERNST, J., KELLIS, M., MASUDA, T., ZACK, D., RICHARDS, J. E., PERICAK-VANCE, M., PASQUALE, L. R. & HAINES, J. L. 2012. Common variants at 9p21 and 8q22 are associated with increased susceptibility to optic nerve degeneration in glaucoma. *PLoS Genet,* 8**,** e1002654.

WILKINSON, C. H., VAN DER STRAATEN, D., CRAIG, J. E., COOTE, M. A., MCCARTNEY, P. J., STANKOVICH, J., STONE, E. M. & MACKEY, D. A. 2003. Tonography demonstrates reduced facility of outflow of aqueous humor in myocilin mutation carriers. *J Glaucoma,* 12**,** 237-42.

WILLIAMS, S. E., CARMICHAEL, T. R., WAINSTEIN, T., HOBBS, A. & RAMSAY, M. 2015. MYOC Mutations in Black South African Patients with Primary Open-angle Glaucoma: Genetic Testing and Cascade Screening. *Ophthalmic Genet,* 36**,** 31-8.

WILSON, A. M. & DI POLO, A. 2012. Gene therapy for retinal ganglion cell neuroprotection in glaucoma. *Gene Ther,* 19**,** 127-36.

WIRTZ, M. K., SAMPLES, J. R., CHOI, D. & GAUDETTE, N. D. 2007. Clinical features associated with an Asp380His Myocilin mutation in a US family with primary open-angle glaucoma. *Am J Ophthalmol,* 144**,** 75-80.

WIRTZ, M. K., SAMPLES, J. R., KRAMER, P. L., RUST, K., TOPINKA, J. R., YOUNT, J., KOLER, R. D. & ACOTT, T. S. 1997. Mapping a gene for adult-onset primary open-angle glaucoma to chromosome 3q. *Am J Hum Genet,* 60**,** 296-304.

WIRTZ, M. K., SAMPLES, J. R., RUST, K., LIE, J., NORDLING, L., SCHILLING, K., ACOTT, T. S. & KRAMER, P. L. 1999. GLC1F, a new primary open-angle glaucoma locus, maps to 7q35-q36. *Arch Ophthalmol,* 117**,** 237-41.

WIRTZ, M. K., SAMPLES, J. R., TOUMANIDOU, V., CHARLESWORTH, J., MIKROPOULOS, D. G., KALTSOS, K., ECONOMOU, A., DIMOPOULOS, A., GEORGIADOU, I. N., MOUMTZIS, G., PAPANASTASIOU, A., KRAMER, P. L., DYER, T., BLANGERO, J. & KONSTAS, A. G. 2010. Association of POAG risk factors and the Thr377Met MYOC mutation in an isolated Greek population. *Invest Ophthalmol Vis Sci,* 51**,** 3055-60.

WISTOW, G. 2006. The NEIBank project for ocular genomics: data-mining gene expression in human and rodent eye tissues. *Prog Retin Eye Res,* 25**,** 43-77.

WOLFS, R. C., KLAVER, C. C., RAMRATTAN, R. S., VAN DUIJN, C. M., HOFMAN, A. & DE JONG, P. T. 1998. Genetic risk of primary open-angle glaucoma. Population-based familial aggregation study. *Arch Ophthalmol,* 116**,** 1640-5.

WONG, T. Y., KLEIN, B. E., KLEIN, R., KNUDTSON, M. & LEE, K. E. 2003. Refractive errors, intraocular pressure, and glaucoma in a white population. *Ophthalmology,* 110**,** 211-7.

WONG, Y. C. & HOLZBAUR, E. L. 2014. Optineurin is an autophagy receptor for damaged mitochondria in parkin-mediated mitophagy that is disrupted by an ALS-linked mutation. *Proc Natl Acad Sci U S A,* 111**,** E4439-48.

WOOD, J. P., CHIDLOW, G., TRAN, T., CROWSTON, J. G. & CASSON, R. J. 2010. A comparison of differentiation protocols for RGC-5 cells. *Invest Ophthalmol Vis Sci,* 51**,** 3774-83.

WU, G. L., YUAN, J. L., HUANG, X. D., RONG, J. F., ZHANG, L. X., LIU, Y. P. & WANG, F. L. 2013. Evaluating the expression of CARMA3 as a prognostic tumor marker in renal cell carcinoma. *Tumour Biol,* 34**,** 3431-5.

WU, J., HEWITT, A. W., GREEN, C. M., RING, M. A., MCCARTNEY, P. J., CRAIG, J. E. & MACKEY, D. A. 2006. Disease severity of familial glaucoma compared with sporadic glaucoma. *Arch Ophthalmol,* 124**,** 950-4.

WU, M. C., LEE, S., CAI, T., LI, Y., BOEHNKE, M. & LIN, X. 2011. Rare-variant association testing for sequencing data with the sequence kernel association test. *Am J Hum Genet,* 89**,** 82-93.

WU, S. Y., NEMESURE, B. & LESKE, M. C. 1999. Refractive errors in a black adult population: the Barbados Eye Study. *Invest Ophthalmol Vis Sci,* 40**,** 2179-84.

XIA, C. H., CHANG, B., DEROSA, A. M., CHENG, C., WHITE, T. W. & GONG, X. 2012. Cataracts and microphthalmia caused by a Gja8 mutation in extracellular loop 2. *PLoS One,* 7**,** e52894.

XIE, C., HAN, Y., FU, L., LI, Q., QIU, X. & WANG, E. 2014. Overexpression of CARMA3 is associated with advanced tumor stage, cell cycle progression, and cisplatin resistance in human epithelial ovarian cancer. *Tumour Biol,* 35**,** 7957-64.

XU, L., WANG, Y., WANG, S. & JONAS, J. B. 2007. High myopia and glaucoma susceptibility the Beijing Eye Study. *Ophthalmology,* 114**,** 216-20.

XU, L., ZHANG, H., WANG, Y. X. & JONAS, J. B. 2008. Central corneal thickness and glaucoma in adult Chinese: the Beijing Eye Study. *J Glaucoma,* 17**,** 647-53.

YAM, G. H., GAPLOVSKA-KYSELA, K., ZUBER, C. & ROTH, J. 2007a. Aggregated myocilin induces russell bodies and causes apoptosis: implications for the pathogenesis of myocilin-caused primary open-angle glaucoma. *Am J Pathol,* 170**,** 100-9.

YAM, G. H., GAPLOVSKA-KYSELA, K., ZUBER, C. & ROTH, J. 2007b. Sodium 4-phenylbutyrate acts as a chemical chaperone on misfolded myocilin to rescue cells from endoplasmic reticulum stress and apoptosis. *Invest Ophthalmol Vis Sci,* 48**,** 1683-90.

YAMAMOTO, M., WAKATSUKI, T., HADA, A. & RYO, A. 2001. Use of serial analysis of gene expression (SAGE) technology. *J Immunol Methods,* 250**,** 45-66.

YAN, X., YUAN, F., CHEN, X. & DONG, C. 2015. Bioinformatics analysis to identify the differentially expressed genes of glaucoma. *Mol Med Rep*.

YING, H., SHEN, X., PARK, B. & YUE, B. Y. 2010. Posttranslational modifications, localization, and protein interactions of optineurin, the product of a glaucoma gene. *PLoS One,* 5**,** e9168.

YING, H., TURTURRO, S., NGUYEN, T., SHEN, X., ZELKHA, R., JOHNSON, E. C., MORRISON, J. C. & YUE, B. Y. 2015. Induction of autophagy in rats upon overexpression of wild-type and mutant optineurin gene. *BMC Cell Biol,* 16**,** 14.

YING, H. & YUE, B. Y. 2012. Cellular and molecular biology of optineurin. *Int Rev Cell Mol Biol,* 294**,** 223-58.

ZAIDI, A. A. 1980. Trabeculectomy: a review and 4-year follow-up. *Br J Ophthalmol,* 64**,** 436-9.

ZHAO, S., FUNG-LEUNG, W. P., BITTNER, A., NGO, K. & LIU, X. 2014. Comparison of RNA-Seq and microarray in transcriptome profiling of activated T cells. *PLoS One,* 9**,** e78644.

ZHAO, T., MIAO, Z., WANG, Z., XU, Y., WU, J., LIU, X., YOU, Y. & LI, J. 2013. CARMA3 overexpression accelerates cell proliferation and inhibits paclitaxel-induced apoptosis through NF-kappaB regulation in breast cancer cells. *Tumour Biol,* 34**,** 3041-7.

ZHAVORONKOV, A., IZUMCHENKO, E., KANHERKAR, R. R., TEKA, M., CANTOR, C., MANAYE, K., SIDRANSKY, D., WEST, M. D., MAKAREV, E. & CSOKA, A. B. 2016. Pro-fibrotic pathway activation in trabecular meshwork and lamina cribrosa is the main driving force of glaucoma. *Cell Cycle,* 15**,** 1643-52.

ZHOU, M., WANG, W., HUANG, W. & ZHANG, X. 2014. Diabetes mellitus as a risk factor for open-angle glaucoma: a systematic review and meta-analysis. *PLoS One,* 9**,** e102972.

ZHOU, T., SOUZEAU, E., SHARMA, S., LANDERS, J., MILLS, R., GOLDBERG, I., HEALEY, P. R., GRAHAM, S., HEWITT, A. W., MACKEY, D. A., GALANOPOULOS, A., CASSON, R. J., RUDDLE, J. B., ELLIS, J., LEO, P., BROWN, M. A., MACGREGOR, S., LYNN, D. J., BURDON, K. P. & CRAIG, J. E. 2017a. Whole

exome sequencing implicates eye development, the unfolded protein response and plasma membrane homeostasis in primary open-angle glaucoma. *PLoS One,* 12**,** e0172427.

ZHOU, T., SOUZEAU, E., SHARMA, S., SIGGS, O. M., GOLDBERG, I., HEALEY, P. R., GRAHAM, S., HEWITT, A. W., MACKEY, D. A., CASSON, R. J., LANDERS, J., MILLS, R., ELLIS, J., LEO, P., BROWN, M. A., MACGREGOR, S., BURDON, K. P. & CRAIG, J. E. 2016. Rare variants in optic disc area gene CARD10 enriched in primary open-angle glaucoma. *Mol Genet Genomic Med,* 4**,** 624-633.

ZHOU, T., SOUZEAU, E., SIGGS, O. M., LANDERS, J., MILLS, R., GOLDBERG, I., HEALEY, P. R., GRAHAM, S., HEWITT, A. W., MACKEY, D. A., GALANOPOULOS, A., CASSON, R. J., RUDDLE, J. B., ELLIS, J., LEO, P., BROWN, M. A., MACGREGOR, S., SHARMA, S., BURDON, K. P. & CRAIG, J. E. 2017b. Contribution of Mutations in Known Mendelian Glaucoma Genes to Advanced Early-Onset Primary Open-Angle Glaucoma. *Invest Ophthalmol Vis Sci,* 58**,** 1537-1544.

ZHOU, Y., GRINCHUK, O. & TOMAREV, S. I. 2008. Transgenic mice expressing the Tyr437His mutant of human myocilin protein develop glaucoma. *Invest Ophthalmol Vis Sci,* 49**,** 1932-9.

ZHOU, Z. & VOLLRATH, D. 1999. A cellular assay distinguishes normal and mutant TIGR/myocilin protein. *Hum Mol Genet,* 8**,** 2221-8.

ZHU, G., WU, C. J., ZHAO, Y. & ASHWELL, J. D. 2007. Optineurin negatively regulates TNFalpha-induced NF-kappaB activation by competing with NEMO for ubiquitinated RIP. *Curr Biol,* 17**,** 1438-43.

ZODE, G. S., BUGGE, K. E., MOHAN, K., GROZDANIC, S. D., PETERS, J. C., KOEHN, D. R., ANDERSON, M. G., KARDON, R. H., STONE, E. M. & SHEFFIELD, V. C. 2012. Topical ocular sodium 4-phenylbutyrate rescues glaucoma in a myocilin mouse model of primary open-angle glaucoma. *Invest Ophthalmol Vis Sci,* 53**,** 1557-65.

ZODE, G. S., KUEHN, M. H., NISHIMURA, D. Y., SEARBY, C. C., MOHAN, K., GROZDANIC, S. D., BUGGE, K., ANDERSON, M. G., CLARK, A. F., STONE, E. M. & SHEFFIELD, V. C. 2011. Reduction of ER stress via a chemical chaperone prevents disease phenotypes in a mouse model of primary open angle glaucoma. *J Clin Invest,* 121**,** 3542-53.